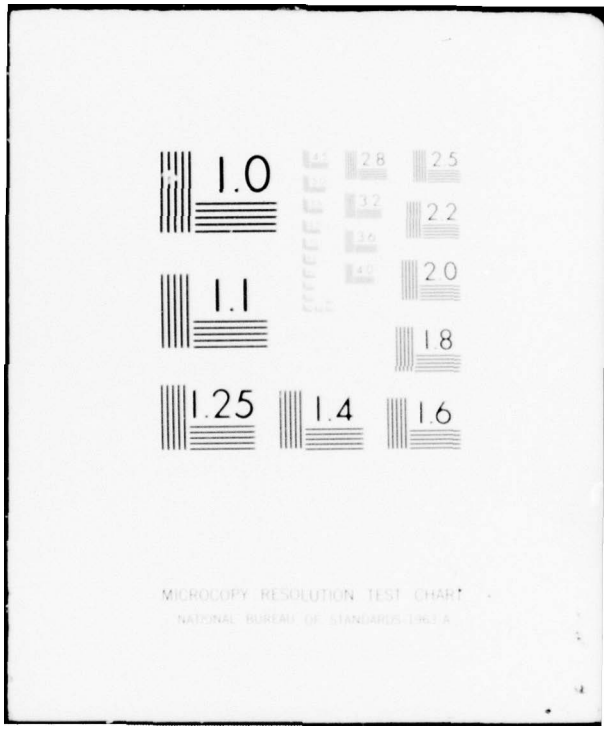
AD-A042 517 TELEDYNE CAE TOLEDO OHIO F/G 21/5
ADVANCED SMALL AXIAL TURBINE TECHNOLOGY.(U)
MAY 77 H F DUE, C ROGO, C L KOSIER DAAJ02-72-C-0117
UNCLASSIFIED TCAE-1508 USAAMRDL-TR-77-1 NL

1 OF 4
AD A042517




1.0
1.1
1.25
1.4
1.6
2.0
2.2
2.5
2.8
3.2
3.6
4.0
1.8
MICROCOPY RESOLUTION TEST CHART
NATIONAL BUREAU OF STANDARDS-1963-A

AD A042517

USAAMRDL-TR-77-1

(12)

ADVANCED SMALL AXIAL TURBINE TECHNOLOGY

DDC
RECEIVED
AUG 4 1977
A

Teledyne CAE
1330 Laskey Road
Toledo, Ohio 43612

May 1977

Final Report for Period July 1972 - June 1976

Approved for public release;
distribution unlimited.

Prepared for

EUSTIS DIRECTORATE
U. S. ARMY AIR MOBILITY RESEARCH AND DEVELOPMENT LABORATORY
Fort Eustis, Va. 23604

AD NO.
DDC FILE COPY

EUSTIS DIRECTORATE POSITION STATEMENT

This report provides experimental data obtained from cold air annular cascade testing and full-round cold air rig testing of a single-stage, high-work, axial-flow turbine. The specific parameters that were evaluated include meridional nozzle constriction, inlet boundary layer, inlet velocity gradients, turbulence intensity, nozzle and rotor cooling, rotor-to-nozzle axial spacing, nozzle and rotor solidity, Reynolds number and Mach numbers. It is expected that the results of this program will be used in future programs to improve the performance of advanced small axial-flow turbines.

This report has been reviewed by technical personnel from this Directorate, and the conclusions and recommendations contained herein are concurred in by this Directorate. The Project Engineers for this effort were Mr. Albert E. Easterling and Mr. LeRoy T. Burrows, Propulsion Technical Area, Technology Applications Division.

DISCLAIMERS

The findings in this report are not to be construed as an official Department of the Army position unless so designated by other authorized documents.

When Government drawings, specifications, or other data are used for any purpose other than in connection with a definitely related Government procurement operation, the United States Government thereby incurs no responsibility nor any obligation whatsoever; and the fact that the Government may have formulated, furnished, or in any way supplied the said drawings, specifications, or other data is not to be regarded by implication or otherwise as in any manner licensing the holder or any other person or corporation, or conveying any rights or permission, to manufacture, use, or sell any patented invention that may in any way be related thereto.

Trade names cited in this report do not constitute an official endorsement or approval of the use of such commercial hardware or software.

DISPOSITION INSTRUCTIONS

Destroy this report when no longer needed. Do not return it to the originator.

UNCLASSIFIED

SECURITY CLASSIFICATION OF THIS PAGE (When Data Entered)

REPORT DOCUMENTATION PAGE	READ INSTRUCTIONS BEFORE COMPLETING FORM
1. REPORT NUMBER: USAAMRDL-TR-77-1	2. GOVT ACCESSION NO. / 3. RECIPIENT'S CATALOG NUMBER
4. TITLE (and Subtitle): ADVANCED SMALL AXIAL TURBINE TECHNOLOGY	5. TYPE OF REPORT & PERIOD COVERED: FINAL REPORT, JULY 1972-JUNE 1976
	6. PERFORMING ORG. REPORT NUMBER: 1508
7. AUTHOR(s): H. F. DUE, JR., C. L. KOSIER, C. ROGO, G. B. JASAS	8. CONTRACT OR GRANT NUMBER(s): DAAJ02-72-C-0117
9. PERFORMING ORGANIZATION NAME AND ADDRESS: TELEDYNE CAE, 1330 LASKEY ROAD, TOLEDO, OHIO 43612	10. PROGRAM ELEMENT, PROJECT, TASK AREA & WORK UNIT NUMBERS: 62207A 1G162207AA71 02 011 EK
11. CONTROLLING OFFICE NAME AND ADDRESS: EUSTIS DIRECTORATE, U.S. ARMY AIR MOBILITY RESEARCH AND DEVELOPMENT LABORATORY, FORT EUSTIS, VIRGINIA	12. REPORT DATE: May 1977 / 13. NUMBER OF PAGES: 330
14. MONITORING AGENCY NAME & ADDRESS (if different from Controlling Office)	15. SECURITY CLASS. (of this report): UNCLASSIFIED / 15a. DECLASSIFICATION/DOWNGRADING SCHEDULE

16. DISTRIBUTION STATEMENT (of this Report)

Approved for public release; distribution unlimited.

DDC RELEASED AUG 4 1977 A

17. DISTRIBUTION STATEMENT (of the abstract entered in Block 20, if different from Report)

18. SUPPLEMENTARY NOTES

19. KEY WORDS (Continue on reverse side if necessary and identify by block number)

SMALL AXIAL TURBINE, HIGHLY LOADED COOLED TURBINE
ADVANCED TURBINE TECHNOLOGY, LOW ASPECT RATIO,
FLOW PERTURBATIONS, TURBINE DESIGN TECHNIQUE

20. ABSTRACT (Continue on reverse side if necessary and identify by block number)

The objective of the program was to provide the advanced technology small axial-flow turbine designer with empirically derived techniques to improve the accuracy of predicting losses, flow condition, velocity triangles and design point matching. The techniques addressed practical mechanical constraints typical of small, highly loaded cooled turbines, such as: (1) cooling system type and injection method or location, (2) blade fabrication, (3) wall thickness and tolerances, (4) engine integration requirements, (5) life, and (6) maintainability. An advanced turbo-shaft gas generator application established a realistic turbine environment.

next page

DD FORM 1 JAN 73 1473 EDITION OF 1 NOV 65 IS OBSOLETE

UNCLASSIFIED

SECURITY CLASSIFICATION OF THIS PAGE (When Data Entered)

405711

The turbine was designed for a work level of 180 Btu/lb, a nozzle inlet temperature of 2400°F and 4.8 lb/sec airflow.

The program was conducted in five phases:

Phase I - Preliminary Design
Phase II - Turbine Cascade Investigation
Phase III - Stage Investigation - Full-Round Rig Test
Phase IV - Design Technique Assessment
Phase V - Modification and Test

For the particular turbine application chosen, experimental data have been obtained for the effects of meridional nozzle constriction, inlet boundary layer, inlet velocity gradients, turbulence intensity, nozzle and rotor cooling, rotor-to-nozzle spacing, nozzle and rotor solidity and Mach number effects. Correlations were obtained and differences between cascade and full-stage test data established. An aerodynamic modeling system was formulated and verified, resulting in an improved turbine design.

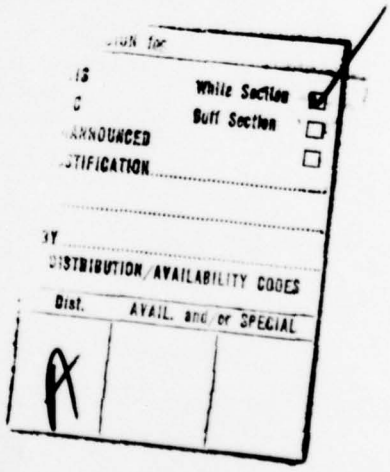
PREFACE

The Advanced Small Axial Turbine Technology Program was sponsored by the U.S. Army Air Mobility Research and Development Laboratory under Contract DAAJ02-72-C-0117.

The intent of the program was to aid the designer of small, highly loaded, axial flow turbines by investigating the variables which effect losses and improve our understanding of the design criteria.

We wish to acknowledge the contributions of the following Teledyne CAE personnel: Leroy (Roy) Neal, Ernest Ortiz, John Berg and George Richardson.

The program was monitored by Messrs. Albert (Gene) Easterling and LeRoy (Roy) Burrows of AMRDL. Their support was fully appreciated.



Data Contained in Appendix C was the best available copy. Users of this report may obtain verification of this data by contacting the Eustis Directorate, US Army Air Mobility R&D Laboratory (AVRADCOM), Ft. Eustis, Va. 23604

TABLE OF CONTENTS

	Page
PREFACE	3
LIST OF ILLUSTRATIONS	9
LIST OF TABLES	28
INTRODUCTION	30
PHASE I - TECHNICAL DISCUSSION	35
PRELIMINARY DESIGN	35
OBJECTIVES	35
CURSORY ENGINE DESIGN	35
CYCLE ANALYSIS	37
COMPRESSOR	37
COMBUSTOR	37
TURBINE PRELIMINARY DESIGN	38
TURBINE DETAIL DESIGN	47
SUMMARY OF PRELIMINARY ENGINE ANALYSIS	83
PHASE II - TURBINE CASCADE INVESTIGATION	85
OBJECTIVE	85
CASCADE RIG AND INSTRUMENTATION DESIGN	85
MOMENTUM TRANSFER SYSTEM	88
NOZZLE MERIDIONAL CONSTRICTION	91
TURBULENCE SCREEN SIZING	97
VANE AND BLADE FABRICATION	98
INSTRUMENTATION	98
INSTRUMENTATION CALIBRATION AND ACCURACY	107
TEST FACILITY, PROCEDURES AND DATA ACQUISITION	109
TEST FACILITY	109
TEST PROCEDURES	110

PRECEDING PAGE BLANK-NOT FILMED

TABLE OF CONTENTS (continued)

	Page
DATA ACQUISITION	113
CASCADE TEST RESULTS	115
TEST SERIES A - EVALUATION OF MERIDIONAL CONSTRICTION ON NOZZLES	115
TEST SERIES B - EVALUATION OF HIGH STATOR MEAN EXIT MACH NUMBER ON STATOR AND ROTOR PERFORMANCE	122
TEST SERIES C - EFFECT OF INLET TURBULENCE	123
TEST SERIES E AND F - E: EVALUATION OF STATOR EXIT FLOW DISTORTION AND SIMULATED LABYRINTH SEAL LEAKAGE ON ROTOR CASCADE PERFORMANCE F: EVALUATION OF SECOND ROTOR LOADING	132
TEST SERIES G - EFFECT OF COOLING AND SOLIDITY ON STATOR PERFORMANCE	133
TEST SERIES H - EFFECT OF STATOR COOLING ON TWO ROTOR SOLIDITIES AND AXIAL SPACING	136
CONCLUSIONS	139
TEST SERIES A - EVALUATION OF MERIDIONAL CONSTRICTION ON NOZZLES	139
TEST SERIES B - EFFECT OF STATOR MACH NUMBER ON LOSSES	140
TEST SERIES C - EFFECT OF INLET TURBULENCE INTENSITY ON STATOR PERFORMANCE	140
TEST SERIES D - EFFECT OF STATOR BOUNDARY LAYER AND DISTORTION ON PERFORMANCE	140
TEST SERIES E - EVALUATION OF STATOR EXIT FLOW DISTORTION AND SIMULATED LABYRINTH SEAL LEAKAGE ON ROTOR CASCADE PERFORMANCE	141
TEST SERIES F - ROTOR LOADING EFFECTS	141
TEST SERIES G - EFFECT OF COOLING AND SOLIDITY ON STATOR PERFORMANCE	141
TEST SERIES H - EFFECT OF STATOR COOLING ON TWO ROTOR SOLIDITIES AND AXIAL SPACING	141
PHASE III - STAGE INVESTIGATION	143
OBJECTIVE	143
TURBINE STAGE DESIGN AND INSTRUMENTATION	143
TURBINE RIG DESIGN	147
TEST FACILITY, INSTRUMENTATION, AND PROCEDURE	151
TEST FACILITY	151
INSTRUMENTATION AND ACCURACY	154
TEST PROCEDURE	156

TABLE OF CONTENTS (continued)

Page

PHASE III - (continued)

TURBINE STAGE TEST RESULTS 158

TEST 1.0 - NOZZLE PERFORMANCE 158
TEST 2.0 - DISK WINDAGE, BEARING LOSSES AND ROTOR COOLANT PUMPING LOSSES 176
TEST 3.0 - EVALUATION OF PERFORMANCE OF PRESSURE SURFACE LOADED TURBINE 178
TEST 4.0 - DETERMINATION OF COOLING FLOW LOSSES ON NOMINAL PLR TURBINE 184
TEST 5.0 - EVALUATION OF BLADE LOADING 188
TESTS 6 and 7 - EFFECT OF LEAKAGE (BYPASS) FLOW ON PERFORMANCE OF TWO ROTOR DESIGNS 196
TESTS 8 and 9 - EFFECTS OF INCREASED NOZZLE/ROTOR AXIAL SPACING AND EFFECT OF NOZZLE BYPASS FLOW ON PERFORMANCE OF SLR TURBINE 197
TESTS 10 and 11 - EFFECT OF INLET BOUNDARY LAYER AND DISTORTION ON PERFORMANCE OF NOMINAL PLR TURBINE 201
TEST 12 - EFFECT OF DECREASED ROTOR SOLIDITY ON PERFORMANCE OF PLR TURBINE 206
TEST 13 - REYNOLDS NUMBER EFFECT ON PERFORMANCE 207

PHASE III DATA EVALUATION 208

PHASE IV - DESIGN TECHNIQUE ASSESSMENT 213

OBJECTIVES 213
REVIEW OF AVAILABLE LOSS SYSTEMS AND DATA - ANALYTICAL AND EXPERIMENTAL 213
DESCRIPTION OF DESIGN TECHNIQUES 215

MERIDIONAL CONSTRICTION 218
NOZZLE EXIT MACH NUMBER 219
INLET TURBULENCE 220
INLET BOUNDARY LAYER AND FLOW DISTORTION 220
NOZZLE COOLING AND ROTOR COOLING INJECTION EFFECTS 221
REYNOLDS NUMBER 221
SOLIDITY EFFECTS OF NOZZLE AND ROTOR ON PERFORMANCE 224
BLADE LOADING ENVELOPE 224
MODIFICATION OF DESIGN TECHNIQUE 225

PHASE V - TURBINE STAGE REDESIGN AND TEST 230

TEST RIG DESIGN MODIFICATION 230

TABLE OF CONTENTS (continued)

	Page
PHASE V - (continued)	
TEST FACILITY, PROCEDURE AND DATA ACQUISITION	230
TEST FACILITY	230
TEST PROCEDURE	230
DATA ACQUISITION	234
TURBINE STAGE REDESIGN TEST RESULTS	234
PHASE V, TEST 1 - NOZZLE PERFORMANCE	234
PHASE V, TEST 2 - TURBINE STAGE PERFORMANCE WITH PLR ROTOR	241
PHASE V, TEST 3 - TURBINE STAGE PERFORMANCE WITH SLR ROTOR	248
PHASE V SUMMARY AND CONCLUSIONS	257
CONCLUSIONS AND RECOMMENDATIONS	263
CONCLUSIONS	263
RECOMMENDATIONS	263
CASCADE TESTING	263
FULL ROUND COLD FLOW RIG TESTING	264
FULL ROUND HOT RIG TESTS	264
LITERATURE CITED	266
APPENDIX A - COMPUTER OUTPUT FOR CYCLE ANALYSIS OF TURBOSHAFT CONFIGURATIONS	271
APPENDIX B - COMPUTER OUTPUT FOR PRELIMINARY TURBINE DESIGN	279
APPENDIX C - COMPUTER OUTPUT FOR FLOWPATH STREAMLINE ANALYSIS	283
APPENDIX D - TESTING SEQUENCE FOR PHASE II	317
APPENDIX E - PROBLEM AREAS ENCOUNTERED DURING PHASE III TESTING	321
LIST OF SYMBOLS	327

LIST OF ILLUSTRATIONS

Figure		Page
1	Small, High Work Turbines Cover a Wide Spectrum of Core Air Flow	31
2	Turbine Efficiency Shows a Strong Dependency on Blade Height and Tip Clearance	32
3	Dunham & Came Turbine Efficiency Prediction vs. Data	32
4	Candidate Engine Configuration No. 1	36
5	Candidate Engine Configuration No. 2	36
6	Turboshaft Engine Cycle Performance at 100 Percent Power	38
7	Axial-Centrifugal Stage Matching Criteria	38
8	Effect of Design Parameters on Turbine Efficiency . . .	42
9	Performance Effects for 2200°F - 170 BTU/lb Turbine . .	43
10	Performance Effects for 2500°F - 200 BTU/lb Turbine . .	43
11	Nozzle and Rotor Velocity Variation with Stage Loading	43
12	Effect of Loading on Rotor Blade Geometry	43
13	Turbine Cooling Requirements	44
14	Effect of Loading on Blade Number and Height	46
15	Effect of Loading on Turbine Weight	46
16	Performance Effects on 2400°F - 180 BTU/lb Turbine . .	47
17	Preliminary Turbine Flowpath	48
18	Preliminary Velocity Triangles (Free-Vortex)	48
19	Division of Total Pressure Loss	50

LIST OF ILLUSTRATIONS

Figure		Page
20	Estimate of Radial Loss Distribution	50
21	Radial Work Distribution for Runs 4 through 9	50
22	Inlet Temperature Distribution for Streamline Analysis - Run 6	50
23	Stator Exit Tangential Velocity Distributions for Streamline Analysis	53
24(a)	Velocity Triangles for Streamline Analysis - Runs 1, 5, 6	54
24(b)	Velocity Triangles for Streamline Analysis - Runs 7, 7a, 8	54
25	Rotor Exit Axial Velocity Radial Distributions	56
26	Radial Work Distribution Resulting from Constant Total Pressure at the Rotor Exit	57
27	Radial Distribution of Absolute Mach Number at Stator Exit	57
28	Radial Distribution of Rotor Relative Mach Number . . .	57
29	Radial Distribution of Absolute Flow Angle at Stator Exit	57
30	Radial Distribution of Rotor Relative Flow Angle . . .	58
31	Radial Distribution of Static Pressure Reaction	58
32	Comparison of Streamline Analyses	59
33	Stator Airfoil Section Coordinates	62
34	Stator Critical Velocity Ratio Distribution	62
35	Stator Boundary Layer Properties Surface Suction . . .	62
36	Effect of Mach No. on Loss for Various Contours (Reference 41).	62
37	Optimum/Geometry Relationship for Minimum Loss (Reference 41).	63

LIST OF ILLUSTRATIONS

Figure		Page
38	Definition of Geometry for a Nozzle with Meridional Constriction	65
39	Rotor Hub Section - Pressure-Side Loaded - 12.5 Percent Span	67
40	Rotor Hub Section - Suction-Side Loaded - 12.5 Percent Span	67
41	Rotor Hub Section - Velocity Distributions	67
42	Rotor Hub Section Boundary Layer Shape Factor on Suction Surface	67
43	Rotor Hub Section Boundary Layer Shape Factor on Pressure Surface	68
44	Rotor Tip Section	68
45	Rotor Tip Section - Surface Velocity Distribution	68
46	Rotor Tip Section Boundary Layer Shape Factor	68
47	Rotor Sections Stacked on C.G. - Pressure Side-Loaded	71
48	Rotor Sections Stacked on C.G. - Suction Side-Loaded	71
49	Gas Generator Turbine Disk Assembly	72
50	Tensile Properties Comparison of Powder Metal Rene' 95 and Forged Waspaloy. (Reference: Teledyne CAE, IR&D Brochure 76-07)	72
51	Stress Rupture Strength for the Candidate Turbine Rotor Materials	72
52	Turbine Disk Stress and Temperature as a Function of Radius	73
53	Strength Properties of IN100	74
54	Turbine Blade Stresses for Case 1 (Upper Limit for Cycle Study Engine)	74
55	Turbine Blade Stresses for Case 2 (Lower Stress Limit for Cycle Study Engine)	74

LIST OF ILLUSTRATIONS

Figure		Page
56	Turbine Blade Stress Distribution for Selected Blade .	74
57	Turbine Blade Root Attachment, Firtree Detail	75
58	Modified Goodman Diagram for the Firtree	77
59	Nozzle Cooling Flow Injection Location	77
60	Vane Heat Transfer Coefficient and Surface Temperature Distribution	78
61	Turbine Rotor Blade Cooling Configurations Selected for Evaluation	79
62	Rotor Blade Surface Heat Transfer Coefficient	81
63	Effect of Cooling Flow Injection on Efficiency	81
64	Turbine Cooling Air Flow Distribution	82
65	Preliminary ASATT Turbine Flowpath	84
66	Selected ASATT Turboshaft Engine Configuration	84
67	Cascade Rig Cross Section	87
68	Traversing Mechanism Layout	87
69	Momentum Transfer Principle	89
70	Momentum Transfer Torque Measurement System	91
71	Momentum Transfer Slave Installed	92
72	Cascade Mounting Plate - Rear View	93
73	Vane Meridional Constriction Configurations	93
74	Nozzle Shroud Configurations, Test Hardware	94
75	Cascade Hardware - Disassembled	95
76(a)	Cascade Outer Shroud - Contoured Wall	96
76(b)	Cascade Inner Shroud - Contoured Wall	96
77	Turbulence Intensity Induced Upstream of Nozzle Inlet .	98

LIST OF ILLUSTRATIONS

Figure		Page
78	Cascade Inlet Distortion, Turbulence and Blockage Plates	99
79(a)	Suction Side Gill Slots	100
79(b)	Pressure Side Gill Slots	100
79(c)	Trailing Edge Slots	100
80	Cooling Supply Holes	101
81(a)	Rotor Cascade - Pressure Loaded - Rear View	102
81(b)	Rotor Cascade - Pressure Loaded - Front View	102
82(a)	Rotor Cascade - Suction Loaded - Rear View	103
82(b)	Rotor Cascade - Suction Loaded - Front View	103
83(a)	Rotor Cascade - Reduced Solidity - Rear View	104
83(b)	Rotor Cascade - Reduced Solidity - Front View	104
84	Cascade Instrumentation Detail	105
85(a)	Hot Film Anemometer	106
85(b)	Anemometer Accessory Equipment	106
86	Momentum Transfer Slave Inlet	107
87	Cobra Head Traverse Probes	108
88	Load Cell Force Correction Error	109
89	Slave Force Calculation Error	110
90	Hot Film Calibration Curve	111
91	Discharge Survey Cobra Probe	111
92	Schematic of Test Arrangement	111
93	ASATT Turbine Cascade Facility	112
94	IBM 1800 Data Acquisition and Control System	114

LIST OF ILLUSTRATIONS

Figure		Page
95	Data Acquisition System - ASATT Cascade	116
96	Test Series A - Configuration 1 - Nozzle Local Total Pressure Loss Distribution	120
97	Test Series A - Configuration 2 - Nozzle Local Total Pressure Loss Distribution	120
98	Test Series A - Configuration 3 - Nozzle Local Total Pressure Loss Distribution	120
99	Test Series A - Configuration 4 - Nozzle Local Total Pressure Loss Distribution	120
100	Test Series A - Configuration 2 - Nozzle Exit Mach Number Distribution.	121
101	Test Series A - Configuration 2 - Nozzle Exit Flow Angle Distribution	121
102	Test Series A - Configuration 4 - Nozzle Exit Mach Number Distribution	122
103	Test Series A - Configuration 4 - Nozzle Exit Flow Angle Distribution	123
104	Normalized Total Pressure Contours	124
105	Test Series A - Pressure Loss Coefficient Comparison of Wall Configurations	125
106	Test Series A - Configuration 1 - Blade Loading Diagram at $\approx P_{inlet}/P_{Sexit}$ = Design - Cylindrical Walls	125
107	Test Series A - Configuration 2 - Blade Loading Diagram at $\approx P_{inlet}/P_{Sexit}$ = Design	125
108	Test Series A - Configuration 3 - Blade Loading Diagram at $\approx P_{inlet}/P_{Sexit}$ = Design	125
109	Test Series A - Configuration 4 - Blade Loading Diagram at $\approx P_{inlet}/P_{Sexit}$ = Design	126
110	Test Series A - Configuration 1 - Exit Pressure Distribution of Inner and Outer Walls	126

LIST OF ILLUSTRATIONS

Figure		Page
111	Test Series A - Configuration 2 - Exit Pressure Distribution on Inner and Outer Walls	126
112	Test Series A - Configuration 3 - Exit Pressure Distribution on Inner and Outer Walls	126
113	Test Series A - Configuration 4 - Exit Pressure Distribution on Inner and Outer Walls	127
114	Test Series B - Nozzle Efficiency From Momentum Transfer System Versus Exit Mach Number	127
115	Test Series C - Configuration 4 - Effect of Inlet Reynolds Number on Turbulent Intensity	128
116	Test Series C - Effect of Reynolds Number on Turbulence Intensity for Configuration 2	128
117	Measurement of Fluctuating Turbulent Components in a Wind Tunnel (Reference 39)	129
118	Hot Film Anemometer Output - Typical Oscilloscope Trace	130
119	Test Series C - Effect of Inlet Turbulence	131
120	Effects of Turbulence on Nozzle Performance (Configuration 2)	131
121	Test Series D - Configuration 2 - Effect of Stator Inlet Boundary Layer	131
122	Test Series D - Configuration 2 - $\bar{\omega}$ Midpassage Versus Radius Versus Boundary Layer Based on 8° Circumferential Surveys	131
123	Test Series D - Configuration 4 - Effect of Stator Inlet Flow Distortion	132
124	Nozzle Efficiency Decrement as a Function of Blockage Plate Height	133
125	Test Series E - Actuator Nozzle Discharge Angle at 12° Circumferential Survey	135
126	Test Series G - The Effect of Cooling and Solidity on Stator Performance	135

LIST OF ILLUSTRATIONS

Figure		Page
127	Test Series H - Effect of Total Cooling on Actuator Performance	137
128	Test Series H - Effect of Axial Spacing and Solidity on Rotor Performance	137
129	Phase III Stator Airfoil Section Coordinates	144
130	Cooling Flow Slot Definition for Phase III Nozzle Vanes	145
131(a)	Test 4.0 - Determination of Cooling Flow Losses on a Nominal PLR Turbine	146
131(b)	Cooling Flow Slot Definition for Phase III Rotor Blade	146
132	ASATT Phase III Turbine Rig	148
133	Nozzle Inlet Housing.	149
134	Bladed Rotor Configurations	150
135	Critical Speed Dependence on Bearing Spring Rates	152
136	Turbine Air Flow Facility - Environmental System Supplies Conditioned Air to Turbine Test Rigs and Exhaust System Provides High Turbine Pressure Ratios	152
137	Kahn Water Brake Dynamometer Installed in the Turbine Test Facility	153
138	Schematic of Phase II ASATT Turbine Rig Instrumentation	156
139	Turbine Rig Instrumentation	157
140	Test 1.0 - Nozzle Performance - Sketch of Flowpath for Nozzle Exit Survey	161
141	Test 1.0 - Nozzle Performance - Flow Pressure Ratio Function, A Comparison of Test Data and Design	161
142	Test 1.0 - Nozzle Performance - Comparison of Nozzle Running Conditions for Both Nominal Rotor Configurations, Test 3.0 and Test 5.0, at Design Speed	163
143	Test 1.0 - Nozzle Performance - Comparison of Design and Test Radial Nozzle Exit Mach Number Distribution	163

LIST OF ILLUSTRATIONS

Figure		Page
144	Test 1.0 - Nozzle Performance - Comparison of Design and Test Data Radial Absolute Gas Angle Profiles at Rotor Inlet	164
145	Test 1.0 - Nozzle Performance - Local Nozzle Pressure Loss Coefficient Contours for Survey With No Coolant and With Measuring Station 0.25 Inch Axially Behind the Trailing Edge	165
146	Test 1.0 - Nozzle Performance - Local Nozzle Pressure Loss Coefficient Contours for Survey with Coolant Flow Injection on Pressure Surface and With Measuring Station 0.25 Inch Axially Behind the Trailing Edge.	165
147	Test 1.0 - Nozzle Performance - Average Nozzle Loss Distribution for Survey Plane 0.25 In. Behind the Trailing Edge With and Without Cooling Compared to Design. .	166
148	Test 1.0 - Nozzle Performance - Exit Pressure Distribution on Inner and Outer Walls for Uncooled Nozzle and With Flow Injection Through Pressure Surface Coolant Holes	166
149	Test 1.0 - Nozzle Performance - Normalized Mid-Channel Static Pressure Distribution for Uncooled Nozzle Exit Survey at $P_{T1}/P_4 = 3.33$	167
150(a)	Test 1.0 - Nozzle Performance - Demonstration of Cyclic Raw Data Over 18 Degree Periods for Uncooled Survey 0.25 Inch Behind the Nozzle Trailing Edge	167
150(b)	Test 1.0 - Nozzle Performance - Demonstration of Cyclic Raw Data Over 18 Degree Periods for Uncooled Survey 0.25 Inch Behind the Nozzle Trailing Edge	168
150(c)	Test 1.0 - Nozzle Performance - Demonstration of Cyclic Raw Data Over 18 Degree Periods for Uncooled Survey 0.24 Inch Behind the Nozzle Trailing Edge	168
151(a)	Test 1.0 - Nozzle Performance: Constant Radius Circumferential Nozzle Pressure Loss Coefficient Profiles for Uncooled Survey 0.25 Inch Behind the Nozzle Trailing Edge.	169
151(b)	Test 1.0 - Nozzle Performance: Constant Radius Circumferential Nozzle Pressure Loss Coefficient Profiles for Uncooled Survey 0.25 Inch Behind the Nozzle Trailing Edge	169

LIST OF ILLUSTRATIONS

Figure		Page
151(c)	Test 1.0 - Nozzle Performance: Constant Radius Circumferential Nozzle Pressure Loss Coefficient Profiles for Uncooled Survey 0.25 Inch Behind the Nozzle Trailing Edge.	170
151(d)	Test 1.0 - Nozzle Performance: Constant Radius Circumferential Nozzle Pressure Loss Coefficient Profiles for Uncooled Survey 0.25 Inch Behind the Nozzle Trailing Edge.	170
151(e)	Test 1.0 - Nozzle Performance: Constant Radius Circumferential Nozzle Pressure Loss Coefficient Profiles for Uncooled Survey 0.25 Inch Behind the Nozzle Trailing Edge.	171
152(a)	Test 1.0 - Nozzle Performance: Constant Radius Circumferential Nozzle Pressure Loss Coefficient Profiles for 1.8% Injection Flow Through Coolant Holes on Pressure Surface and Survey Station 0.25 Inch Behind the Nozzle Trailing Edge	171
152(b)	Test 1.0 - Nozzle Performance: Constant Radius Circumferential Nozzle Pressure Loss Coefficient Profiles for 1.8% Injection Flow Through Coolant Holes on Pressure Surface and Survey Station 0.25 Inch Behind the Nozzle Trailing Edge	172
152(c)	Test 1.0 - Nozzle Performance: Constant Radius Circumferential Nozzle Pressure Loss Coefficient Profiles for 1.8% Injection Flow Through Coolant Holes on Pressure Surface and Survey Station 0.25 Inch Behind the Nozzle Trailing Edge	172
152(d)	Test 1.0 - Nozzle Performance: Constant Radius Circumferential Nozzle Pressure Loss Coefficient Profiles for 1.8% Injection Flow Through Coolant Holes on Pressure Surface and Survey Station 0.25 Inch Behind the Nozzle Trailing Edge	173
152(e)	Test 1.0 - Nozzle Performance: Constant Radius Circumferential Nozzle Pressure Loss Coefficient Profiles for 1.8% Injection Flow Through Coolant Holes on Pressure Surface and Survey Station 0.25 Inch Behind the Nozzle Trailing Edge	173

LIST OF ILLUSTRATIONS

Figure		Page
153	Test 1.0 - Nozzle Performance: Exit Pressure Distribution on Inner and Outer Walls With Suction Surface Loaded Rotor Downstream and With Rotor Removed.	174
154	Test 1.0 - Nozzle Performance: Exit Pressure Distribution on Inner and Outer Walls With Pressure Surface Loaded Rotor Downstream and With Rotor Removed.	174
155	Test 1.0 - Nozzle Performance: Comparison of Phase II and Phase III Nozzle Pressure Loss Coefficient Profiles	175
156	Test 1.0 - Nozzle Performance: Comparison of Phase II and Phase III Nozzle Exit Gas Angle Profiles.	175
157	Test 1.0 - Nozzle Performance: Comparison of Phase II and Phase III Nozzle Exit Mach Number Distributions . .	176
158	Test 2.0 - Bladeless Disc Configuration with Coolant Flowpath.	177
159	Test 2.0 - Windage, Bearing Losses and Rotor Coolant Absorbed Power Bladeless Disk Configuration Total Torque vs Speed.	178
160	Test 2.0 - Windage Bearing Losses and Rotor Coolant Absorbed Power. Bladeless Disk Configuration - Windage and Bearing Torque vs Speed	179
161	Test 3.0 - Nominal Solidity - 41 Blades Pressure Loaded Rotor, Baseline Configuration	180
162	Test 3.0 - Baseline Turbine Performance Map	180
163	Test 3.0 - ASATT Turbine Performance.	180
164	Test 3.0 - Evaluation of Nominal Performance Baseline Configuration	182
165	Test 3.0 - Evaluation of Nominal Performance Baseline Configuration	182
166	Test 3.0 - Evaluation of Nominal Performance Baseline Configuration	182
167	Test 3.0 - Evaluation of Nominal Performance Baseline Configuration	182

LIST OF ILLUSTRATIONS

Figure		Page
168	Test 3.0 - Evaluation of Nominal Performance Baseline Configuration.	183
169	Test 5.0 - Evaluation of Blade Loading Radial Efficiency Distribution Based on Nozzle Inlet Rakes and Rotor Exit Survey	183
170	Test 5.0 - Evaluation of Blade Loading Nozzle Inlet and and Rotor Exit Circumferential Temperature Variation . .	183
171	Test 5.0 - Evalution of Blade Loading, Axial Static Pressure Distribution.	183
172	Test 5.0 - Evaluation of Blade Loading, Nozzle Exit and Rotor Discharge Relative Mach Number Distribution. .	184
173	Test 5.0 - Evaluation of Blade Loading, Rotor Incidence Angle Distribution at Nozzle Mach Number M = 1.38. . . .	184
174	Test 1.0 - Nozzle Performance: Average Nozzle Loss Distribution for Survey Plane 0.25 Inch Behind the Trailing Edge With and Without Cooling Compared to Design	185
175	Rotor Loss Distributions	185
176	Test 4.0 - Determination of Cooling Flow Losses on Nominal PLR Turbine.	187
177	Test 4.0 - Determination of Cooling Flow Losses on Nominal PLR Turbine.	189
178	Test 4.0 - Determination of Cooling Flow Losses on Nominal PLR Turbine.	189
179	Test 5.0 - Blade Loading Evaluation: Performance Map for the Suction Loaded Rotor Configuration	191
180	Test 5.0 - Blade Loading Evaluation: SLR Performance Map with Reynolds Number Corrected to Design Point Conditions.	191
181	Test 5.0 - Evaluation of Blade Loading, Inlet Temperature Distribution from Average Circumferential Rakes.	192
182	Test 5.0 - Evaluation of Blade Loading, Inlet Total Pressure Distribution from Average Circumferential Rakes . .	192

LIST OF ILLUSTRATIONS

Figure		Page
183	Test 5.0 - Evaluation of Blade Loading, Rotor Exit Total Temperature Radial Survey.	192
184	Test 5.0 - Evaluation of Blade Loading, Rotor Exit Radial Total Pressure Survey	192
185	Test 5.0 - Evaluation of Blade Loading, Rotor Exit Radial Swirl Angle Survey.	193
186	Test 5.0 - Evaluation of Blade Loading, Radial Efficiency Distribution Based on Nozzle Inlet Rakes and Rotor Exit Survey.	193
187	Test 5.0 - Evaluation of Blade Loading, Circumferential Temperature Gradients at Turbine Inlet and Exit.	193
188	Test 5.0 - Evaluation of Blade Loading, Radial Efficiency Distribution Based on Nozzle Inlet Rakes and Rotor Exit Survey.	193
189	Test 5.0 - Evaluation of Blade Loading, Nozzle Exit and Rotor Discharge Relative Mach Number Distribution. .	195
190	Test 5.0 - Evaluation of Blade Loading, Rotor Loss Distributions.	195
191	Test 5.0 - Evaluation of Blade Loading, Rotor Incidence Angle Distribution at Nozzle Mach No., M = 1.38.	195
192	Test 5.0 - Evaluation of Blade Loading, Axial Static Pressure Distribution.	195
193	Test 5.0 - Evaluation of Blade Loading, Axial Static Pressure Distribution.	196
194	Test 7.0 - Effect of Nozzle Leakage (Bypass) Flow on Performance of Two Rotor Designs	198
195	Partial Inner Wall Flowpath With Axial Spacer.	199
196	Tests 8.0 and 9.0 - Effects of Increased Nozzle/Rotor Axial Spacing and Effect of Nozzle Bypass Flow on Performance of SLR Turbine. Efficiency Drop Due to Spacing at Design Speed.	200

LIST OF ILLUSTRATIONS

Figure		Page
197	Tests 8.0 and 9.0 - Effects of Increased Nozzle/Rotor Axial Spacing and Effect of Nozzle Bypass Flow on Performance of SLR Turbine. Efficiency Drop Due to Increased Axial Spacing at 90 Percent Design Speed. . .	200
198	Tests 8.0 and 9.0 - Effects of Increased Nozzle/Rotor Axial Spacing and Effect of Nozzle Bypass Flow in Performance of SLR Turbine. Efficiency Drop Due to Increased Spacing at 70 Percent Design Speed.	201
199	Tests 8.0 and 9.0 - Effects of Increased Nozzle/Rotor Axial Spacing and Effects of Nozzle Bypass Flow on Performance of SLR Turbine. Efficiency Drop Due to Increased Spacing and Bypass Flow at Two Power Levels .	201
200	Inlet Flow Distortion Devices	202
201	ASATT Phase III Turbine Rig	204
202	Tests 10 and 11 - Distribution of Induced Turbulence at Turbine Inlet.	205
203	Effect of Inlet Distortion Plate on Overall Efficiency.	205
204	Effect of Inlet Distortion Plates on Overall Efficiency .	205
205	Effect of Inlet Distortion Plates on Overall Efficiency .	205
206	Test 12 - Effect of Rotor Solidity, PLR Rotor	207
207	Test 13 - Reynolds Number Effect on Performance	209
208	Comparison of Teledyne CAE Predicted and Experimental Turbine Efficiencies.	217
209	Division of Total Pressure Loss by the Teledyne CAE Loss System	219
210	Inlet Flowpath for Inlet Distortion and Boundary Layer Tests	222
211	Effect of Nozzle and Rotor Cooling Flow on Turbine Stage Efficiency.	222
212	Blading Loss Profile Model Compared to Phase III, Test Data	228

LIST OF ILLUSTRATIONS

Figure		Page
213	Model of ASATT SLR Turbine; Profiles of Input Throat Coefficients.	228
214	Mach Number Comparisons; Model and Phase III SLR Turbine Stage Data.	228
215	Nozzle Exit Mach Number Comparison; Model and Nozzle Blowdown Test	228
216	Wall Static Pressure Distribution; Model Compared to SLR Turbine	229
217	Turbine Model Flowpath Comparison	229
218	Model II Efficiency Profile Compared to Test Data . . .	229
219	Rotor Exit Swirl for Model II Compared to Test Data . .	229
220	Definition of ASATT Nozzle Trailing Edge Cutback	231
221	Blading Loss Profiles	232
222	Mach Number Distributions	232
223	Predicted Wall Static Pressure Distributions.	232
224	Phase V Predicted Stage Efficiency Distribution	232
225	Test 1.0 - Nozzle Performance - Diagram of Flowpath for Nozzle Exit Survey.	236
226	Phase V Turbine Inlet Nozzle Modification	237
227	Phase V ASATT Nozzle Blowdown	238
228	Phase V, Test L, Nozzle Performance	238
229	Phase V, Test 1, Nozzle Performance	238
230	ASATT Phase V Nozzle Exit Survey Iso-Mach Number Lines for Nozzle Total-Static Pressure Ratio of 3.33.	239
231	ASATT Phase V Nozzle Exit Survey Iso-Pressure Loss Coefficient Lines for Nozzle Total-Static Pressure Ratio of 3.33	239

LIST OF ILLUSTRATIONS

Figure		Page
232	ASATT Phase V Nozzle Exit Survey Iso-Exit Mach Number Lines for Design Nozzle Total-Static Pressure Ratio of 2.7.	240
233	ASATT Phase V Nozzle Exit Survey Iso-Pressure Loss Coefficient Lines for Design Nozzle Total-Static Pressure Ratio of 2.7.	240
234	ASATT Phase V Pressure Surface Loaded Rotor Configuration Test Map	242
235	ASATT Phase V Pressure Surface Loaded Rotor Configuration Test Map Corrected to Design Reynolds Number . . .	243
236	Test 3.0 - Baseline Turbine Performance Map. Corrected to Design Reynolds Number - Phase III	244
237	Design Prediction - ASATT Turbine Performance	244
238	ASATT Phase V, Test 2 Axial Static Pressure Distribution - Pressure Side Loaded Rotor, PLR.	246
239	ASATT Phase V, Test 2 Mid-Channel Pressure Distribution Pressure Side Loaded Rotor (PLR).	246
240	ASATT Phase V, Test 2 Axial Static Pressure Distribution Pressure Side Loaded Rotor, P/N 604673 (PLR).	247
241	Phase V, Test 2: Stage Performance with Pressure Loaded Rotor Turbine Configuration	249
242	Phase V, Test 2: Stage Performance with Pressure Loaded Rotor Turbine Configuration	249
243	Phase V, Test 2: Stage Performance with Pressure Loaded Rotor Turbine Configuration	249
244	Phase V, Test 2: Stage Performance with Pressure Loaded Rotor Turbine Configuration	249
245	Phase V, Test 2: Stage Performance with Pressure Loaded Rotor Turbine Configuration	250
246	Phase V, Test 2: Stage Performance with Pressure Loaded Rotor Turbine Configuration	250

LIST OF ILLUSTRATIONS

Figure		Page
247	ASATT Phase V, Test 2: Rotor Loss Coefficient Distribution.	250
248	ASATT Phase V, Test 2: Nozzle Exit & Rotor Discharge Relative Mach No. Distributions.	250
249	Phase V, Test 2: Stage Performance with Pressure Loaded Rotor Configuration.	251
250	Phase V, Test 2: Stage Performance with Pressure Loaded Rotor Turbine Configuration.	251
251	Phase V, Test 2: Stage Performance with Pressure Loaded Rotor Turbine Configuration.	251
252	Phase V, Test 2: Stage Performance with Pressure Loaded Rotor Turbine Configuration.	251
253	Phase V, Test 2: Stage Performance with Pressure Loaded Rotor Turbine Configuration.	252
254	Phase V, Test 2: Stage Performance with Pressure Loaded Rotor Turbine Configuration.	252
255	Test 5.0 - Evaluation of Blade Loading. Rotor Incidence Angle Distribution.	252
256	Suction Surface Loaded Rotor After Severe Hub Encountered During Phase III Testing.	253
257	ASATT Phase V Suction Surface Loaded Rotor Configuration Test Map	254
258	ASATT Phase V Suction Surface Loaded Rotor Configuration Test Map Corrected to Design Reynolds Number .	254
259	Phase III, Test 3.0 - ASATT Turbine Performance . . .	255
260	Blade Loading Evaluation SLR Phase III, Test 3.0, Performance	255
261	Phase V, Test: Axial Static Pressure Distribution. .	255
262	Phase V, Test 3: Mid-Channel Pressure Distribution .	256

LIST OF ILLUSTRATIONS

Figure		Page
263	Phase V, Test 3: Vane-to-Vane Static Pressure Distribution at Trailing Edge.	256
264	Phase V, Test 3: Stage Performance with Suction Loaded Rotor Turbine Configuration. Rotor Exit Total Pressure Survey.	258
265	Phase V, Test 3: Stage Performance with Suction Loaded Rotor Turbine Configuration. Rotor Exit Total Temperature Survey.	258
266	Phase V, Test 3: Stage Performance with Suction Loaded Rotor Turbine Configuration. Rotor Exit Swirl Angle Survey	258
267	Phase V, Test 3: Stage Performance with Suction Loaded Rotor Configuration. Stage Inlet Total Pressure Gradient	258
268	Phase V, Test 3: Stage Performance with Suction Loaded Rotor Turbine Configuration. Stage Inlet Total Temperature Gradient.	259
269	Phase V, Test 3: Stage Performance with Suction Loaded Rotor Turbine Configuration. Radial Efficiency Distribution.	259
270	ASATT Phase V, Test 3: Rotor Loss Distribution. . . .	259
271	ASATT Phase V, Test 3: Rotor Discharge Relative and Nozzle Exit Mach No. Distribution.	259
272	Phase V, Test 3: Stage Performance with Suction Loaded Rotor Configuration.	260
273	Phase V, Test 3: Stage Performance with Suction Loaded Rotor Turbine Configuration.	260
274	Phase V, Test 3: Stage Performance with Suction Loaded Rotor Turbine Configuration.	260
275	Phase V, Test 3: Stage Performance with Suction Loaded Rotor Turbine Configuration.	260
276	Phase V, Test 3: Stage Performance with Suction Loaded Rotor Turbine Configuration.	261

LIST OF ILLUSTRATIONS

Figure		Page
277	Phase V, Test 3: Stage Performance with Suction Loaded Rotor Turbine Configuration.	261
278	Test 3.0 - Evaluation of Blade Loading. Rotor Incidence Angle Distribution.	261
E-1	Test 1 (Nozzle Performance) Facility Installation and Test Equipment.	322
E-2	Axial Shift in Measurement Plane as a Result of Nulling	323
E-3	Regions of Data Taken During Survey Shows Concentration in Mid-Channel and Reduces Value of Contour Plots . .	324
E-4	Redesigned Total Pressure Probe Installed in Traverse Mechanism	324
E-5	Water Brake Operating Envelope.	326

LIST OF TABLES

Table		Page
1	Turboshaft engine Design Analysis - 100% Power.	39
2	Combustor Design Parameters	40
3	Design Point Selection Comparison	46
4	Summary of Streamline Analysis Variations	51
5	Comparison of Rotor Relative Velocity Ratio	55
6	Summary of Static Pressure Reaction	55
7	Summary of Vane Aerodynamic and Geometric Design Data	60
8	Summary of Rotor Blade Aerodynamic and Geometric Data.	69
9	Firtree and Disk Stresses	75
10	Vane Cooling Flow Distribution.	77
11	Turbulence Produced by Various Screen Sizes	99
12	Phase II Cascade Test Sequence.	117
13	Test Configuration Geometry	118
14	Summary of Pressure Loss for Boundary Layer and Flow Distortions	134
15	Summary of Evaluation of Stator Exit Flow Distortion and Leakage Effects on Rotor Cascade Performance.	134
16	Phase III Test Program.	159
17	Inlet Conditions of Primary and Coolant Flows	186
18	Performance Parameter Comparison of PIR Turbine and SLR Turbine at Design Speed	190
19	Performance Changes Due to Increased Inlet Boundary or Increased Outer Wall Gradients at Turbine Inlet	206
20	Phase III Summary of Test Results at Design Speed and Work.	210

LIST OF TABLES

Table		Page
21	Hot Wire Anemometer Measurement of Nozzle Inlet Boundary Layer.	223
22	Nozzle Loss Distribution.	224
23	ASATT Turbine Phase V Test Points	234

INTRODUCTION

Prior to about 1966, turbine aerodynamic design was considered to be a well-proven technology; major analytical design effort was being applied to compressor aerodynamics, because high turbine efficiencies could be achieved on an assured basis. This is still relatively true for uncooled designs or very large stages.

The advent of requirements for increased turbine inlet temperature, to increase specific horsepower and improve fuel consumption, resulted in the experimental discovery of high secondary loss effects as well as deficiencies in the design system. These losses exist in all highly loaded cooled turbines, irrespective of size, but are especially severe for the small (under one-inch blade span) axial flow machines. Both basic aerodynamic (cascade/channel) effects and accentuated cooling flow interaction effects contribute to the degradation.

The degradation of anticipated efficiency levels even without air cooling injection losses, detracts strongly from the cycle benefits of the increased temperatures, and in extreme circumstances, could result in achieving "temperature for the sake of temperature only".

Discussions in 1971 with Dr. Taylor of M.I.T. and Mr. R. Novak of Dynatech, then performing a review of the total available literature on the subject for the Air Mobility Research and Development Laboratory (AMRDL), were unsuccessful in arriving at a succinct definition of the nature of the problem. It was an opinion whether the problem was purely an "aspect ratio" effect - secondary flow losses introduced by the (relatively) long chord, or a result of using conventional design limits and criteria for detail blade loading analysis and boundary layer buildup, and without sufficient attention to details of the endwall phenomena.

It was also found that there was a general lack of appreciation for the special and unique requirements of small cooled turbines, because of the far higher attention and investment in large engines (Reference 4). The recent increased level of requirements for small, high performance engines in USA, USN and USAF missions has given rise to the need for research of this nature - to fill in the vacant corners of detail aerodynamic knowledge in blade designs which must do the same aerothermodynamic jobs as similar blades of four to eight times the equivalent size. Figure 1 graphically depicts the turbine blade height for advanced high work turbines over a wide range of engine sizes.

A widely used procedure to estimate turbine efficiency is to relate turbine blade loss characteristics to turbine mean section velocity diagrams (Stewart[5] and Smith[6]). The Smith data is expanded in References 7 and 8. An alternate approach still using mean line parameters is to consider a breakdown into individual losses such as profile, secondary, trailing-edge wakes, Reynolds and Mach number, and incidence, and to correct for annulus

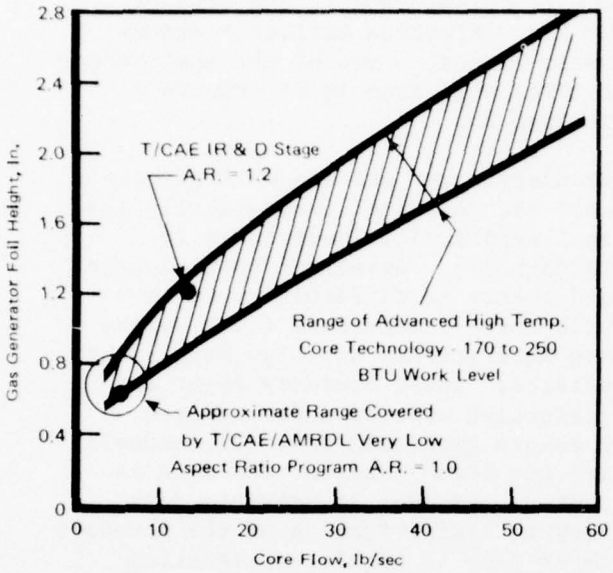


Figure 1. Small, High Work Turbines Cover a Wide Spectrum of Core Air Flow.

and tip clearance effects. Ainley[9,10] and Balje'[11,12] and Cooke[13] give extensive data on this approach.

Cold flow rig test evaluation of the fluid cooled high temperature gas generator turbine (5 lb/sec, 2300°F, 138 Btu/lb) designed by Teledyne CAE under contract to the Army (Reference 14) provided observations on aerodynamic problems unique to small cooled turbines. This turbine was designed by conventional approach to yield an efficiency of over 85 percent yet tested to only a peak of 82 percent. Deterioration of performance was attributed to high secondary losses arising from short, thick blading, low aspect ratios and wall effects. Schlichting and Das[15] suggests that blading with aspect ratio less than 2.0 will have losses mainly comprised of end wall or secondary type. Test data on aspect ratio and tip clearance effects of the turbine of Reference 14 is given in References 16 and 17. This data also suggests a trade-off of increased hub work for longer blading to produce similar performance as a turbine with higher rim speeds but shorter blading.

Figure 2 summarizes the results of the aspect ratio testing (References 16 and 17) and indicates a strong correlation of efficiency with aspect ratio. The addition of cooling injection flows compounds the situation, because higher percentages are required for small, compared to large turbines.

Dunham and Came[18] made improvements to the Ainley-Mathieson prediction technique to better account for secondary and tip losses; Figure 3 shows a comparison of the predicted to test results of Reference 16. Burrows[19] also did extensive testing and correlated data on the low aspect ratio stator of Reference 16 for improvements in efficiency prediction.

Northern Research Engineering Corporation (NREC)[20], was contracted to do cascade testing on the same family of turbines. They chose a rectilinear cascade and concluded that short blades were more efficient. However, the data also showed that small irregularities (0.001 inch step in flow path and small leakages) were found to increase total loss coefficients by as much as a factor of 5. The method of defining the loss coefficients from a simple survey can also lead to very poor accuracy (Reference 21) and makes this data suspect.

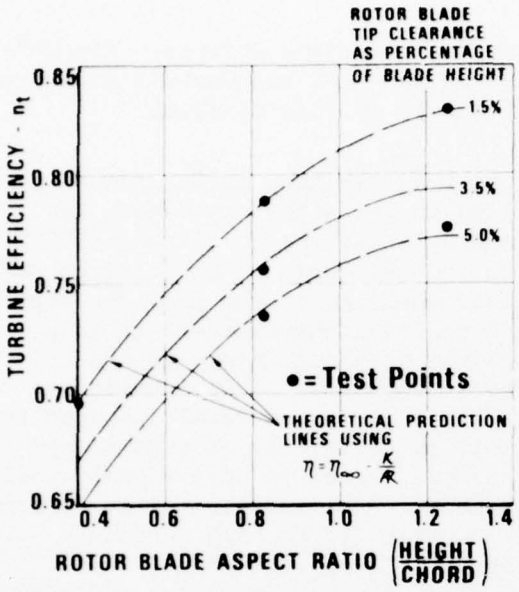


Figure 2. Turbine Efficiency Shows a Strong Dependency on Blade Height and Tip Clearance.

The location, amount, and type of cooling injection influence aerodynamic losses. Some of the most recent studies are given in References 21 through 25.

Boundary layer and end-wall effects have been examined theoretically and semi empirically (References 26 through 31). Agreement between test and theory is difficult to achieve with three-dimensional flows, blade row interactions and high Mach number effects. Inlet boundary layer and distortion effects under adverse pressure gradients in small channels are not documented, or the data is scarce. Launder 28 presents data showing laminarization of the boundary layer flow in highly accelerating channels, and Turber[27] concludes that the end-wall boundary-layer inside a stator passage is essentially independent of the boundary layer entering the cascade.

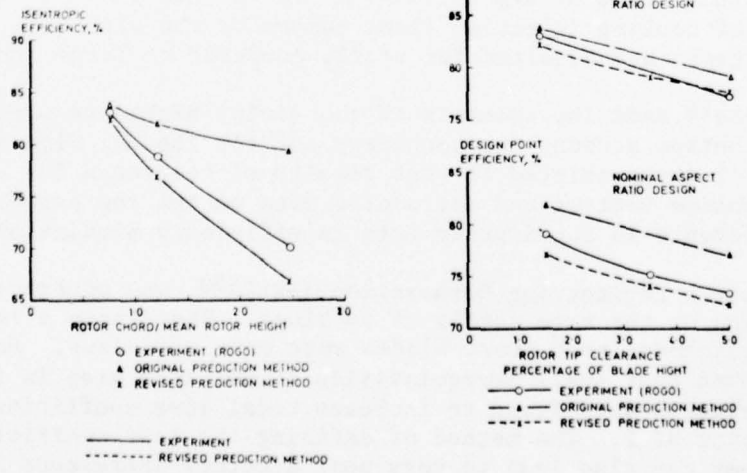


Figure 3. Dunham & Came Turbine Efficiency Prediction Vs. Test Data.

Design and test of a highly loaded turbine is given in References 32 through 34. Boundary layer analysis is used to define blade and wall shapes, and tests demonstrate high performance capabilities. High aspect ratios, thin trailing edges, and thin airfoils characteristic of the large uncooled turbofan turbine could not be used in a "small" cooled machine. The approach shows potential, but application of a simple free vortex turbine in the same flow path and with the same mean velocity triangles was projected to produce the same efficiency as the tested forced vortex turbine of Reference 32.

Allison, under contract to NASA (Reference 35), performed cascade and full-round testing on a high work factor ($\Omega_H = 5.5$) turbine using vortex flow generators, tandem blading, tangential blowing, and jet flaps. They showed that the jet flap has significant potential for improved performance in cooled and uncooled configurations (Reference 36).

Turbulence, intensity and Reynolds number effects on cascade losses are given in References 37 and 38. Interestingly, stator losses were found to increase, whereas rotor losses decreased with increases in inlet turbulence. Decreased rotor losses were attributed to a reduction of off-design incidence. Test data on this subject is scarce.

From the above literature survey it was concluded that there are two main technical approaches that can be made.

1. Use of the simpler methods of analysis allows design of a turbine whose performance is readily predictable in large turbine sizes and high aspect ratios. Small turbines incur additional losses due to factors not considered, or due to inherent losses of size and wall effects. Small turbine blade losses can be modified by inclusion of an end-wall or similar semiempirical factors for performance prediction. This means that small turbines are accepted to be inherently poor in performance, and the test program and correlations should define extent and provide inputs for accurate prediction.

2. A modified design approach can be made to include local cooling losses, mass flow mixing, blockage factors and detailed blade loss definition in each stream-tube. Iterating this procedure against detailed airfoil shape definition with boundary layer calculations in the separate stream-tubes (walls and blade surfaces) will result in blading that is a significantly better match from stator to rotor, and will not result in additional penalities that must be solely accounted for in small turbines.

The latter approach was selected for the Advanced Small Axial Turbine Technology (ASATT) program supplemented by cascade and full round test programs. The data correlations obtained during testing can be added to existing procedures to satisfy the first approach as a natural sequence and consequence of events.

The ASATT program was planned to fill part of the data void with respect to the design of small, highly loaded, cooled turbines. The program was arranged in five phases described briefly as follows:

Phase I: Preliminary Design

A baseline turbine geometry was established by a preliminary turboshaft engine design study.

Phase II: Turbine Cascade Investigation

The baseline turbine aerodynamics were tested in an annular sector cascade. Various perturbations to the flow channel aided evaluation of loss mechanisms.

Phase III: Stage Investigations

The baseline turbine aerodynamics were tested in the turbine stage and turbine performance was evaluated for a number of variables.

Phase IV: Design Technique Assessment

The data correlations from Phases II and III were examined against the original design model. Modifications of the model were performed to achieve satisfactory agreement.

Phase V: Modifications and Test

The modified design technique was used to predict the performance of the turbine after a geometric modification was made to improve performance. The turbine was retested to verify the predicted performance.

A detailed discussion of each phase appears in the next section, followed by some pertinent conclusions drawn from the overall program and recommendations for future effort in this area.

PHASE I - TECHNICAL DISCUSSION

PRELIMINARY DESIGN

The Phase I effort was directed toward the preliminary design of the research turbine and was divided into the following tasks:

1. Cursory Engine Design
2. Turbine Preliminary Detail Design

OBJECTIVES

The primary objectives of the Phase I effort were:

1. To establish a valid turboshaft engine environment and define the engine interface constraints within which to design a realistic small, highly loaded, cooled turbine.

2. To choose one turbine design of maximum value to the purposes of the program, optimize its design within current knowledge, and lay the foundation for overall program aerodynamic analyses.

CURSORY ENGINE DESIGN

Several turboshaft engine configurations were investigated between 12:1 (170 Btu/lb) and 16.3:1 (200 Btu/lb) pressure ratio and temperature levels of 2200° and 2500°F as to their influence on turbine cooling requirements, airfoil and passage shapes, life and manufacturability. One design was chosen, representative of the most highly loaded, highest temperature level, single-stage turbine, deemed practical for the program.

The engine configurations consisted of the following component arrangement.

Axial-centrifugal compressor combination (2-stage and 3-stage axials)
Reverse-flow/annular, vaporizing combustor
Single-stage, axial-flow, gas generator turbine
Two-stage power turbine with a front drive shaft
Two-bearing, gas generator shaft configuration

Two engine cross-sections complying with the above stated arrangements are shown in Figures 4 and 5. The major difference in the configurations is the number of axial compressor stages required for the higher work, higher pressure ratio configuration.

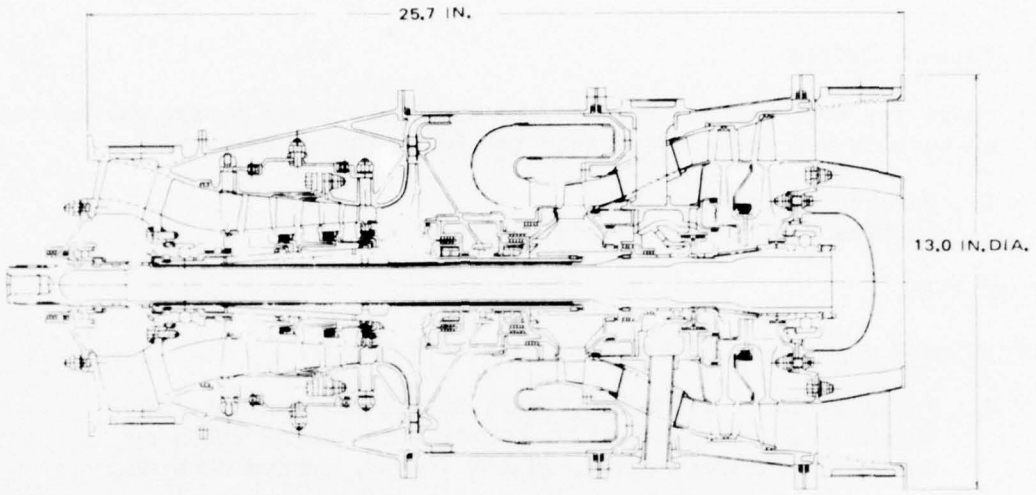


Figure 4. Candidate Engine Configuration No. 1.

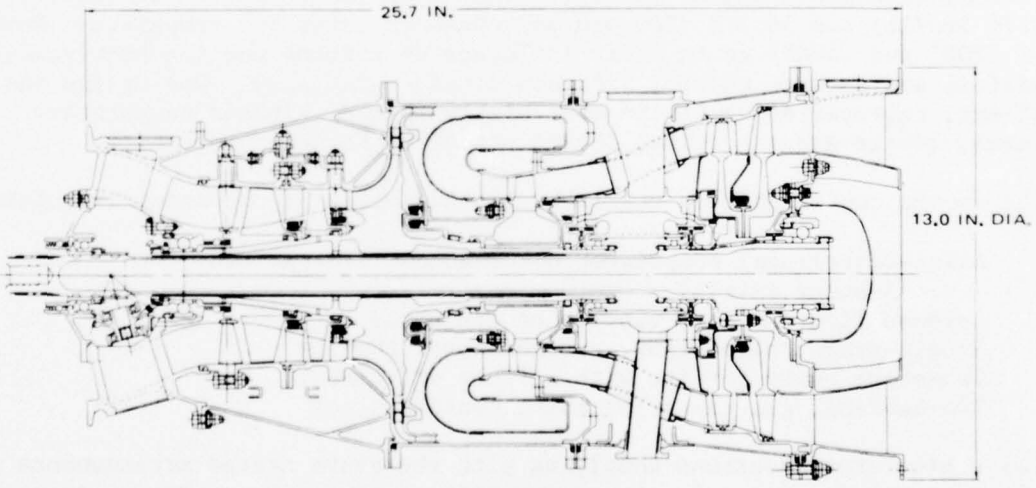


Figure 5. Candidate Engine Configuration No. 2.

CYCLE ANALYSIS

Table 1 lists the performance of the various candidate engine cycles investigated. The component efficiencies are based on technology representative of Teledyne CAE experience in the development of small components. The parasitic losses such as overboard leakage, windage, seal friction, bearing friction, and duct pressure loss are expected to be realistic for a well manufactured and well assembled engine, with particular attention paid to sealing high pressure flanges. The computer output for each of the cycle points listed is included in Appendix A.

The cycle performances for the various engines is shown in Figure 6 in terms of specific power and specific fuel consumption as a function of compressor pressure ratio. The band shown for the two turbine inlet temperatures is caused by the varied component efficiencies and the turbine cooling requirements.

The cycle design point was selected at a cycle pressure ratio of 13.3 (total-static) and a turbine inlet temperature of 2400°F. The rationale for the selection was based on component constraints.

The constraints of turbine work (170-200 Btu/lb) and nozzle inlet temperature (2200-2500°F) were imposed by the work statement, and the wheel speed range (54,000-62,000 rpm) was implied from specific speed and compressor matching analysis. A selection of 180 Btu/lb, 2400°F, 60,000 rpm design point reflected a best judgment choice within the imposed and implied constraints.

COMPRESSOR

Axial-centrifugal stage matching analysis of the compressor was performed to determine the best pressure ratio split between the axial and centrifugal (Figure 7). The matching analysis yielded an axial compressor pressure ratio of 3.0 (total-static) and a centrifugal compressor pressure ratio of 4.43 (total-static). The selected split was aided by setting the following bounds: WN^2 limit (2.3), an indictator of maximum stress; a minimum specific speed limit of 70, to achieve good centrifugal efficiency; and a pressure ratio of 3.0 (total-static) for the axial as the maximum pressure ratio for two axial stages.

COMBUSTOR

The selection of a combustor type and flow path was determined by a tradeoff between envelope requirements, compressor and turbine geometry, combustor loading parameters, and relative experience with various combustor configurations.

The flow paths of the centrifugal compressor and axial flow turbine blend well with the reverse-flow, annular combustor. This combination has the added benefit of minimizing engine length. In addition, the combustor envelope allowed by the centrifugal compressor diameter precludes the

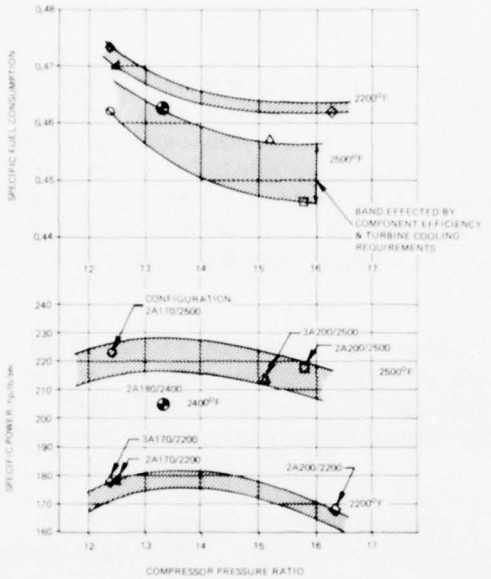


Figure 6. Turboshaft Engine Cycle Performance at 100 Percent Power.

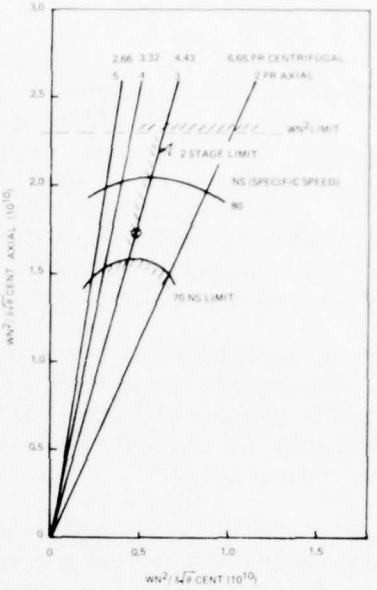


Figure 7. Axial-Centrifugal Stage Matching Criteria.

necessity for an advanced technology combustor, thus loading parameters can be kept within or near demonstrated experience. Consequently, the reverse-flow, annular type combustor is well suited for this application.

The flow path of the reverse-flow, annular, vaporizer combustor is shown in the engine layout (Figure 4), and the design point parameters are presented in Table 2. Also included in Table 2, for comparison, are the design point parameters of several similar combustors which form the basis for this design.

A preliminary estimate of the flow split indicates that approximately 39 percent of the engine airflow is required for combustion and 32 percent for cooling the static and rotating components. This leaves 29 percent for dilution and tailoring of the exit temperature profile to achieve the design point pattern factor (TDF) of 0.23. This is well within the experience level indicated in Table 2.

TURBINE PRELIMINARY DESIGN

During the cursory engine design some preliminary turbine design was performed to assure that the combinations of turbine inlet temperature, turbine work level and wheel speed would provide a turbine design close to optimum. A free-vortex, simple radial equilibrium computer program was used for the preliminary design study. The program calculates hub, mean and tip velocity triangles parameters at the turbine nozzle inlet, exit and rotor inlet and exit. (Phase IV discussion of this report includes a

TABLE 1

TURBOSHAFT ENGINE DESIGN ANALYSIS
100% POWER

A-Axial + Centrif Configuration C-Centrifugal		2A170/ 2200	3A170/ 2200	2A200/ 2500	3A200/ 2500	2A170/ 2500	2A200/ 2200	2A180/ 2400
Gas Generator Speed	rpm	58,230	58,000	60,880	54,700	58,230	60,880	60,000
Airflow	lb/sec	4.8	4.8	4.8	4.8	4.8	4.8	4.8
Overall Pressure Ratio	t-s	12.5	12.4	15.8	15.2	12.4	16.3	13.3
Overall Efficiency	t-s%	80.4	80.0	78.9	77.0	80.4	78.9	79.3
Turbine Inlet Gas Temp.	°F	2,200	2,200	2,500	2,500	2,500	2,200	2,400
Gas Generator Turbine Horsepower	Btu/lb	170.2 857.5	170 851.9	198.4 1047.0	200 1021.0	170.5 1070.0	199.5 809.0	180.0 982.1
Specific Power	Shp/lb/sec	178.5	177.5	218.0	213.0	223.0	168.5	205.0
SFC	lb/hp-hr	0.470	0.473	0.446	0.457	0.462	0.462	0.463
Axial Section RP		3.0	4.2	3.1	4.2	3.0	3.1	3.0
Axial Section Efficiency	%	85.0	84.0	84.9	84.0	85.0	84.9	85.0
Centrif. Section RP	t-s	4.17	2.95	5.10	3.6	4.17	5.10	4.43
Centrif. Section Efficiency	t-s%	81.7	82.5	80.0	81.0	81.7	80.0	80.3
Combustor Section	%	3.5	3.5	3.0	3.0			3.5
Combustor Efficiency	%	99.0	99.0	99.0	99.0			99.0
Gas Generator Turb. Eff.*	%	85.0	85.0	84.0	84.5	84.0	84.5	84.5
Equiv. Cooling Leakage - o.b.	%	0.5	0.5	0.5	0.5	0.5	0.5	0.5
- Bypass	%	3.2	3.2	4.6	4.6	4.1	3.7	4.0
Windage HP		28.0	28.0	38.0	58.0	34.0	30.0	35.0
Turbine Δh/Hcr	Btu/lb	33.3	34.7	35.4	35.3	30.1	38.8	33.7
Turbine Pressure Ratio	t-t	3.54	3.543	3.866	3.854	3.111	4.676	3.477
Turbine $WN_c/\delta 60$	lb/rpm/sec	381.0	382.6	310.3	289.8	382.6	301.8	367.1
Turbine $N\sqrt{\theta}$ T4	rpm	26,120	26,010	25,920	23,290	24,810	27,300	25,980
Turbine $W\sqrt{\theta_{Cr}}\epsilon/\delta$	lb/sec	0.900	0.908	0.747	0.777	0.953	0.688	0.880
Power Turbine Speed	rpm	25,000	25,000	25,000	25,000	25,000	25,000	25,000
Inter Turbine Temperature	°F	1598	1598	1798	1796	1891	1496	1762
Power Turbine Efficiency	%	88.8	88.8	88.8	88.8	88.8	88.8	88.8
Total-Static Back Pressure		1.040	1.040	1.040	1.040	1.040	1.040	1.040
Exhaust Gas Temperature	°F	1143	1143	1254	1265	1341	1060	1250
Accessory HP		9.0	9.0	9.0	9.0	9.0	9.0	9.0
Power Turb. Mech. Shaft		0.985	0.985	0.985	0.985	0.985	0.985	0.985

* This is an uncooled thermodynamic efficiency which when combined with the indicated bypass is estimated to yield equivalent cooled turbine performance.

TABLE 2

COMBUSTOR DESIGN PARAMETERS

COMBUSTOR DESIGN PARAMETERS					
Parameter	Units	TCAE Models			AMRDL
		A	B	C	
CDP	psia	173.3	185.2	323.2	195.38
CDT	^{o}R	1141	1179	1386	1216
Combustor Corrected Flow $\frac{W\sqrt{\theta}}{\delta}$	lb/sec	2.35	1.40	0.98	0.5
Fuel Flow	lb/hr	1533	1365	1573	454.7
Fuel-Air Ratio	----	0.0229	0.0326	0.0331	0.0291
Reference Velocity	ft/sec	91.3	55.4	48.4	54.0
Residence Time	millisecs.	8.1	11.3	13.0	7.91
Air Loading (DP)	lb air/ sec/$ft^3$$atm^2$	0.365	0.236	0.10	0.304
Fuel Loading (PZ)	lb fuel/ sec/ft^3/atm^2	0.0309	0.0225	0.0087	0.0185
Total		0.00835	0.00768	0.0033	0.00883
Heat Release (PZ)	Btu/ hr/ft^3/atm	24.1×10^6	18.7×10^6	12.6×10^6	16.1×10^6
Total		6.53×10^6	6.4×10^6	4.8×10^6	7.72×10^6
Pressure Loss	%	5.5	4.0	3.0	3.5 Liner
Temperature Rise	^{o}F	1436	1936	1909	1751
Temperature Ratio	--	2.26	2.64	2.38	2.44
Pattern Factor	--	0.23	0.2	0.2	0.23
Inlet Mach No.	--	0.15	0.15	0.08	0.16
Dilution Air	% Wa	46.9	19.4	11.6	28.6
Efficiency	%	98.5	99.0	98.5	99.0

detailed description of the modified Ainley procedure). The effect of rotor tip clearance, rotor exit swirl, axial velocity ratio, trailing edge radii, incidence, profile loss, Reynolds, Mach number and endwall loss are included in the calculation. A base turbine design was established. Various design configurations were investigated by allowing only one parameter to vary from its base value. Figure 8 shows the relative effect on efficiency as a result of the variation of some of these parameters. The base value for each parameter corresponds to the $\Delta\eta = 0$ value for these curves, (i.e., base rotor tip clearance = 0.01 inch, base stage exit axial velocity ratio, Vx/Vc_{rg}, = 0.45).

Two cycle points representative of the extremes were chosen for the preliminary turbine design study: 2200°F - 170 Btu/lb and 2500°F - 200 Btu/lb. Various hub stage loadings (Ω_H) were investigated over a range of flow coefficients to obtain maximum efficiency. An exit swirl of 18 degrees was set as the maximum permissible in a gas generator turbine application. Relative efficiency variations for the two turbine cycle points are shown in Figures 9 and 10. The results showed that the efficiency continued to increase with higher loading and higher flow coefficient until limit load or rotor choking occurred. In both cases limit load was indicated beyond a hub loading factor of 5.0. The velocity triangle parameters of interest are shown as a function of hub stage loading for the two cases in Figures 11 and 12. The nozzle discharge critical velocity ratios at the hub for both cases were well into the transonic-supersonic region over most hub stage loadings. The rotor relative critical velocity ratios at the hub inlet at loadings above 5.0 result in values above 0.80. At the rotor discharge tip, the relative critical velocity ratios decrease with increased loadings and are transonic at a hub loading near 5.0. There is no appreciable difference between the two cases on the basis of the velocity comparison. The effect of loading on rotor blade geometry in terms of inlet angle and turning is shown in Figure 12. At hub stage loadings between 4.0 and 5.0 there is very little difference in the two turbine cases; however, above a loading of 5.0, rotor hub turning increases above 120 degrees.

Excessive hub turning, particularly when associated with low hub reaction, should be avoided since the combination leads to thicker boundary layers, larger secondary losses and possible separation of flow (10). Figure 11 demonstrates the increase in rotor hub inlet relative velocity ratio and therefore implied decrease in hub reaction which was associated with the increase in turning as rotor hub loading was increased.

The preliminary turbine design process also includes an initial estimate of turbine cooling requirements to achieve a desired life, the flow path size and number of vanes and blades, and the weight of the blades and disk.

The structural design of the turbine is based on a life of at least 750 hours at 100 percent power, and 15,000 cycles of low cycle fatigue life. Figure 13 shows the variation of required cooling for the two cases of fatigue life as a function of hub stage loading. The material strength properties of IN713C were used for the purposes of this preliminary

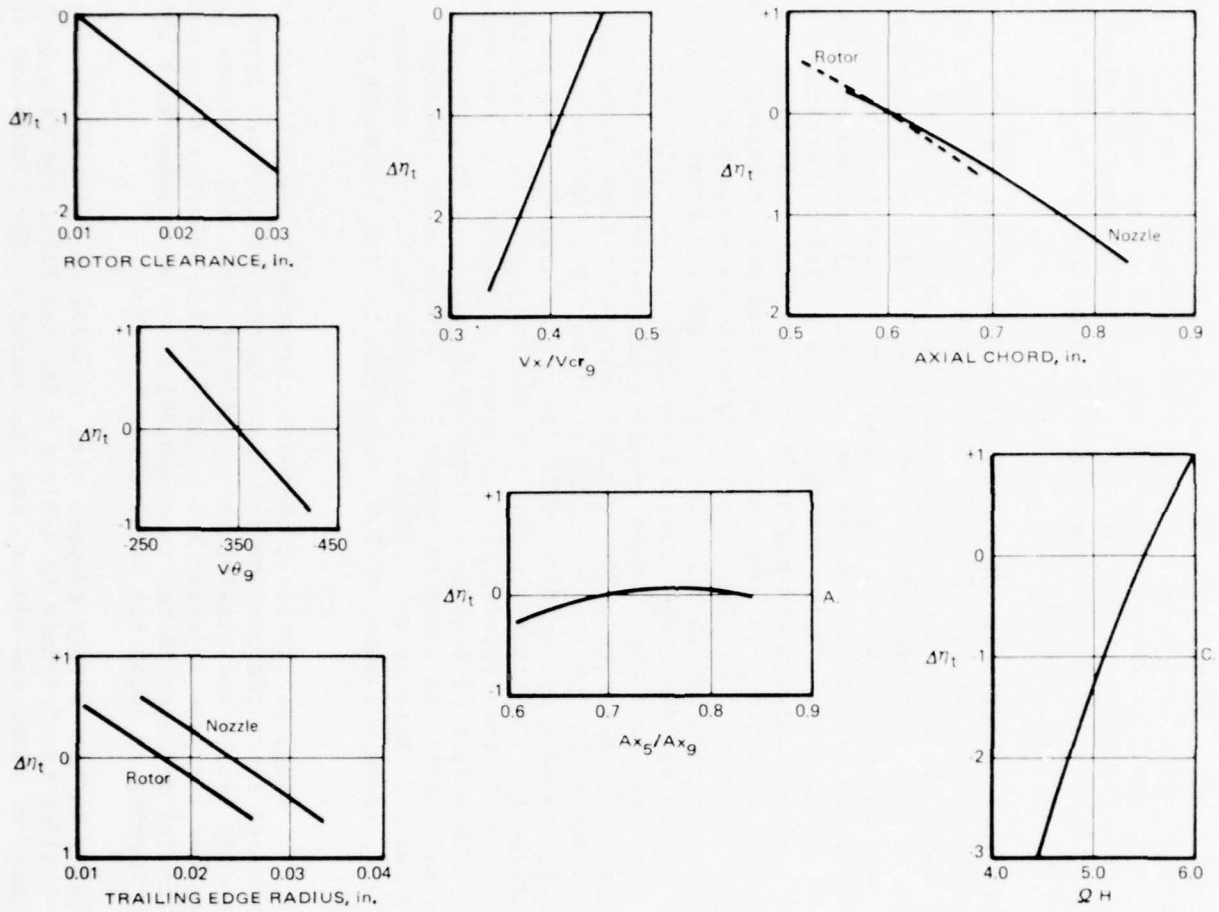


Figure 8. Effect of Design Parameters on Turbine Efficiency.

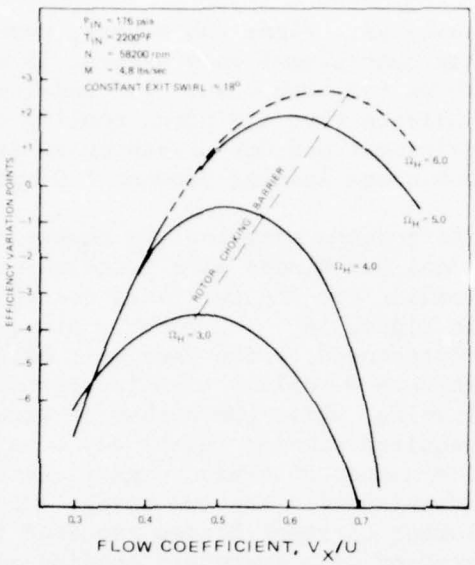


Figure 9. Performance Effects for 2200°F - 170 Btu/lb Turbine.

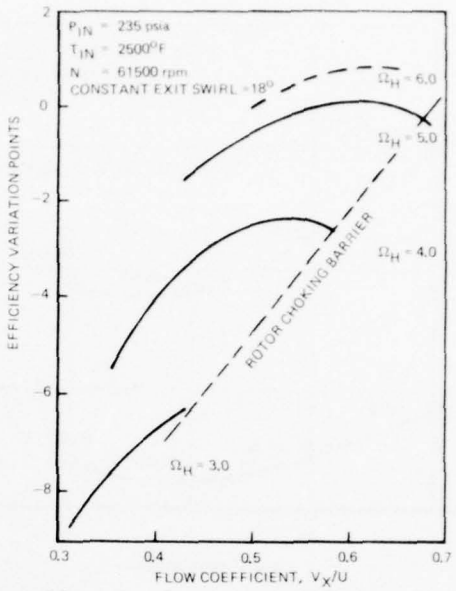


Figure 10. Performance Effects for 2500°F - 200 Btu/lb Turbine.

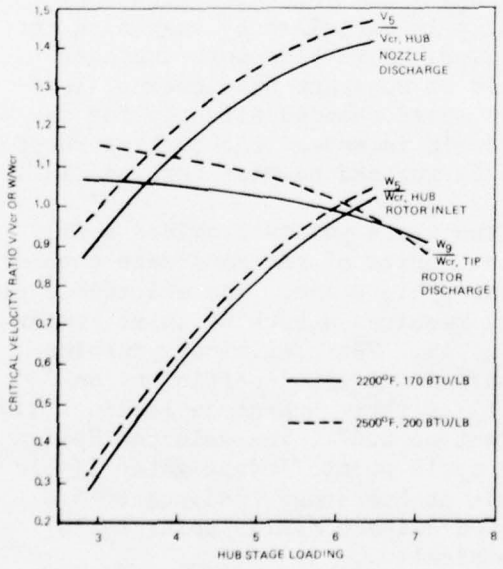


Figure 11. Nozzle and Rotor Velocity Variation with Stage Loading.

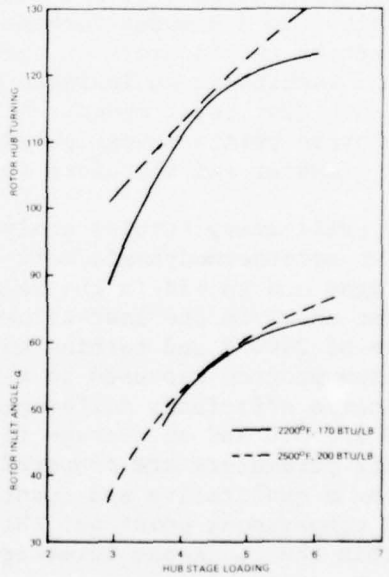


Figure 12. Effect of Loading on Rotor Blade Geometry.

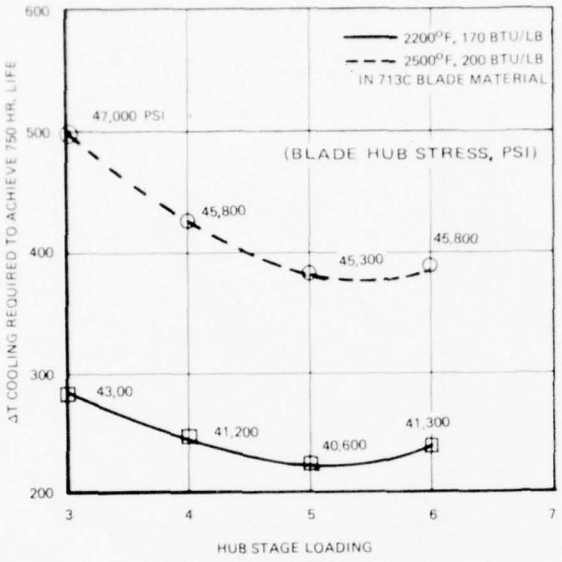


Figure 13. Turbine Cooling Requirements.

analysis. Blade hub stress, considering centrifugal only stress, is also shown for each case. The results indicate that a minimum cooling requirement and hub stress exist at a hub stage loading between 5.0 and 6.0.

The turbine size and the number of vanes and blades as a function of loading for the two cases are shown in Figure 14. The turbine size, represented by the vane exit height, increases rapidly with increasing loading, while the number of vanes required remains relatively constant. The number of vanes required were identical for the two cases. The number of rotor blades required increased with increased loading and remained nearly identical for the two cases up to a loading of 5.0. The effect of loading on turbine rotor weight is shown in Figure 15. The weight decreases with increased loading for both cases up to a loading of 5.0. Beyond 5.0, the 2500°F, 200 Btu/lb turbine increases while the 2200°F, 170 Btu/lb turbine continues to decrease. It is interesting to note that the 2500°F, 200 Btu/lb turbine had a smaller vane height but resulted in a heavier turbine. This result is explained by examining the effect of turbine work on turbine hub radius. A turbine work increase (ΔH) results in an increase of hub radius at constant hub loading (Ω_H) and constant rotor speed. Although rotor speed changed slightly for the two cycle points investigated, the net result increased the turbine rotor hub diameter and therefore resulted in a larger and heavier turbine disk.

The preliminary turbine analysis of the two cycle points provided sufficient aerothermodynamic data to assess the merits of the candidate turbine designs and to aid in the selection of the cycle point. The selected cycle point shown in the last column of Table 1 requires a turbine inlet temperature of 2400°F and turbine work of 180 Btu/lb. The preliminary turbine design program was used to generate the effect of flow coefficient on relative efficiency difference (Figure 16) at three hub stage loadings 3.0, 4.0 and 5.0 and an average flow coefficient of 0.67. The selected design point parameters are compared to the two cycle points investigated (Table 3) on a qualitative and quantitative basis at hub stage loadings of 5.0. The comparisons point out that the selected turbine design point falls within the two cases investigated parametrically.

Subsequent turbine analysis based on Ainley/Mathieson (Ref. 9 & 10) and Teledyne CAE experience (Appendix B) indicated that the required turbine work of the selected cycle (2A 180/2400) should be more realistically provided with a 3.75 pressure ratio turbine stage at a minimum uncooled turbine efficiency of 80.2 percent. As a result, this was adopted as the design goal. Other widely accepted works of S. F. Smith[6] and W. L. Stewart[5] indicate significantly higher performance potential. Based on the Smith correlation a turbine efficiency better than 91 percent could be expected from stage loading and flow coefficient (Figure 16) at zero tip clearance. In terms of velocity diagram parameters, the Stewart correlations predict on efficiency of 84.5 percent. With the 80.2 percent uncooled efficiency goal, the impact on the cycle (2A 180/2400) is approximately a 3.4 percent reduction of power turbine work and a like increase in engine specific fuel consumption. This loss, however, could be partially recovered with the increased performance potential indicated by Smith and Stewart. Consequently, the results of the engine cycle analysis was considered sufficiently accurate and further cycle iterations discontinued.

Based on the above a summary of the gas generator turbine parameters at the 100 percent power design point is shown in the following table (ASATT Turbine Design Point Summary excerpted from Appendix B).

Physical Airflow - lb/sec	4.8
Corrected Flow - lb/sec	0.90
*Efficiency (T-T) - percent	80.2
Actual Work - Btu/lb	180
Referred Work ($\Delta H/\theta_{cr}$) - Btu/lb	33.4
Nozzle Inlet Temperature - ^{o}F	2400
Nozzle Inlet Pressure - psia	188.6
Physical Speed - rpm	60,000
Referred Speed - rpm	26,010
Pressure Ratio (Hot) - (T-T)	3.75

*Uncooled Thermodynamic Efficiency.

TABLE 3

DESIGN POINT SELECTION COMPARISON			
	170/2200	200/2500	180/2400
Efficiency at Optimum Flow Coefficient - Relative to Nominal	+2.0	0	+0.3
Approximate Best Work Coefficient	5.0	5.0	5.0
Approximate Best Flow Coefficient	0.6	0.6	0.67
Choking, Reaction and Swirl Limits	Good	Poor	Good
Blade Rows Choked	Nozzle	Nozzle & Rotor	Nozzle
Nozzle Hub Exit Velocity Ratio (Ω = 5.0)	1.28	1.34	1.28
Rotor Hub Inlet Velocity Ratio (Ω = 5.0)	0.81	0.83	0.80
Rotor Tip Exit Velocity Ratio (Ω = 5.0)	1.03	1.08	1.02
Rotor Gas Inlet Angle (Ω = 5.0)	60	61	56
Rotor Hub Turning Angle (Ω = 5.0)	120	123	115
Rotor Hub Centrifugal Stress - psi	40,600	45,300	42,000
Rotor Cooling Requirements - ΔT	220	380	290
Rotor Cooling Flow and Leakage	3.0	5.0	4.0
Nozzle Cooling Flow and Leakage	3.0	5.0	4.0
Nozzle Vanes/Rotor Blades (Ω = 5.0	27/47	27/46	26/42
Total Weight of Blades and Disc (Ω = 5.0)	4.65	5.2	5.06
Referred Work $\left(\frac{\Delta H}{\theta_{cr}}\right)$ - BTU/lb.	34.8	35.8	33.7

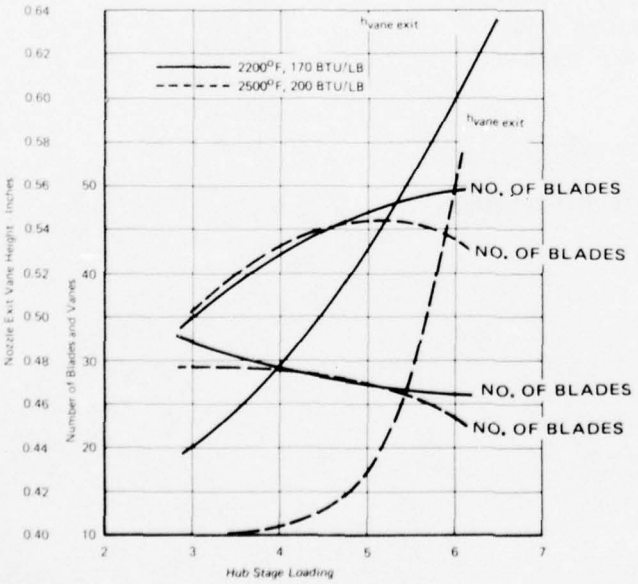


Figure 14. Effect of Loading on Blade Number and Height.

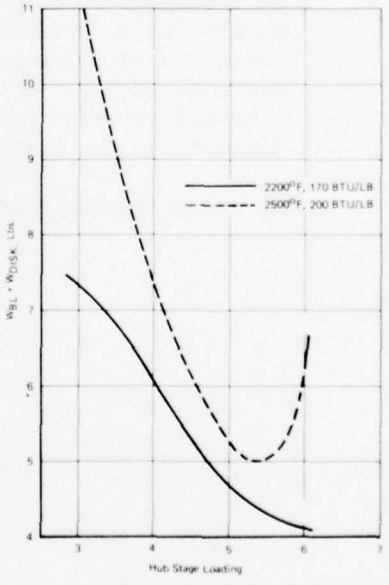


Figure 15. Effect of Loading on Turbine Weight.

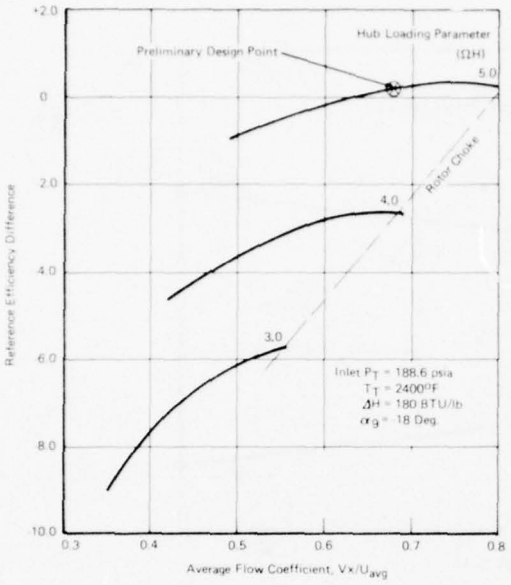


Figure 16. Performance Effects on 2400°F - 180 Btu/lb Turbine.

The preliminary turbine flow path selected for detail analysis is shown in Figure 17. The initial preliminary design investigation for the 180/2400 turbine design with 5.0 hub stage loading and 0.67 flow coefficient indicated a 26 vane and 42 blade requirement (Table 3). Subsequent heat transfer analysis and design of the nozzle coolant scheme lead to a necessary increase in nozzle axial chord. In order to maintain an axial solidity of 1.0, the number of vanes was decreased to 20. Stress analysis required a prime number of blades and therefore the nearest prime number, 41, was chosen. The flow path in Figure 17 represents the resultant 20 vane; 41 blade configuration. Velocity triangles corresponding to this flow path at hub, mean and tip sections are shown in Figure 18.

TURBINE DETAIL DESIGN

The baseline flow path, based on the free-vortex, constant work, and mean-line design, was analysed using streamline analysis techniques. The effects of radial distributions of pressure loss, whirl velocity, and work on the flow field were investigated and an optimum final design was selected. Additional discussion of design technique is presented in Phase IV.

Flow Path

The Teledyne CAE axial flow turbomachinery flow path design technique consists of an axisymmetric streamline analysis which gives a solution along arbitrary straight lines in the meridional plane. Station calculations are not independent in this solution but are tied to each other by a spline fit through streamline radii and another curve fit, to compute gradients in meridional velocity.

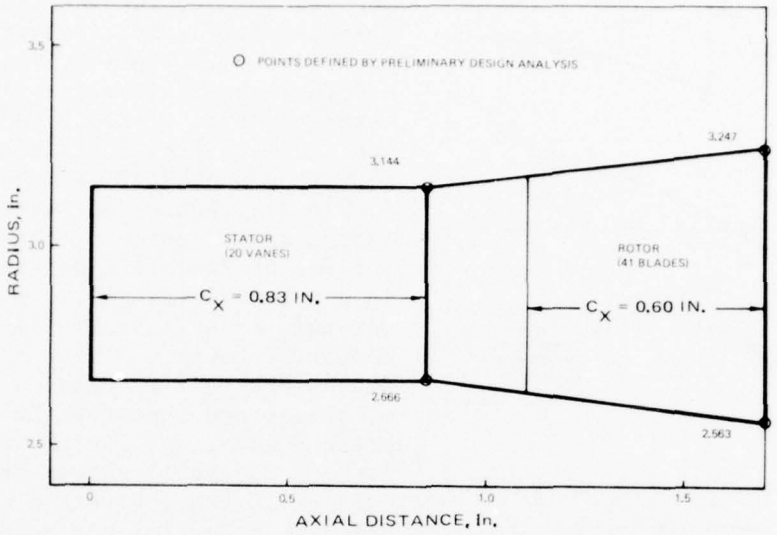


Figure 17. Preliminary Turbine Flow Path.

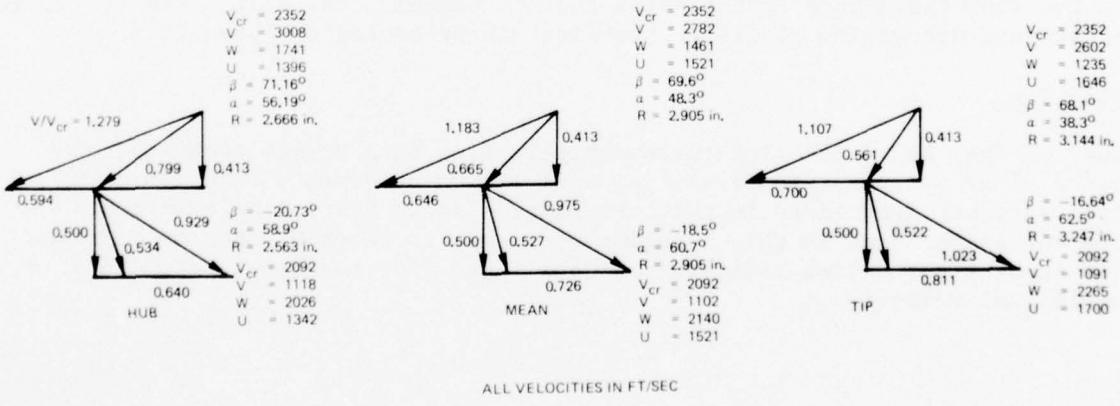


Figure 18. Preliminary Velocity Triangles (Free-Vortex).

Velocity calculations along an arbitrary line in the meridional plane are based on the momentum equation, which accounts for streamline curvature and entropy gradients. The expression for velocity is obtained from consideration of three-dimensional flow-through turbomachines in a cylindrical coordinate system.

Once the velocity distribution calculations are performed at a given station, a continuity calculation is made and the calculated flow is checked against the flow design. If the comparison is not satisfied, then the velocity distribution calculation is repeated by assuming a new value at the hub station. This process is repeated until the continuity check is satisfied. When the continuity check is completed, streamline shaft calculations are then performed at all stations. When continuity, streamline shaft and velocity checks are satisfied, the solution is considered to be complete.

In the program the stators are described by inputing distributions of loss coefficient and tangential velocity or angle. For rotors, input distributions of loss coefficient and exit total temperature or total pressure are given. The program also handles inlet profiles for inlet total temperature and/or pressure.

A radial distribution of pressure loss was estimated for the stator and rotor to arrive at a more realistic flow field. The distribution was tailored after the division of total pressure loss determined by the loss system during preliminary design. Figure 19 shows the stator and rotor loss divided into endwall, profile, mixing and tip clearance on an average basis. The loss distributions estimated for the streamline analysis are shown in Figure 20. The distributions are biased to account for the expected high loss regions. The stator loss distribution was biased to the inner and outer flow-path regions to reflect the increased loss caused by secondary flows. The rotor was heavily biased over the hub to the mid-span region to account for the high loss expected due to high blade loading and relatively low reaction.

Nine streamline analysis computer solutions (Table 4) were processed using various combinations of stator exit tangential velocity, radial work gradient, pressure loss, and inlet temperature distortion (TDF).

Computer runs 1 through 5 were performed with various combinations of stator and rotor pressure loss and stage work gradients, either constant or as a function of radius. Computer run 3 did not converge because of severe axial velocity gradients imposed by the radial losses and high work in the hub region.

Run 6 was performed with radial distributions of pressure loss and work with an inlet temperature distribution introduced, typical of combustor exit pattern (Figure 22) (TDF = 0.23). The radial distribution of work used for runs 4 through 9 is shown in Figure 21. Run 7 was performed with the

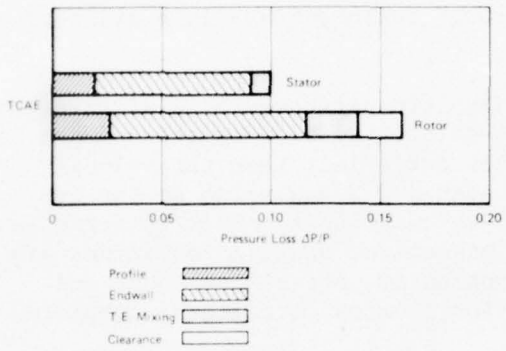


Figure 19. Division of Total Pressure Loss.

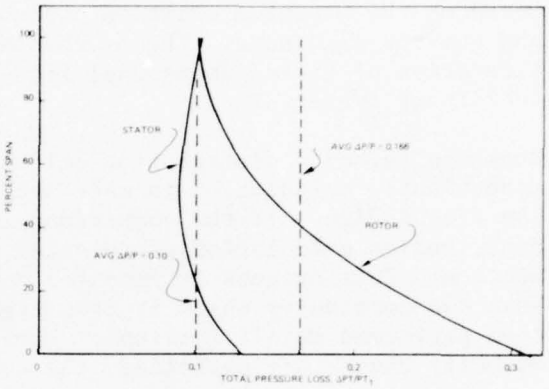


Figure 20. Estimate of Radial Loss Distribution.

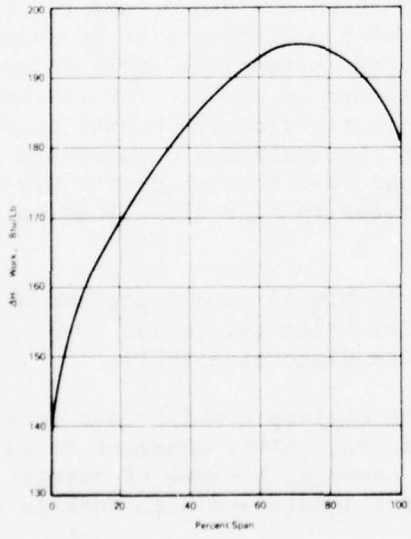


Figure 21. Radial Work Distribution For Runs 4 through 9.

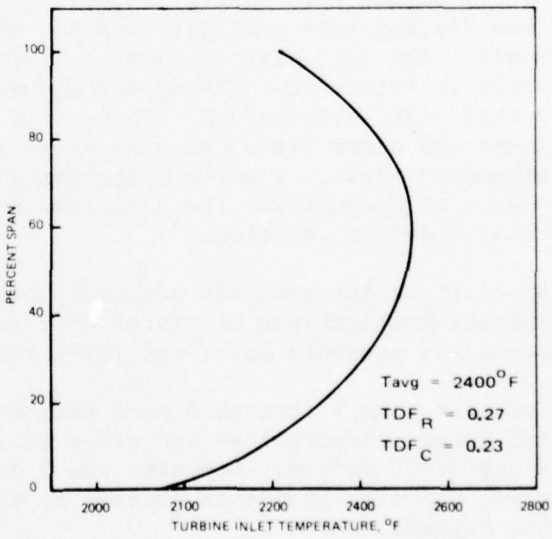


Figure 22. Inlet Temperature Distribution for Streamline Analysis - Run 6.

TABLE 4

SUMMARY OF STREAMLINE ANALYSIS VARIATIONS

Run	Configuration	Total Pressure Loss		Work
		Stator	Rotor	
		Constant Meanline		
1	Const. Meanline	Constant*	Constant	Constant
2	Const. Meanline	f (R)**	Constant	Constant
3	Const. Meanline	f (R)	f (R)	Constant
4	Const. Meanline	f (R)	Constant	f (R)
5	Const. Meanline	f (R)	f (R)	f (R)
		With Combustor Exit Temperature Distribution Factor Included		
6	Const. Meanline	f (R)	f (R)	f (R)
		Constant Tip Radius Flow Path		
7	Const. Tip Radius	f (R)	f (R)	f (R)
		With Stator Exit Tangential Velocity Imposed Radially		
8	Const. Meanline	f (R)	Constant	f (R)
		With Cooling Air Injection		
9	Const. Meanline	f (R)	f (R)	f (R)

* Parameter is Constant with Radial Span.
** Parameter Varies with Radial Span.

flow path modified for a constant tip radius rotor. Run 7A was later obtained as a variation on Run 7, with radially constant exit total pressure, and was the solution selected for the continued design analysis. Runs 1 through 7 were performed using a free-vortex stator exit velocity distribution, and a specified vortex distribution (Figure 23) was used in Run 8. The streamline analysis program was modified to permit cooling air injection. Run 9 was attempted to evaluate that effect on the flow field; however, the run did not converge. The computer output for all cases is included in Appendix C.

The various cases were evaluated by comparing the velocity triangles at 12.5, 50 and 87.5 percent span. Figure 24(a) shows the velocity triangles for Runs 1, 5 and 6, and Figure 24(b) for Runs 7, 7A, and 8. Runs 2 and 4 were not constructed since they were primarily intermediate steps to achieve Run 5 with radial stator and rotor pressure loss distributions. Comparisons of Run 1 and 5 do not show much difference in the velocity triangles. Only slight differences in velocity and angles were noted. When the case was run with an inlet temperature distribution (Run 6), it was noted that the mean and tip axial velocities at the stator exit increased from 71 to 76 degrees. However, at the rotor exit the hub axial velocities were higher in Run 6 than Run 5, while the mean and tip were lower. In terms of rotor relative velocity ratio the hub and tip increased in the presence of TDF, while the mean decreased as shown in Table 5.

Run 7 velocity triangles were similar to Run 5 even though the flow path was modified from the flared tip to a constant radius tip rotor. However, the radial mass flow shift, did result in an increase in relative velocity ratio at the mean and tip sections (Table 5). Run 7A was performed to arrive at a more uniform axial velocity profile leaving the rotor.

A uniform total pressure was specified as the program input in place of the radial work distribution. The results show that the hub axial velocity increased to provide a very uniform profile at the rotor exit (Figure 25) and that the rotor still exhibited good acceleration in terms of relative velocity ratio (Table 5).

The specified stator exit vortex distribution (Run 8) resulted in velocity triangles which showed large mass flow shifts in both the stator and rotor. Although the rotor hub acceleration was the highest of any case run, the extreme flow shift to the hub caused very large stator exit angles so this case was not considered for further analysis.

All of the cases were compared on the basis of stage reaction defined in terms of static pressures. It is widely accepted that a major source of inefficiency in flow channels is the result of adverse static pressure gradients within the flow field (Reference 39, Ch. 24, pp. 615-630). The stage static pressure reaction was calculated for all cases at the hub streamline since it is minimum at that location (Table 6).

It was noted that the highest static pressure reaction was achieved by the specified vortex run; however, since the stator exit angle at the tip was

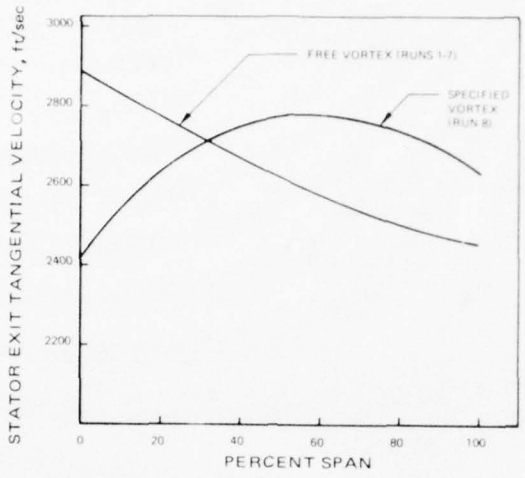


Figure 23. Stator Exit Tangential Velocity Distributions for Streamline Analysis.

higher than desirable from the manufacturability aspect, that case was not considered further. Further comparisons of the cases led to the following generalizations:

Change to Flow Field	Static Pressure Reaction
A. Radial Loss Distribution	Decreases
B. Radial Loss and Work Distribution	Decreases
C. A & B above with TDF at inlet	Decreases
D. A & B with constant tip rotor	Increases
E. D with constant exit total pressure	Increases
F. A & B with specified Vortex	Increases

A constant tip radius blade was desired for the design since it has the advantage of constant tip clearance regardless of axial shaft movement. The streamline analysis showed that it also has the highest potential to achieve the best efficiency of the cases investigated.

Run 7 represented the configuration with a realistic turbine environment; however, the axial velocity gradient was more severe than desired. Therefore, Run 7A was performed with constant rotor exit total pressure. The results showed that a uniform axial velocity was achieved and that the static pressure reaction also improved slightly. Therefore, Run 7A was chosen for further detail design analysis.

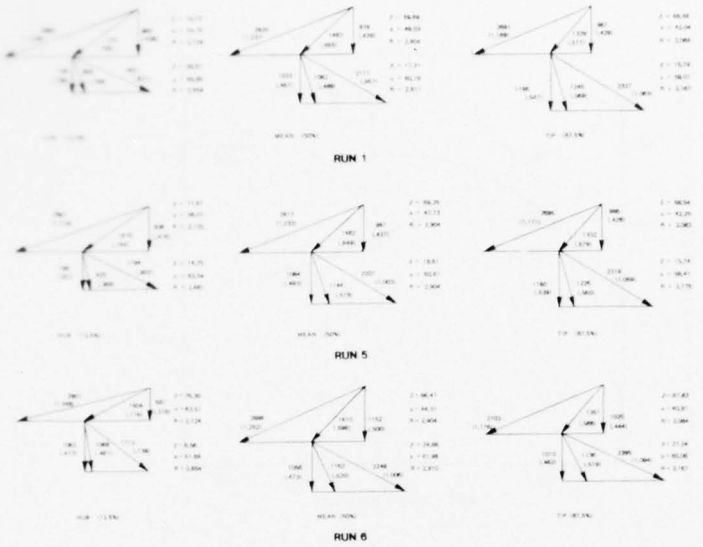


Figure 24(a). Velocity Triangles for Streamline Analysis Runs 1, 5, 6.

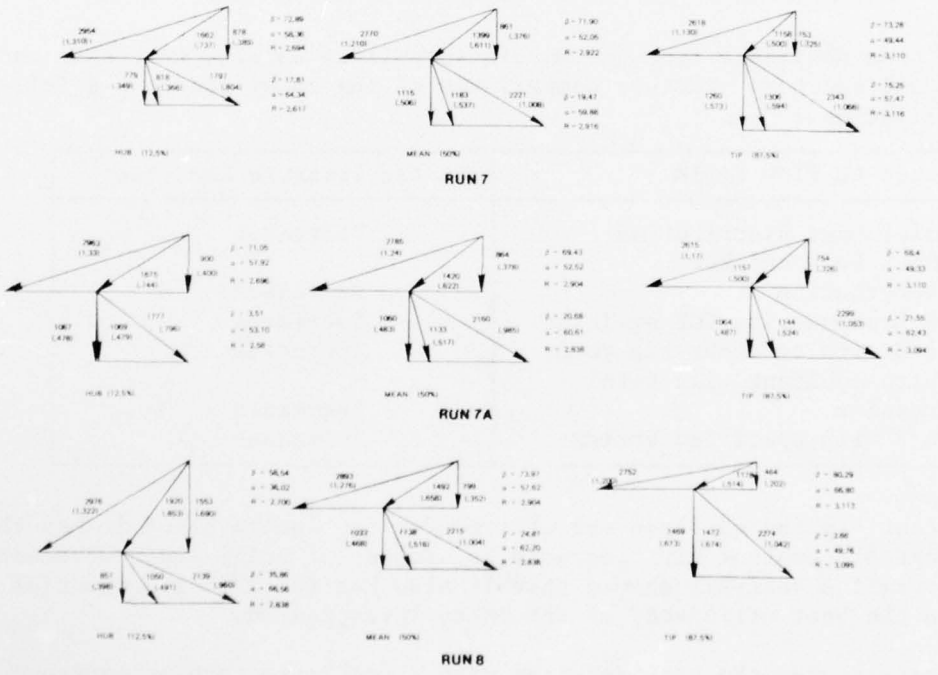


Figure 24(b). Velocity Triangles for Streamline Analysis Runs 7, 7A, 8.

TABLE 5

COMPARISON OF ROTOR RELATIVE VELOCITY RATIO

RUN	HUB	MEAN	TIP
1	1.07	1.42	1.75
5	1.07	1.49	1.74
6	1.14	1.39	1.77
7	1.08	1.58	2.02
7A	1.06	1.52	1.99
8	1.11	1.48	1.93

TABLE 6

SUMMARY OF STATIC PRESSURE REACTION

CASE (RUN)	STATIC PRESSURE REACTION
1	0.0967
2	0.0936
3	NO SOLUTION
4	0.0845
5	0.0913
6	0.717
7	0.0932
7A	0.0992
8	0.1255
9	NO SOLUTION

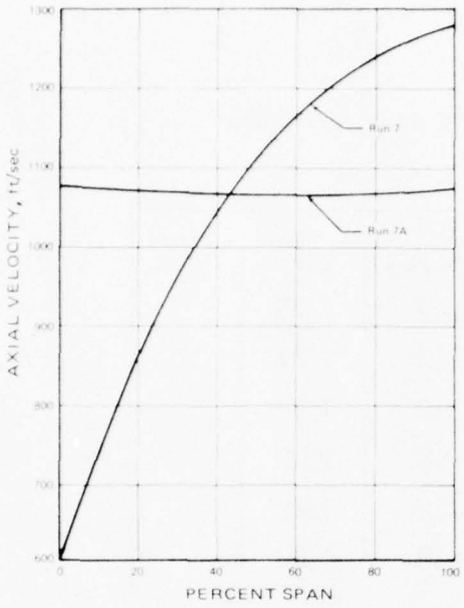


Figure 25. Rotor Exit Axial Velocity Radial Distributions.

The radial work gradient required to satisfy the flow solution and the constant radial total pressure constraint is shown in Figure 26. The velocity triangles for the hub (12.5 percent span), mean (50) and tip (87.5) (Figure 25), were used for the design of the nozzle and rotor blade sections. Various parameters of interest, such as absolute Mach number, rotor relative Mach number, absolute gas flow angle, rotor relative gas flow angle and reaction are shown as a function of percentage span to aid in the analysis (Figures 27 through 31).

A visual comparison of the variance of streamlines is shown in Figure 32 for the constant meanline flow path and the constant tip radius blade. These are eleven streamlines from hub to tip, with a division of 10 percent of the mass flow between each line. The distribution of streamlines for both flow paths indicates relatively uniform flow throughout the entire flow path.

Of the cases investigated, the choice of Run 7A for the design velocity triangles represents the optimum flow path and velocity triangles for the following reasons:

1. The radial work distribution was tailored to provide nearly constant axial velocity and exit total pressure.

2. The stage static pressure reaction over the entire span was favorable in the presence of the radial pressure loss distributions for both the stator and rotor.

3. A constant radius blade affords the best control of minimum running tip clearance.

Nozzle Vanes

The nozzle vanes were designed to the mean section velocity triangle selected from the flow path streamline analysis. The design procedure consisted of a preliminary estimate of the number of vanes usine Zweifel's criteria of loading (Reference 40).

The [illegible] loading criteria considers a rectangular pressure loading with zero diffusion. This produces the maximum tangential blade force (and ideally, the optimum number of blades).

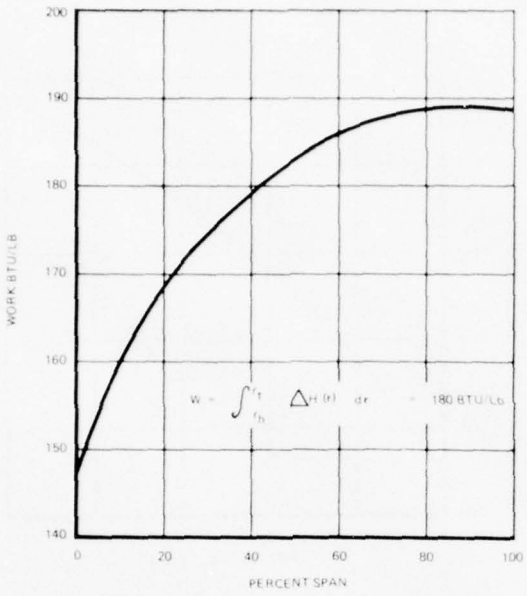


Figure 26. Radial Work Distribution Resulting from Constant Total Pressure at the Rotor Exit.

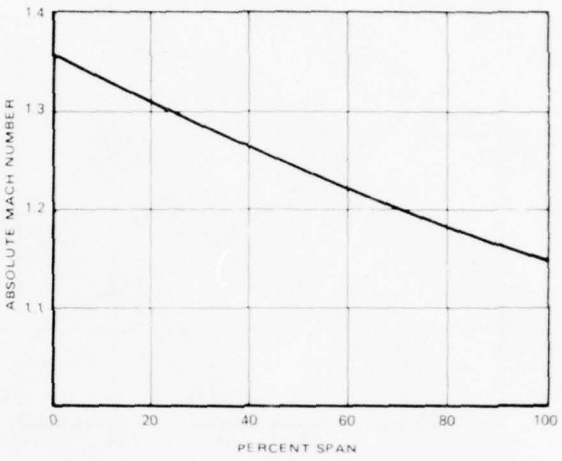


Figure 27. Radial Distribution of Absolute Mach Number at Stator Exit.

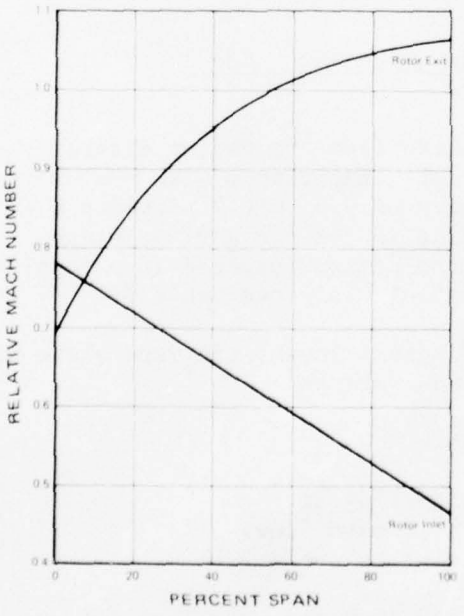


Figure 28. Radial Distribution of Rotor Relative Mach Number.

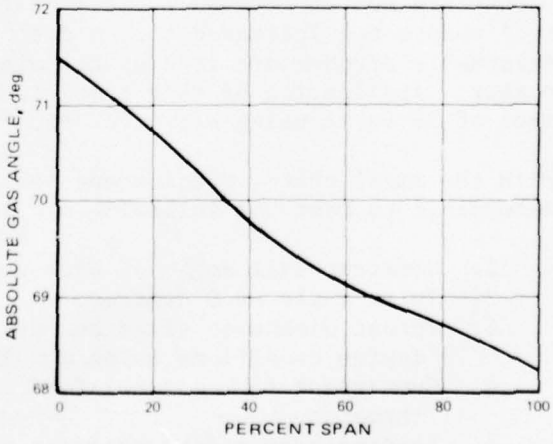


Figure 29. Radial Distribution of Absolute Flow Angle at Stator Exit.

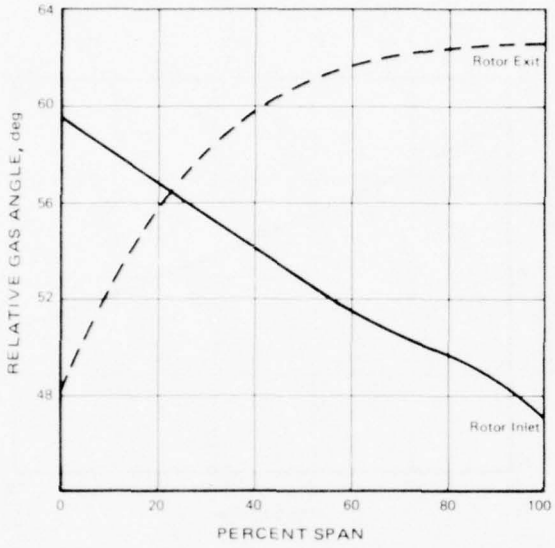


Figure 30. Radial Distribution of Rotor Relative Flow Angle.

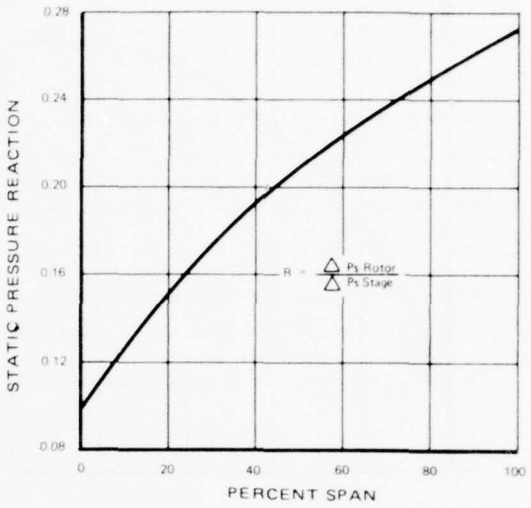


Figure 31. Radial Distribution of Static Pressure Reaction.

In terms of the axial chord to spacing (solidity), the equation is defined as:

$$\frac{Cx}{s} = \frac{2 \cos^2 \beta 5 \ (\text{Tan } \beta 1 - \text{Tan } \beta 5)}{\psi t}$$

The optimum number of blades can be calculated from the vector diagram parameters and an assumed Zweifel coefficient. Experience with vane airfoil shapes has indicated that a coefficiency of 0.5 to 0.7 provides a reasonable aerodynamic loading for minimizing losses for a first-stage nozzle. Application of this criterion to the design resulted in a complement of 20 vanes using a Zweifel coefficient of 0.65 (see Table 7).

With the axial chord, spacing and vector diagrams known, the vane shape was determined to meet the following section requirements.

1. Constant exit angle of 69.5 degrees.
2. Inlet angle of 0 degrees.
3. Throat dimension sized to pass design flow at design conditions using continuity of mass flow.
4. Convergent flow channel from the inlet to the throat.
5. Leading-edge radius constant at 0.070 inch and trailing-edge radius constant at 0.015 inch.
6. An airfoil velocity distribution to assure separation free flow.

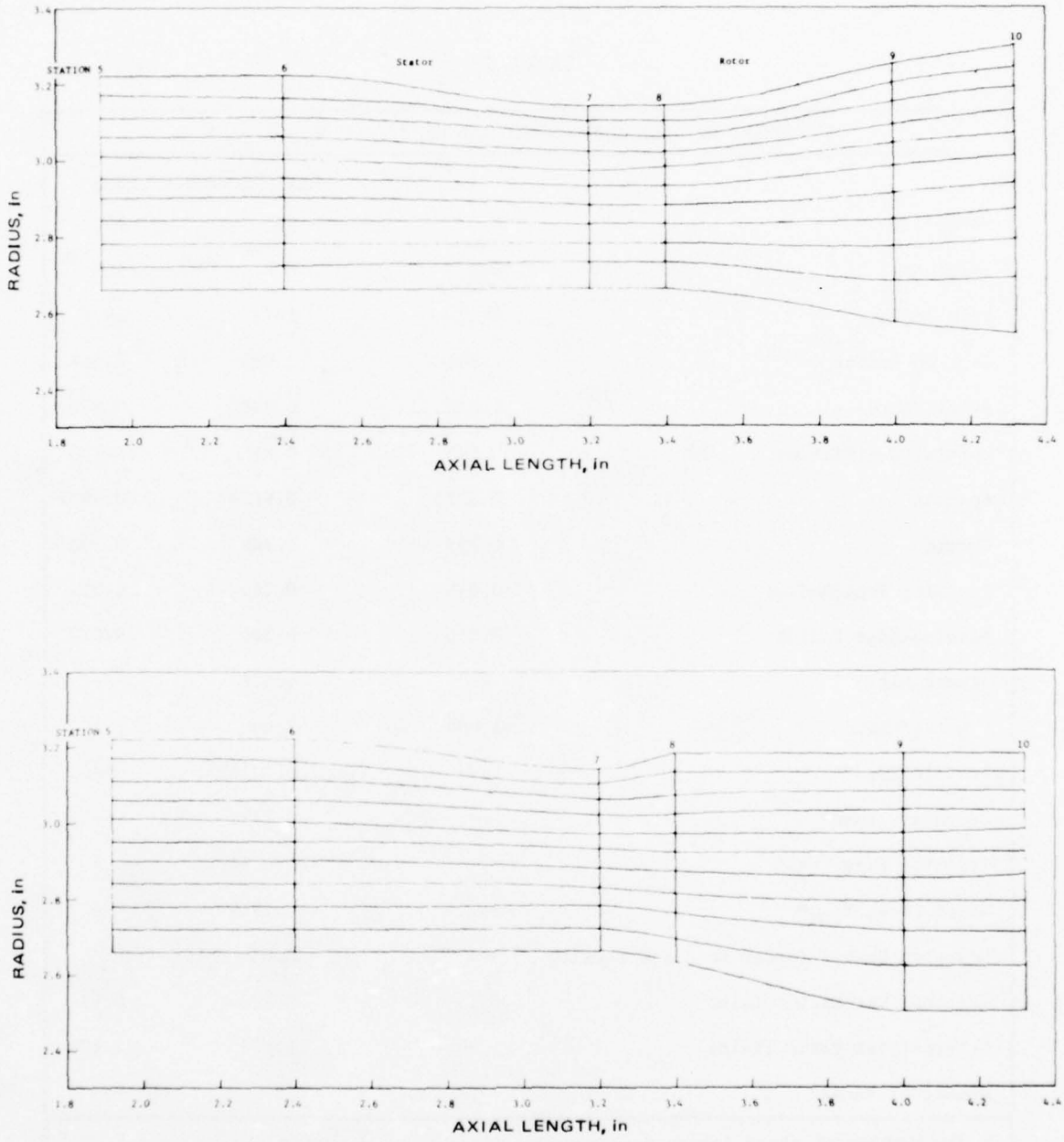


Figure 32. Comparison of Streamline Analyses.

TABLE 7

SUMMARY OF VANE AERODYNAMIC AND GEOMETRIC DESIGN DATA

	Percent Span at Exit		
Parameter	0	50	100
Inlet Angle	0.0	0.0	0.0
Exit Angle	69.7	69.7	69.7
Section Radius	2.666	2.905	3.144
Axial Chord	0.830	0.830	0.830
Zwiefel Coefficient	0.595	0.65	0.703
Spacing	0.8375	0.9126	0.9877
Throat	0.255	0.281	0.303
Trailing Edge Radius	0.015	0.015	0.015
Leading Edge Radius	0.070	0.070	0.070
Aspect Ratio	---	0.576	---
Spacing/Chord	1.009	1.099	1.190
Profile Loss*	---	0.0376	---
Secondary Loss*	---	0.1412	---
Trailing Edge Loss*	---	0.0191	---
Total Loss, Y_{TOT}*	---	0.1979	---
Reynolds Number (refer to C and V exit)	---	8.034×10^5	---
Critical Vel Ratio (Inlet)	0.15	0.15	0.15
Critical Vel Ratio (Exit)	1.28	1.183	1.106
Number of Vanes	---	20	---

* Derivation of these losses is discussed under the Phase IV Section, Design Technique Assessment, which is based on Appendix B data, computer output for preliminary turbine design.

The vane shape was constructed by contouring the suction and pressure surfaces to satisfy the above requirements, and the resulting flow channel was analyzed using a blade-to-blade flow analysis as reported in Reference 42. The flow analysis produced surface velocity distributions which enabled a calculation (Reference 43) of the boundary layer parameters. Satisfactory surface velocity distributions were judged by the amount of suction surface diffusion downstream of the throat and by boundary layer analysis to assure separation free flow along the entire vane surface.

The design contour which met the requirements is shown in Figure 33. The surface velocity distribution for the mean section is shown in Figure 34. Note that a small amount of diffusion occurs downstream of the throat on the suction surface. In terms of suction side diffusion factor, which serves as a cross check for the more elaborate boundary layer analysis,

$$Ds = 1 - \frac{V5}{Vmax},$$

this equals a factor of 0.077.

In the past, NASA has generally recommended that a high-efficiency turbine be designed for suction surface D factors less than or equal to 0.10. Using NASA's guidelines, the suction surface diffusion for this design is considered.

The boundary layer analysis for the velocity distribution is shown in Figure 34 and produced the variation of momentum and displacement thickness shown in Figure 35. Also shown in Figure 35 is the form factor which is an indication of separation.

The distribution of form factor along the suction surface shows a late transition from laminar to turbulent flow as indicated by the rapid decrease from 2.6 to 1.4. Separation is generally considered incipient when the form factor reaches 2.8 (Reference 39, pp. 576-582).

Table 7 lists the important geometric and aerodynamic data of the vane.

The tip loading is also shown in Figure 34. The diffusion of suction side is also less than 0.10 and did not require a boundary layer analysis. The hub section is loaded the least with a Zweifel coefficient of 0.595, as compared to mean and tip values of 0.65 and 0.703, respectively (Table 7). Diffusion was, therefore, assumed to be negligible and a boundary analysis was not conducted.

Meridional Constriction

Meridional constriction analysis was applied to the nozzle endwall design to minimize the secondary flow losses in the nozzle. The technique has been experimentally developed by Deich[41], however, no known analytical verification exists. The reported data (Figure 36) includes working curves (Figure 37) for designing the endwall contour to achieve minimim loss.

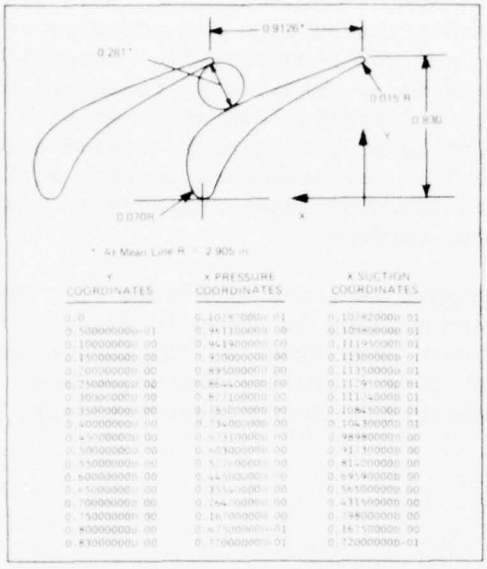


Figure 33. Stator Airfoil Section Coordinates

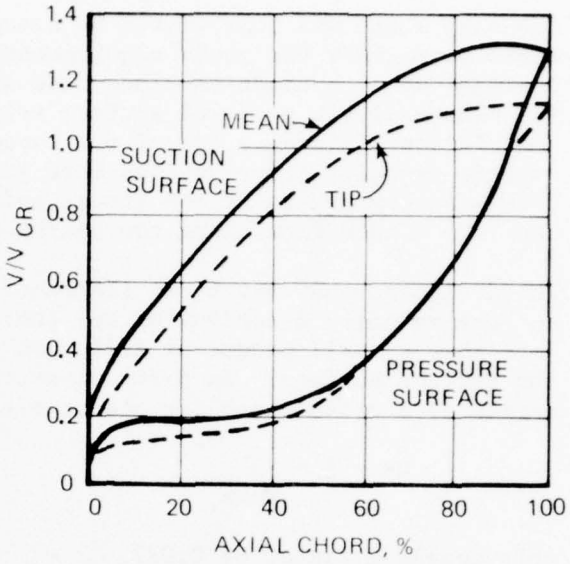


Figure 34. Stator Critical Velocity Ratio Distribution.

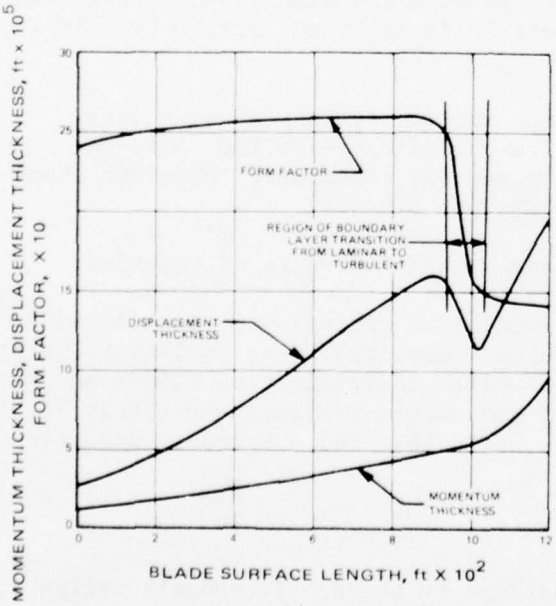


Figure 35. Stator Boundary Layer Properties Surface Suction.

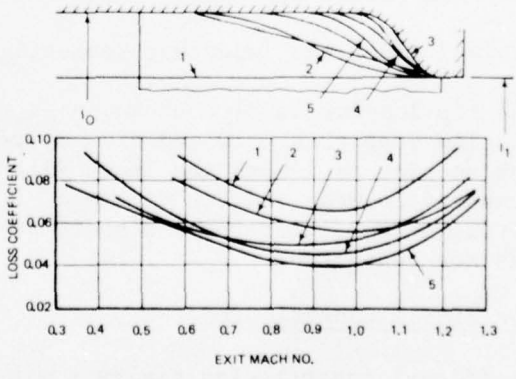


Figure 36. Effect of Mach No. on Loss for Various Contours (Reference 41).

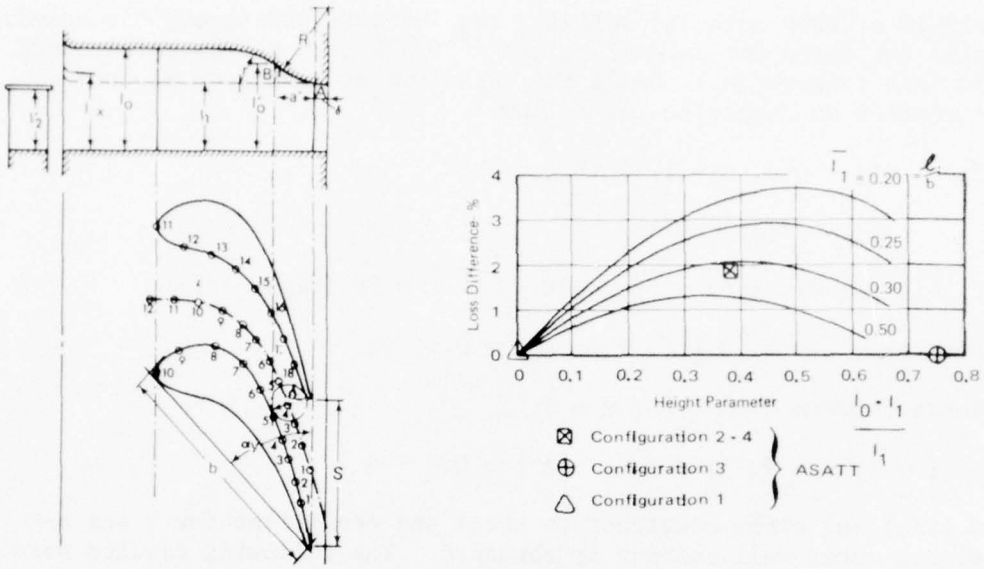


Figure 37. Optimum/Geometry Relationship for Minimum Loss (Reference 41).

It is theorized that the reduction of losses occurs as a result of:

1. Fluid turning is accomplished at lower velocities. This results in lower blade-to-blade static pressure gradients and hence lower intensity secondary flows.

2. Radial static pressure gradients are relieved at the nozzle exit. This decreases the flow of low energy fluids on the suction surface near the exit plane.

3. More intensive fluid acceleration toward the end of the channel and thinning of the boundary layer. Since boundary layer thickness has been shown (Reference 39) to affect endwall losses, a thinner boundary layer would tend to reduce those losses.

The reported data (Figure 36) shows that as the exit Mach number increases for each contour configuration, the loss coefficient decreases to a minimum and then increases.

Of the contours reported, the straight wall (1) created the highest loss and the moderately sloping contour (5) achieved the lowest loss.

Part of the Phase II experimental turbine cascade investigation is involved with testing four contour configurations to determine the minimum loss contour. Therefore, for the Phase I effort, the nozzle was designed to the optimim contour (based on Figure 37), and variations from that configuration were determined in Phase II.

On the basis of flow path and solidity requirements previously discussed, the nozzle was sized for an exit height of 0.478 inch and an axial chord of 0.830 inch (Figure 38). Using the technique of Reference 41, the optimum contour is determined as follows:

Since, $\bar{\ell}_1 = 0.4$, b = 1.30 (Figure 38)

$$\bar{\ell}_1 - \ell_1/b = 0.367$$

at ℓ_1, for max loss difference $\Delta\bar{\ell}_o = 0.38$ (Figure 37)

Therefore, $\ell_o = \ell_1 (1 + \Delta\bar{\ell}_o) = 0.66$ in

From Reference 41 $R \simeq \ell_o$, $r \simeq R$,

$$\xi = (\ell_o - \ell_o') / (\ell_o - \ell) \simeq 0.3 - 0.4$$

Perform trial and error construction until the conditions for ξ are met and a smooth outer wall contour is obtained. The following results were obtained:

R = 0.78 in
r = 0.50 in
ℓ_o = 0.60 in
ξ = 0.33 (meets requirement listed above)

The completed construction is shown in Figure 38. The estimated maximum loss difference (improvement) (from Figure 37) is approximately 1.5 percent.

Rotor Blade

The rotor blade airfoil design procedure followed a similar method as the nozzle vane. The relative velocity triangles in Figure 25 were used to generate the hub and tip sections. Intermediate sections were straight-line interpolated from the defined hub and tip sections. The Zweifel criteria was again used to determine an initial estimate for blade spacing, and the loading was checked using flow analysis and boundary layer analysis.

The Zweifel coefficient is defined for rotor blades in terms of the relative velocity triangles. The axial chord to spacing ratio (solidity) is:

$$\frac{CX}{S} = \frac{2 \cos^2 \alpha_9 \quad (\tan \alpha_5 - \tan \alpha_9)}{\psi t}$$

The Zweifel loading coefficient ψt, for highly loaded rotor blading, has been pushed to values exceeding unity. A Zweifel coefficient of 1.10 was used for a preliminary estimate of the meanline loading for the ASATT rotor. This value resulted in an axial solitity of 1.348, and for an axial chord of 0.60 in. (from the flow path study) the number of blades was determined as 41 blades. A check on the blade attachment practicality was required to insure that 41 blades would fit within the hub periphery.

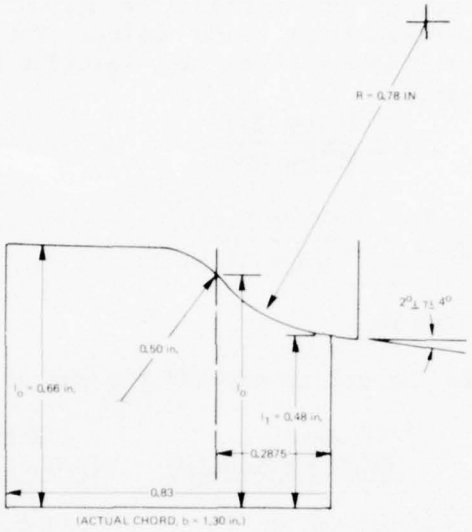


Figure 38. Definition of Geometry for a Nozzle with Meridional Constriction.

This was performed using a scaled hub section of an existing high work turbine and it confirmed a 41 blade configuration.

The rotor airfoil contours were constructed by contouring the suction and pressure surfaces to satisfy the requirements listed below:

1. Three blade sections consisting of two hub sections at 12-1/2 percent span and one tip section at 87-1/2 percent span to yield the relative velocity triangle at those locations.

2. Throat dimensions sized to pass design flow for each section.

3. Linear faired sections between the defined hub and tip sections.

4. Hub leading edge radius of 0.035 in., tip leading edge radius of 0.025 in., and trailing radius of 0.015 in., constant spanwise.

5. Incidence on leading edge to be determined to satisfy aerodynamic loading requirements.

Two hub sections (12.5 percent span) were designed to exhibit different loadings but both satisfying the velocity diagrams in Figure 25. A linear fair was selected to satisfy realistic constraints of manufacturability of a very small airfoil with intricate cooling passages. A recognized aerodynamic penalty, to be evaluated experimentally in the Phase III/IV efforts, was therefore incurred.

The two rotor blade loadings were achieved by contouring the suction and pressure surfaces to various inlet blade angles. The incidence variations were analyzed using the blade-to-blade flow solution and compared on the basis of diffusion factor.

$$\text{Suction Surface } D_S = 1 - \frac{W/W_{CR}\ \text{EXIT}}{W/W_{CR}\ \text{MAX.}}$$

$$\text{Pressure Surface } D_P = 1 - \frac{W/W_{CR}\ \text{MIN.}}{W/W_{CR}\ \text{INLET}}$$

$$\text{Total D Factor} = D_S + D_P$$

The resulting D factors for rotors one and two hub sections were:

	Rotor 1 (Suction Loaded)	Rotor 2 (Pressure Loaded)
D_S	0.36	0.23
D_P	0.49	0.52
D_T	0.85	0.75

Although the suction surface loaded hub section had a D factor higher than the pressure loaded hub, both rotors were configured to avoid separation over the entire blade surface on the basis of boundary layer analyses. A common tip section was designed to the 87.5 percent blade span velocity triangle with a 4-degree positive incidence for minimum loss. The flow analysis showed that all diffusion occurred on the pressure surface and that separation should not occur.

The losses predicted for the rotor are shown in Table 8. The losses are divided into profile, secondary (endwall), clearance, and trailing edge, and are dependent on inlet and exit velocity triangles and geometric characteristics. The effect of loading does not show up in the present loss system since both loadings produce the same exit velocity triangle.

The two hub sections defined at the 12.5 percent span location are shown in Figures 39 and 40. The surface velocity distributions, calculated using the two-dimensional compressible flow technique of Reference 42, are shown in Figure 41. The suction boundary layer shape factor was calculated using the method of Reference 43 to investigate possible separation regions on the airfoil. This plot is shown as Figure 42 for both hub sections and it can be noted that the shape factor indicates an early transition to a turbulent boundary layer and that the flow is attached along the entire surface since the shape factor never exceeds 2.8. Analysis of the pressure surfaces for both sections also confirmed that the flow would remain attached as shown in Figure 43.

The tip section was constructed in a similar manner as described above for the hub and is shown in Figure 44. Flow analysis produced the velocity distributions shown in Figure 45 and the boundary layer parameter shown in Figure 46.

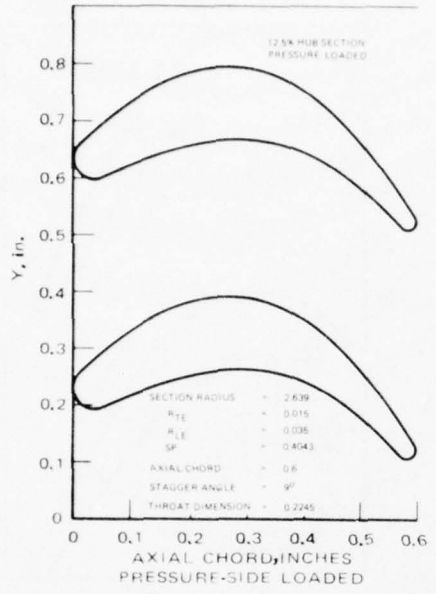


Figure 39. Rotor Hub Section - Pressure-Side-Loaded - 12.5 Percent Span.

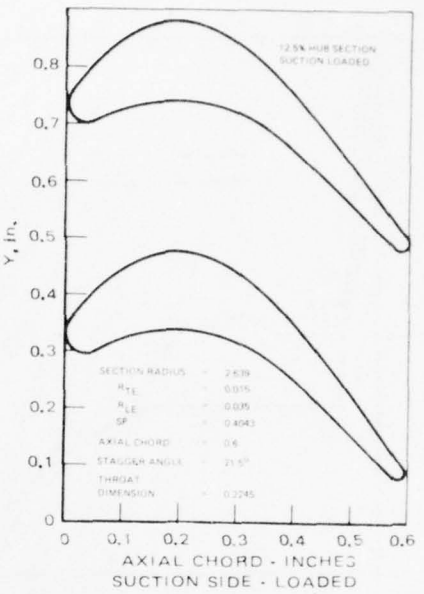


Figure 40. Rotor Hub Section - Suction-Side-Loaded - 12.5 Percent Span.

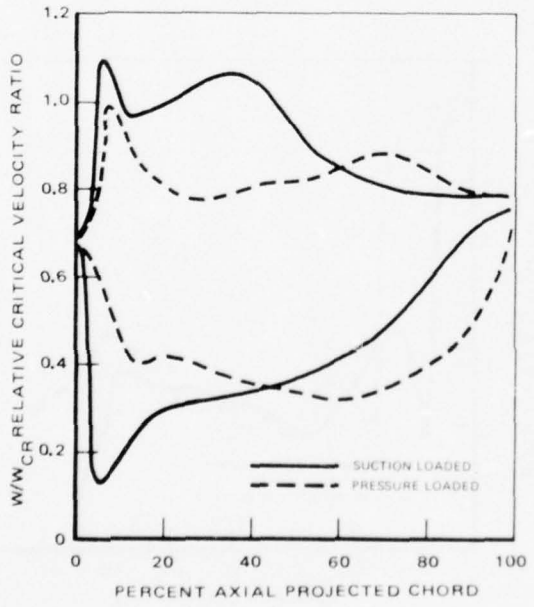


Figure 41. Rotor Hub Section - Velocity Distributions.

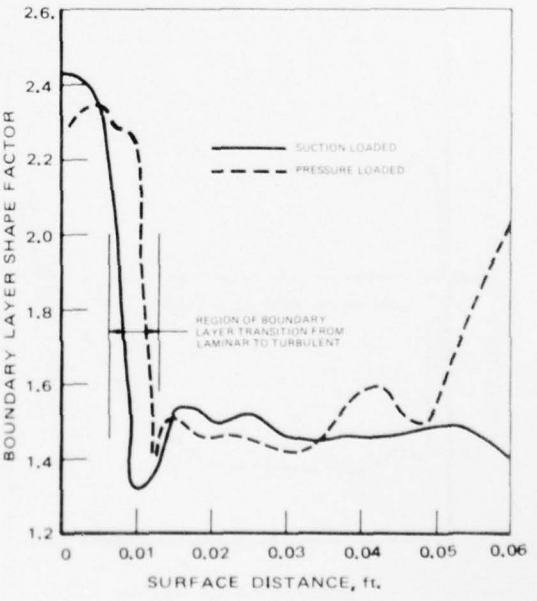


Figure 42. Rotor Hub Section Boundary Layer Shape Factor on Suction Surface.

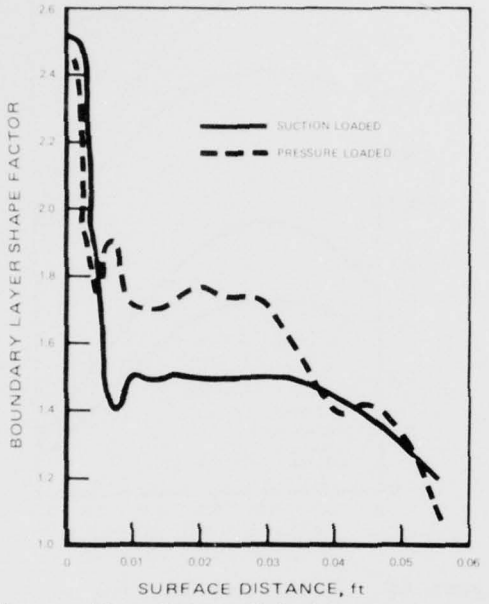


Figure 43. Rotor Hub Section Boundary Layer Shape Factor on Pressure Surface.

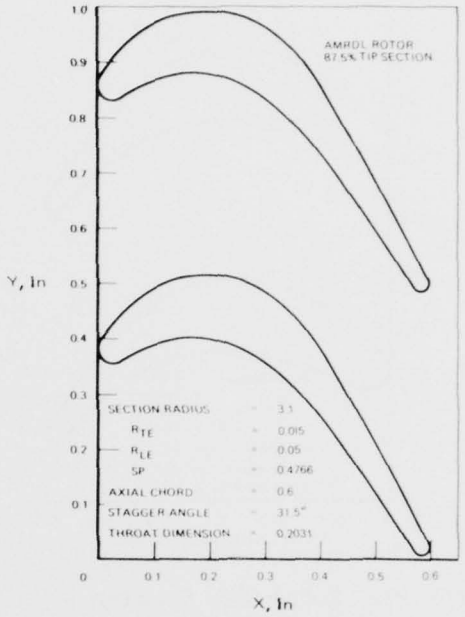


Figure 44. Rotor Tip Section

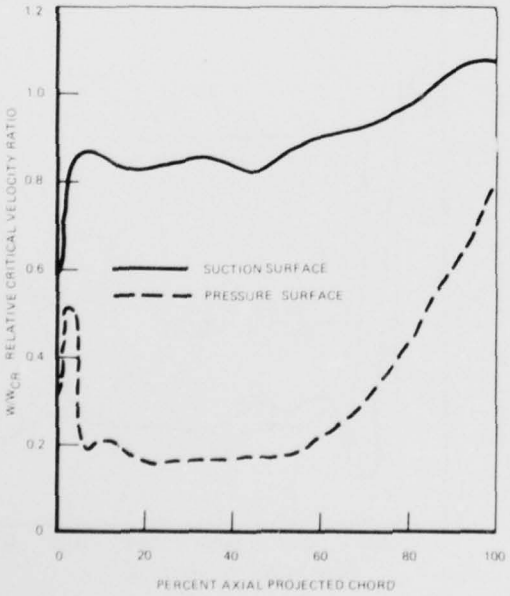


Figure 45. Rotor Tip Section - Surface Velocity Distribution.

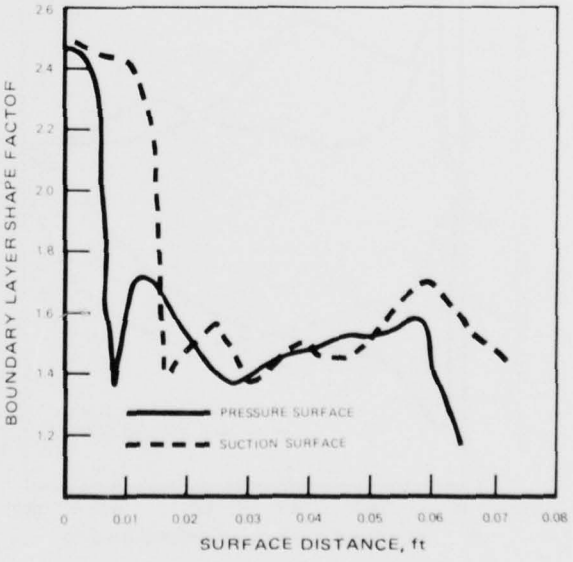


Figure 46. Rotor Tip Section Boundary Layer Shape Factor.

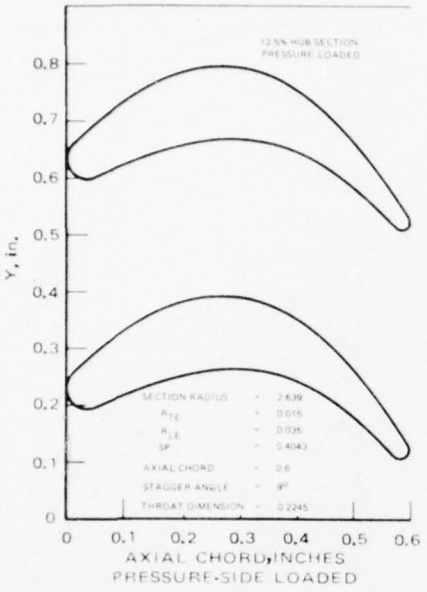


Figure 39. Rotor Hub Section - Pressure-Side-Loaded - 12.5 Percent Span.

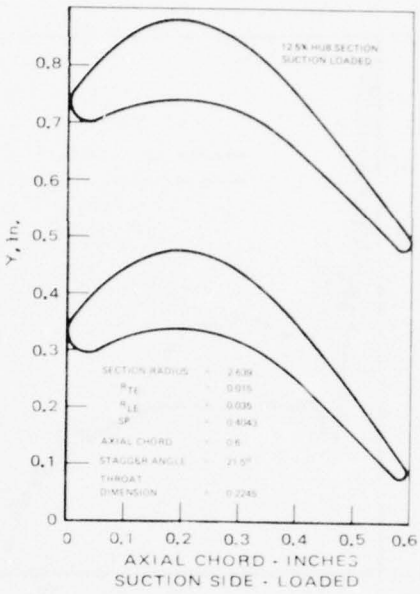


Figure 40. Rotor Hub Section - Suction-Side-Loaded - 12.5 Percent Span.

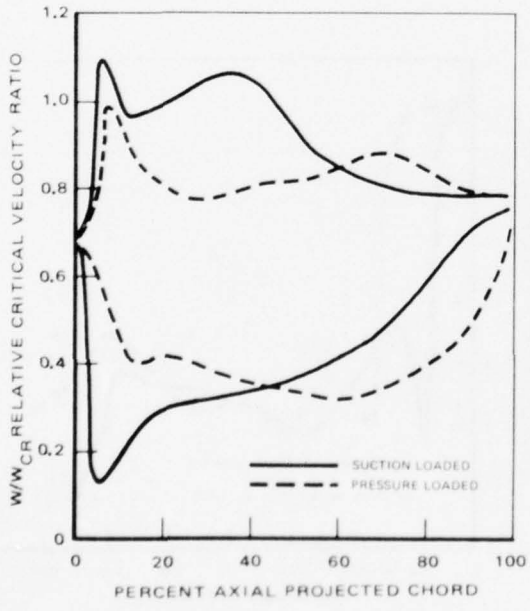


Figure 41. Rotor Hub Section - Velocity Distributions.

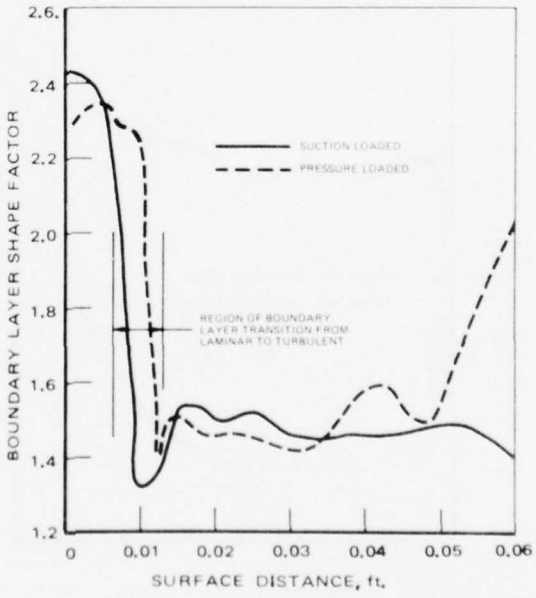


Figure 42. Rotor Hub Section Boundary Layer Shape Factor on Suction Surface.

TABLE 8

SUMMARY OF ROTOR BLADE AERODYNAMIC AND GEOMETRIC DESIGN DATA

Parameter	Pressure Loaded Hub	Suction Loaded Hub	Tip
Percent Span	12.5	12.5	87.5
Inlet Angle	37.9	47.9	45.2
Exit Angle	53.1	53.1	62.4
Incidence	+20	+10	+4
Section Radius	2.58	2.58	3.09
Axial Chord	0.60	0.60	0.60
Zweifel Coefficient	1.34	1.34	1.04
Spacing	0.404	0.404	0.477
Throat	0.224	0.224	0.203
Trailing Edge Radius	0.015	0.015	0.015
Leading Edge Radius	0.035	0.035	0.025
Aspect Ratio	1.07	1.07	1.07
Spacing/Axial Chord	0.673	0.673	0.795
Profile Loss (Meanline Avg. Loss)*	0.077	0.077	0.077
Secondary Loss (Meanline Avg. Loss)*	0.279	0.279	0.279
Clearance Loss (Meanline Avg. Loss)* (cl = 0.010)	0.0509	0.0509	0.0509
Trailing Edge Loss (Meanline Avg. Loss)*	0.0644	0.0644	0.0644
Total Loss, Y_{TOT}	0.4713	0.4713	0.4713
Reynolds Number	1.88×10^5	1.88×10^5	1.88×10^5
Rel. Critical Vel. Ratio (Inlet)	0.744	0.744	0.50
Rel. Critical Vel. Ratio (Exit)	0.796	0.796	1.05
Number of Blades	41	41	41

* Derivation of these losses is discussed under the Phase IV section, Design Technique Assessment, which is based on Appendix B data, computer output for preliminary turbine design.

The tip section boundary layer analysis also exhibited separation free flow as indicated by the shape factor on both the suction and pressure surfaces. The designed airfoils were considered to be satisfactory since they met the preliminary criteria of the selected Zwiefel loading coefficients and were confirmed by the blade-to-blade analysis.

Since the most critical rotor sections, hub and tip, were already incorporated in the blade analysis, further analysis of the resultant mean interpolation was considered unnecessary.

The two rotor blades were formed by stacking the different hub sections with the same tip sections at the center of gravity of the solid section. The sections were faired, and interpolated sections were generated at 0, 25, 50, 75 and 100 percent span relative to the stacking line. An overlay of the stacked sections is shown for the pressure-side-loaded blade in Figure 47 and for the suction-loaded blade in Figure 48.

Mechanical Design

Structural integrity of the turbine was based on satisfying 750 hours life and 15,000 cycles low cycle fatigue at the 100-percent power rating.

The mechanical design of the turbine disk and blade assembly (Figure 49) is based upon a turbine inlet temperature of 2400°F (with the disk cooled to 1200°F at the live rim and 800°F at the bore) and a speed of 60,000 rpm (100 percent power). The blades are designed with cooling passages to maintain a metal temperature of 1200°F at the airfoil root and a maximum temperature of 1730°F at 80 percent of the blade height. The heat transfer analysis and cooling technique is presented in the next section.

The analysis performed considers the centrifugal stresses in the blades, the gas bending and the centrifugal untwist stresses.

A preliminary estimate of the metal temperature profiles over the blade and disk was based upon that cooling necessary to provide minimum yield stress safety factors of 1.1 for the blade and 1.4 for the disk and 750 hours of life, considering only centrifugal stresses.

The gas generator turbine disk is assumed to be fabricated from a Rene' 95 powder metal alloy by the hot isostatic pressing process. The tensile, yield and elongation are shown in Figure 50 compared to a conventional turbine disk alloy, forged Waspalloy. Stress rupture data is shown in Figure 51 for both Rene'95 and the candidate blade material cast IN100. Data from an alternate disk material (AF2-1DA) is also shown for comparison.

The radial and tangential stress distribution in the disk is shown in Figure 52 as a function of radius. A maximum tangential stress of 176,000 psi occurred at the bore of the disk. A maximum radial stress of 62,000 psi occurred near the disk rim. Even though the peak tangential stress exceeded the material yield slightly, it is still well below the ultimate. In addition, the 750-hour rupture stress estimated from the data in Figure 51

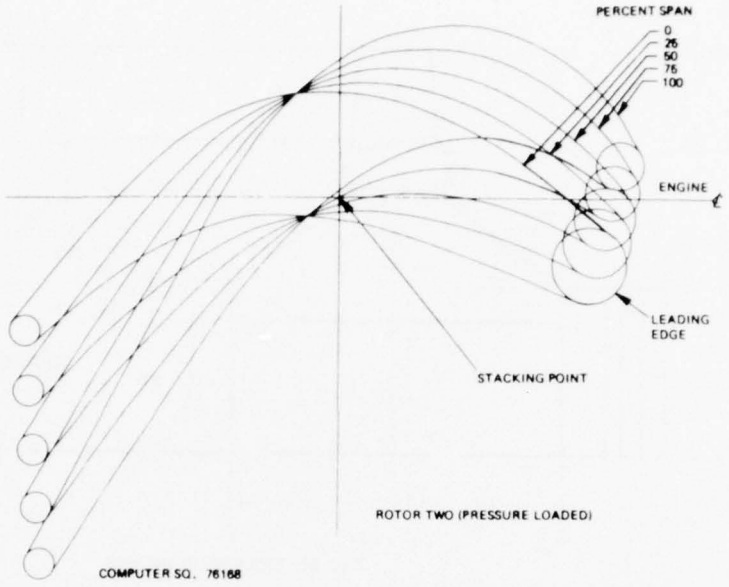


Figure 47. Rotor Sections Stacked on C.G. - Pressure-Side-Loaded.

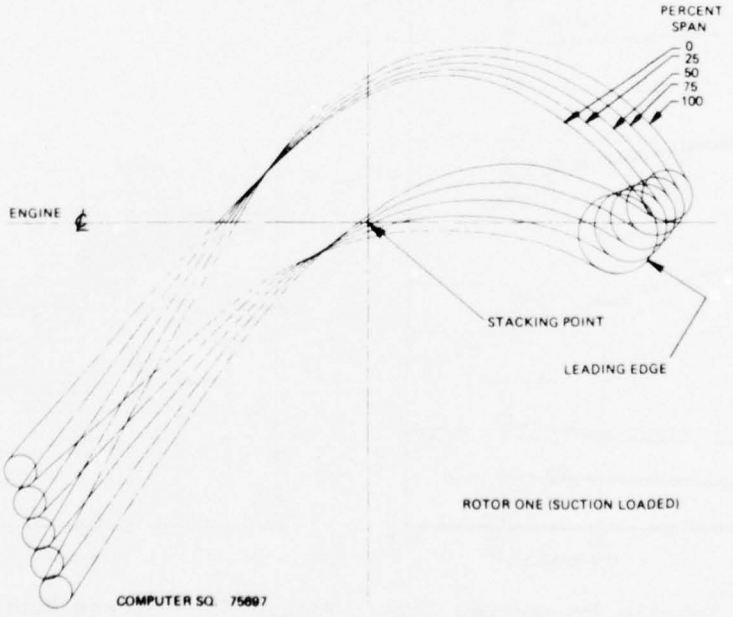


Figure 48. Rotor Sections Stacked on C.G. - Suction-Side-Loaded.

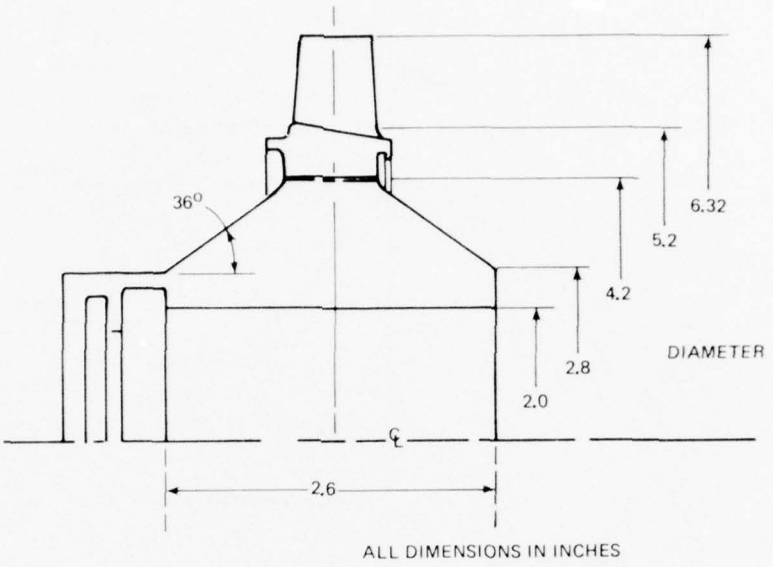


Figure 49. Gas Generator Turbine Disk Assembly.

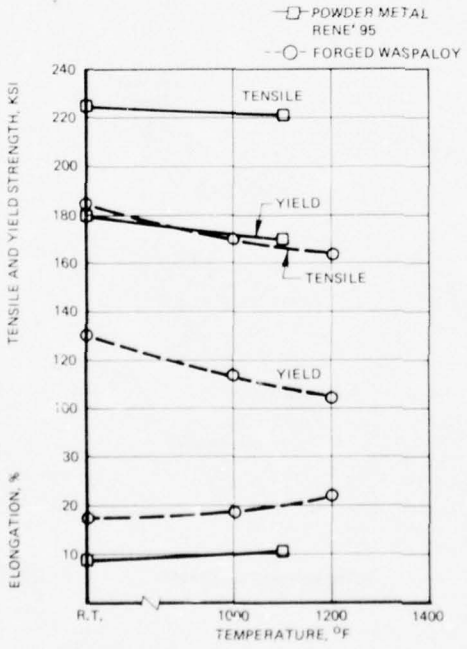


Figure 50. Tensile Properties Comparison of Powder Metal Rene' 95 and Forged Waspaloy. (Reference: Teledyne CAE, IR&D Brochure 76-07.)

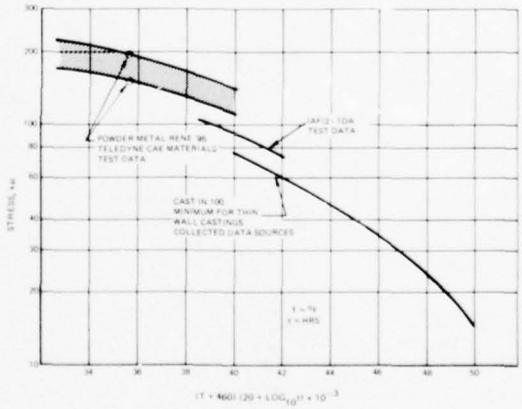


Figure 51. Stress Rupture Strength for the Candidate Turbine Rotor Materials.

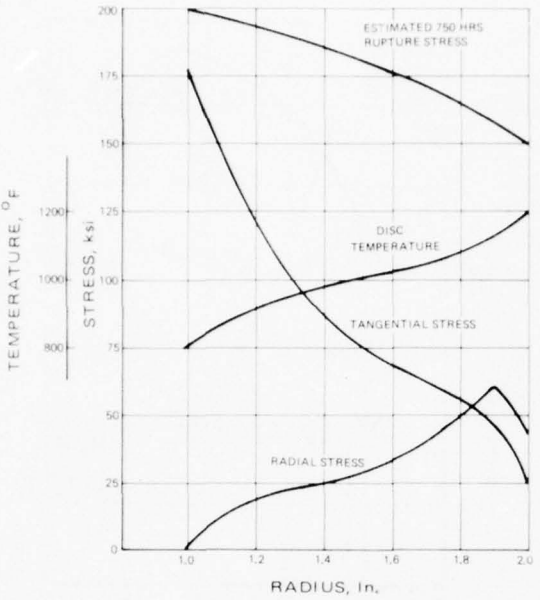


Figure 52. Turbine Disk Stress and Temperature as a Function of Radius.

shows that adequate margin exists over the entire disk radius.

The turbine blades incorporate conventional cooling and are fabricated from cast IN100 material. Figure 53 shows the average material properties for IN100 at various temperatures. Cooling air is introduced into the blades through internally cast passages in the airfoil and fir tree root attachment. During the preliminary engine cycle studies two design cases were analyzed: Case 1, 2500°F turbine inlet temperature at 61,500 rpm; and Case 2, 2200°F T.I.T. at 58,230 rpm. These cases represented the upper and lower stress limits. Figures 54 and 55 show the centrifugal P/A stresses and the maximum permissible airfoil metal temperature profile, together with the allowable stress rupture stresses for 750 hours of life for both cases.

Figure 56 shows the centrifugal P/A stresses, the maximum permissible airfoil metal temperature profile, and the stress rupture stresses for 750 hours of life for the turbine blade of the selected turbine configuration/cycle of 2A180/2400.

The analysis indicates that the turbine blade will meet the requirements with an adequate margin over most of the span and with small margin in the 70-percent span region.

The blade root attachment consists of a three-lobe fir tree directly scaled from an existing blade. A calculated scale factor of 0.87 is used to accommodate 41 blades of a 2.49-inch disk radius. A three-lobe fir tree was selected since this design provides maximum disk tenon cross-sectional area and minimizes the centrifugal stress in the tenon lower neck. Three passages in the blade fir tree allow cooling air to be introduced into the blades (Figure 57). The fir tree portion of the blade case, from IN100 material, is designed for an assumed metal temperature of 1200°F at 60,000 rpm using Heywood's method of fir tree analysis. Based on the allowable stress rupture properties of IN100, a life of 750 hours is obtainable. The maximum nominal combined stress in the fir tree is equal to 80,500 psi and occurs in the upper neck (A-A of Figure 57 of the fir tree (Table 9)). The maximum nominal combined stress that the disk tenon (D-D of Figure 57) is equal to, is 108,900 psi. The points of maximum steady-state stress are

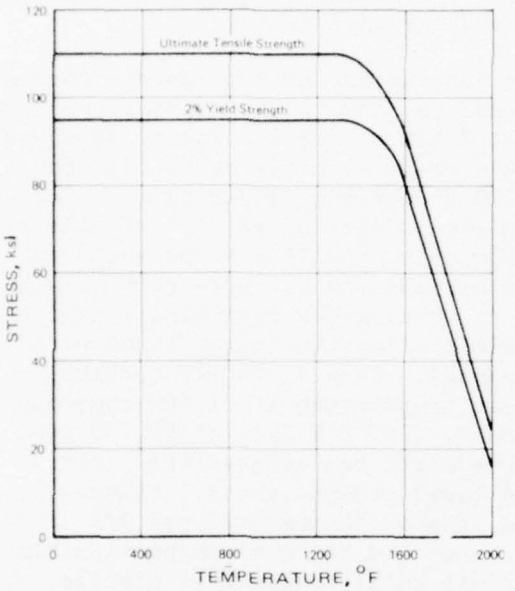


Figure 53. Strength Properties of IN100.

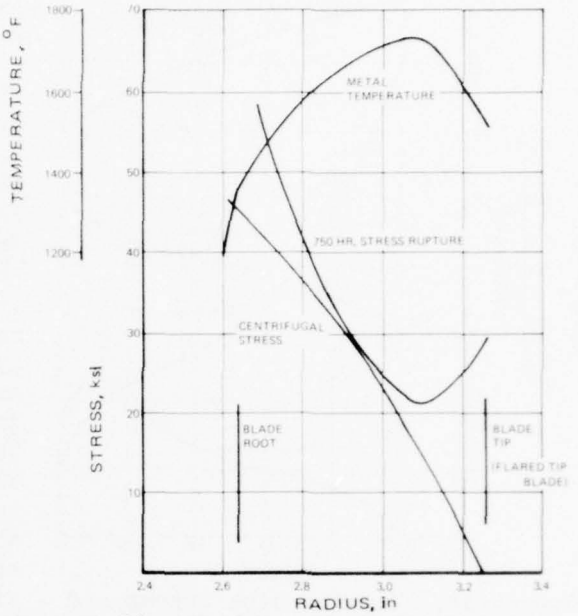


Figure 54. Turbine Blade Stresses for Case 1 (Upper Limit for Cycle Study Engine).

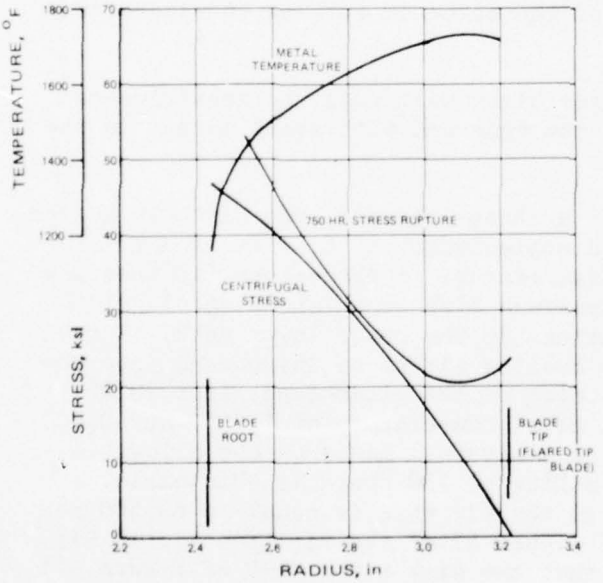


Figure 55. Turbine Blade Stresses For Case 2 (Lower Stress Limit for Cycle Study Engine).

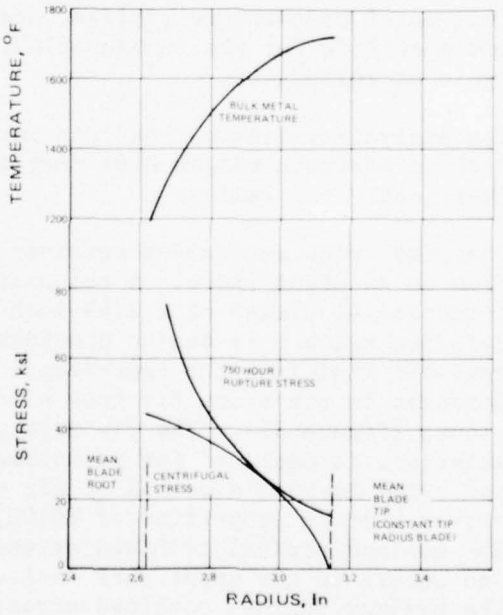


Figure 56. Turbine Blade Stress Distribution for Selected Blade.

TABLE 9

FIRTREE AND DISK STRESSES

Location	Assumed Temperature - °F	Nominal Neck Stress - psi	Nominal Fillet Stress - psi	Nominal Combined Stress - psi	Ultimate Stress - psi	Yield Stress - psi	Safety Factor
A-A	1200	43,600	44,800	80,500	110,000	95,000	1.18
B-B	1200	32,600	43,600	66,800	110,000	95,000	1.42
C-C	1200	23,900	46,100	56,800	110,000	95,000	1.67
DISK - TENON STRESSES							
D-D	1200	66,300	49,100	108,900	220,000	161,000	1.48

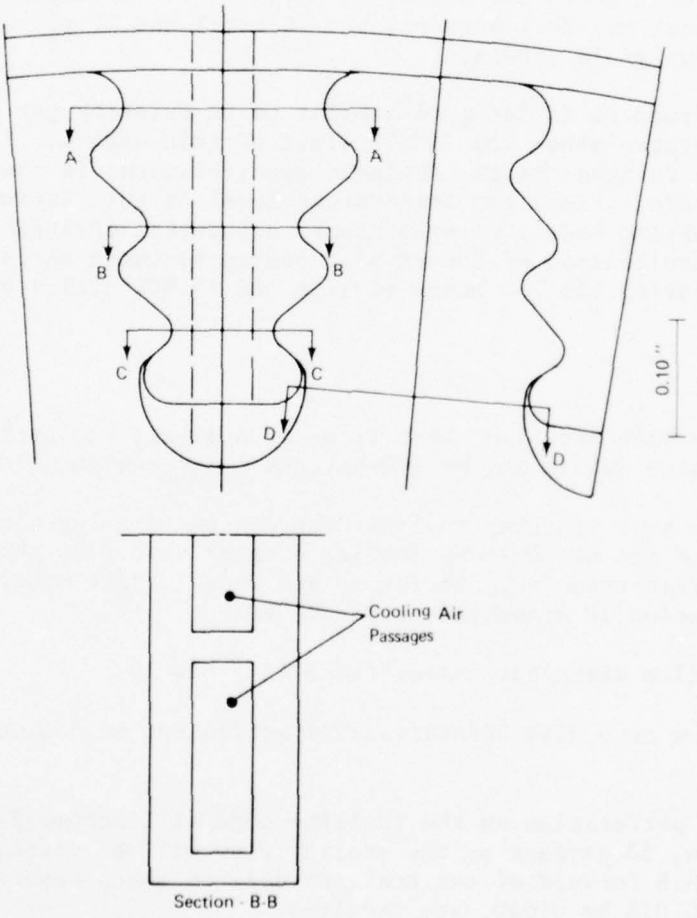


Figure 57. Turbine Blade Root Attachment, Fir Tree Detail.

presented on a modified Goodman diagram (Figure 58) and are defined by the equation:

$$\left(\frac{\sigma_A}{\sigma_{EAL}}\right)^{1.35} + \left(\frac{\sigma_M}{\sigma_{RAL}}\right)^{1.35} = 1$$

Where: σ_A = applied vibratory stress
σ_{EAL} = endurance limit
σ_M = applied mean stress
σ_{RAL} = rupture stress

The analysis shows that the fir-tree attachment and disk tenon fall well within the 1.4 factor-of-safety envelope and meet the life requirements.

The calculated fir tree and disk tension stresses are based on the centrifugal pull of a solid airfoil. The stresses and safety factor for the fir tree and disk tenon are presented in Table 9. Section A-A of the fir tree is the most critical section, but it still has 18 percent margin over the 0.2 percent yield stress.

The nozzle structure is designed similar to an existing gas generator turbine that operates above the 2400°F limit of this engine. Thermal stress and low-cycle fatigue are the dominate considerations in the design of the nozzle structure. Since the temperature level of this engine is less than the similar engine model, no preliminary structural analysis was deemed necessary. Application of the similar design features satisfied the concerns of achieving the 750 hours of life and 15,000 cycles of low-cycle fatigue.

Heat Transfer

A preliminary vane and blade heat transfer analysis was performed for the selected turbine design at the 100-percent power design point.

A preliminary heat transfer analysis was conducted using the preliminary vane shape and the preliminary loading diagram to define the distribution of external heat transfer coefficient and vane surface metal temperature. This distribution is presented in Figure 60.

The cooling flow distribution is listed in Table 10.

The total flow of 0.0144 lb/sec/vane is equivalent to 6.0 percent engine flow.

A 50-percent perforation on the trailing edge will accommodate 0.007 lb/sec/blade. Hence, 50 percent of the cooling flow will be discharge approximately 0.3 inch forward of the trailing edge on the pressure-side of the vane. Four slots, 0.075 by 0.020, are required.

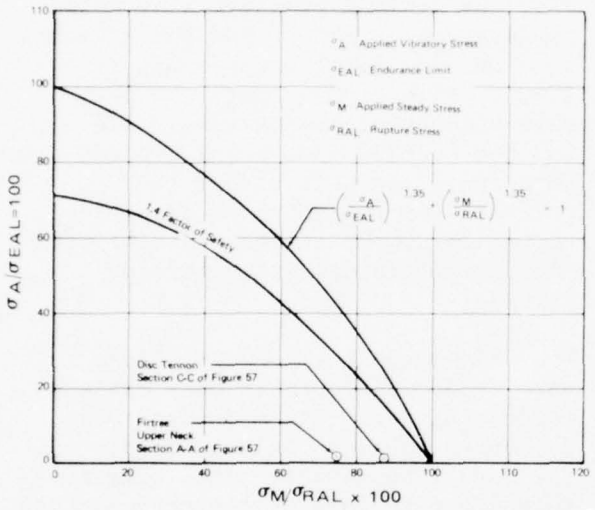


Figure 58. Modified Goodman Diagram for the Fir Tree.

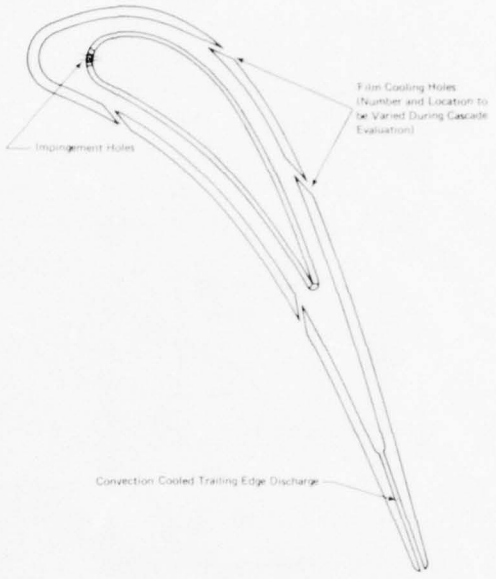


Figure 59. Nozzle Cooling Flow Injection Locations.

TABLE 10

VANE COOLING FLOW DISTRIBUTION

Nozzle Local Gas Temp. °R	Location	Orifice Pattern	Flow Lb/Sec/Blade
2768	Suction Side	4 Slots @ 0.010 x 0.107	0.0070
2768	Pressure Side-Forward	1 Slot @ 0.010 x 0.116	0.0010
2768	Pressure Side-Aft	12 Holes @ 0.010 Dia.	0.0016
2400	Suction Side	2 Slots @ 0.010 x 0.080	0.0020
2400	Pressure Side-Forward	9 Holes @ 0.010 Dia.	0.0012
2400	Pressure Side-Aft	6 Holes @ 0.010 Dia.	0.0008
2768	Leading Edge	4 Holes @ 0.010 Dia.	0.0004

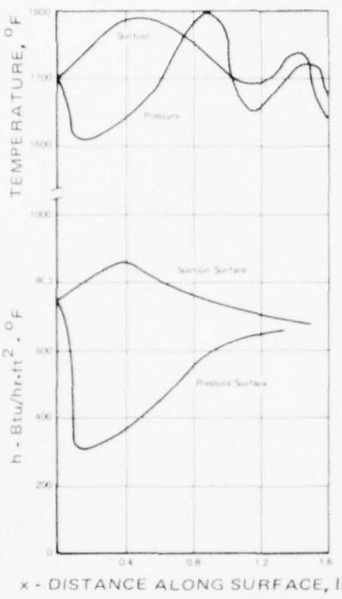


Figure 60. Vane Heat Transfer Coefficient and Surface Temperature Distribution.

The preliminary heat balance shows that the maximum pressure side metal temperature is 1800°F and the maximum suction side metal temperature is 1780°F (Figure 60). Both the pressure side metal temperature range and the suction side metal temperature range are well within the criteria for the 750-hour life required by comparison to the similar higher temperature gas generator turbine.

Four blade cooling configurations were selected as preliminary designs for evaluation. These designs are presented schematically in Figure 61. The resulting surface metal temperature distributions at the mean section are listed on the figure for the selected configuration.

The preliminary design consists of a series of one-dimensional heat balance calculations to determine the distribution of local heat transfer coefficient at the mean section. The section average temperature is 1640°F.

Configuration 1 presents a two-pass convection cooling scheme with bleed through chordwise holes in both the leading edge and the trailing edge. This configuration allows simple cooling of narrow leading edges typical of highly curved blades and results in high cooling airflow. This design was eliminated from further consideration when cursory heat balance indicated excessive (0.6 percent) cooling flow requirements.

Configuration 2 presents a three-pass convection cooling scheme with bleed through chordwise holes in the trailing edge and discharge through the tip at the trailing edge. A preliminary analysis indicated a 4.5-percent coolant flow requirement, and a feasible design. This system was chosen as the second candidate for preliminary analysis.

Configuration 3 presents a two-pass convection cooling system, with discharge through chordwise holes in the trailing edge, in parallel with a straight-through convection cooling system in the leading edge with discharge at the tip. The preliminary analysis shows a coolant flow requirement of 3.6 percent and a feasible design.

Configuration 4 presents the favored two-pass convection cooling system with impingement cooling at the leading edge, and discharge through chordwise holes in the trailing edge. The preliminary analysis shows a low coolant flow requirement of 1.9 percent and a feasible design. This design

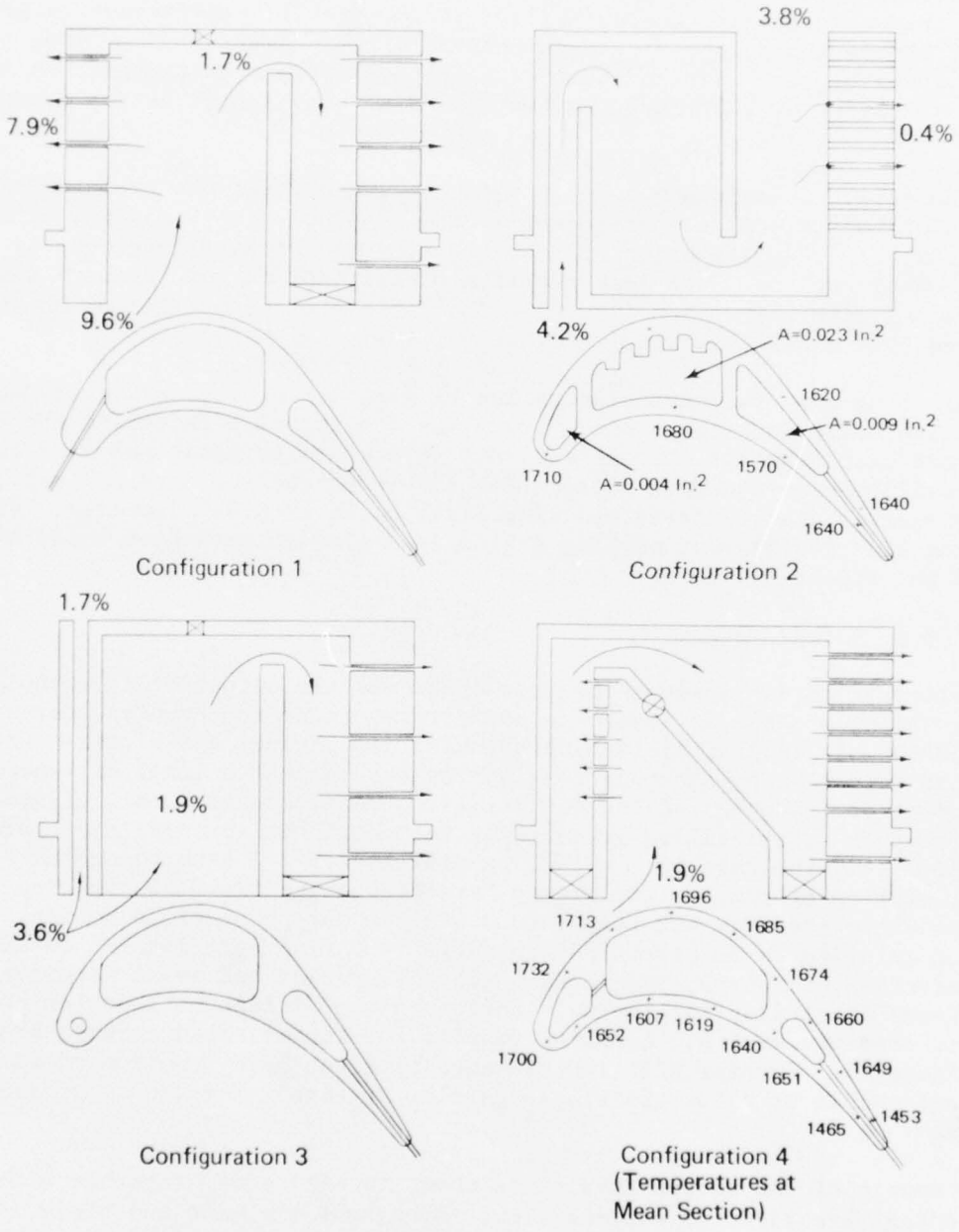


Figure 61. Turbine Rotor Blade Cooling Configurations Selected for Evaluation.

was selected for detailed analysis.

The distribution of heat transfer coefficient (Figure 62) shows the anticipated characteristics. The peak (1200 Btu/hr-ft^2-°F) coefficient occurs at the stagnation point which decreases as a cubic distribution along the blade surface. The level of heat transfer coefficient on the suction side is on the order of 1.5 times the heat transfer coefficient on the pressure side.

For the selected impingement-convection cooling system, the cubic distribution of heat transfer coefficient at the leading edge is matched with the bell-shaped distribution of heat transfer coefficient developed by impingement cooling. The heat transfer coefficient on the pressure side is matched with convection flow, and the 1.5 higher heat transfer on the suction side should not require internal fins.

The trailing edge is convection cooled by ejection of the coolant through chordwise holes into the blade wakes. The coolant flow rates and the local internal heat transfer coefficients are determined by sonic velocity through the trailing-edge ejection holes. The flow area and the internal surface area requirements are satisfied with eight holes at 0.010 diameter. The leading-edge impingement cooling system is satisfied with five holes of 0.020 in. diameter.

Cooling Flow Analysis

A cooling injection analysis program that uses the output of an uncooled design point program as input was used to determine incremental loss variations for air cooling of turbine shrouds, disk, vanes and blades. Calculations were made by assuming that mixing occurs over a small distance at the point of injection of the cooling air. Vertical components of velocity with respect to streamline are assumed to contribute no axial or angular momentum. In the case of a rotor, pumping losses are also accounted for by an assumption of pumping efficiency for the cooling flow and a subroutine to calculate pressure and temperature rise to the point of injection. The mixing solution is an iterative procedure involving equations of continuity, conservation of energy, and conservation of angular and axial momentum. Treatment is similar to Shapiro's influence coefficient methods for constant static pressure mixing. Computer results for the selected turbine are shown in Figure 63. Turbine efficiency change is given as a function of independent nozzle or rotor trailing-edge flow at either suction or pressure surface.

A schematic of the cooled turbine is shown in Figure 64, together with the percentage breakdown of cooling flows throughout the vane and blade. The division of vane cooling flows consists of: (1) film cooling through gill and trailing edge holes as shown in Figure 59, 4.0 percent; (2) tip shroud flow, 0.5 percent; and (3) hub shroud flow, 0.5 percent, for a total of 6.0 percent of engine flow. The division of blade cooling flows consists of: (1) inner disk flow, 1.3 percent; (2) outer disk flow, 0.7 percent; and

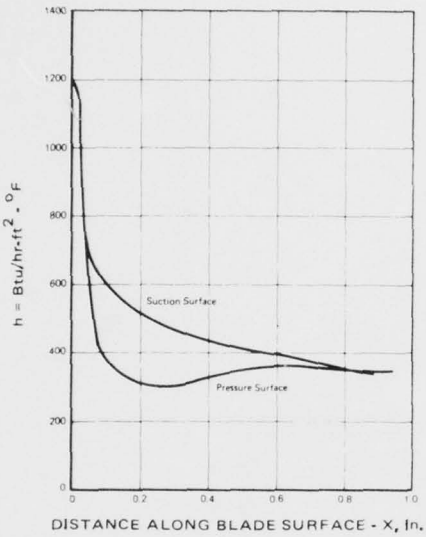


Figure 62. Rotor Blade Surface Heat Transfer Coefficient.

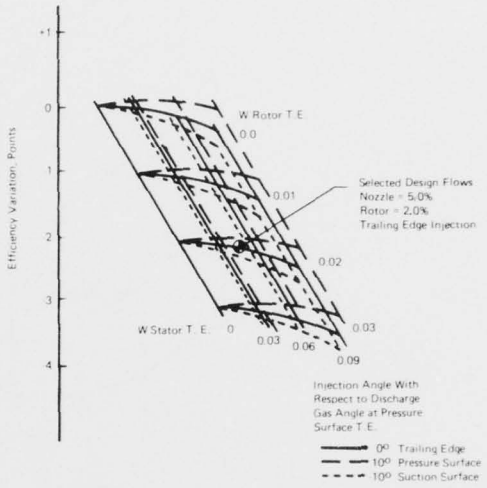
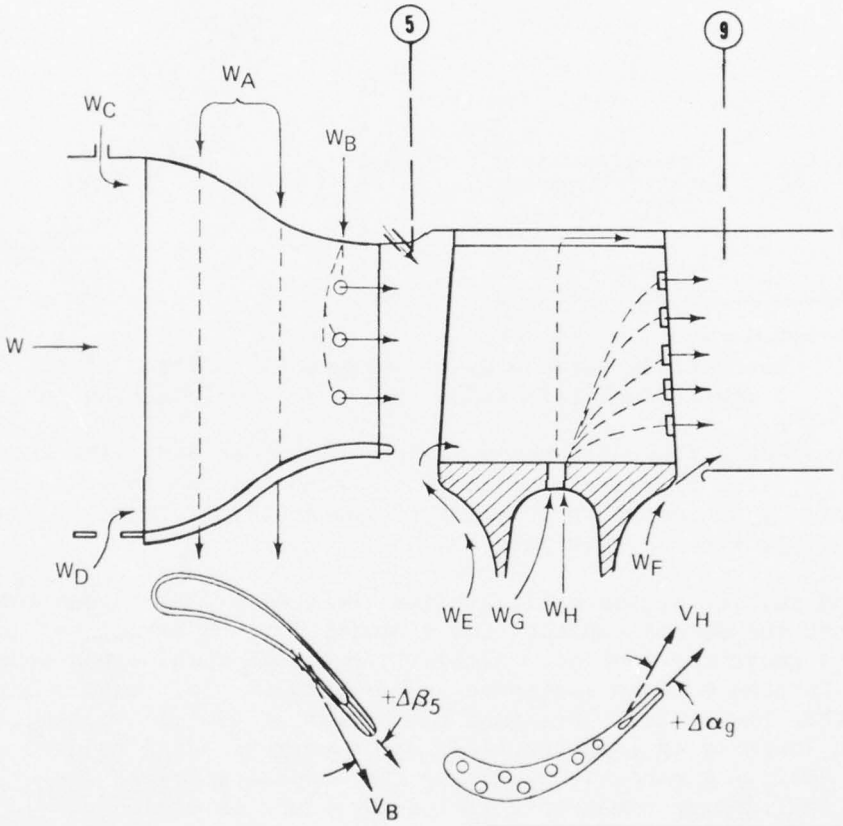


Figure 63. Effect of Cooling Flow Injection on Efficiency.

(3) trailing-edge flow, 2.0 percent, for a total of 4.0. The total vane and blade cooling flow amounted to 10.0 percent of the inlet engine airflow. The efficiency decrement as a result of the cooling (Figure 63) was predicted as approximately 2.0 percent.

During the initial engine cycle studies the engine thermodynamic models did not reflect the detail coolant flow distribution and associated losses of a cooled gas generator turbine. Rather, the cooled turbine was modeled as an uncooled turbine with an estimated bypass flow to yield equivalent performance within the cycle. The final gas generator cooled turbine design required an increase in pressure ratio and a corresponding reduction in efficiency goals. A comparison between the candidate engine cycle (2A 180/2400) and the final design parameters including effect on engine output is as follows:

	2A180/2400	Final Design Point
Engine Airflow, lb/sec.	4.8	4.8
Actual Work, Btu/lb	180.	180.
Pressure Ratio, Total-to-Total	3.48	3.75
Efficiency, uncooled	84.5	80.2
Bypass, %	4.0	0
Coolant Flow, %	0	10%(Fig. 64)
Inlet Pressure, psia	188.6	188.6
Rotor Inlet Temp., ^{o}F	2400.	2400.
Engine SFC, lb/Hp-Hr	0.463	0.479
Power Turbine Output, Hp.	982.1	949.8



		170/2200	200/2500	180/2400
W_A	Combustor Primary & Nozzle Cooling Flow	0	0	0
W_B	Nozzle Film Cooling Flow	3	6	5.0
W_C	Nozzle Tip Shroud Cooling Flow	0	0.5	0.5
W_D	Nozzle Hub Shroud Cooling Flow	0	0.5	0.5
W_E	Inner Disc Cooling Flow	1	1.3	1.3
W_F	Outer Disc Cooling Flow	0.5	0.7	0.7
W_G	Rotor Blade Flow	0	0	0
W_H	Rotor Blade Trailing Edge Flow	1.5	3	2.0
	Total Cooling Flow (percent of Wa)	6	12	10.0

Figure 64. Turbine Cooling Airflow Distribution.

SUMMARY OF PRELIMINARY ENGINE ANALYSIS

The preliminary engine and turbine design analysis resulted in a gas generator turbine flow path shown in Figure 65. The flow path and blading analysis performed in Phase I was deemed acceptable to meet the ASATT Program objectives and carried on the Phase II to investigate the aerodynamic performance in an annular cascade.

The candidate turboshaft engine cross-section revised to reflect the results of the preliminary turbine design analysis is shwon in Figure 66.

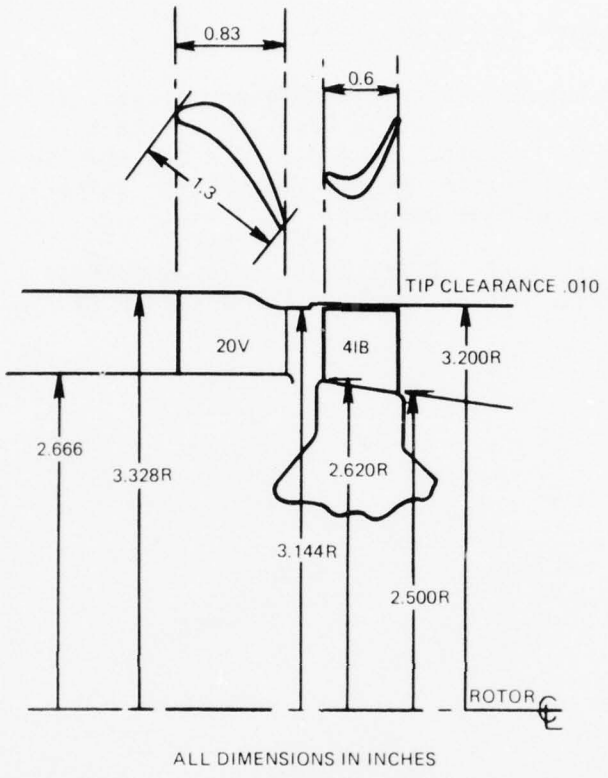


Figure 65. Preliminary ASATT Turbine Flow Path.

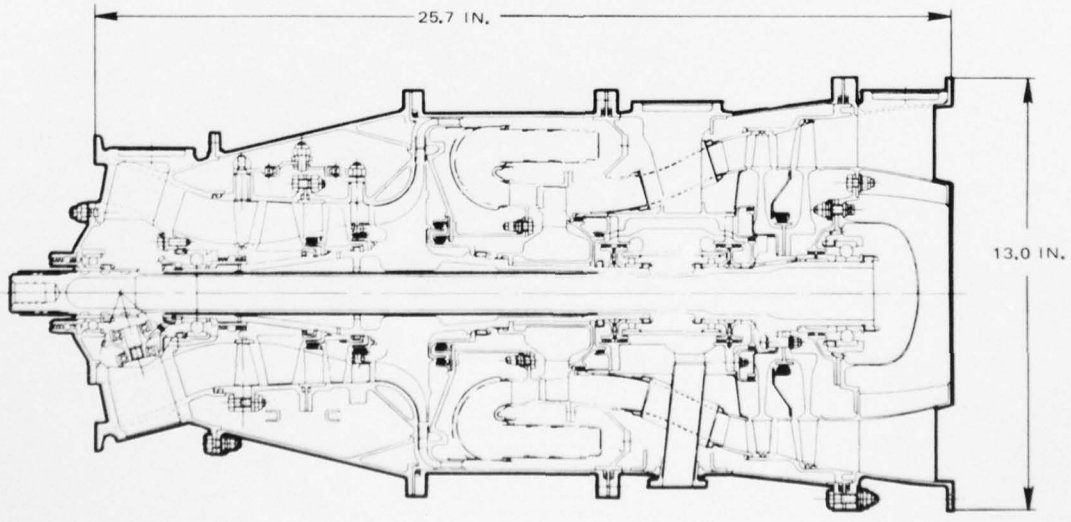


Figure 66. Selected ASATT Turboshaft Engine Configuration.

PHASE II - TURBINE CASCADE INVESTIGATION

The Phase II effort was directed toward determining the aerodynamic performance of the turbine designed in Phase I, using a cold flow, stationary, annular cascade. The Phase II effort was divided into the following tasks:

1. Cascade rig and instrumentation control layout
2. Rig detail design
3. Manufacture test rig hardware
4. Test plan
5. Rig assembly, Instrumentation and checkout
6. Cascade rig testing
7. Data correlation

OBJECTIVE

The objective of Phase II, Turbine Cascade Investigation, was to investigate the aerodynamic performance of the turbine design in a stationary, annular sector, cascade with various geometric and aerodynamic perturbations. The perturbations included nozzle endwall contour, inlet turbulence and velocity distortion, stator and rotor solidity, rotor loading and nozzle cooling flow and point of injection.

CASCADE RIG AND INSTRUMENTATION DESIGN

An annular sector cascade rig was designed for cold flow operation to test and evaluate the performance of the Phase I turbine vane and blade shapes. A sequential test program was devised to evaluate the various effects of:

A. Meridional constrictions on vanes.
B. High vane exit Mach number.
C. Vane inlet turbulence.
D. Vane inlet boundary layer and distortion.
E. Vane exit flow distortion and leakage on rotor performance.
F. Rotor blade loading.
G. Vane cooling and solidity.
H. Vane cooling on two rotor solidities and axial spacing.

The rig was instrumented to provide: (1) airflow, (2) inlet total pressure and temperature distribution, (3) wall static pressures throughout the flow channel, (4) circumferential and radial traverse of pressure, (5) temperature and angle at two axial planes (vane exit and turning vane exit), (6) hot film radial traverse at the vane inlet, and (7) torque produced by the tangential momentum change in the turning vane sector (Momentum Transfer System).

The ASATT Cascade Rig was designed to test the Phase I turbine vane and blade shapes in an annular cascade section and to determine the performance under various operating conditions. The rig is configured to permit systematic variations of inlet flow conditions, cooling flow injection,

solidity, and inner and outer wall shape.

The cascade rig consisted of four main assemblies: the inlet plenum, the nozzle plate, the momentum transfer slave, and the exhaust plenum. A cross-section of the rig is shown in Figure 67. Several mechanical changes made to the rig during the initial testing to achieve satisfactory momentum transfer data included:

1. Replacing the air bearing with ball bearings and removing the cable system.

2. Adding a honeycomb straightener section to the axial portion of the slave.

3. Replacing the flexible diaphragm seal with a pressurized labyrinth seal.

4. Adding splitter vanes to the slave.

5. Adding hard line exhaust plumbing to permit vacuum exhaust operation.

The principal objectives in developing the rig's mechanical design concept were to:

Minimize the possibility of air leakage into the cavity on the inlet side of the momentum transfer rotor

Achieve a high degree of accuracy in the torque measurement system

The possibility of air leakage through the circumferential transferring mechanism housing slot was of considerable concern. In the conventional construction, a sliding seal is used to effect the closure, but since the seal drag resists the traversing action, the seal compression is necessarily low. In contrast, the design shown in Figure 68 has the seal compressive load applied after the traverse has been completed. In this manner, the seal compression can be set as high as necessary without affecting the traversing mechanism.

The proper operation of the momentum transfer system depends on all of the airflow entering and leaving through the vane sector. This requires positive sealing at the sector rotor periphery.

Initially, air circulation from the exhaust plenum back to the inlet side of the momentum transfer rotor was prevented by sealing the rotor periphery with a flexible diaphragm. The diaphragm material was a polyester reinforced nitryl rubber. The anistropic reinforcement supports the hoop tension developed by the pressure differential across the diaphragm without affecting the diaphragm's circumferential flexibility. However, during initial testing it was found that the nitryl rubber diaphragm induced

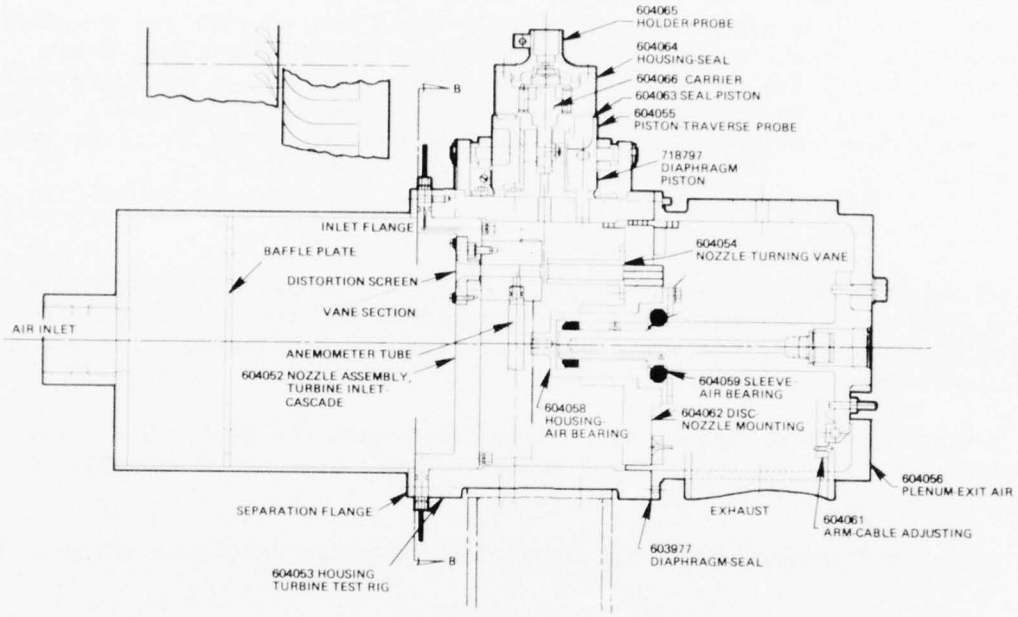


Figure 67. Cascade Rig Cross Section.

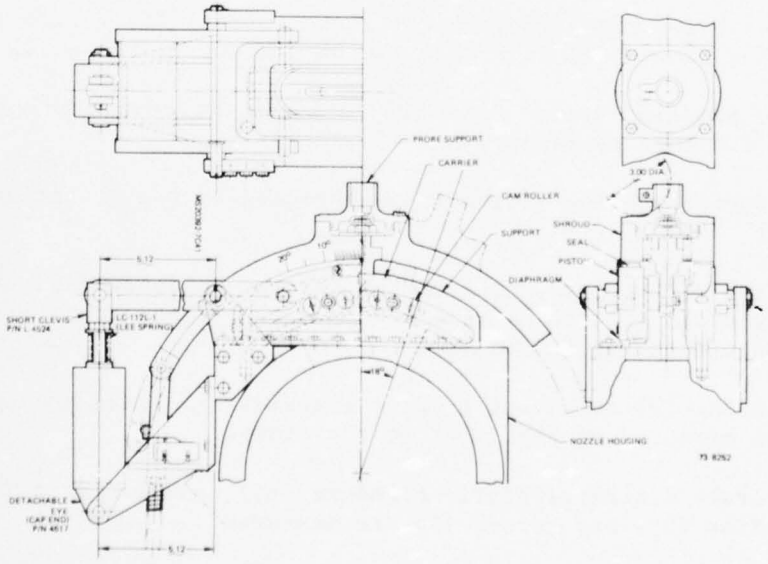


Figure 68. Traversing Mechanism Layout.

torques into the system which were not consistent and calibration attempts were not repeatable. The diaphragm was replaced with the pressurized labyrinth seal as shown in Figure 67. In operation, an external pressure was supplied to the rearward seal space so that the forward seal space pressure equalled the nozzle exit plenum cavity pressure. The balance was controlled manually using a differential transducer for the sensor. This modification was found to work very well and repeatable calibrations were achieved.

MOMENTUM TRANSFER SYSTEM

The momentum-transfer system, which is based on the principles of continuity, energy, and momentum, is utilized to accurately measure cascade performance and to eliminate inconsistent performance results attributed to conventional instrumentation techniques.

The momentum-transfer system accurately determines the stator and rotor tangential velocities from torque measurements. A detailed analysis of this concept can be found in Reference 44.

The momentum-transfer system is composed of five main elements (Figure 69):

(a) A design stator or nozzle cascade (DN), which has the same physical geometry as the turbine stator.

(b) An actuator nozzle (AN), which simulates the relative velocity vector to the turbine rotor.

(c) A gimbaled momentum-transfer slave rotor (MTS), which turns the inlet tangential flow from the DN cascade to the axial direction.

(d) The gimbaled design rotor (DR) cascade, which has the same geometry as the turbine rotor.

(e) A torque sensing device (τ) connected to the stationary MTS or DR.

Losses or the efficiency of the stator cascade is determined very accurately, reliably, and simply with no reliance on survey probe data. The principle of loss measurement is as follows:

(a) Airflow (W) and inlet total temperature (T_o) and pressure (P_o) are measured at the inlet to the stator.

(b) Average discharge static pressure (p_5), annulus area (A_{x5}), mean radius (R_5) and torque (T) are measured.

(c) Continuity equation $W = A_{x5}\, V_5 \cos \beta_5 \, \frac{P_5}{Rt_5}$

and $t_5 = T_5 - \frac{V_5^2}{2gJC_p}$

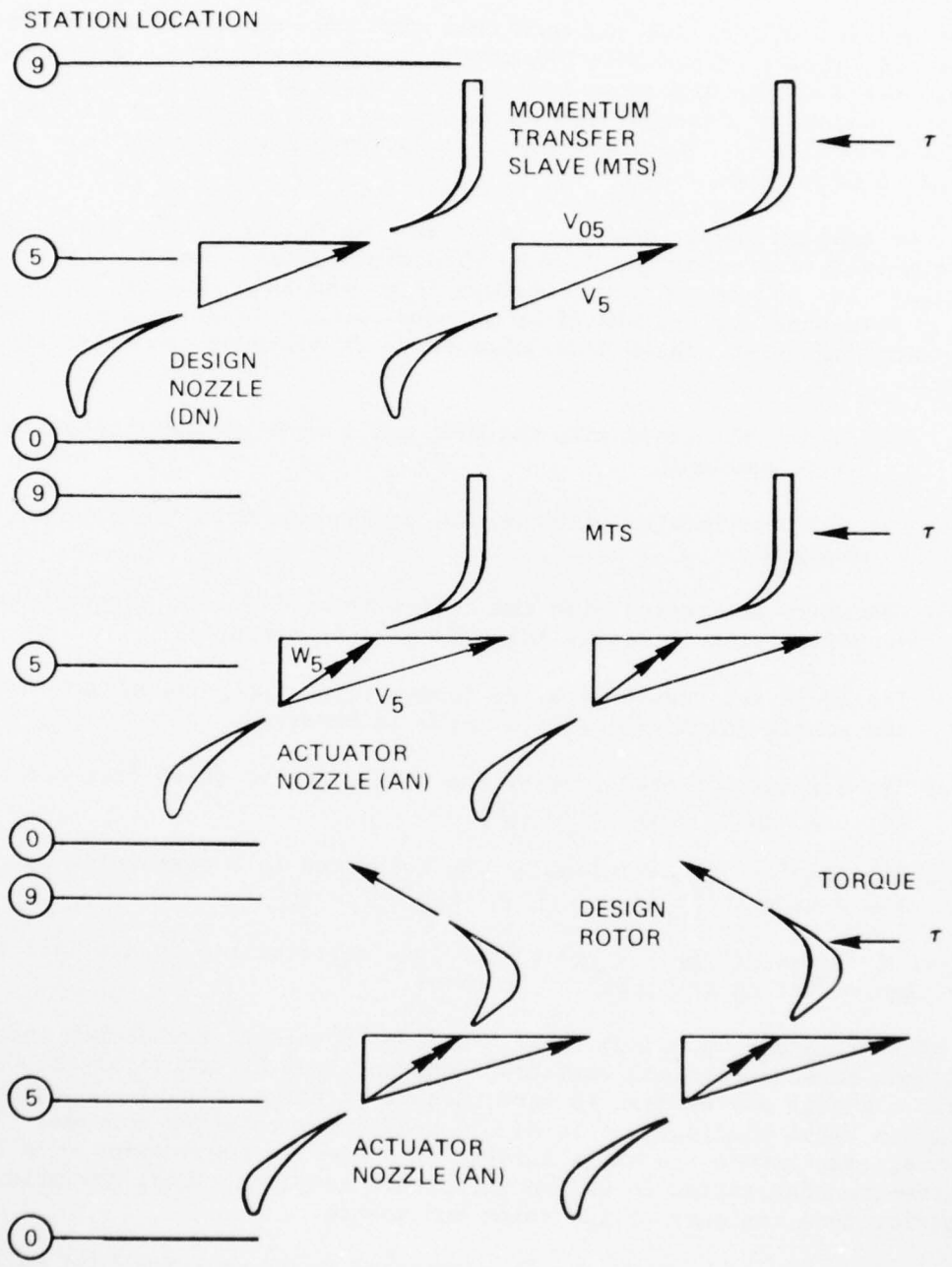


Figure 69. Momentum Transfer Principle.

(d) Momentum equation, $\tau = \frac{w}{g} \quad V_5 \ \text{Sin} \ \beta_5$

Expressions (c) and (d) are two equations with two unknowns resulting in a solution of average stator exit velocity and discharge angle. Knowing pressure ratio across the cascade, the ideal velocity and efficiency is readily calculated. Average deviation angle and changes are extremely accurate because of reliable and simple measurements without surveys and integration procedures.

Effects of cooling flows, boundary layer and distortion on the stator were similarly evaluated using the Momentum-Transfer System. Use of the system to evaluate the nozzle cooling, boundary layer and inlet distortion on the rotor is determined by the use of an actuator nozzle (AN). The procedure for determining inlet nozzle distortion on performance of the rotor is as follows:

(a) The AN is calibrated with the MTS, and torque without distortion (τ_{AN}) is measured.

(b) The AN is calibrated with the MTS, and torque with distortion (τ_{AN^D}) is measured.

(c) The AN is calibrated with the design rotor (DR), and torque without distortion at nozzle inlet (τ_{DR°) is measured.

(d) The AN is calibrated with the design rotor (DR), and torque with the nozzle inlet distorted (τ_{DR^D}) is measured.

(e) The angular momentum lost by the nozzle due to inlet distortion is $\Delta \tau_{AN} = \tau_{AN^\circ} - \tau_{AN^D}$.

(f) The angular momentum lost by the rotor due to a distortion on the nozzle inlet is $\Delta \tau_{DR} = \tau_{DR^\circ} - \tau_{DR^D}$.

The loss in torque ($\tau_{DR} - \tau_{AN}$) is the loss attributable to a nozzle inlet distortion effect on the loss of the rotor.

In a similar manner, boundary layer, cooling injection, turbulence intensity, meridional constriction and variations thereof, can be accurately be determined. Although survey data is very inaccurate for a total loss determination (in small blading), it is highly useful for relative changes. Total pressure, temperature and angle surveys were used in combination with the momentum-transfer system to define efficiency contours, local deviations and performance contours of the rotor and nozzle.

The momentum transfer rotor torque was reacted by a precision load cell as shown in Figure 70. This particular orientation of the load cell was selected in order to nominally cancel all the in-plane loads acting on the rotor, thereby relieving the bearing system of all but unavoidable spurious radial loads. A photo of the slave bearing on the rotor with the nozzle plate removed is shown in Figure 71.

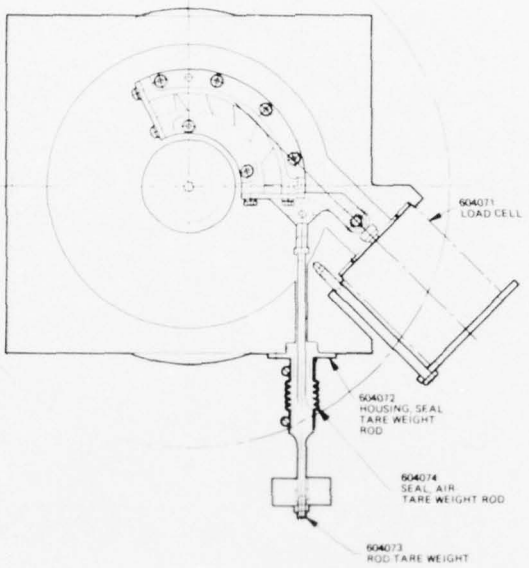


Figure 70. Momentum Transfer Torque Measurement System.

In order to minimize the "downtime" between different nozzle tests, the nozzle, instrumentation and cooling flow plumbing were provided as a complete replaceable assembly. All the instrumentation and cooling flow connections were made on the periphery of the nozzle plate. All the connections between the nozzle and the nozzle plate were accomplished as a bench assembly. All of the instrumentation tubing connected to the plate was bench assembled to the nozzle cascade parts using an epoxy resin bond. A view of the nozzle plate showing all instrumentation lines connected is shown in Figure 72.

NOZZLE MERIDIONAL CONSTRICTION

Several wall configurations were designed for evaluation during the test sequence in order to determine optimum meridional constriction on the nozzle annulus. Figure 73 shows the various wall configurations tested and Figure 74 shows photographs of the configuration with the actual hardware test pieces.

The Phase I section described the analysis used to determine the meridional constriction for the ASATT turbine. The effect of exit Mach number as reported by Deich, et al (Reference 41), shows that the profiling technique is effective in the supersonic as well as the subsonic flow regime. Of the contours reported (Reference 41), contours 5 and 7 appear to be geometrically most similar to the configurations tested in the ASATT

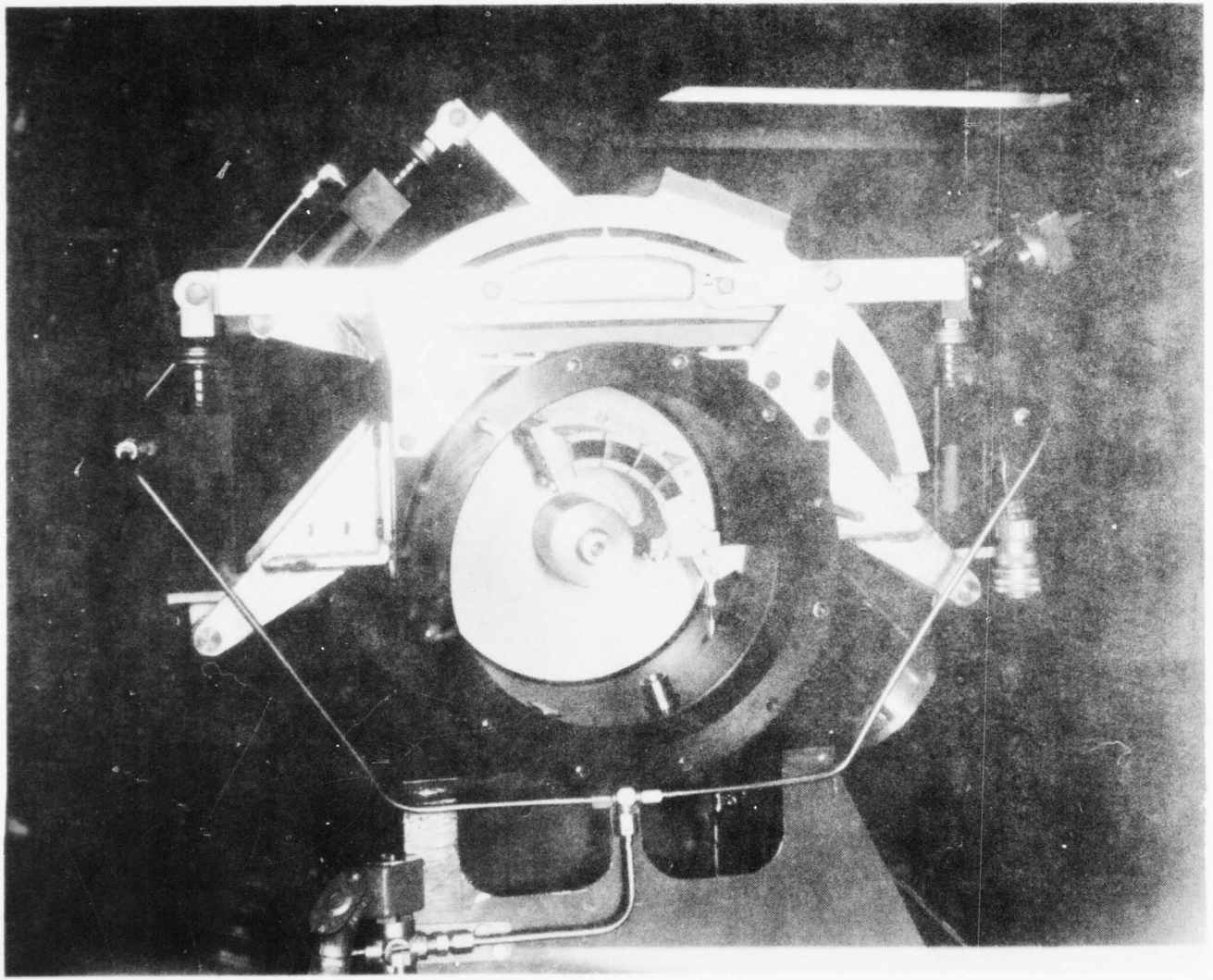


Figure 71. Momentum Transfer Slave Installed.

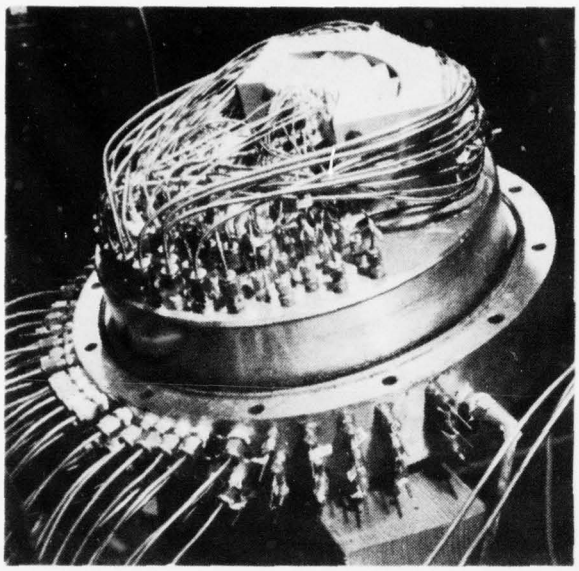


Figure 72. Cascade Mounting Plate - Rear View.

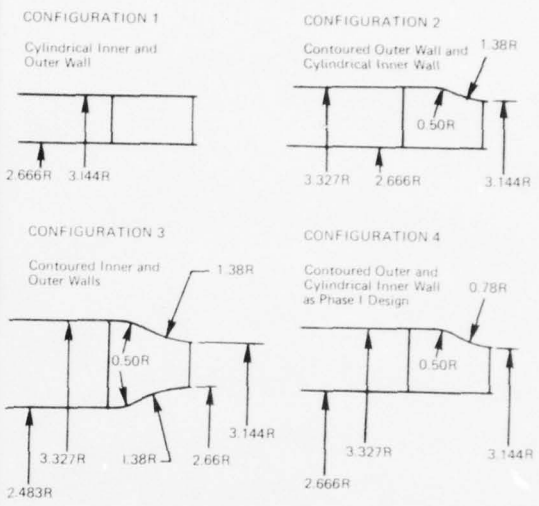


Figure 73. Vane Meridional Constriction Configurations.

program. Contour 5 is shown to exhibit the lowest loss, and it was used as a model to design the ASATT configuration 2. It has the constriction closest to the trailing edge very near the throat.

The nozzle cascade sector consisted of an annular sector with parallel walls leading to the cascade of five vanes fixed at the spacing determined during the Phase I turbine design. Particular attention was given to the length of the passage to minimize the boundary layer growth into the cascade. Some finite length was necessary to accommodate the inlet pressure and temperature rakes and a hot film anemometer traverse probe. The boundary layer thickness entering the cascade was estimated from flat plate theory to be 3 percent of the inlet passage height with the cylindrical wall inlet.

A view of the parts which made up the cascade assembly for the cylindrical wall configuration is shown in Figure 75. The channel wall static holes are shown in Figure 76 in the inner and outer contoured wall configurations. Also evident are the large holes which ocntained the inlet pressure and temperature rakes on the outer wall and the hot film traverse access hole on the inner wall. All of the configurations used the same foil and cascade geometry with the only difference being the outer and inner wall shape. Some of the pertinent measured data of each configuration in addition to

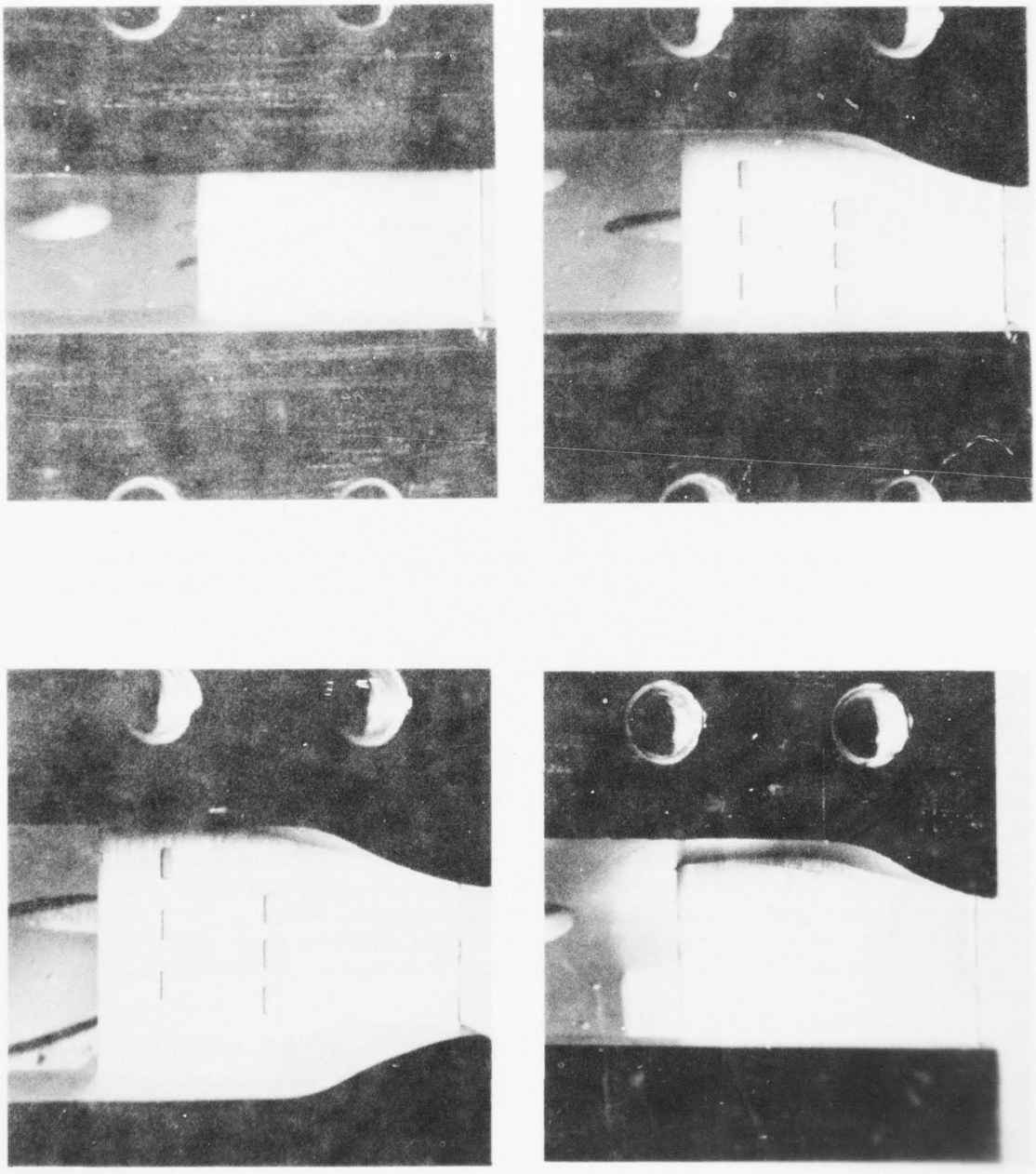
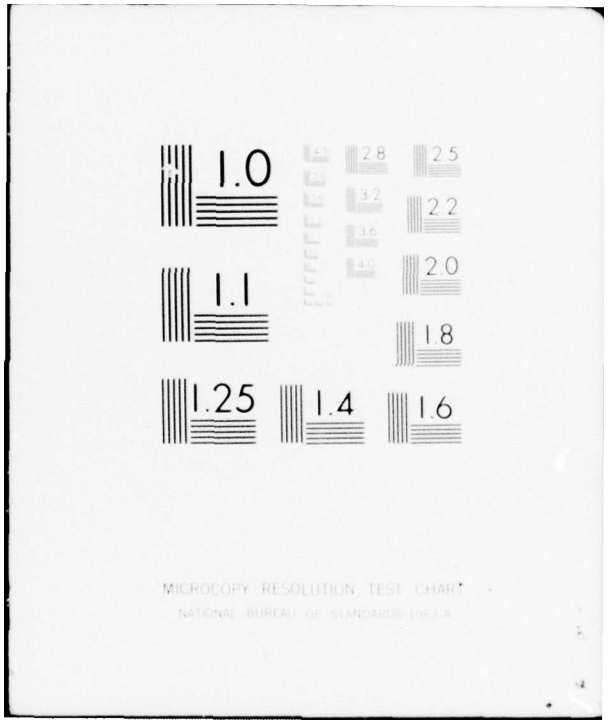


Figure 74. Nozzle/Shroud Configurations, Test Hardware.

AD-A042 517 TELEDYNE CAE TOLEDO OHIO F/G 21/5
ADVANCED SMALL AXIAL TURBINE TECHNOLOGY.(U)
MAY 77 H F DUE, C ROGO, C L KOSIER DAAJ02-72-C-0117
UNCLASSIFIED TCAE-1508 USAAMRDL-TR-77-1 NL

2 OF 4
AD A042517




1.0
1.1
1.25
1.4
1.6
2.8
2.5
3.2
2.2
3.6
2.0
4.0
1.8
MICROCOPY RESOLUTION TEST CHART
NATIONAL BUREAU OF STANDARDS 1963-A

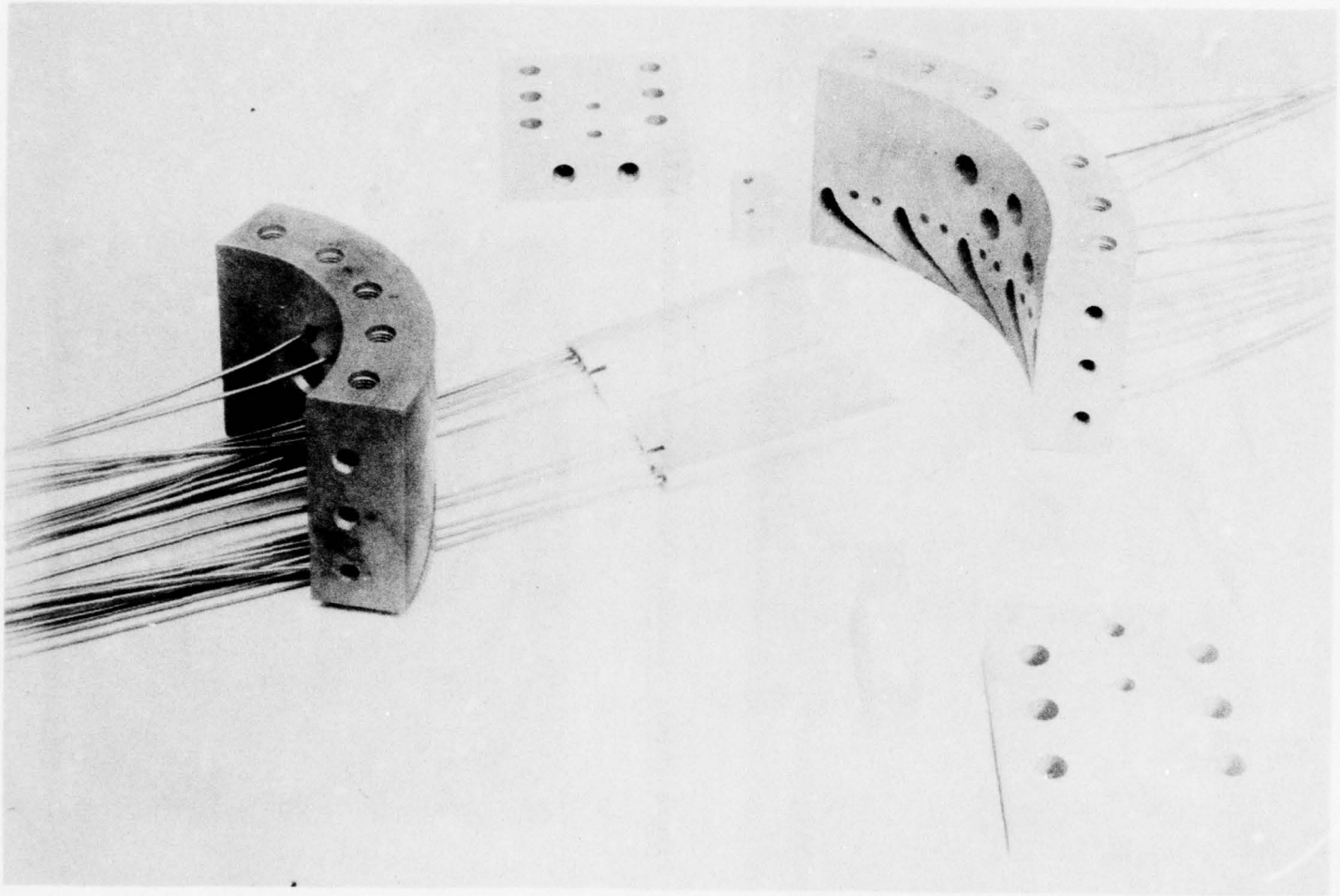


Figure 75. Cascade Hardware - Disassembled.

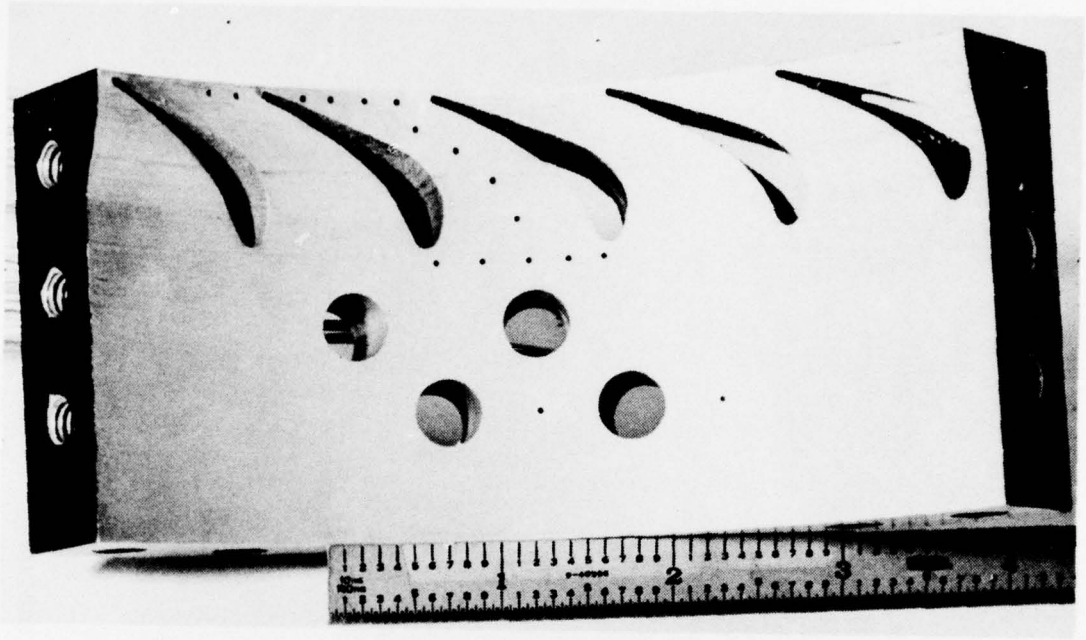


Figure 76(a). Cascase Outer Shroud - Contoured Wall.

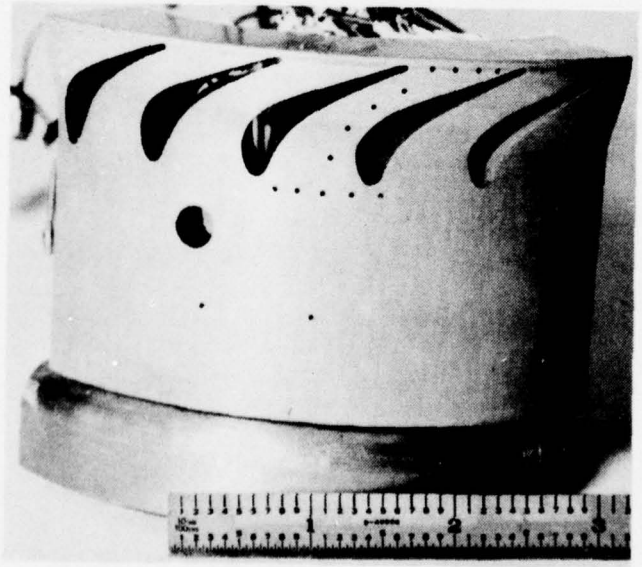


Figure 76(b). Cascase Inner Shroud - Contoured Wall.

Figure 73 (design) is:

Configuration	1	2	3	4
Outer Wall Radius, Exit, (in.)	3.148	3.141	3.115	3.075
Inner Wall Radius, Exit, (in.)	2.670	2.660	2.615	2.595
Arc of Inside Wall Sector (deg.)	69.66	72.08	70.55	70.62
Exit Annulus Area (in^2)	1.560	1.619	1.764	1.586
Inlet Annulus Area (in^2)	1.747	2.484	3.031	2.430
Throat Area (in^2)	0.536	0.589	0.640	0.624

TURBULENCE SCREEN SIZING

Turbulence is the irregular random motion of small fluid masses. Turbulence intensity is a measure of the "degree of disturbance" in the flow stream. It is the ratio of the RMS (Root Mean Square) value of the fluctuating components (u', v', w') of turbulent velocities to the mean velocity (U) of flow (Figure 77). In general, at a certain distance from the screens, the turbulent motion has a tendency to assume isotropy, i.e., the mean oscillations in all the directions become equal. Mathematically, y' = v' = w'. Therefore, under such a condition, the turbulence intensity becomes:

$$T = \sqrt{1/3\ (u'2 + v'2 + w'2)/U}$$

$$T = \sqrt{u'2/U}$$

Experimental data for the turbulence intensity (T) versus the ratio of the distance from the screen (x) to the diameter of grid wire (d) has been reported in References 45, 46 and 47. A formula to calculate turbulence intensity (T) with known values of x/d has been given by Dryden[45] and can be written as:

$$T = \frac{1}{\sqrt{400\ \ [1 + 0.4\ (x/d - 80)]}}$$

The above formula is not valid for x/d less than about 60; in such cases, Dryden's graphical results as presented in his paper are used.

For various sizes of the available wire cloth, calculations were made for the turbulence intensity at the nozzle inlet. The results of these calculations are summarized in Table 11. Wire sizes of 40 mesh x 0.012 in. dia. and 14 mesh x 0.02 in. dia. for the screen were estimated to yield intensities that would fulfill the test objectives.

The screens designed to produce average values of turbulence intensity of 3.7 and 11.2 percent are shown in Figure 78 together with the distortion and blockage plates used in the inlet velocity profile variations.

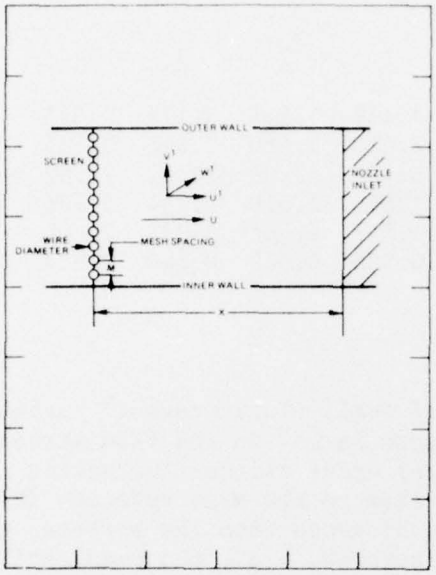


Figure 77. Turbulence Intensity *Induced Upstream of* Nozzle Inlet.

VANE AND BLADE FABRICATION

The vane was extruded from aluminum as a constant section. The Phase I turbine design vane exit angle variation was only 4 degrees across the span, therefore the constant section vane was designed to yield the meanline exit air angle of 69.5 degrees. The airfoil contour was checked with a 20-times size comparator and was within 0.002 inch.

The cooled vane configuration tested is shown in Figure 79 installed in the inner cyclindrical wall. A top view of the cooled vanes shown in Figure 80 shows the supply holes for the cooling slots and the inner shroud cooling holes. A cooling manifold arrangement was used to valve-off the different cooling circuits for various test runs.

The rotor cascade sector was machined from free-machining brass on a contour mill in an integral wheel. The airfoil contours were checked with the 20 times size mylars and were within the 0.002 inch tolerance band for nearly all all sections checked. The few sections falling outside the tolerance band had a maximum deviation of 0.003 inch. Front and rear views of the pressure loaded rotor are shown in Figure 81, and the suction loaded rotor is shown in Figure 82.

A third rotor cascade was designed to test a lower solidity pressure loaded configuration. Since the same sector space had to accommodate the decreased solidity configuration, the choice of solidity was dictated by removing one or more blades and spacing the remaining equally within the sector. Removal of two blades produced a solidity reduction of 22 percent and was deemed an adequate change. The reduced solidity rotor was designed to the same vector triangles as the baseline rotor so that the rotor reaction for both rotors would be identical for the rotor cascade configuration. The reduced solidity rotor is shown in Figure 83.

INSTRUMENTATION

The instrumentation for the cascade rig was provided to enable the measurements of inlet total temperature and pressure airflow, channel wall static pressures, boundary layer velocity profile, inlet passage distribution of turbulence, vane exit, and rotor exit radial and circumferential traverse of total pressure and temperature and angle and torque reaction due to momentum change. The majority of the pressure measurements were made using transducers and a few using Wallace and Tierman absolute pressure gauges



Figure 78. Cascade Inlet Distortion, Turbulence and Blockage Plates.

TABLE 11

TURBULENCE PRODUCED BY VARIOUS SCREEN SIZES

Wire Size Detail	x (In.)	d (In.)	M (In.)	x/d	x/M	d/M	T
40-0.009	1.2	0.009	0.016	133	75	0.56	0.028
40-0.012	1.2	0.012	0.013	100	92.3	0.92	0.037*
14-0.016	1.2	0.016	0.055	75	21.8	0.29	0.056
12-0.02	1.2	0.02	0.051	60	23.5	0.39	0.112*
8 -0.028	1.2	0.028	0.097	42.8	12.4	0.29	0.125
6 -0.023	1.2	0.023	0.142	52.6	8.45	0.16	0.120

* Screens Chosen to Fulfill Test Objectives.

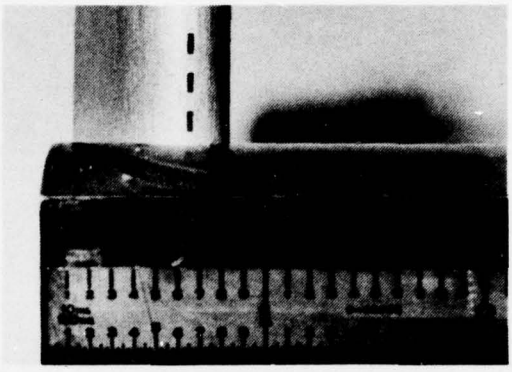


Figure 79(a). Suction Side Gill Slots.

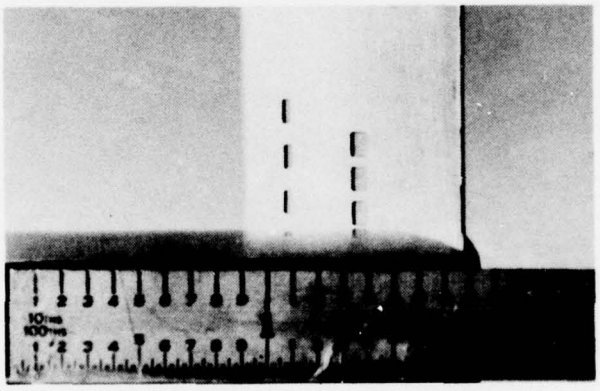


Figure 79(b). Pressure Side Gill Slots.

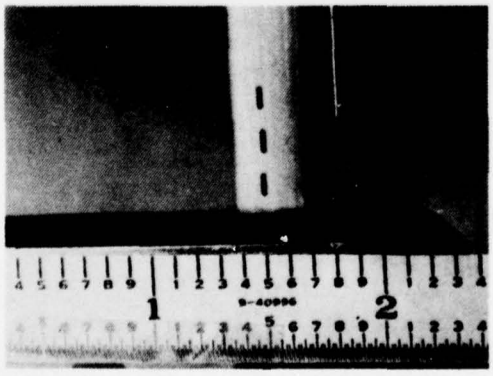


Figure 79(c). Trailing Edge Slots.

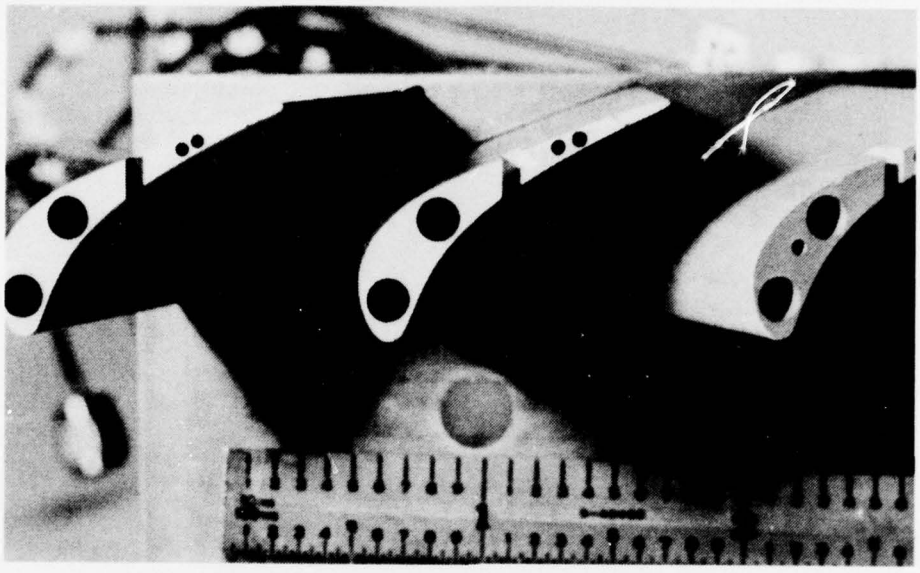


Figure 80. Cooling Supply Holes.

for test stand monitoring. Temperatures were measured using iron-constant thermocouples. A table of instrumentation shown in Figure 84 lists location of measurement, ranges and expected accuracy.

The hot film anemometer traverse located immediately in front of the vane leading edge, consisted of a radial survey between the center vanes to ascertain the velocity profile, turbulence intensity level and boundary layer thickness. Forty-two surface static pressure taps were located at the inner and outer wall, passage, and at the vane meanline suction and pressure surfaces.

Turbulence and boundary layer measurements were made using a hot-film probe as shown in Figure 85(a) together with the electronic equipment in Figure 85(b). The equipment used for these measurements consisted of:

1. RMS Voltmeter (Thermal System Incorporated TSI Model No. 1060).
2. Digital Voltmeter (Weston Model 1240).
3. Monitor and hot-film power supply for constant temperature anemometers with signal linearizer (TSI Models 1051-6, 1050 and 1052).
4. Oscilloscope (Tektronic type 535 with camera attachment).

Traverse data was taken initially with a wedge type probe shown in Figure 86 as installed in front of the slave. Initial tests proved that the

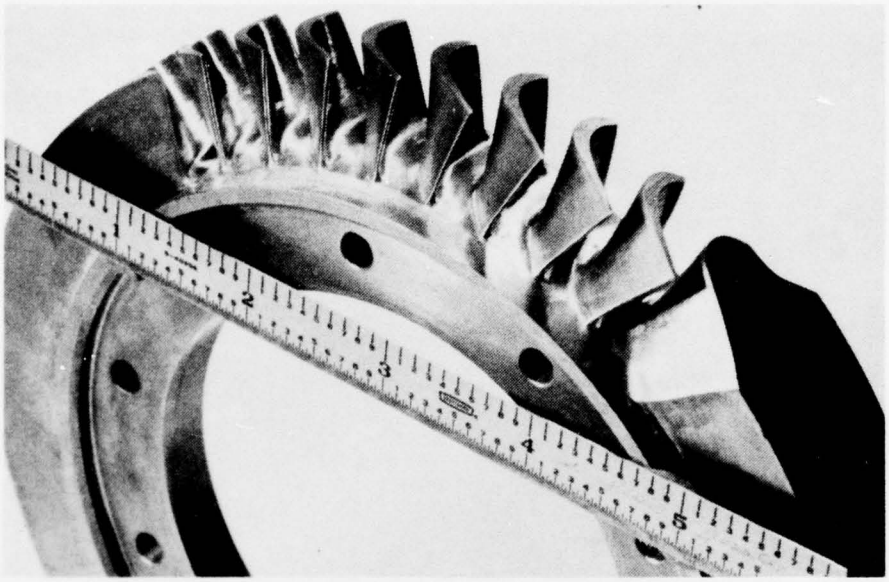


Figure 81(a). Rotor Cascade - Pressure Loaded - Rear View.

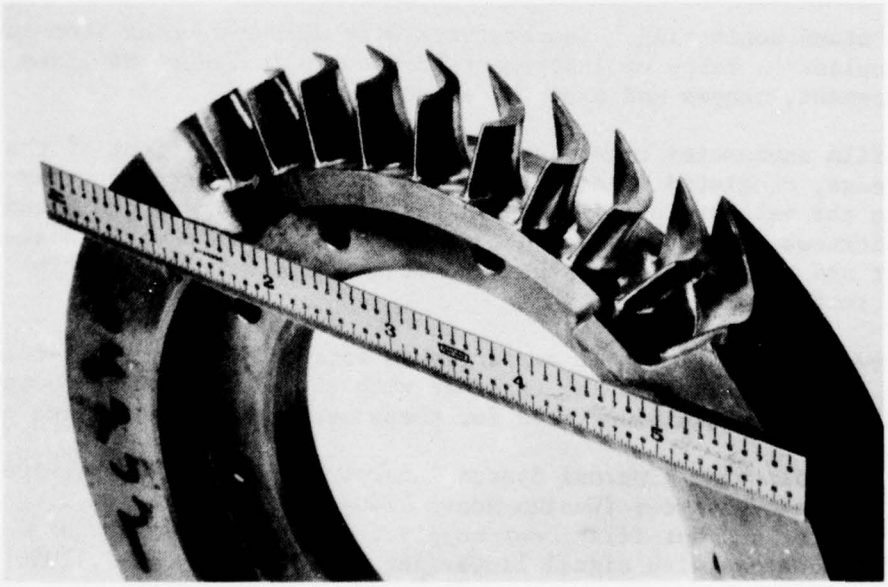


Figure 81(b). Rotor Cascade - Pressure Loaded - Front View.

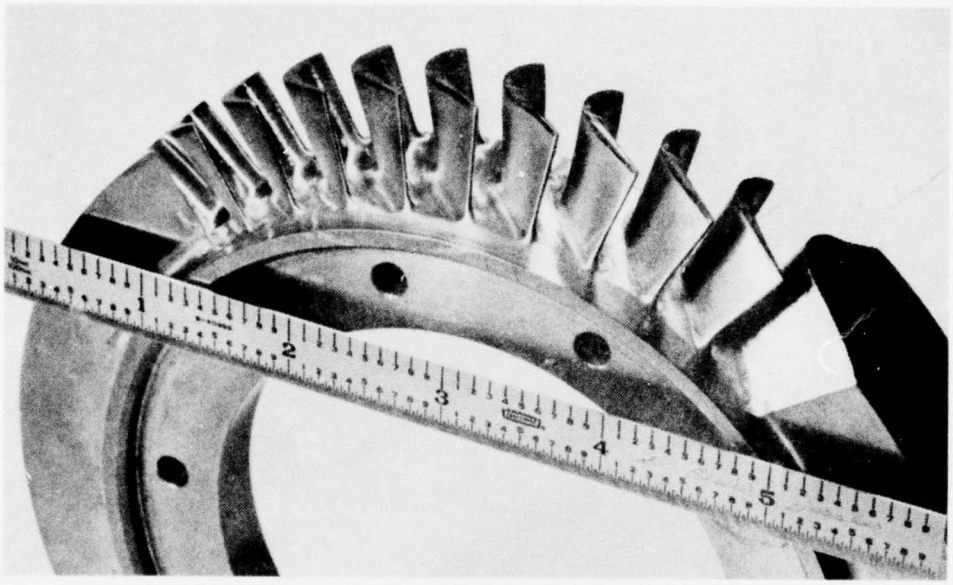


Figure 82(a). Rotor Cascade - Suction Loaded - Rear View.

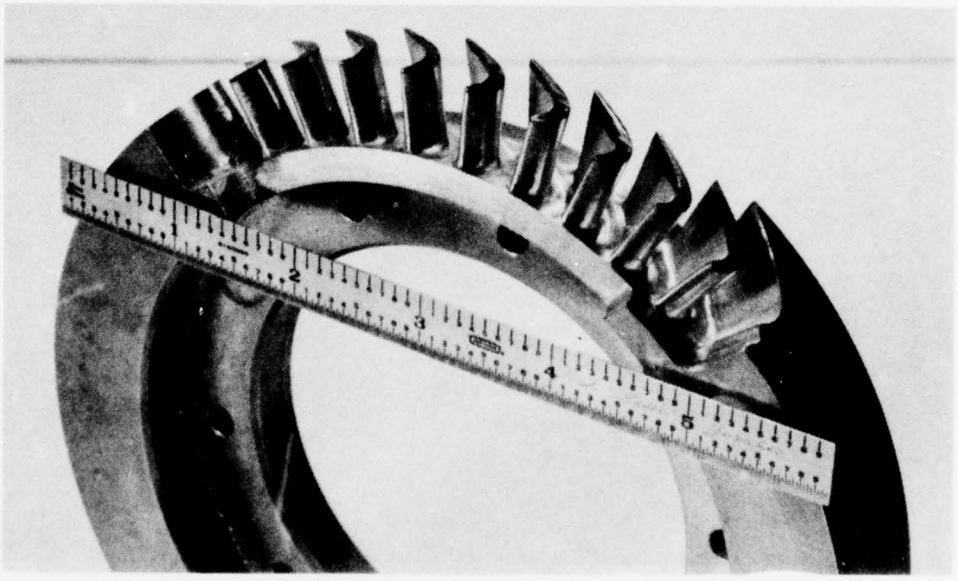


Figure 82(b). Rotor Cascade - Suction Loaded - Front View.

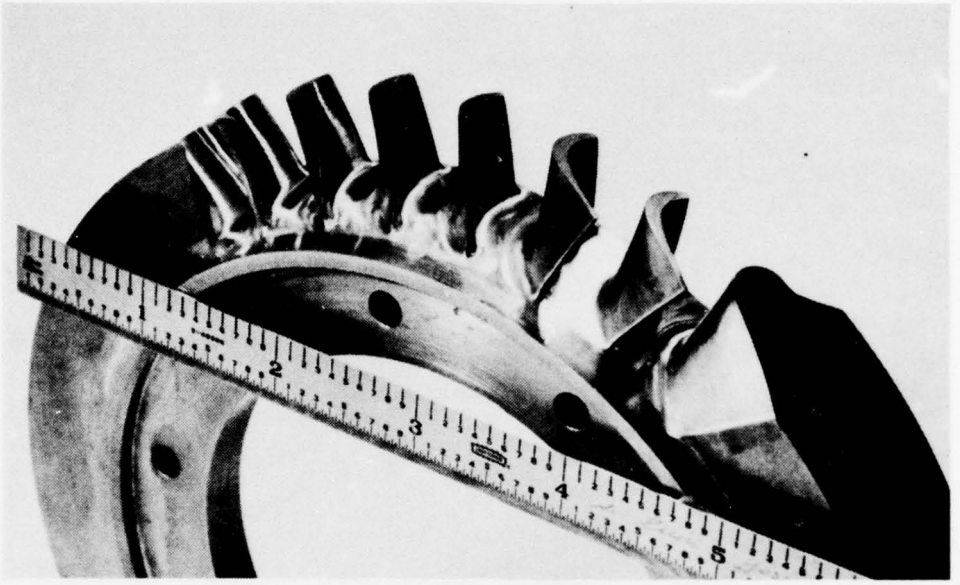


Figure 83(a). Rotor Cascade - Reduced Solidity - Rear View.

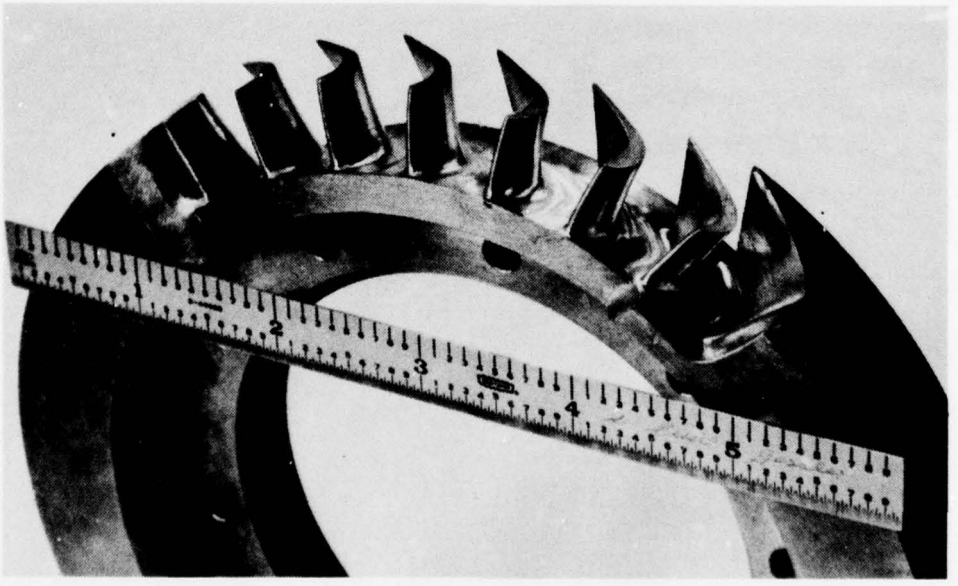


Figure 83(b). Rotor Cascade - Reduced Solidity - Front View.

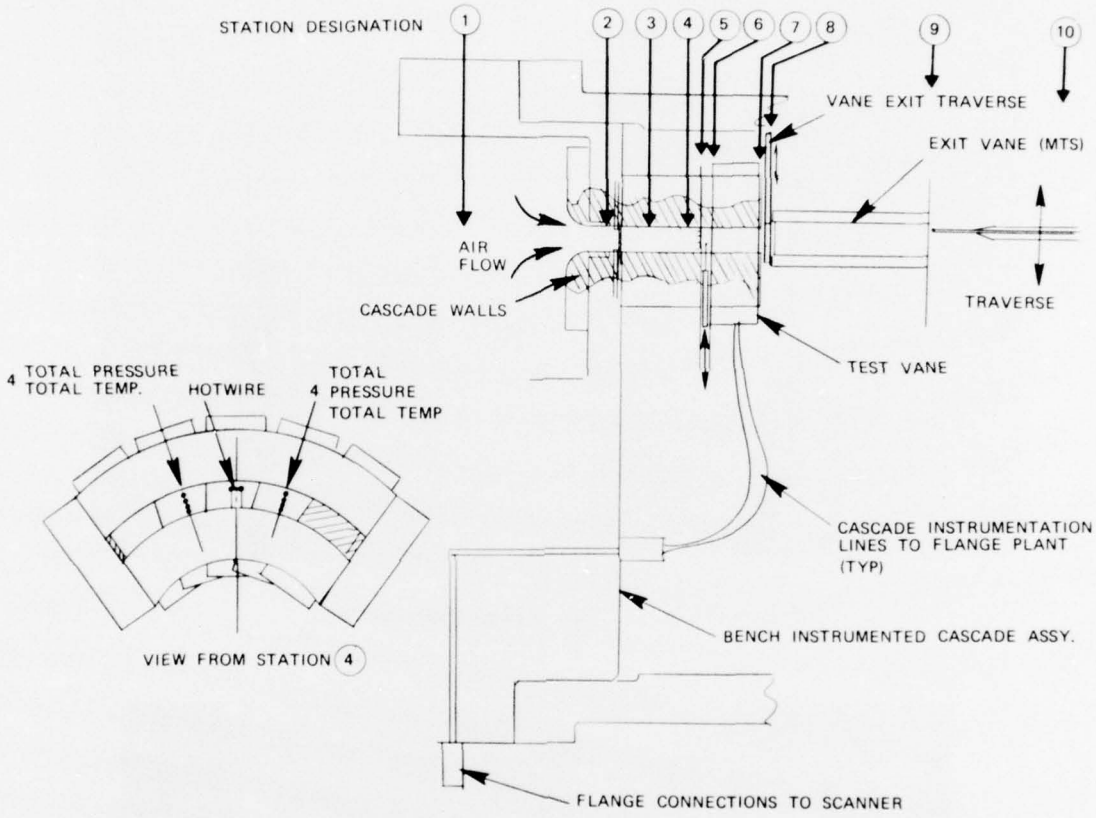


TABLE OF INSTRUMENTATION

Station	Instrument/Parameter	Quantity of Instrumentation	Range	Accuracy
0	Orifice Inlet Temperature Orifice/Inlet Flow	1-thermocouple 1-orifice (2 statie pressures)	60-180 F 0.3-0.6 pps.	±2 Deg ±1% Max.
1	Pressure Gage/Inlet Pressure	1-Gage	0-100 psia	± 1 psi
1	Inlet Temperature	1-thermocouple	60-180°F	± 2 deg
2	Inlet to Distortion Screen	None	N.A.	N.A.
3	Screen Exit	None	N.A.	N.A.
4	Hot Wire Anemometer/Turbulence Intensity	1-Anemometer	3-12% turbulence	±1%
5	Total Pressure Rake/P_T (Transducer)	8-Total Pressures	0-50 psia	±½ F.S.
5	Pressure Transducer/Wall P_S	4-Static Pressures	0-50 psia	±½ F.S.
5	Thermocouple Rake/T_T	8-Total Temperatures	60-180 F	±2 °F
6	Pressure Transducers/P_S Wall	42 Static Pressures	0-50 psia	±½ F.S.
7	Flow Nozzle/Cooling Flow Bypass Flow	1-Flow Nozzle (2 Static Pressures)	0-0.1 lb/sec	±1 % F.S.
7	Pressure Transducers/P_S Wall	42 Static Pressures	0-50 psia	±½ F. S.
8	Pressure Transducers & Thermocouples/T_T, P_T, P_S, Angle (Rad & Cir Traverse)	1-Total Pressure 2-Static Pressures 1-Total Temperature	0-50 psia -160/ 60-180 F	±½ F. S. ± 2 deg
9	Pressure Transducer/P_T, P_S, T_T Angle, Traverse	1-Total Pressure 2-Static Pressures 1-Total Temperature	0-50 psia -160/ 60-180 F	±½ F.S. ± 2 deg
9	Load Cell/Torque	1-Load Cell	0-100 lb	0.10% F.S.
10	Pressure Gage/Exit Pressure Thermocouple/Exit Temperature	1-Gage 1-Thermocouple	0-50 psig 60-180 F	± 1 psi ± 2 Deg

Figure 84. Cascade Instrumentation Detail.

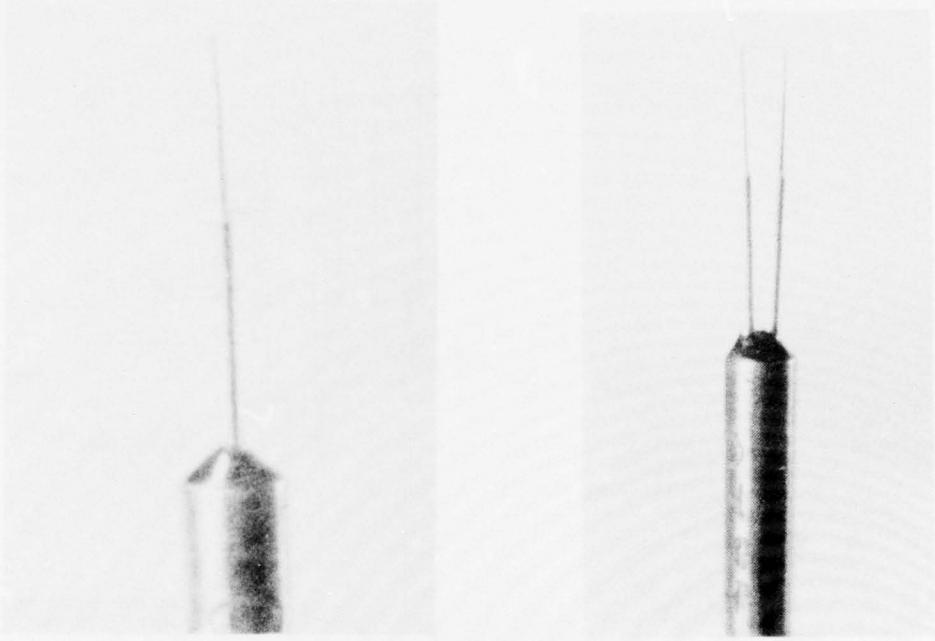


Figure 85(a). Hot Film Anemometer.

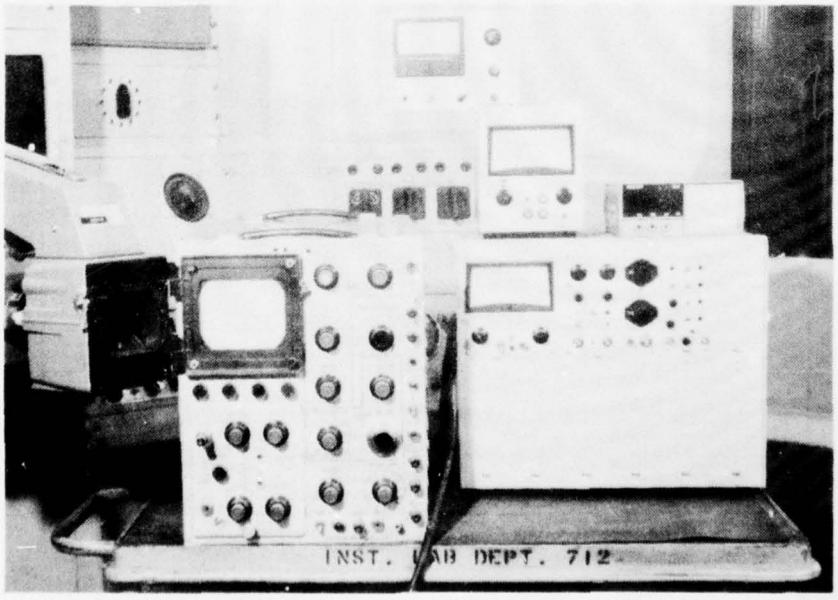


Figure 85(b). Anemometer Accessory Equipment.

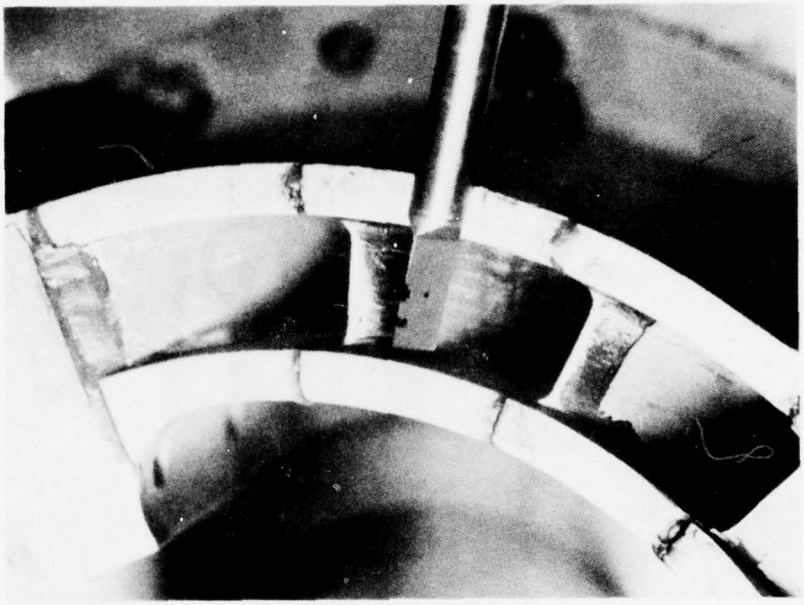


Figure 86. Momentum Transfer Slave Inlet.

blockage required by the probe shank affected the flow field, and subsequent testing was performed using a small cobra head probe of the type shown in Figure 87 (circled).

INSTRUMENTATION CALIBRATION AND ACCURACY

The instrumentation was selected and calibrated to accurately measure cascade performance and to determine local performance variations.

The momentum transfer slave torque measurement system was calibrated over a 50-pound force range and 10 psig rig pressure range to yield a maximum error of 0.35 percent of full scale. Figures 88 and 89 present the M.T.S. correction data as a function of slave force.

The inlet turbulence and boundary layer velocity profile were measured with a constant temperature hot film probe. The probe consisted of a quartz-coated platinum film sensor on a 0.002-inch glass rod (TSI Model 1210). The hot film probe was tunnel calibrated to 500 ft/sec velocity and the hot film voltage was normalized to standard pressure ($E_{HOT\ FILM}/\delta^{1/4}$). Figure 90 shows a typical hot film calibration curve. Turbulence intensity was determined using the measurement of RMS voltage and the velocity/voltage relationship determined from Figure 90, a function of the corrected hot film voltage, as follows:

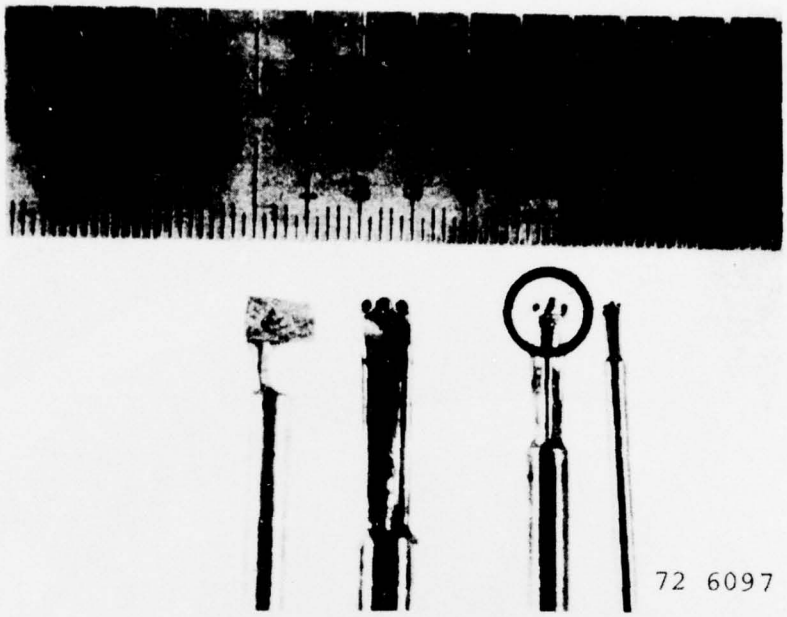


Figure 87. Cobra Head Traverse Probes.

$$T = \frac{RMS}{U} \quad \frac{\Delta V}{\Delta e} \quad \text{turbulence intensity}$$

Where: RMS = root mean square of the axial velocity fluctuations measured with an RMS voltmeter (TSI Model 1060).

U = free stream velocity

$\frac{\Delta V}{\Delta e}$ = velocity-voltage relationship described in Figure 90

The nozzle exit angle, total pressure, and temperature were measured by a standard cobra type probe. The probe consisted of a 0.125-inch support stem and 0.040-inch angle and total pressure sensing tubes. Also, a bare wire iron-constantan thermocouple was placed at the probe center line, 0.050 inch above the total pressure element. The probe was tunnel calibrated over a range of Mach numbers for pressure and temperature recovery factors. Figure 91 shows the recover data obtained.

The pressure transducers and thermocouples were calibrated to the IBM Data Acquisition and Control (DAC) system. Each pressure transducer was pressurized in steps throughout its range of operation with a Mensor pressure controller, Model 10095-00X quartz pressure sensor. The DAC system read and recorded each pressure data point and generated a slope and intercept

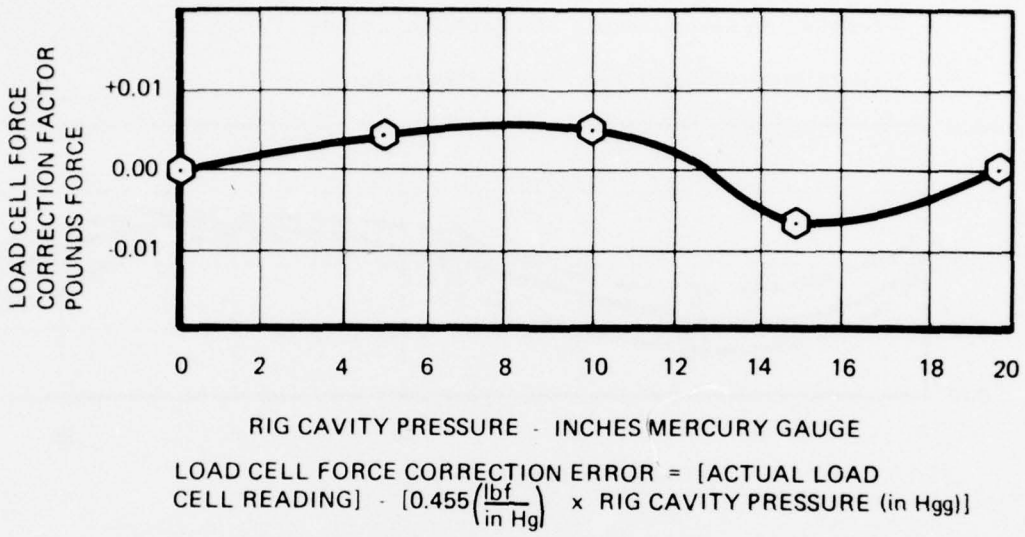


Figure 88. Load Cell Force Correction Error.

type calibration. Each transducer was then check-calibrated to ensure accuracy within ±0.25 percent of reading. The thermocouples were calibrated in a similar manner to within ±2°F of reading.

TEST FACILITY, PROCEDURES AND DATA ACQUISITION

TEST FACILITY

The test equipment consisted of a line from the facility shop air supply, an inlet control valve, an inlet electrical resistance heater, a filter, a cascade rig and instrumentation, and the vacuum exhaust line. This arrangement is shown schematically in Figure 92. A photograph showing the facility is presented in Figure 93.

The rig was stationed on a portable stand shown in the test facility schematic, Figure 93. Air from the shop air supply flowed through a 25-micron filter, a 15-KW electrical resistance heater, an ASME sharp-edged orifice with flange taps, and into the rig plenum through a 2-inch flex hose. The airflow impinged on a baffle plate which served as a dampener to minimize flow pulsations at the cascade inlet. The flow proceeded through the cascade section, the momentum transfer slave (MTS), and was exhausted to the laboratory exhaust system.

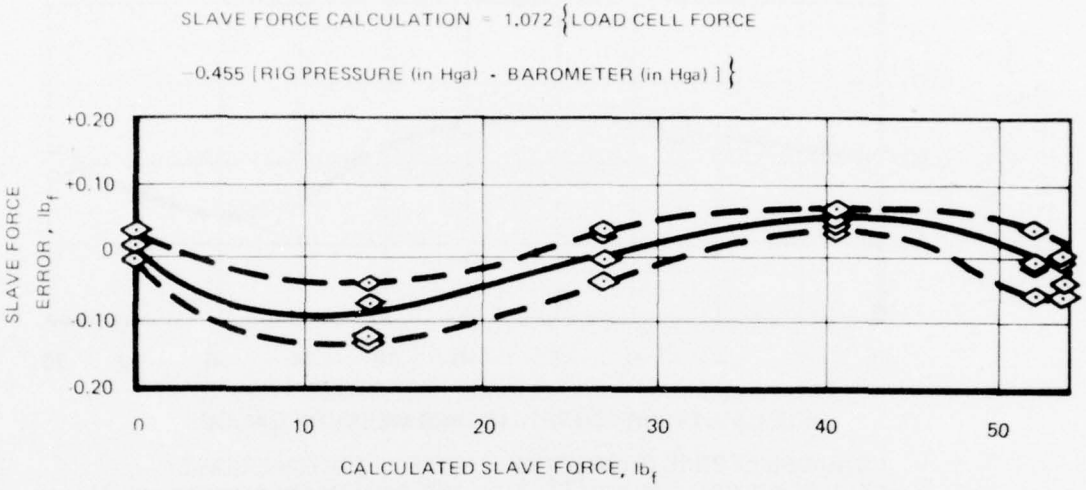


Figure 89. Slave Force Calculation Error.

Initial testing showed that a higher-than expected total pressure loss was occurring across the momentum transfer slave. The exhaust was hardline plumbed to the vacuum exhaust system to allow the rig to operate at a variety of inlet pressures and overall pressure ratios. With this facility modification the rig was capable of operating over a range of inlet pressures between 20 psia to 50 psia with any exhaust pressure as low as 1 psia.

TEST PROCEDURES

The rig was installed in the test facility and leak checked at 50 psia with the exhaust port capped. The data acqusition system was brought on line and ambient readings of all recorded measurements were taken. Flow was initiated by opening the upstream control valve and setting the inlet pressure at a predetermined value depending on the test run. Inlet pressure was varied during the test program from 20 psia to 50 psia. The nozzle pressure ratio was set using the vacuum exhaust control valve. The exhaust pressure was varied from ambient (14.7 psia) to 1 psia to yield the desired pressure ratio and nozzle exit Mach number.

Gaseous nitrogen was expanded from high pressure bottles to provide the flow for the cooling effects test sequence. Air inlet temperature was controlled using an electrical resistance heater in the line. The inlet temperature was maintained between 120° and 140°F to prevent condensation at the nozzle exit. Thirty-eight test configurations were run including seven test reruns, and over 200 hours of test time was accumulated on the cascade rig.

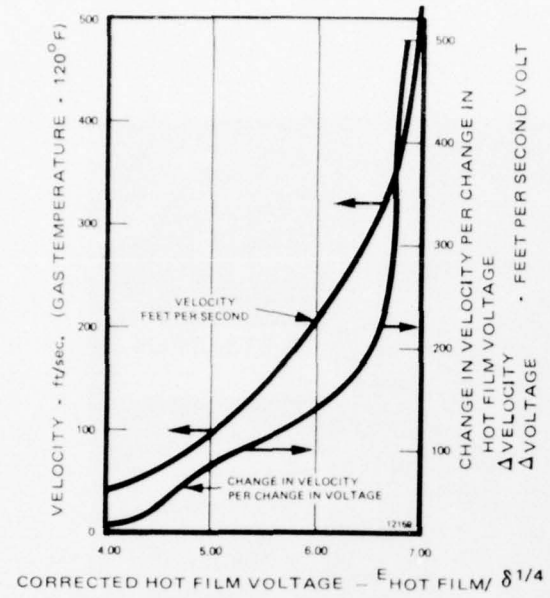


Figure 90. Hot Film Calibration Curve.

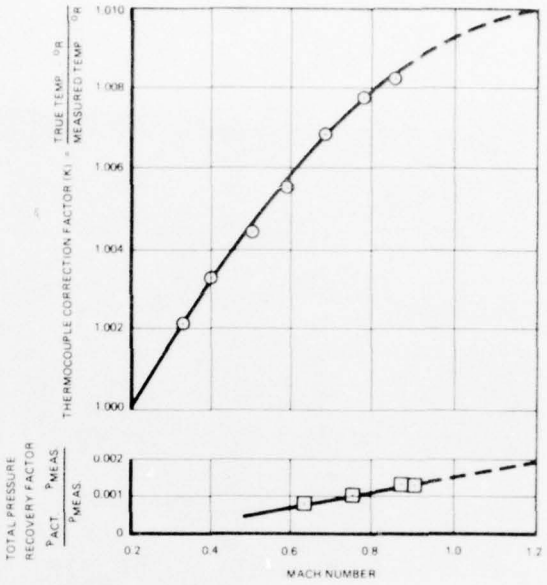


Figure 91. Discharge Survey Cobra Probe Recovery Calibration.

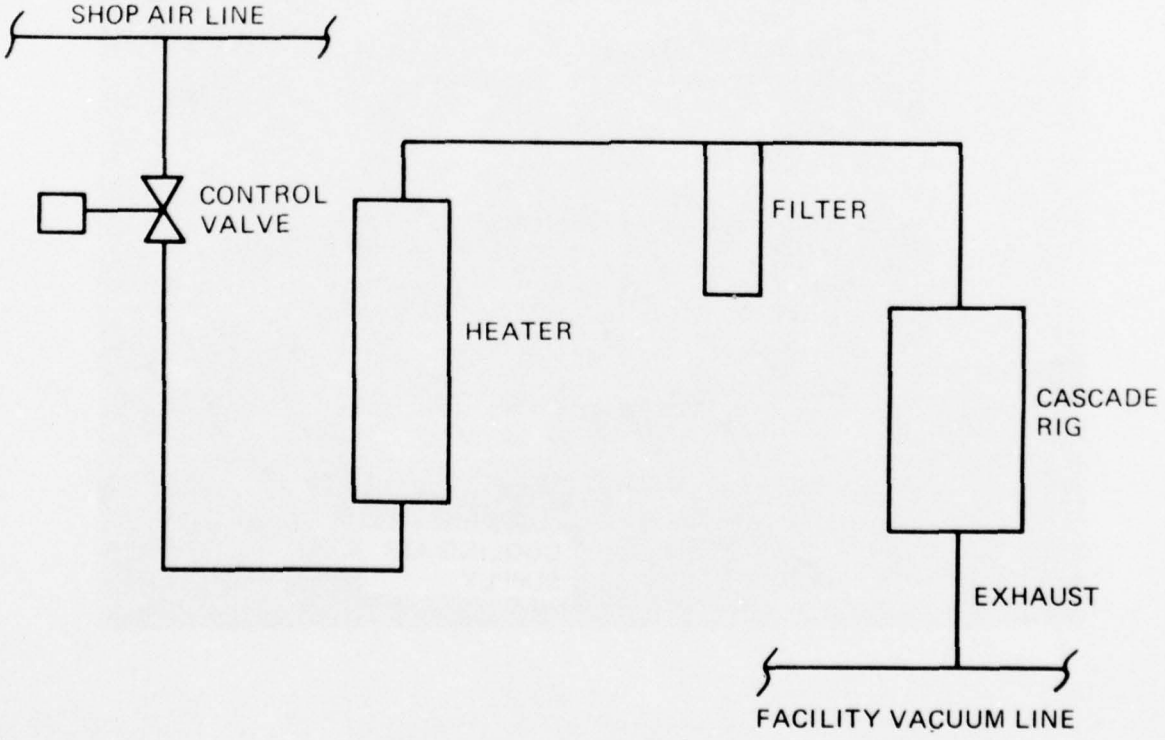


Figure 92. Schematic of Test Arrangement.

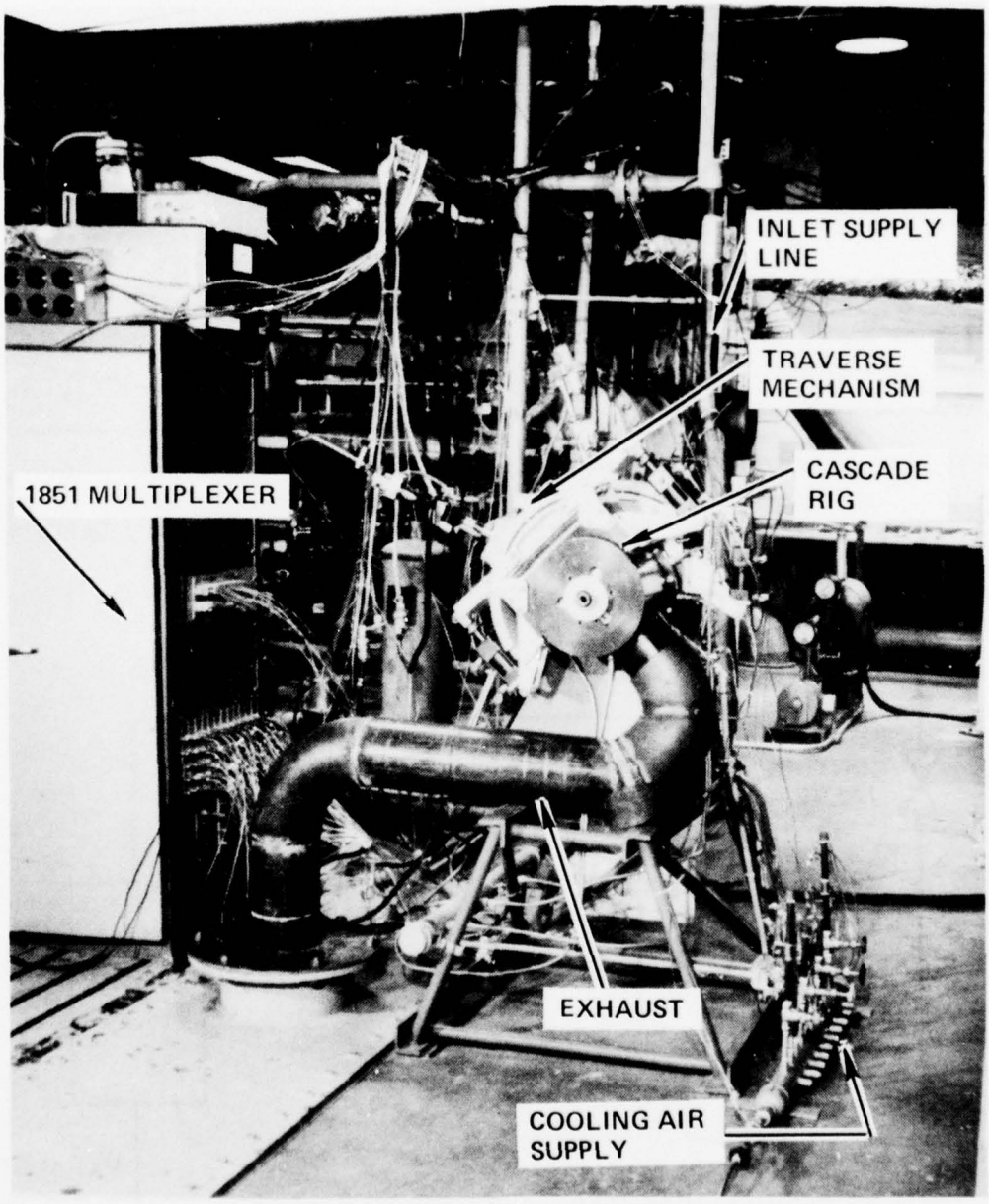


Figure 93. ASATT Turbine Cascade Facility.

The desired test point was set by determining the nozzle exit Mach number from the momentum transfer calculation. When a desired test point was achieved, all instrumentation was scanned with the traverse probes retracted from the air passage and the data was printed on the console typewriter and recorded on magnetic tape.

The radial traverse of the hot film probe, located mid-channel at the vane inlet, consisted of: (1) determining the input voltage/velocity characteristic at the mid-passage and (2) traversing at 2 percent span intervals, starting at the inner wall and recording RMS and input voltage at each interval. Selected points were displayed on the oscilloscope and photographed using the Polaroid camera attachment.

The radial and circumferential traverse performed at the nozzle exit consisted of sampling eight radial and circumferential locations. Inlet pressure and flow was continually monitored during each traverse to insure that the set point was maintained. Approximately 30 seconds was required at each traverse point for pressure stabilization to occur.

A radial and circumferential total pressure and angle survey was performed at the slave exit to determine whether all of the tangential momentum was transferred. When it was determined that the flow was axial, this traverse was omitted from the test procedure for the remaining test sequence.

DATA ACQUISITION

The data acquisition procedure adopted for collecting and assimilating the cascade data consisted of implementing the IBM 1800 data acquisition and control system (DACS).

The IBM 1800 DACS, Figure 94, is basically a digital computer with specific hardware features designed to facilitate interaction with real time processes. The 1800 system is a 16-bit word machine with cycle times of two or four micro seconds. A full range of data processing peripherals is supported. These include card and paper tape readers and punches, typewriters, line printers, and magnetic tape and disc storage devices. System control is enhanced by a multilevel hardware interrupt capability along with flexible and digital modes. Analog to digital converters (ADC) are available with speeds of 10,000 or 20,000 samples per second. Signal multiplexers, interfacing with the ADC, are available in solid state (high level only) and relay (high and low level) types with switching rates of 1000 points/second and 100 points/second, respectively. Standard digital input/output capability is enhanced by pulse counter and electronic contact switching features.

All the above-mentioned hardware features are fully supported in the FORTRAN IV high-level language under the control of the Multiprogramming Executive System (MPX).

The DACS presently features a 32K, four micro second 1800 computer, paper tape punch, 1-console typewriter keyboard, 4-remote typewriter printers,

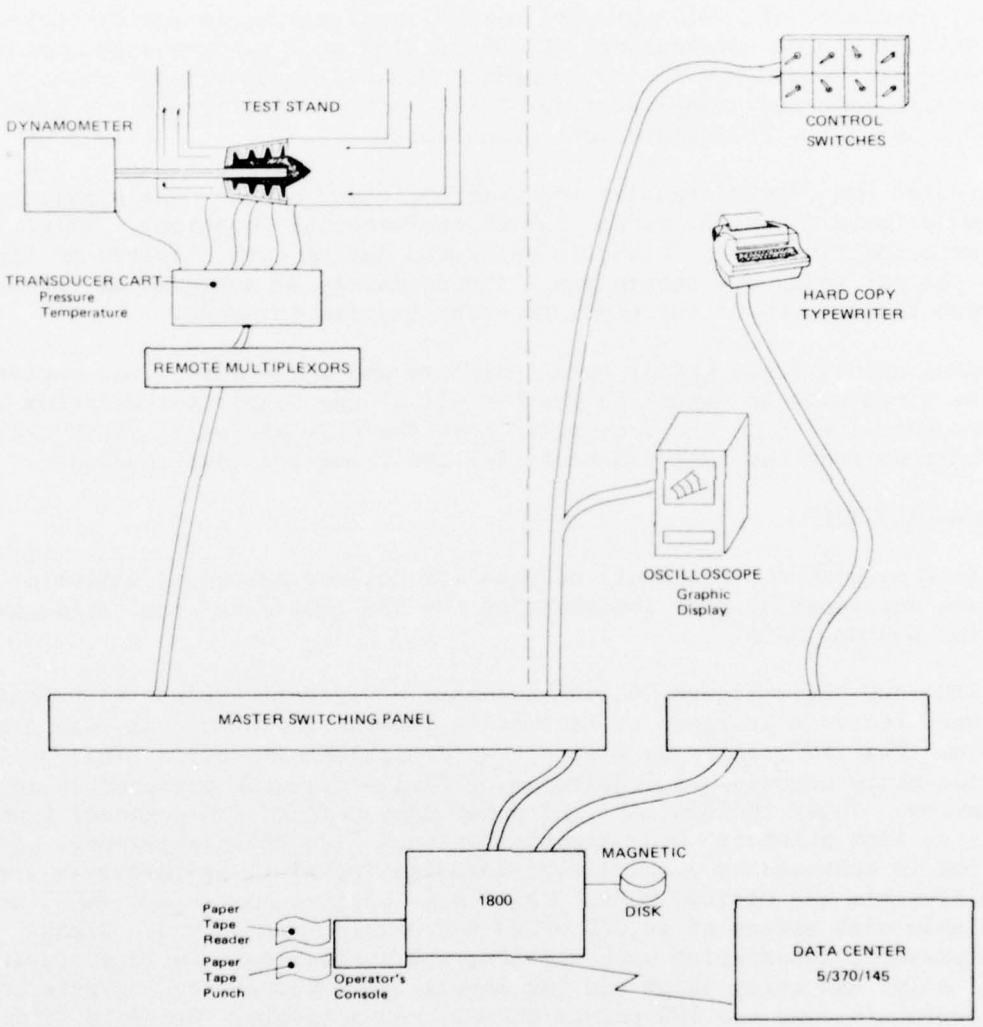


Figure 94. IBM 1800 Data Acquisition and Control System.

1-card reader/punch, 2-magnetic tape drive. Process input/output includes 10,000 point per second ADC, 320 points of remote analog input, 97 digital inputs, 48 digital outputs, 48 process interrupts, 16 electronic contact operate switches and 2 points of analog output. A solenoid operated master switching panel combined with remote multiplexers affords remote access (maximum of 10,000 feet) to all test areas in the network.

The system as configured for the cascade testing is shown in Figure 95. This setup utilizes five pressure scanner valves connected to transducers which are connected to the IBM 1851 Multiplexer. The scanners have twelve input pressures, each one of which is reserved for calibration. Through a unique switching arrangement, various segments of the test measurements are recorded, printed or stored, or used for calculations to aid in establishing the test point and the cascade performance.

Data was available immediately for inspection and cursory analysis through the on-line typewriter output. The data recorded on magnetic tape was reduced on the IBM 370 where velocity, Mach number, pressure loss, and other salient calculations were performed. The cal-comp plotter was utilized for plotting the radial and circumferential traverse data. Air was supplied to the rig from the factory air supply.

CASCADE TEST RESULTS

The testing was phased to provide aerodynamic performance data in a systematic sequence considering: (1) application of the momentum transfer principles, and (2) expedient use of assembly and test time. The test sequence is shown in Table 12. During the test program it was deemed expedient to revise the test program. The testing performed deviated somewhat from the sequence shown in Table 12. A detailed breakdown of the test sequence, as run, is given in Appendix D.

A summary of the test configuration geometry is given in Table 13. The table lists the dimensional measurements taken for each test configuration.

The test results are presented in the form of inlet and exit pressure, velocity and mass flow distributions and contour plots of loss coefficient and efficiency for the test sequences. The vane meanline and channel inlet and exit velocity distributions are also shown. Comparisons are made between the momentum data and the conventional pressure and angle traverse data. The calculation procedure used in determining nozzle efficiency from momentum transfer (MTS) data is given in Reference 2, Appendix III for one of the data points. The deviations from the predicted performance and impact on the Phase III full-round rotating turbine design are discussed in the cascade data evaluation section.

TEST SERIES A - EVALUATION OF MERIDIONAL CONSTRICTION ON NOZZLES

Test Objective

The purpose of this test series was to evaluate four wall configurations and to ascertain which of the four wall configurations would have the best meridional constriction for performance. These configurations consisted

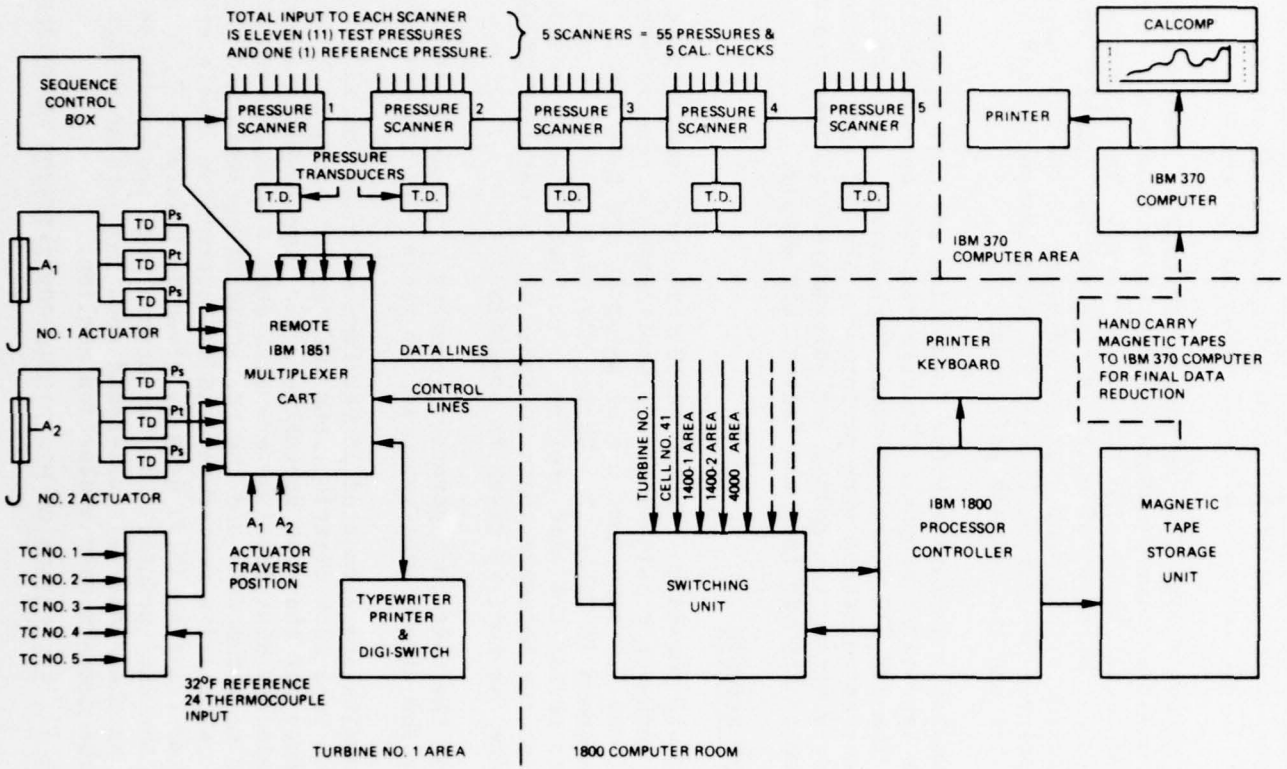


Figure 95. Data Acquisition System - ASATT Cascade.

TABLE 12

PHASE II CASCADE TEST SEQUENCE

TEST SERIES AND OBJECTIVE	TEST NUMBER	VARIABLE	MOMENTUM RIG CONFIGURATION	
			NOZZLE	ROTOR
A. EVALUATION OF MERIDIONAL CONSTRICTION ON NOZZLES	1	CYLINDRICAL WALLS	NOMINAL	SLAVE
	2	BEST OUTER WALL INNER WALL VARIATION NO. 1	NOMINAL	SLAVE
	3	BEST OUTER WALL INNER WALL VARIATION NO. 2	NOMINAL	SLAVE
	4	OUTER WALL VARIATION NO. 2 BEST INNER WALL OF TESTS 1 AND 2	NOMINAL	SLAVE
B. EFFECT OF HIGH STATOR MEAN EXIT MACH NUMBERS	5	PRESSURE	NOMINAL	SLAVE
C. EFFECT OF INLET TURBULENCE	6	TURBULENCE SCREEN NO. 2	NOMINAL	SLAVE
D. EFFECT OF STATOR INLET BOUNDARY LAYER AND FLOW DISTORTION	7	INNER BOUNDARY INCREASED TO 5% OF BLADE HEIGHT	NOMINAL	SLAVE
	8	OUTER BOUNDARY LAYER INCREASED TO 5% OF BLADE HEIGHT	NOMINAL	SLAVE
	9	INNER AND OUTER BOUNDARY INCREASED 10% OF BLADE HEIGHT	NOMINAL	SLAVE
	10	PIPE FLOW OR NOMINAL VELOCITY DISTRIBUTION	NOMINAL	SLAVE
	11	HIGH VELOCITY ON OUTER WALL	NOMINAL	SLAVE
	12	HIGH VELOCITY ON INNER WALL	NOMINAL	SLAVE
E. EVALUATION OF STATOR EXIT FLOW DISTORTION AND LEAKAGE EFFECTS ON ROTOR CASCADE PERFORMANCE	13	PIPE FLOW OR NOMINAL VELOCITY DISTRIBUTION	ACTUATOR	SLAVE
	14	HIGH VELOCITY ON OUTER WALL	ACTUATOR	SLAVE
	15	HIGH VELOCITY ON INNER WALL	ACTUATOR	SLAVE
	16	HIGH VELOCITY ON INNER WALL	ACTUATOR	LOCKED NOMINAL
	17	HIGH VELOCITY ON OUTER WALL	ACTUATOR	LOCKED NOMINAL
	18	PIPE FLOW OR NOMINAL VELOCITY DISTRIBUTION	ACTUATOR	LOCKED NOMINAL
	18a	SEAL LEAKAGE VARIED FROM 0 TO 10% MAIN FLOW	ACTUATOR	LOCKED NOMINAL
F. EVALUATION OF SECOND ROTOR LOADING	19	SECOND ROTOR BLADE DESIGN OF PHASE I	ACTUATOR	PHASE I SECOND DESIGN - LOCKED
G. EFFECT OF COOLING AND SOLIDITY ON STATOR PERFORMANCE	20	NO FLOW-CALIBRATION CHECK	NOMINAL	SLAVE
COOLING EFFECTS	21	PRESSURE AND SUCTION SIDE HOLES ONLY	NOMINAL	SLAVE
	22	TRAILING EDGE HOLES ONLY	NOMINAL	SLAVE
	23	OUTER WALL HOLES AND INNER WALL HOLES ONLY	NOMINAL	SLAVE
	24	ALL CONFIGURATIONS SIMULTANEOUSLY WITH DESIGN FLOWS	NOMINAL	SLAVE
	24a	SUCTION AND PRESSURE HOLES ADDED DOWNSTREAM - ALL COOLING HOLES FLOWING	NOMINAL	SLAVE
NOZZLE SOLIDITY EFFECT ON PERFORMANCE	24b	NOZZLE SOLIDITY REDUCED 20% COOLING FLOW VARIED	REDUCED SOLIDITY	SLAVE
H. EFFECT OF STATOR COOLING ON TWO ROTOR SOLIDITIES AND AXIAL SPACING	25	TOTAL COOLING FLOW	ACTUATOR	SLAVE
	26	TOTAL COOLING FLOW	ACTUATOR	LOCKED NOMINAL
	27	EVERY OTHER ROTOR BLADE REMOVED	ACTUATOR	LOCKED NOMINAL
	28	INCREASED AXIAL SPACING	ACTUATOR	LOCKED NOMINAL

TABLE 13

TEST CONFIGURATION GEOMETRY

TEST SERIES AND OBJECTIVE	TEST NUMBER	VARIABLE	INLET GEOMETRY						EXIT GEOMETRY				COOLING CIRCUIT EXIT AREA	BLADE TIP CLEARANCE
			ANNULUS		BLOCKAGE PLATES				ANNULUS		THROAT	VANE SPACING		
					O. D.		I. D.							
			HEIGHT INCHES	AREA (INCHES)^2	HEIGHT INCHES	%	HEIGHT INCHES	%	HEIGHT INCHES	AREA (INCHES)^2	AREA (INCHES)^2	* INCHES	INCHES^2	INCHES
A. EVALUATION OF MERIDIONAL CONSTRICTION ON NOZZLES	1	CYLINDRICAL WALLS	0.478	2.747					0.478	1.484	0.536	0.910		
	2	BEST OUTER WALL INNER WALL VARIATION NO. 1	0.491	2.484					0.491	1.746	0.389	0.910		
	3	BEST OUTER WALL INNER WALL VARIATION NO. 2	0.850	3.043					0.500	1.806	0.440	0.900		
	4	OUTER WALL VARIATION NO. 2 BEST INNER WALL OF TESTS 1 AND 2	0.660	2.430					0.480	1.711	0.624	0.890		
B. EFFECT OF HIGH STATOR MEAN EXIT	5	PRESSURE	0.491	2.484					0.491	1.746	0.549	0.910		
C. EFFECT OF INLET TURBULENCE	6	TURBULENCE SCREEN NO. 2												
D. EFFECT OF STATOR INLET BOUNDARY LAYER AND FLOW DISTORTION	7	INNER BOUNDARY INCREASED TO 5% OF BLADE HEIGHT			0.063	9.5								
	8	OUTER BOUNDARY LAYER INCREASED TO 5% OF BLADE HEIGHT					0.059	8.8						
	9	INNER AND OUTER BOUNDARY INCREASED 10% OF BLADE HEIGHT			0.063	9.5	0.059	8.8						
	10	PIPE FLOW OR NOMINAL VELOCITY DISTRIBUTION	0.660	2.430	0.171	25.8	0.160	24.2	0.480	1.711	0.624	0.890		
	11	HIGH VELOCITY ON OUTER WALL					0.160	24.2						
	12	HIGH VELOCITY ON INNER WALL			0.171	25.8								
E. EVALUATION OF STATOR EXIT FLOW DISTORTION EFFECTS ON ROTOR CASCADE PERFORMANCE	13	PIPE FLOW OR NOMINAL VELOCITY DISTRIBUTION	0.666	2.522	0.174	26.3	0.163	24.5	0.485	1.759	1.204	0.818		
	14	HIGH VELOCITY ON OUTER WALL												
	15	HIGH VELOCITY ON INNER WALL												
	16	HIGH VELOCITY ON INNER WALL												0.010
	17	HIGH VELOCITY ON OUTER WALL												
	18	PIPE FLOW OR NOMINAL VELOCITY DISTRIBUTION												
F. EVALUATION OF SECOND ROTOR LOADING	19	SECOND ROTOR BLADE DESIGN OF PHASE I												0.031
G. EFFECT OF COOLING ON STATOR PERFORMANCE	20	NO FLOW-CALIBRATION CHECK	0.660	2.430					0.480	1.711	0.624	0.890		
	21	a. PRESSURE SIDE HOLES ONLY b. SUCTION SIDE HOLES ONLY											0.0519	
	22	TRAILING EDGE HOLES ONLY											0.1139	
	23	OUTER WALL HOLES AND INNER WALL HOLES ONLY											0.6225	
	24	ALL CONFIGURATIONS SIMULTANEOUSLY WITH DESIGN FLOWS											0.6942	
	24a	SUCTION & PRESSURE HOLES ADDED DOWNSTREAM - ALL COOLING HOLES FLOWING											0.7461	
NOZZLE SOLIDITY EFFECT ON PERFORMANCE	24b	NOZZLE SOLIDITY REDUCED 30%, COOLING FLOW VARIED	0.670	2.545	0.176	26.5	0.165	24.6	0.490	1.736	0.704	1.225	0.6942	
H. EFFECT OF STATOR COOLING ON TWO ROTOR SOLIDITIES AND AXIAL SPACING	25	TOTAL COOLING FLOW	0.666	2.522	0.174	26.3	0.163	24.5	0.485	1.759	1.204	0.818	0.6942	
	26	TOTAL COOLING FLOW											0.6942	0.020
	27	EVERY OTHER ROTOR BLADE REMOVED												0.031
	28	INCREASED AXIAL SPACING												0.069

of: (1) cylindrical inner and outer walls, (2) a contoured outer wall with a cylindrical inner wall, (3) the same contoured outer wall as Configuration 2 with a contoured inner wall, and (4) the second contoured outer wall and a cylindrical inner wall (Figure 74).

Test Results

Test data was reduced in the form of Calcomp plots, exit contour plots, blade loading diagrams for the nozzle as a function of static pressures, and exit static pressure distributions. In addition, average total efficiencies were calculated for the particular configuration.

The nozzle vane pressure loss radial distributions obtained from the four endwall configurations are shown in Figures 96 through 99. Initial difficulties with the operation of the MTS system, explained in a previous section, clouded the comparisons of average loss. The radial distribution and the loss level appear to be consistent with the loss indicated from the MTS in terms of nozzle efficiency. The comparison of the configurations is summarized as follows:

NOZZLE EFFICIENCY

Configuration	Traverse (Area Average)	MTS	P1/P4 (Cascade Total Pressure Ratio)
Design	87.4	87.4	2.70
1	80.1	78.0	2.90
2	89.1	87.5	2.56
3	83.3	78.0	2.27
4	85.9	78.0	2.30

The comparison of the measured radial pressure loss distribution with the design distribution showed that the endwall losses were substantially higher than anticipated. The data also shows that a large variation exists in the circumferential direction, indicating the presence of strong three-dimensional flows. All of the data comparisons were made at conditions which were as close to the design value as practical within the rig stabilization time.

The survey data indicated that of the four configurations, Configurations 2 and 4 showed the best or closest to design efficiency distributions. Figure 100 shows Mach number versus radius at the exit as compared to the design requirements for Configuration 2. It was noted that the tip section meets design requirements, whereas the hub shows definite underturning and an indication of high loss. This is confirmed in Figure 101, which shows the flow angle distributions versus radius.

A similar set of curves is presented for Configuration 4 in Figures 102 and 103. In this case, the data presented is at a total-to-static pressure ratio of 2.3, which is somewhat lower than design. The survey data indicates that this configuration shows much higher losses than Configuration 2.

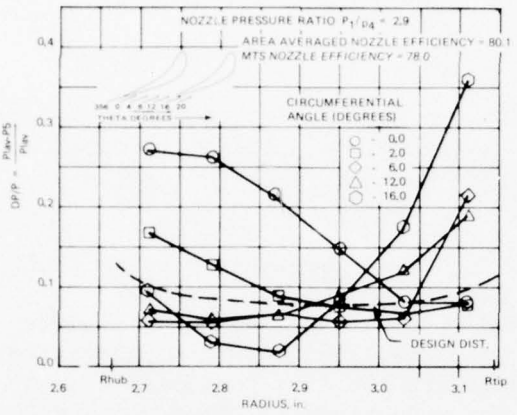


Figure 96. Test Series A - Configuration 1 - Nozzle Local Total Pressure Loss Distribution.

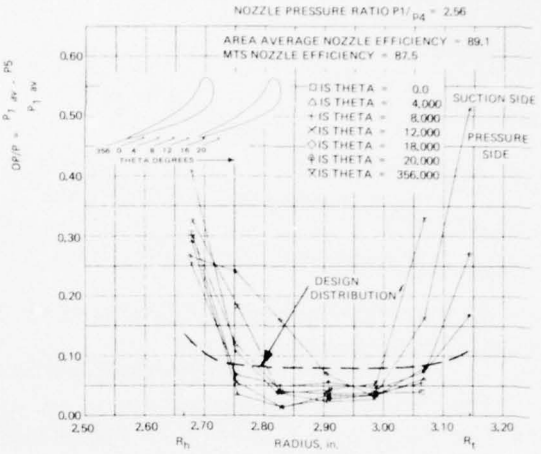


Figure 97. Test Series A - Configuration 2 - Nozzle Local Total Pressure Loss Distribution.

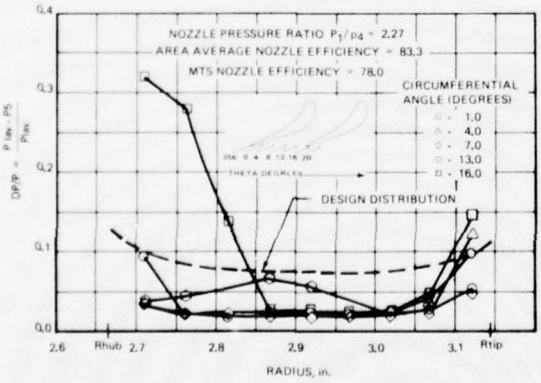


Figure 98. Test Series A - Configuration 3 - Nozzle Local Total Pressure Loss Distribution.

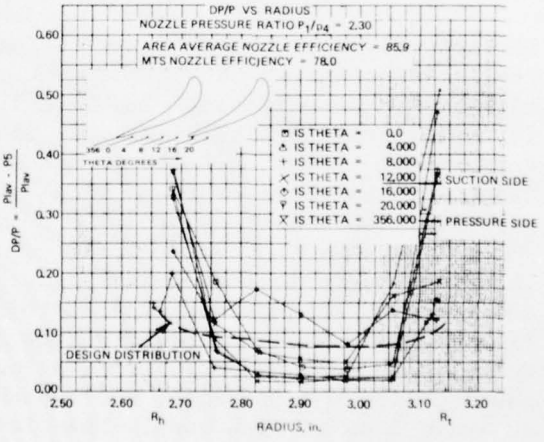


Figure 99. Test Series A - Configuration 4 - Nozzle Local Total Pressure Loss Distribution.

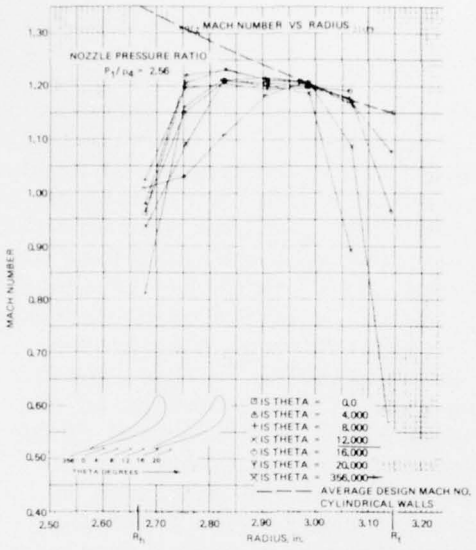


Figure 100. Test Series A - Configuration 2 - Nozzle Exit Mach Number Distribution.

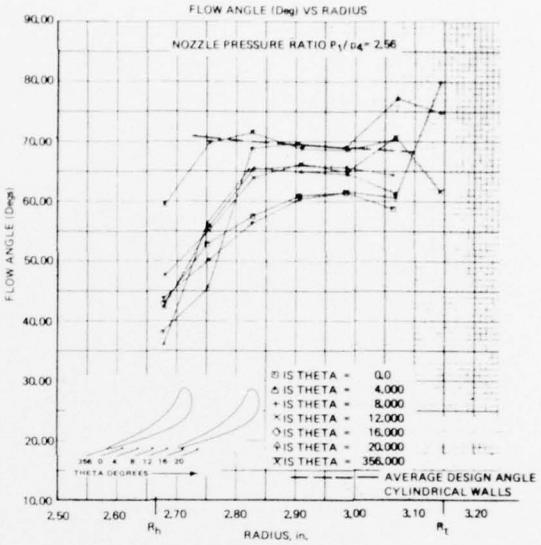


Figure 101. Test Series A - Configuration 2 - Nozzle Exit Flow Angle Distribution.

Figure 103 also shows that underturning in the hub at some circumferential positions is as low as 30°, which would be indicative of hub separation.

Figure 104 summarizes the exit total pressure contour as a function of radius and circumferential angle for the four configurations. The data is presented for cascade total pressure ratios as close to design value as could be achieved with various configurations. The contour plots are given in terms of local exit pressure average. As such, they represent a pressure defect when the value becomes less than zero. The contour plots illustrate a total pressure loss defect in the inner and outer walls, and the total pressure loss appears to be significantly higher at the inner radii in each of the four configurations. Of the four configurations, number 2 appears to have the lowest loss in terms of total pressure parameter and the most uniform total pressure distribution as a function of radius.

A comparison of all four configurations on the basis of total pressure loss coefficient versus percentage blade span at mid-passage is given in Figure 105. This survey data shows that, by comparison, the lowest losses here are incurred by the wall configurations of geometry 2 and geometry 4. Cylindrical wall configuration 1 shows substantially larger losses in the region of the outer radii. Configuration 3, on the other hand, shows high losses on both walls. Of the two remaining configurations under consideration, only one data point separates the performance superiority of Configuration 4 over Configuration 2.

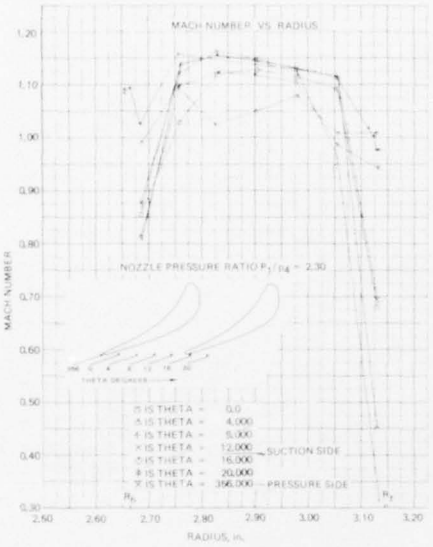


Figure 102. Test Series A - Configuration 4 - Nozzle Exit Mach Number Distribution.

Local static pressure distributions at the mid-passage of the nozzle, as a function of axial chord, are given in Figures 106 through 109. The most significant feature of these curves is the static pressure distribution on the suction side in the near 80 to 100 percent section. The curves indicate that with the exception of Configuration 1, which has cylindrical walls, there is little or no indication of separation on the suction side of the blading in this region. In the case of Configuration 1, the static pressure at a location of 82 percent chord shows a lower static pressure than at the discharge of 100 percent chord. The remaining configurations show either acceleration or minor differences in static pressure at this station.

The set of curves showing the exit static pressure distribution on the inner and outer walls, Figures 110 through 113, are most interesting from the standpoint of indicators of separation. Any change in inner or outer static pressure which constitutes a step increment would be an indicator of separation. With the exception of Configuration 2, on its outer wall, all four wall configurations indicate this separation trend. Configuration 2 does indicate, however, a separation trend on the inner wall on the suction side of the vane which is consistent with the outer three wall configurations. It is judged that of the four configurations, however, Configuration 2 is the least separation prone over the entire vane surface.

Additional information indicating that Configuration 2 has the best overall characteristics of the four tested is given in Test Series B. Here a comparison from the momentum transfer system efficiencies is given as a function of high stator exit mean Mach numbers.

TEST SERIES B - EVALUATION OF HIGH STATOR MEAN EXIT MACH NUMBER ON STATOR AND ROTOR PERFORMANCE

Test Objective

The test objective of this sequence was to determine the nozzle cascade performance at several Mach numbers. In this case, torque was recorded on all runs and converted to a loss curve as a function of Mach number. This test series, as in the previous set of runs, incorporated turbulence screen 1, which was designed to produce a turbulence intensity of 3.7 percent at the vane inlet.

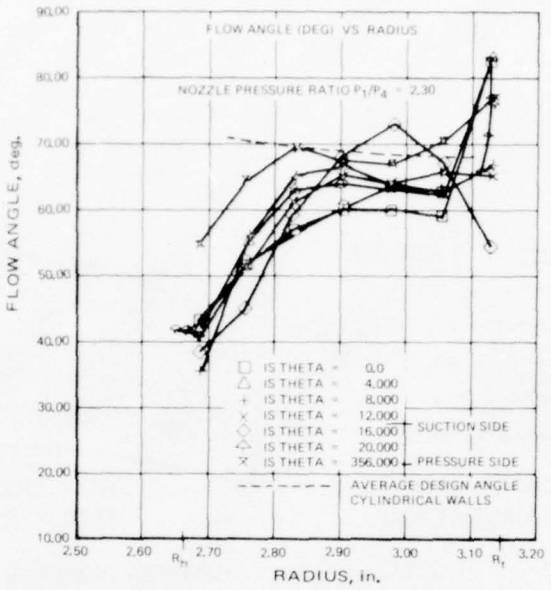


Figure 103. Test Series A - Configuration 4. Nozzle Exit Flow Angle Distribution.

Test Results

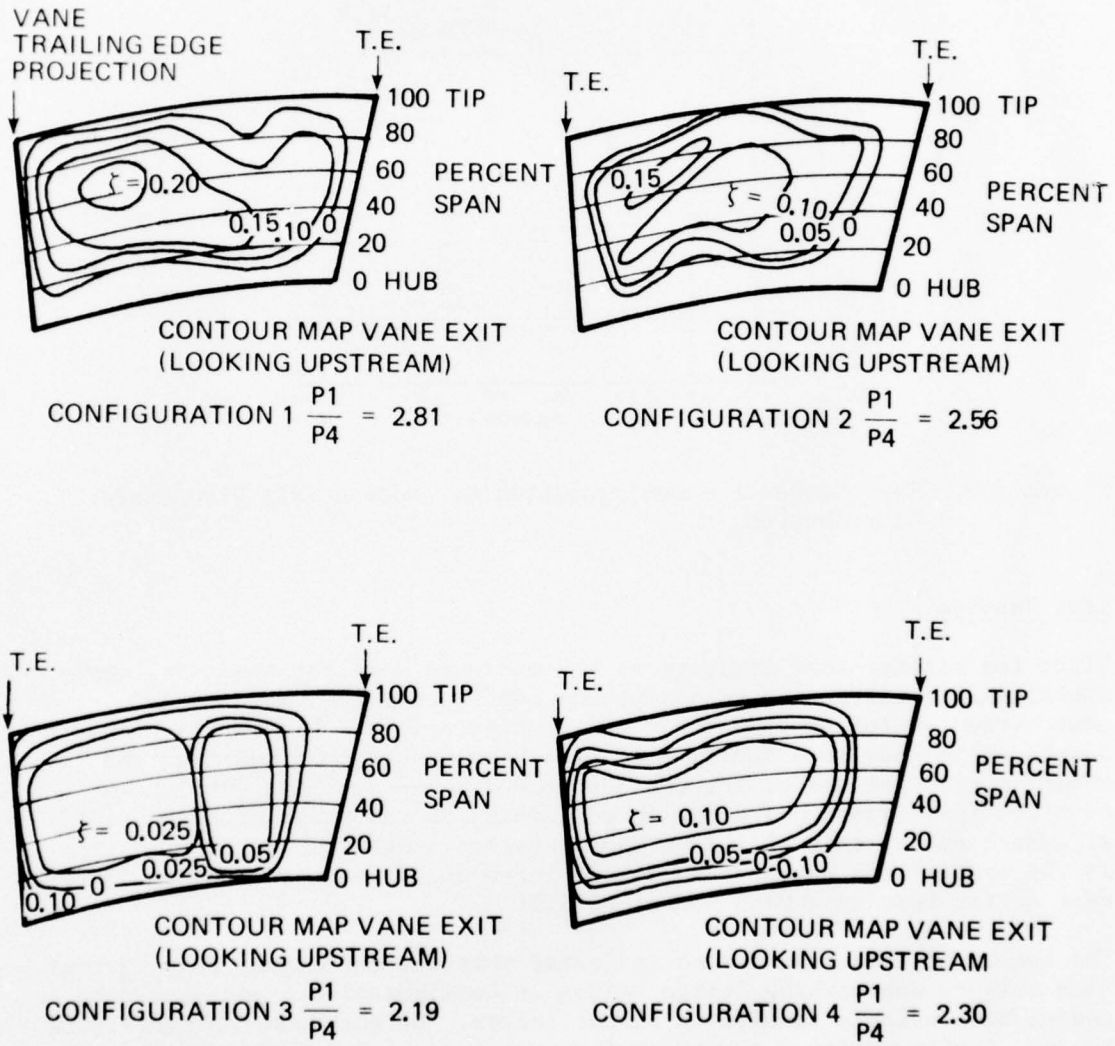
Since the earlier test evaluations had narrowed down the candidate meridional wall constriction to an optimum configuration, 2 or 4, this test series evaluated only these two configurations. Figure 114 presents nozzle efficiency as a function of exit Mach number obtained from the momentum transfer system for Configurations 2 and 4. This data shows that Configuration 4 peaks out in efficiency on the order of 80 percent at a Mach number exit of 1.15. Configuration 2 again shows superiority at the higher Mach numbers and demonstrates an efficiency level of 93 percent at the test exit Mach number of 1.3.

The result of this test series indicated that the efficiency peaks out at Mach numbers approaching design values on Configuration 4 and exceeding design Mach numbers results in higher losses. Of the four configurations tested, Configuration 2 showed performance approximating that which was desired.

TEST SERIES C - EFFECT OF INLET TURBULENCE

Test Objective

Test Series C evaluates the effect of different inlet turbulence intensity levels on the nozzle cascade performance. Turbulence intensity levels were artifically induced using screens of different wire size and mesh placed



$$\zeta = \frac{P_{5_{LOCAL}} - P_{5_{AVERAGE}}}{P_{5_{AVERAGE}}}, \quad P_{5_{AVERAGE}} = \text{AREA AVERAGE OVER ONE PITCH SECTOR OF MEASURING PLANE}$$

Figure 104. Normalized Total Pressure Contours.

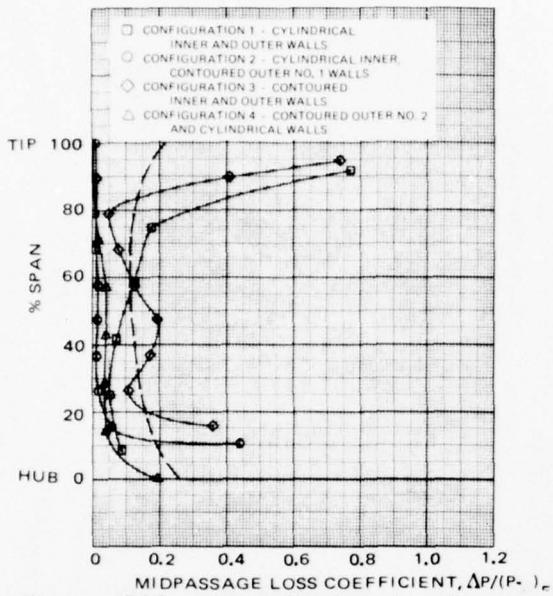


Figure 105. Test Series A - Pressure Loss Coefficient Comparison of Wall Configurations.

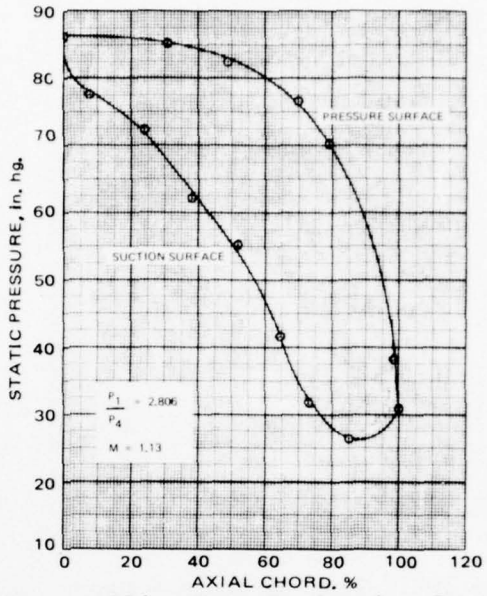


Figure 106. Test Series A - Configuration 1 - Blade Loading Diagram at ≃ Pinlet/Psexit = Design - Cylindrical Walls.

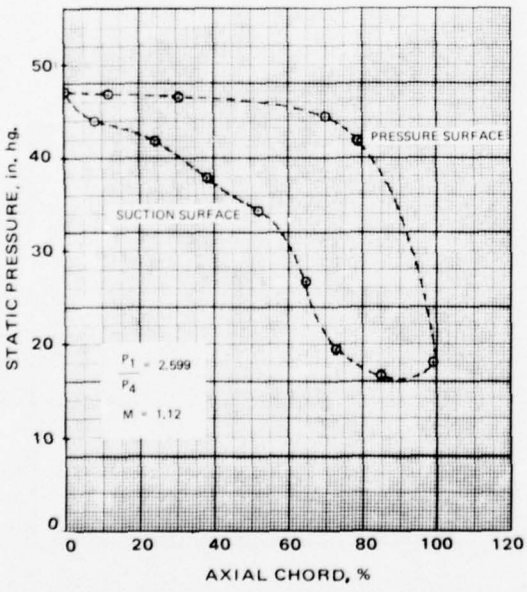


Figure 107. Test Series A - Configuration 2 - Blade Loading Diagram at ≃ Pinlet/Psexit = Design.

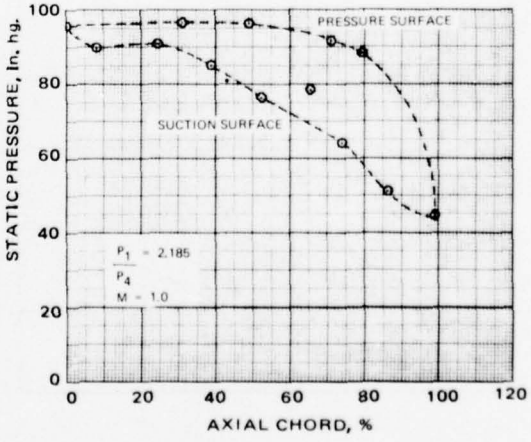


Figure 108. Test Series A - Configuration 3 - Blade Loading Diagram at ≃ Pinlet/Psexit = Design.

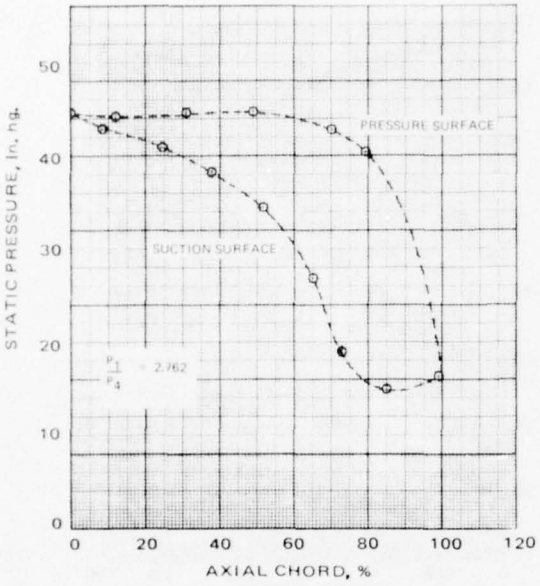


Figure 109. Test Series A - Configuration 4 - Blade Loading Diagram at P_{inlet}/P_{sexit} = Design.

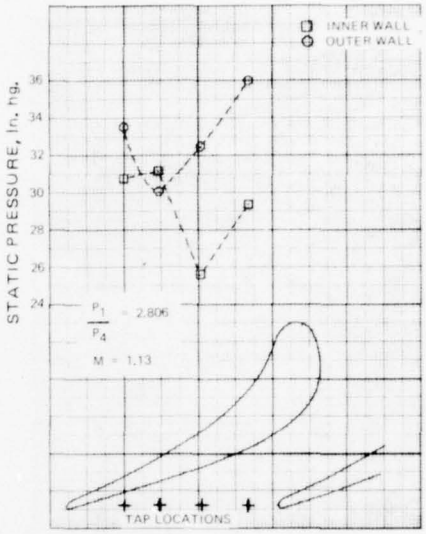


Figure 110. Test Series A - Configuration 1. Exit Pressure Distribution on Inner and Outer Walls.

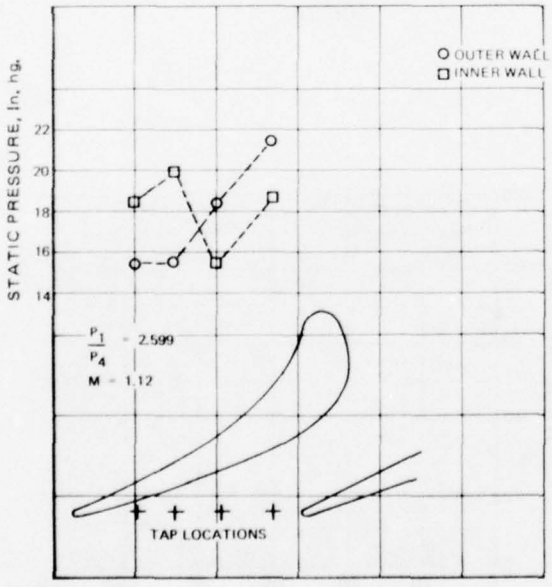


Figure 111. Test Series A - Configuration 2. Exit Pressure Distribution on Inner and Outer Walls.

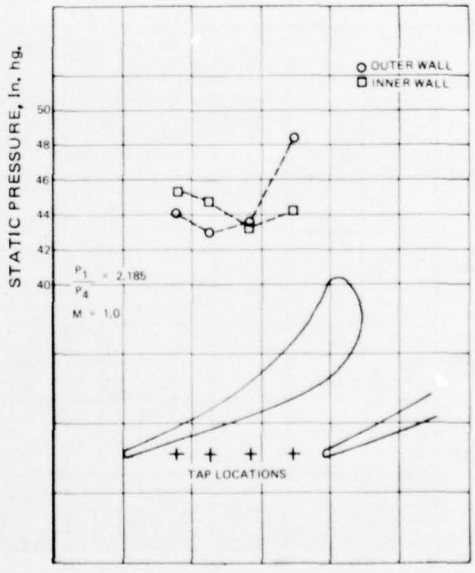


Figure 112. Test Series A - Configuration 3 - Exit Pressure Distribution on Inner and Outer Walls.

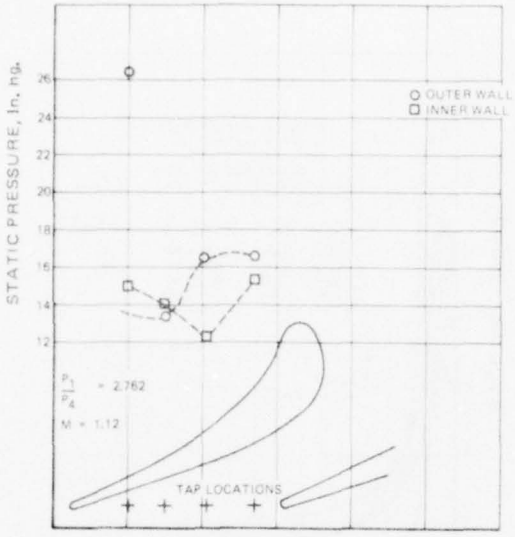


Figure 113. Test Series A - Configuration 4 - Exit Pressure Distribution on Inner and Outer Walls.

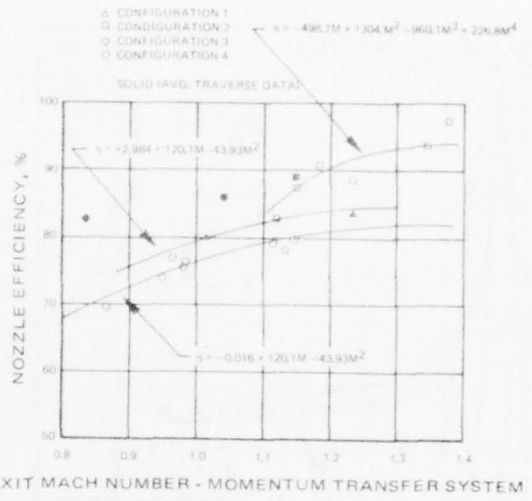


Figure 114. Test Series B - Nozzle Efficiency From Momentum Transfer System Versus Exit Mach Number.

upstream of the nozzle leading edge. The turbulence intensity was calculated from measured values of bridge voltage and RMS voltage using equipment described in the previous section in conjunction with a hot film anemometer which was calibrated in the Teledyne CAE flow facility.

Test Results

The inlet turbulence measurements for Test Series C are shown in Figure 115 and 116 together with the baseline low turbulence screen. The wall configurations tested were the contoured outer and cylindrical inner, number 2 and number 4. Also listed is the inlet Mach number and Reynolds number and the nozzle exit absolute Mach number. Several Reynolds numbers were run by varying the inlet pressure over the range from 18 psia to 36 psia. Nozzle pressure ratio was set for each test by using the vacuum exhaust control.

Examination of Figures 115 and 116 shows that high turbulence intensity exists near the wall, the value being several times that near mid-channel. This phenomenon is well known (Reference 39, pp. 466), as is shown in Figure 117; however, no analytical procedure was available to include that effect during the design analysis. The low intensity screen, screen one, produced nearly the expected value of 3.7 percent near mid-channel with a peak near the wall of 11 percent, while screen two produced much less than expected. The intensity showed a strong dependence on Reynolds number, particularly near the wall, with the higher Reynolds number producing the greater turbulence.

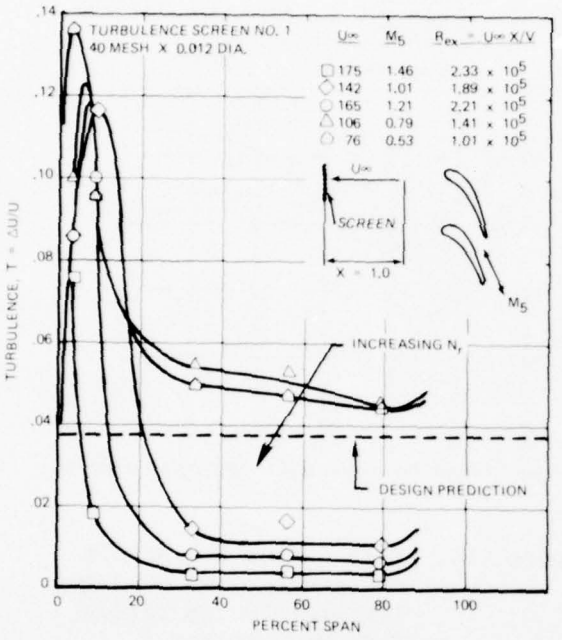


Figure 115. Test Series C - Configuration 4 - Effect of Inlet Reynolds Number on Turbulent Intensity.

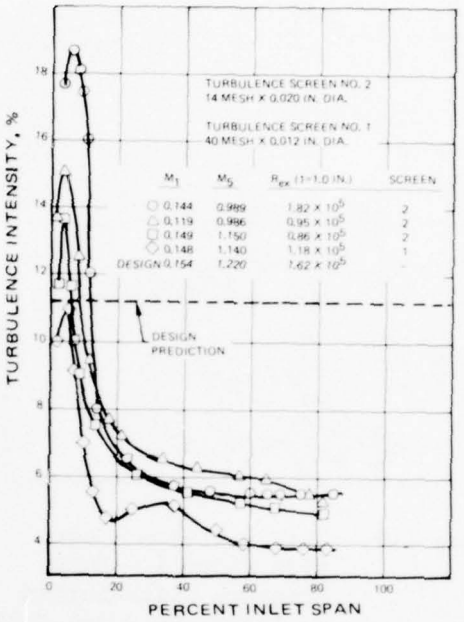


Figure 116. Test Series C - Effect of Reynolds Number on Turbulence Intensity for Configuration 2.

The traverses were performed from the inner toward the outer wall so that the inner wall boundary layer wall was always penetrated. The outer wall boundary layer was penetrated on only one test, and the hot film anemometer bumped the outer wall failing the instrument. All other tests were traverses to approximately 80 percent passage height to prevent hot film failures. The test which did traverse the complete span indicated significantly lower outer wall turbulence with respect to the inner wall.

A TSI-Model 1060 RMS voltmeter was used to record the root mean square of the axial velocity fluctuations detected by the hot wire anemometer. As a visual check, an oscilloscope was wired into the hot film circuit. Figure 118 shows photographs of some oscilloscope traces from the hot film output at various locations through the inner boundary layer. The low frequency peaks represent noise which is filtered out in the RMS voltmeter. High frequency data, which appear as thick trace lines, represent the RMS value of the axial velocity fluctuations. The corresponding voltmeter reading is shown by each picture. Comparison of the readings at 6 percent height and at 20 percent height, illustrates the decrese in magnitude of fluctuations as the probe moved away from the inner wall.

Figure 119 presents the measured inlet turbulence intensity at the midspan as a function of Reynolds number for the two nozzle wall configurations and the two screens. Over the range of Reynolds numbers tested, turbulence intensity was little affected in the mid-passage by variations in this

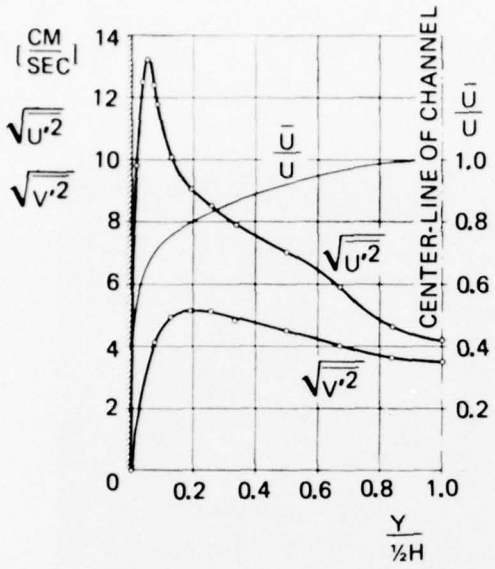


Figure 117. Measurement of Fluctuating Turbulent Components in a Wind Tunnel (Reference 39).

parameter. This is contrary to the strong effects as measured near the wall extremeties of Figures 115 and 116.

Figure 120 gives the efficiency fall off of nozzle wall Configuration 2 due to screen turbulence intensity changes. Increasing turbulence intensity results in increased nozzle losses. Similar data, presented in Reference 38, confirms this trend.

TEST SERIES D - EVALUATION OF STATOR INLET BOUNDARY LAYER AND FLOW DISTORTION

Test Objective

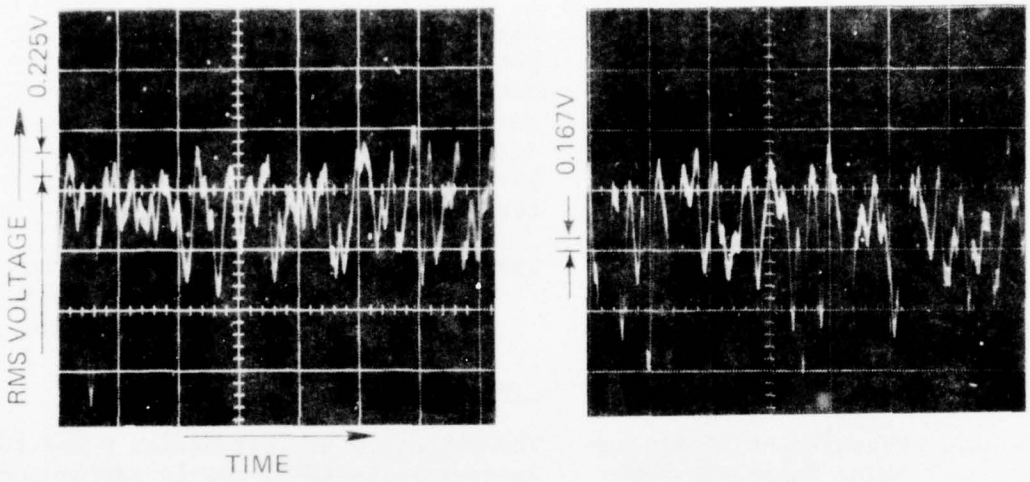
The objective of Test Series D was to determine the ASATT nozzle performance under various inlet velocity perturbations. Hot film anemometer measurements were taken as described in the preceding sequence dealing with inlet turbulence. Six tests were performed in this sequence, each producing a different inlet velocity profile.

Test Results

The velocity profile was artifically induced using blockage plates located in the plane of the distortion screen. The magnitude of the induced velocity defect was estimated using a superposition of the plate height on the boundary layer at the screen as calculated from flat plate theory. A geometric summary of the blockage plates used at the inner and outer walls is given in Table 13.

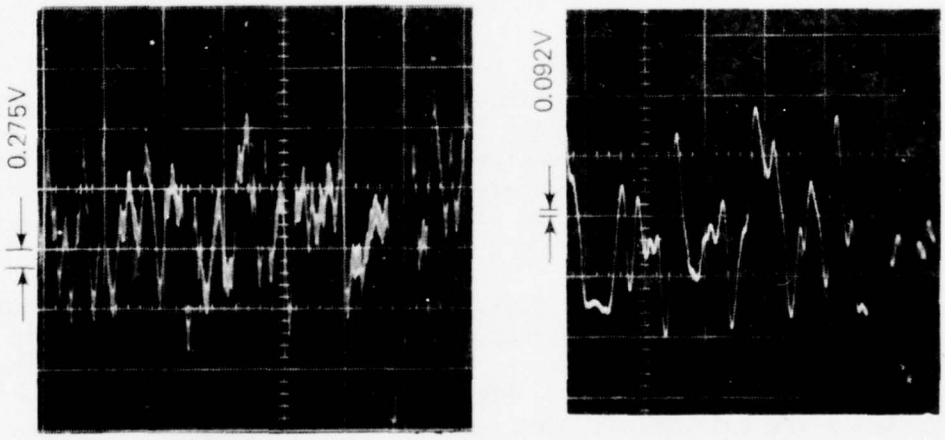
Figure 121 shows the inlet velocity distribution measured for the baseline (zero blockage), together with the inner, outer, and inner and outer combined plates. The performances of these configurations are summarized in Table 14. The traverse data shown in Figure 122 was area averaged and a nozzle efficiency was calculated. The results show that the increased boundary layer on the inner wall causes the largest decrease in efficiency. Inner and outer wall boundary layer increase caused a lesser reduction in nozzle efficiency compared to the inner and outer alone. Figure 123 shows the velocity distributions produced using a blockage plate to significantly distort the inlet flow field in three distinct modes, high outer wall, high inner wall and pipe flow velocity distributions.

The efficiencies of the flow distortion tests are also shown in Table 14. It is interesting to note that the decrement in nozzle efficiency was greater for the inner wall blockage and least for the inner and outer combined.



3 PERCENT HEIGHT
RMS = 0.225V
τ = 17.5%

10 PERCENT HEIGHT
RMS = 0.167V
τ = 16.0%



6 PERCENT HEIGHT
RMS = 0.275V
τ = 18.6%

20 PERCENT HEIGHT
RMS = 0.092V
τ = 7.3%

Figure 118. Hot Film Anemometer Output - Typical Oscilloscope Trace.

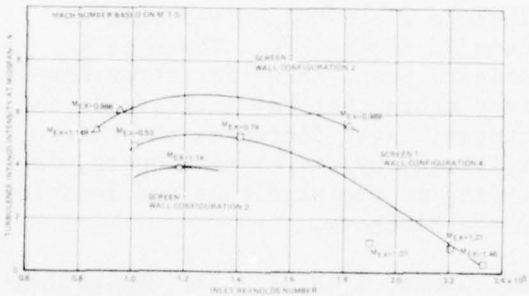


Figure 119. Test Series C - Effect of Inlet Turbulence.

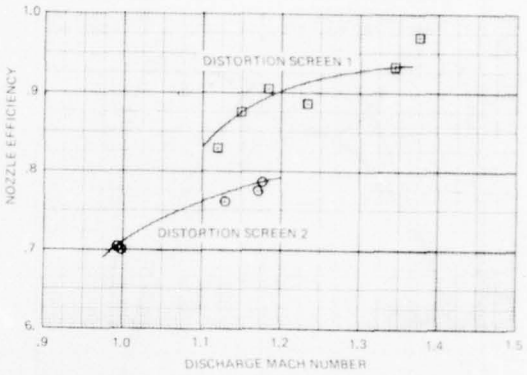


Figure 120. Effects of Turbulence on Nozzle Performance (Configuration 2).

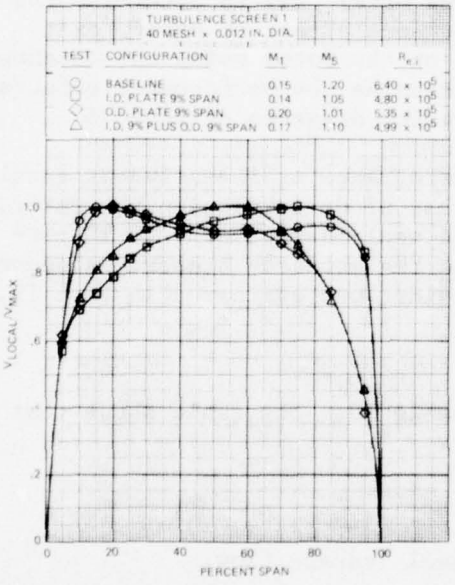


Figure 121. Test Series D - Configuration 2 - Effect of Stator Inlet Boundary Layer.

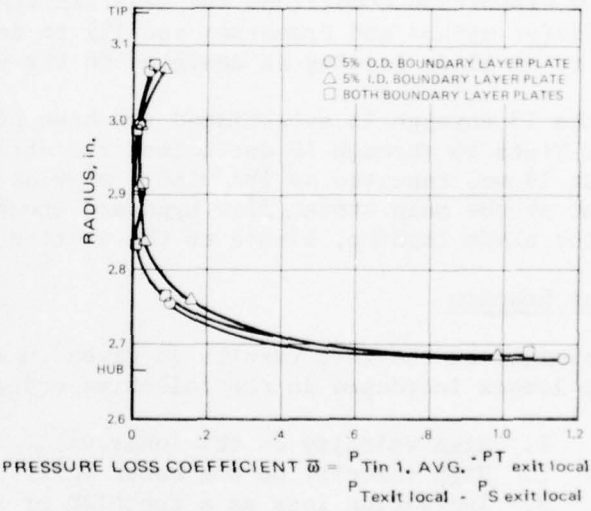


Figure 122. Test Series D - Configuration 2 - $\bar{\omega}$ Midpassage Versus Radius Versus Boundary Layer Based on 8° Circumferential Surveys.

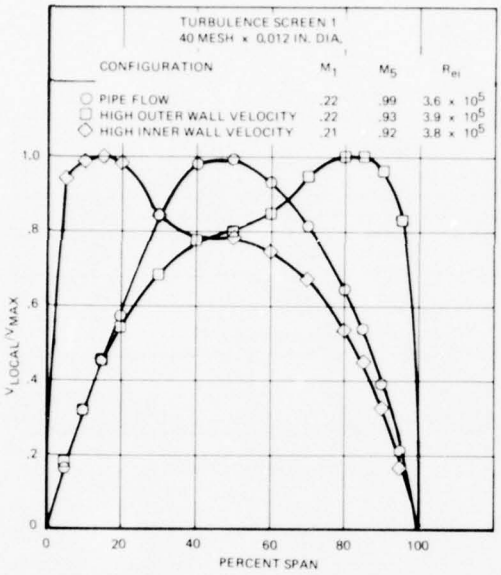


Figure 123. Test Series D - Configuration 4 - Effect of Stator Inlet Flow Distortion.

A method to show the effect of inlet boundary layer thickness on nozzle efficiency was sought, and a graph of efficiency decrement as a function of blockage plate height was made as shown in Figure 124. There is a definite trend shown for three distinct cases that the increase in inlet boundary layer decreases the nozzle efficiency by differing amounts, depending on the magnitude and location of the blockage.

TEST SERIES E AND F - E: EVALUATION OF STATOR EXIT FLOW DISTORTION AND SIMULATED LABYRINTH SEAL LEAKAGE ON ROTOR CASCADE PERFORMANCE
F: EVALUATION OF SECOND ROTOR LOADING

Test Objectives

The test objectives of these two sequences were: (1) to determine the performance effect of stator exit flow distortion conditions and seal leakage on the rotor using the momentum transfer method and traverse; and (2) to determine the performance effects of rotor blade loading as designed to the vector diagrams of Phase I.

Tests 13 through 15 established the base performance of the actuator nozzle, and Tests 16 through 18 determined the effects of distortion on the rotor. Test 18 was repeated as 18A with a simulated seal leakage of 0 to 10 percent of the main stream flow bypassed around the actuator stator. A second rotor blade loading, biased to the suction side, was evaluated in Test 19.

Test Results

A summary of the test results is given in Table 15. The table shows that the losses increased in the following order:

1. High velocity on the inner wall.
2. High velocity on the outer wall.
3. Increasing loss as a function of seal leakage flow.

A corresponding decrement in efficiency due to each parameter variation is provided and ranges from 1.8 to 6.0 points.

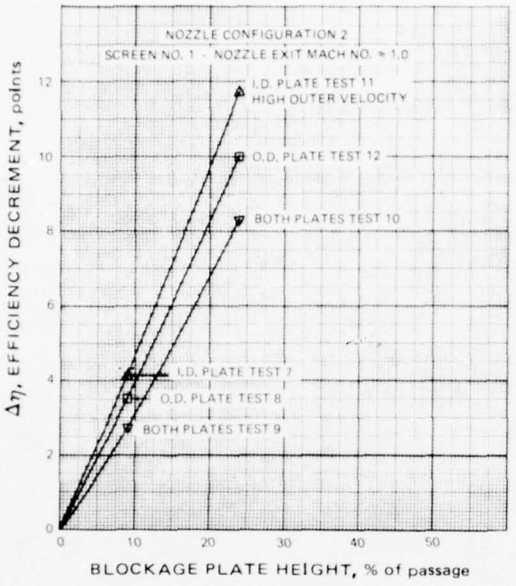


Figure 124. Nozzle Efficiency Decrement as a Function of Blockage Plate Height.

The efficiency of the stator cascade was determined without reliance on survey probe data by applying the momentum transfer principle of loss measurement as described previously. The actuator stator performance was determined from survey and momentum methods and was found to produce the desired rotor relative characteristics. The measured angle distribution is shown in Figure 125.

In a similar manner, the effect of loading distribution on the rotor was determined in Test Series F. Reference to Table 15 and comparing the corrected torque on configurations with a pressure side loading and suction side loading shows that torques on the SLR rotor are 0.9 percent higher than those on the PLR rotor.

Seal leakage was varied from 0 to 10 percent main flow. The effect on the rotor is also shown in Table 15. In this case, 7 percent of the main stream flow bypassed the nozzle and entered the rotor. The change in rotor efficiency amounted to a loss of 6 points. This is an equivalent in stage performance of nearly one point for each percent bypass leakage across the nozzle.

TEST SERIES G: EFFECT OF COOLING AND SOLIDITY ON STATOR PERFORMANCE

Test Objective

The effects of solidity and cooling injection on the performance of the nozzle were, primarily, determined from the momentum-transfer system. Inlet conditions were set on the nozzle to produce the approximate design exit Mach number and this Mach number was maintained constant with and without cooling injection.

Test Results

The test results of the entire test series G are summarized in Figure 126. Efficiency change from the nominal nozzle to efficiency with cooling injection or nozzle solidity effects are plotted as a function of percent cooling flow to primary flow. A curve corresponding to Test 21 shows the loss in efficiency on the nozzle as a function of pressure and suction side cooling holes only. One data point was taken to simulate a total pressure side and suction side cooling of 4.5 percent. The loss in efficiency was shown to be 2.5 points.

TABLE 14

SUMMARY OF PRESSURE LOSS FOR BOUNDARY LAYER AND FLOW DISTORTION

Configuration	M1	M5	η Traverse	$\Delta \eta$
Baseline Configuration 2 (Screen 1)	0.15	1.20	89.73	---
Inner Wall Baseline	0.14	1.05	85.65	4.08
Outer Wall Baseline	0.29	1.01	86.20	3.53
Inner and Outer Baseline	0.17	1.10	86.84	2.89
Pipe Flow Blockage Plates	0.22	0.995	81.30	8.43
High Velocity Inner Wall	0.22	0.93	79.60	10.13
High Velocity Outer Wall	0.21	0.90	77.90	11.83

TABLE 15

SUMMARY OF EVALUATION OF STATOR EXIT FLOW DISTORTION
AND LEAKAGE EFFECTS ON ROTOR CASCADE PERFORMANCE

TEST NO.	VARIABLE	MOMENTUM RIG CONFIG. NOZZLE	ROTOR	TORQUE/LB. INLET FLOW ** (CORRECTED)	TORQUE CHANGE (NORMALIZED)	TORQUE CHANGE - ROTOR (NORMALIZED)	CHANGE IN EFFICIENCY	LEAKAGE BY-PASS FLOW
13	Pipe Flow - Nominal Velocity Distribution	Actuator	Slave	45.08	0	---	---	0
14	High Velocity on Outer Wall	Actuator	Slave	43.06	2.02	---	---	0
15	High Velocity on Inner Wall	Actuator	Slave	41.02	4.06	---	---	0
16	High Velocity on Inner Wall	Actuator	Locked Nominal	93.89	6.49	2.45	-1.8 points	0
17	High Velocity on Outer Wall	Actuator	Locked Nominal	92.54	7.84	5.82	-4.35 points	0
18	Pipe Flow or Nominal Velocity Distribution	Actuator	Locked Nominal	100.38	0	0	0	0
18a	Seal Leakage Test	Actuator	Locked Nominal	92.29	8.09	8.09	-6 points	7.0%
19*	No. 2 Rotor	Actuator	Locked Nominal #2	101.26	0.88	---	+0.9 points	0

* Evaluation of Second Rotor Loading
** Torque in inch/lbf

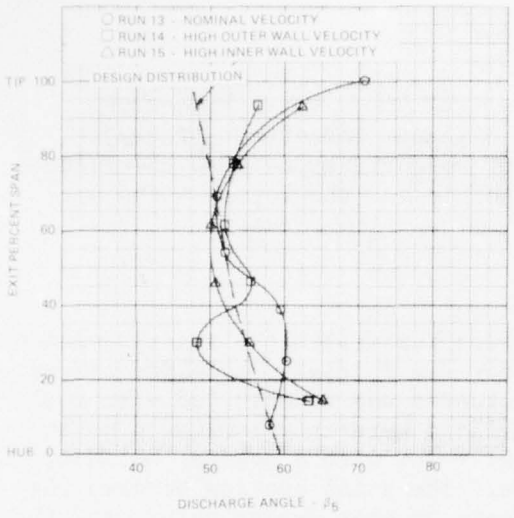


Figure 125. Test Series E - Actuator Nozzle Discharge Angle at 12° Circumferential Survey.

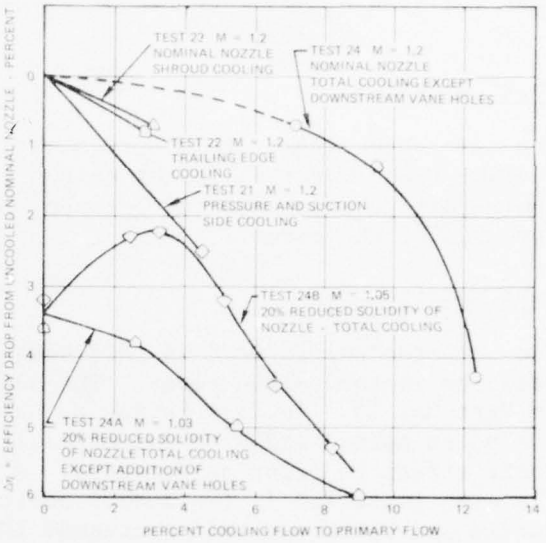


Figure 126. Test Series G - The Effect of Cooling and Solidity on Stator Performance.

Test 22 evaluated the effect of trailing-edge cooling alone. In this case, 3 percent trailing-edge cooling was ejected from the nozzle. The loss in efficiency corresponded to less than one percentage point.

Test 23 gives the effect of shroud cooling alone. In this test, three percent of the mainstream flow was used for cooling the shrouds. Again, less than one point loss in efficiency can be attributed to shroud cooling.

Test 24 gives the combined effect on the nominal nozzle with shroud cooling, trailing-edge cooling, suction side cooling, and pressure side cooling. It may be noted that the loss with combined cooling is less than the loss for the individually injected cooling flows. This result may be attributed to the possible maldistribution of the individual flows as compared to the redistribution of combined cooling flow and main flow causing a beneficial net effect on the flow field.

Test 24B gives the combined effect of a reduction of 20 percent in nozzle solidity and the total cooling effects. A 20-percent reduction in nozzle solidity alone results in a 3.8-point loss in efficiency. As the cooling flow was increased from 0 to 10 percent, a minor increase in efficiency occurs on the reduced solidity nozzle configuration. This can be attributable to a pressure to suction side cross flow occurring at zero percent cooling flow. In any case, the increase appears to be within experimental accuracy. The additional downstream suction side cooling holes resulted in further decreases in nozzle efficiency. At a total cooling flow of 6 percent, the decrement amounts to about 1.4 percent loss in efficiency.

TEST SERIES H - EFFECT OF STATOR COOLING ON TWO ROTOR SOLIDITIES AND AXIAL SPACING

Test Objective

The test objective on this series was to evaluate the effect of stator cooling flow injection losses on two rotor solidities and also to evaluate the effect of axial spacing between the nozzle and the rotor on the performance of the rotor.

Test Modification

The actuator nozzle used in this test series duplicates the relative inlet velocity vector to the rotor. The actuator was initially baseline tested in Test No. 13. In Test Series H, the actuator was reinstalled with cooling holes opened and a series of cooling flows were then evaluated as to their effect on rotor performance. A test rotor with a nominal solidity was also installed in the locked position. The axial spacing between the nozzle and rotor was then increased 100 percent over design value, and the tests were repeated. In a similar manner, an alternate rotor solidity was also evaluated. The test sequence consisted of:

Test No. 25 - With slave rotor in place, the total cooling flow rate was varied in four steps, from 0 to 50 percent over maximum, and surveys were taken at the nozzle exit.

Test No. 26 - With the design rotor in place of the slave, Test No. 25 was repeated.

Test No. 27 - The nominal rotor was replaced by a 30 percent reduced solidity rotor, and Test No. 25 was repeated at nominal and zero cooling flow only.

Test No. 28 - The axial space between the stator trailing edge and the rotor leading edge was increased by 100 percent, and Test No. 25 was repeated at nominal and zero cooling flows.

Test Results

The effect of total cooling flow on the actuator performance is given in Figure 127. There, nozzle efficiency as a function of percent cooling to primary flow is given as evaluated from momentum transfer system data. Base efficiency of the actuator nozzle at the mean, design, inlet relative Mach number (0.65) is 95 percent and agrees with predicted values. Increases in cooling flow result, initially, in almost a linear decrease in efficiency. Figure 128 shows the effects of increased axial spacing and reduced rotor solidity as a function of cooling flow for the actuator nozzle. Data is presented in terms of momentum torque changes which approximate efficiency loss.

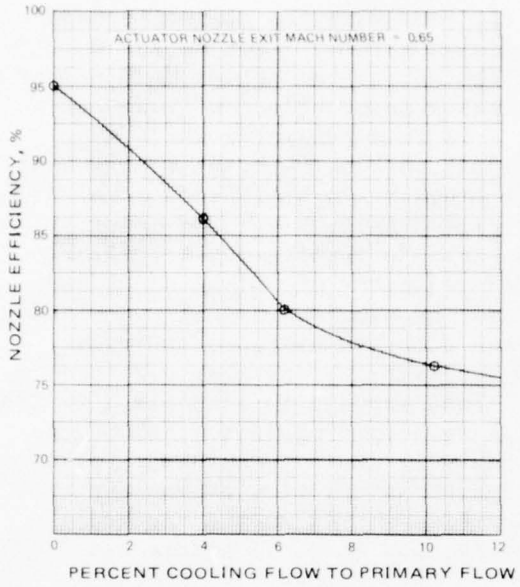


Figure 127. Test Series H - Effect of Total Cooling on Actuator Performance.

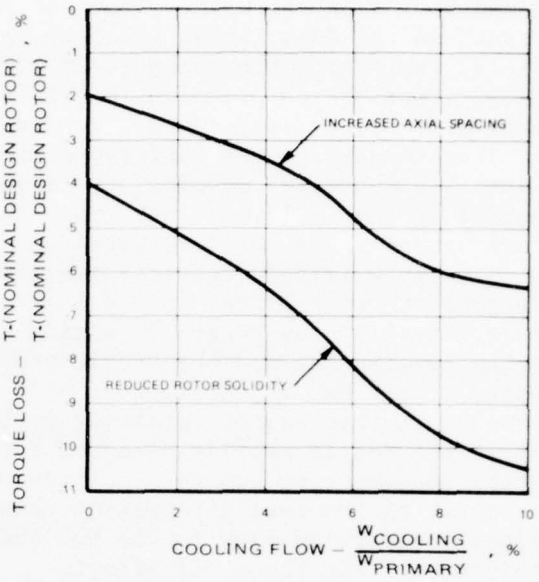


Figure 128. Test Series H - Effect of Axial Spacing and Solidity on Rotor Performance.

A performance comparison of the design rotor with no cooling flow and an increased axial spacing between the nozzle and rotor from 0.25 inch to 0.55 inch shows a loss in efficiency of 2 percent. As cooling flow is increased, the effect becomes more significant, and larger increases in performance loss may be noted at higher cooling flows. This effect is approximately doubled with a cooling flow of roughly 7 percent of the total primary flow.

With no cooling flow, the effect of reducing the rotor solidity by 30 percent is to decrease the torque by four points as obtained from momentum transfer data (Figure 128). This test data indicates that the selection of rotor solidity for design from the ASATT turbine is near optimum.

Additional testing was conducted on the reduced solidity rotor to evaluate the effects of cooling flow in Test No. 27. It may be noted that as cooling flow is increased, the performance fall-off increases substantially. The fall-off on the reduced solidity rotor, however, is smaller than the fall-off on the design rotor, indicating a sensitivity to cooling flow injection when maximum performance is desired.

Cascade Data Evaluation

Phase II test effort consisted of an evaluation of the parameters which would have an impact on the ASATT full round turbine design. Test series A, which evaluated the meridional wall constriction on the nozzles, results in an optimum wall section of Configuration 2, which has a contoured outer

wall and a cylindrical wall. The test efficiency with the nominal screen was confirmed at 89.1, which is close to design values. Test series B confirmed that the performance could still be met at the design Mach number of 1.24. Test series C showed that there was a major effect of turbulence intensity on stator performance; however, this is a parameter which was again investigated in the full-round Phase III testing reported in the next section. In a similar fashion, the stator boundary layer effects were evaluated in the full-round and cross-correlated between cascade information. The nozzle and rotor solidity tests on the cascade verified that the loadings were approximately correct; therefore the number of nozzle vanes and the number of rotor blades can be maintained the same as initially designed. A major impact of the Phase II testing comes from the discharge surveys from the nozzle test and the static pressure distributions that were measured at the hub on the suction side. These surveys indicated a definite separation in this region resulting in high underturning in the hub of the nozzle. The nozzle profile selected for Phase II testing, consisted of a constant section from hub to tip, primarily from simplicity of manufacture. As a result of the test information showing high losses in the tip and completely separated flow in the hub sections, the Phase II nozzle was redesigned for the Phase III effort.

Since most of the test information on the rotor design showed that objectives were met, the rotors of Phase II were preserved for Phase III testing.

CONCLUSIONS

Thirty-eight tests were conducted on the nozzle cascade and rotor cascade combinations. Seven of these tests were rerun, which brought the total test time to over 200 hours. Eight major sequences in testing were conducted to accomplish the program objective as described in the Statement of Work. These test series A through H are described below with the conclusions and test results.

TEST SERIES A - EVALUATION OF MERIDIONAL CONSTRICTION ON NOZZLES

Four wall configurations, including cylindrical walls, were tested over a range of Mach numbers. Inlet conditions were fixed by a nominal screen which produced an average turbulence intensity of about 3.7 percent. Approximate test inlet Reynolds number was 650,000. Test data was obtained with the momentum transfer system and survey information at inlet and exit to the nozzles. The nozzle efficiencies obtained for the four meridional wall configurations are as follows:

Test No. 1 - Cylindrical walls produced a nozzle efficiency of 83.5 percent.

Test No. 2 - Contoured outer wall and a cylindrical inner wall produced a nozzle efficiency of 89.1 percent.

Test No. 3 - Contoured outer wall and inner wall variation No. 2 produced a nozzle efficiency of 83.3 percent.

Test No. 4 - Contoured outer wall variation No. 2 and a cylindrical inner wall produced a nozzle efficiency of 85.9 percent.

Survey data indicated that the highest losses were incurred through the use of cylindrical walls. The highest efficiency was obtained by wall configuration 2, which has a meridional constriction on the outer wall and a cylindrical inner wall. The efficiency of configuration 2 was slightly higher than the design value of 87.4 percent. Blade loading diagrams at the midpassage showed that design requirements were achieved.

However, static pressure data on the inner and outer walls along with survey information indicated that wall losses were still high, and there was a definite indication of separation in the hub region. It is concluded, based on the combination of survey data, static pressure distributions, and the momentum transfer system data, that underturning does occur in the hub region due to the separated flow.

TEST SERIES B - EFFECT OF STATOR MACH NUMBER ON LOSSES

The best wall configurations of test series A were rig evaluated over a range of Mach numbers. Stator exit Mach number was varied from 0.9 to 1.4 on wall configurations 2 and 4. The efficiency on both configurations increased with increasing Mach numbers to a limiting value. Configuration 4 appeared to peak out in efficiency at a Mach number of 1.15, whereas configuration 2 showed increasing efficiencies to a Mach number of 1.4. The design point Mach number for the stator is 1.24. This set of results showed that configuration 2 was the optimum meridional constriction of the four geometries tested and produced an efficiency of over 90 percent.

TEST SERIES C - EFFECT OF INLET TURBULENCE INTENSITY ON STATOR PERFORMANCE

Turbulence intensity on the nozzle configurations was varied by a change in screens at the inlet. Two screens were used: (1) a low-intensity 40 mesh by 0.012 inch diameter, to produce a turbulence intensity of 3.7 percent; and (2) a 14-mesh by 0.020-inch diameter turbulence screen, to produce an average turbulence intensity of 11 percent. The low-intensity screen produced the nearly expected value of 3.7 percent near mid-channel, whereas screen two produced somewhat less turbulence than expected. The intensity showed a strong dependence on Reynolds number near the walls, whereas the turbulence intensity at mid-span varied very little as a function of the average inlet Reynolds number.

Wall configuration 2 was tested with both screens and showed a significant efficiency fall-off with increasing turbulence intensity. Based on survey and momentum transfer system data, the stator loss is nearly doubled, with 11 percent turbulence intensity as compared to the screen producing 3.7 percent turbulence intensity when tested at a nozzle exit Mach number of 1.18. An accurate assessment of turbine performance should, therefore, not only include the nozzle performance decrement due to turbulence intensity, but the transfer of the effect to the rotor and the decrement on the rotor itself.

TEST SERIES D - EFFECT OF STATOR BOUNDARY LAYER AND DISTORTION ON PERFORMANCE

The inlet boundary layer in configuration 2 was biased to the outer wall and also to the inner wall by using blockage plates located at the plane of the distortion screen. The inlet velocity biasing followed the boundary layer increase bias; that is, an inner wall boundary layer increase produced an inner span velocity decrease, and a similar effect occurred in the tip. Both boundary layer biases substantially increased losses over the uniform flow conditions. The use of a 9-percent span plate on the inner wall produced a decrement in efficiency of 4.1 percent based on survey data. Similar usage of a boundary plate on the outer wall produced a decrement of 3.5 percent.

TEST SERIES E - EVALUATION OF STATOR EXIT FLOW DISTORTION AND SIMULATED LABYRINTH SEAL LEAKAGE ON ROTOR CASCADE PERFORMANCE

Inlet velocity to the cascade was distorted in a similar manner to test series D except larger blockage plates were used. In this case, an actuator nozzle was used to simulate the entrance conditions to the rotor. Biasing the velocity to either high inner wall or high outer wall decreased the torque produced on the momentum transfer system by values corresponding to a loss of 1.8 to 4.4 percent in efficiency. The effect of imposing a high velocity on the inner wall on the actuator reduced rotor efficiency by 1.8 percent. The effect of high velocity on the outer wall produced an even higher loss in performance of 4.4 percent in efficiency.

The seal leakage or flow bypassing the nozzle but entering the rotor was varied from zero to 10 percent main flow. This resulted in an equivalent loss in stage performance of nearly 1 percent for each percent in bypass leakage across the nozzle.

TEST SERIES F - ROTOR LOADING EFFECTS

The pressure-side-loaded rotor of test series E was replaced with a suction side-loaded rotor. Torque measurements on the two rotor cascades showed the SLR rotor to be higher than the PLR by 0.9 point. These tests were conducted with the actuator nozzle which simulates the design relative angle into the blades (Figure 69). This cascade was lightly loaded and provided a uniform flow into the blade row. If the two rotor configurations were unequally sensitive to entrace flow imperfections, this indicated performance advantage could have been negated.

TEST SERIES G - EFFECT OF COOLING AND SOLIDITY ON STATOR PERFORMANCE

Stator efficiency decreases with any increase of cooling flow for a given Mach number. The nominal nozzle showed a 3.5-point decrease in efficiency with a 12-percent total cooling flow as shown in Figure 126. Efficiencies are given in terms of a ratio of total energy output to total energy input of all the flow. When the nozzle solidity was reduced 20 percent, the efficiency loss varied from 2 to 4 percent with total cooling flows of 4 to 8 percent of main flow at the inlet. Trailing-edge cooling produced the lowest decrement in performance.

TEST SERIES H - EFFECT OF STATOR COOLING ON TWO ROTOR SOLIDITIES AND AXIAL SPACING

The base efficiency of the actuator nozzle at design relative Mach number was 95 percent with no cooling and agrees with predicted values. Increases in cooling flow decrease the performance in an almost linear fashion. This effect, when transferred to the rotor, for example, shows a loss in efficiency of 5.5 percent when 8 percent total cooling flow was used on the nozzle.

The effect of increasing the axial spacing between the stator and rotor was to decrease the efficiency. Two percent in nozzle efficiency was lost for doubling the axial spacing from 0.25 inch to 0.55 inch. When cooling flow is injected, a parallel curve is obtained for efficiency decrement with cooling flow. The effect of reducing rotor solidity by 30 percent resulted in a reduction of efficiency of 2 percent. This indicates that the rotor solidity selection for the ASATT turbine was near optimum and will be maintained for the Phase III design effort.

PHASE III - STAGE INVESTIGATION

The high-work, single-stage, cooled turbine designed in Phase I was investigated in a full-round stage configuration using the cold-flow turbine test facility. A test program was devised to investigate the effects of:

1. Rotor blade aerodynamic loading
2. Rotor solidity
3. Rotor axial spacing
4. Leakage past the nozzle
5. Inlet boundary layer
6. Inlet distortion
7. Cooling flow
8. Reynolds number

on overall performance. Separate tests defined the nozzle performance so that stator and rotor performance could be separated. Tests were also performed to identify and quantify the bearing, windage and seal losses so that the parasitic losses could be separated from the turbine performance and thus permit an evaluation of the aerodynamic performance of the turbine.

OBJECTIVE

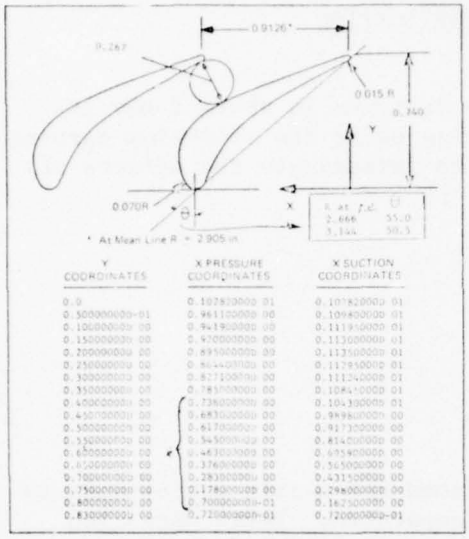
The objective of the Phase III effort was to investigate the performance of the turbine in a stage configuration. The baseline aerodynamics of the Phase I turbine design were modified based on the results of the Phase II testing. The effects of inlet flow field distortion, blade loading, leakage and nozzle-rotor cooling on performance were also investigated in the Phase III, stage, configuration.

TURBINE STAGE DESIGN AND INSTRUMENTATION

The Phase II nozzle cascade tests indicated overturning near the tip and underturning as a result of flow separation at the inner wall region. Also, tests of various meridional nozzle restriction configurations indicated that configuration 2 yields the best performance under the ASATT operating conditions. This background and additional consideration given to aero-loading parameters, solidity correlations and limit loading of transonic vane shapes, led to the Phase III nozzle airfoil and flow path designs.

Figure 129 shows a two-dimensional construction of the mean section, listing the coordinates for both the suction and pressure surfaces of the Phase III vane. This is identical to the Phase II stator except for the change in pressure side coordinates and the radial stagger angle distribution.

The hub stagger angle determined provided a throat angle of 71.5 degrees. The solidity and discharge angle results in the geometry being close to minimum loss. The pressure surface was tailored to allow for the increase in throat angle and to decrease the unguided turning from 6 degrees to 3 degrees.



Y COORDINATES	X PRESSURE COORDINATES	X SUCTION COORDINATES
0.0	0.107820000 01	0.107820000 01
0.500000000-01	0.961100000 00	0.109400000 01
0.100000000 00	0.941900000 00	0.111950000 01
0.150000000 00	0.920000000 00	0.113500000 01
0.200000000 00	0.895000000 00	0.113500000 01
0.250000000 00	0.864400000 00	0.112950000 01
0.300000000 00	0.827100000 00	0.111240000 01
0.350000000 00	0.785000000 00	0.108430000 01
0.400000000 00	0.738000000 00	0.104300000 01
0.450000000 00	0.683000000 00	0.099800000 00
0.500000000 00	0.617000000 00	0.093700000 00
0.550000000 00	0.545000000 00	0.814200000 00
0.600000000 00	0.463000000 00	0.695900000 00
0.650000000 00	0.376000000 00	0.565000000 00
0.700000000 00	0.283000000 00	0.431500000 00
0.750000000 00	0.178000000 00	0.298000000 00
0.800000000 00	0.700000000-01	0.162500000 00
0.830000000 00	0.720000000-01	0.720000000-01

*Changed From Phase II Stator

Figure 129. Phase III Stator Airfoil Section Coordinates.

The tip stagger angle was decreased to yield a throat angle of 68°, and like the hub, it has 3 degrees of unguided turning along the suction surface.

The cooling hole goemetry for the Phase III stator is shown in Figure 130. Compared to the Phase I hot flow path design (Figure 59), this hole geometry is considerably simplified on the Phase III cold flow turbine rig. Since heat transfer/structural life studies are not the principal areas of investigation in this rig, simulation of the coolant injection may be achieved through a single set of gill slots positioned mid-chord on the pressure surface side of the vanes. This change in coolant injection distribution in view of Phase II results is considered to have minimal effect on overall turbine performance. and will provide the basic data on vane coolant flow effects at a significantly reduced prototype acquisition cost. The supply holes were EDMed straight through each stator, maintaining a minimum wall thickness of 0.030 inch.

The three rotor blade shapes tested in the Phase II cascade were chosen to be tested in the full-round rotating, Phase III, rig. The blades were generated using the same mylars as the Phase II blades, since no significant defects were noted from the Phase II testing. The three shapes were designed to demonstrate the effects of loading and solidity on blade efficiency. The test variations included:

1. Nominal solidity (s/C_X = 0.734) pressure-side loading.
2. Nominal solidity (s/C_X = 0.734) high suction-side loading.
3. Low solidity (s/C_X = 0.587) high pressure-side loading.

The three rotors were designed to perform the same work output (i.e., identical velocity triangles) so that any efficiency differences determined from testing will be a result of the flow field effect on the viscous losses and fluid turning. Two of the three rotors, with nominal solidity, were fabricated with pressure-side slots for cooling air injection (Figure 131). The departure from the trailing-edge holes as originally designed in the Phase I effort was necessary due to the manufacturing limitations heretofore not addressed for a machined blade. Casting the internal geometry of the Phase I design permitted the use of trailing-edge holes. However, for a prototype wheel, cast blades were cost-prohibitive, and the tolerances imposed by the machining process renders trailing-edge holes impractical.

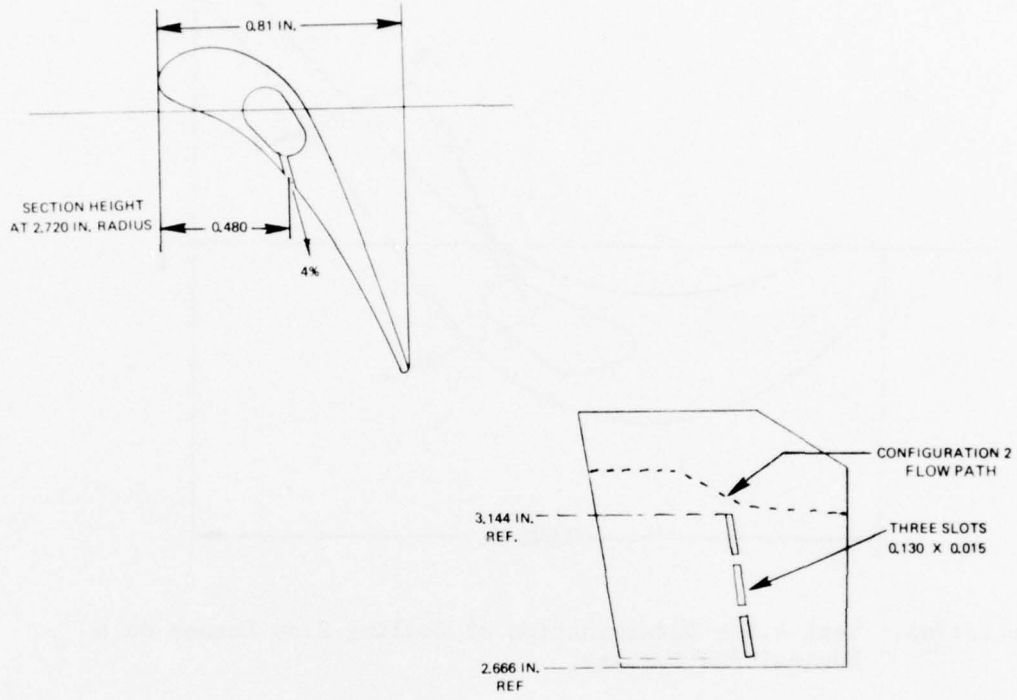


Figure 130. Cooling Flow Slot Definition for Phase III Nozzle Vanes.

As a result, the coolant flow injection is simulated by a single set of slots at about mid-chord on the pressure-side of the blade. Compared to the hot Phase I coolant flow path through the blade (Figure 61), this is less torturous with the impingement cooled leading edge and two pass radial flow not duplicated. This change in internal flow path, like the vane, is considered minimal in terms of its effect on turbine performance. To investigate the validity of pressure-side injection, as opposed to trailing edge, a cursory heat transfer analysis was performed. The results indicate that a trade-off exists between the temperature gradients and stress levels in the blade trailing-edge region. The pressure-side cooling yields slightly higher metal temperatures at the trailing edge but lower stresses due to the absence of stress concentration around the trailing-edge holes. The combination of higher temperature and lower stress results in approximately 10 percent greater margin at 750 hr stress rupture life.

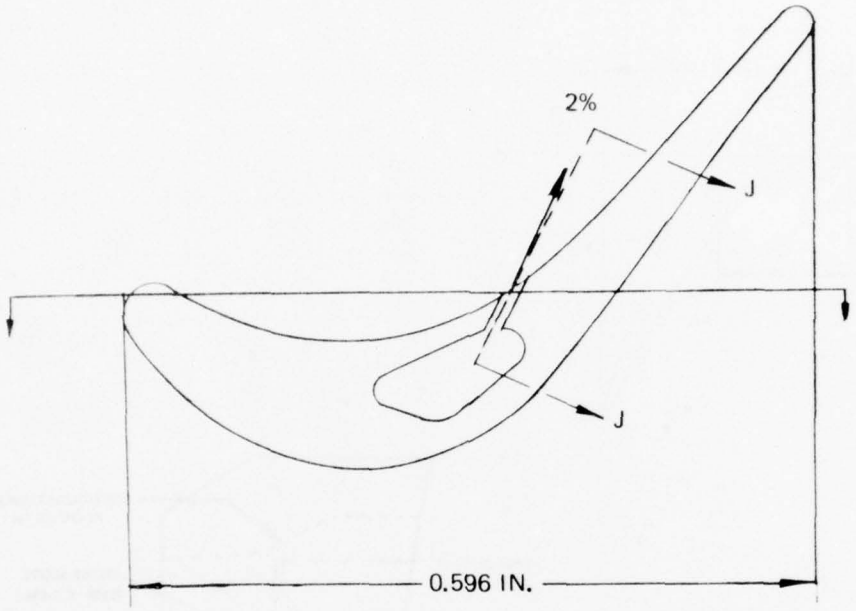


Figure 131(a). Test 4.0 - Determination of Cooling Flow Losses on a Nominal PLR Turbine.

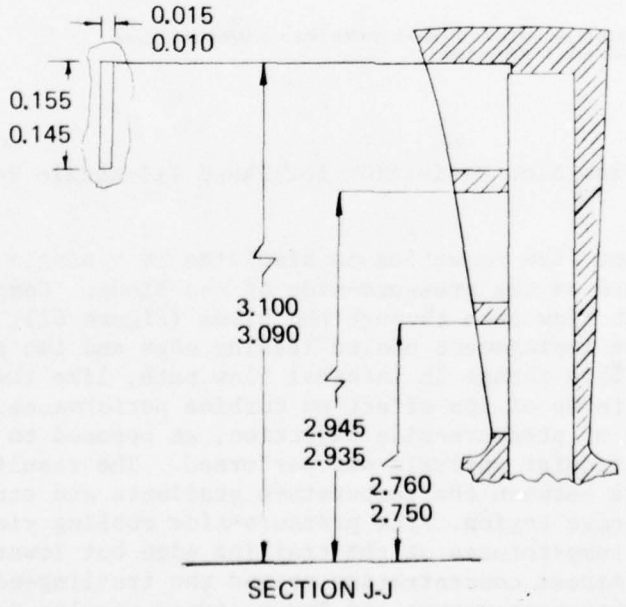


Figure 131(b). Cooling Flow Slot Definition for Phase III Rotor Blade.

TURBINE RIG DESIGN

A cross-section of the turbine rig is shown in Figure 132. The major part numbers are listed and some of the pertinent instrumentation is shown. Basically, the turbine rig consists of the following major assemblies:

1. The transition housing adapts the nozzle inlet housing to the test stand plenum. It contains four hollow support struts to supply nozzle bypass air to the rotor disk for labyrinth seal leakage simulation.

2. The nozzle air inlet housing contains twenty vanes designed to produce the desired air angle distribution and pass corrected flow. It has twenty-eight surface static pressure taps built into the housing with connections at flange periphery as shown in Figure 133. Secondary supply feeds simulated cooling air to the vanes.

3. The exhaust duct housing contains discharge surface static pressure taps on the inner wall. It has four support struts that feed the inner body instrumentation to the exterior bosses for quick assembly and turnaround. It also contains the air supply line for simulated rotor cooling air. A carbon face seal interfaces with the rotor air supply cavity. The rear flange mates with the facility exhaust piping.

4. The turbine wheels (Figure 134) fit a common hub so that changing the wheel for a different test configuration requires only that the exhaust duct be removed. The hub is bolted to the two-bearing shaft assembly which drives a water brake dynamometer. A pressurized oil system provides oil-mist lubrication for the conrad type ball bearing and roller bearing using impingement on the bearing races.

Turbine rotor blade tip clearance was monitored using four contact type, electrical circuits, exposed at different heights (0.004, 0.006, 0.008, 0.010) and equally spaced around the turbine outer shroud. The minimum running clearance was estimated to be 0.012 in.

A critical speed analysis was performed on the turbine rig shaft system. The analysis utilizes a matrix solution for the critical speeds and natural frequencies of shaft systems, considering bending and shear effects, mount flexibility, inter-shaft connnections, and gyroscopic effects of attached disks. The rotor is modeled by a series of disks connected by sections of elastic, massless beams. A set of linear equations, relating deflection, slope, moment, and shear, is generated in a manner similar to the Holzer method. With this set of equations and the boundary conditions taken as free-free, a determinant is defined which must vanish at a natural frequency. Relative deflection, slope, moment and shear are printed out

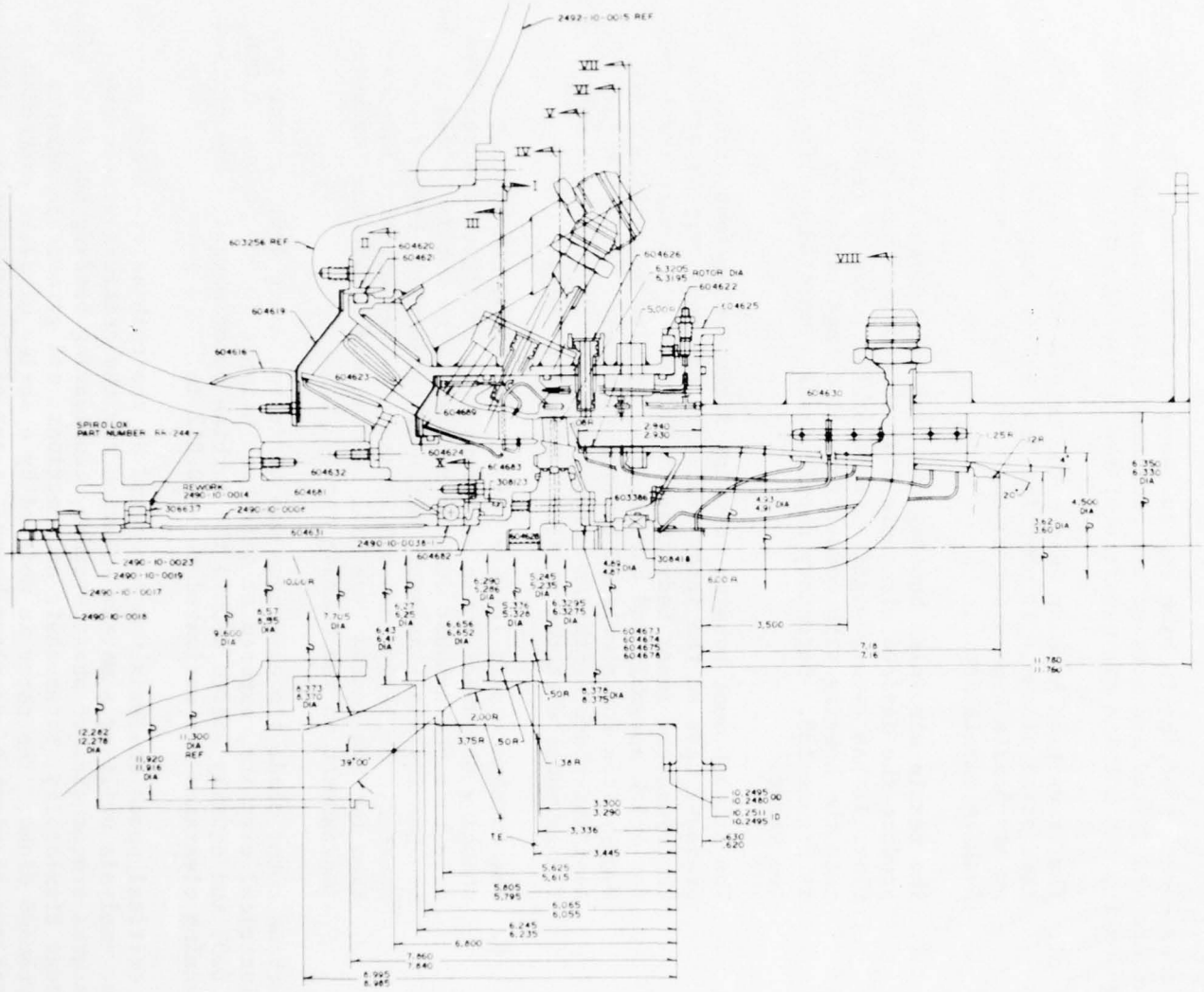
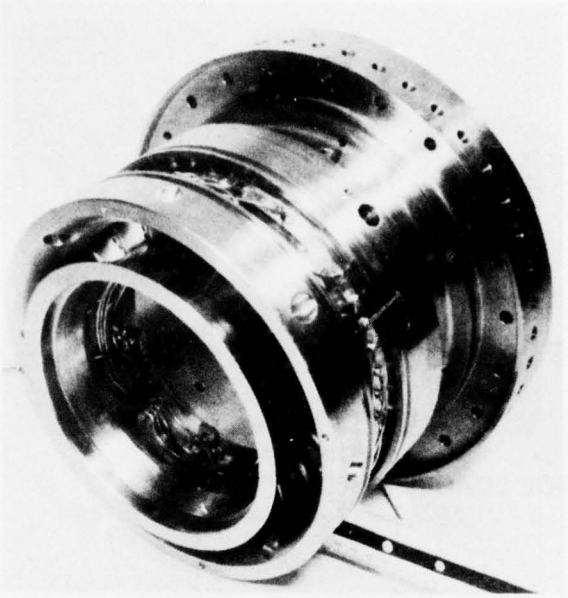
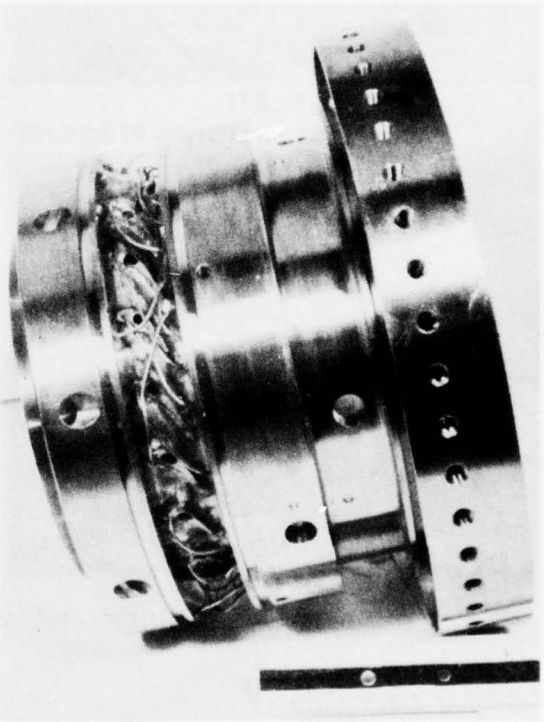


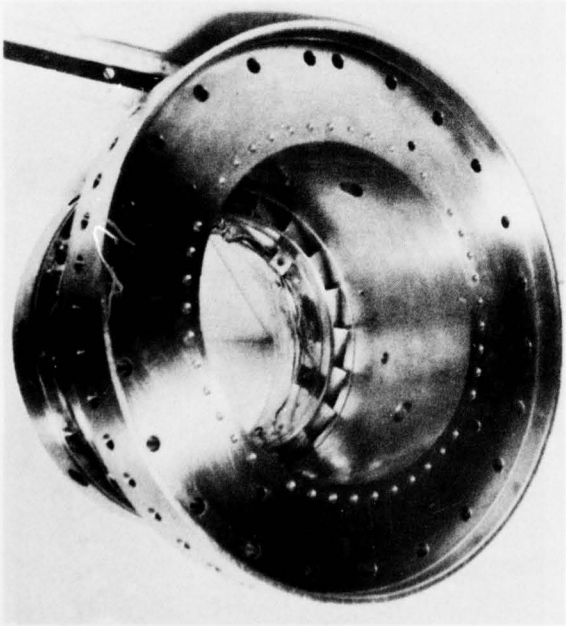
Figure 132. ASATT Phase III Turbine Rig.



(a) INLET VIEW

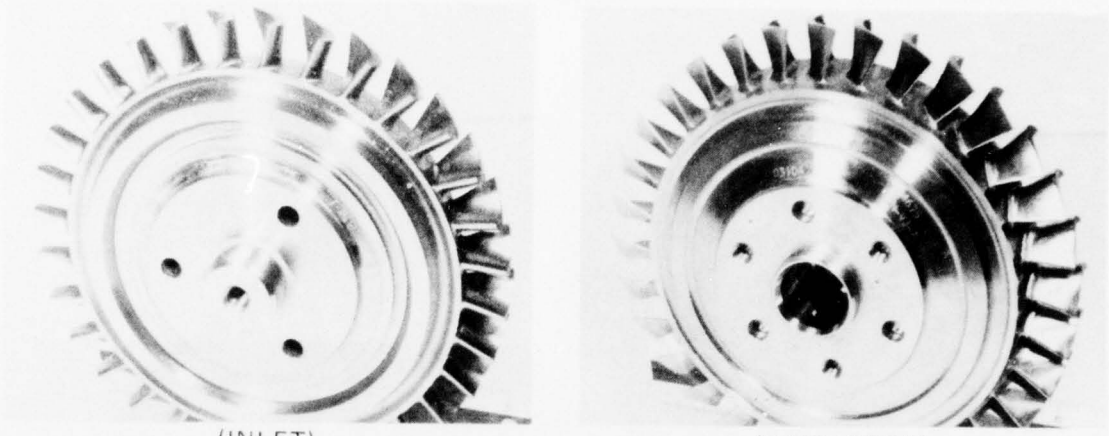


(b) SIDE VIEW



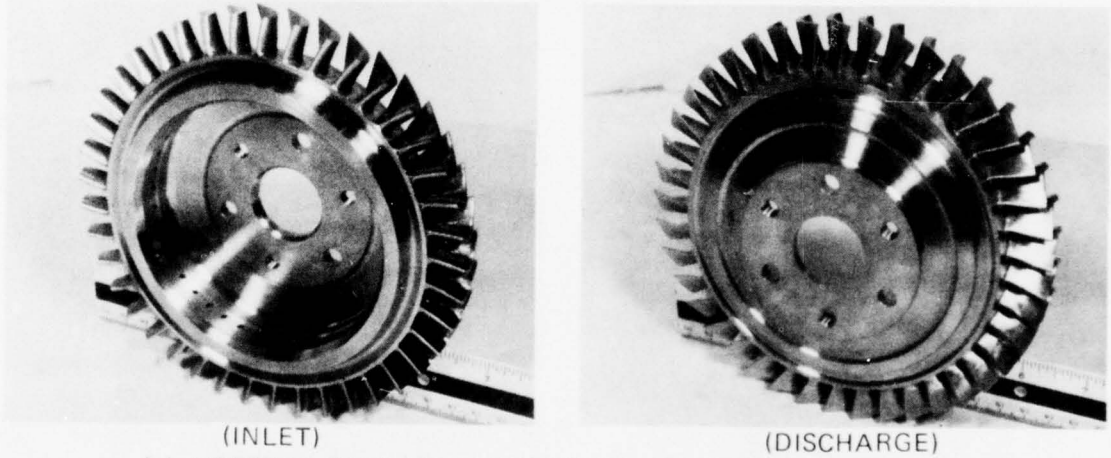
(c) DISCHARGE VIEW

Figure 133. Nozzle Inlet Housing - 604625.



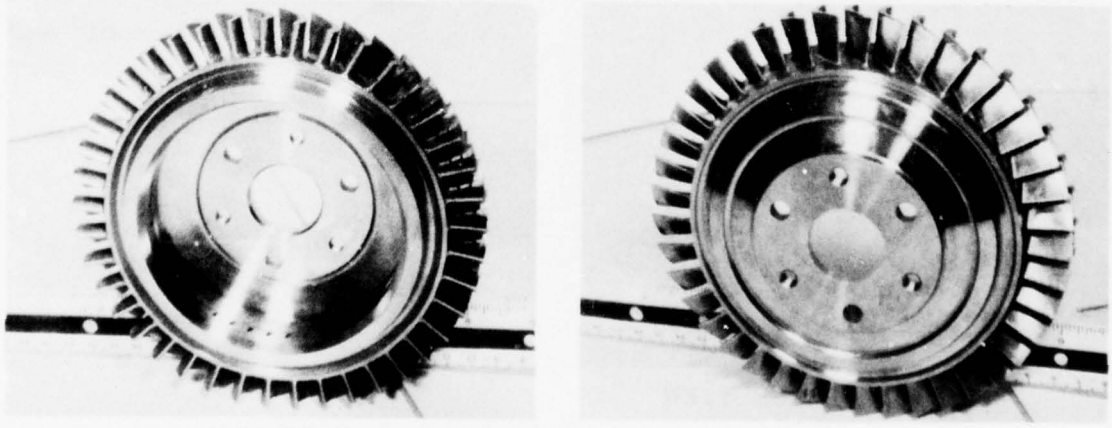
(INLET) (DISCHARGE)

(a) LOW SOLIDITY- PRESSURE SIDE LOADED PN604675



(INLET) (DISCHARGE)

(b) NOMINAL SOLIDITY - PRESSURE SIDE LOADED PN604673



(INLET) (DISCHARGE)

(c) NOMINAL SOLIDITY SUCTION - SIDE LOADED PN604674

Figure 134. Bladed Rotor Configurations.

for each frequency.

Figure 135 shows the results of the critical speed analysis plotted parametrically, with critical speed as a function of the bearing spring rate. The ball bearing chosen has a spring rate of approximately 10^5 lb-in. It may be noted that if both bearings have spring rates of 10^5 (K1 = K2 = 100,000 lb-in), the first critical occurs at 14,000 rpm and the second critical at 33,000 rpm. The required operating speed of the rig is from 60 to 110 percent design speed or 18,500 rpm to 34,000 rpm. Since 34,000 rpm is too close to the second critical, the spring rate of K1 was increased to 10^6 by using a roller bearing in place of the ball bearing. The increased spring rate did not appreciably change the speed location of the first critical; however, the second critical was moved to 66,000 rpm, well out of the rig operating range.

TEST FACILITY, INSTRUMENTATION, AND PROCEDURE

TEST FACILITY

The plant air supply and exhaust system are comprised of five centrifugal compressors and 14 positive displacement vane pumps with associated ducting, heaters, and refrigeration (Figure 136).

Air enters from atmosphere and passes through a series of oil curtain filters to remove dust and airborne particles. Manifolding, valving, and intercoolers allow a wide choice of compressor flow paths from a single ram to four parallel rams, or a set of series rams, or any combination thereof. Each compressor is capable of delivering 11 lb/sec airflow at a pressure ratio of 1.33:1. A stage pair will provide a 1.77:1 pressure ratio at a slightly lower weight flow.

Inlet and discharge valving at the individual test cells provides the test operator with pressure and flow control as dictated by the test plan.

Prior to conducting the cold flow turbine rig tests, a series of tests are conducted to determine bearing losses and disk windage losses. These tests are run by driving the turbine disk with an air turbine torque indicated by using an in-line rotary torquemeter.

The power absorption for the ASATT turbine testing is provided by a water brake dynamometer installed as shown in Figure 137. The reacted torque on the brake stationary frame is measured using the in-line torquemeter. Readout is accomplished using an electronic digital counter at the test console. The signal is also recorded by the 1800 DACS (described in the Phase II Data Acquisition section).

Various power absorption levels of the water brake dynamometer are available at particular speeds by regulation of the water level within the water brake housing. Control is achieved by opening or closing the valve at the inlet to the water brake. Limits of power and speed are imposed by the heat absorption characteristics of water and the maximum rotational speeds allowable for the bearings; however, all required points fall within the limits of the anticipated turbine operating envelope.

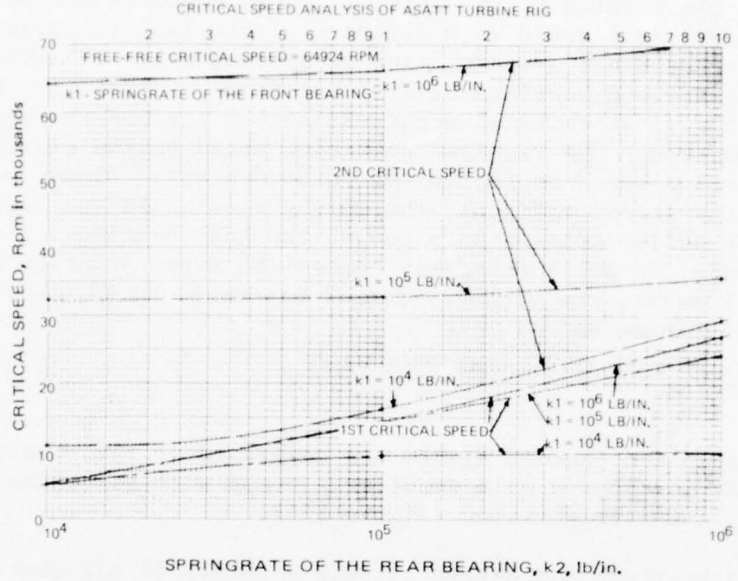


Figure 135. Critical Speed Dependence on Bearing Spring Rates.

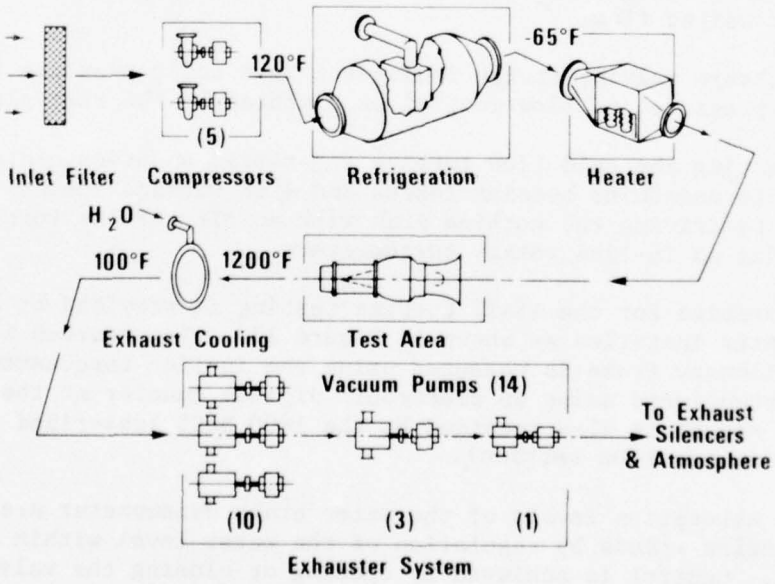


Figure 136. Turbine Air Flow Facility - Environmental System Supplies Conditioned Air to Turbine Test Rigs, and Exhaust System Provides High Turbine Pressure Ratios.

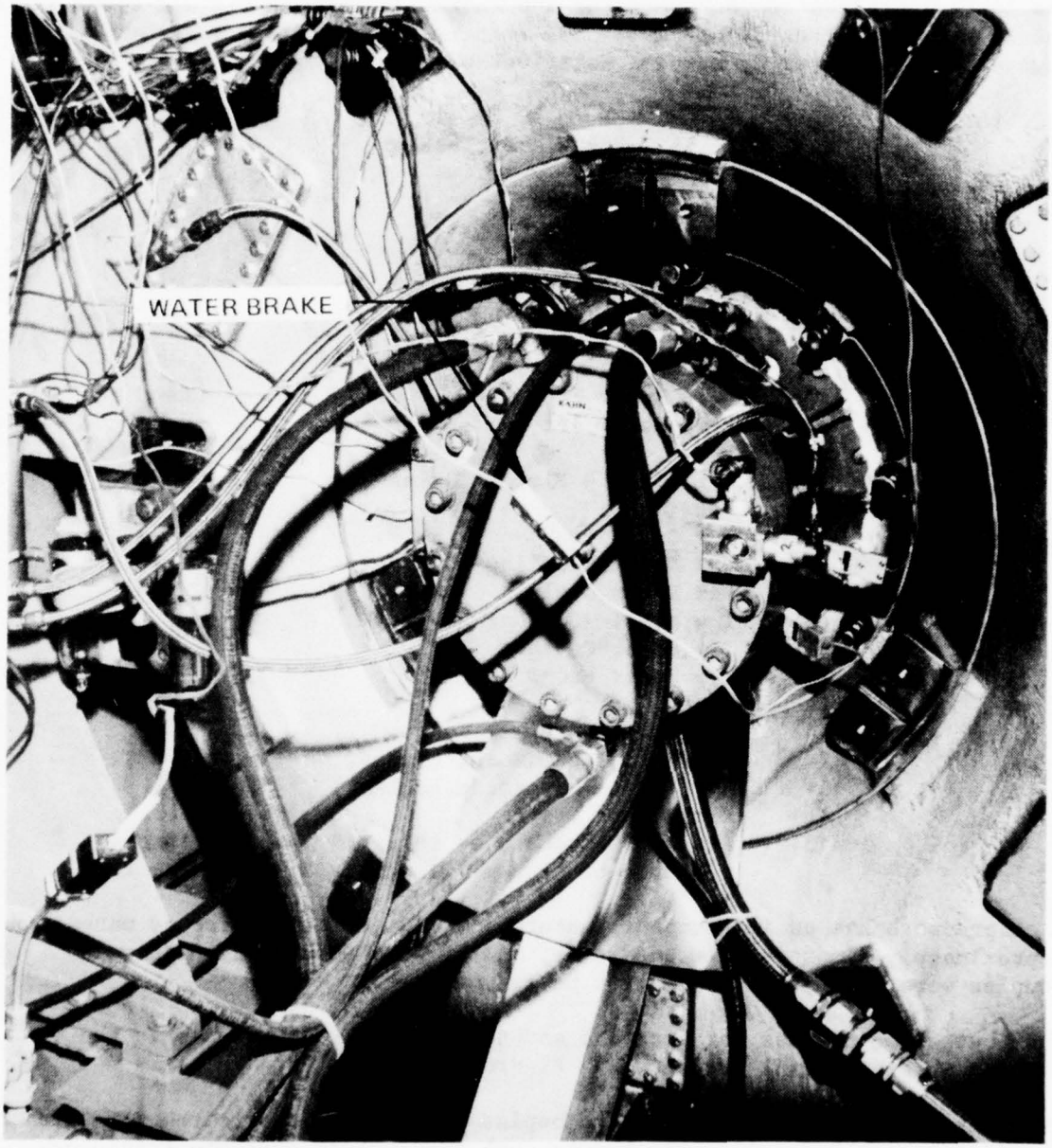


Figure 137. Kahn Water Brake Dynamometer Installed in the Turbine Test Facility.

INSTRUMENTATION AND ACCURACY

The instrumentation requirements for the Phase III turbine rig are shown in the flow path sketch, Figure 138. The various instrumentation shown in Figure 138 are listed by station location as follows:

Station 1 Inlet
- (4) P_{T1} & T_{T1} 4 Element Rakes
- (8) Ps1
- (6) Hot Film Probes

Station 2, 3, 4 Nozzle Instrumentation
- (20) Ps1-2
- Nozzle Exit Survey System; P_T, α, T_T

Station 5 Rotor Exit
- (2) Rotor Exit Survey Probes
- (8) Ps5
- (2) P_{SRF} Rotor Front
- (2) P_{SRR} Rotor Aft

Station 6 Exit Duct
- (4) P_{T6} & T_{T6} 4 Element Rakes
- (8) Ps6

Cooling Air Circuits
- (2) PsN Nozzle Cooling
- (1) PsR Rotor Cooling
- (2) T_{CN} Nozzle Coolant
- (1) T_{CR} Rotor Coolant
- (2) T_{RF} Rotor Front

Miscellaneous
- (4) Tip Indicators
- (4) Flow Orifices (main, bypass, nozzle, coolant, rotor coolant)
- (1) Air Bypass System
- (3) Actuator Readout, as required, in-line torque measurement system (Himmelstein Model MCRT 2-04)

Each pressure has an independent measurement, either transducer or manometer. Approximately 80 pressure transducers, and 12 manometers and 40 thermocouples were employed for the test measurements.

The four element rakes for pressure and temperature measurements at the turbine inlet and exit are shown in Figure 139.

The pressure transducers and thermocouples were calibrated to the IBM Data Acquisition and Control system before each test. Each pressure transducer pressurized in steps throughout its range of operation with a Mensor pressure controller, Model 10095-00X quartz pressure sensor. The DAC system reads and records each pressure data point and generates a slope and intercept type calibration. Each transducer is then check-calibrated to ensure accuracy within $\pm$0.25 percent of maximum reading. The thermocouple circuits are calibrated in a similar manner to within $\pm$2°F of reading.

Assuming that during testing the average true temperature and pressure is within these calibration bands, an estimate may be made of the uncertainty in the calculated value of total-to-total adiabatic efficiency (η). This is obtained by accumulating the potential errors due to each measured variable that enter into the efficiency calculation and consists of the following:

$$\eta = \frac{T_1 - T_9}{T_1 \left[1 - (P_9/P_1)^{(\gamma - 1)/\gamma}\right]}$$

$$\frac{\partial \eta}{\partial T_1} = \frac{T_9}{(T_1)^2 \left[1 - P_9/P_1)^{(\gamma - 1)/\gamma}\right]}$$

$$\frac{\partial \eta}{\partial T_9} = \frac{-1}{T_1 \left[1 - (P_9/P_1)^{(\gamma - 1)/\gamma}\right]} = -\frac{T_1}{T_9}\left(\frac{\partial \eta}{\partial T_1}\right)$$

$$\frac{\partial \eta}{\partial P_1} = \frac{(T_9/T_1 - 1)\left(\frac{\gamma - 1}{\gamma}\right)(P_9/P_1)^{-\frac{1}{\gamma}} P_9}{(P_1)^2 \left[1 - (P_9/P_1)^{(\gamma - 1)/\gamma}\right]^2}$$

$$\frac{\partial \eta}{\partial P_9} = \frac{(1 + T_9/T_1)\left(\frac{\gamma - 1}{\gamma}\right)(P_9/P_1)^{\frac{-1}{\gamma}}}{(P_1)\left[1 - (P_9/P_1)^{(\gamma - 1)/\gamma}\right]^2} = -\frac{P_1}{P_9}\left(\frac{\partial \eta}{\partial P_1}\right)$$

$$\text{Uncertainty} = \pm\sqrt{\left(\frac{\partial \eta}{\partial T_1} \cdot S_T\right)^2 + \left(\frac{\partial \eta}{\partial T_9} \cdot S_T\right)^2 + \left(\frac{\partial \eta}{\partial P_1} \cdot S_P\right)^2 + \left(\frac{\partial \eta}{\partial P_9} \cdot S_P\right)^2}$$

Where S_T = Potential error in temperature measurement
= $\pm 2°$
Sp = Potential error in pressure measurement
= ± 0.061 psid ($\pm 0.25\%$ of 24.6 psia)

For the ASATT turbine rig at near design point (4.0 pressure ratio) with inlet pressure and temperature of 24.6 psia and 690°R, the above yields an uncertainty of ± 2.4 points on efficiency. This is for any single data point and is reduced by averaging the results of a number of data scans at the same rig operating conditions (Reference 48). During the performance mapping, each data point is actually the average of 4 to 5 data scans with the special interest points being obtained more than once. This reduces the uncertainty by approximately 48 percent to ± 1.2 points on efficiency for the bulk of the data and down to ± 0.7 point at design point and other special interest data points. It should be noted that the above uncertainties are increased when the rig is operated at lower pressure and temperature differentials across the turbine stage. That is, with the same inlet pressure and temperature, rig operation at a stage pressure ratio of 2.0 increases this uncertainty by nearly a factor of two.

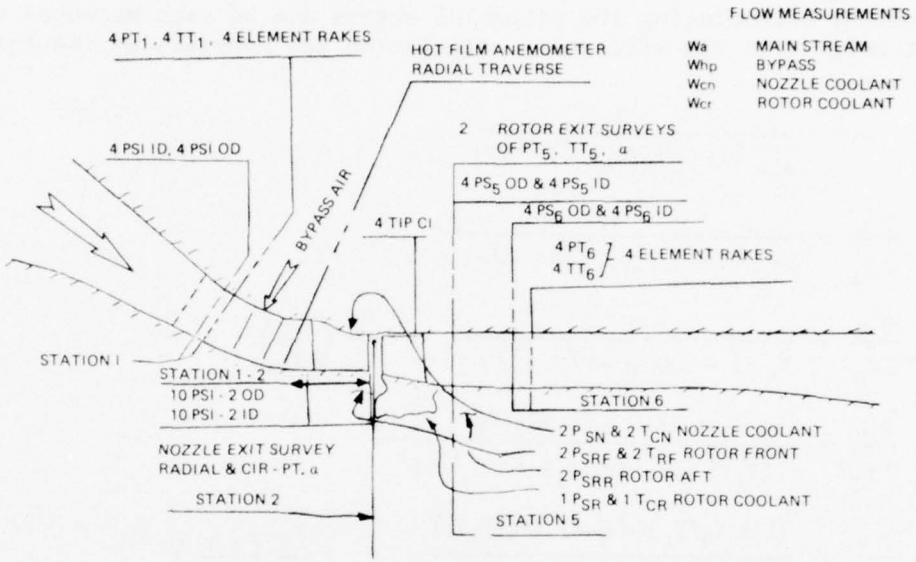


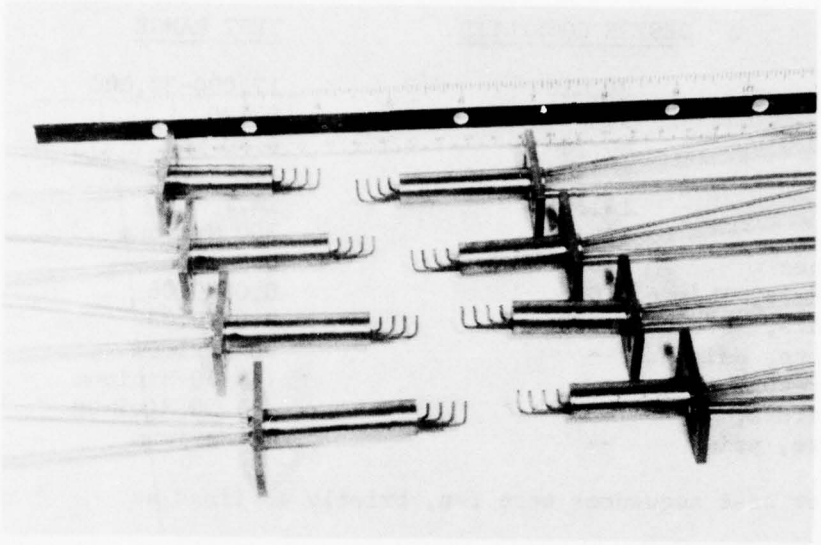
Figure 138. Schematic of Phase III ASATT Turbine Rig Instrumentation

The inlet turbulence and boundary layer velocity profile was measured with a constant temperature hot film probe similar to the Phase II measurements. The probe consists of a quartz-coated platinum film sensor on a 0.002 inch glass rod (TSI Model 1210). The hot film probe was tunnel calibrated to 500 ft/sec velocity, and the hot film voltage was normalized to standard pressure (Voltage $P/\delta^{1/4}$).

The inlet turbulence intensity was determined for the baseline rotor tests and boundary layer effects tests using the procedure developed in Phase II with the hot film anemometer.

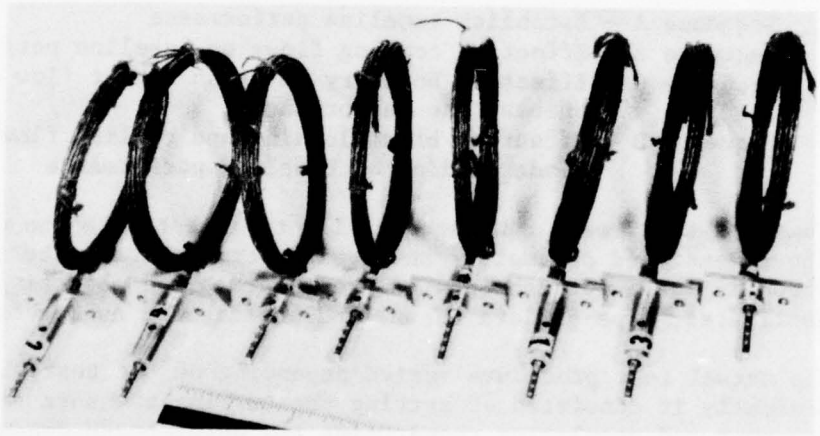
TEST PROCEDURE

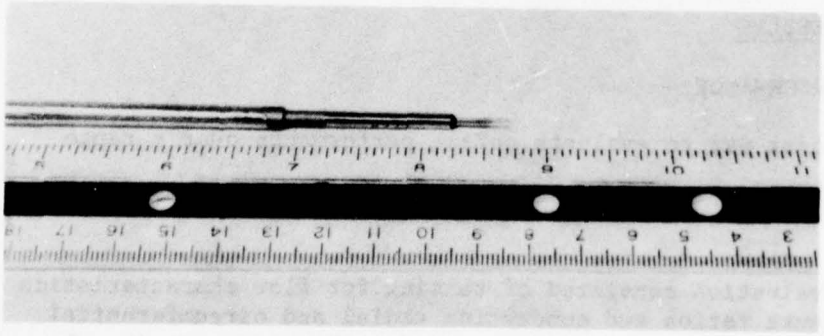
Airflow was initiated through the stand piping by operation of the vacuum pumps located in the exhaust line. The supply pressure was regulated using the ram air blowers located at the facility inlet. The main supply air temperature level was modulated by electric air heaters to prevent icing conditions while running at high pressure ratios. Turbine power output was absorbed by a Kahn smooth disk water brake dynamometer. Torque measurement was made using an in-line torquemeter with integral speed pickup. Main supply airflow was measured using a sharp edge orifice located in the inlet line immediately upstream of the inlet plenum. The turbine was operated over the range of parameters listed as follows:



(a) INLET & EXIT FIXED TOTAL PRESSURE RAKES

(b) TOTAL TEMPERATURE RAKES





(c) HOT FILM ANEMOMETER

Figure 139. Turbine Rig Instrumentation

PARAMETER	DESIGN CORRECTED	TEST RANGE
Speed, rpm	26,010	17,000-32,000
Torque, in-lb	90	0-130
Power, HP	40.56	0-50 hp
Pressure Ratio (cold)-TT	4.2	1.2-4.6
Inlet Pressure, psia	14.696	14.7
Inlet Temperature, °F	59	300 Maximum
Inlet Flow Rate, lb/sec	0.862	0.3-1.0
Nozzle Coolant Flow Rate, lb/sec	0.042	0.03-0.06
Rotor Coolant Flow Rate, lb/sec	0.020	0.01-0.03
Nozzle Coolant Pressure, psia	--	30 Maximum
Nozzle Coolant Temperature, °F	--	(-) 50 Minimum
Rotor Coolant Temperature, °F	--	(-) 50 Minimum
Rotor Coolant Pressure, psia	--	30 Maximum

A series of four major test sequences were run, briefly outlined as follows:

Sequence A - Establish baseline performance
Sequence B - Effect of cooling flows on baseline performance
Sequence C - Effect of boundary layer and inlet flow distortion on baseline performance
Sequence D - Effect of blade loading and cooling flows including blade loading on baseline performance

Thirteen tests were run sequentially to investigate the effects of the above mentioned parameters on turbine performance. The testing sequence shown in Table 16 describes the test series and objective, variable investigated, type of data taken, and anticipated number of data points.

The actual test procedure varied depending on the test objective, but basically it consisted of setting the turbine pressure ratio and inlet pressure and regulating speed using the water brake dynamometer.

TURBINE STAGE TEST RESULTS

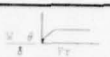
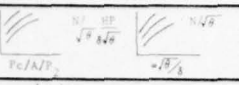
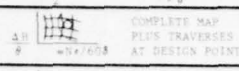
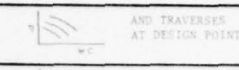
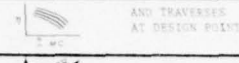
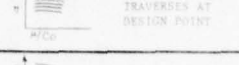
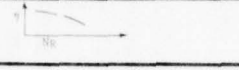
TEST 1.0 - NOZZLE PERFORMANCE

The purpose of this test was to evaluate nozzle performance over a range of pressure ratios.

Test Configuration

Nozzle performance evaluation consisted of testing for flow characteristics over a range of pressure ratios and conducting radial and circumferential surveys at nozzle exit to establish pressure loss and flow angles for the nominal uncooled nozzle. Full surveys also were conducted with cooling flow (equal to 1.8 percent primary flow) injected through the nozzle pressure surface cooling holes. The purpose of this test was to determine

TABLE 16 - PHASE III TEST PROGRAM

SERIES AND OBJECTIVE	TEST	VARIABLE	CONFIGURATION	DATA POINTS	TYPE OF DATA
DETERMINE NOZZLE PERFORMANCE	1	PRESSURE RATIO	NOZZLE ONLY	8 PRESSURE RATIOS TRAVERSE AT DESIGN POINT	
DEFINE DISK WINDAGE, BEARING LOSSES AND ROTOR COOLANT ABSORBED POWER	2	PRESSURE CHECK FOR LEAKAGE AT N=0 CHANGE PRESSURE WITH SPEED VARY ROTOR COOLANT FLOW	BLADELESS DISK	5 SPEEDS 3 PRESSURES	
EVALUATION OF NOMINAL PERFORMANCE	3	NOMINAL SOLIDITY - 41 BLADES PRESSURE LOADED ROTOR (604673)	BASELINE	TOTAL OF 30 POINTS OF SPEED AND PRESSURE RATIO	 COMPLETE MAP PLUS TRAVERSES AT DESIGN POINT
DETERMINE COOLING FLOW	4	VARY NOZZLE COOLING FLOW ONLY VARY ROTOR COOLING FLOW ONLY VARY NOZZLE + ROTOR FLOW	SAME AS 3	3 FLOWS AT DESIGN PT. 3 FLOWS AT DESIGN PT. 1 FLOW AT DESIGN PT.	 AND TRAVERSES AT DESIGN POINT
EVALUATION OF BLADE LOADING	5	FULL ASSEMBLY WITH SECOND ROTOR AIRFOIL DESIGN	SECOND ROTOR BLADE DESIGN (604674)	TOTAL OF 30 POINTS OF SPEED AND PRESSURE RATIO	 COMPLETE MAP PLUS TRAVERSES AT DESIGN POINT
DETERMINE COOLING FLOW EFFECTS	6	VARY NOZZLE COOLING FLOW ONLY VARY ROTOR COOLING FLOW ONLY VARY NOZZLE AND ROTOR FLOW	SAME AS 5	3 FLOWS AT DESIGN PT. 3 FLOWS AT DESIGN PT. 1 FLOW AT DESIGN PT.	 AND TRAVERSES AT DESIGN POINT
EFFECT OF LEAKAGE	7	LEAKAGE BETWEEN NOZZLE AND ROTOR VARIED 0 TO 10%	BEST ROTOR OF TESTS 3 AND 5	6 FLOWS AT DESIGN POINT; 6 FLOWS AT 30% POWER RATING	
EFFECT OF LARGE AXIAL SPACING	8	INCREASE AXIAL SPACING 0.2 INCHES	SAME AS 7 WITH LARGE AXIAL SPACER	5 SPEEDS 4 PRESSURE RATIOS	PARTIAL MAP
EFFECT OF LEAKAGE AT INCREASED AXIAL SPACING	9	LEAKAGE BETWEEN NOZZLE AND ROTOR VARIED 0 to 10%	SAME AS 8	6 FLOWS AT DESIGN POINT; 6 FLOWS AT 30% POWER RATING	
EFFECT OF INLET BOUNDARY LAYER	10	INCREASE INLET BOUNDARY LAYER ON INNER AND OUTER WALLS	SAME AS 7 EXCEPT WITH B.L. PLATES	3 SPEEDS 4 PRESSURE RATIOS	PARTIAL MAP
EFFECT OF INLET DISTORTION	11	HIGH VELOCITY ON OUTER WALL	SAME AS 7 EXCEPT WITH I.D. DISTORTION PLATE	3 SPEEDS 4 PRESSURE RATIOS	PARTIAL MAP
EFFECT OF ROTOR SOLIDITY	12	ROTOR SOLIDITY LESS THAN NOMINAL (604675 ROTOR)	NUMBER OF BLADES DECREASED TO 32	NUMBER OF BLADES DECREASED TO 32	 TRAVERSES AT DESIGN POINT
REYNOLDS NUMBER EFFECT	13	REYNOLDS NUMBER	SAME AS 7	2 DESIGN POINT RUNS AT DIFFERENT REYNOLDS NUMBERS	

if flow added upstream of the nozzle throat would affect the performance. All testing used a full-round twenty-vane nozzle with a measured throat area of 2.614 square inches. The nominal inlet distortion screen was used. No inlet boundary layer plates were present. Nozzle flow was fixed by setting a fixed inlet pressure based on the average of sixteen total pressure rake readings and a downstream static pressure based on the average of six static in the nozzle exit plane.

Twenty-one radial positions were surveyed circumferentially over a 36-degree sector. Hardware restrictions limited the radial surveys to within 7 percent of both walls. The local exit total pressure sensed by the pitot tube, inlet total pressure from a representative inlet rake element, and their differences were recorded continuously by oscillograph plots as each radial position was maintained and the probe moved circumferentially through the exit stream. Continuous recording of these data insured wake detection. Other pertinent parameters were monitored on a discrete basis using the Data Acquisition System.

Nozzle flow for the surveys was set with an inlet total pressure of 50 inch Hg. and a total-static pressure ratio of 3.33. For the survey with injected flow through coolant holes, flow at inlet primary conditions was bypassed to the nozzle coolant system (see Figure 140).

Test Results

Testing indicated that nozzle choked flow was 6.4 percent less than design flow. This was expected since the nozzle passage, as fabricated, was small with respect to the design. The flow pressure ratio function in Figure 141 compares design flow to a set of test data accumulated from Test 5.0 (nominal suction surface loaded rotor turbine configuration with ambient inlet pressure) and test 1.0 (rotorless nozzle exit survey configuration at an inlet pressure of 50-inch Hg). Both sets of data indicate choked corrected airflow, $W\sqrt{\theta}\,\epsilon/\delta$, of 0.846. Other data throughout Phase III testing indicate this level. These data demonstrate the repeatability at extreme conditions.

The exit survey probe was calibrated at NASA/Lewis supersonic flow tunnel at a Mach number of 1.30 with results indicating Rayleigh Normal Shock Equations could be applied to measured data. With knowledge of the upstream unshocked local exit static pressure and measured local exit total pressure behind the shock wave of the pitot tube, the unshocked local total pressures were calculated and used in all other calculations.

In addition to the corrections applied for local inlet total pressure and local exit total pressure, the following assumptions were used in all test results: (1) local nozzle exit static pressure was based on discrete nozzle exit wall static pressures with linear interpolation radially and no circumferential gradient; (2) uniform mass flow; and (3) constant inlet temperature from discrete inlet rake readings.

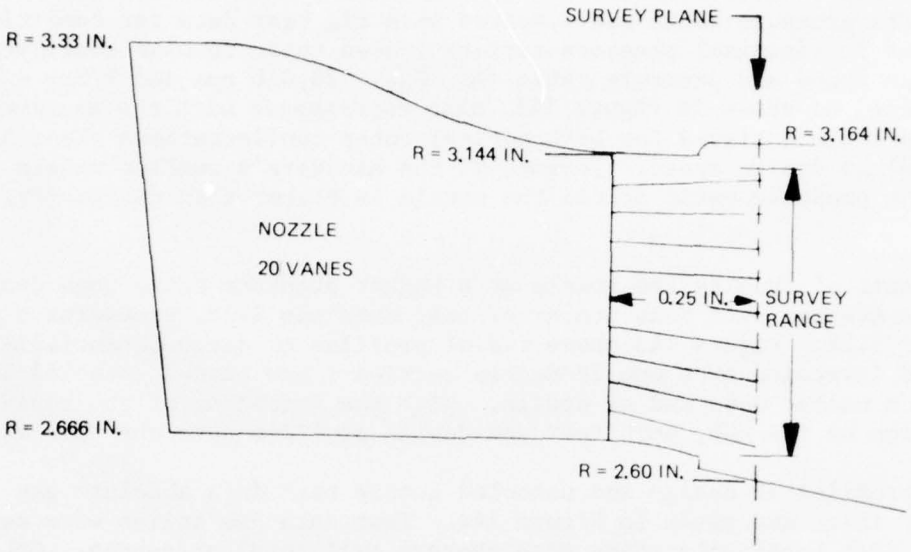


Figure 140. Test 1.0 - Nozzle Performance - Sketch of Flow Path for Nozzle Exit Survey.

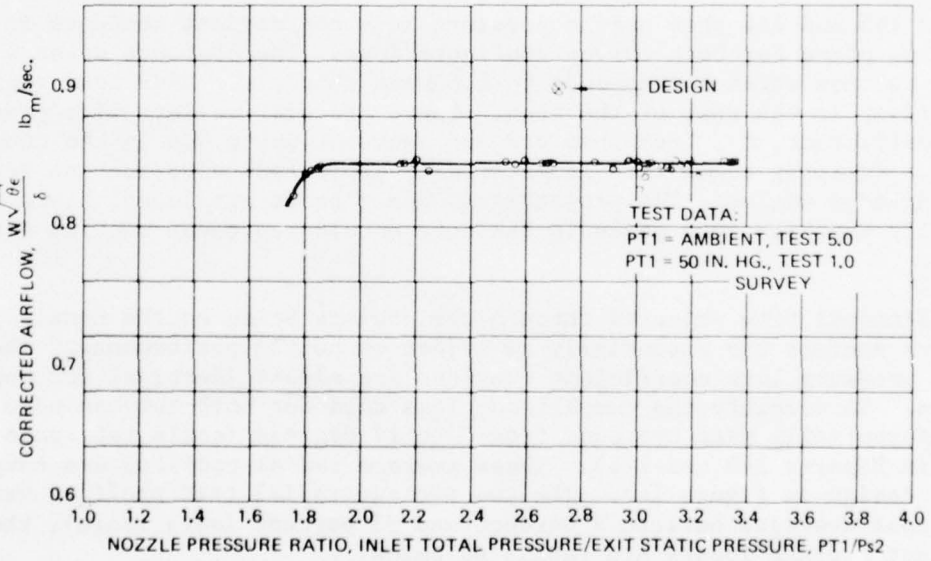


Figure 141. Test 1.0 - Nozzle Performance: Flow Pressure Ratio Function, A Comparison of Test Data and Design.

Nozzle total-to-static pressure ratio for nozzle exit surveys was set at 3.33. The pressure ratio was compared with rig test data for conditions from Test 3.0 (nominal pressure surface loaded rotor turbine configuration) at design speed and pressure ratio ($N/\sqrt{\theta_{cr}}$ = 26,010 rpm and P/P_{TT} = 4.2). This value, as shown in Figure 142, also corresponds with the maximum nozzle pressure ratio achieved for both nominal rotor configurations (Test 3.0 and Test 5.0) at design speed. Because of the hardware's smaller nozzle throat area, the pressure ratio across the nozzle is higher than design ($P_{T1}/P4$ = 2.72).

As a result of running the nozzle at a higher pressure ratio than design, the mass average exit Mach number of test data was 1.38, exceeding a design value of 1.24. Figure 143 shows radial profiles of circumferentially mass averaged (averaged over one 18-degree section = one pitch) uncooled local exit Mach number data and of design. With the exception of the rapid deceleration at the hub, both test and design profiles have the same slope.

Radial profiles of design and uncooled nozzle test data absolute gas angle at rotor inlet are given in Figure 144. Test data gas angles were calculated from continuity using mass average exit total pressures. Other necessary parameters were as previously discussed. The underturning at the hub is indicative of separation or high secondary losses. This makes the uniform mass flow assumption somewhat invalid; however, this assumption is conservative, since the difference between design and test data would decrease if flow is assumed to be increased over the low loss region.

Figures 145 and 146 show nozzle pressure loss coefficient contours in the measuring plane for both survey configurations. The contours cover a 27-degree section which corresponds to 1.5 vane channels. High loss regions are evident in the rest of the span. There are wide valleys with pressure loss coefficient, $\overline{\omega}$, less than 0.2 and peaks of up to 0.4 in the core region. Trailing edges were geometrically projected using suction surface trailing-edge angles. The projections appear to be displaced, since typically the high loss peaks in the core should represent suction surface losses.

The additional flow injected through the coolant holes on the nozzle pressure surface had essentially no effect on nozzle performance. The nozzle pressure loss coefficient contours are almost identical for both surveys. To simplify the comparison, loss data for both surveys were circumferentially mass averaged from 0 to 18 degrees (angle reference as shown in Figures 145 and 146). These average radial profiles are compared to the design in Figure 147. The two average radial test profiles were again mass averaged between 7 percent and 93 percent (data range), the resultant average losses are tabulated below.

Configuration	Pressure Loss Coefficient, $\overline{\omega}$
Without Cooling	0.154
With 1.8% Cooling	0.157
Design	0.179

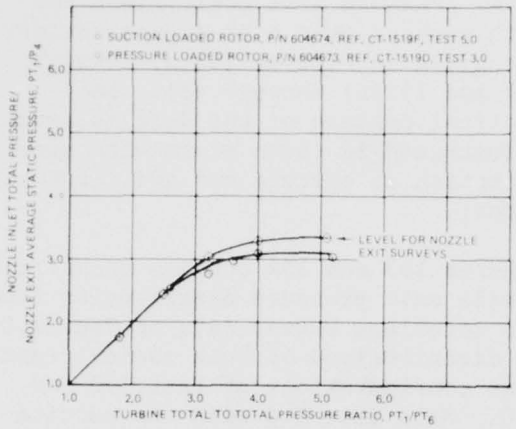


Figure 142. Test 1.0 - Nozzle Performance: Comparison of Nozzle Running Conditions for Both Nominal Rotor Configurations, Test 3.0 and Test 5.0, at Design Speed.

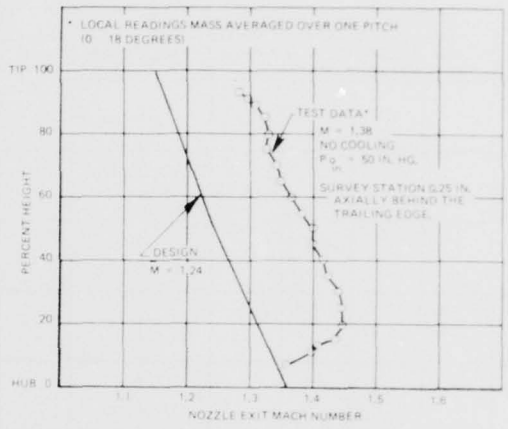


Figure 143. Test 1.0 - Nozzle Performance: Comparison of Design and Test Radial Nozzle Exit Mach Number Distribution.

The true average profiles for test data will be somewhat larger when the remaining wall loss is also added in. Note the test data indicates the core loss is less than the original design prediction.

A high hub loss region is also indicated in static pressure distributions at the nozzle exit. Figure 148 shows identical distributions for both cooled and uncooled surveys.

The high corner static pressure on the suction surface at the hub indicates a separation or a high secondary loss region. Hub losses detected in the rotor inlet surveys are complicated by the flairing nozzle duct and also a step in the hub flow path, which is visible in Figure 140.

Figure 149 shows the normalized mid-channel static pressure distribution for pressure ratio $P_{T1}/P4 = 3.33$. This data, although taken from uncooled nozzle exit survey data, is representative of mid-channel acceleration for choking nozzle conditions. Good acceleration is evident on both walls all the way to the trailing edge of the nozzle.

Repeatability of data from channel to channel was assumed in mass averaging data after only one 18 degree sector. Figures 150(a), (b) and (c) illustrate the cyclical pattern of local exit total pressure survey data over

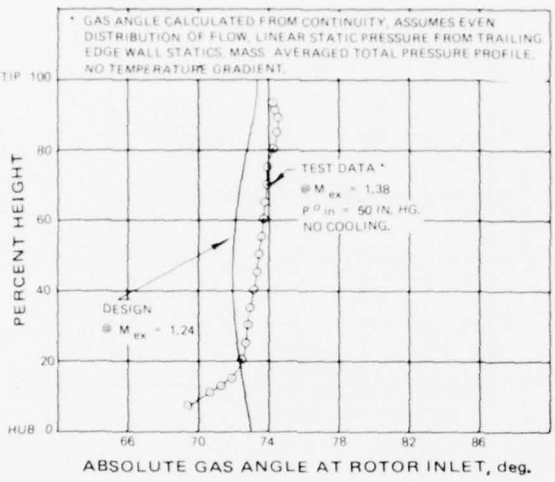


Figure 144. Test 1.0 - Nozzle Performance: Comparison of Design and Test Data Radial Absolute Gas Angle Profiles at Rotor Inlet.

36 degrees. Circumferential traces of local pressure loss coefficient for both surveys over a 27-degree sector are given in Figures 151(a) through (e) and 152(a) through (e). The cyclical pattern of the data is again illustrated in these plots with some exception at extreme hub and tip conditions.

Figures 153 and 154 compare normalized nozzle exit pressure distribution from the rotorless survey data of Test 1.0 to distributions of both nominal rotor test configurations of Test 3.0 and 4.0. Note Test 5.0 with the suction surface loaded rotor achieved a maximum nozzle total-to-static pressure ratio of 3.02, which is less than the 3.33 pressure ratio at which surveys were conducted. High loss at the hub is visible in all three tests. This is detected by increase in static pressure from mid-channel to suction surface. The larger slope of the outer wall data for both Tests 3.0 and 5.0 compared to 1.0 suggest that the tip was better when rotors were present.

A brief comparison of Phase III and Phase II nozzle performance data is presented in Figures 155 through 157; Phase II test results as reported in the previous section, included cascade nozzle performance data for meridional constriction on nozzles. Wall configuration 2 in Phase II corresponds to the full-round wall configuration of Phase III. Figure 155 illustrates low nozzle pressure loss coefficient profiles in the core region. Gas angles for Phase III, as shown in Figure 156, are larger than Phase II; however, the tests were conducted at different pressure ratios. Underturning at the hub is indicated in both sets of data. Mach number radial distributions at the nozzle exit, Figure 157, illustrate the same slopes for both tests. The difference in the levels is again caused by the differences in pressure ratios.

In summary, the test results of Test 1, nozzle performance, showed that:

1. Although high in the hub region, the mass average loss coefficient was measured to be 14 percent lower than design,

2. The highest losses were concentrated in the hub on the suction side, indicative of a localized high vortex loss,

3. The nozzle throat area is 6.4 percent smaller than design,

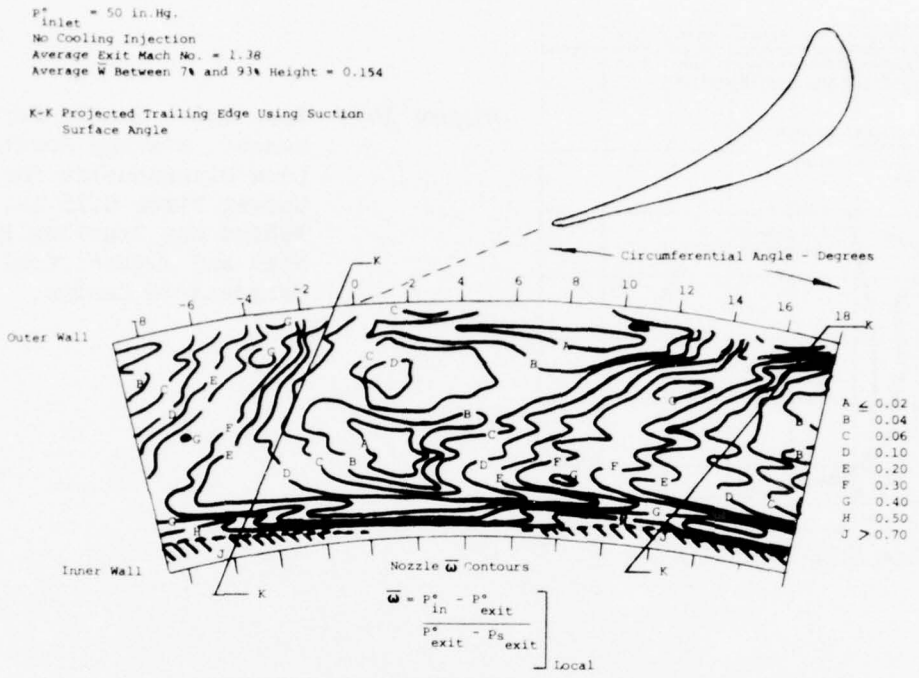


Figure 145. Test 1.0 - Nozzle Performance: Local Nozzle Pressure Loss Coefficient Contours for Survey With No Coolant and With Measuring Station 0.25 Inch Axially Behind the Trailing Edge.

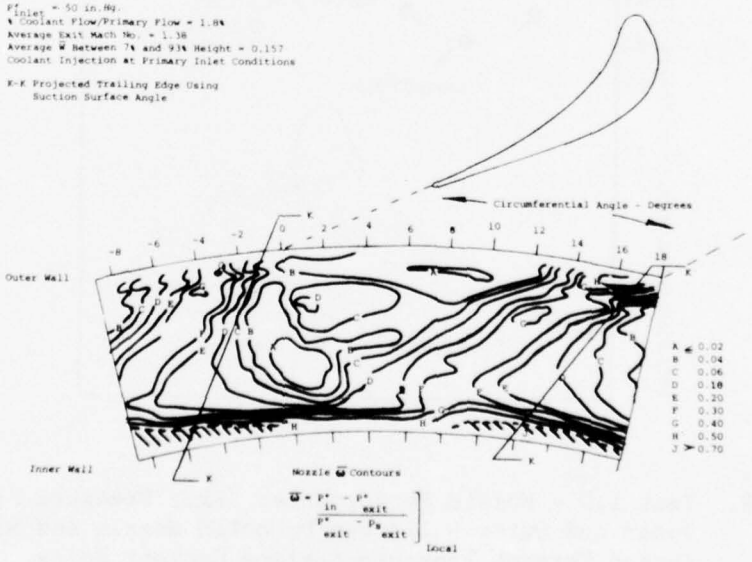


Figure 146. Test 1.0 - Nozzle Performance: Local Nozzle Pressure Loss Coefficient Contours for Survey with Coolant Flow Injection on Pressure Surface and With Measuring Station 0.25 Inch Axially Behind the Trailing Edge.

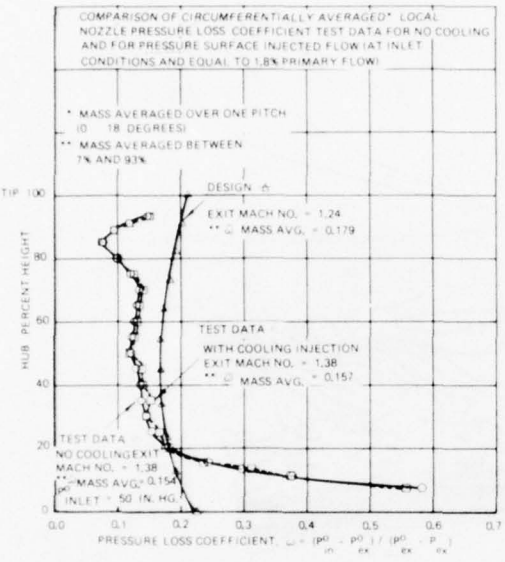


Figure 147. Test 1.0 - Nozzle Performance: Average Nozzle Loss Distribution for Survey Plane 0.25 In. Behind the Trailing Edge With and Without Cooling Compared to Design.

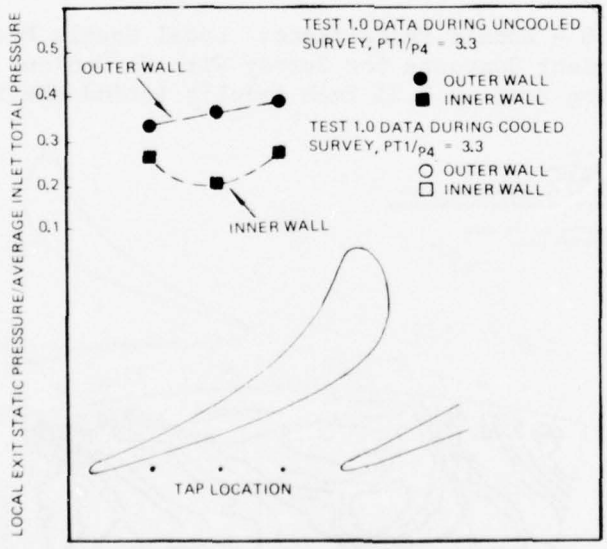


Figure 148. Test 1.0 - Nozzle Performance: Exit Pressure Distribution on Inner and Outer Walls for Uncooled Nozzle and With Flow Injected Through Pressure Surface Coolant Holes.

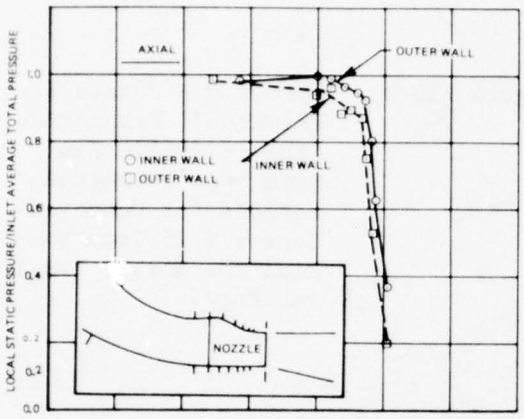


Figure 149. Test 1.0 - Nozzle Performance: Normalized Mid-Channel Static Pressure Distribution for Uncooled Nozzle Exit Survey at P_{T1}/P_4 = 3.33.

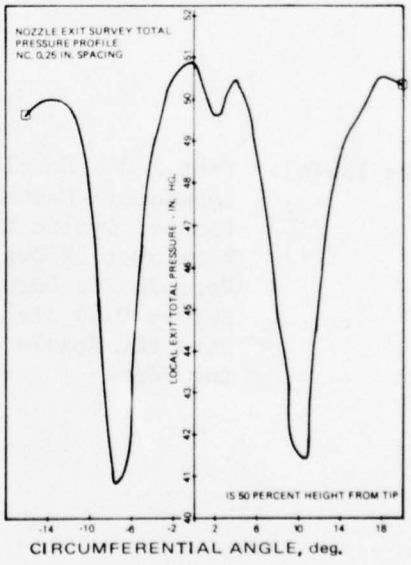


Figure 150(a). Test 1.0 - Nozzle Performance: Demonstration of Cyclic Raw Data Over 18-Degree Periods for Uncooled Survey 0.25 Inch Behind the Nozzle Trailing Edge.

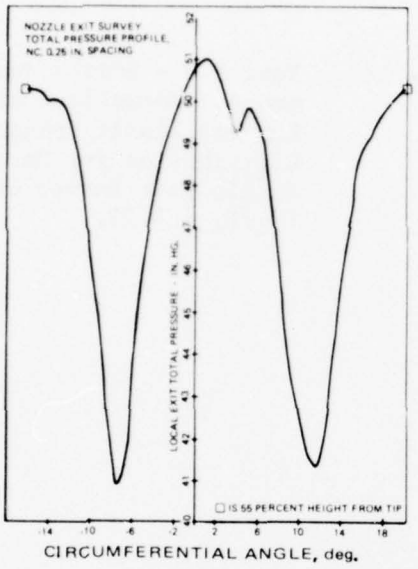


Figure 150(b). Test 1.0 - Nozzle Performance: Demonstration of Cyclic Raw Data Over 18-Degree Periods for Uncooled Survey 0.25 Inch Behind the Nozzle Trailing Edge.

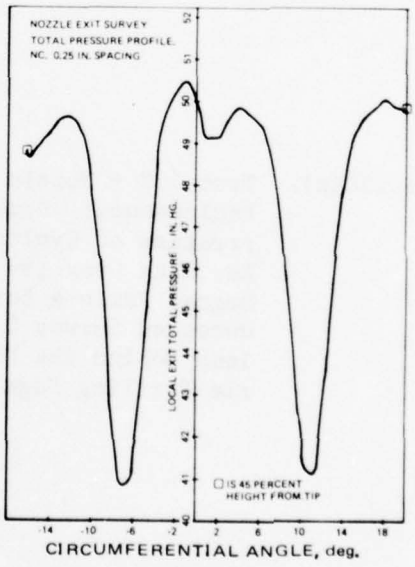


Figure 150(c). Test 1.0 - Nozzle Performance: Demonstration of Cyclic Raw Data over 18 Degree Periods for Uncooled Survey 0.25 Inch Behind the Nozzle Trailing Edge.

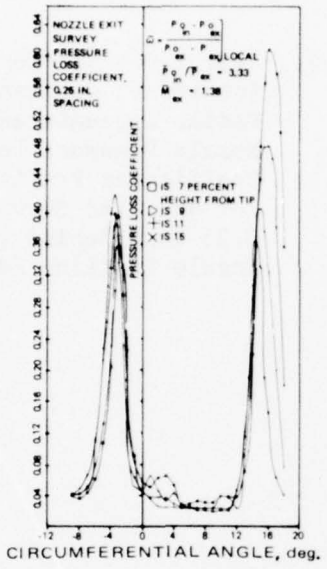


Figure 151(a). Test 1.0 - Nozzle Performance: Constant Radius Circumferential Nozzle Pressure Loss Coefficient Profiles for Uncooled Survey 0.25 Inch Behind the Nozzle Trailing Edge.

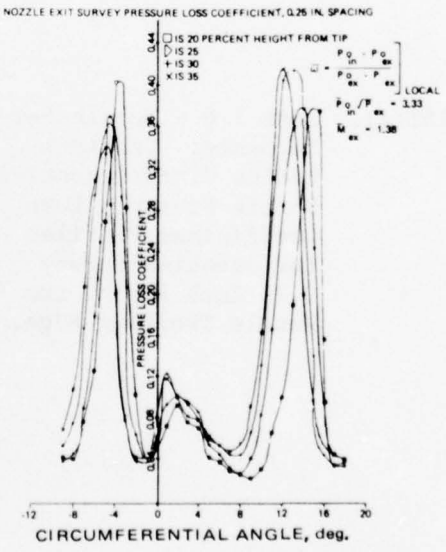


Figure 151(b). Test 1.0 - Nozzle Performance: Constant Radius Circumferential Nozzle Pressure Loss Coefficient Profiles for Uncooled Survey 0.25 Inch Behind the Nozzle Trailing Edge.

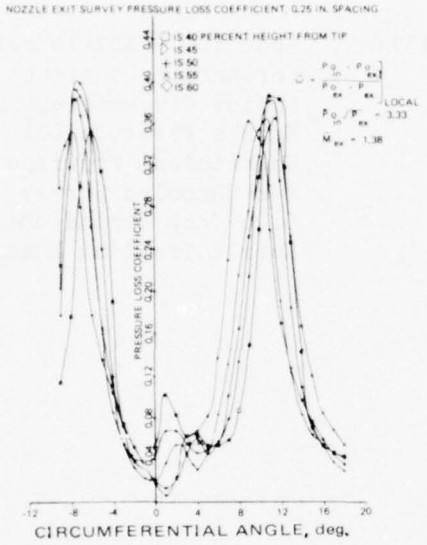


Figure 151(c). Test 1.0 - Nozzle Performance: Constant Radius Circumferential Nozzle Pressure Loss Coefficient Profiles For Uncooled Survey 0.25 Inch Behind the Nozzle Trailing Edge.

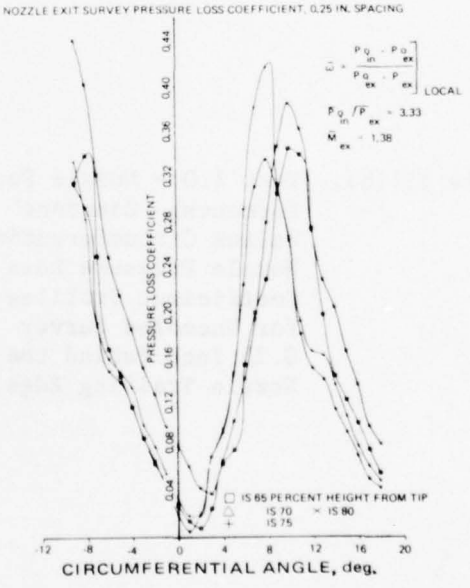


Figure 151(d). Test 1.0 - Nozzle Performance: Constant Radius Circumferential Nozzle Pressure Loss Coefficient Profiles for Uncooled Survey 0.25 Inch Behind the Nozzle Trailing Edge.



Figure 151(e). Test 1.0 - Nozzle Performance: Constant Radius Circumferential Nozzle Pressure Loss Coefficient Profiles for Uncooled Survey 0.25 Inch Behind the Nozzle Trailing Edge.

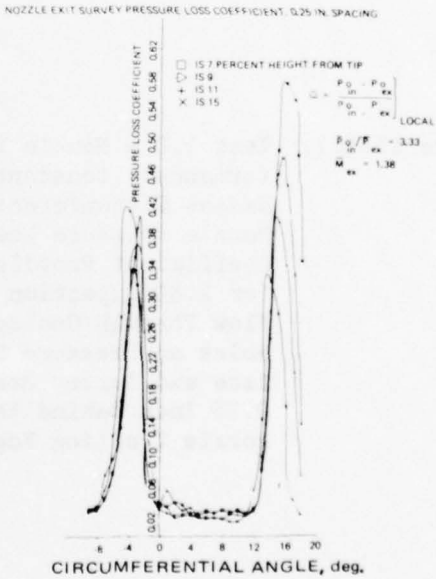


Figure 152(a). Test 1.0 - Nozzle Performance: Constant Radius Circumferential Nozzle Pressure Loss Coefficient Profiles for 1.8% Injection Flow Through Coolant Holes on Pressure Surface and Survey Station 0.25 Inch Behind the Nozzle Trailing Edge.

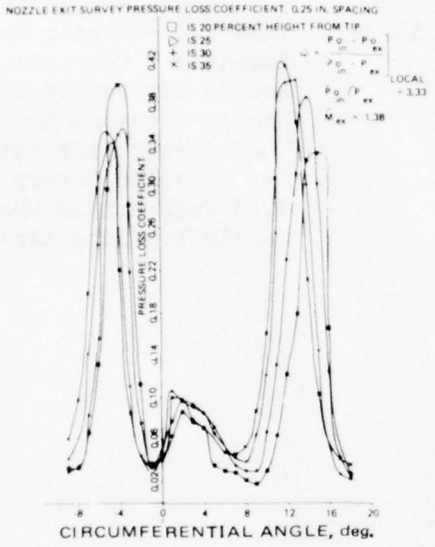


Figure 152(b). Test 1.0 - Nozzle Performance: Constant Radius Circumferential Nozzle Pressure Loss Coefficient Profiles for 1.8% Injection Flow Through Coolant Holes on Pressure Surface and Survey Station 0.25 Inch Behind the Nozzle Trailing Edge.

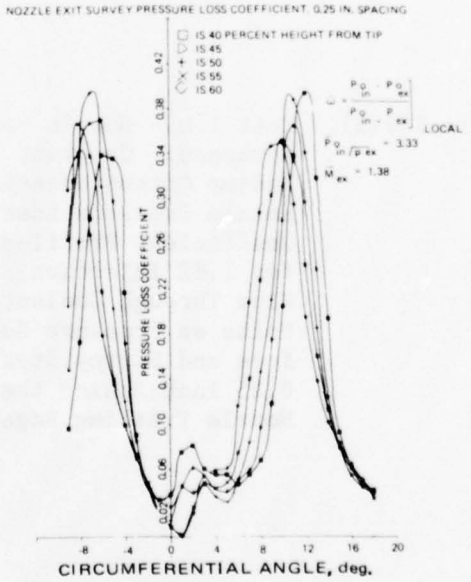


Figure 152(c). Test 1.0 - Nozzle Performance: Constant Radius Circumferential Nozzle Pressure Loss Coefficient Profiles for 1.8% Injection Flow Through Coolant Holes on Pressure Surface and Survey Station 0.25 Inch Behind the Nozzle Trailing Edge.

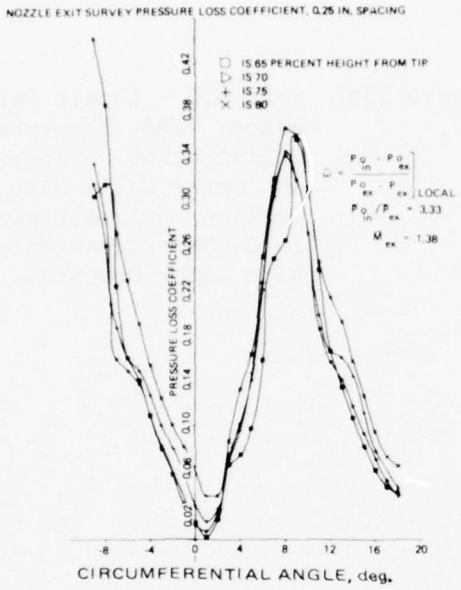


Figure 152(d). Test 1.0 - Nozzle Performance: Constant Radius Circumferential Nozzle Pressure Loss Coefficient Profiles for 1.8% Injection Flow Through Coolant Holes on Pressure Surface and Survey Station 0.25 Inch Behind the Nozzle Trailing Edge.

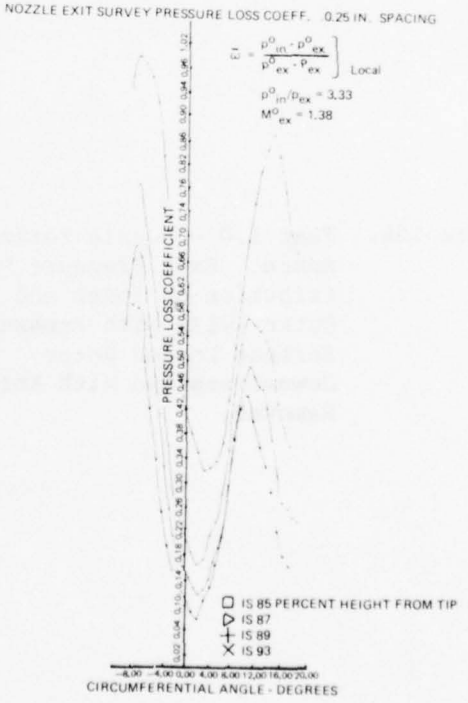


Figure 152(e). Test 1.0 - Nozzle Performance: Constant Radius Circumferential Nozzle Pressure Loss Coefficient Profiles for 1.8% Injection Flow Through Coolant Holes on Pressure Surface and Survey Station 0.25 Inch Behind the Nozzle Trailing Edge.

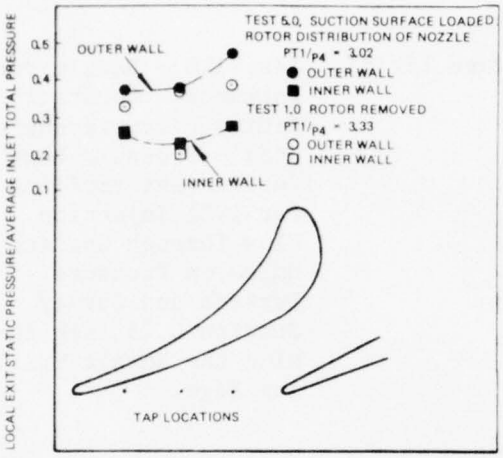
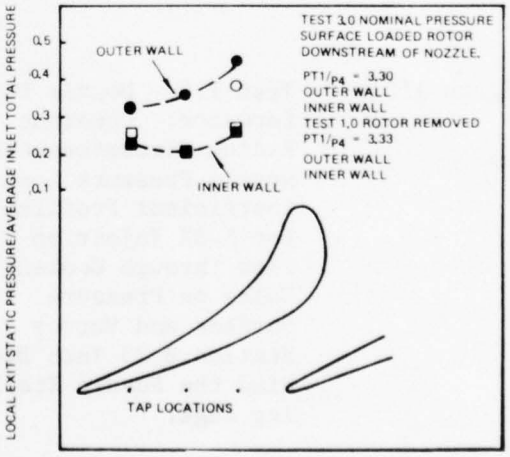


Figure 153. Test 1.0 - Nozzle Performance: Exit Pressure Distribution on Inner and Outer Walls With Suction Surface Loaded Rotor Downstream and With Rotor Removed.

Figure 154. Test 1.0 - Nozzle Performance: Exit Pressure Distribution on Inner and Outer Walls With Pressure Surface Loaded Rotor Downstream and With Rotor Removed.



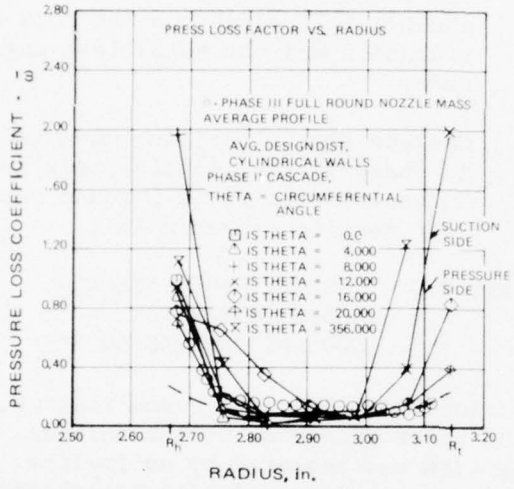
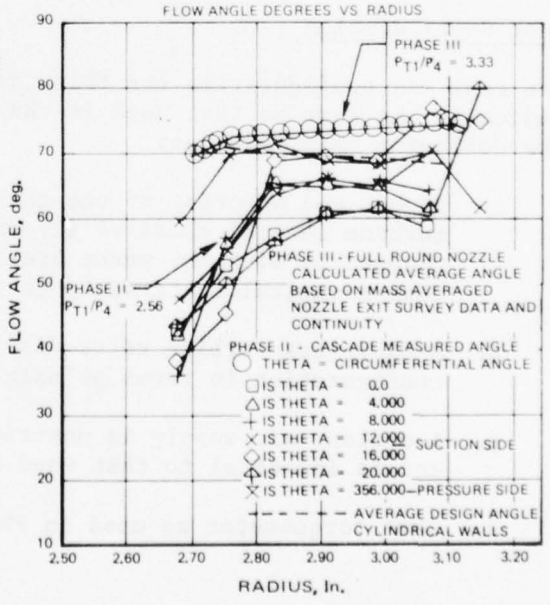


Figure 155. Test 1.0 - Nozzle Performance: Comparison of Phase II and Phase III Nozzle Pressure Loss Coefficient Profiles.

Figure 156. Test 1.0 - Nozzle Performance: Comparison of Phase II and Phase III Nozzle Exit Gas Angle Profiles.



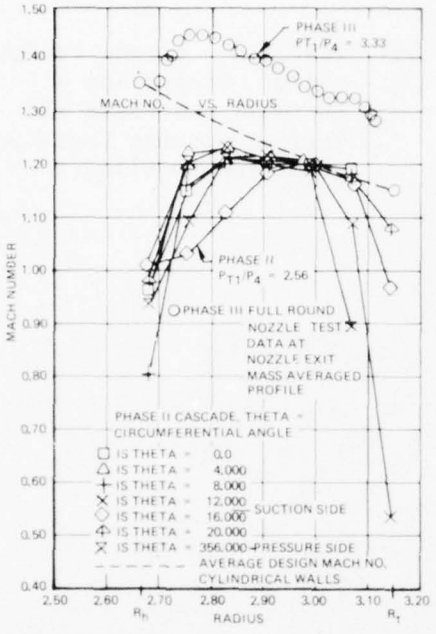


Figure 157. Test 1.0 - Nozzle Performance: Comparison of Phase II and Phase III Nozzle Exit Mach Number Distributions.

4. The injection of cooling flow from the pressure side of the vane had a negligible effect on the loss distribution and the total loss magnitude,

5. Cascade sector testing conducted in Phase II gave similar test results compared to full round cascade results of Phase III.

Test 2.0 - DISK WINDAGE, BEARING LOSSES AND ROTOR COOLANT PUMPING LOSSES

During Phase III full-round testing, the power generated by the turbine section was measured by an in-line torquemeter integral with the shafting and located between the turbine disk and the power-absorbing water brake. As a result, the indicated torque measurement is that produced by the turbine blades less the torque required to overcome windage on the shaft/disk, bearing/seal friction, and blade coolant pumping. The purpose of this test was to determine the magnitude of these windage/friction/pumping losses and, hence, provide for a more accurate assessment of the actual torque generated by the blades.

Test Configuration

The test rig configuration for this testing is shown in Figure 158 and is basically the same as that used in the subsequent performance testing with the following main features:

a. High-speed motoring of the shaft is provided by an air driven turbine located ahead of the torquemeter. This drive is interchangeable with the water brake used in performance testing, thus identical shaft seal/bearing layout is retained.

b. A bladeless turbine rotor disk duplicates the bladed disk configuration in terms of main flowpath hub and mounting geometry.

c. A coolant air supply is positively sealed from the main flow path and is identical to that used throughout the Phase III testing.

d. Same torquemeter as used in Phase III.

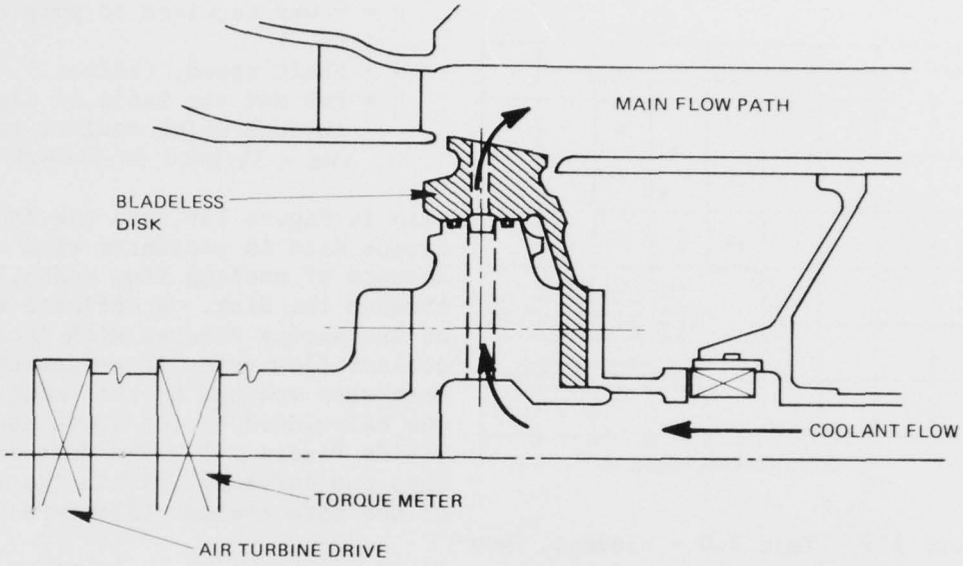


Figure 158. Test 2.0 - Bladeless Disk Configuration with Coolant Flow Path.

Test Results

Specific data points were set by motoring the shaft at a given speed and then setting the desired levels of surrounding pressure (main flow path) and coolant flow rate. The results in terms of absorbed torque vs. mechanical shaft speed is shown in Figure 159, with the following observations.

a. Windage/bearing/seal losses are nearly constant throughout the shaft speed range, with the bulk of the data falling between 3 to 4 in-lb torque (Figure 159). This is nominally 3.6 percent $\pm$0.52 percent of the design turbine work at one atmosphere rig inlet total pressure.

b. Ambient pressure surrounding the bladeless disk was set at three levels of 17, 50 and 100 percent of barometric pressure (Figure 159). No significant change in torque is observed, thus indicating that windage effects alone are small in this particular rig.

c. Coolant pumping losses correlate well with that calculated by the Euler equation where:

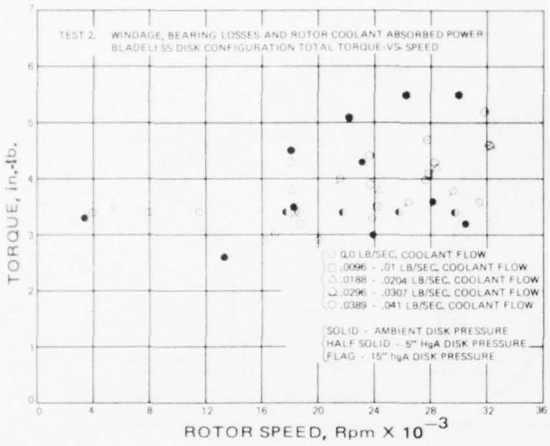


Figure 159. Test 2.0 - Windage, Bearing Losses and Rotor Coolant Absorbed Power Bladeless Disk Configuration Total Torque vs. Speed.

$$P = \frac{W_a N^2}{g\ 550} \left(R_t^2 - R_h^2\right)$$

P = Power required to pump coolant, Hp.
N = Shaft speed, rad/sec.
R = Hub and tip radii of disk through which coolant air (Wa - lb/sec) is pumped, feet.

Also in Figure 159, the raw indicated torque data is presented with various amounts of cooling flow radially through the disk. A definite trend of increasing torques with increasing coolant flow rates is evidenced. This data when reduced by the pumping torque calculated by the above equation yields Figure 160. The data collapses into one curve and within the scatter of the zero coolant flow data.

Based on this test, a least square polynominal fit (third order) of the torque data together with Euler's equation where applicable was used throughout Phase III data reduction in correcting indicated torque for mechanical/windage and pumping losses.

TEST 3.0 - EVALUATION OF PERFORMANCE OF PRESSURE SURFACE LOADED TURBINE

The purpose of this test was to define the stage performance of the baseline turbine configuration and evaluate the blade element performance from wall static pressures and rotor exit traverse measurements.

Test Configuration

The nominal 41 blade pressure-side loaded rotor (Figure 134) and the 20 vane nozzle (Figure 133) were used throughout this test. Coolant holes in the blades and nozzle vanes were closed and the surface was smoothed to the 0.0126 inch with axial spacing between the nozzle and rotor at a nominal design of 0.25 inch.

Instrumentation for performance evaluation included the following (Figure 138):

- Nozzle inlet total temperature and pressure
- Rotor exit total temperature and pressure
- Rotor exit radial traverse (2 locations) of temperature, pressure and swirl angle

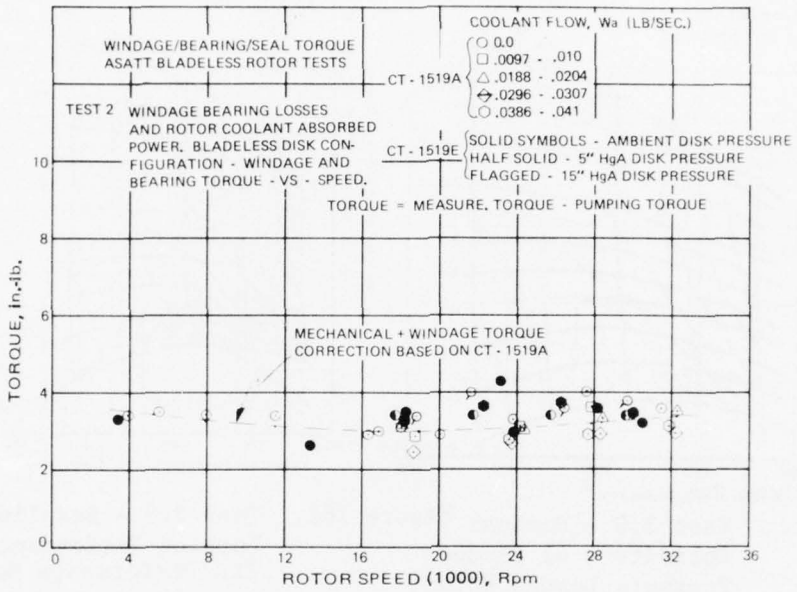


Figure 160. Test 2.0 - Windage Bearing Losses and Rotor Coolant Absorbed Power. Bladeless Disk Configuration - Windage and Bearing Torque vs. Speed.

- In-line torquemeter (Himmelstein Model McRT 2-04)
- Static pressures at stage inlet and exit total measuring planes, nozzle exit, nozzle vane mid-channel, and rotor exit locations on both inner and outer walls.

Test Results

With turbine stage inlet conditions maintained at nominal one atmosphere and 220°-230°F temperature, twenty-five data points were taken at various speed - pressure ratio settings and the overall stage performance was defined based on dynamometer data, as shown in the map on Figure 161. For comparison to design performance, this map was then adjusted to reflect increased performance at design values of Reynolds number per the correlations established during subsequent testing in test 13. The resulting map is shown in Figure 162 and except for tip clearance, is directly comparable to the design map (Figure 163). The tip clearance difference between these two maps is 0.0086 in. (0.0126 in. for Figure 162, and 0.004 in. design for Figure 163). An estimate of tip clearance effects on performance is shown in Figure 8 and yields approximately a 1.0 point efficiency change for a 0.0086 in. change in clearance. Hence, for a common comparison to Figure 162, the performance shown on the design map (Figure 163) may be decreased by 1.0 efficiency points and yields 80.3 percent. This is also

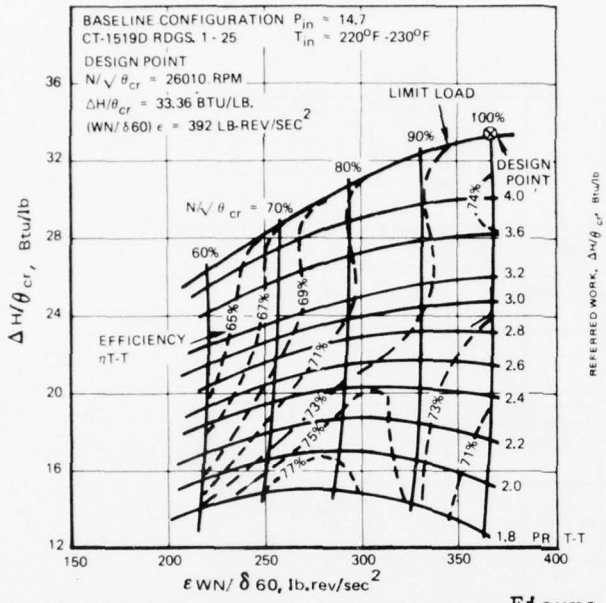


Figure 161. Test 3.0 - Nominal Solidity - 41 Blades Pressure Loaded Rotor, Baseline Configuration.

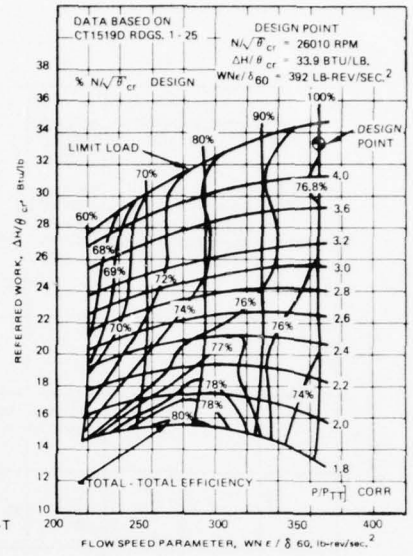


Figure 162. Test 3.0 - Baseline Turbine Performance Map: PLR Performance Map With Reynolds Number Corrected to Design Point Conditions.

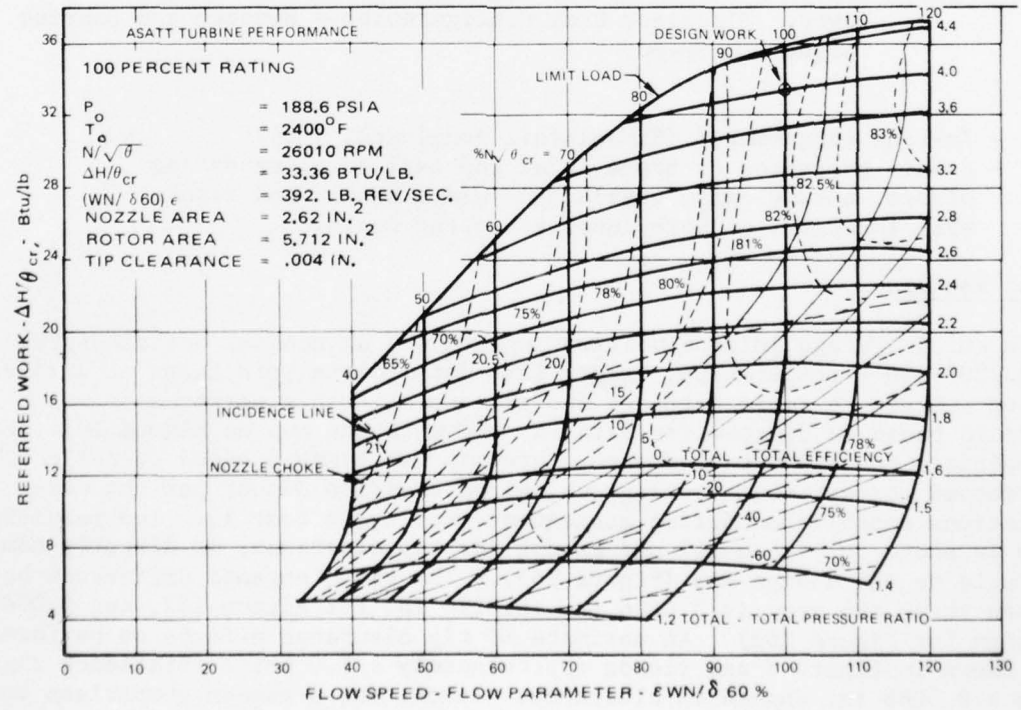


Figure 163. Test 3.0 - ASATT Turbine Performance.

consistent with the 80.2 percent efficiency predicted during Phase I (Appendix B) at a slightly lower rotor tip clearance of 0.011 in. The overall performance comparison between test and design at work level and shaft speed is summarized below:

	TEST	DESIGN	Δ, PERCENT
Referred Work, $\Delta H/\theta_{cr}$, Btu/lb.	33.4	33.4	0
Efficiency, η, Percent	76.5	80.2	-3.7
Flow Speed Parameter, $(WN/\delta 60)\varepsilon$, lb-rev/sec^2	367	392	-6.4
Referred Work at Limit Load, $\Delta H/\theta_{cr}$, Btu/lb.	34.6	35.8	-1.2

With respect to design values, the efficiency is down 3.7 percentage points with a similar trend at limit load conditions where work is 3.4 percent low. Also, the flow speed parameter indicates a 6.4-percent small nozzle throat, which is in agreement with the nozzle blowdown tests of test 1. More specific data as to blade element performance as indicated by the static pressure taps and rotor exit traverses is as follows:

a. Radial distribution of stage performance was determined from total temperature, pressure, and angle surveys at rotor exit and rake total temperature/pressure conditions at the nozzle inlet. Using a radial distribution of the circumferential average of local inlet values and the local radial distribution of the traverses, a radial adiabatic efficiency gradient was determined. These data are shown in Figures 164 through 169. The absolute level of efficiencies indicated in Figure 169 are substantially higher than that of the map data. This is in part due to significant circumferential and radial temperature gradients at the inlet which are in turn propagated through the turbine (Figure 170). Since the traverse is sensing only circumferential conditions and the turbine inlet is taken as the average, the calculated efficiencies will be high. However, the efficiency distribution is significant in that it reflects near design gradients from 30 to 90 percent span. The hub, 10 to 30 percent span, data is inconclusive.

b. The axial static pressure distribution through the stage is shown in Figure 171 and is compared to design values. Good correlation is obtained near the outer wall. However, the inner wall indicates substantially greater expansion at nozzle discharge, hence higher flow Mach numbers than design intent (Figure 172). This has the effect of increasing incidence at the rotor blade leading edge (Figure 173) and reducing the reaction through rotor hub, both tending to reduce hub performance. Increasing the nozzle throat area to design levels with most of the increase near the hub should improve the performance.

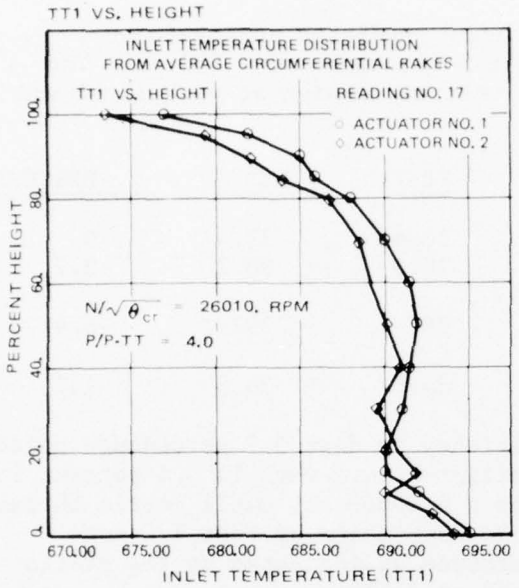


Figure 164. Test 3.0 - Evaluation of Nominal Performance Baseline Configuration: Inlet Total Temperature Vs. Height.

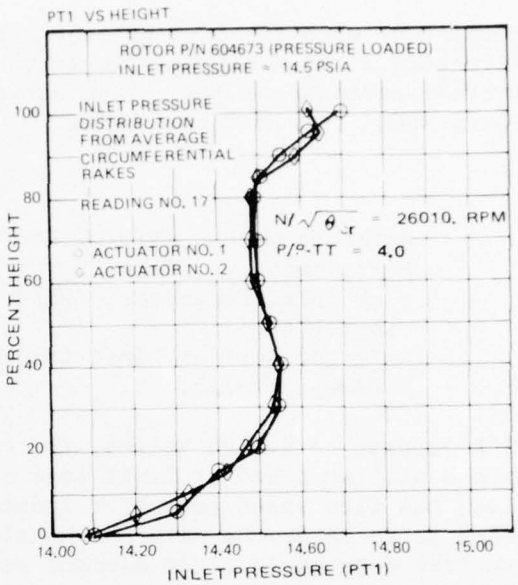


Figure 165. Test 3.0 - Evaluation of Nominal Performance *Baseline Configuration.*

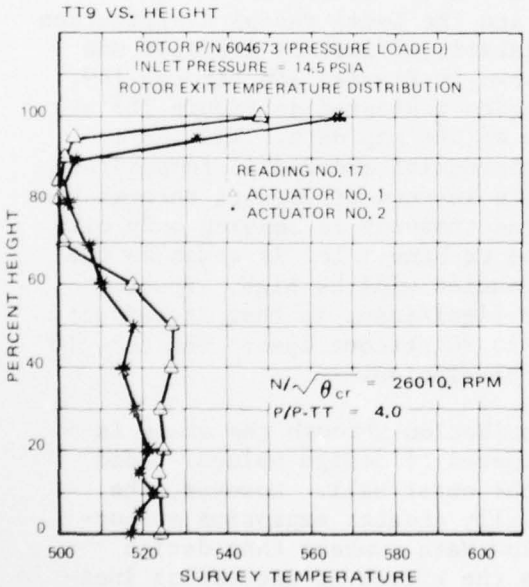


Figure 166. Test 3.0 - Evaluation of Nominal Performance Baseline Configuration: Exit Total Temperature Vs. Height.

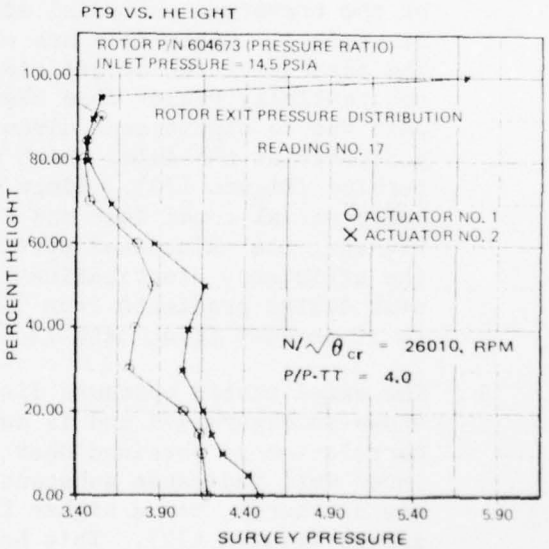


Figure 167. Test 3.0 - Evaluation of Nominal Performance Baseline Configuration.

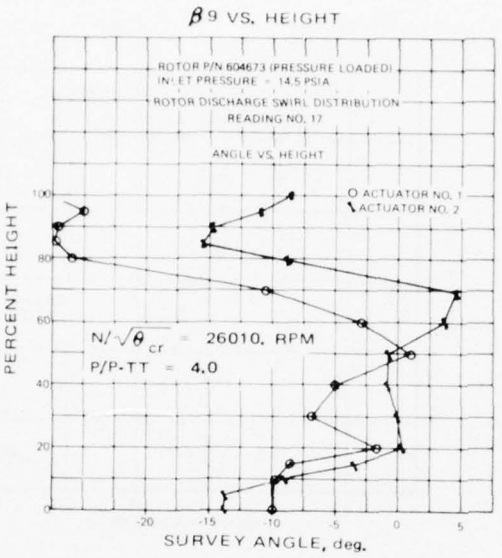


Figure 168. Test 3.0 - Evaluation of Nominal Performance Baseline Configuration: Exit Swirl Vs. Height.

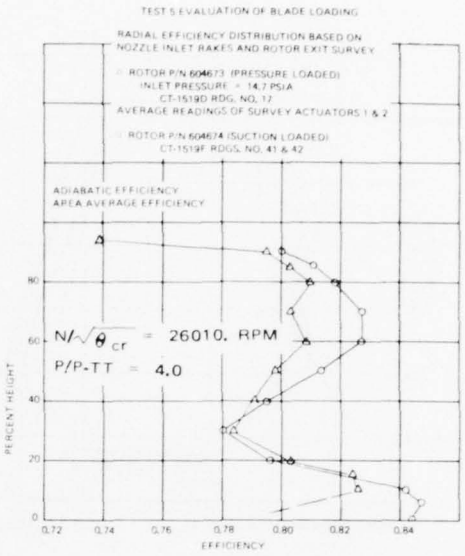


Figure 169. Test 5.0 - Evaluation of Blade Loading Radial Efficiency Distribution Based on Nozzle Inlet Rakes and Rotor Exit Survey.

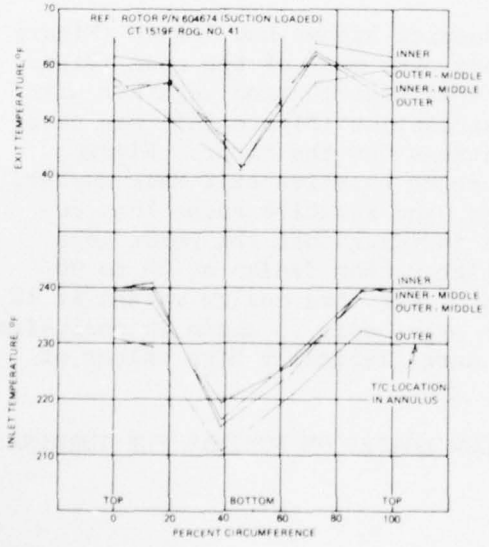


Figure 170. Test 5.0 - Evaluation of Blade Loading Nozzle Inlet and Rotor Exit Circumferential Temperature Variation.

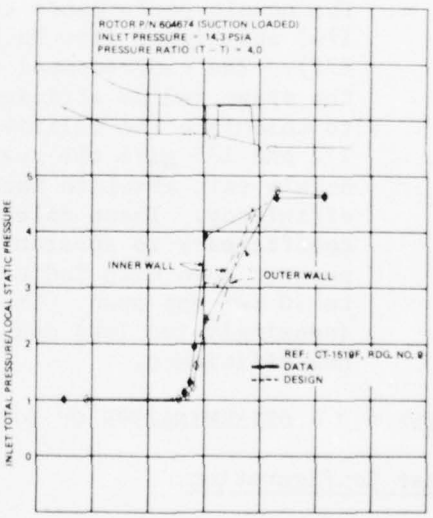


Figure 171. Test 5.0 - Evaluation of Blade Loading, Axial Static Pressure Distribution.

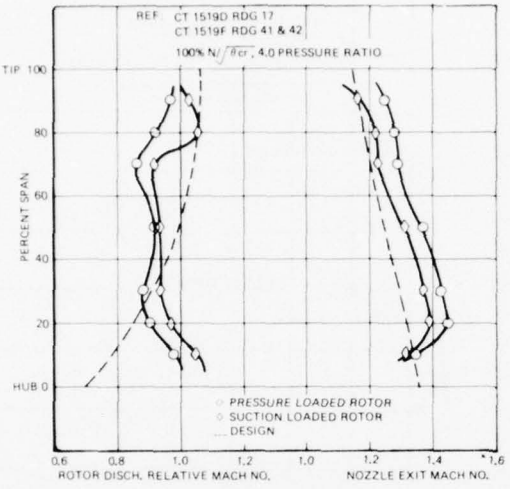


Figure 172. Test 5.0 Evaluation of Blade Loading. Nozzle Exit and Rotor Discharge Relative Mach Number Distribution.

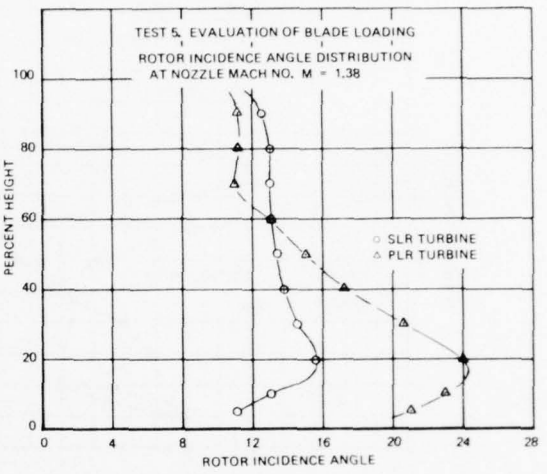


Figure 173. Test 5.0 - Evaluation Blade Loading. Rotor Incidence Angle Distribution at Nozzle Mach Number M = 1.38.

c. The nozzle performance tests measured higher hub losses (Figure 174) and higher flow Mach numbers over most of the span (Figure 172). The experimental nozzle loss distribution together with the stage radial efficiency distribution (Figure 169) was used to calculate the relative conditions for the rotor. Figures 172 and 175 give the resulting rotor relative exit Mach number, nozzle exit absolute Mach number, and relative rotor loss coefficiency. These calculations indicate that the rotor loss coefficiency is substantially higher than design at 30 to 90 percent span with indications of lower than design values at 10 to 30 percent span. The latter hypothesis is again inconclusive (seemingly too low) due to the unrealistically high values of hub efficiency.

TEST 4.0 - DETERMINATION OF COOLING FLOW LOSSES ON NOMINAL PLR TURBINE

Test Configuration

Testing for coolant effect was conducted using the same hardware as Test 3 (Evaluation of Performance of PLR Turbine) with the exception of installing supply lines to stator and rotor coolant inlet fittings. The rig assembly used the full-round 20-vane nozzle and 41-blade (nominal solidity) pressure surface loaded rotor with a nominal running tip clearance of 0.013 inch, a nominal inlet distortion screen, no inlet boundary layer plates, and a nominal nozzle/rotor axial spacing of 0.25 inch.

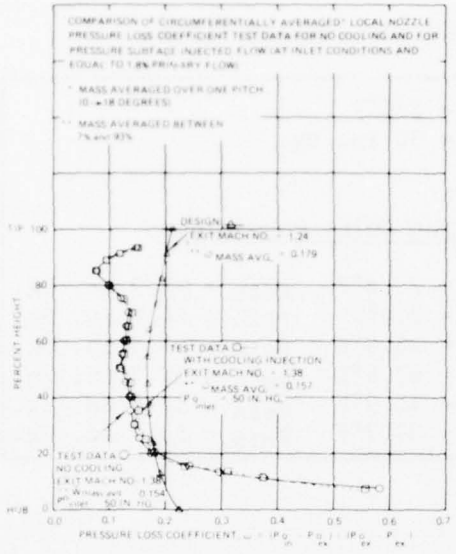


Figure 174. Test 1.0 - Nozzle Performance: Average Nozzle Loss Distribution for Survey Plane 0.25 In. Behind the Trailing Edge with and without Cooling Compared to Design.

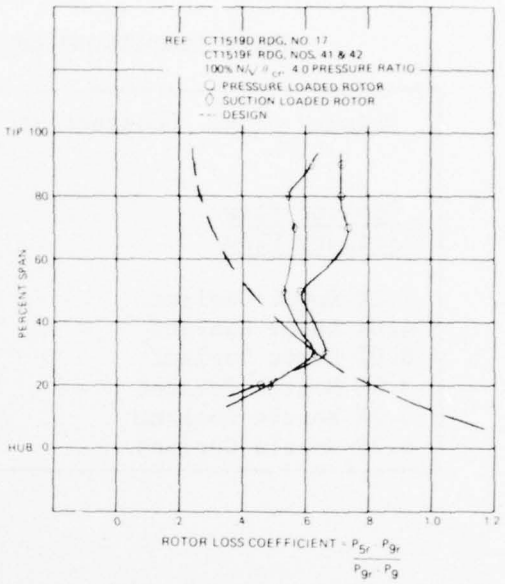


Figure 175. Rotor Loss Distributions.

The turbine was set at design speed and pressure ratio, $N/\sqrt{\theta_{cr}}$ = 26,010 rpm and P/PTT = 4.2. Sixteen total pressure rake readings at both nozzle inlet and rotor exit were averaged to set the turbine total-total pressure ratio. Speed was regulated with a Kahn water brake, having a design maximum speed of 35,000 rpm. However, a maximum limit of 30,000 rpm was imposed to maintain a safe operating margin. Primary flow inlet total temperature (averaged from sixteen rake readings) was maintained slightly below 230 degrees fahrenheit. This temperature was the maximum inlet temperature for running at a referred speed of 26,010 rpm without exceeding the 30,000-rpm mechanical speed limitation. Inlet total pressure was set at 50 inches Hg.

Nozzle and rotor coolant was injected through holes on the pressure surface of the blading. Figures 130 and 131(a) and 131(b) illustrated the size and locations of these holes. Each coolant flow was set by its percentage with respect to the primary inlet flow. Coolant inlet conditions, total temperature and static pressure, were measured in cavities downstream of their flow measuring orifices. These conditions varied by the amount of coolant flow; that is, higher percentage of coolant flow resulted in higher inlet pressure and cooler inlet temperature. Table 17 illustrates this effect.

TABLE 17

INLET CONDITIONS OF PRIMARY AND COOLANT FLOWS

Primary Flow: Constant at T°_{in} = 230°F, P°_{in} = 50 in. Hg.		
Coolant Flow %Primary Flow	Coolant Inlet Conditions	
2.2% Rotor Coolant	T°_{in} = 23.8°F	Psin = 19.7 in. Hg.
4.0% Rotor Coolant	T°_{in} = 3.4°F	Psin = 26.8 in. Hg.
8.0% Rotor Coolant	T°_{in} = 16.4°F	Psin = 47.5 in. Hg.
3.5% Nozzle Coolant	T°_{in} = 67.5°F	Psin = 50.7 in. Hg.
5.7% Nozzle Coolant	T°_{in} = 41.9°F	Psin = 52.9 in. Hg.
6.2% Nozzle Coolant	T°_{in} = 37.7°F	Psin = 53.7 in. Hg.

Radial rotor exit surveys of total pressure, total temperature and exit gas angle were conducted at several coolant rates.

Test Results

A comparison of theoretical and test data total discharge flow as a function of nozzle and rotor coolant flow is given in Figure 176. Previous test results from Test 1, Nozzle Performance, indicated the maximum corrected airflow which the nozzle could pass was approximately $(W\sqrt{\theta_{cr}}/\delta)\ \varepsilon = 0.847$. Since nozzle coolant is injected upstream of the nozzle throat, this choked value includes both primary and nozzle coolant flow. Theoretical corrected total discharge flow is the sum of 0.847 plus the rotor coolant contribution. Theoretical discharge flow lines are shown in Figure 176. Note, for zero percent rotor coolant corrected total discharge flow is constant 0.847. As rotor coolant is introduced, lines representing constant percent rotor coolant decrease as nozzle coolant increases. This is because the definition of percent coolant is coolant flow compared to inlet primary flow. As nozzle coolant increases, the inlet primary flow decreases. Therefore, for the same percent rotor coolant by definition, there is less actual rotor coolant flow as nozzle coolant increases. Test data, with the exception of one reading, agreed within 0.5 percent of the theoretical curves.

In evaluating performance, the turbine system was treated as a control volume with energy inputs of primary flow, nozzle coolant flow and rotor coolant flow and with energy output of mixed total discharge flow. Torque

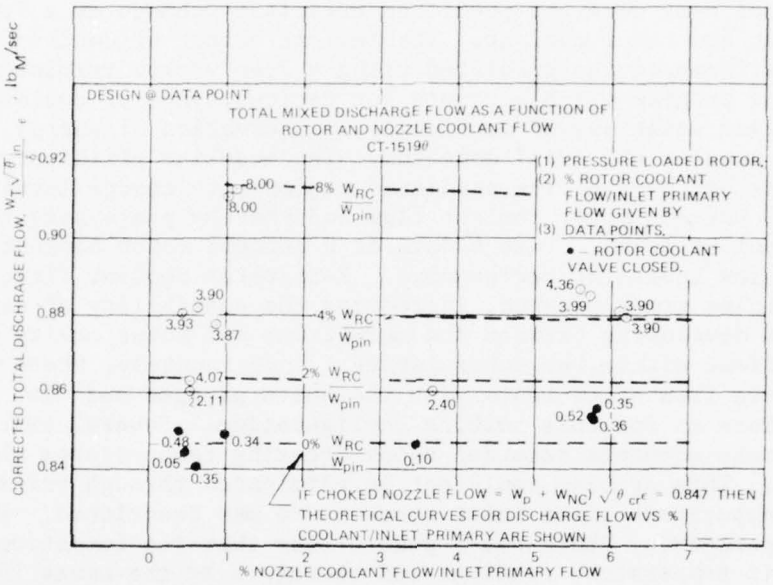


Figure 176. Test 4.0 - Determination of Cooling Flow Losses on Nominal PLR Turbine: Discharge Flow vs. Cooling Flow.

data for this test was unstable; therefore, rake temperatures and coolant cavity temperatures were used to calculate energy change. Inlet and exit rake temperature readings were corrected for conduction, convection and ram recovery, using equations derived from thermocouple calibration data. Efficiency is defined as:

$$\eta = \frac{\text{Net Work}}{\text{Ideal Work}}$$

with, Net Work = Mass Flow$_i$ (Enthalpy$_{in}$ - Enthalpy$_{out}$)$_i$

i = Input Source

Ideal work assumes isentropic expansion of each source from their respective inlet conditions to the mixed exit state:

Ideal Work = Σ_iMass Flow$_i$ (Enthalpy$_{in}$ - Isen. Enthalpy$_{out}$)$_i$

i = Input Source.

Results indicate 0.05 percent loss in efficiency for every one percent nozzle cooling and approximately 1.1 percent loss in efficiency for every one percent rotor coolant injection. Since the design point calls for

4 percent nozzle cooling and 2 percent rotor cooling (Ref. Figure 130), efficiency drop due to cooling is 2.4 percent for design. Figure 177 is a comparison of test data and predicted efficiency change as a function of nozzle coolant and rotor coolant. Theoretical effect of coolant flow injection on performance was predicted using a free vortex turbine design point computer program which accounts for various types of cooling. The program involves equations of continuity, conservation of energy and conservation of angular and axial momentum. The baseline efficiency of Figure 177 was set by applying predicted performance change levels to 4 percent and 8 percent rotor coolant flow and thereby projecting the 0 percent rotor coolant level. Test 4 data at 0 percent rotor coolant flow gave suspiciously low levels of performance. Zero rotor coolant flow, when the coolant holes are unplugged, introduces the possibility of secondary flow patterns developing between the mainstream and rotor cavity due to the pressure gradient within the rotor cavity. Unfortunately, there was no comparable data from other tests with the holes plugged and with the same inlet conditions as for this turbine configuration. Several exit total temperature rake elements recorded below freezing temperatures when coolant was injected. This problem could not be eliminated through raising the primary inlet temperature since inlet temperature was restricted. With below freezing temperatures, there was a possibility that ice formation may have distorted exit temperature readings and therefore be the cause for data scatter shown in Figure 177.

Rotor exit traverse data for several coolant rates is shown in Figure 178. The exit total pressure profile shows no change due to coolant which is consistent with results of Test 1 (Nozzle Performance) in which nozzle exit surveys indicated no difference in pressure loss coefficient between the nominal uncooled nozzle and the nozzle with 1.8 percent coolant flow injected. Exit gas angle profiles within the range of data scatter show no coolant effect. Differences in the exit total temperature profiles result from the percent of coolant injected and its inlet temperature.

TEST 5.0 - EVALUATION OF BLADE LOADING

The purpose of this test was to experimentally evaluate the effect of a variation in rotor blade loading on the overall performance of the turbine.

Test Configuration

The build consisted of the full-round nominal nozzle with the suction surface loaded rotor (SLR) turbine assembly. The cooling holes on the nozzle and rotor were closed off.

The axial spacing between the nozzle trailing edge and the rotor leading edge was set at the nominal 0.25 inch, and the average radial rotor static tip clearance was 0.012 inch. Instrumentation and test variables were the same as for the PLR turbine. The two rotor geometries tested were shown in Figure 134.

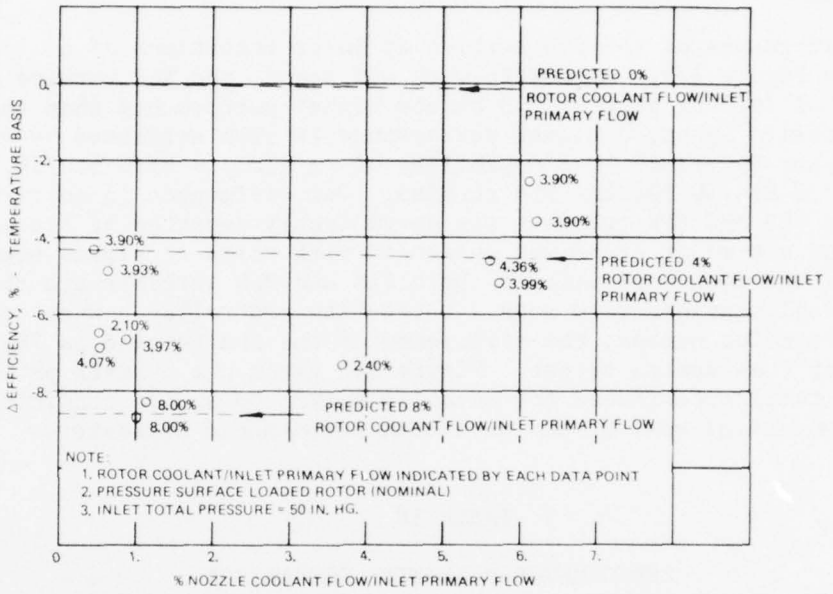


Figure 177. Test 4.0 - Determination of Cooling Flow Losses on Nominal PLR Turbine : Efficiency Drop vs. Cooling Flow

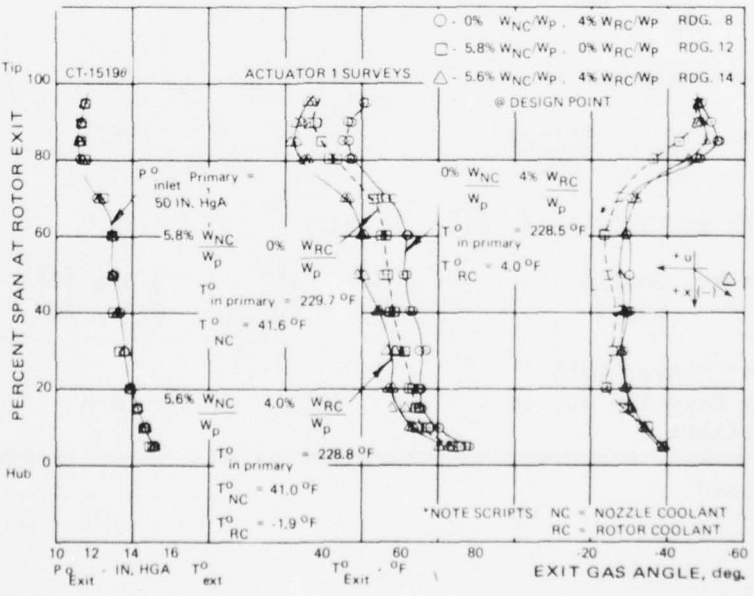


Figure 178. Test 4.0 - Determination of Cooling Flow Losses on Nominal PLR Turbine. Rotor Exit Pressure, Temperature and Swirl Surveys.

Test Results

Overall performance of the SLR turbine at inlet conditions of 14.7 and 230°F is given in Figure 179. At design work and speed, the SLR turbine shows an efficiency of 76.3 percent or 3.3 points higher performance than the PLR turbine. At design speed, a higher performance is also evidenced by a 5.4 percent higher SLR limit load capability of $\Delta H/\theta_{cr}$ = 35.0 btu/lb, as compared to 33.2 Btu/lb for the PLR turbine. The difference in performance between the PLR and SLR turbines was consistently repeated at atmospheric testing, and a similar trend was evidenced with tests at higher pressures (Test 13). The flow capacities of both SLR and PLR turbines are the same and both configurations were nozzle choke-flow controlled. When corrected to engine Reynolds number, the efficiency of the SLR turbine is 78.8 or 1.4 points lower than design target. Figure 180 gives the overall performance of the SLR turbine corrected for Reynolds number to engine conditions. Table 18 summarizes some of the pertinent aerodynamic parameters.

TABLE 18

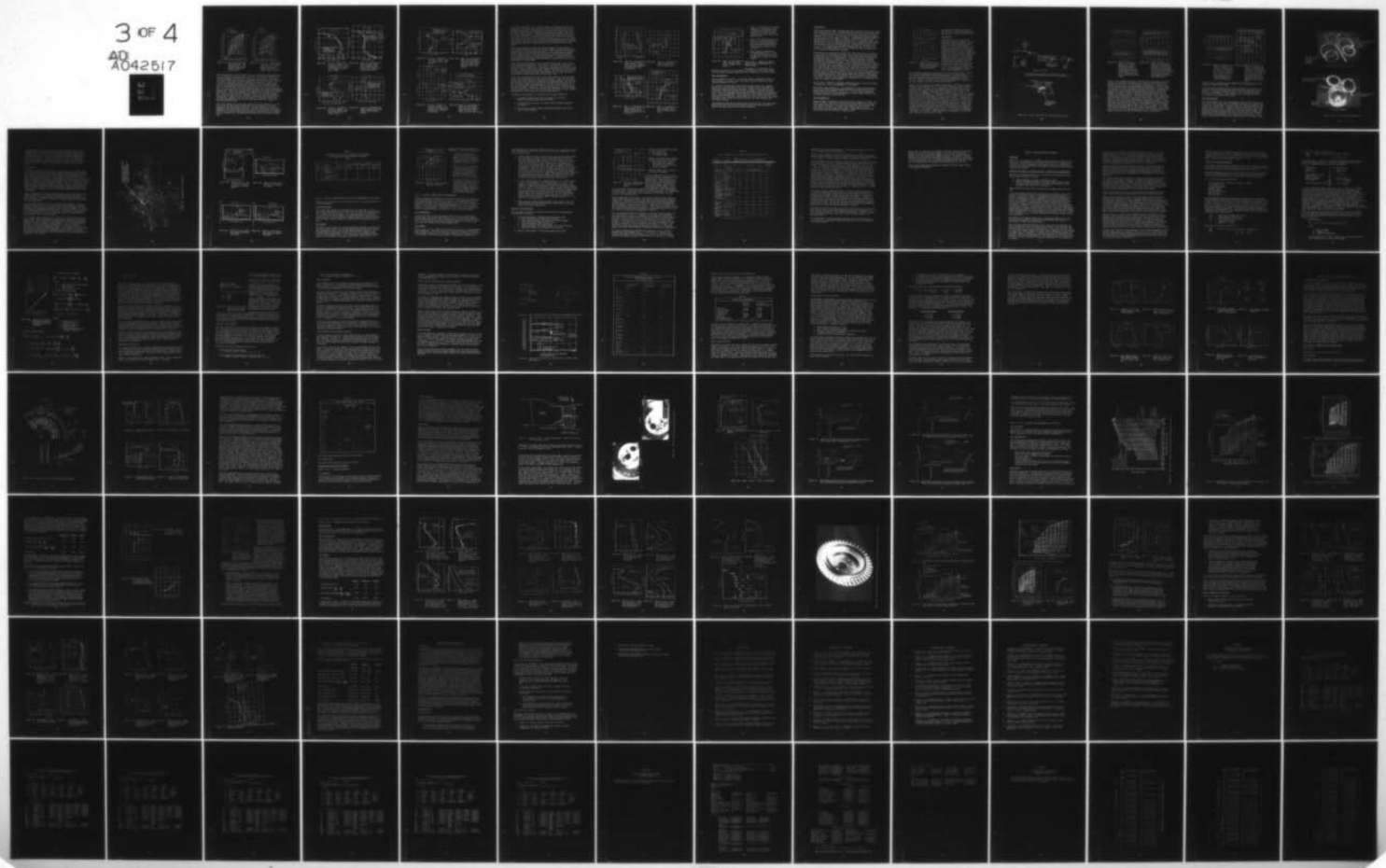
PERFORMANCE PARAMETER COMPARISON
OF PLR TURBINE AND SLR TURBINE AT DESIGN SPEED

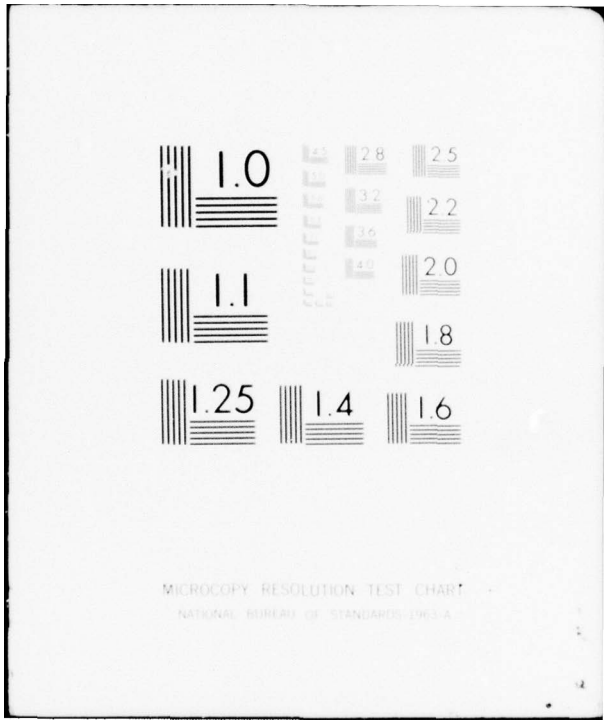
Parameter	PLR Turbine	SLR Turbine	Design
Referred Work, $\frac{\Delta H}{\theta_{cr}}$, $\frac{Btu}{lb}$	33.4	33.4	33.4
Efficiency at Design Work	73.0*	76.3	80.2
Referred Flow, $\frac{WN}{\delta 60}\sqrt{\theta}$, $\frac{lb\text{-}rev}{sec^2}$	367	367	392
Referred Work at Limit Load, $\frac{Btu}{lb}$	33.2	35.0	35.8
Reynolds Number, Nozzle	3.3×10^5	3.3×10^5	8.03×10^5
Rotor	0.8×10^5	0.8×10^5	1.88×10^5
Efficiency at Design Work Corrected by Reynolds No. to Engine Conditions	76.5	78.8	80.2

* At Limit Load

AD-A042 517 TELEDYNE CAE TOLEDO OHIO F/G 21/5
ADVANCED SMALL AXIAL TURBINE TECHNOLOGY.(U)
MAY 77 H F DUE, C ROGO, C L KOSIER DAAJ02-72-C-0117
UNCLASSIFIED TCAE-1508 USAAMRDL-TR-77-1 NL

3 OF 4
AD A042517




1.0
1.1
1.25
1.4
1.6
1.8
2.0
2.2
2.5
2.8
3.2
3.6
4.0
MICROCOPY RESOLUTION TEST CHART
NATIONAL BUREAU OF STANDARDS 1963-A

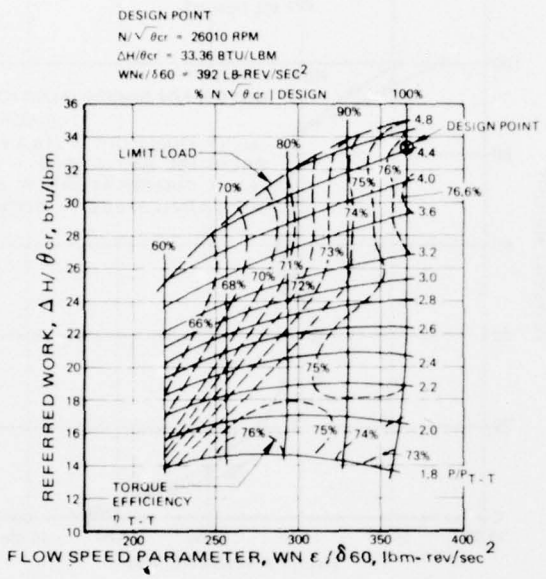


Figure 179. Test 5.0 - Blade Loading Evaluation: Performance Map for the Suction Loaded Rotor Configuration.

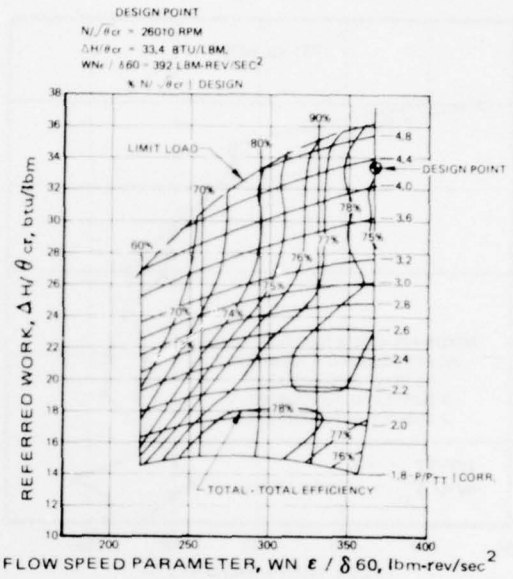


Figure 180. Test 5.0 - Blade Loading Evaluation: SLR Performance Map with Reynolds Number Corrected to Design Point Conditions.

Radial distribution of performance of the two turbines was determined from total temperature, pressure, angle surveys at rotor exit, and rake total pressure temperature conditions at the nozzle leading edge. Individual inlet probe values were averaged circumferentially and plotted as a function of radius to calculate radial distribution of efficiency. Figures 181 through 186 show the data taken and resulting radial efficiency distribution. Good agreement between the two surveys is shown from 30 percent span to 90 percent span with substantial differences in efficiency in the hub. The two surveys are located 84 degrees apart, and large circumferential differences in rake inlet and rake exit conditions were noted during testing (Figure 187). These rake temperature circumferential gradients are due to heat conduction losses through the probe stem to the large inlet plenum. Survey hub efficiency data is, therefore, suspect and absolute values are questionable. However, since the SLR and PLR turbines were tested with the same instrumentation and the same operating conditions, comparative observations may be made.

Figure 188 compares the design point radial efficiency distribution of the two turbine configurations as determined from the average of two total temperature and total pressure surveys. The SLR turbine shows higher performance in the extreme hub region and in the 40 to 80 percent span sections. Differences in the two turbine performances are probably due to a combined effect of loading due to incidence and loading due to differences of blade shape.

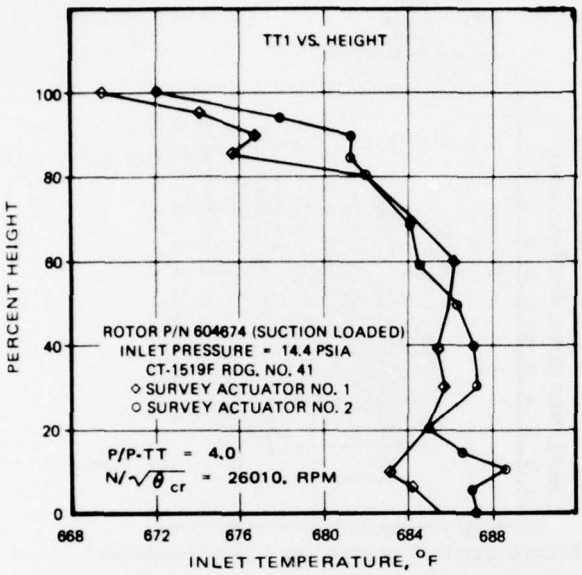


Figure 181. Test 5.0 - Evaluation of Blade Loading. Inlet Temperature Distribution from Average Circumferential Rakes.

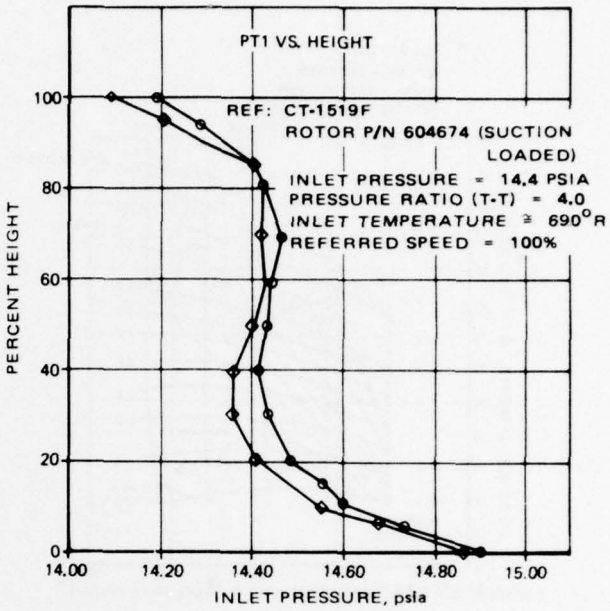


Figure 182. Test 5.0 - Evaluation of Blade Loading. Inlet Total Pressure Distribution from Average Circumferential Rakes.

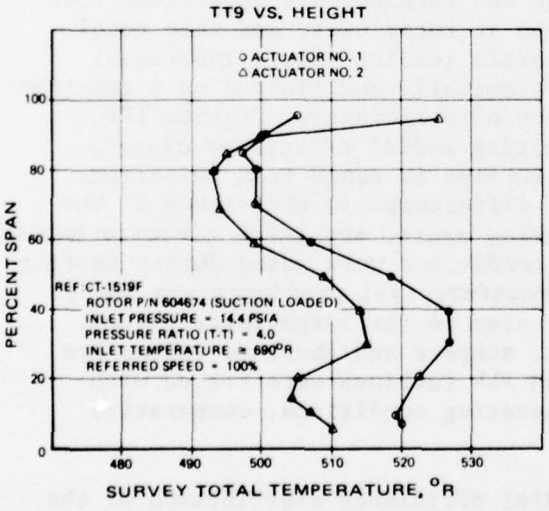


Figure 183. Test 5.0 - Evaluation of Blade Loading. Rotor Exit Total Temperature Radial Survey.

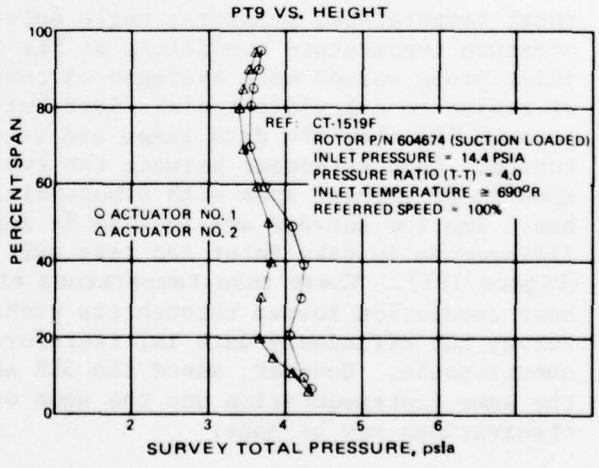


Figure 184. Test 5.0 - Evaluation of Blade Loading. Rotor Exit Radial Total Pressure Survey.

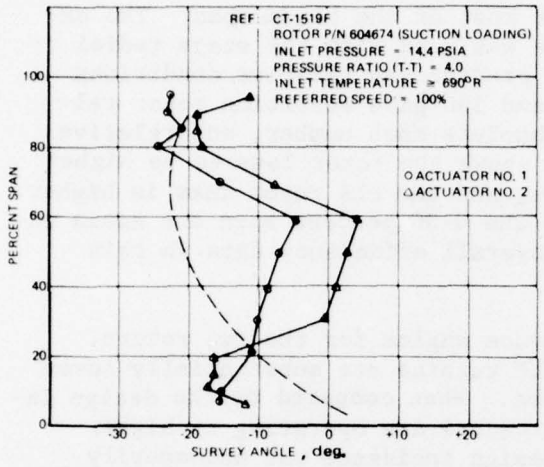


Figure 185. Test 5.0 - Evaluation of Blade Loading. Rotor Exit Radial Swirl Angle Survey.

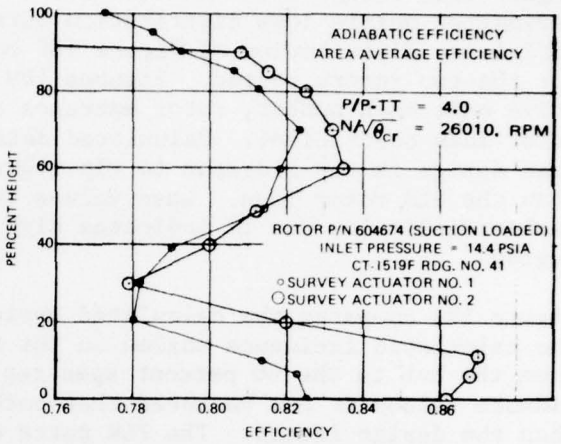


Figure 186. Test 5.0 - Evaluation of Blade Loading. Radial Efficiency Distribution Based on Nozzle Inlet Rakes and Rotor Exit Survey.

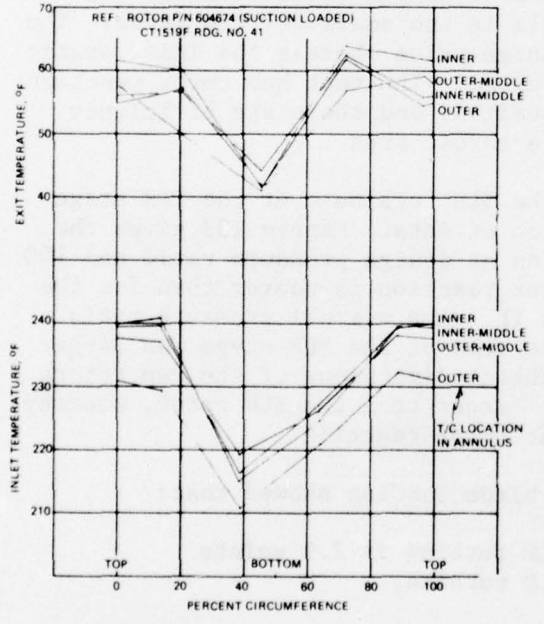


Figure 187. Test 5.0 - Evaluation of Blade Loading: Circumferential Temperature Gradients at Turbine Inlet and Exit.

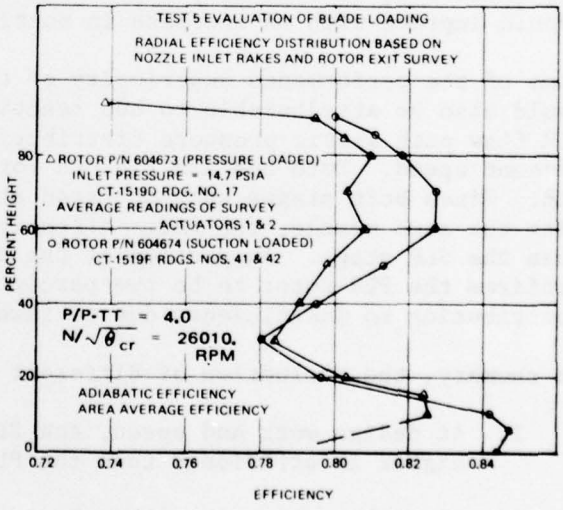


Figure 188. Test 5.0 - Evaluation of Blade Loading. Radial Efficiency Distribution Based on Nozzle Inlet Rakes and Rotor Exit Survey.

The nozzle performance, Test 1, showed higher than design hub losses and higher than design exit Mach numbers over most of the blade span. The experimental nozzle loss distribution curve was used with the stage radial efficiency distribution of Figure 188 to predict the relative conditions for the two rotors tested. Figures 189 and 190 give resulting rotor relative exit Mach number, rotor entrance absolute Mach number, and relative rotor loss coefficient. Calculated data shows the rotor loss to be higher than design in the mid-span to tip region, and the PLR rotor loss is higher than the SLR rotor loss. Loss values in the 0-30 percent span are again unrealistically low due to indicated high overall efficiency data in this region.

Figure 191 compares the calculated incidence angles for the two rotors. The calculated incidence angles on the SLR turbine are substantially lower from the hub to the 60 percent span region. When compared to the design incidence values it can be noted that both rotors are operating at higher than the design intent. The PLR rotor design incidence was necessarily high to obtain the pressure loaded shape, however, it appears that the increase observed from the test had the effect of increasing the losses substantially in the hub region.

Figure 192 gives the measured static pressure distribution in the SLR flow path at design pressure ratio. *Comparison to design* value confirms the results of Test 1, showing that the nozzle is too small for the rotor. The outer wall nozzle static exit is near design value whereas the inner static pressure is substantially below design values. The test hub rotor reaction is, therefore, considerably lower than desired, and the stage efficiency should improve with an increase in nozzle throat area.

Some of the performance superiority of the SLR turbine over the PLR stage could also be attributable to hub reaction effects. Figure 193 gives the PLR flow path static pressure distribution at design pressure ratio and 100 percent speed. Both hub and tip PLR rotor reaction is poorer than for the SLR. Since both stages were operated at the same overall pressure ratio with the same nozzle, the rotor effective area of the PLR stage was larger than the SLR stage. Inspection of the throat dimensions of the two rotors confirms the PLR rotor to be two percent larger than the SLR rotor, thereby contributing to inefficiency due to lower rotor reaction.

In summary, the evaluation of different blade loading showed that:

1. At design work and speed, the SLR turbine is 2.9 points higher in efficiency than the PLR turbine,

2. The SLR turbine is within 1.4 points (low) of design prediction efficiency,

3. Flow capacity of both turbines was down 6.4 percent from design due to a small nozzle,

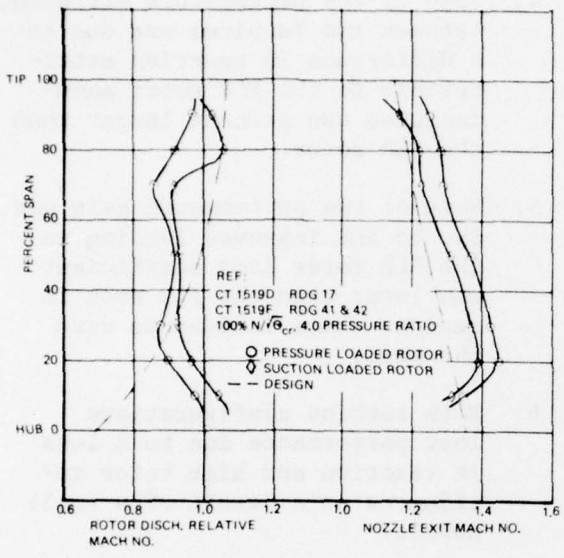


Figure 189. Test 5.0 - Evaluation of Blade Loading. Nozzle Exit and Rotor Discharge Relative Mach Number Distribution.

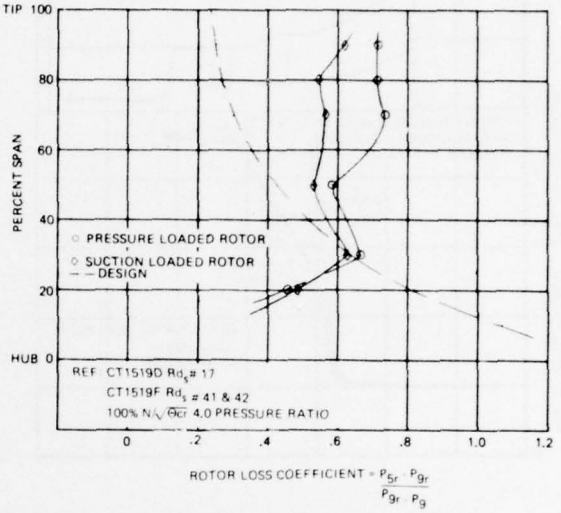


Figure 190. Test 5.0 - Evaluation of Blade Loading: Rotor Loss Distributions.

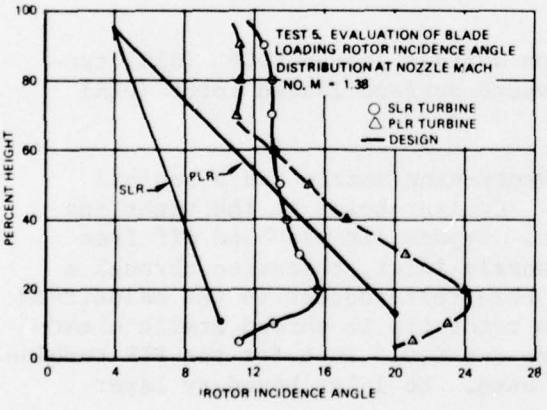


Figure 191. Test 5.0 - Evaluation of Blade Loading: Rotor Incidence Angle Distribution at Nozzle Mach No. M = 1.38.

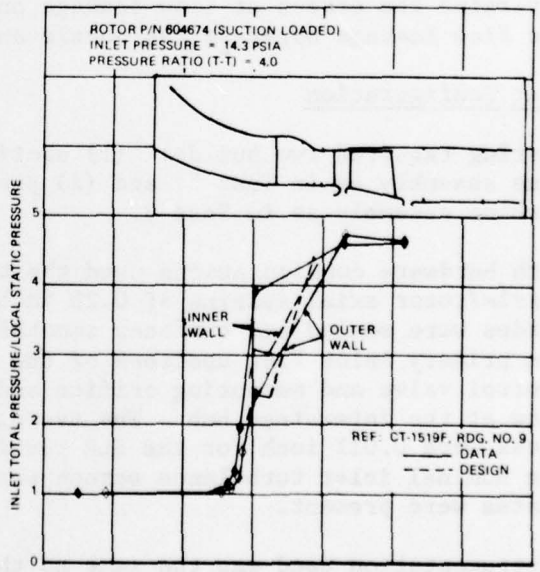


Figure 192. Test 5.0 - Evaluation of Blade Loading: Axial Static Pressure Distribution.

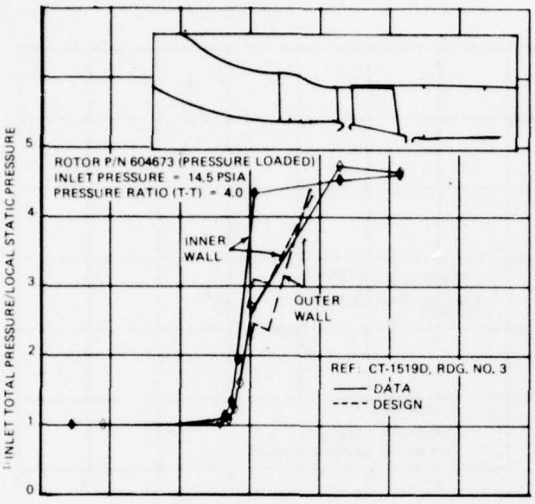


Figure 193. Test 5.0 - Evaluation of Blade Loading: Axial Static Pressure Distribution.

4. Some of the performance difference between two turbines was due to a difference in reaction attributable to the PLR rotor manufactured two percent larger than the SLR rotor.

5. Some of the performance gain was due to SLR improved loading as the SLR rotor loss coefficient was lower than the PLR even in regions where incidences were the same.

6. Both turbine configurations lost performance due to a loss in reaction and high rotor incidences as a result of a small nozzle.

TESTS 6 and 7 - EFFECT OF LEAKAGE (BYPASS) FLOW ON PERFORMANCE OF TWO ROTOR DESIGNS

The purpose for these tests was to determine the effect of flow leakage on performance of two rotor designs. The flow leakage bypasses the nozzle and is readmitted to the rotor inlet.

Test Configuration

Testing required two builds: (1) suction surface loaded rotor (SLR) turbine assembly as in Test 5; and (2) pressure surface loaded rotor (PLR) turbine assembly as in Test 3.

Both hardware configurations used the twenty-vane nozzle and a nominal nozzle/rotor axial spacing of 0.25 inch. Coolant holes on the vanes and blades were sealed and surfaces smoothed. Bypass air was bled off from the primary inlet flow upstream of the nozzle inlet, channeled through a control valve and measuring orifice and then reintroduced to the mainstream flow at the interstage hub. The average rotor tip to shroud static clearances were 0.011 inch for the SLR turbine and 0.013 inch for the PLR turbine. The nominal inlet turbulence screen was used. No inlet boundary layer plates were present.

Instrumentation used was the same as that of Tests 3 and 5, except no rotor exit surveys were performed and additional instrumentation was added to monitor the bypass flow rate and inlet conditions.

Test Results

Tests were conducted with a average inlet total pressure of 50 in. Hg. and a total temperature of 230°F. Each configuration was run at 100 percent power; that is, design referred speed ($N/\sqrt{\theta}$ = 26,010 rpm) and design total-total pressure ratio (P/P_{TT} = 4.2), and also at a reduced power rating of approximately 60 percent with respect to design. The 60-percent power setting was approximated on the SLR stage at a referred speed of 70 percent and a pressure ratio of 2.5. The same power was set at a 10-percent higher speed (80 percent) on the PLR stage and required a lower pressure ratio of 2.27. The two setting points at 60 percent power, although not identical, are in a U/Co. vs. η region where efficiency changes are small and still comparable. The percent bypass flow to total discharge flow was varied from 0 to 10 percent for both power settings.

Test results are illustrated in Figure 194, which shows loss in torque efficiency due to nozzle bypass flow for both turbine configurations at 100 percent power and at the reduced power. Torque efficiency was calculated (discussed in Test 4 - Determination of Cooling Flow Losses on Nominal PLR Turbine) with energy inputs of primary flow through the nozzle and secondary flow bypassing the nozzle. For 100 percent power, the SLR turbine efficiency falls more rapidly than PLR turbine efficiency with the addition of bypass flow. As discussed in Test 5 (Evaluation of Blade Loading), one reason the SLR turbine efficiency was higher than the PLR turbine was that rotor reaction for the PLR was poorer than that of the SLR. It is possible that introduction of bypass flow to rotor inlet hub increased the PLR hub reaction, thereby making up for some of the penalty imposed with the flow bypassing the nozzle. The combined improved hub reaction and bypass flow penalty resulted in PLR performance drop rate which was less than that of the SLR. All four curves indicate an increasing rate of performance decline as the bypass flow increases.

TESTS 8 and 9 - EFFECTS OF INCREASED NOZZLE/ROTOR AXIAL SPACING AND EFFECT OF NOZZLE BYPASS FLOW ON PERFORMANCE OF SLR TURBINE

These tests were conducted to: (1) determine the overall turbine performance with increased spacing between the stator trailing edge and rotor leading edge from a nominal 0.25 inch to 0.45 inch; and (2) determine the effect on overall turbine performance of nozzle bypass flow with the increased nozzle/rotor axial spacing.

Test Configuration

Nominal hardware consisted of the suction surface loaded rotor (SLR), the turbine of Test 5, and the SLR turbine with nozzle bypass flow of Test 7. Three spacers were used to increase the nozzle/rotor axial spacing from 0.25 inch to 0.45 inch: (1) nozzle inner shroud spacer, (2) rotor shaft spacer, and (3) exhaust duct spacer. Figure 195 illustrates the turbine flow path with the axial spacers present.

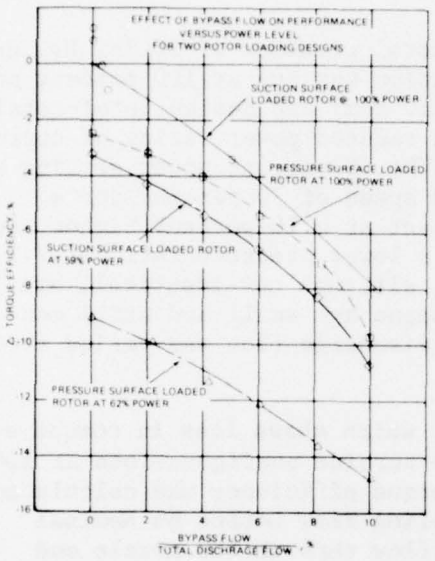


Figure 194. Test 7.0 - Effect of Nozzle Leakage (Bypass) Flow on Performance of Two Rotor Designs.

Instrumentation used was the same as that of Test 7 (nominal nozzle/rotor axial spacing nozzle bypass flow tests).

Test Results

Testing with the increased nozzle/rotor axial spacing included: (1) the turbine set at design speed and pressure ratio ($N/\sqrt{\theta}$ = 26,010 rpm and P/P_{TT} = 4.2) while nozzle bypass flow/total discharge flow was varied from 0 percent to 10 percent, (2) turbine at reduced power (70 percent $N/\sqrt{\theta}]_{design}$ P/P_{TT} = 2.5) with the same variance of bypass flow, and (3) turbine running conditions varied for a partial map without the nozzle bypass flow (data at 100 percent, 90 percent and 70 percent design corrected speed over a total-total pressure ratio range of 1.8 to 4.2). Inlet conditions were set at a total pressure of 50 in. Hg and a total temperature of 230°F.

Test results are presented in terms of loss in torque efficiency. The torque efficiency calculation is (discussed in Test 4 - Determination of Cooling Flow Losses on the Nominal PLR Turbine) with energy inputs of primary flow through the nozzle and secondary flow bypassing the nozzle. Net work, however, is based on power from measured speed and measured torque with windage correction (as discussed in Test 2).

Figures 196, 197 and 198 are constant speed lines of change in torque efficiency versus pressure ratio. For a valid comparison, nominal spacing data, the Test 5 SLR map, which was generated with ambient inlet total pressure, was corrected with the Reynolds number effect equations (from Test 13) to correspond to an inlet total pressure of 50 in. Hg. Each speed line is compared to its respective speed line data of Test 5. Design point (100 percent $N/\sqrt{\theta}]_{design}$ and P/P_{TT} = 4.2) on Figure 196 indicates 3.2 points loss in efficiency due to increased axial spacing. Minimal effect of axial spacing for the 100-percent speed line occurs at a pressure ratio range of 2.9 to 3.3 with a loss of 2.2 points in efficiency. The 90 percent speed line data (Figure 197 shows minimal effect at a pressure ratio range of 3.4 to 3.7 with loss of 2.4 points in efficiency). Figure 198 (70 percent $N/\sqrt{\theta}$ design line) indicates a wide pressure ratio range with minimal effect on efficiency from 3.2 to 4.0 and a loss of 4.8 percent in efficiency. At 70 percent speed and P/P_{TT} = 2.5 there is a 5.6-percent difference in efficiency. This running point corresponds to the reduced power setting for the bypass flow data.

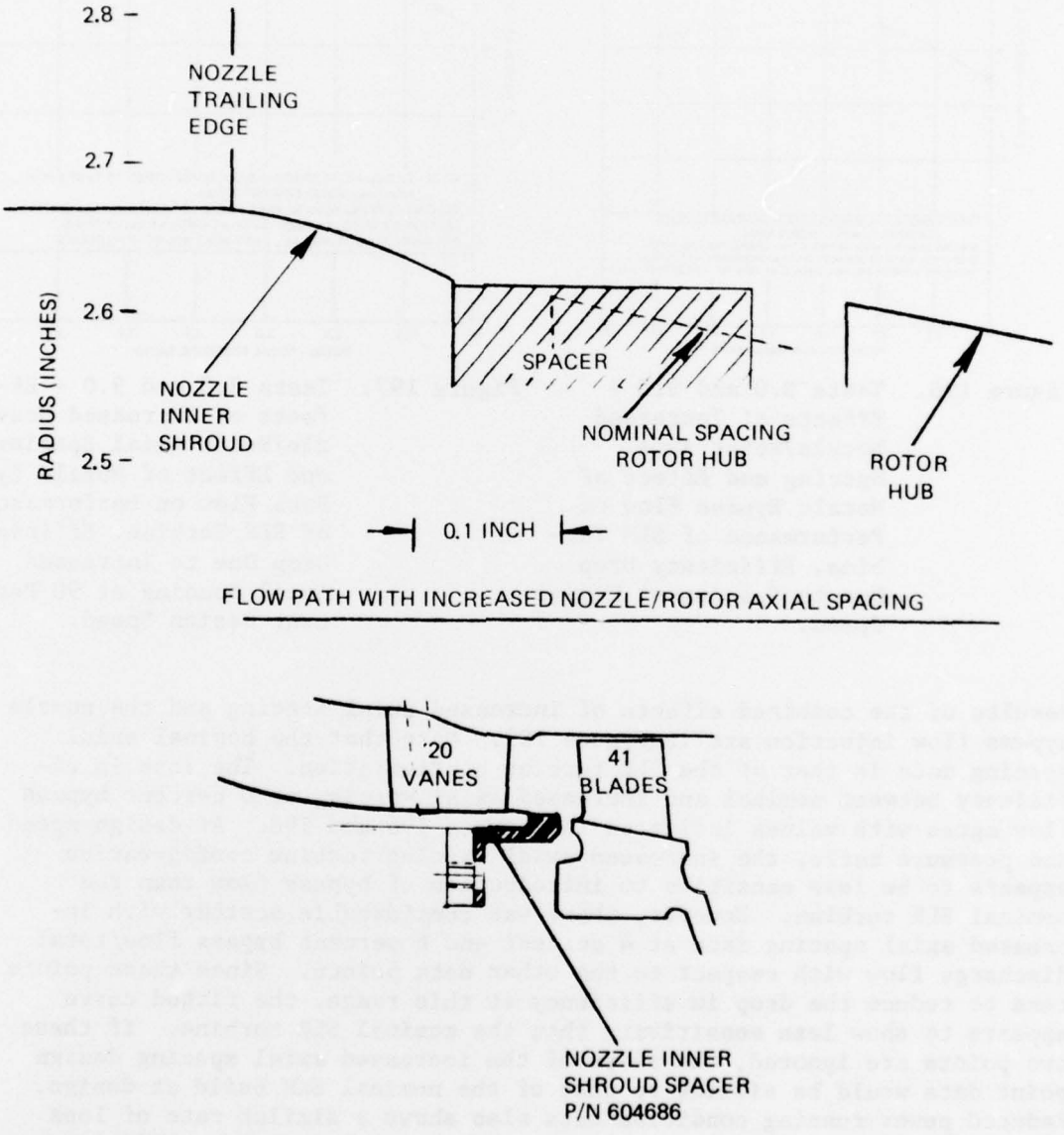


Figure 195. Partial Inner Wall Flow Path with Axial Spacer.

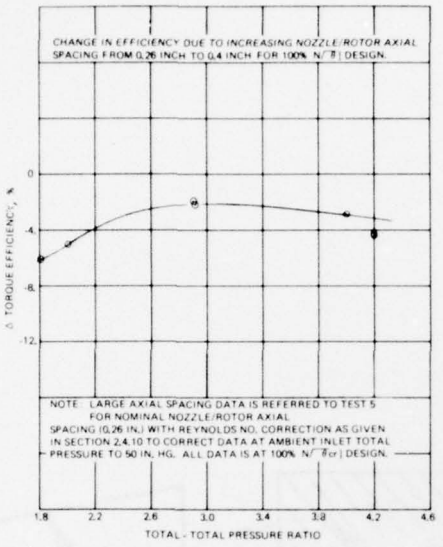


Figure 196. Tests 8.0 and 9.0 - Effects of Increased Nozzle/Rotor Axial Spacing and Effect of Nozzle Bypass Flow on Performance of SLR Turbine. Efficiency Drop Due to Spacing at Design Speed.

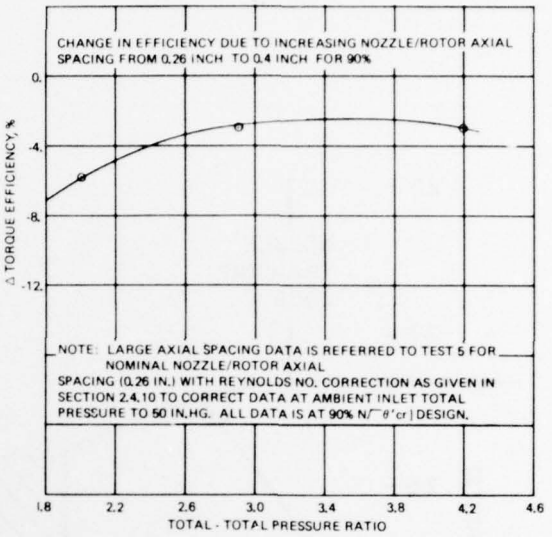


Figure 197. Tests 8.0 and 9.0 - Effects of Increased Nozzle/Rotor Axial Spacing and Effect of Nozzle By-Pass Flow on Performance of SLR Turbine. Efficiency Drop Due to Increased Axial Spacing at 90 Percent Design Speed.

Results of the combined effects of increased axial spacing and the nozzle bypass flow injection are in Figure 199. Note that the nominal axial spacing data is that of the SLR turbine configuration. The loss in efficiency between nominal and increased axial spacing at 0 percent bypass flow agree with values indicated in Figures 196 and 198. At design speed and pressure ratio, the increased axial spacing turbine configuration appears to be less sensitive to introduction of bypass flow than the nominal SLR turbine. However, there was considerable scatter with increased axial spacing data at 4 percent and 6 percent bypass flow/total discharge flow with respect to the other data points. Since these points tend to reduce the drop in efficiency at this range, the fitted curve appears to show less sensitivity than the nominal SLR turbine. If these two points are ignored, the slope of the increased axial spacing design point data would be similar to that of the nominal SLR build at design. Reduced power running condition data also shows a similar rate of loss with bypass flow injection for both turbine configurations. Efficiency drop for each curve is approximately linear up to 6 percent bypass flow. Beyond this point, the rate of efficiency drop is accelerated.

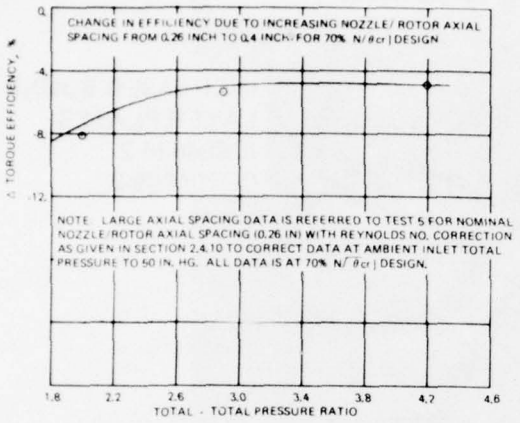


Figure 198. Tests 8.0 and 9.0 - Effects of Increased Nozzle/Rotor Axial Spacing and Effect of Nozzle Bypass Flow in Performance of SLR Turbine. Efficiency Drop Due to Increased Spacing at 70 Percent Design Speed.

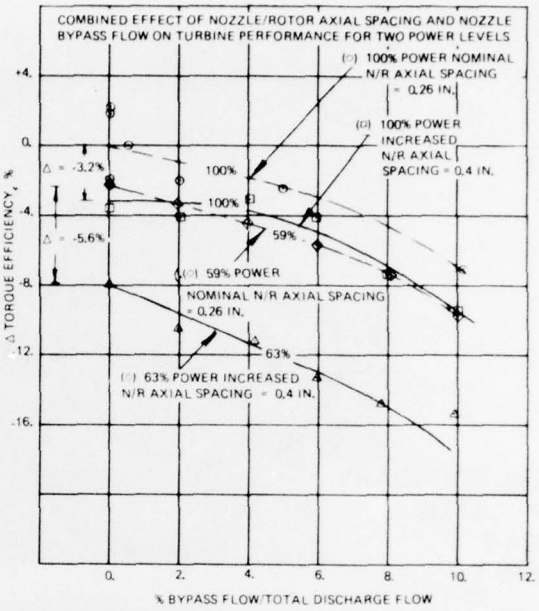


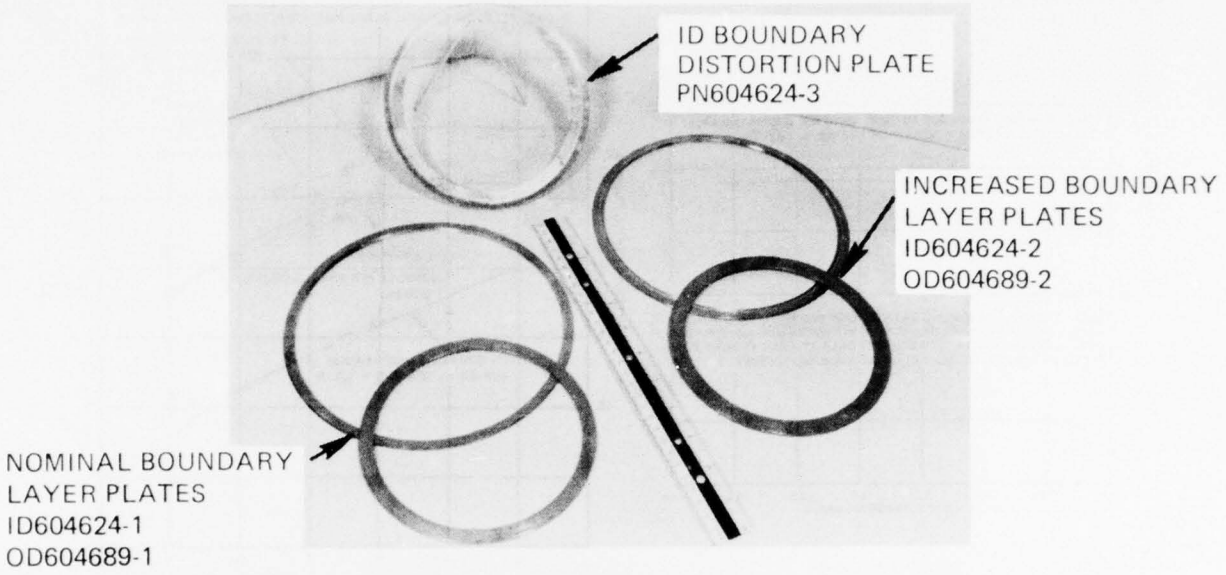
Figure 199. Tests 8.0 and 9.0 - Effects of Increased Nozzle/Rotor Axial Spacing and Effects of Nozzle Bypass Flow on Performance of SLR Turbine. Efficiency Drop Due to Increased Spacing and Bypass Flow at Two Power Levels.

TESTS 10 and 11 - EFFECT OF INLET BOUNDARY LAYER AND DISTORTION ON PERFORMANCE OF NOMINAL PLR TURBINE

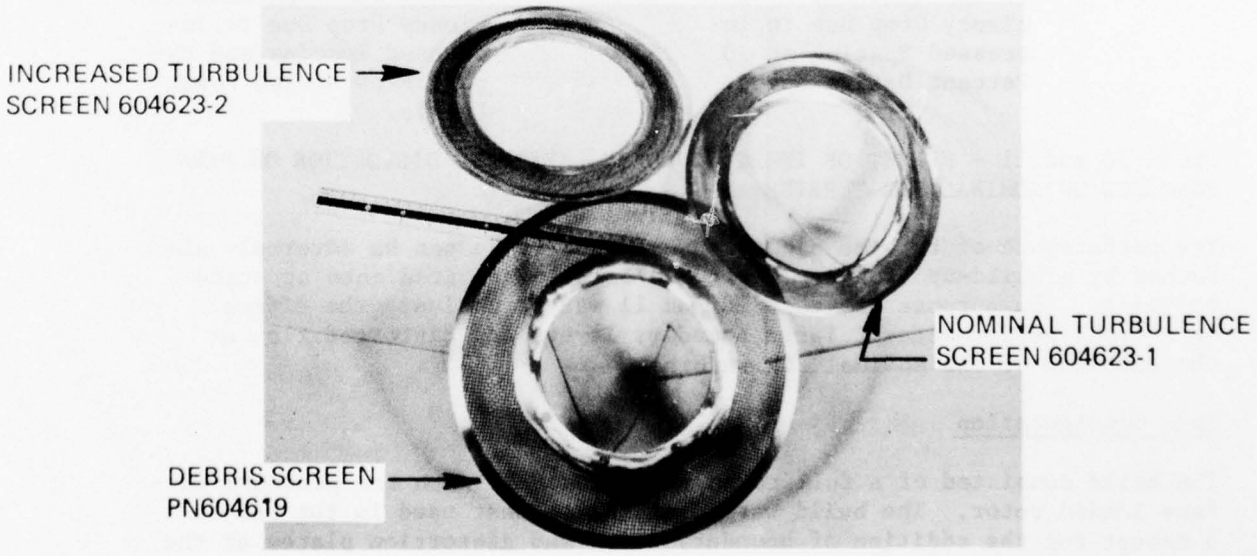
The performance of turbine blade rows and the stage can be adversely affected by a build-up boundary layer and/or velocity gradients at state entrance. The purpose of tests 10 and 11 was to evaluate the effect on overall performance of large boundary layers and distorted flow at the entrance of the nominal PLR turbine.

Test Configuration

The build consisted of a full round nominal nozzle with the pressure surface loaded rotor. The build was identical to that used in the PLR Test 3 except for the addition of boundary layer and distortion plates at the nozzle inlet (Figure 200). Turbulence intensity levels were artifically induced using a screen placed upstream of the nozzle leading edge. The turbulence intensity was calculated from measured values of bridge voltage and RMS voltage equipment described previously with a hot film anemometer which was calibrated in the Teledyne CAE flow facility. Test 10 was conducted with turbulence screening (nominal 40 x 40 mesh x 0.012



(a) INLET BOUNDARY LAYER PLATES



(b) INLET SCREENS

Figure 200. Inlet Flow Distortion Devices.

diameter wire) and 8 percent blockage boundary plates, on both inner and outer walls, to artifically induce a thicker boundary layer at the turbine inlet. Test configuration 11 was the same as 10 except the ID and OD boundary layer plates were replaced by a single blockage plate, on the inner annulus. This plate, occupying 24 percent of the inlet annulus area located 1.7 inches upstream of the nozzle leading edge, was used to induce a distorted turbine inlet velocity profile. Plates and a screen were located in the same nozzle upstream plane (Figure 201).

Test Results

The inlet turbulence measurements for Tests 10, 11 and no blockage Test 3 are shown in Figure 202. Much higher turbulence intensities are generated near the walls for all configurations tested. This is consistent with data obtained from the Phase II cascade testing, and Reichardt's data from Schlichting (Reference 39). The addition of boundary layer or distortion plates increased the turbulence substantially along the wall where they were placed. The Phase II cascade testing showed a fall off of nozzle efficiency with increased turbulence intensity and also a fall off in performance with a given screen, but differing boundary layer or velocity gradient plates. Since the plates themselves produce a turbulence increase, changes in performance due to a singular variable such as increased boundary layer could be separated.

Figures 203 through 205 give the total changes in performance due to inlet velocity gradient or increased inlet boundary layer with the turbine operating over a range of pressure ratio of 100, 90 and 80 percent speeds. Data is presented in terms of decrement efficiency change over the nominal PLR stage performance.

At near design pressure ratio of 4.2 and 100 percent speed, 1.2 points in efficiency were lost with increased boundary layer thickness, whereas no change was observed due to a high outer wall velocity gradient. As speed is decreased at fixed design pressure ratio, the inlet gradient also begins to have performance effect; at 80 percent, it results in 1.7 points loss in turbine efficiency. Table 19 summarizes some of the observed performance changes on the PLR turbine stage.

At off-design pressure ratios in some cases actual performance increases may be noted. This is not unlike the test data of Elsner and Porochnicki, Reference 38, where increases in performance were obtained with increased turbulence on rotor blading at high incidence. It was theorized that reduction in losses with increased turbulence occurred as a result of elimination of local flow separation zones. At off-design there will be some operating conditions where increased local gradients or boundary layers will result in improved rotor incidence and higher overall performance. In general however, gradients, increased boundary layer, and turbulence are detrimental to performance.

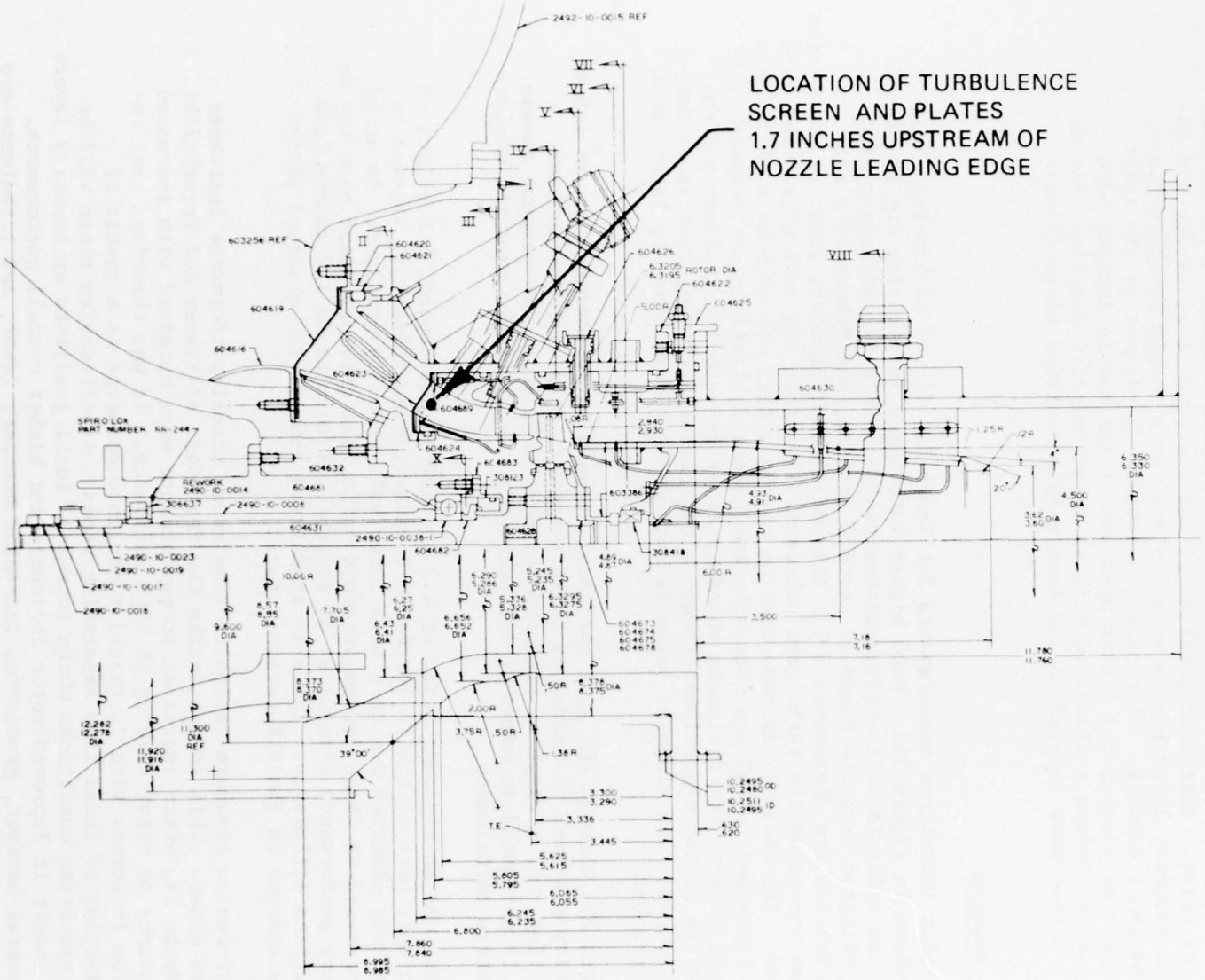


Figure 201. ASATT Phase III Turbine Rig.

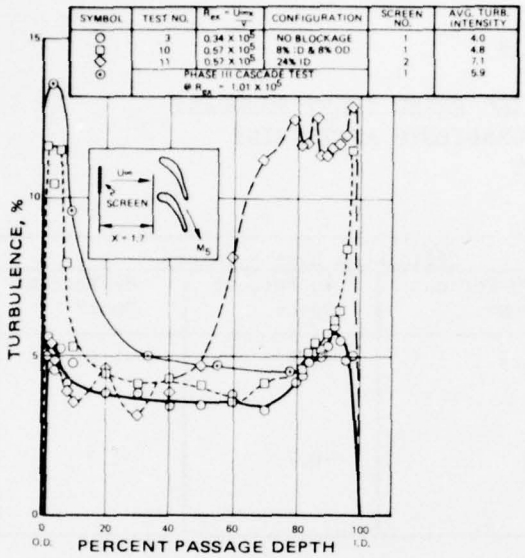


Figure 202. Tests 10 and 11 - Distribution of Induced Turbulence at Turbine Inlet.

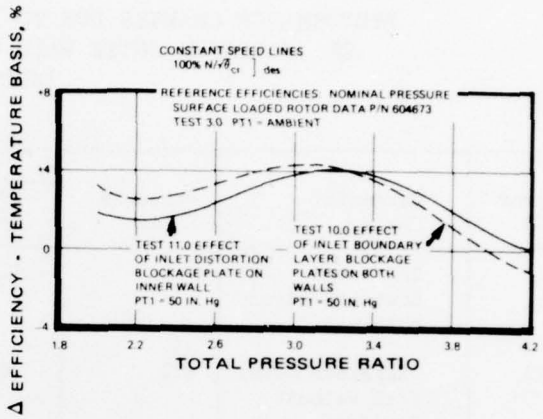


Figure 203. Effect of Inlet Distortion Plate on Overall Efficiency.

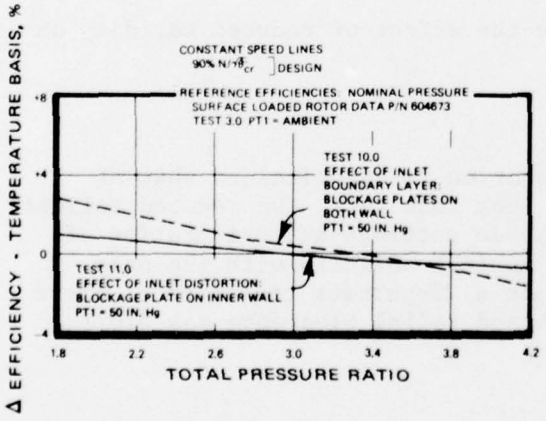


Figure 204. Effect of Inlet Distortion Plates on Overall Efficiency.

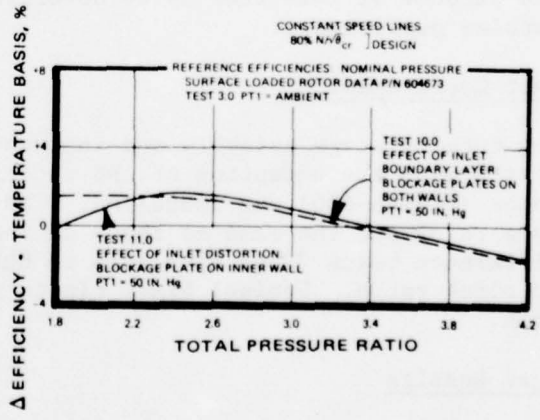


Figure 205. Effect of Inlet Distortion Plates on Overall Efficiency.

TABLE 19

PERFORMANCE CHANGES DUE TO INCREASED INLET BOUNDARY OR INCREASED OUTER WALL GRADIENTS AT TURBINE INLET

Test No.	Parameter Change	Pressure Ratio	Efficiency Loss - Points		
			100 Percent Speed	90 Percent Speed	80 Percent Speed
10	Increased Boundary Layer Both Walls	4.2	-1.2	-1.6	-1.8
11	Increased Outer Wall Velocity Gradient	4.2	0	-0.7	-1.7

TEST 12 - EFFECT OF DECREASED ROTOR SOLIDITY ON PERFORMANCE OF PLR TURBINE

The purpose of this test is to determine the effect of reduced solidity on turbine performance.

Test Configuration

The turbine stage assembly and instrumentation is identical to that of Test 3 with the exception of the rotor. For this test, the reduced solidity rotor (Figure 130) was installed. The blade sections and orientation of this rotor are the same as those of the nominal solidity with the only difference being 32 vs 41 blades to obtain a 22-percent reduction of chord to pitch ratio. Nominal blade tip to shroud radial clearance was 0.011 inch.

Test Results

To obtain a direct comparison of stage performance between the nominal and reduced solidity rotors, a partial performance map was generated. Figure 206 compares this data to that of the nominal solidity rotor on an efficiency change vs isentropic velocity ratio plot at a constant stage total-to-total pressure ratio. All of the data is normalized for airflow variation and corrected for Reynolds number effect (per Test 13) to a

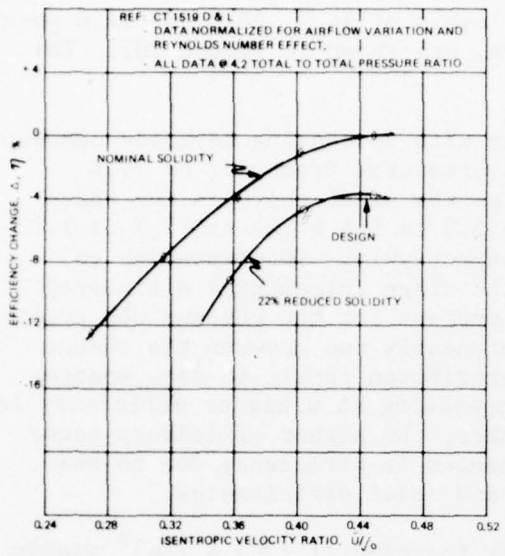


Figure 206. Test 12 - Effect of Rotor Solidity, PLR Rotor.

common turbine inlet pressure of one atmosphere. The results indicate:

a. A 22-percent reduction of solidity from the nominal 41-blade configuration yields a nearly a four-point reduction of stage efficiency at design isentropic velocity ratio.

b. The use of Zweifel's loading criteria, Reference 40, for setting optimum solidities is verified to the extent that performance dropped when a solidity less than that suggested by Zweifel was treated.

c. The data also shows that the performance decrement increases to approximately six points when shaft speed is reduced to 75 percent design; this indicates an increased sensitivity to incidence angles at the rotor blade leading edge.

TEST 13 - REYNOLDS NUMBER EFFECT ON PERFORMANCE

Dimensional analysis indicates that gas turbine efficiency for a given uncooled configuration is primarily a function of three parameters: total-to-total stage pressure ratio, corrected shaft speed, and Reynolds number. Compared to the effect of speed and pressure ratio, the effect of Reynolds number is very small, with considerable uncertainty as to the basis and accuracy of its prediction. The purpose of this test was to determine the effect of Reynolds number on the Phase III ASATT turbine performance.

Test Configuration

In this test, the two rotors, pressure (PLR) and suction (SLR) surface loaded blades, were tested individually in the full round stage assembly. Axial spacing between the nozzle trailing edge and the rotor was the design 0.25 inch with nominal tip clearance (static) measured at 0.012 inch and 0.013 inch for the PLR and SLR rotors respectively.

Test Results

Prior to each test the turbine test facility was heated to a stable 220°-230°F inlet temperature. This was followed by progressive increases of pressure ratio and shaft speed until the specified nominal data conditions of P_1/P_9 = 4.0 and $N/\sqrt{\theta}_{cr}$ = 26,010 rpm were attained. Seventy-eight complete data

scans were taken at three inlet pressure levels of 14.7, 20.0 and 24.6 psia. The averaged results, based on torque data, are shown in Figure 207. The results indicate that:

a. Turbine stage efficiency increases with increasing Reynolds number. With the above variation of inlet pressures from 14.7 to 24.6 psia, the Reynolds number, based on the axial chord as the characteristic dimension, varied from 3.3 to 5.5 x 10^5 and 0.7 to 1.3 x 10^5 for the nozzle and rotor respectively. Corresponding to this change in Reynolds number, the stage incremental efficiency increase was 1.7 percent and 0.9 percent for the PLR and SLR rotors respectively. This is a factor of nearly two between the change on the PLR vs SLR rotors and is attributed partly to data scatter and to the fact that the SLR is operating at a higher efficiency level. For equal changes in Reynolds number, the higher efficiency rotor is expected to reflect smaller changes in efficiency due to the reduced margin between operating and ideal efficiencies.

b. A fit of the PLR data with a power function $(1 - \eta) \alpha (N_R)^{\alpha}$ yields a value of the exponent of the Reynolds number of -0.123. This compares favorably with Ainley's (Reference 10) empirical correlations of turbine stage efficiency variation with Reynolds numbers above 0.5 x 10^5. For comparative purposes, Ainley's proportionality, $(1 - \eta) \alpha (N_R)^{-0.2}$, is also shown through the PLR data (Figure 207) and indicates higher efficiency gains with increasing Reynolds numbers due to the larger exponent on N_R. For the same Reynolds number change as in (a) above, Ainley predicts a 2.6-percent increase or 55 percent greater change in efficiency than by $(1 - \eta) \alpha (N_R)^{-0.123}$ for the PLR rotor.

c. Extrapolating to design Reynolds number with the above -0.123 exponent on N_R yields efficiencies of 0.77 and 0.788, for both the PLR and SLR rotors respectively.

PHASE III DATA EVALUATION

Thirteen separate tests were conducted on three turbine configurations, evaluating the following:

A. Baseline Performance - Pressure Side-Loaded Rotor (PLR)
   a. Nozzle performance with and without cooling
   b. Disc windage, bearing losses and rotor coolant pumping
   c. Stage performance without cooling flow
   d. Stage performance with cooling flow
   e. Stage performance with inlet boundary layer and distortion
   f. Stage performance with decreased rotor solidity

B. Effect of Blade Shape - Suction-Side-Loaded Rotor (SLR)

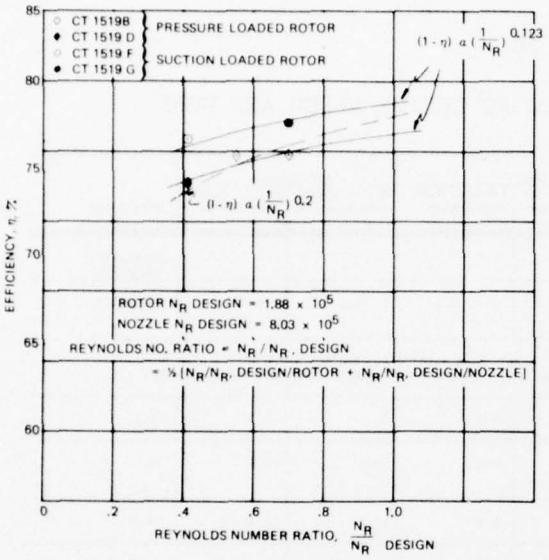


Figure 207. Test 13 - Reynolds Number Effect on Performance.

C. Effect of Inter-Blade Row Leakage or Disk Cooling on:
   1. SLR turbine stage
   2. PLR turbine stage

D. Effect of Increased Axial Spacing Between Turbine Nozzle and Rotor
   1. SLR turbine stage without inter-blade row leakage
   2. SLR turbine stage with inter-blade row leakage

E. Reynolds Number Effect on PLR and SLR Stage Performance

Table 20 summarizes the test results and gives relative performances of the configurations and a comparison to design values. Wherever applicable, data is presented at 100 percent referred speed, design referred work, and design Reynolds number. For a given turboshaft engine application, the gas generator turbine must produce its design work during the development phase even if efficiency levels are well below targets. The comparisons in Table 20 were, therefore, made at design work rather than at design total-to-total pressure ratio.

The best efficiency, 78.8 percent, was shown by the SLR stage and was 2.3 points higher than the PLR stage. This turbine produced a limit load work $\Delta H/\theta_{cr}]_{LL}$ = 34.6 Btu/lb or 3.6 percent more than the design requirement. Cooling injection tests showed a 0.05-point loss in stage efficiency for each percentage of nozzle cooling and a 1.1-point loss in efficiency for each percentage increase in rotor coolant. Inter-blade row leakage or front disk cooling flow additionally penalizes the stage performance at a rate of 0.65 point in efficiency per percentage of coolant.

The stage performance was very sensitive to the axial spacing between the rotor and nozzle. A loss of 3.2 points in efficiency was incurred by doubling the axial spacing (trailing edge of the nozzle to leading edge of the rotor) from 0.25 to 0.45 inch. This high loss is partially attributable to an irregularity of the hub flow path when the axial spacer is in place. Since the rotor hub is flared, the flow path geometry is aerodynamically optimum at only one design axial spacing of 0.2 inch. The free vortex nozzle space mixing losses are also high due to high Mach numbers and radial static gradients imposed by turbine design requirements.

The stage performance was comparatively insensitive to inlet velocity gradients and inlet boundary layer. A loss of only 1.2 points in efficiency was incurred by the placement of 8 percent ID and OD blockage plates (total annulus blockage of 16 percent) at a station of 1.7 inches

TABLE 20

PHASE III SUMMARY OF TEST RESULTS AT DESIGN SPEED AND WORK

Test No.	Parameter or Effect of:	Configuration and Change	Exit Flow-Speed Parameter $\epsilon(W\sqrt{\theta}/\delta)$	Flow		Efficiency		Efficiency
				Percent Change from Baseline	Percent Diff. from Design	Points Change from Baseline	Points Diff. from Design	
--	None-Design	Design	392	--	--	--	--	Nozzle 90.1 Stage 80.2
1	Cooling Flow on Nozzle	Nozzle Alone: Cooling Flows of 0 and 1.8 Percent		0, 1.8	-6.4, -4.6	0, -0.1	2.4/2.3	92.5/92.4
2	Disk Windage Bearing and Cooling Pumping Losses	Nozzle Plus Bladeless Disk Assembly	Stage Efficiency Loss in Points @ P = 1 Atmos.	(a) Disk Windage and Bearing = 3.4 (b) Disk Windage, Bearing with 1.8% Rotor Cooling = 4.2				
3	None - Baseline PLR	PLR Stage: No Cooling	367	0	-6.4	0	-3.7	76.5
4	Cooling Flow on PLR Stage	PLR-Stage with Cooling, W_{CN} = 4% W_{CR} = 2%	374	+2.0	-4.6	-2.2	-5.9	74.3
5	Rotor Blade Loading	SLR Stage: No Cooling	367	0	-6.4	+2.3	-1.4	78.8
6	Nozzle Bypass Flow on SLR Stage Performance	SLR Stage with W_{BP} = 4%	382	+4.0	-2.6	-2.6 *	-4.0	76.2
7	Nozzle Bypass Flow on PLR Stage Performance	PLR Stage with W_{BP} = 4%	382	+4.0	-2.6	-1.6	-5.3	74.9
8	Increased Nozzle/ Rotor Axial Spacing on performance of SLR Turbine	SLR Stage with Increased Nozzle/Rotor Axial Spacing from 0.25 to 0.45 in.	367	0	-6.4	-3.2 *	-4.6	75.6
9	Increased Nozzle/ Rotor Axial Spacing on Performance of SLR Turbine with Nozzle Bypass Flow	SLR Stage with 0.2 in. Increased Nozzle/ Rotor Axial Spacing and W_{BP} = 4%	382	+4.0	-2.6	-3.7 *	-5.1	75.1
10	Increased Boundary Layer on Both Walls	PLR-Stage: 8% Annulus Blockage Plates on ID and OD Walls 40x40x0.012 Screen	367	0	-6.4	-1.2	-4.9	75.3
11	Increased Outer Wall Velocity Gradient	PLR-Stage: 24% Annulus Blockage Plate on ID 12x12x0.020 Screen	367	0	-6.4	0	-3.7	76.5
12	Decreased Rotor Solidity on Performance of PLR Turbine	PLR Blading with 22% Reduced Solidity	367	0	-6.4	-3.7	-7.4	72.8
13	Reynolds Number on Performance of PLR Turbine	PLR Stage at $N_R/N_{R_{Design}}$ = 0.41	367	0	-6.4	-2.7	-6.4	73.8
13	Reynolds Number on Performance of SLR Turbine	SLR Stage at $N_R/N_{R_{Design}}$ = 0.41	367	0	-6.4	-2.5 *	-3.9	76.3

* Baseline is SLR stage with no cooling, Test 5.

upstream of the nozzle leading edge. A 24-percent blockage at the ID only did not change performance measurably.

When PLR rotor solidity was reduced 22 percent, the efficiency dropped 3.7 points, indicating that the use of Zweifel's loading criteria was reasonable for the design. A similar trend was found in the Phase II cascade.

Reynolds number effect on the stage was evaluated by inlet pressure increases from atmospheric to effect a Reynolds number increase from 0.41 to 0.7 of design. The test data was found to fit a power function of $(1 - \eta) \alpha N_R^{-0.123}$, as compared to Ainley's (Reference 10) empirical correlation $(1 - \eta) \alpha N_R^{-0.2}$. This factor accounts for some of the difference between the predicted and the test efficiency of 1.4 points of the SLR stage, Test 5. Surveys and calibration conducted in Test 1 showed the nozzle to be small with respect to design by 6.4 percent. The nozzle Mach number was also measured high with respect to design and resulted in a low rotor reaction. Although the nozzle mass average loss coefficient was measured to be 14 percent lower than design, higher-than-design losses were concentrated in the nozzle hub on the suction side of the vane, indicative of a localized vortex. The high nozzle hub loss and small nozzle throat area were strong contributors to a nozzle-to-rotor mismatch and stage inefficiency. A high hub loss region was also found in the Phase II cascade testing of a similar meridional wall constriction nozzle.

The nozzle loss data obtained in Phase II, Sector Cascade Investigations, obtained by combining the results from the momentum transfer data and survey data, also showed underturning in the hub regions. Therefore, the constant section Phase II nozzle was modified for Phase III to improve hub deficiency. This was done by maintaining the existing efficient tip sections and recontouring the lower half of the hub suction side to reduce afterthroat turning. The hub sections were also restaggered for greater turning and the vane lean was also adjusted so that the trailing-edge line would project through the turbine rotational centerline.

The Phase III (full-round nozzle performance evaluation) survey data showed that the high hub loss was still present; however, the average loss was lower than the design value (and lower than the Phase II nozzle). In addition, the Phase III nozzle turned out to be 6.4 percent smaller than the design intent.

The combination of high hub region losses and small throat contributed to a nozzle-to-rotor aerodynamic mismatch causing the rotor hub to operate at a low reaction level.

Several factors complicate the analysis to describe the flow analytically; namely, the relatively high Mach number (1.4), the large effect that secondary flow has on the small passage, and the highly three-dimensional nature of the flow passage (meridional profiling). In Phase IV, the distribution of the throat area is varied to improve the reaction distribution of the turbine state, using a compressible stream filament solution of the flow and incorporating the measured loss distributions of Phase III.

Some of the problems associated with the Phase III turbine stage testing are discussed in Appendix E.

PHASE IV - DESIGN TECHNIQUE ASSESSMENT

OBJECTIVES

Based on the data generated in Phase II Cascade Testing and Phase III Full Round Tests, the objectives of the Phase IV effort were to integrate the available test data and empirical correlations into the existing design technique and to establish more valid design procedures for advanced small axial cooled turbines.

REVIEW OF AVAILABLE LOSS SYSTEMS AND DATA - ANALYTICAL AND EXPERIMENTAL

The design of advanced turbines can be viewed from the standpoint that to achieve high performance one must:

A. Have the ability to predict conventional losses.
B. Apply aerodynamic processes to the blade design (profile shape, loading, radial distribution) and have proper profiling of the meridional flow path for loss reduction.

These methods can all be traced to some form of boundary layer flow control.

It has been determined by previous investiations (Reference 29) that the majority of losses occurring in a turbomachine are directly linked to boundary layer growth. Hence, to understand the various phenomena occurring in a turbomachine from the standpoint of aerodynamic performance, and to have the ability to apply this knowledge to preliminary and final design calculations, an understanding of fluid boundary layer behavior is required. However, this problem has been very elusive due to the complex nature of the flow. The complete description of even two-dimensional incompressible turbulent boundary layer flow over a flat plate under strong adverse pressure gradients is not complete, as was observed by many investigators (Reference 26). In flow-through turbine cascades, the flow is mostly of the accelerating type, and hence boundary layer analysis becomes practically applicable.

The object of the research was to aid in establishing improved loss computing methods as based on fundamental fluid behavior when applied, in particular, to small gas turbine engines.

One of the most widely used methods today is the Ainley and Mathieson procedure (Reference 9) which has gained favor because of its simplicity and relatively good accuracy (for large machines). Its success is based on the fact that only vector triangles and basic turbine geometric data are required for computation. This makes it a valuable tool in preliminary design calculations. However, the method is basically empirical in nature and cannot properly reflect new blading designs. This method is good only under the restrictions for which the data are taken and, therefore, by its application is limited.

Another widely used procedure to estimate turbine efficiency is to relate turbine blade loss characteristics to turbine mean section velocity diagrams (References 5 and 6). An alternate approach using meanline parameters is to consider a breakdown into individual losses such as profile, secondary, trailing-edge wakes, Reynolds and Mach number, and incidence, and to correct for annulus and tip clearance effects. Extensive data on this approach is presented in References 11, 12, 13, 14, 16 and 17.

Dunham and Came (Reference 18) made improvements to the Ainley-Mathieson prediction technique to better account for secondary and tip losses. Figure 3 shows a comparison of predicted and test results (Reference 16). Burrows (Reference 19) also did extensive testing and correlated data on the low aspect ratio stator of Reference 16 for improvements in efficiency prediction.

NREC (Reference 20) was contracted to do cascade testing on the same family of turbines. They chose a rectilinear cascade and concluded that short blades were more efficient. However, the data also showed that small irregularities (0.001 in. step-in flow path and small leakages) were found to increase total loss coefficients by as much as a factor of five. The method of defining the loss coefficients from a simple survey can also lead to very poor accuracy (Reference 21) and makes this data suspect.

The location, amount, and type of cooling injection influence aerodynamic losses. Some of the most recent studies are given in References 21-25.

Boundary layer and end wall effects have been examined theoretically and semiempirically (References 26-31). Agreement between test and theory is difficult to achieve with three-dimensional flows, blade row interactions, and high Mach number effects. Inlet boundary layer and distortion effects under adverse pressure gradients in small channels are not documented, or data is scarce. Launder (Reference 28) presents data showing laminarization of the boundary layer flow in highly accelerating channels, and Turbine (Reference 27) concludes that the endwall boundary layer inside a stator passage is essentially independent of the boundary layer entering the cascade.

Design and test of a highly loaded turbine is given in References 32-34. Boundary layer analysis is used to define blade and wall shapes, and tests demonstrate the high performance capabilities. High aspect ratios, thin trailing edges, and thin airfoils characteristic of the large uncooled turbofan turbine could not be used in a small cooled machine. The approach shows potential, but application of a simple free-vortex turbine in the same flow path and with the same mean velocity triangles is projected to produce the same efficiency as the test forced vortex turbine of Reference 32.

Allison, under contract to NASA (Reference 35), performed fundamental cascade and full-round testing on a high work factor ($\Omega_H = 5.5$) turbine using vortex plow generators, tandem blading tangential blowing, and jet flaps. They showed that the jet flap has significant potential for improved performance in cooled and uncooled configurations.

Turbulence, intensity and Reynolds number effects on cascade losses are given in References 37 and 38. Interestingly, stator losses were found to increase, whereas rotor losses decreased with increases in inlet turbulence. Decreased rotor losses were attributed to a reduction of off-design incidence. Test data on this subject is scarce.

DESCRIPTION OF DESIGN TECHNIQUE

The design procedure used in the Phase I effort used a streamline curvature method with a variable work distribution and entropy gradient in the radial direction applied to the basic turbine flow path (Reference 1).

The detail design required loss buckets at each station, local cooling influences, meridional constriction, inlet temperature/pressure gradients, axial spacing, boundary layer, and radial work distribution effects.

The loss analysis system incorporated:

Profile losses (t/c, deflection, reaction, solidity)
Mach number losses
Trailing-edge losses
Incidence losses
Reynolds number
Tip clearance effects
Endwall losses
Cooling losses

The computerized design point program used was essentially an outgrowth and modification of the Ainley blade-loss treatment. One of the more important modifications that allowed a better agreement of predicted to experimental efficiency on short-blade turbines was that of secondary loss and the sum of incidence, profile, clearance, trailing edge, and disk losses. Data were accumulated on a number of recent turbine stages, covering a broad range of blade geometries. The information was then correlated as a function of mean deflection angle, solidity and aspect ratio, based on the expression given in Reference 15.

ΔY^{**} = Correlation secondary loss factor
h/c = Blade height-to-chord ratio
C_L = Lift coefficient of the blade
N = Subscript for nozzle
R = Subscript for rotor

Nozzle data was found to correlate as:

$$\frac{\Delta Y^{**}}{C_{LN}} = 0.077 - 0.085\, C_{LN} + 0.0035\, C_{LN}^2 - 0.00486\, C_{LN}^3$$

$$1.0 \leq C_{LN} \leq 2.60$$

The rotor was found to correlate as:

$$\frac{\Delta Y^{**}}{C_{LR}} = 0.368 - 0.281\ C_{LR} + 0.076\ C_{LR}^2 - 0.007\ C_{LR}^3$$

$$1.0 < C_{LR} < 4.1$$

Figure 208 shows a comparison of predicted and experimental efficiencies of 18 different uncooled turbines. The range of geometry covered by the analysis is demonstrated by the following parameters:

Blade height	h	=	0.1 to 3.5 in.
Solidity	σ	=	0.97 to 2.6
Aspect Ratio	$\frac{h}{c}$	=	0.34 to 3.3
Blade height-to-throat opening ratio	$\frac{h}{do}$	=	1.1 to 5.3
Wheel tip diameter	d	=	4.0 to 22 in.
Flow parameter	$\frac{WN}{\delta\theta}$	=	54 to 3700 $\frac{lb\ rev}{sec^2}$
Single stage specific work	$\frac{\Delta H}{\Theta cr}$	=	8.8 to 29 $\frac{Btu}{lb}$

A cooling injection analysis program that uses the output of an uncooled design point program as input was used to determine incremental loss variations for air cooling of turbine shrouds, disk, vanes and blades. Calculations were made by assuming that mixing occurs over a small distance at the point of injection of the cooling air. Vertical components of velocity with respect to streamline were assumed to contribute no axial or angular momentum. In the case of a rotor, pumping losses were also accounted for by an assumption of pumping efficiency for the cooling flow and a subroutine to calculate pressure and temperature rise to the point of injection. The mixing solution is an iterative procedure involving equations of continuity, conservation of energy and conservation of angular and axial momentum (Ref. 55). Treatment is similar to Shapiro's influence coefficient methods for constant static pressure mixing.

Within this program the governing equations that account for the mixing of coolant mass with mainstream flow are as follows. Results on the effect of coolant flow injection through the rotor and/or stator are presented in Figure 63.

1. Energy Balance:

$$(\dot{m}\ C_p\ T_o)_m + (\dot{m}\ C_p\ T_o)_i = (\dot{m}_m + \dot{m}_i)\ (C_p\ T_o)_f$$

Where:

$\dot{m}$ - Mass Flow Rate
C_p - Specific Heat
T_o - Stagnation Temperature

and the subscripts m, i and f, respectively, stand for mainstream flow, injected flow and final mixing states.

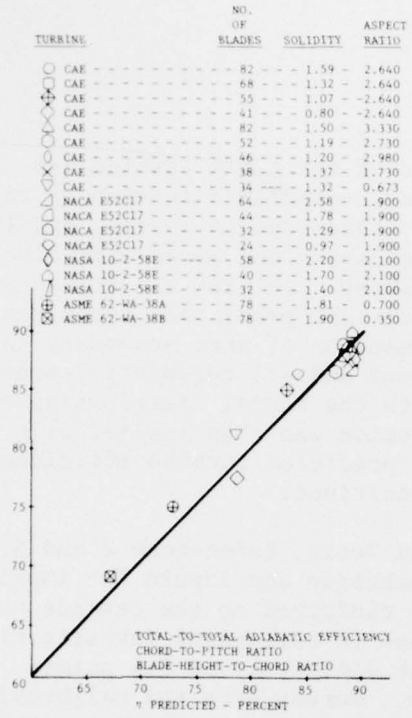


Figure 208. Comparison of Teledyne CAE Predicted and Experimental Turbine Efficiencies.

2. Stagnation Pressure Change:

$$\frac{dPo}{Po} = -kM^2 \left[\left(1 - \frac{V' \cos\beta}{V}\right) \frac{dW}{W} + \frac{dTo}{2To} \right]$$

Where:

V' = Total Velocity of Injected Flow
V = Total Velocity
β = Angle Between V and V'

3. Static Pressure Change:

$$\frac{dP}{P}(1 - M^2 \sin^2\alpha) = \left(\frac{dA}{A} - \frac{dW}{W}\right) kM^2 \sin^2\alpha$$

$$- \left(1 + \frac{k-1}{2} M^2\right) \left(\frac{dTo}{To}\right) kM^2 \sin^2\alpha$$

$$- \left[\frac{dr}{r} + (1 - \gamma_\theta) \frac{dW}{W}\right] \left[(k-1) \frac{kM^4}{4} \sin^2 2\alpha\right]$$

$$- \left[(-kM^2 \cos^2\alpha)\frac{dr}{r} + (kM^2 \sin^2\alpha)(1 - \gamma_x)\frac{dW}{W}\right]$$

$$x[1 + (k-1) M^2 \sin^2\alpha]$$

Where:

γ_x = Meridional Injection Velocity Ratio
γ_θ = Azimuthal Injection Velocity Ratio
α = Flow Angle Measured from Azimuthal Direction

4. Static Pressure Change:

$$\frac{dT}{T}(1 - M^2 \sin^2\alpha) = -(k-1) M^2 \sin^2\alpha \left(\frac{dW}{W} - \frac{dA}{A}\right)$$

$$+ (1 - kM^2 \sin^2\alpha) \left[1 + \frac{k-1}{2} M^2\right] \frac{dTo}{To}$$

$$+ (k-1) M^2 \cos^2\alpha (1 - kM^2 \sin^2\alpha) \left[\frac{dr}{r} = (1 - \gamma_\theta) \frac{dW}{W}\right]$$

$$- (k-1) M^2 \sin^2\alpha \left[(-kM^2 \cos^2\alpha) \frac{dr}{r} + kM^2 \sin^2\alpha (1 - \gamma_x) \frac{dW}{W}\right]$$

5. Equation of State:

$$\frac{P}{\rho} = RT$$

The predicted average stage loss distribution of the ASATT turbine (no cooling) as given in Figure 209 was biased in the radial direction to reflect high endwall losses and high rotor hub losses due to loading and low reaction. The distribution of the losses was determined by an iterative process on velocity triangles whereby the turbine flow path was broken into four streamtube turbines. The one-dimensional loss prediction technique was applied to each stream tube with the assumption of zero secondary loss occurring in the two middle streamtube turbines and all secondary losses incurred in the hub and tip streamtubes. With the radial distribution of losses defined, the streamline curvature solution was then applied with the number of streamtubes increased to ten. The predicted turbine efficiency was 80.2 percent at the hot engine design conditions.

The Phase II Cascade and Phase III Full Round Tests, References 2 and 3, provided verification data for the design technique and inputs for improvement of the system. In total, 38 tests were conducted on the cascade and thirteen tests on three turbine configurations in full-round investigations. The baseline SLR rotor tested at 78.8 percent efficiency or 1.4 points below prediction and 6.4 percent low in flow. Survey data and calibrations showed the nozzle to be small by 6.4 percent, thereby accounting for the flow deficiency.

Since the nozzle was undersize, part of the 1.4 points in stage inefficiency could be attributable to nozzle/rotor mismatch. The accuracy of the instrumentation for efficiency measurement is $\pm$ 1.2 points. The prediction given by the design technique for this particular configuration is therefore within the accuracy of measurement and was considered to be adequate.

A number of other effects on turbine performance were experimentally evaluated that are not considered in the modified Ainley loss treatment in the Phase II and Phase III test program. Obtaining generalized data applicable to all turbine designs was beyond the scope of the present contract; however, certain trends and observations can be made: (Reference Phase II and Phase III for details).

MERIDIONAL CONSTRICTION

Four nozzle meridional wall constriction geometries were evaluated, Figure 73. Cylindrical walls gave the poorest efficiency, 83.5 percent @ M = 1.24. Double constriction, inner and outer walls configuration 3, showed little or no improvement (Figure 105). This effect can be compared with the findings of Deich, Reference 41.

Figure 37, from Reference 41, shows performance gains of outer constricted walls over cylindrical walls as a function of $L_0 - L_i$ where:

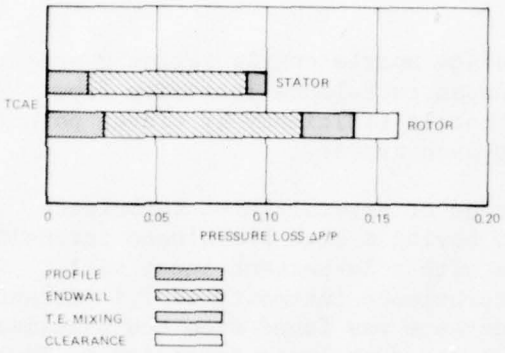


Figure 209. Division of Total Pressure Loss by the Teledyne CAE Loss System.

L_0 = flow path height at nozzle inlet
L_1 = flow path height at nozzle exit.

Configuration 3 with $L_1 = 0.367$ inch and $\frac{L_0 - L_1}{L_1} = 0.844$ would fall in the region of no return on Figure 37. Although the Deich data was obtained on outer wall meridional constriction only, the ASATT configuration 3 data confirms the trend of little or no improvement for large constriction values of $\frac{L_0 - L_1}{L_1}$. Configuration 2 showed a substantial improvement over cyclindrical walls with a test nozzle efficiency of 89.1 at the design Mach number. This improvement in terms of pressure loss is over four percent and substantially greater than would be predicted by the Deich curve.

Configuration 4 with a more rapid constriction near the throat gave an improvement of roughly two percent and falls close to the prediction of Figure 37. It may be concluded that Figure 37 is adequate to predict meridional constriction gains on the nozzle for preliminary design with additional improvements obtainable by detail design and cascade verification.

NOZZLE EXIT MACH NUMBER

The nozzle efficiency is correlated as a function of Mach number in Figure 114. The general trend for all configurations was to increase efficiency at a decreasing rate with Mach number. At lower exit Mach numbers, $M \cong 0.8$, the flow losses may be expected to be high due to near throat shock losses and shock boundary layer separation on the suction side. At the higher exit Mach numbers, $M = 0.8$ to $M = 1.3$, the shock becomes more oblique more of the nozzle passage flows full (suction side flow reattachment). With near-constant shock boundary layer losses, efficiencies peak out at $M \gtrsim 1.3$, as trailing edge shocks and mixing losses become predominate with higher Mach numbers.

The nozzle efficiency correlations obtained are:

Cylindrical Wall Configuration 1

$$\eta = 2.984 + 120.1M - 43.93M^2; \quad 1.0 \leq M \leq 1.3$$

Outer Constriction Configuration 2 (same as Phase III)

$$\eta = -498.7 + 1304M^2 - 960.1M^3 + 226.8M^4; \quad 1.05 \leq M \leq 1.4$$

Outer Wall Constriction Configuration 4

$\eta = -0.016 + 120.1M - 43.93M^2$; $0.8 \leq M \leq 1.2$

INLET TURBULENCE

Inlet turbulence effects on the best cascade nozzle configuration 2 are given in Figure 120. An increase in midspan turbulence intensity from four percent to six percent reduced the nozzle efficiency by eleven points to an efficiency of 80 percent at design Mach number.

This same nozzle was tested in a full stage at several inlet turbulence intensities, Figure 202. In addition to having a high turbulence intensity screen, Test 11, Phase III was conducted with a 24-percent inner wall blockage plate resulting in an average turbulence intensity of 7.1 percent. At design point no change in stage performance was found from the baseline Test 3, Phase III, which had an average inlet turbulence intensity of four percent.

Differences between cascade and full round testing turbulence effects are partially attributable to Reynolds numbers. The cascade tests were conducted at high exit $N_r \cong (4.75 \text{ to } 6) \times 10^5$, whereas stage tests were conducted at low $N_r = (1.7 \text{ to } 2.85) \times 10^5$. Reference 15 showed that at low Reynolds number, the effect of increased turbulence, T, was to improve the efficiency of a cascade row. However, Reference 38 shows nozzle cascade losses increasing with T = 0.7 to 4.8 percent and $N_r = 6.1 \times 10^5$ down to $N_r = 2.8 \times 10^5$ and T = 15.4 to 20.4 percent.

Turbine stage performance is further complicated by multiple blade row interaction, and insufficient data is available to generalize a loss variation with turbulence intensity. The ASATT tests and data in the open literature suggest that a turbulence loss correlation should have a strong dependency on Reynolds number.

INLET BOUNDARY LAYER AND FLOW DISTORTION

Nozzle cascade test results on inlet boundary layer and flow distortion are summarized in Figure 124. Substantial decreases in nozzle efficiency were incurred. The use of a 9-percent span blockage plate on the inner wall, for example, produced a decrement in nozzle efficiency of 4.1 percent, whereas a similar outer wall plate produced a smaller decrement of 3.5 percent.

These nozzle losses did not appear in a direct relationship in full stage tests. At near design work and 100 percent speed no stage efficiency loss was observed due to a high outer wall gradient (hub blockage plate occupying 24 percent of inlet annulus was used). With increased boundary layer on both walls, stage efficiency was reduced by 1.2 points, Table XX. At off design conditions, however, the turbine performance, in some cases, actually increased. This may be due to reduction of separation losses due to increased turbulence or incidence changes attributed to shifts in velocity

gradients. The data available was insufficient to obtain a correlation. Table 21 summarizes the measured inlet boundary layers and Figure 210, the geometries tested.

NOZZLE COOLING AND ROTOR COOLING INJECTION EFFECTS

Cascade test results are summarized in Figures 126, 128 and Table 15. The nozzle efficiency loss with cooling flow was small, i.e., 3.5 points decrease with 12 percent total cooling flow. Trailing edge ejection was more efficient by a factor of two over combined upstream pressure and suction side ejection. The trailing edge cooling efficiency loss was 0.25 points per one percent of flow.

The effect of interstage seal leakage or disk cooling on rotor efficiency as obtained in cascade test is given in Table 15. The measured influence factor was 0.86 point loss in rotor efficiency per percent of flow. A similar full-stage test in Phase III yielded 1.6 points loss in stage efficiency with 4-percent flow, (Table 20). In terms of rotor efficiency, the influence factor was 0.76 points in efficiency per percent of flow; an excellent agreement with cascade results.

Overall stage nozzle and rotor cooling effects are given in Table 20. The Phase III test results were compared to predicted values using the mixing loss cooling performance evaluation technique, Figures 176 and 177. Good agreement is shown on flow capacity and efficiency loss prediction. Additional verification has been obtained on an in-house turbine. A comparison of predicted to test data of cooling effects on an independent research turbine program conducted on contractor test facilities is given in Figure 211 and also shows good agreement. It was concluded that the loss prediction system used to evaluate cooling injection losses has been test validated for the range of variables of interest.

REYNOLDS NUMBER

Full-stage tests were conducted at three Reynolds numbers of 0.41, 0.55 and 0.71 of design on the PLR turbine and Reynolds numbers of 0.41 and 0.71 of design on the SLR turbine. The test data was found to fit a power function of $(1 - \eta) \alpha Nr^{-0.123}$ as compared to Ainley's (Reference 10) empirical correlation $(1 - \eta) \alpha Nr^{-0.2}$. At the lowest test inlet pressure, the blade row Reynolds numbers were 3.65×10^5 for the nozzle and 0.811×10^5 for the rotor. Transition from laminar to turbulent flow may be expected at $Nr \approx 2 \times 10^5$, Figure 42.

Since the rotor was below critical throughout the test range and rotor losses are higher than nozzle losses to begin with, the stage performance degradation with decreasing Reynolds numbers was primarily attributable to the rotor.

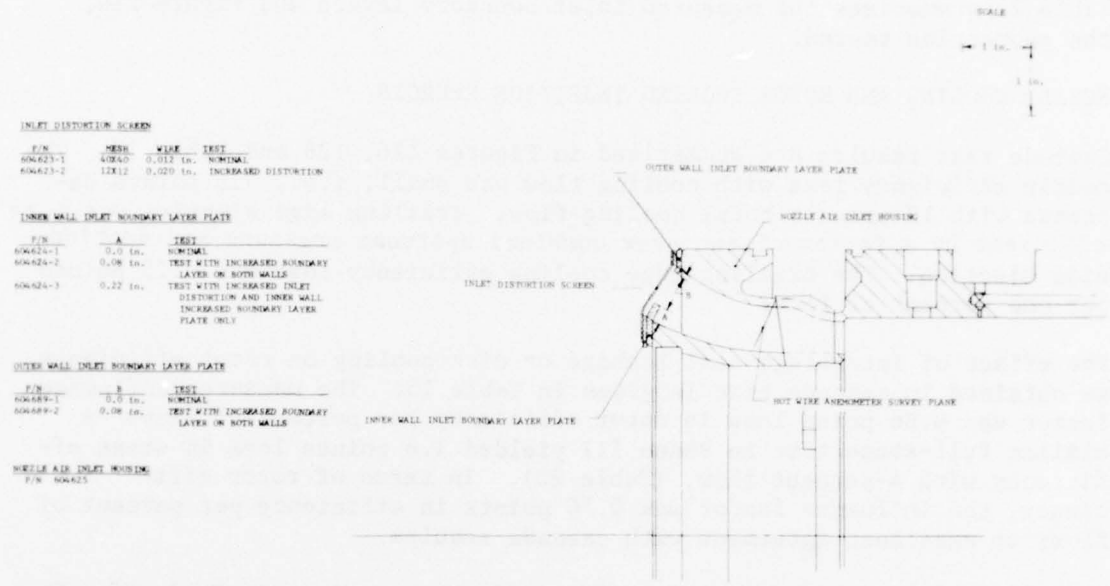


Figure 210. Inlet Flow path for Inlet Distortion and Boundary Layer Tests.

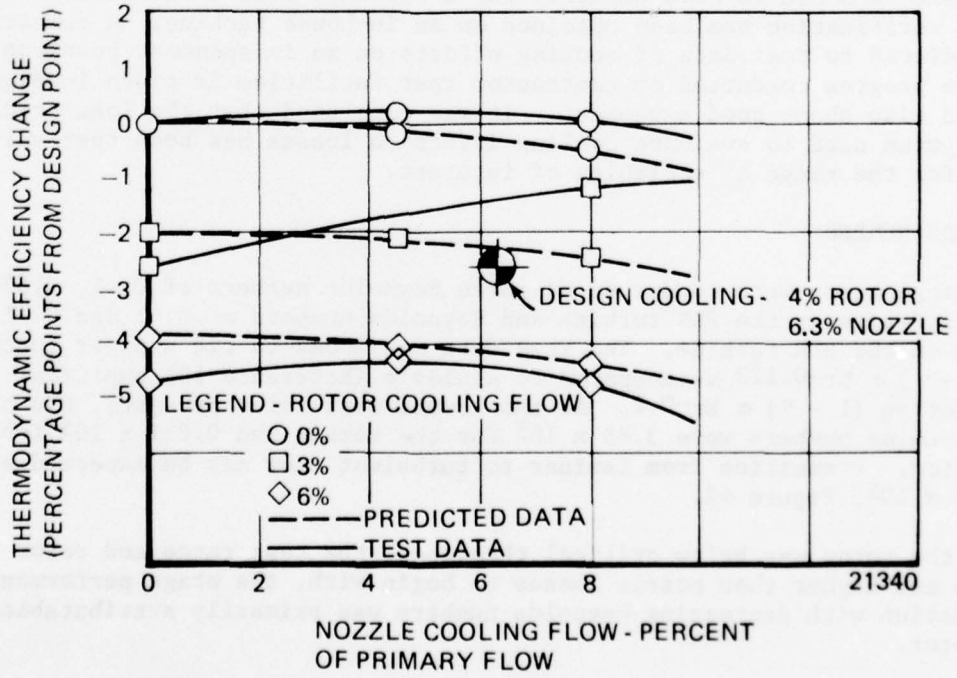


Figure 211. Effect of Nozzle and Rotor Cooling Flow on Turbine Stage Efficiency.

TABLE 21

HOT WIRE ANEMOMETER MEASUREMENT OF NOZZLE INLET BOUNDARY LAYER

	NOMINAL CONFIGURATIONS		
	(1) Nom. Distortion Screen (2) No. Boundary Layer Plates	(1) Nom. Distortion Screen (2) Boundary Layer Plates on Both Walls	(1) Distortion Screen 2 (2) Boundary Layer Plate on Inner Wall Only
Screen P/N	604623-1	604623-1	604623-2
Mesh Wire Dia. (in)	40 x 40 0.012	40 x 40 0.012	12 x 12 0.020
Inner Wall B.L. Plate P/N	604624-1	604624-2	604624-3
Length of Penetration into Stream (in) = A	0.0	0.08	0.22
% of Mean Passage Height	0.0	8.78	24.15
S = Boundary Layer Thickness (% H)	29.0	30.0	52.0
S* = Displacement Thickness (% H)	3.04	6.70	13.22
Θ = Momentum Thickness (% H)	2.43	4.05	8.54
Outer Wall B.L. Plate P/N	604689-1	604689-2	604689-1
Length of Penetration into Stream (in) = B	0.0	0.08	0.0
% of Mean Passage Height	0.0	8.78	0.0
S = Boundary Layer Thickness (% R)	16.0	26.0	13.0
S* = Displacement Thickness (% R)	1.56	5.5	1.9
Θ = Momentum Thickness (% R)	1.27	3.3	1.34
Inlet Reynolds No. Rx Based on X = 1.63 in.	1.25×10^5	1.41×10^5	1.65×10^5
Inlet Total Pressure ("Hg)	50	50	50
Inlet Total Temp. (°F)	215	230	228
Inlet Core Mach No.	0.111	0.130	0.150
Avg. Turbulence Intensity (%)	0.041	0.0526	0.0725

SOLIDITY EFFECTS OF NOZZLE AND ROTOR ON PERFORMANCE

Cascade tests conducted in Phase II on a 20-percent reduced solidity nozzle showed a loss in efficiency of 3.4 points with zero cooling flow, Figure 126. The low solidity tests were conducted at M = 1.03 due to facility limitations. Assuming a Mach number correction, Figure 114, $\Delta N/\Delta M = 120.1 - 87.86M = 4.2$ points for M = 1.23 or a net increase in efficiency of 0.8 point. A comparison of the predicted solidity with the modified Ainley loss system at this same Mach number is given in Table 22. An efficiency loss of 1.04 points is predicted. Although the measured trend is opposite to prediction, a measurement error of ± 1 point places the two values within the same accuracy band.

TABLE 22

NOZZLE LOSS DISTRIBUTION

	Nominal Solidity	20 Percent Reduced Solidity
Profile, $\bar{\omega}$	0.0380	0.0390
Trailing Edge, $\bar{\omega}$	0.0230	0.0113
Clearance, $\bar{\omega}$	0	0
Secondary, $\bar{\omega}$	0.1318	0.1652
Total, $\bar{\omega}$	0.1928	0.2155
Efficiency, η	90.34	89.30
Efficiency Change	1.04	

A similar test was conducted in cascade with a 30-percent reduced rotor solidity and also a full-round test with a 22 percent reduced solidity rotor. The corresponding stage efficiency losses were 4.0 and 3.6 points loss. The respective cascade and full-round influence factors are 1.33 and 1.64 points loss in stage efficiency per 10 percent reduction of rotor solidity. Good agreement was obtained from cascade to full round testing. The use of Zweifel's loading criteria, Reference 40, for setting optimum solidities is verified to the extent that performance dropped when a solidity less than that suggested by Zweifel was treated.

BLADE LOADING ENVELOPE

Cascade and full-round tests were conducted on the two rotor shapes selected, Figures 39 through 48. The rotor cascade tests showed the SLR rotor to be higher in efficiency than the PLR rotor by 0.9 point (Table 15). Phase III full-stage test numbers, Table 20, showed the SLR stage to be 2.3 points higher than the PLR stage. The more pronounced stage results may be due to Coriolis' effects, tip clearance flows, relative flow fields and centrifugal fields not simulated in cascade. Although performance levels were different, the trends were in the same direction from the cascade and full-round tests.

The reason for higher performance from the SLR configuration was probably due to having lower incidence losses. The hub was selected to be highly loaded to minimize size and blade numbers. Structural limitations fixed the hub section area requirements. These constraints lead to a hub passage area that is nearly constant with a leading-edge throat unless positive incidences are employed. The resulting gas foils for the PLR had higher design incidences than SLR, and the blade loading as a singular variable cannot be separated from these tests. It may be concluded, however, that the SLR rotor with less design incidence, but front loaded, had better performance in stage and cascade than the PLR high incidence rear loaded rotor.

MODIFICATION OF DESIGN TECHNIQUE

The parameters experimentally evaluated yielded a substantial store of data, some of which followed predictable trends and some which did not. New information has been generated; however, the tests were conducted on basically one turbine flow path. Some of the trends are peculiar to the ASATT geometry alone and the data acquired was not general enough nor complete enough to propose a new quantitative loss formulation. Since the predicted efficiency and test efficiency of the SLR configuration were within 1.4 points, the basic loss system was considered adequate. Additional cooling injection losses are readily predictable, whereas effects of increased inlet turbulence, velocity distortion, boundary layer, and rotor to nozzle axial spacing effects are "add on" losses which can be treated on an individual basis. Emphasis was, therefore, placed on modifications to the design technique incorporating the results of the experimental investigation. An analytical turbine model was initiated that incorporated Phase III measured values of:

1. Nozzle Radial Distribution of Loss.
2. Rotor Radial Distribution of Loss.
3. Nozzle and Rotor Throat Openings as a Function of Radius.
4. Flow-Path Dimensions and Geometry.
5. Expansion Ratio and Average Inlet Conditions.

A modified NASA off-design multi-sector computer program (Reference 53), was used to model the test data. The turbine flow path was broken into five annular sectors and the above measured data was used as input. Each sector is treated as a quasi-one-dimensional element and is joined spanwise by radial equilibrium and chordwise by continuity. A trial and error procedure was used to match measured test data. This procedure was used on those variables not completely defined by test in the stage model (nozzle and rotor flow coefficients, for example) until close agreement was obtained on all measured data.

Rotor incidence losses were calculated at all radial stations based on an input option requiring:

1. An optimum loss (ω OPT) corresponding to zero incidence.
2. A normalizing incidence (i_s) for which stalling incidence was used.
3. Coefficients for a fourth-order polynomial to correct for incidence effect (positive and negative incidence are treated separately).
4. Incidence boundaries for the polynomial fit beyond which linear extrapolation occurs.

The actual loss ($\bar{\omega}$) is computed using the following equation:

$$\bar{\omega} = \bar{\omega}_{OPT} \left[1 + A\left(\frac{i}{i_s}\right)^2 + B\left(\frac{i}{i_s}\right)^3 + C\left(\frac{i}{i_s}\right)^4\right]$$

Ainley[10] incidence loss predictions were used to calculate the polynomial coefficients for the equation above. In Ainley's prediction, the total profile loss ($\bar{\omega} = \Delta P^o/(P^o - p)$ exit) is based on (1) i_s, a stalling incidence calculated using blade geometry, (2) $\bar{\omega}_{opt}$, the profile loss of incidence is zero, and (3) i is measured incidence. For our model, positive and negative incidence ranges were treated separately. For each range, the Ainley data was fit to a fourth degree polynomial representing the full range of i/i_s presented. The resultant coefficients were:

POSITIVE INCIDENCE	NEGATIVE INCIDENCE
A = 0.4116	A = 0.8200
B = 0.4373	B = 0.2550
C = 0.1511	C = 0.0350

The objective of the modeling was to match Phase III test results. The total rotor loss coefficient from Phase III test data included incidence effects. The test data total loss coefficient was calculated from: (1) turbine inlet rake total temperature and pressure data radial profiles, (2) nozzle performance testing total pressure loss and exit swirl, (3) linear radial static pressure based on wall statics at nozzle exit and rotor exit, (4) total temperature, pressure and swirl from rotor exit survey, (5) geometrical areas at measuring stations, and (6) blade speed. By applying continuity at rotor inlet and rotor exit with the assumptions listed, vector triangles along constant percent height streamtubes were constructed; and from the resultant relative parameters, the rotor loss coefficient was calculated.

The off-design program (Reference 53), which was used for the modeling, required the zero incidence loss, $\bar{\omega}_{opt}$, as input. As an initial value, the calculated total rotor loss coefficient was used. $\bar{\omega}_{opt}$ was then iteratively adjusted until the total loss (with incidence penalty) calculated in the off-design program best matched the test data total loss profile. Figure 212 demonstrates that fair agreement of rotor total loss coefficient was achieved.

The ASATT models used an effective throat area option, which uses measured throat openings, measured total blading losses from Phase III test data, and throat flow coefficients (Shown in Figure 213) to calculate a subsonic

effective relative exit gas angle. Flow coefficient profiles were varied to best match blading exit Mach number distributions and total airflow of Phase III test data. The final flow coefficient profiles are presented in Figure 213. Resultant Mach number distributions are compared to SLR test data in Figure 214. In Figure 215, nozzle exit Mach number distributions are also compared to nozzle blow down test data which has been scaled to the same pressure ratio as the base model. Figure 216 shows a comparison of model and test data acceleration at the walls. Good agreement is shown with all parameters.

For verification, this model was then applied to an unrelated IR&D turbine three times larger in swallowing capacity. Figure 217 shows a comparison of the ASATT turbine flow path to a scaled version of the IR&D turbine flow path. Efficiency and rotor exit swirl profiles for the IR&D model and test data are shown in Figures 218 and 219. Fair agreement in these preliminary results lends credibility to the ASATT models. The ASATT model was then used to define flow path modifications to improve performance, Section V.

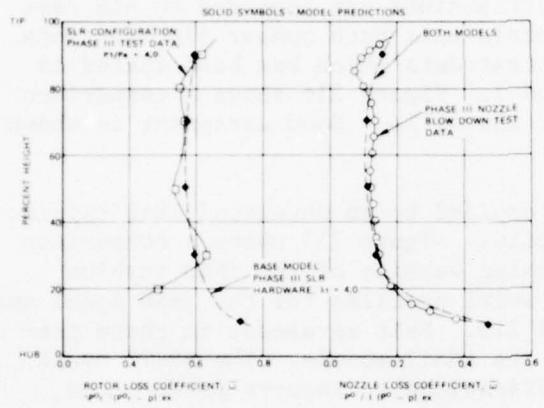


Figure 212. Blading Loss Profile Model Compared to Phase III Test Data.

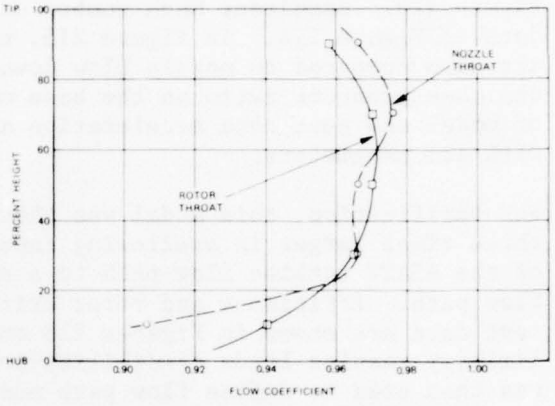


Figure 213. Model of ASATT SLR Turbine; Profiles of Input Throat Coefficients.

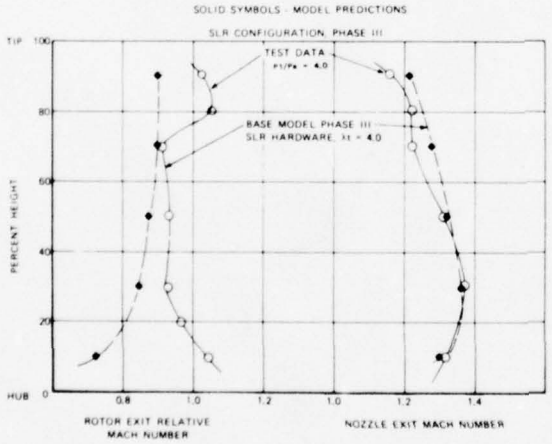


Figure 214. Mach Number Comparisons; Model and Phase III SLR Turbine Stage Data.

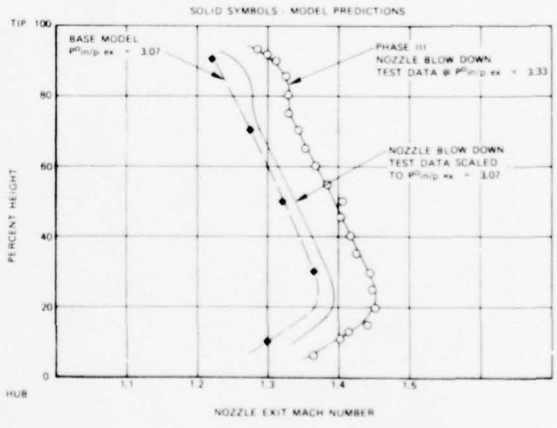


Figure 215. Nozzle Exit Mach Number Comparison; Model and Nozzle Blowdown Test.

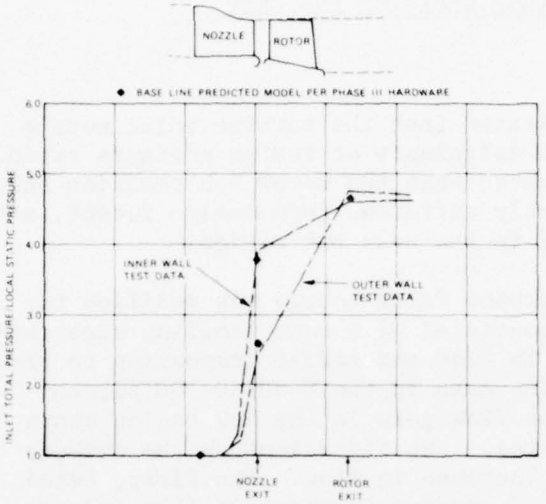


Figure 216. Wall Static Pressure Distribution; Model Compared to SLR Turbine.

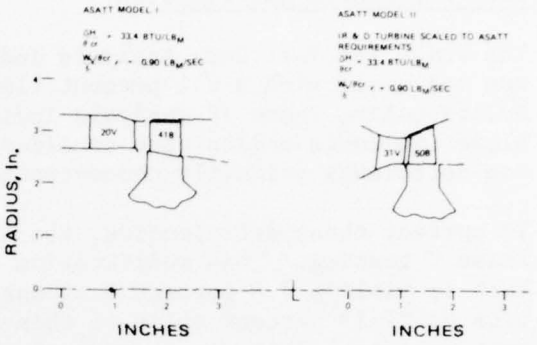


Figure 217. Turbine Model Flow Path Comparison.

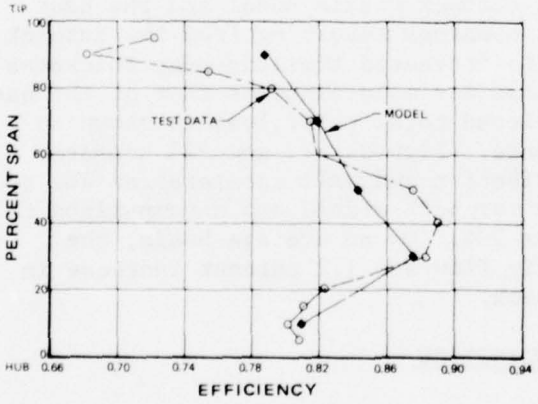


Figure 218. Model II Efficiency Profile Compared to Test Data.

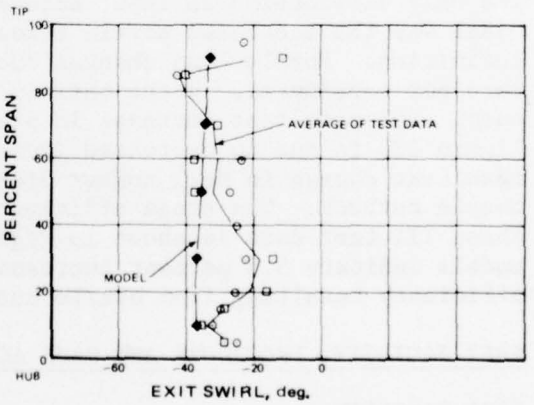


Figure 219. Rotor Exit Swirl for Model II Compared to Test Data.

PHASE V - TURBINE STAGE REDESIGN AND TEST

TEST RIG DESIGN MODIFICATION

The Phase III Test Data Analysis indicated that the turbine inlet nozzle was too small with a 6.4 percent flow deficiency at design pressure ratio. Additionally, Phase IV analysis indicated that the rotor hub reaction and blade incidence angles were considerably different from design intent, with the deficiency primarily concentrated in the near hub region.

To correct these deficiencies, the turbine inlet nozzle was modified for Phase V testing. This modification consisted of a vane trailing edge cutback to yield a 6.4 percent increase in flow and radial contouring to provide an 87/13 percent split of this increase in the 0-50/50-100 percent span regions. This places most of the flow gain in the hub region where the Phase III deficiencies are indicated. Two iterations on the cutback were required to achieve the desired increase in flow. The first, based on blueprint dimensions, yielded a 14.2-percent increase in flow and was considered to be unsatisfactory for Phase V testing. The second and final cutback (actually addition of vane trailing edge) iteration, Figure 220, passed design flow of 0.90 lb/sec and was consequently used throughout the Phase V test program.

The analytical model procedure defined in Phase IV, Modification of Design Technique, was used to predict the performance of the turbine. The flow path was broken into five equal height annular sectors joined spanwise by radial equilibrium and chordwise by continuity.

The only distinction in input between cutback nozzle model and the base model was the increased nozzle throat openings resulting from the cutback definition. Nozzle loss changes due to increased trailing-edge thickness were not considered. Rotor optimim loss was maintained as that of the base case. The resultant decrease in predicted total rotor loss as shown in Figure 221 is due to decreased incidence. Figures 222 and 223 compare resultant change in Mach number distribution and wall acceleration due to nozzle cutback. The stage efficiency for both models and a comparison to Phase III test data is shown in Figure 224. On an average basis, the models indicate 5.6 percent increase in flow and 1.2 percent increase in efficiency resulting from nozzle cutback.

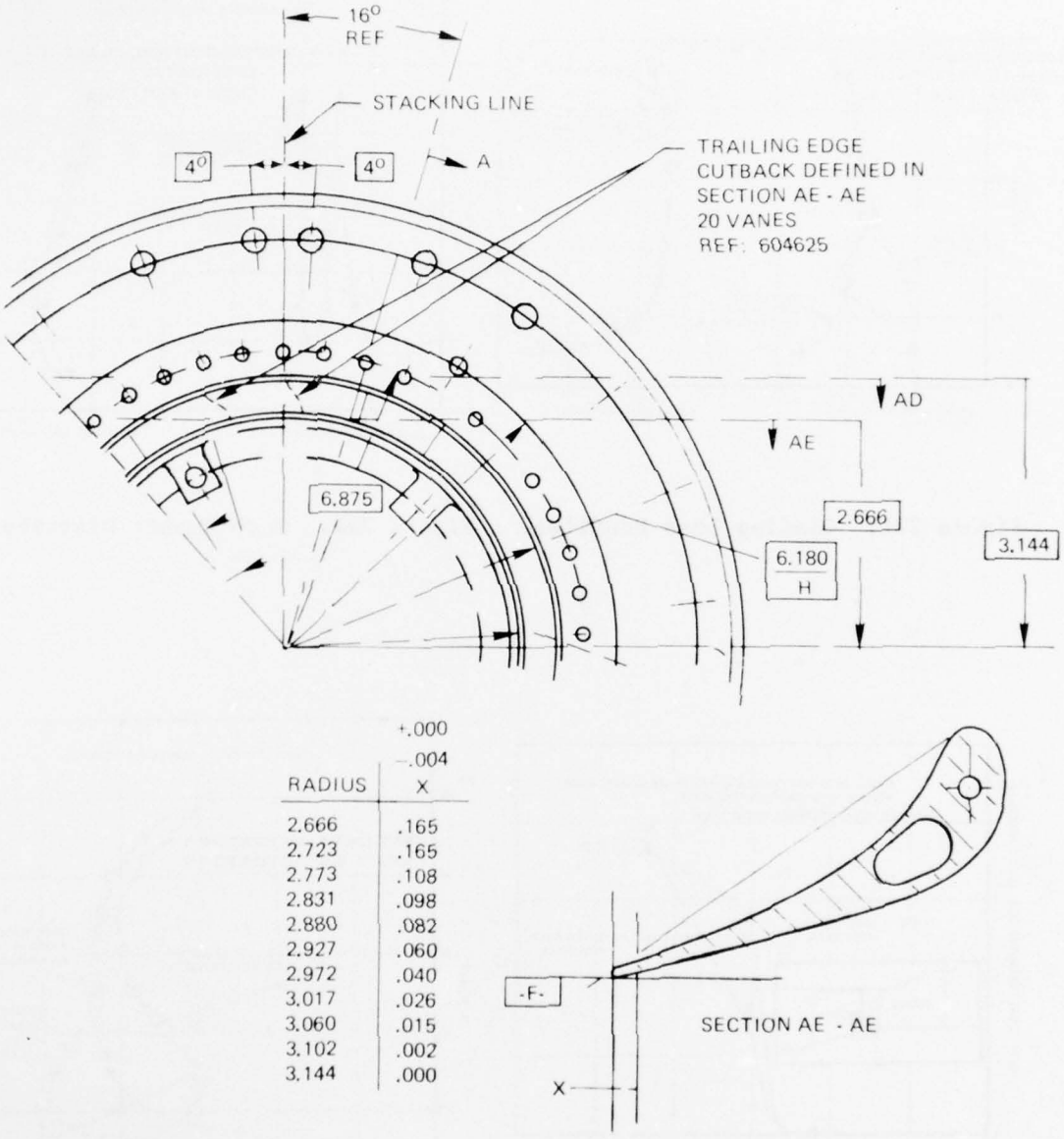
TEST FACILITY, PROCEDURE AND DATA ACQUISITION

TEST FACILITY

Discussed in Test Facility section, Phase III.

TEST PROCEDURE

The Phase V test program consisted of basically two test procedures, that of turbine inlet nozzle calibration and full turbine stage performance.



RADIUS	X +.000 −.004
2.666	.165
2.723	.165
2.773	.108
2.831	.098
2.880	.082
2.927	.060
2.972	.040
3.017	.026
3.060	.015
3.102	.002
3.144	.000

Figure 220. Definition of ASATT Nozzle Trailing-Edge Cutback.

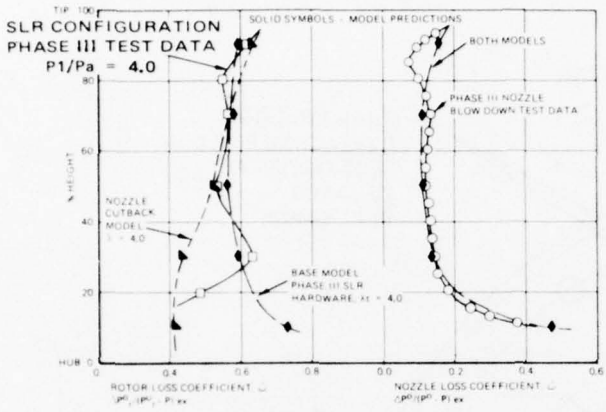


Figure 221. Blading Loss Profiles.

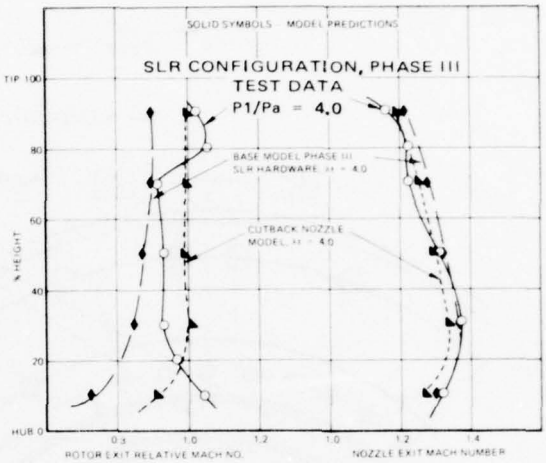


Figure 222. Mach Number Distributions.

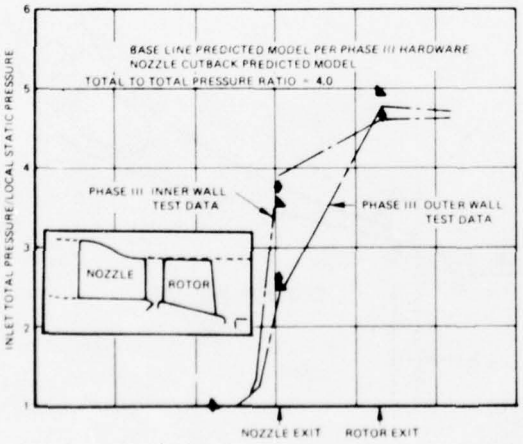


Figure 223. Predicted Wall Static Pressure Distributions.

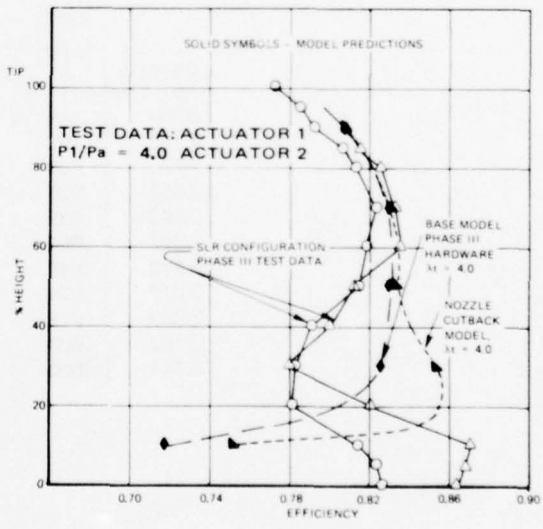


Figure 224. Phase V Predicted Stage Efficiency Distribution.

During the nozzle calibration test, the procedure for determing the flow rate/pressure ratio characteristic of the Phase V nozzle consisted of setting an inlet pressure of 24.6 psia and reducing the discharge pressure incrementally to achieve the desired pressure ratio. At least 12 pressure ratios were set between 1.2 and 4.7 (inlet total average/discharge static average). Data recorded at each pressure ratio point consists of inlet total temperature and pressures, wall static pressures (nozzle inner and outer wall, flow passage and trailing edge) and mass flow rate using the 1800 data acquisition and controls system (DACS).

The nozzle total pressure loss was determined at two pressure ratios, 3.33 and 2.72 (inlet total pressure average/discharge static average). The pressure ratio was set by fixing the inlet total pressure average at 24.6 psia and adjusting the discharge average static pressure to yield the desired pressure ratio.

The total pressure probe was located at a fixed radial position and continuously traversed circumferentially over an arc of 36 degrees (2 vane pitches) to assure the capture of two trailing-edge wakes. At least sixteen radial positions were surveyed over the blade span. Data were recorded on an X-Y plotter and consisted of inlet total pressure and a ΔP total (P total inlet - P total exit local).

During the full-stage performance tests, airflow was initiated through the test turbine by combined operation of the laboratory exhaust vacuum pumps and inlet rams. The inlet pressure was set at 24.6 psia. Turbine speed was gradually increased to corrected level by decreasing the exhaust pressure with the turbine load maintained using the Hydra-Brake adjustments. Accelerometers located on the bearing housing were monitored to assure operation free from destructive resonances. Turbine rotor tip clearance indicators were monitored to assure rub-free operation (0.012 in. minimum radial) during the test. Other standard parameters which monitored during the test included: bearing lube oil pressure and temperature, water brake discharge pressure and temperature, torque, speed, turbine air inlet temperature and pressure, and turbine air exit pressure and temperature. The inlet pressure was maintained at near 24.6 psia and air temperature near 230°F. The turbine was stabilized at speed and pressure ratio for a period of several minutes, and readings of all static pressures and rakes were obtained using the 1800 DACS. Radial surveys of total pressure, temperature and angle were taken at the two circumferential locations at the rotor discharge. The surveys consisted of thirteen point surveys, eleven points at equal radial intervals and two at 5 and 95-percent spans from the inner to outer walls.

A series of approximately thirty operating points were run to define the performance map. These points were set by varying exhaust pressure and water brake load to cover a speed range from 60 percent (17,290 rpm) to 100 percent and pressure ratios from 1.8 to limit load. The test points are shown in Table 23 as a function of percent speed and pressure ratio. The nominal stator and rotor cooling flow was turned on at design

TABLE 23

ASATT TURBINE PHASE V TEST POINTS

Pressure Ratio	PERCENT SPEED 60	70	80	90	100
Limit Load	X	X	X	X	X
4.4				X	X
4.0			X	X	X Cooling & Survey
3.6	X	X	X	X	X
3.2	X		X		X
2.8		X Survey		X	X
2.4	X		X	X	
2.1		X	X	X	
1.8	X		X		X

point speed, and performance/survey data were taken.

DATA ACQUISITION

Discussed in Data Acquisition section, Phase III

TURBINE STAGE REDESIGN TEST RESULTS

PHASE V, TEST 1 - NOZZLE PERFORMANCE

Test Objective

The objective of this test was to determine the nozzle flow characteristic of the modified nozzle assembly over a range of pressure ratios and to measure the total pressure loss across the nozzle using a radial and circumferential survey of total pressure at the nozzle discharge.

Test Configuration

The test configuration was similar to that used during the Phase III Test 1 nozzle performance evaluations. The same survey probe was used with the tip set 0.25 inch axially behind the trailing edge of the nozzle vane tip. Due to the nozzle modification, a trailing edge cutback that increases with decreasing radius, the axial distance between the stator trailing edge and the probe, is not constant and reaches a maximum of 0.29 inch at the inner wall. The survey probe tip, aligned with its axis parallel to the stator suction surface, was traversed in a plane normal to the rig shaft and corresponds to the location of the rotor blade leading edges. Data over the entire span (16 radial positions) was obtained by positioning the probe at a prescribed radius and then traversing circumferentially over a 36° arc (Figures 225 and 226). This arc includes a full vane channel, two vane trailing-edge wakes, and part of the adjacent channels.

Test Results

Phase III test data indicated that the turbine inlet nozzle was 6.4 percent smaller than the design. The most significant throat area deficiency appeared in the hub region, where a high rotor incidence and a low hub reaction resulted. The Phase V hardware modification was directed toward correcting this deficiency by cutting back the nozzle trailing edge to open the nozzle area 6.4 percent, with most of the opening required in the hub region (see section "Test Rig Design Modification").

The first iteration on the cutback yielded a 14.2 percent increase in flow. Throat specification for this cutback defined from the trailing edge, assuming that the nozzle was made to print and stacked on a radial line. Subsequent dimensional checks showed the nozzle vanes to be stacked incorrectly in manufacture, which resulted in openings that were too large. A second iteration on the cutback yielded the correct flow, $W\sqrt{\theta}/\delta/\epsilon$ = 0.9 lb/sec, and was used throughout Phase V testings. Figure 227 shows the flow rate vs pressure ratio characteristics of both nozzle cutback iterations. To check for rig leakage (flow bypassing nozzle), flow through the nozzle was measured at two levels of inlet pressure - ambient and 24.6 psia. No appreciable rig leakage was indicated with both the pressurized and the ambient flow being within data scatter of each other.

The results of the total pressure and total pressure loss surveys at nozzle total-to-static pressure ratios of 2.72 and 3.33 are shown in Figures 228 through 233. The radial distributions of the vane-to-vane integrated average nozzle pressure loss coefficients are compared in Figure 228 for design, Phase III and Phase V. Cutting back the vanes increased the loss to $\bar{\omega}$ = 0.184 vs $\bar{\omega}$ = 0.154 for the original nozzle at pressure ratio of 3.33. The radial gradient changed significantly in that the near hub (0-30 percent span) losses were reduced, and beyond 30 percent span the losses were increased on the average. The 3.33 pressure ratio setting was determined from the PLR full-stage tests (4.2 total-to-total pressure ratio and 100 percent $N/\sqrt{\theta_{cr}}$) during Phase III and provides a common point of

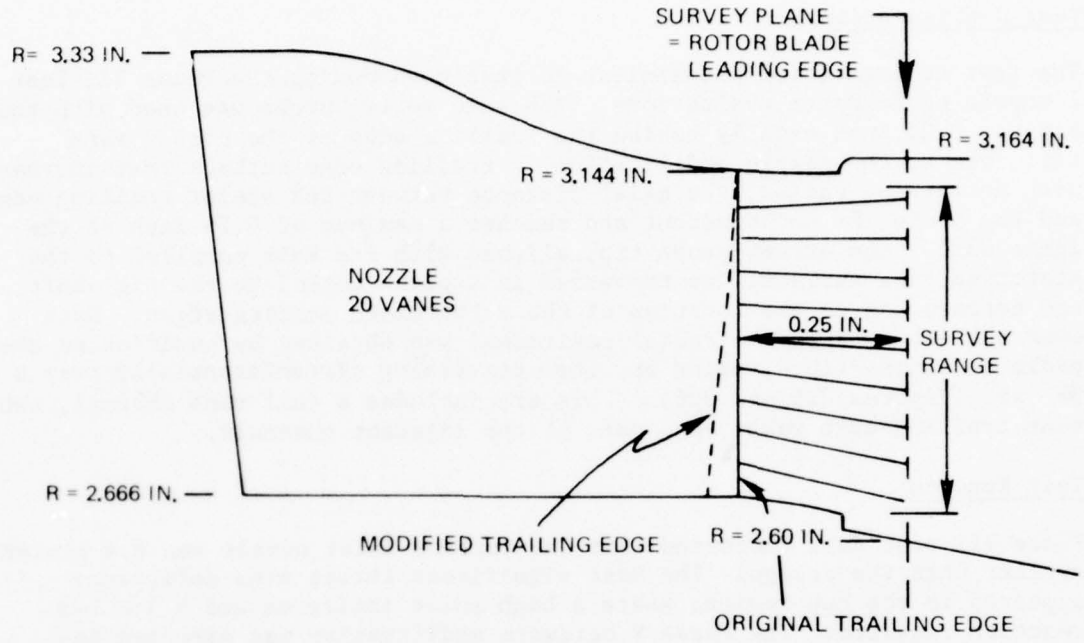
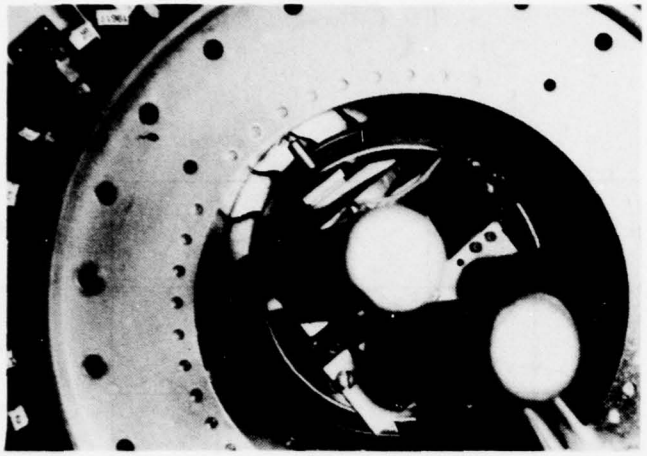


Figure 225. Phase V, Test 1 - Nozzle Performance - Diagram of Flow Path for Nozzle Exit Survey.

comparison. The same trends are indicated at the design pressure ratio of 2.72, with the average loss showing an improvement with respect to design goals, $\overline{\omega}$ = 0.145 vs $\overline{\omega}$ design = 0.179.

The results of the average nozzle exit Mach number calculations are shown in Figure 229 and indicate a slight reduction with respect to Phase III, 1.36 vs 1.38, at a pressure ratio of 3.33. The radial gradient remained essentially the same except for the higher Mach numbers near the hub (0-25 percent span). At design pressure ratio (2.72), the average Mach number (1.22) and its gradient are near design goals.

In the plane of measurement, the constant loss coefficient and Mach number contours are shown in Figures 230 through 233. At a pressure ratio of 3.33 (Figures 230 and 231), which is near the full-stage operating point when stage total-to-total pressure ratio is 4.0 at 100% $N/\sqrt{\theta_{cr}}$, the Mach number and loss contours show good periodicity. Highest losses are concentrated near the inner wall in the mid-channel region with a maximum local loss coefficient of 1.1 indicative of potential flow separation from the inner wall. Most of the channel core region was below 0.1 with increasing losses around the channel periphery towards the walls. Localized higher loss regions were present near the trailing-edge wakes. One was



(Phase V)

Phase III

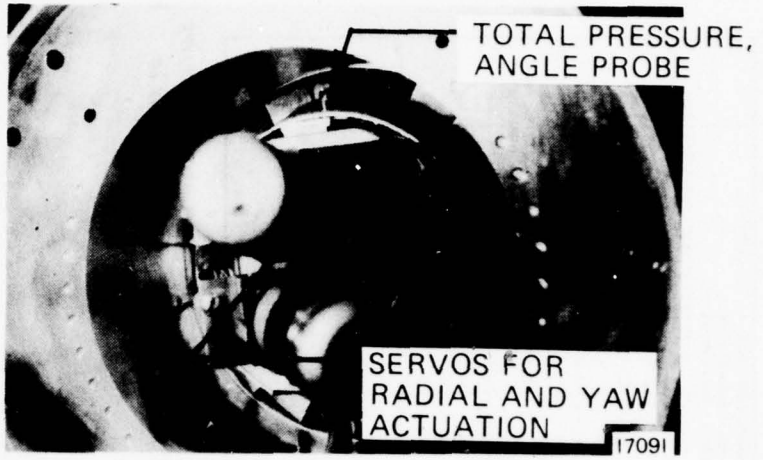


Figure 226. Phase V Turbine Inlet Nozzle Modification.

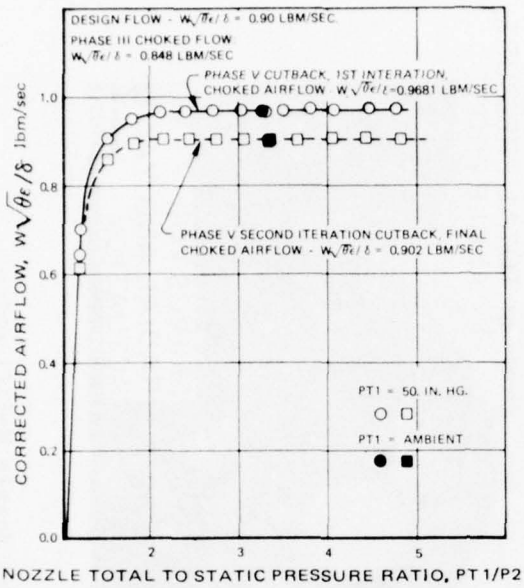


Figure 227. Phase V - ASATT Nozzle Blowdown.

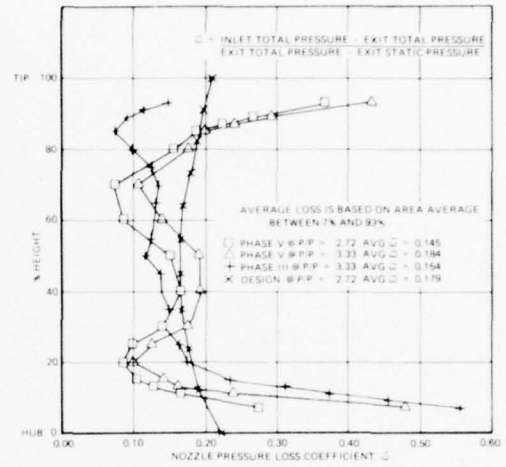


Figure 228. Phase V, Test 1: Nozzle Performance.

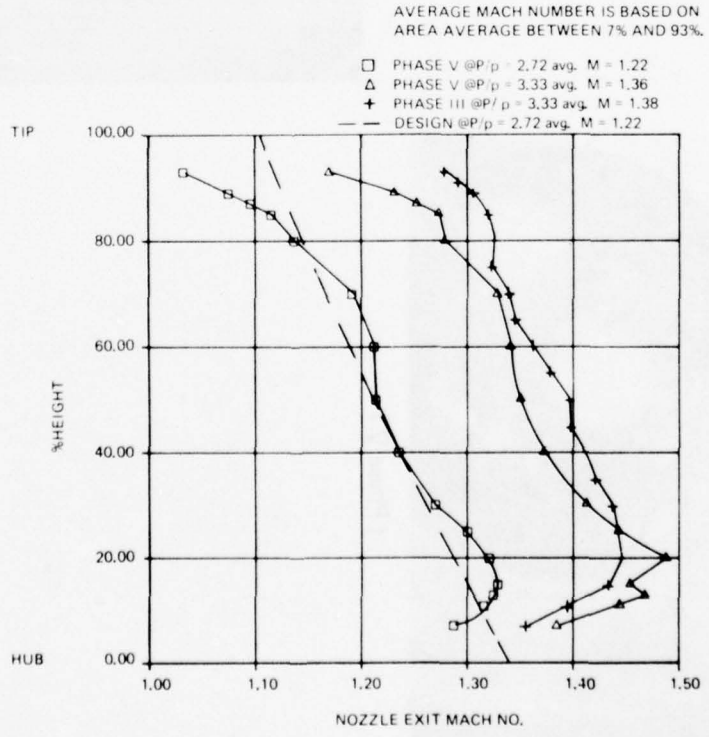


Figure 229. Phase V, Test 1: Nozzle Performance.

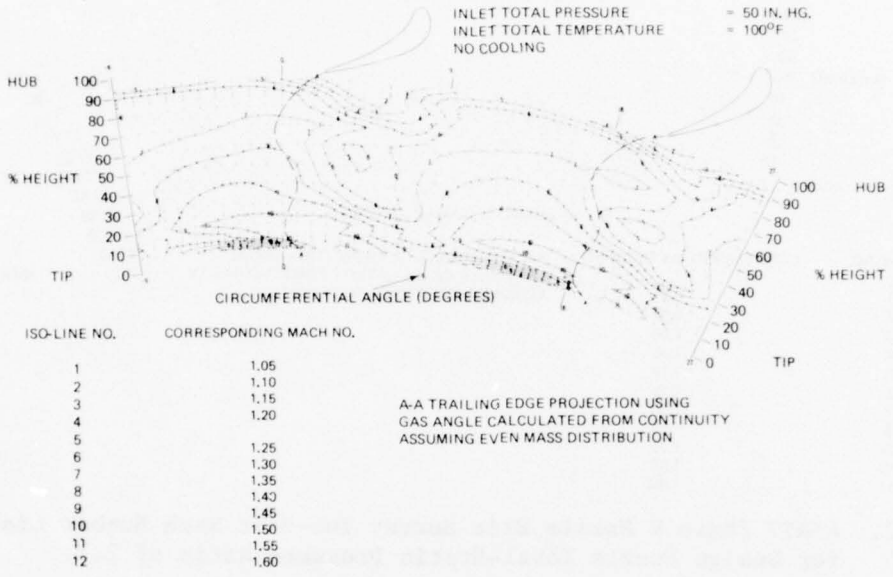


Figure 230. ASATT Phase V Nozzle Exit Survey Iso-Mach Number Lines for Nozzle Total-Static Pressure Ratio of 3.33.

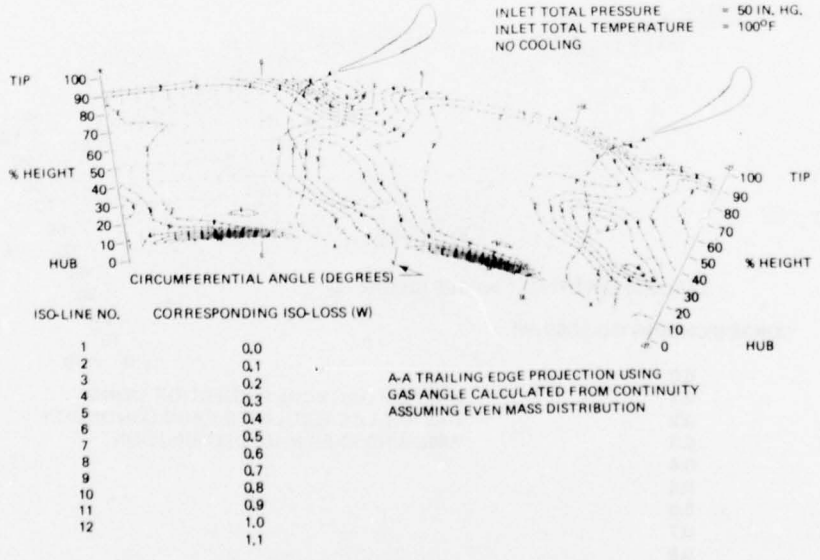
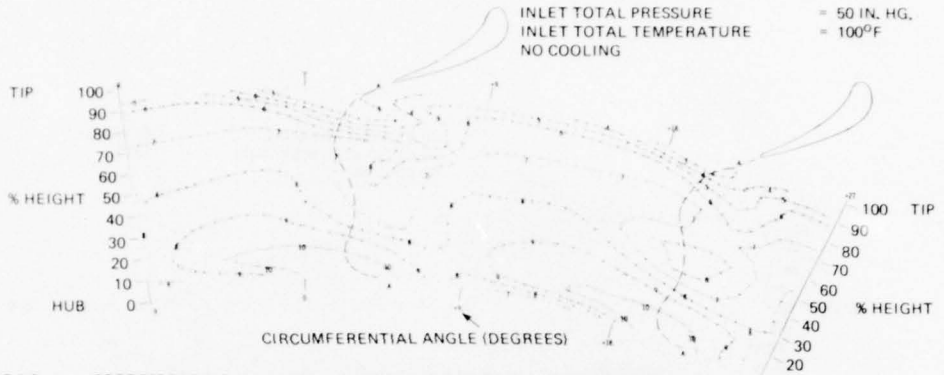


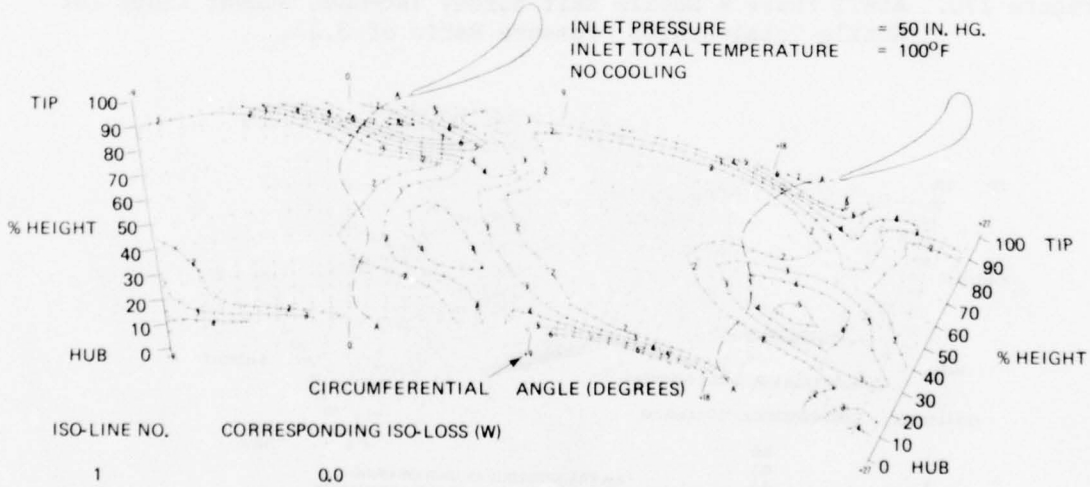
Figure 231. ASATT Phase V Nozzle Exit Survey Iso-Pressure Loss Coefficient Lines for Nozzle Total-Static Pressure Ratio of 3.33.



ISO-LINE NO.	CORRESPONDING MACH NO.
1	0.9
2	0.95
3	1.00
4	1.05
5	1.10
6	1.15
7	1.20
8	1.25
9	1.30
10	1.35
11	1.40

A-A TRAILING EDGE PROJECTION USING GAS ANGLE CALCULATED FROM CONTINUITY ASSUMING EVEN MASS DISTRIBUTION.

Figure 232. ASATT Phase V Nozzle Exit Survey Iso-Exit Mach Number Lines for Design Nozzle Total-Static Pressure Ratio of 2.7.



ISO-LINE NO.	CORRESPONDING ISO-LOSS (W)
1	0.0
2	0.1
3	0.2
4	0.3
5	0.4
6	0.5
7	0.6
8	0.7
9	0.8

A-A TRAILING EDGE PROJECTION USING GAS ANGLE CALCULATED FROM CONTINUITY ASSUMING EVEN MASS DISTRIBUTION

Figure 233. ASATT Phase V Nozzle Exit Survey Iso-Pressure Loss Coefficient Lines for Design Nozzle Total-Static Pressure Ratio of 2.7.

centered near the outer wall at 85-90 percent span with a maximum loss coefficient of 0.4-0.5; both may be attributed to localized vortex flow.

At a design pressure ratio of 2.72, the above trends are duplicated (Figures 232 and 233) but at lower levels of loss coefficients and Mach numbers.

The survey probe was calibrated at NASA/Lewis supersonic flow tunnel a Mach number of 1.3. The results showed that the Rayleigh normal shock equations can be applied to the measured total pressures to account for the shock losses ahead of the tip. The above data includes this correction and incorporates a linear hub-to-tip static pressure distribution as measured 0.25 inch ahead of the survey plane.

PHASE V, TEST 2 - TURBINE STAGE PERFORMANCE WITH PLR ROTOR

Test Objective

Define effect on stage performance of the Phase V turbine modification with the PLR rotor and evaluate the blade element performance using the wall static pressures and rotor exit radial traverse measurements.

Test Configuration

The turbine stage configuration consisted of the modified turbine inlet nozzle assembly and the nominal 41 blade pressure surface loaded rotor. The stator assembly to blade axial spacing was 0.25 inch. (The same as Test 3 of Phase III evaluations). Measured static rotor tip to shroud clearance was 0.012 to 0.013 inch radial. The instrumentation was also identical to that of the Phase III tests and included the following:

- Nozzle inlet total temperature and pressure
- Rotor exit total temperature and pressure
- Rotor exit radial traverse (2 locations) of temperature, pressure, and swirl angle
- In-Line torque meter
- Static pressures at stage inlet and exit total measuring planes, nozzle exit, nozzle vane mid-channel, and rotor exit locations on both inner and outer walls.

Test Results

The Phase V tests were conducted with 24.6 psia and 220°-230°F inlet pressures and temperatures. The resultant performance map with the modified turbine inlet nozzle and pressure surface loaded rotor is shown in Figure 234. For comparison of performance to Phase III data (Figure 236) and design (Figure 237), this map is corrected for Reynolds Number according to $(1 - \eta) \alpha (N_R)^{-0.123}$ as correlated in Phase III and is shown in Figure 235. The tip clearance difference between the design map (Figure 237) and the Phase V test map (Figure 235) is 0.0085 in. (0.0125 for Figure 235 and 0.004

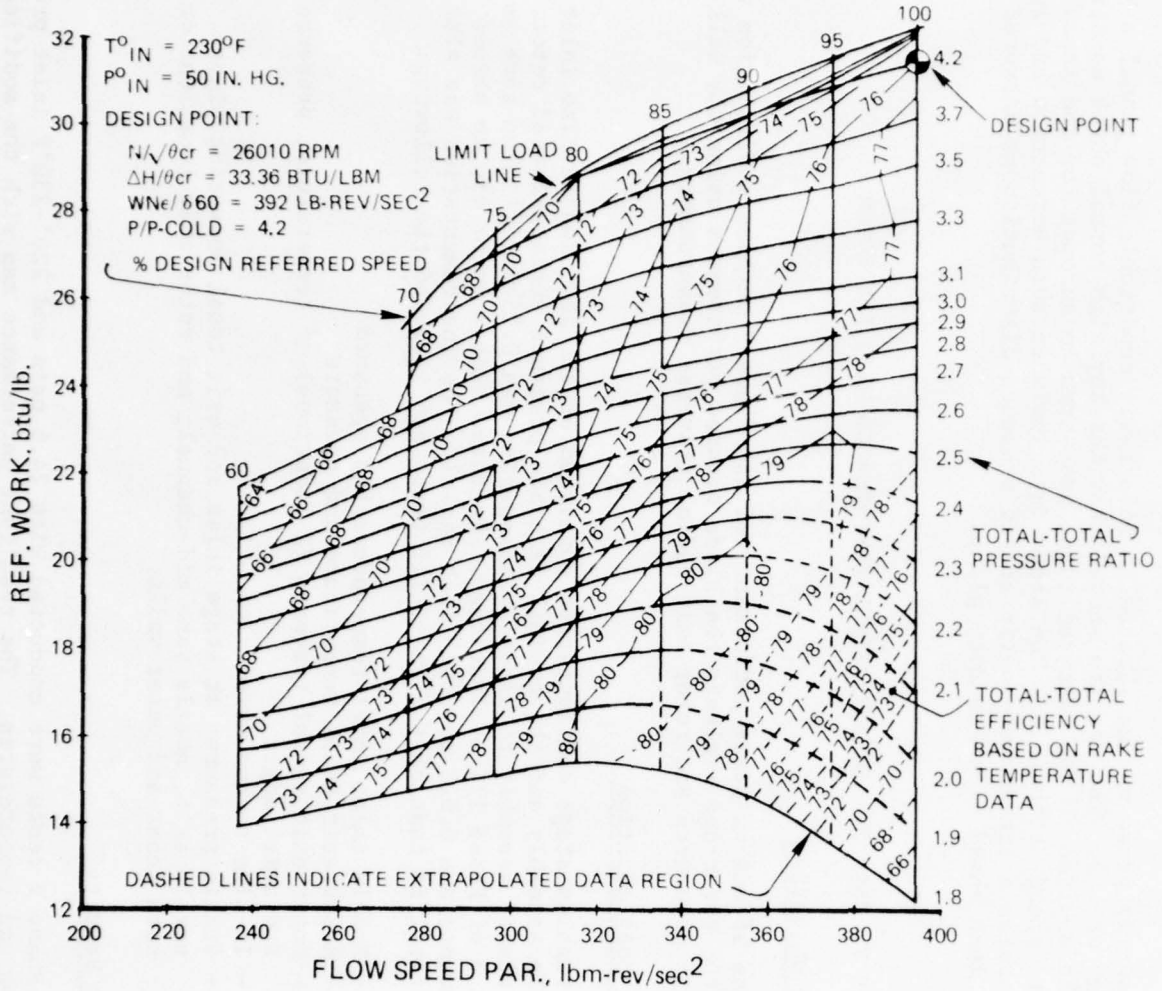


Figure 234. ASATT Phase V Pressure Surface Loaded Rotor Configuration Test Map.

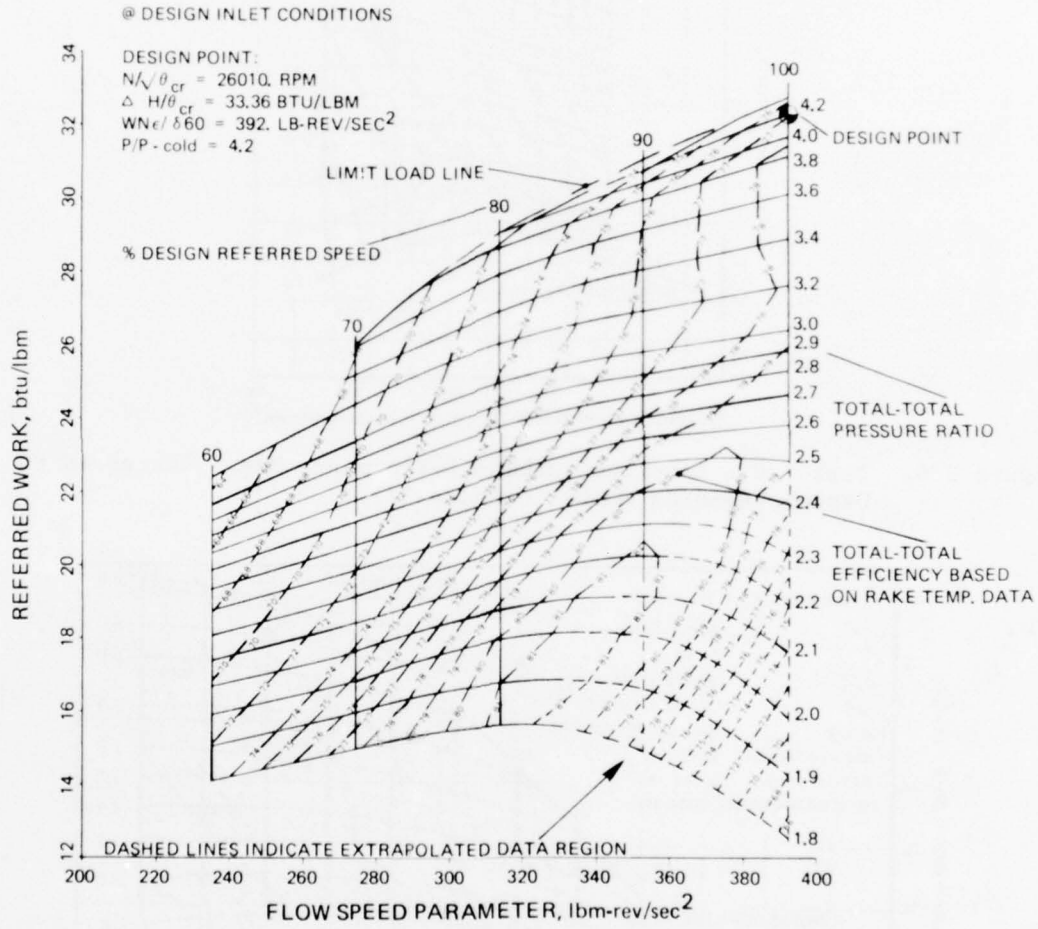


Figure 235. ASATT Phase V Pressure Surface Loaded Rotor Configuration Test Map Corrected to Design Reynolds Number.

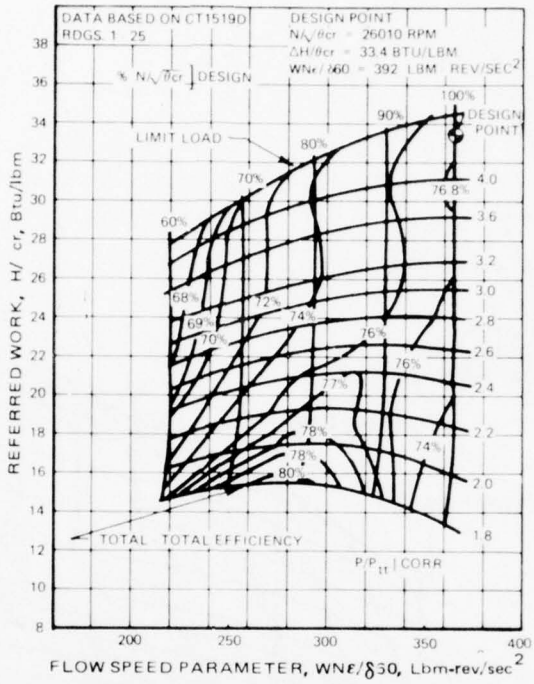


Figure 236. Test 3.0 - Baseline Turbine Performance Map. Corrected to Design Reynolds Number - Phase III.

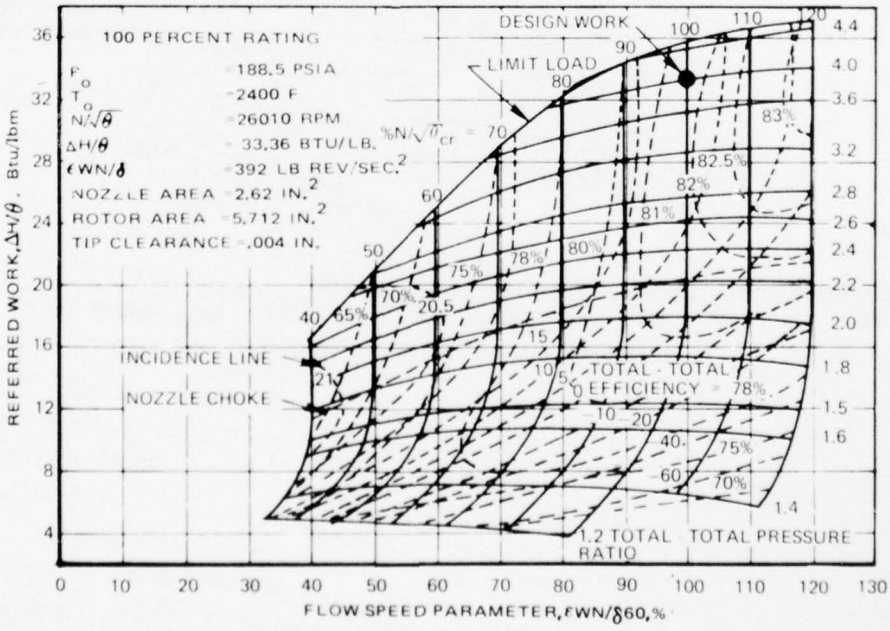


Figure 237. Design Prediction - ASATT Turbine Performance.

in. for Figure 237). An estimate of tip clearance effects on performance is shown in Figure 8 and yields approximately a 1.0 point efficiency change for a 0.0085 in. change in tip clearance. Hence, for a common comparison to Figure 235, the performance shown on the design map (Figure 237) may be reduced by 1.0 efficiency points and yields 80.3 percent. This is also consistent with the 80.2 percent efficiency predicted during Phase I (Appendix B) at a slightly lower rotor tip clearance of 0.011 in. A listing of the performance at 100 percent $N/\sqrt{\theta_{cr}}$ and 4.0 total-to-total pressure ratio yields the following:

	PHASE III	PHASE V	DESIGN
Pressure Ratio (Total to Total)	4.0	4.0	4.0
Referred Work $\frac{\Delta H}{\theta_{cr}}$, $\frac{Btu}{lb}$	31.2	31.6	33.4
Flow Speed Parameter, $\frac{WN\epsilon}{\delta 60}$, $\frac{lb\text{-}rev}{sec^2}$	367	392	392
Efficiency, η	76.8	77.8	*80.2

Comparing Phase V vs Phase III performance indicates that at near design flow and pressure ratio, stage efficiency increased by 1.0 point due to the nozzle modification. The limit load work, however, dropped to 32.0 Btu/lb or a 7.5-percent reduction compared to the original nozzle configuration.

Wall static pressure distribution comparisons are shown in Figures 238 through 240 and indicate the following:

a) A 3.4-percent increase in average static pressure at the inner wall of nozzle discharge (Figure 238), which agrees in trend with the Phase IV model predictions and yields increased reaction through the rotor by a factor of 3.8. (Reaction defined as the ratio of local static pressure change across the rotor to the local stage static pressure change.)

b) A 15.4-percent reduction in average static pressure at the outer wall (Figure 238) of the nozzle discharge with a reduction in rotor tip reaction by a factor of 0.77.

c) An average reduction of static pressures at rotor discharge (Figure 238) of 8 percent which can be attributed in part to the 6.4 percent increase in flow and an increase of approximately four degrees (Figure 243) swirl at rotor discharge. This resultant increase in flow Mach number at rotor discharge agrees with stage performance data in that limit load work shows a reduction with increasing rotor discharge velocities.

* NOTE: Efficiency at a tip clearance of 0.011 inch, Figure 237, performance given at a tip clearance of 0.004 inch.

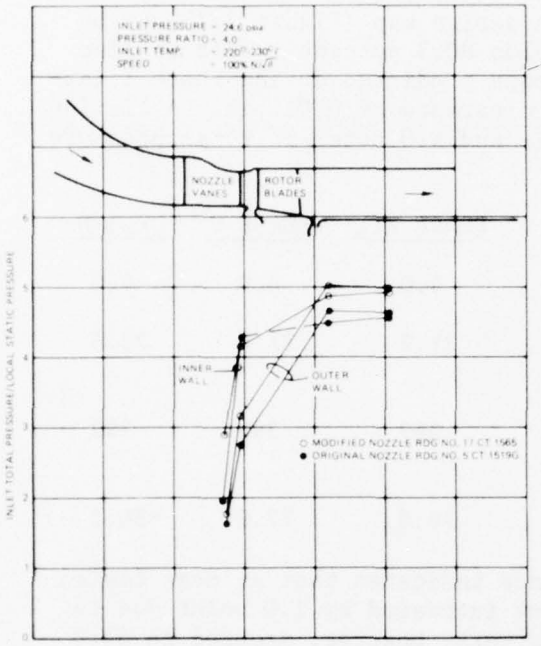
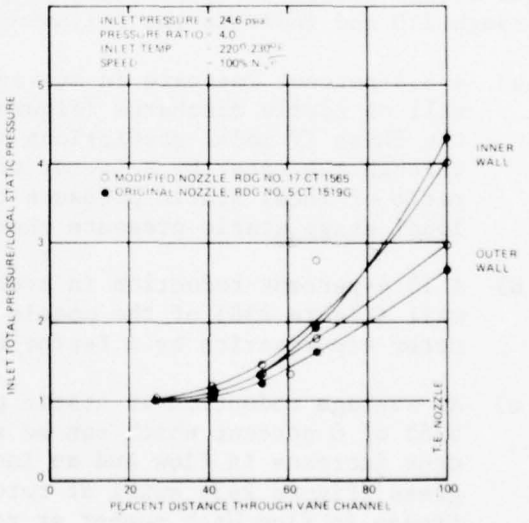


Figure 238. ASATT Phase V, Test 2 Axial Static Pressure Distribution - Pressure Side Loaded Rotor (PLR)



Pressure 239. ASATT Phase V, Test 2 Mid-Channel Pressure Distribution, Pressure-Side-Loaded Rotor (PLR).

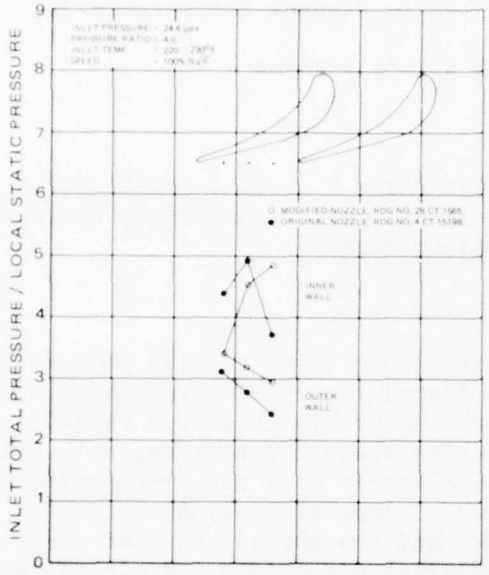


Figure 240. ASATT Phase V, Test 2 Nozzle Trailing Edge Static Pressure Distribution - Pressure Side Loaded Rotor, (PLR).

d) The nominal mid-span/mid-channel velocity distribution through the nozzle vane channels did not change appreciably as indicated by the pressure distribution of Figure 239. The radial velocity gradient shifted in the direction of reduced hub to tip difference. Nozzle vane to vane pressure distribution near the trailing edge (Figure 240) follows the same trend as above and also indicates significantly more expansion on the pressure surface side of the channel at the hub.

The rotor exit survey data on the distribution of total pressure, temperature and swirl angle is shown in Figures 241 and 243. Stage inlet radial gradients, averaged circumferentially, of total pressure and temperature are shown in Figures 244 and 245. Using the above data combined with the experimental nozzle loss data of Test 1, calculations were performed to obtain distributions of adiabatic efficiency (Figure 246), rotor loss coefficient (Figure 247), nozzle exit Mach number, and relative rotor discharge Mach number (Figure 248). The results, compared to the Phase III data with the original nozzle, are summarized as follows:

a) Stage performance in terms of efficiency at 4.0 total-to-total pressure ratio and 100 percent $N/\ \theta_{cr}$ was increased, with the bulk of the improvement occurring in the 10 to 60 percent span region. Rotor loss coefficients have also been reduced in the same radial span.

b) Nozzle discharge Mach number has generally increased ($\sim 4.5\%$) over the entire span. This is somewhat contradictory to the nozzle blowdown data at nearly the same total to static pressure ratio and suggests nozzle-rotor interactions at above critical Mach numbers. With the modified nozzle, an increased nozzle discharge Mach Number can occur if the effective air turning angle through the stators is reduced toward the axial direction. To obtain this additional expansion, a reduction in angle varying approximately 4° to 1° from hub to tip is indicated, when compared to the original Phase III data. The resultant rotor incidence angle reduction is shown in Figure 255.

Rotor exit survey data taken at 70 percent power with 70 percent $N/\sqrt{\theta_{cr}}$

and 2.8 total-to-total pressure ratio is shown in Figures 249 through 254.

PHASE V, TEST 3 - TURBINE STAGE PERFORMANCE WITH SLR ROTOR

Test Objective

Define the effect on stage performance of the Phase V turbine modification with the SLR rotor and evaluate the blade element performance using the wall static pressures and rotor exit traverse measurements.

Test Configuration

The configuration is identical to the previous test (Test 2) with the exception of the rotor. The suction surface loaded rotor (SLR) is substituted for the pressure surface loaded (PLR) rotor. Rotor tip to shroud radial clearance measured 0.012 to 0.013 inch. During Phase III testing, this SLR rotor was severely damaged (Figure 256), as a result of a rig overspeed and associated high vibration/rig bearing failure. Approximately 45 percent of the blades rubbed. Both the rotor blades and the shroud required resurfacing to bring the rig back into the original dimensions and clearances.

Test Results

The reduced performance map of the modified turbine, Phase V, with the SLR rotor is shown in Figure 257. As with the PLR rotor data (Test V-2), this was generated with 24.6 psia and 220°-230°F air inlet pressure and temperature. Thirty-one data points were taken throughout the map, including limit load per the test schedule outlined in Table 23 (under test facility, procedure, and data acquisition). This map corrected to ASATT design conditions by the Reynolds Number correction correlated in Phase III is shown in Figure 258 and is directly comparable to the design map, Figure 258, and the similarly corrected Phase III map (Figure 260) with the original nozzle configuration. At near design operation 4.0 total-to-total pressure ratio and 100 percent $N/\sqrt{\theta_{cr}}$, the following listing compares the performance from these three maps.

	PHASE V	PHASE III	DESIGN
Pressure Ratio (T-T)	4.0	4.0	4.0
Referred Work, $\frac{\Delta H}{\theta_{cr}}$, $\frac{Btu}{lb}$	32.5	32.2	33.4
Flow Speed Parameter, $\frac{WN\epsilon}{\delta 60}$, $\frac{lb\text{-}rev}{sec^2}$	392	367	392
Efficiency, η	79.9	79.1	80.2

A comparison of Phase V vs Phase III performance shows that efficiency increased by 0.8 point to 79.9 percent and is close to design goal as a result of the nozzle modification. Limit load decreased by 9.1 percent to

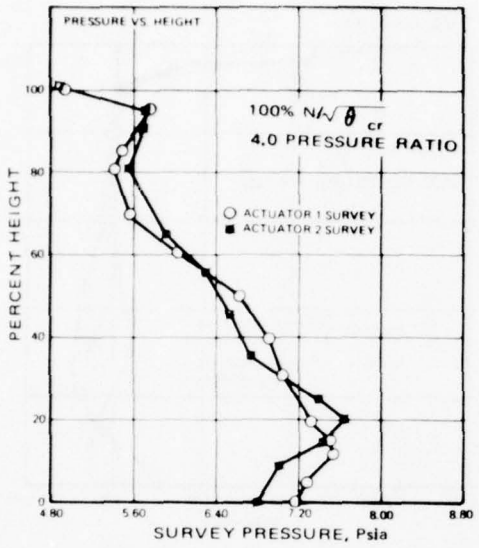


Figure 241. Phase V Test 2: Stage Performance with Pressure Loaded Rotor Turbine Configuration. Rotor Exit Total Pressure Survey.

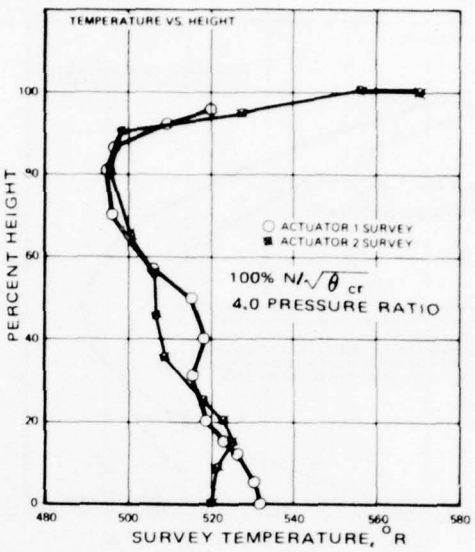


Figure 242. Phase V Test 2: Stage Performance with Pressure Loaded Rotor Turbine Configuration. Rotor Exit Total Temperature Survey.

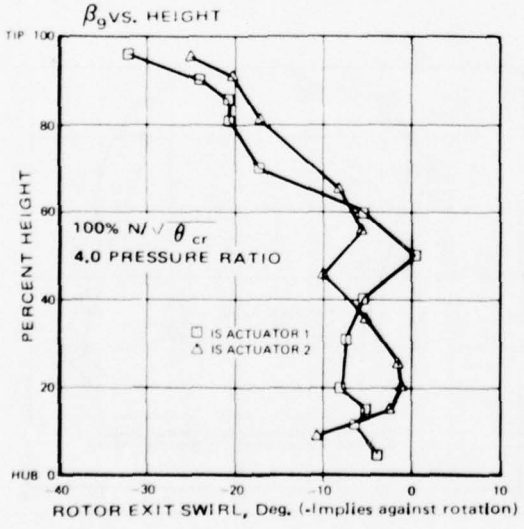


Figure 243. Phase V Test 2: Stage Performance with Pressure Loaded Rotor Turbine Configuration. Rotor Exit Swirl Angle Survey.

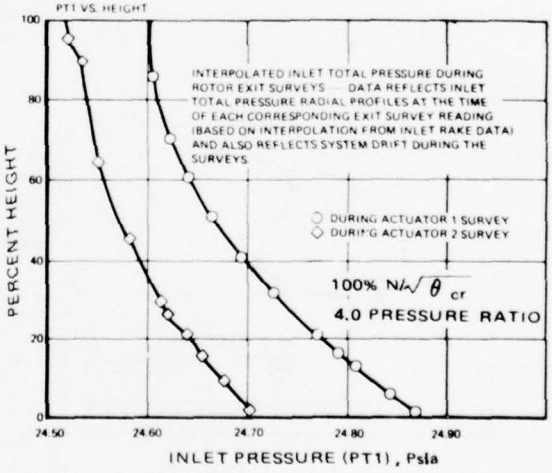


Figure 244. Phase V, Test 2: Stage Performance with Pressure Loaded Rotor Configuration. Stage Inlet Total Pressure Gradient.

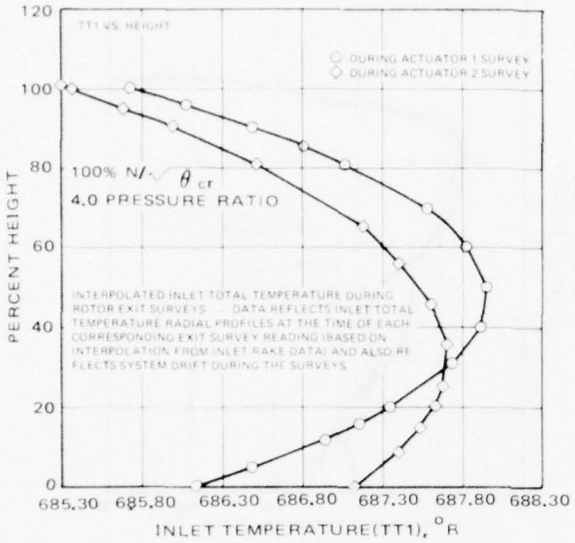


Figure 245. Phase V Test 2: Stage Performance with Pressure Loaded Rotor Turbine Configuration. Stage Inlet Total Temperature Gradient.

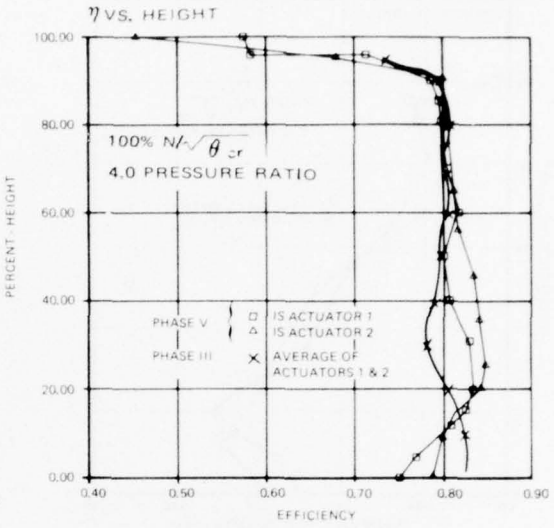


Figure 246. Phase V Test 2: Stage Performance with Pressure Loaded Rotor Turbine Configuration. Radial Efficiency Distribution.

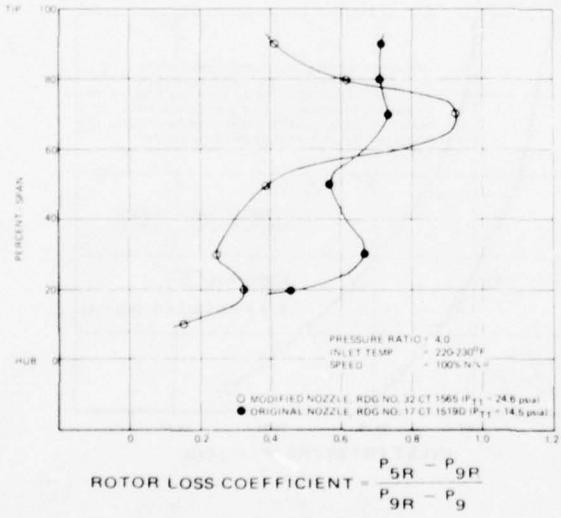


Figure 247. ASATT Phase V Test 2: Rotor Loss Coefficient Distribution.

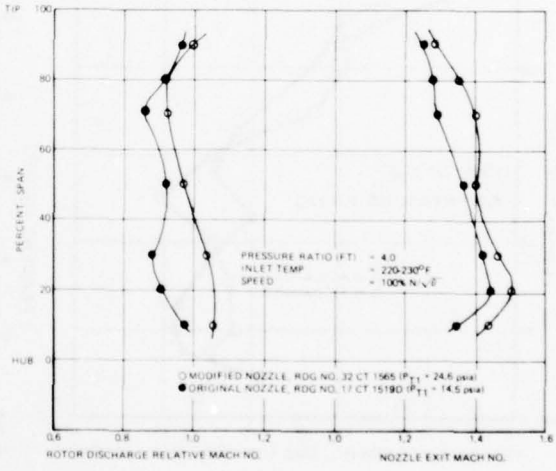


Figure 248. ASATT Phase V Test 2: Nozzle Exit & Rotor Discharge Relative Mach No. Distributions.

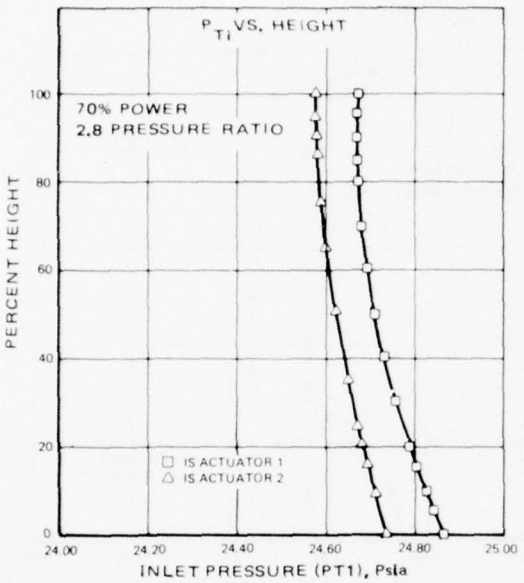


Figure 249. Phase V Test 2: Stage Performance with Pressure Loaded Rotor Configuration.

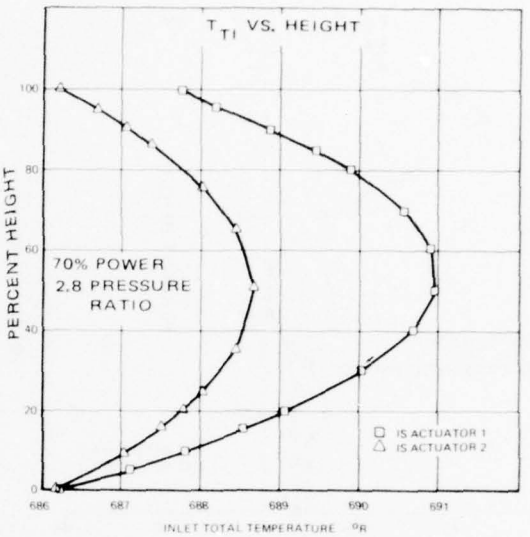


Figure 250. Phase V, Test 2: Stage Performance with Pressure Loaded Rotor Turbine Configuration.

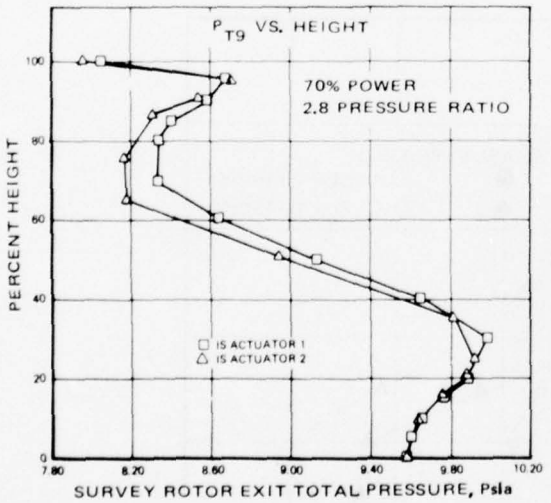


Figure 251. Phase V, Test 2: Stage Performance with Pressure Loaded Rotor Turbine Configuration.

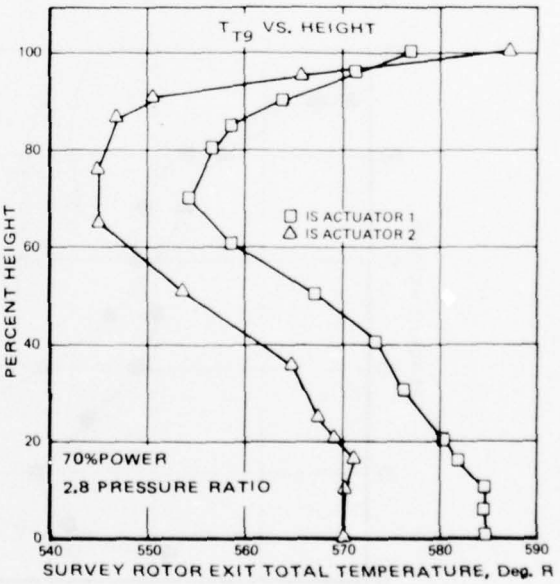


Figure 252. Phase V, Test 2: Stage Performance with Pressure Loaded Rotor Turbine Configuration.

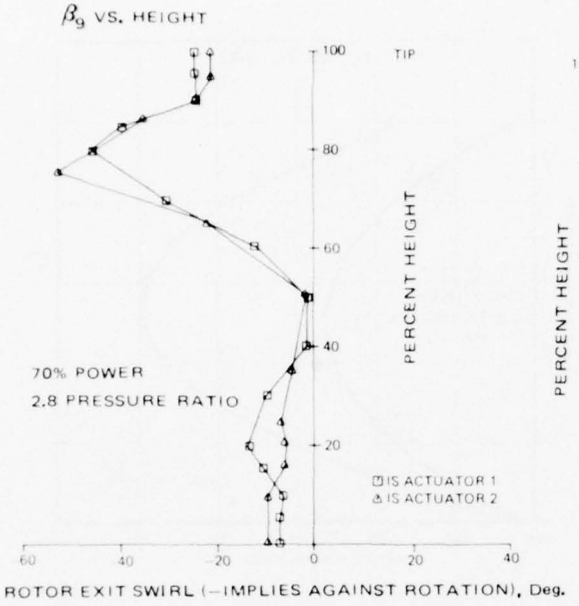


Figure 253. Phase V, Test 2: Stage Performance with Pressure Loaded Rotor Turbine Configuration. Rotor Exit Swirl Survey.

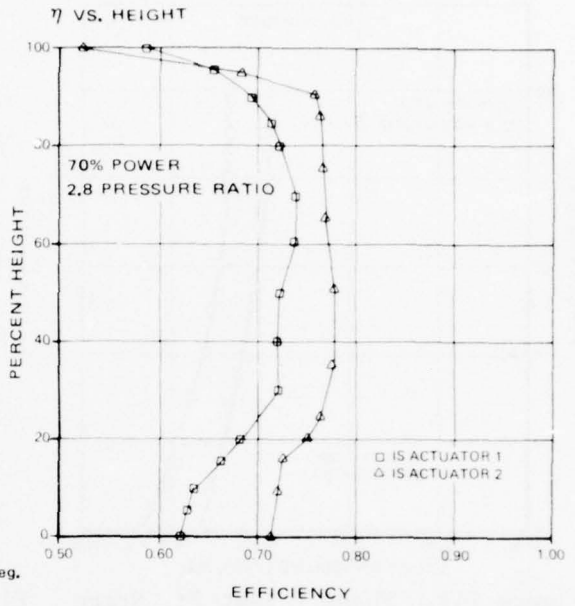


Figure 254. Phase V, Test 2: Stage Performance with Pressure Loaded Rotor Turbine Configuration. Radial Stage Efficiency Distribution.

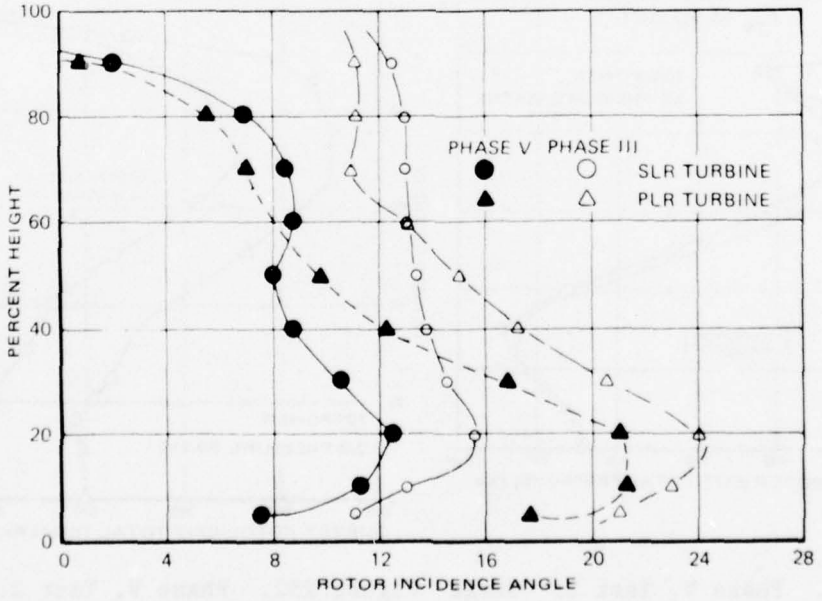


Figure 255. Test 5.0 - Evaluation of Blade Loading. Rotor Incidence Angle Distribution.

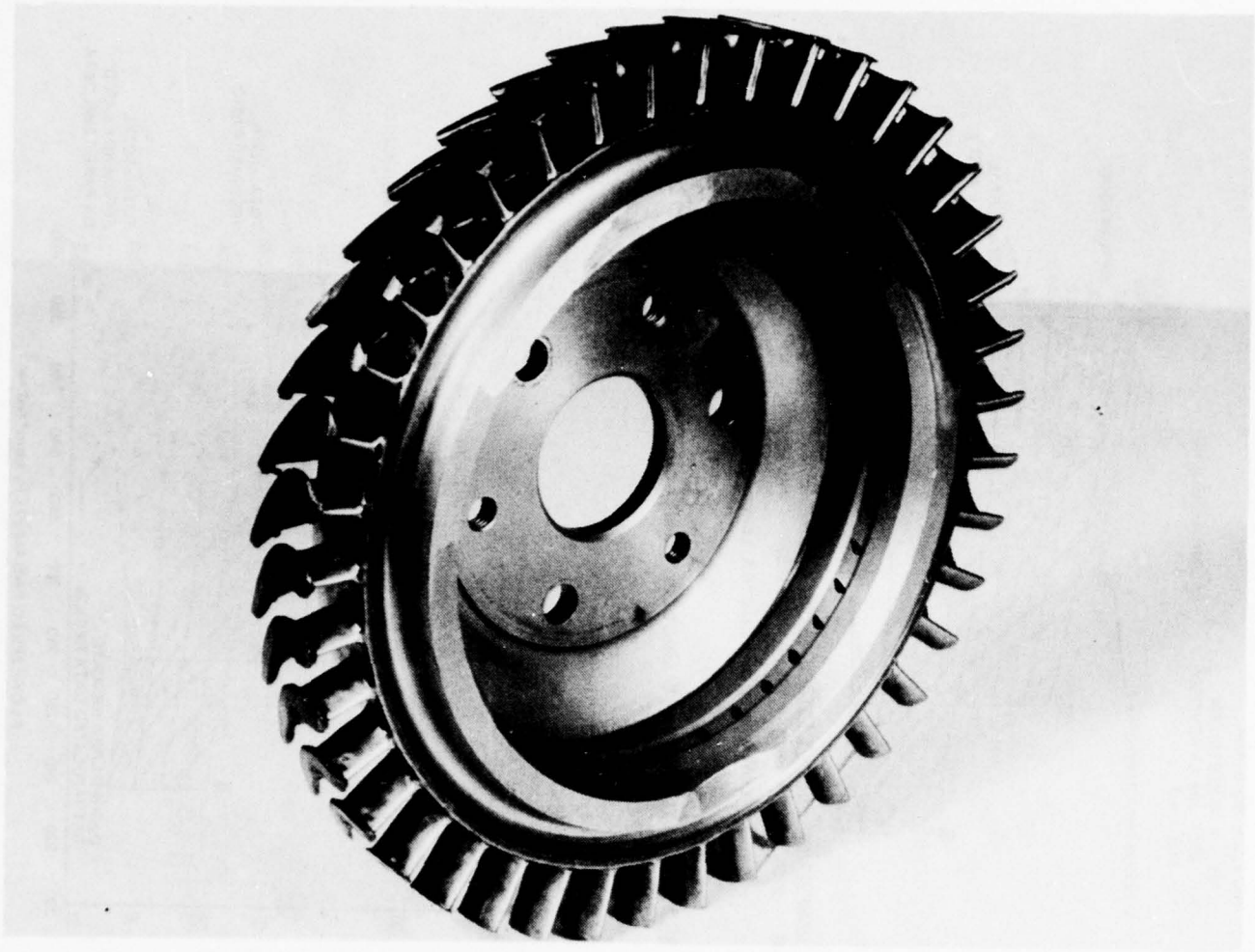


Figure 256. Suction Surface Loaded Rotor After Severe Rub Encountered During Phase III Testing.

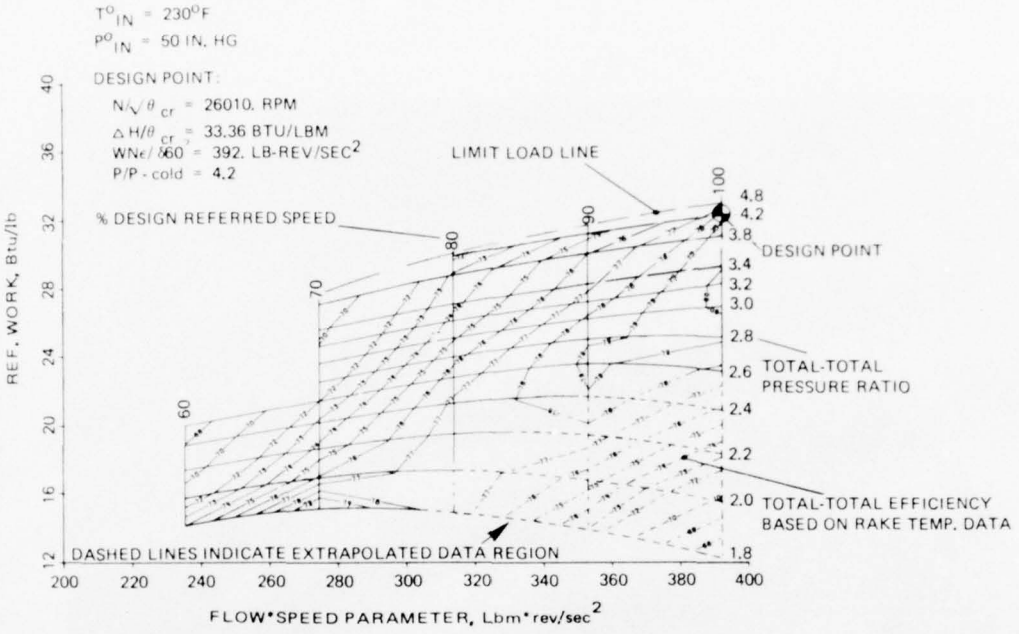


Figure 257. ASATT Phase V Suction Surface Loaded Rotor Configuration Test Map.

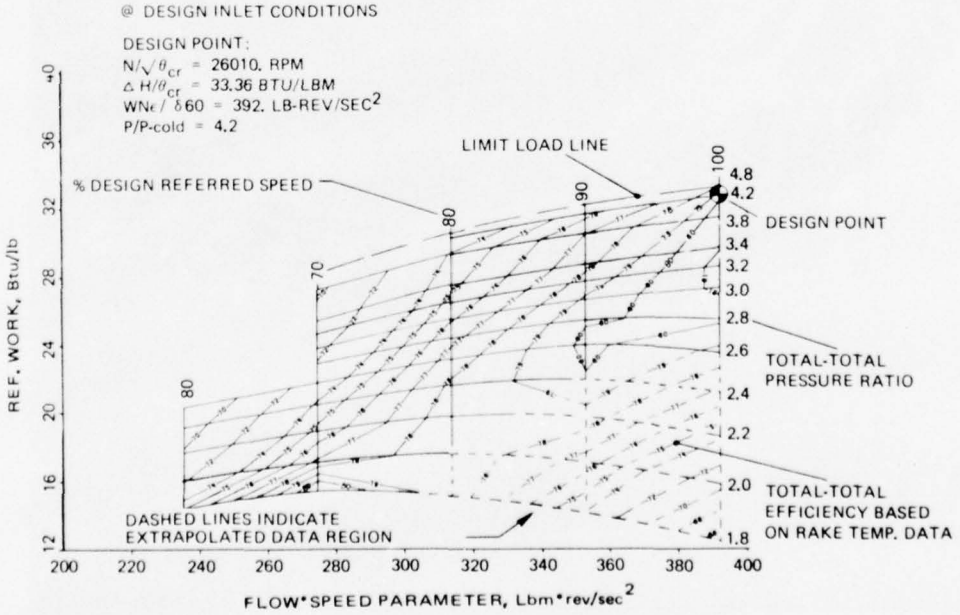


Figure 258. ASATT Phase V Suction Surface Loaded Rotor Configuration Test Map Corrected to Design Reynolds Number.

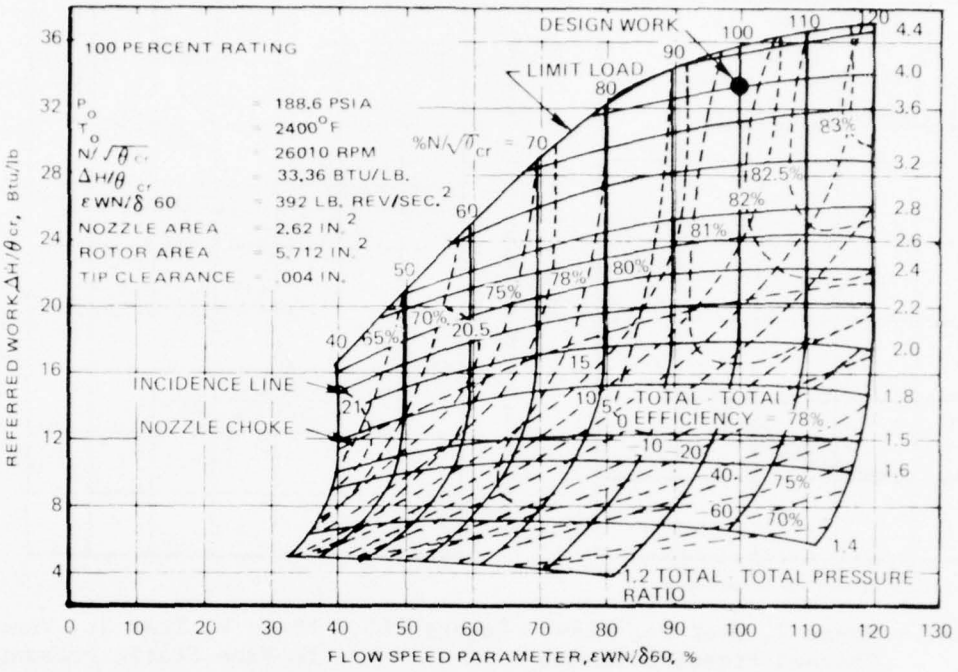


Figure 259. Phase III, Test 3.0 - ASATT Turbine Performance.

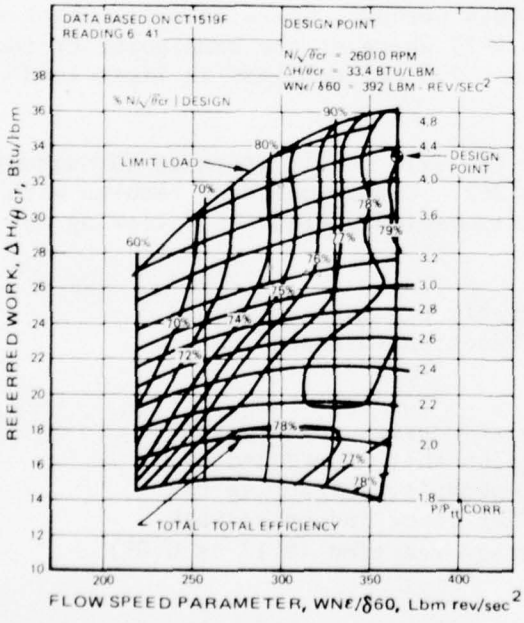


Figure 260. Blade Loading Evaluation. SLR Phase III, Test 3.0, Performance.

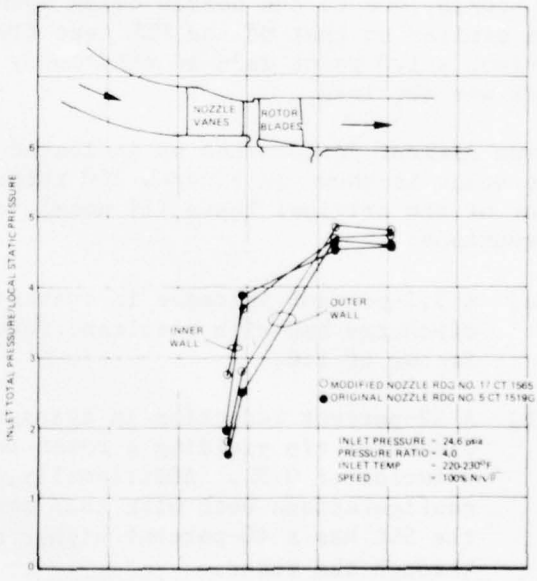


Figure 261. Phase V, Test: Axial Static Pressure Distribution.

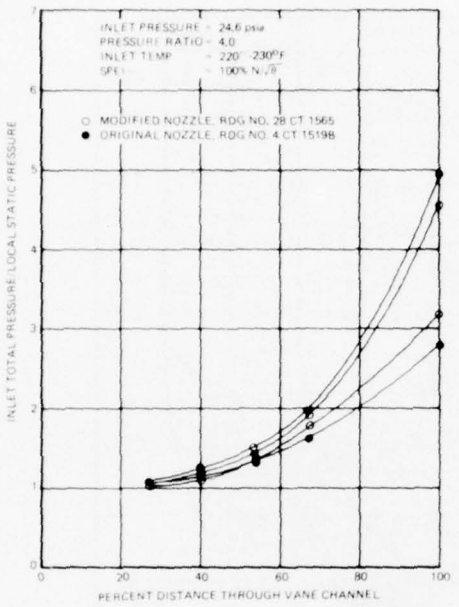


Figure 262. Phase V, Test 3: Mid-Channel Pressure Distribution.

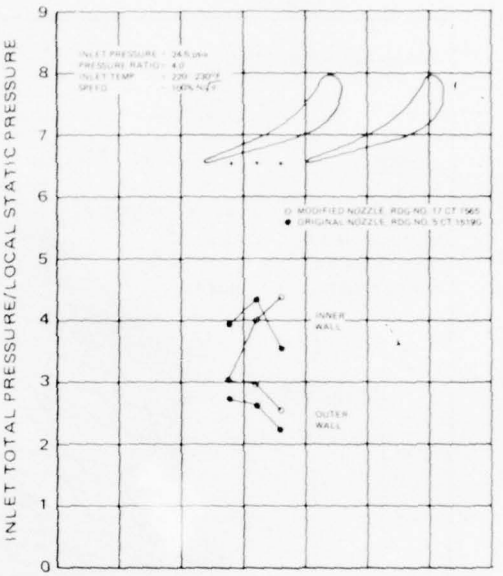


Figure 263. Phase V, Test 3: Vane-to-Vane Static Pressure Distribution at Trailing Edge.

33 Btu/lb, due to the nozzle being opened 6.4 percent. These relative changes are similar to that of the PLR test (Test V-2) where at the same point of comparison a 1.0 point gain in efficiency and a 7.5 percent loss in limit load work was obtained.

Blade element performance as indicated by the wall static pressure throughout the stage is shown in Figures 260 through 262. Comparing these results with that of the original Phase III nozzle configuration yields the following observations:

a) A 5.3-percent increase in average static pressure at nozzle discharge hub with resultant rotor reaction increased by a factor of 1.6.

b) A 12-percent reduction in average static pressure at nozzle discharge tip yielding a rotor reaction that is reduced by a factor of 0.81. Additionally, a comparison of SLR vs PLR configurations both with this modified rotor indicates that the SLR has a 40-percent higher average reaction (0.13 vs 0.09) through the rotor.

c) A reduction of average static pressures at a rotor exit of 4.0 percent yields a higher stage discharge Mach number. This is consistent with the reduced limit load performance as indicated by the map and is in part due to the increased flow through the turbine. Stage exit swirl remained the same on the average.

d) The nominal mid-span/mid-channel velocity distribution, like the PLR data, did not change appreciably (Figure 262). The hub to tip average gradient is reduced. Vane-to-vane static pressure distribution (Figure 263) also shows reduced average hub to tip gradient; however, trailing edge vane-to-vane gradient near the hub increased significantly with additional expansion near the pressure surface and less expansion near the suction surface.

The rotor exit survey data at 4.0 total-to-total pressure ratio and 100 percent $N/\sqrt{\theta_{cr}}$ is shown in Figures 264 through 266 (P_9, T_9, & β_9). Circumferentially averaged total pressure and temperature radial gradients at stage inlet are shown in Figures 267 and 268. This data, combined with the experimental nozzle loss data of Test 1, permits calculations on the radial distribution of adiabatic efficiency (Figure 267), rotor loss coefficient number (Figure 271). The results, compared to the original nozzle SLR configuration (Phase III), are as follows:

a) Adiabatic efficiency has increased and rotor losses have been reduced in the 20 to 60 percent span region. This is the same trend as obtained with the PLR rotor (Phase V, Test 2) and is consistent with a reduction of rotor incidence per Phase IV modeling (Figure 278).

b) Nozzle discharge Mach number did not change significantly on the average. The gradient, however, shows slightly reduced velocities in the 20 to 60 percent span region with a crossover to higher velocities towards the outer wall. Rotor discharge relative Mach number also shows minimal change on the average with the gradient shifting to yield increased velocities in the 20 to 70 percent span.

Survey data taken at a 70-percent power point with 70 percent $N/\sqrt{\theta_{cr}}$ and 2.8 total-to-total pressure ratio is shown in Figures 272 through 277.

Part of this test also included the introduction of coolant air through the nozzle (4 percent of primary flow) and rotor (2 percent of primary flow) at near design point total-to-total stage pressure ratio of 4.0 and 100 percent $N/\sqrt{\theta_{cr}}$. The results of this show a 2.0-point reduction in efficiency and a 2.7-percent reduction of turbine inlet nozzle main flow. This agrees closely to the coolant flow test correlations of the Phase III tests.

PHASE V SUMMARY AND CONCLUSIONS

The Phase V testing consisted of three major tests:

1. Flow calibration and pressure loss survey of modified turbine inlet nozzle.

2. Definition of stage performance with pressure surface loaded rotor and modified nozzle assembly.

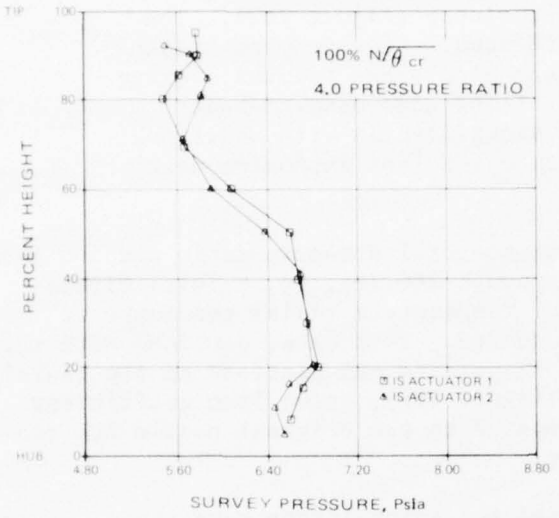


Figure 264. Phase V, Test 3: Stage Performance with Suction Loaded Rotor Turbine Configuration. Rotor Exit Total Pressure Survey.

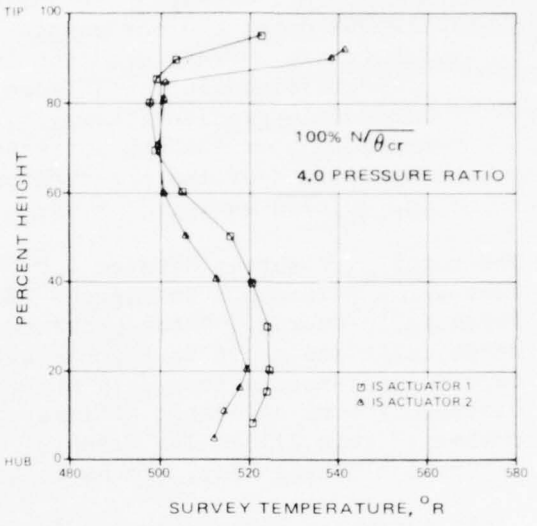


Figure 265. Phase V, Test 3: Stage Performance with Suction Loaded Rotor Turbine Configuration. Rotor Exit Total Temperature Survey.

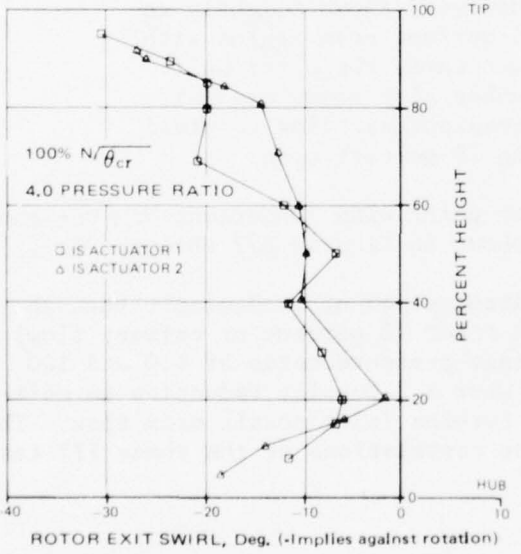


Figure 266. Phase V, Test 3: Stage Performance with Suction Loaded Rotor Turbine Configuration. Rotor Exit Swirl Angle Survey.

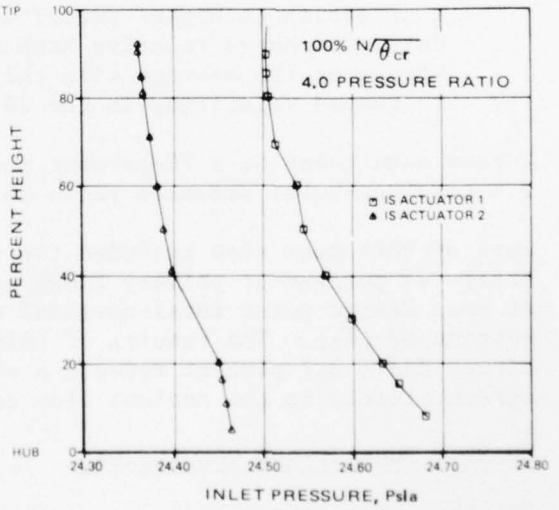


Figure 267. Phase V, Test 3: Stage Performance with Suction Loaded Rotor Configuration. Stage Inlet Total Pressure Gradient.

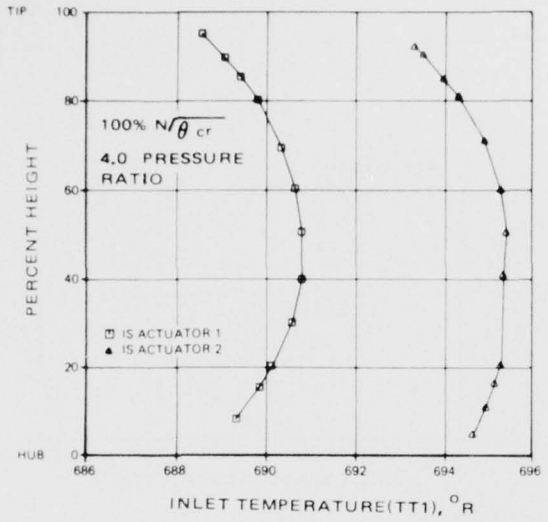


Figure 268. Phase V, Test 3: Stage Performance with Suction Loaded Rotor Turbine Configuration. Stage Inlet Total Temperature Gradient.

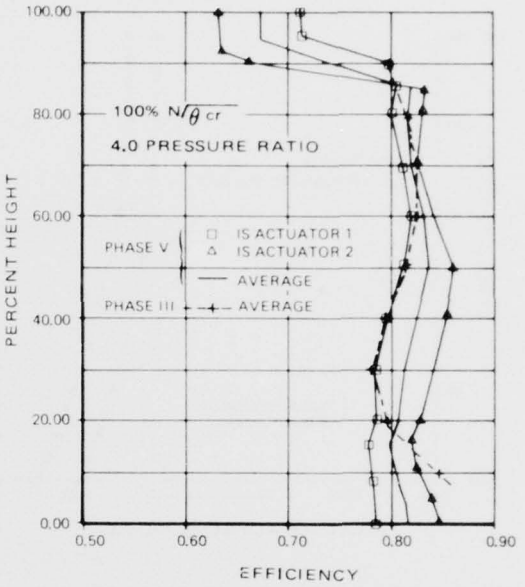


Figure 269. Phase V, Test 3: Stage Performance with Suction Loaded Rotor Turbine Configuration. Radial Efficiency Distribution.

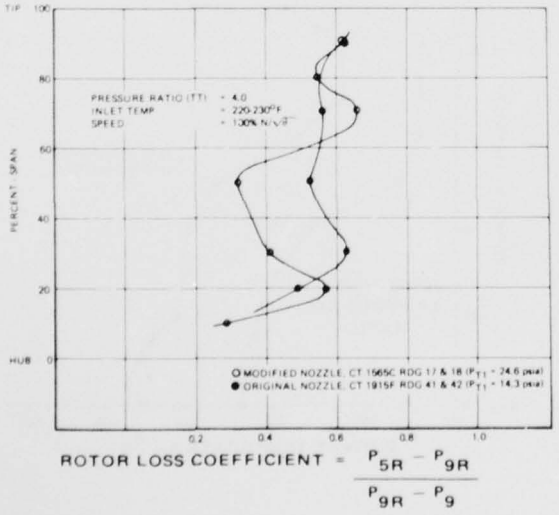


Figure 270. ASATT Phase V, Test 3: Rotor Loss Distribution.

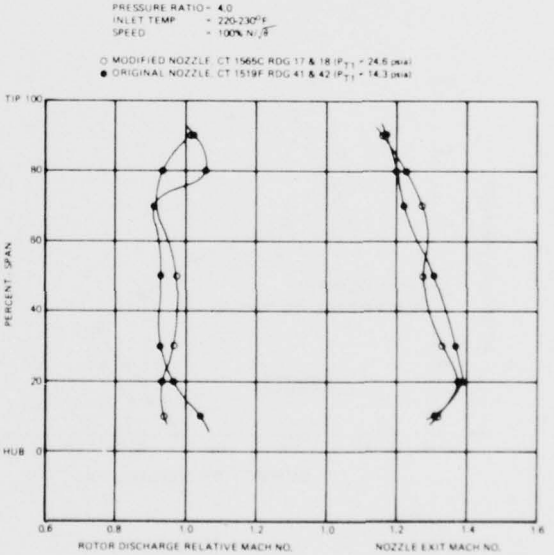


Figure 271. ASATT Phase V, Test 3: Rotor Discharge Relative and Nozzle Exit Mach No. Distribution.

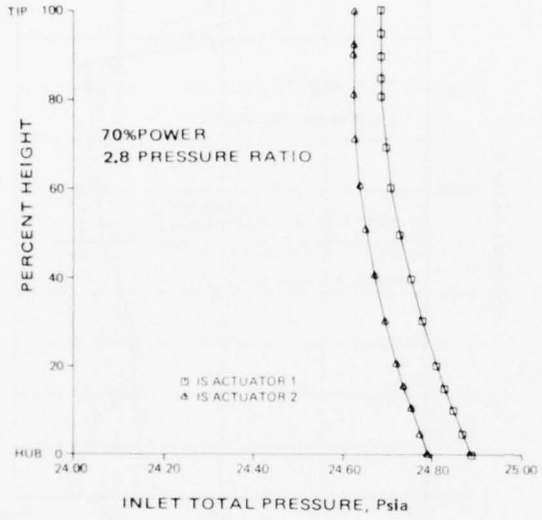


Figure 272. Phase V, Test 3: Stage Performance with Suction Loaded Rotor Configuration.

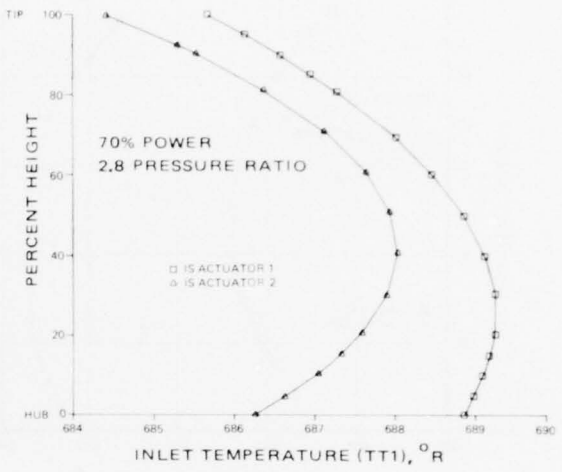


Figure 273. Phase V, Test 3: Stage Performance with Suction Loaded Rotor Turbine Configuration.

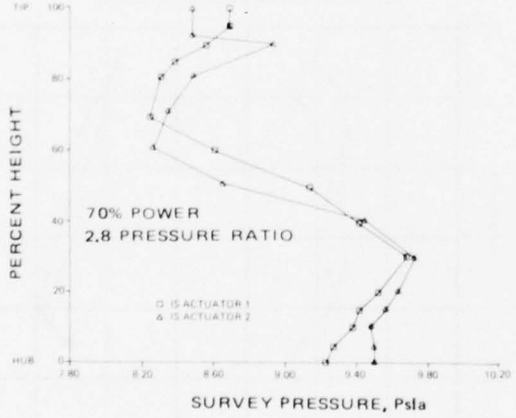


Figure 274. Phase V, Test 3: Stage Performance with Suction Loaded Rotor Turbine Configuration.

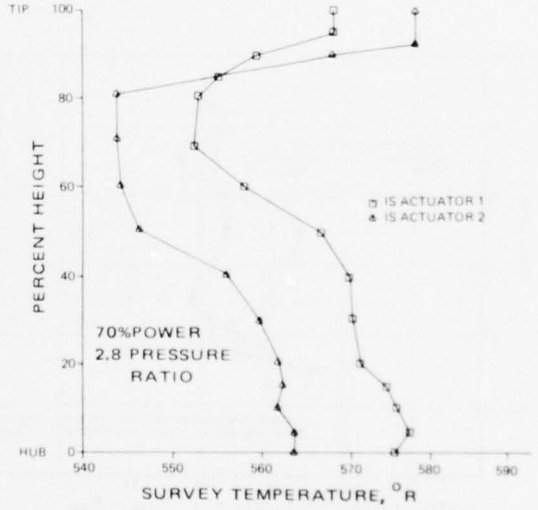


Figure 275. Phase V, Test 3: Stage Performance with Suction Loaded Rotor Turbine Configuration.

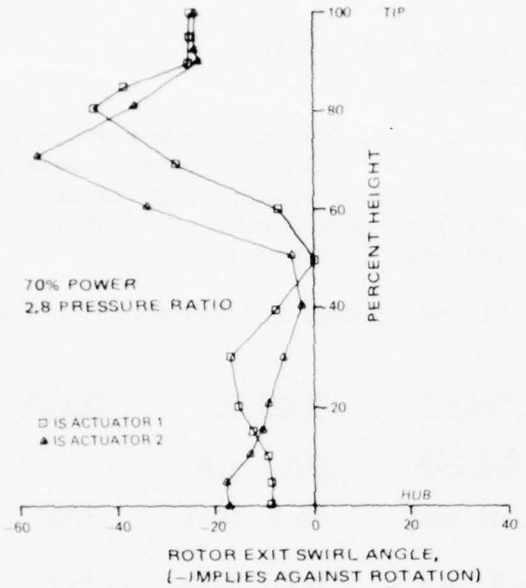


Figure 276. Phase V, Test 3: Stage Performance with Suction Loaded Rotor Turbine Configuration.

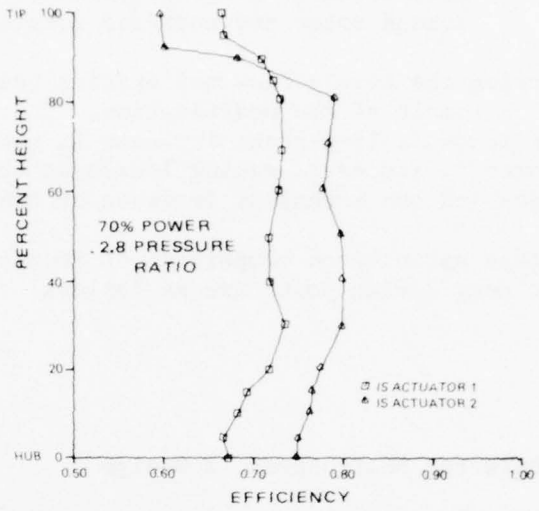


Figure 277. Phase V, Test 3: Stage Performance with Suction Loaded Rotor Turbine Configuration.

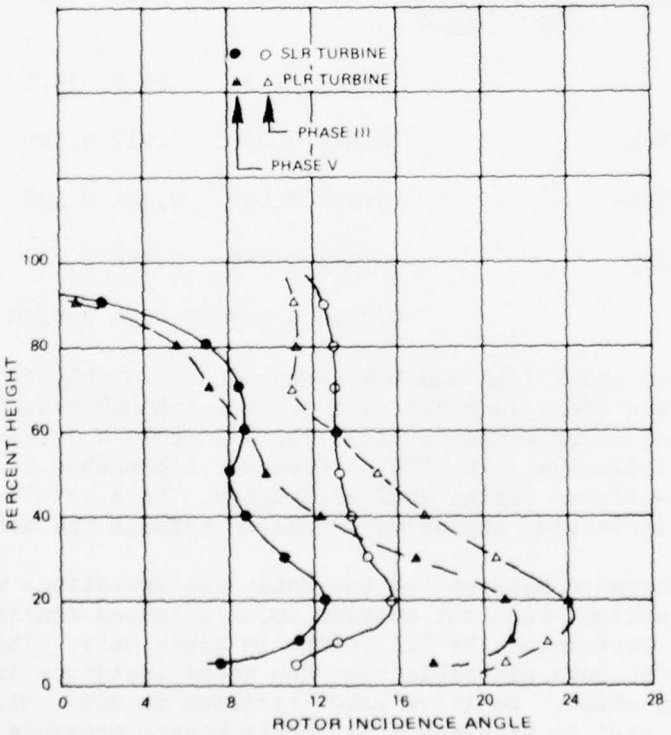


Figure 278. Test 3.0 - Evaluation of Blade Loading. Rotor Incidence Angle Distribution.

3. Definition of stage performance with suction surface loaded rotor and modified nozzle assembly.

During the nozzle flow calibration tests (Test 1), design flow was achieved as a result of the modification. The total pressure loss surveys, however, indicated a 19-percent increase in nozzle loss coefficient. This is attributed to increased mixing losses at the trailing edge due to the stator cutback and the attendant increase of trailing-edge thickness.

Stage performance comparison of Phases III and V tests and design objectives at near design point are as follows:

	PHASE V		PHASE III		DESIGN
	PLR	SLR	PLR	SLR	
Referred Shaft Speed, % Design	100%	100%	100%	100%	100%
Pressure Ratio (Total to Total)	4.0	4.0	4.0	4.0	4.0
Referred Work, $\Delta H/\theta_{cr}$, Btu/lb	31.6	32.5	31.2	32.2	33.4
Flow Speed Parameter, $\frac{WN\epsilon}{\delta 60}$, $\frac{lb\text{-}rev}{sec^2}$	392	392	367	367	392
Efficiency, η	77.8	79.9	76.8	79.1	80.2
Rotor Reaction, Hub	0.044	0.072	0.012	0.046	0.11
Rotor Reaction, Mean	0.094	0.130	0.101	0.139	0.17
Rotor Reaction, Tip	0.145	0.188	0.190	0.233	0.24
Tip Clearance	0.0125	0.0125	0.0126	0.0120	0.011

Both stage configurations (SLR and PLR) responded favorably to the nozzle modification. Rotor blade incidence was reduced and hub reaction through the rotor increased as expected to yield approximately a 1.0-point improvement in stage efficiencies. The SLR performance approached to within 0.3 point of the 80.2-percent design goal efficiency. As a result of the nozzle cutback, air deflection angles were reduced through the nozzle case.

The relative performance between the two rotor configurations was the same as in Phase III testing, with the suction surface loaded configuration yielding superior performance by 2.1 points in efficiency. This is attributed in part to the more favorable near hub rotor incidence and reaction of the SLR configuration. Positive rotor reaction is desirable on highly loaded blading in that it provides a favorable static pressure gradient through the blade to blade passages. Flow inefficiencies, such as boundary layer growth and flow separation characteristic of diffusing flow, are therefore minimized.

CONCLUSIONS AND RECOMMENDATIONS

CONCLUSIONS

An advanced small axial cooled (2400°F) turbine with a referred work, $\frac{\Delta H}{\theta_{cr}}$, of 33.4 Btu/lb (actual work of 180 Btu/lb) has been rig tested to within 0.3 points of a design point efficiency of 80.2 percent. This gas generator turbine, typical of that for 982 HP turboshaft engine, was tested to obtain the effects of meridional nozzle constriction, inlet boundary layer, inlet velocity gradients, turbulence intensity, nozzle and rotor cooling, rotor to nozzle spacing, nozzle and rotor solidity, and Mach number effects. Cascade data were also obtained from a momentum transfer rig that could discern small performance changes accurately and was supplemented by data from external surveys.

Correlations were obtained, and differences between cascade and full stage test data were established. The experimentally evaluated parameters yielded a substantial store of data - some of which followed predictable trends, while other data did not. A simplistic loss system predicted the performance of the final configuration as 80.2 percent as compared to the test value of 79.9 percent. Additional cooling injection losses were found to be readily predictable, based on a simple mixing loss model. New information was generated on performance effects but the tests were conducted on basically one turbine flow path. Some of the trends were peculiar to the ASATT geometry alone and the data acquired was neither general enough nor complete enough to propose a new quantitative loss formulation. Effects such as increased turbulence, Mach number, velocity distortion, loading form, inlet boundary layer, and rotor to nozzle axial spacing were treated as "add on losses" to the base and will require additional testing and correlation to obtain predictable losses. In general these losses were found to have a significant effect on turbine performance.

A procedure combining an analytical turbine model with experimental data obtained from tests on the nozzle cascade was used to modify the nozzle and improve the efficiency of the Phase III turbine stage. Extending this technique to tailor the rotor for the nozzle discharge conditions can be used to extract the maximum uncooled turbine efficiency potential which is estimated to be 84 percent.

RECOMMENDATIONS

CASCADE TESTING

The experience gained from testing the cascade rig has revealed several important considerations concerning the experimental evaluation of turbine airfoil performance. The following recommendations are presented, based on the rig operations and data analysis:

1. Future momentum transfer cascade rigs should be designed in the full-round configuration to eliminate the critical nozzle-slave alignment problem present in the sector configuration.

2. Nozzle exit traverse data revealed significant blade-to-blade pressure and angle gradients in addition to radial gradients. The momentum transfer technique proved to be a successful method for determining average cascade performance without reliance on radial and circumferential averaging methods. It is recommended that additional blade profiles be tested using this technique. Emphasis during the design and test of these vanes should be placed on the evaluation of loading without encountering incidence loss variations.

FULL ROUND COLD FLOW RIG TESTING

During Phase III and Phase V, full round cold flow tests evaluated the performance of the as-designed and modified ASATT turbine stage. The modification improved performance by improving the match and radial distribution of rotor incidence and reaction. However, the full performance potential has not been reached. Additional gains in performance may be obtained by further improving the stator/blade interface. The following items are recommended to evaluate this potential gain:

1. Redesign turbine inlet nozzle with objective of providing optimum vector triangles consistent with Phase III and V experience and low incidence losses throughout the radial span.

2. If necessary, design a new rotor that is optimally matched to the nozzle flow field.

3. Fabricate and test new hardware with performance evaluations that include:

   a. Flow calibration of nozzle with discharge surveys of total pressure loss and flow angle at design point pressure ratio.

   b. Performance test of new nozzle in full stage configuration with both the SLR and the new matched rotor. Data to include mapping and surveys similar to that of Phase V.

FULL ROUND HOT RIG TESTS

Subsequent to the above cold flow rig tests it is recommended that the performance be validated under hot gas generator flow conditions with the best of the above stage configurations. With the hardware adapted to the hot flow path conditions, these tests will provide data as to the:

a. Validity of Reynolds number performance corrections.

b. Integrity of the turbine components under design pressures, temperatures, and mechanical loads.

c. Vane and blade cooling system performance.

d. Nozzle/stage swallowing capacity at design coolant to main flow path momentum ratios.

e. Design point and off-design performance along the simulated gas generator operating line.

LITERATURE CITED

1. Rogo, C. and Due, H., ADVANCED SMALL AXIAL TURBINE TECHNOLOGY PROGRAM, PHASE I INTERIM REPORT, Teledyne CAE Report number 1249, October 1972.

2. Due, H. and Rogo, C., ADVANCED SMALL AXIAL TURBINE TECHNOLOGY PROGRAM, PHASE II TEST REPORT, Teledyne CAE Report number 1329, February 1974.

3. Due, H. and Rogo, C., ADVANCED SMALL AXIAL TURBINE TECHNOLOGY PROGRAM, PHASE III TEST REPORT, Teledyne Report number 1482, November 1975.

4. Benstein, E. H., SMALL FLYING ENGINES ARE DIFFERENT, American Institute of Aeronautics and Astronautics paper number, 74-1185, October 19

5. Stewart, W. L., A STUDY OF AXIAL-FLOW TURBINE EFFICIENCY CHARACTERISTICS IN TERMS OF VELOCITY DIAGRAM PARAMETERS, ASME Paper number 61-WA-37, November 1961.

6. Smith, S. F., A SIMPLE CORRELATION OF TURBINE EFFICIENCY, Journal of the Royal Aeronautical Society, Vol. 69, p. 467-470, July 1965.

7. ANALYSIS OF GEOMETRY AND DESIGN POINT PERFORMANCE OF AXIAL FLOW TURBINES, PART I - DEVELOPMENT OF THE ANALYSIS METHOD AND THE LOSS COEFFICIENT CORRELATION (NREC Report No. 1125-1), Northern Research and Engineering Corporation, Cambridge, Massachusetts, September 14, 1967.

8. ANALYSIS OF GEOMETRY AND DESIGN POINT PERFORMANCE OF AXIAL FLOW TURBINES, PART II - COMPUTER PROGRAM (NREC Report No. 1125-2), Northern Research and Engineering Corporation, Cambridge, Massachusetts, January 31, 1968.

9. Ainley, D. G., AN APPROXIMATE METHOD FOR THE ESTIMATION OF THE DESIGN POINT EFFICIENCY OF AXIAL FLOW TURBINES, Aeronautical Research Council, C. P. 30, (1950).

10. Ainley, D. G. and Mathieson, G. C. R., AN EXAMINATION OF THE FLOW OF PRESSURE LOSSES IN BLADE ROWS OF AXIAL FLOW TURBINES, Aeronautical Research Council, R&M 2891 (1955).

11. Balje, O. E. R. L. Binsley, AXIAL TURBINE PERFORMANCE EVALUATION. Part A - Loss Geometry Relationships, Paper No. 68-GT-13.

12. Balje, O. E. R. L. Binsley, AXIAL TURBINE PERFORMANCE EVALUATION. Part B - Optimization with and without Constraints, Paper No. 68-GT-14.

LITERATURE CITED - Continued

13. Cooke, D. H., A STUDY OF HIGH-MACH-NUMBER, HIGH-TEMPERATURE APPLICATION OF A SMALL, SINGLE-STAGE, AXIAL-FLOW GAS TURBINE (USAAVLABS TR 68-34), U.S. Army Aviation Material Laboratories, Fort Eustis, Virginia, June, 1968, AD 676184.

14. Gabel, R. M. and Tabbey, A. J., ADVANCEMENT OF HIGH-TEMPERATURE TURBINE TECHNOLOGY FOR SMALL GAS TURBINE ENGINES, USAAVLABS - Technical Report Tr-68-65 N 69-32919, Contract DA-44-177-AMC-184(T) 1968.

15. Schlichting, H., Das, A., RECENT RESEARCH ON CASCADE FLOW PROBLEMS, ASME, Paper No. 65-FE-A, July 12, 1965.

16. Rogo, C., EXPERIMENTAL ASPECT RATIO AND TIP CLEARANCE INVESTIGATION ON SMALL TURBINES 1969 SAE Transaction Paper 6800448.

17. Rogo, C., and R. Marshall, EXPERIMENTAL INVESTIGATION OF LOW ASPECT RATIO AND TIP CLEARANCE ON TURBINE PERFORMANCE AND AERODYNAMIC DESIGN, USAAVLABS, Technical Report 67-80, U.S. Army Aviation Materiel Laboratories, Fort Eustis, Virginia, February 1968, AD674201.

18. Dunham, J. and P. M. Came, IMPROVEMENTS TO THE AINLY-MATHIESON METHOD OF TURBINE PERFORMANCE PREDICTION, Paper number 70-GT-2.

19. Burrows, L. INVESTIGATION OF THE DESIGN AND PERFORMANCE OF SMALL AXIAL FLOW TURBINES, AGARD Report on Advanced Components for Turbojet Engines Part 2, 1968, AD 687774.

20. Carter, A. F., and F. K. Lenherr, AN INVESTIGATION OF EFFICIENCY LIMITS FOR SMALL, COOLED TURBINES, USAAVLABS Technical Report 70-14, August 1970.

21. Provenzale, G. E. and S. N. Thirumalaisamy, EXPERIMENTAL INVESTIGATION OF THE EFFECTS OF TRANSPIRATION COOLING ON TURBINE STATOR BLADE AERODYNAMICS, ASME Paper No. 69-GT-39.

22. Moffitt, T. P. and H. W. Prust, Jr., E. M. Szanca, SUMMARY OF COLD-AIR TESTS OF A SINGLE-STAGE TURBINE WITH VARIOUS STATOR COOLING TECHNIQUES, NASA TM X-52968.

23. Hartsel, J. E. PREDICTION OF EFFECTS OF MASS-TRANSFER COOLING ON THE BLADE-ROW EFFICIENCY OF TURBINE AIRFOILS, AIAA Paper No. 72-11, January 17-19, 1972.

24. Anderson, L. R. and W. H. Heiser, SYSTEMATIC EVALUATION OF COOLED TURBINE EFFICIENCY, ASME Paper No. 69-GT-63.

LITURATURE CITED - Continued

25. Barnes, J. F. and P. M. Came, SOME AERODYNAMIC ASPECTS OF TURBINE BLADE COOLING, ASME Paper number 69-GT-15.

26. Dring, R. P., A MOMENTUM-INTEGRAL ANALYSIS OF THE THREE-DIMENSIONAL TURBINE END-WALL BOUNDARY LAYER, United Aircraft Corp., Pratt & Whitney Aircraft Divison, East Hartford, Conn.

27. Turner, J. R., AN INVESTIGATION OF THE END-WALL BOUNDARY LAYER OF A TURBINE-NOZZLE CASCADE, Phillipsburg, N. J.

28. Launder, Brian E., LAMINARIZATION OF THE TURBULENT BOUNDARY LAYER BY ACCELERATION, GAS TURBINE LABORATORY, MIT Report Number 77, November 1964.

29. Horlock, J. H., BOUNDARY LAYER PROBLEMS IN AXIAL TURBOMACHINES, CUED/A - Turbo/TR11.

30. Mellor, G. L. and G. M. Wood, AN AXIAL COMPRESSOR END-WALL BOUNDARY LAYER THEORY, Paper Number 70-GT-80.

31. A NEW METHOD OF PROFILING THE GUIDE CASCADES OF STAGES WITH SMALL RATIOS OF DIAMETER TO LENGTH, Translation No. 3277, 18 July 1963, Associated Electrical Industries (Manchester) Limited.

32. Welna, H., and D. E. Dahlberg and W. H. Heiser, INVESTIGATION OF A HIGHLY LOADED TWO-STAGE FAN-DRIVE TURBINE, AFAPL-TR-69-92, Volume I, December 1969.

33. Welna, H., D. E. Dahlberg and W. H. Heiser, INVESTIGATION OF A HIGHLY LOADED TWO STAGE FAN-DRIVE TURBINE, AFAPL-TR-69-92, Volume III, December 1969.

34. Welna, H., D. E. Dahlberg and W. H. Heiser, INVESTIGATION OF A HIGHLY LOADED TWO-STAGE FAN-DRIVE TURBINE, TCAE-T-71-27, L-3665, Volume II, December 1969.

35. Lueders, H. G., EXPERIMENTAL INVESTIGATION OF ADVANCED CONCEPTS TO INCREASE TURBINE BLADE LOADING. Volume I, Analysis and Design. NASA CR-735, June 1967.

    Lueders, H. G., EXPERIMENTAL INVESTIGATION OF ADVANCED CONCEPTS TO INCREASE TURBINE BLADE LOADING. Volume II, Performance Evaluation of Plain Rotor Blade. NASA CR-1172, August 1968.

Lueders, H. G., EXPERIMENTAL INVESTIGATION OF ADVANCED CONCEPTS TO INCREASE TURBINE BLADE LOADING. Volume III, Performance Evaluation of Tandem Rotor Blade. NASA CR-1254, December 1968.

Lueders, H. G., EXPERIMENTAL INVESTIATION OF ADVANCED CONCEPTS TO INCREASE TURBINE BLADE LOADING. Volume IV, Performance Evaluation of Plain Rotor Blade with Plow Type Vortex Generators. NASA CR-1342, April 1969.

Lueders, H. G., EXPERIMENTAL INVESTIGATION OF ADVANCED CONCEPTS TO INCREASE TURBINE BLADE LOADING. Volume V, Performance Evaluation of Jet-Flap Rotor Blade. NASA CR-1580, May 1970.

36. Bettner, J. L., DESIGN AND EXPERIMENTAL RESULTS FOR A TURBINE WITH JET FLAP STATOR AND JET FLAP ROTOR (NACA CR2244), May 1973.

37. Zysina-Molozien, L. M., I. D. Vannik, M. A. Korotkov, and M. A. Medvedeva, EFFECT OF TURBULENCE AND THE REYNOLDS NUMBER ON FLOW THROUGH BLADE CASCADES, UDC 621.165.533.6.

38. Elsner, J. and J. Porochnicki, INFLUENCE OF FLOW TURBULENCE ON THE EFFICIENCY OF HEAT TURBINE BLADE SYSTEMS, NASA TT F-13, 180, Accession No. N70-37524.

39. Schlicting, H., BOUNDARY LAYER THEORY, Fourth Edition, McGraw-Hill Copyright 1960.

40. Zweifel, O., THE SPACING OF TURBOMACHINE BLADING ESPECIALLY WITH LARGE ANGULAR DEFLECTIONS, The Brown Boveri Review, Vol. 32, 12 November 1945.

41. Deich, Filipov and Lazqev, ATLAS OF PROFILES FOR AXIAL FLOW TURBINES, Mashinostozoenie, Moscow, USSR, 1965.

42. Katsansis, T., FORTRAN PROGRAM FOR CALCULATING TRANSONIC VELOCITIES ON A BLADE-TO-BLADE STREAM SURFACE OF A TURBOMACHINE, NASA Technical Report, TN D-5427, September 1969.

43. McNally, W. D., FORTRAN PROGRAM FOR CALCULATING COMPRESSIBLE LAMINAR AND TURBULENT BOUNDARY LAYERS IN ARBITRARY PRESSURE GRADIENTS, NASA Technical Report ND D-5681, May 1970.

44. Ohlsson, G. O., CASCADE PERFORMANCE FROM TESTS WITH WHEEL OF AXIAL OUTLET, ASME Paper Number 62WA36.

45. Dryden, Hugh L., A REVIEW OF THE STATISTICAL THEORY OF TURBULENCE, Quarterly of Applied Mathematics, Volume 1, Number 1, April 1943, pp. 7-42.

46. Karman, Th. von, SOME REMARKS ON THE STATISTICAL THEORY OF TURBULENCE, Proceedings of the Fifth International Congress of Applied Mechanics, Cambridge, Massachusetts, 1938, p. 347.

47. Cornell, W. G., LOSSES IN FLOW NORMAL TO PLANE SCREENS, Transactions of the ASME, May 1958, p. 791.

48. Baker, H. D., Ryder, E. A. & Baker, N. H., TEMPERATURE MEASUREMENT IN ENGINEERING - Vol. I, Omega Engineering, Inc., Stamford, Conn., 1975.

49. Deich, M. E., and Zaryankin, A. E., "METHOD OF INCREASING THE EFFICIENCY OF TURBINE STAGES WITH SHORT BLADES." Translations No. 2816, Associated Electrical Industries (Manchester) Ltd., T.P./T2816, April 29, 1960.

50. "METHOD OF INCREASING THE EFFICIENCY OF TURBINE STAGES WITH SHORT BLADES." Translation No. 2816, Associated Electrical Industries (Manchester) Ltd., April 29, 1960.

51. "A NEW METHOD OF PROFILING THE GUIDE CASCADES OF STAGES WITH SMALL RATIOS OF DIAMETER TO LENGTH." Translation No. 3277, Associated Electrical Industries (Manchester) Ltd., July 18, 1963.

52. "EFFECT OF THE CONSTRUCTIONAL FACTORS ON THE CHARACTERISTICS OF GAS TURBINE STAGES WITH A LOW RATIO OF MEAN DIAMETER/HEIGHT." Translation No. 3276, Associated Electrical Industries, Ltd., July 19, 1963.

53. Flagg, E. E., "ANALYTICAL PROCEDURE AND COMPUTER PROGRAM FOR DETERMINING THE OFF-DESIGN PERFORMANCE OF AXIAL TURBINES," NASA CR-710, February 1967.

54. Ainley, D. G., and Mathieson, G. G. R., "AN EXAMINATION OF THE FLOW AND PRESSURE LOSSES IN BLADE ROWS OF AXIAL-FLOW TURBINE." R&M No. 1891, March 1951.

55. Anderson, L. R., Heiser, W. H., and Jackson, J. C., "AXISYMETRIC ONE-DIMENSIONAL COMPRESSIBLE FLOW-THEORY AND APPLICATIONS," Journal of Engineering for Power, Transactions of the ASME, ASME Paper No. 70-GT-82, Feb. 1970.

APPENDIX A

COMPUTER OUTPUT FOR CYCLE ANALYSIS OF TURBOSHAFT CONFIGURATIONS

The computer output of each cycle point run from Program 30.038 for the various turboshaft engine configurations is included in this appendix. Each configuration is identified by a code following the example below:

2A 170/2200

2A = 2-Stage Axial Compressor
170 = 170 BTU/lb Turbine Work
2200 = 2200°F Turbine Inlet Temperature

DESIGN POINT CALCULATIONS-REGENERATED TURBOSHAFT ENGINE
SINGLE SPOOL,FREE TURBINE PROGRAM 30.038

DATE9-7-72 NAMEGOHARA SQ65589
USA AMRDL TURBOSHAFT ENGINE DN.
SLS.

INPUT

2A180/2900

	ALT	M	TA	PA	P2/P1	
100	0.0	C.0	0.5187D 03	0.1470D 02	0.1000D 01	
	ETA COMB	LHV	EM	ETA N	HPE	F/A CONT
200	C.9900D 00	C.1840D 05	C.9850D 00	0.9700D 00	0.4400D 02	0.1000D 01
	BO	EC	BHC	BHH	PL	WA
300	C.5000D-02	C.4000D-01	0.0	0.0	0.0	0.4800D 01
	DP/PHC	DP/PC	DP/PIT	DP/PD	DP/PHH	P10/PA
400	0.0	C.3500D-01	C.5000D-02	0.0	0.0	0.1040D 01
	P3/P2	ETA C	ETA T	T5	ETA PT	EHE
500	0.1330D 02	C.7930D 00	0.8450D 00	0.2860D 04	0.8880D 00	0.0
	NPT	N	(ETA-CP)I	(ETA-TP)I	(ETA-PTP)I	
600	0.2500D 05	C.6000D 05	0.0	0.0	0.0	

OUTPUT 3C.038

TA	0.5187D 03	PA	0.1470D 02	N/RTH2	0.6000D 05	N/RTH5C	0.2598D 05
T2	C.5187D 03	P2	0.1470D 02	WRT/D2	0.4800D 01	WN/D605	0.3671D 03
T3	0.1206D 04	P3	0.1955D 03	NPT/T7C	0.1225D 05	DHT/T5C	0.3374D 02
T4	0.1206D 04	P4	0.1955D 03	WN/D607	0.5563D 03	DHT/N2	0.4997D-07
T5	0.2860D 04	P5	0.1385D 03	DHPT/T7	0.3541D 02	DH/N2PT	0.2361D-06
T6	0.2264D 04	P6	0.5425D 02	P3/P2	0.1330D 02	ETA C	0.7930D 00
T7	0.2222D 04	P7	0.5398D 02	P5/P6	0.3477D 01	ETA T	0.8450D 00
T8	0.1710D 04	P8	0.1528D 02	P7/P8	0.3532D 01	ETA PT	0.8880D 00
		P9	0.1528D 02	P10/PA	0.1040D 01	ETA N	0.9700D 00
T10	0.1710D 04	P10	0.1528D 02	DP/PHC	0.0	ETA COM	0.9900D 00
WA	0.4800D 01	P11	0.1527D 02	DP/PC	0.3500D-01		
W3	C.4554D C1	TAL	0.2063D 03	DP/PIT	0.5000D-02		
W5	0.4710D 01			DP/PD	0.0		
W7	C.4902D C1			DP/PHH	0.0		
W10	0.4902D 01			DP/PN	0.1050D-02		
WRT/P8	0.1327D 02	BO	0.5000D-02	EHE	0.0	F/A	0.2755D-01
FN	0.7198D 02	FG	0.7198D 02	AJ	0.6384D 02	XF	0.4546D 03
SHP	0.9521D 03	BSFC	0.4629D C0	ESHP	0.1011D 04	EBSFC	0.4497D 00
ETA-CP	0.8512D C0	ETA-TP	0.8252D 00	ETA-PTP	0.8719D 00		

$\Delta h_T = 180$

DESIGN POINT CALCULATIONS-REGENERATED TURBOSHAFT ENGINE
SINGLE SPOOL,FREE TURBINE PROGRAM 30.038

DATE8-4-72 NAME L COX SQ68702

U.S. AMRDL ADV. TURBINE STUDY
FREE TURBINE TURBOSHAFT SLS 2A 170/2200

INPUT

	ALT	M	TA	PA	P2/P1	
100	0.0	0.0	0.0	0.0	0.0	
	ETA COMB	LHV	EM	ETA N	HPE	F/A CONT
200	0.9900D 00	0.1840D 05	0.9900D 00	0.9700D 00	0.9000D 01	0.0
	BO	BC	BHC	BHH	BL	WA
300	0.5000D-02	0.3000D-01	0.0	0.0	0.0	0.4800D 01
	DP/PHC	DP/PC	DP/PIT	DP/PD	DP/PHH	P10/PA
400	0.0	0.3500D-01	0.5000D-02	0.0	0.0	0.1040D 01
	P3/P2	ETA C	ETA T	T5	ETA PT	EHE
500	0.1200D 02	0.8040D 00	0.8500D 00	0.2660D 04	0.8880D 00	0.0
	NPT	N	(ETA-CP)I	(ETA-TP)I	(ETA-PTP)I	
600	0.2500D 05	0.5823D 05	0.0	0.0	0.0	

OUTPUT 30.038

TA	0.5187D 03	PA	0.1470D 02	N/RTH2	0.5823D 05	N/RTH5C	0.2612D 05
T2	0.5187D 03	P2	0.1470D 02	WRT/D2	0.4800D 01	WN/D605	0.3978D 03
T3	0.1162D 04	P3	0.1764D 03	NPT/T7C	0.1266D 05	DHT/T5C	0.3335D 02
T4	0.1162D 04	P4	0.1764D 03	WN/D607	0.6036D 03	DHT/N2	0.4889D-07
T5	0.2660D 04	P5	0.1702D 03	DHPT/T7	0.3322D 02	DH/N2PT	0.2072D-06
T6	0.2101D 04	P6	0.4986D 02	P3/P2	0.1200D 02	ETA C	0.8040D 00
T7	0.2074D 04	P7	0.4961D 02	P5/P6	0.3413D 01	ETA T	0.8500D 00
T8	0.1618D 04	P8	0.1528D 02	P7/P8	0.3246D 01	ETA PT	0.8880D 00
		P9	0.1528D 02	P10/PA	0.1040D 01	ETA N	0.9700D 00
T10	0.1618D 04	P10	0.1528D 02	DP/PHC	0.0	ETA COM	0.9900D 00
WA	0.4800D 01	P11	0.1527D 02	DP/PC	0.3500D-01		
W3	0.4632D 01	TAU	0.1819D 03	DP/PIT	0.5000D-02		
W5	0.4745D 01			DP/PD	0.0		
W7	0.4829D 01			DP/PHH	0.0		
W10	0.4889D 01			DP/PN	0.1050D-02		
WRT/P8	0.1287D 02	BO	0.5000D-02	EHE	0.0	F/A	0.2443D-01
FN	0.6981D 02	FG	0.6981D 02	AJ	0.6191D 02	WF	0.4074D 03
SHP	0.8660D 03	BSFC	0.4705D 00	ESHP	0.8939D 03	EBSFC	0.4558D 00
ETA-CP	0.8576D 00	ETA-TP	0.8307D 00	ETA-PTP	0.8728D 00		

DESIGN POINT CALCULATIONS-REGENERATED TURBOSHAFT ENGINE
SINGLE SPOOL,FREE TURBINE PROGRAM 30.038

DATE8-4-72 NAME L CCX SQ68702

U.S. AMRDL ADV. TURBINE STUDY
FREE TURBINE TURBOSHAFT SLS 3A 170/2200

INPUT

	ALT	M	TA	PA	P2/P1	
100	0.0	0.0	0.5187D 03	0.1470D 02	0.1000D 01	
	ETA COMB	LHV	EM	ETA N	HPE	F/A CONT
200	0.9900D 00	0.1840D 05	0.9900D 00	0.9700D 00	0.9000D 01	0.0
	B0	BC	BHC	BHH	BL	WA
300	0.5000D-02	0.3000D-01	0.0	0.0	0.0	0.4800D 01
	DP/PHC	DP/PC	DP/PIT	DP/PD	DP/PHH	P10/PA
400	0.0	0.3500D-01	0.5000D-02	0.0	0.0	0.1040D 01
	P3/P2	ETA C	ETA T	T5	ETA PT	EHE
500	0.1280D 02	0.8000D 00	0.8500D 00	0.2660D 04	0.8880D 00	0.0
	NPT	N	(ETA-CP)I	(ETA-TP)I	(ETA-PTP)I	
600	0.2500D 05	0.5800D 05	0.0	0.0	0.0	

OUTPUT 30.038

TA	0.5187D 03	PA	0.1470D 02	N/RTH2	0.5800D 05	N/RTH5C	0.2601D 05
T2	0.5187D 03	P2	0.1470D 02	WRT/D2	0.4800D 01	WN/D605	0.3713D 03
T3	0.1187D 04	P3	0.1881D 03	NPT/T7C	0.1273D 05	DHT/T5C	0.3470D 02
T4	0.1187D 04	P4	0.1881D 03	WN/D607	0.5997D 03	DHT/N2	0.5128D-07
T5	0.2660D 04	P5	0.1815D 03	DHPT/T7	0.3335D 02	DH/N2PT	0.2058D-06
T6	0.2078D 04	P6	0.5017D 02	P3/P2	0.1280D 02	ETA C	0.8000D 00
T7	0.2051D 04	P7	0.4992D 02	P5/P6	0.3618D 01	ETA T	0.8500D 00
T8	0.1597D 04	P8	0.1528D 02	P7/P8	0.3266D 01	ETA PT	0.8880D 00
		P9	0.1528D 02	P10/PA	0.1040D 01	ETA N	0.9700D 00
T10	0.1597D 04	P10	0.1528D 02	DP/PHC	0.0	ETA COM	0.9900D 00
WA	0.4800D 01	P11	0.1527D 02	DP/PC	0.3500D-01		
W3	0.4632D 01	TAU	0.1807D 03	DP/PIT	0.5000D-02		
W5	0.4743D 01			DP/PD	0.0		
W7	0.4887D 01			DP/PHH	0.0		
W10	0.4887D 01			DP/PN	0.1050D-02		
WRT/P8	0.1278D 02	B0	0.5000D-02	EHE	0.0	F/A	0.2405D-01
FN	0.6934D 02	FG	0.6934D 02	AJ	0.6150D 02	WF	0.4010D 03
SHP	0.8603D 03	BSFC	0.4662D 00	ESHP	0.8880D 03	EBSFC	0.4516D 00
ETA-CP	0.8557D 00	ETA-TP	0.8297D 00	ETA-PTP	0.8726D 00		

DESIGN POINT CALCULATIONS-REGENERATED TURBOSHAFT ENGINE
SINGLE SPOOL,FREE TURBINE PROGRAM 30.038

DATE8-4-72 NAME L COX SQ68702

U.S. AMRDL ADV. TURBINE STUDY
FREE TURBINE TURBOSHAFT SLS 2A 200/2500

INPUT

	ALT	M	TA	PA	P2/P1	
100	0.0	0.0	0.5187D 03	0.1470D 02	0.1000D 01	
	ETA COMB	LHV	EM	ETA N	HPE	F/A CONT
200	0.9900D 00	0.18400 05	0.9900D 00	0.9700D 00	0.9000D 01	0.0
	BO	BC	BHC	BHH	BL	WA
300	0.6000D-02	0.4000D-01	0.0	0.0	0.0	0.4800D 01
	DP/PHC	DP/PC	DP/PIT	DP/PD	DP/PHH	P10/PA
400	0.0	0.3000D-01	0.5000D-02	0.0	0.0	0.1040D 01
	P3/P2	ETA C	ETA T	T5	ETA PT	EHE
500	0.1550D 02	0.7890D 00	0.8400D 00	0.2960D 04	0.8880D 00	0.0
	NPT	N	(ETA-CP)I	(ETA-TP)I	(ETA-PTP)I	
600	0.2500D 05	0.6088D 05	0.0	0.0	0.0	

OUTPUT 30.038

TA	0.5187D 03	PA	0.1470D 02	N/RTH2	0.6088D 05	N/RTH5C	0.2592D 05
T2	0.5187D 03	P2	0.1470D 02	WRT/D2	0.4800D 01	WN/D605	0.3180D 03
T3	0.1265D 04	P3	0.2278D 03	NPT/T7C	0.1211D 05	DHT/T5C	0.3545D 02
T4	0.1265D 04	P4	0.2278D 03	WN/D607	0.5147D 03	DHT/N2	0.5275D-07
T5	0.2960D 04	P5	0.2210D 03	DHPT/T7	0.3731D 02	DH/N2PT	0.2545D-06
T6	0.2316D 04	P6	0.5863D 02	P3/P2	0.1550D 02	ETA C	0.7890D 00
T7	0.2275D 04	P7	0.5834D 02	P5/P6	0.3769D 01	ETA T	0.8400D 00
T8	0.1725D 04	P8	0.1528D 02	P7/P8	0.3817D 01	ETA PT	0.8880D 00
		P9	0.1528D 02	P10/PA	0.1040D 01	ETA N	0.9700D 00
T10	0.1725D 04	P10	0.1528D 02	DP/PHC	0.0	ETA COM	0.9900D 00
WA	0.4800D 01	P11	0.1527D 02	DP/PC	0.3000D-01		
W3	0.4579D 01	TAU	0.2233D 03	DP/PIT	0.5000D-02		
W5	0.4710D 01			DP/PD	0.0		
W7	0.4902D 01			DP/PHH	0.0		
W10	0.4902D 01			DP/PN	0.1050D-02		
WRT/P8	0.1332D 02	BO	0.6000D-02	EHE	0.0	F/A	0.2860D-01
FN	0.7229D 02	FG	0.7229D 02	AJ	0.6412D 02	WF	0.4714D 03
SHP	0.1063D 04	BSFC	0.4435D 00	ESHP	0.1092D 04	EBSFC	0.4318D 00
ETA-CP	0.8509D 00	ETA-TP	0.8184D 00	ETA-PTP	0.8709D 00		

DESIGN POINT CALCULATIONS-REGENERATED TURBOSHAFT ENGINE
SINGLE SPOOL,FREE TURBINE PROGRAM 30.038

DATE8-4-72 NAME L COX SQ68702

U.S. AMRDL ADV. TURBINE STUDY
FREE TURBINE TURBOSHAFT SLS 3A 200/2500

INPUT

	ALT	M	TA	PA	P2/P1	
100	0.0	0.0	0.5187D 03	0.1470D 02	0.1000D 01	
	ETA COMB	LHV	EM	ETA N	HPE	F/A CONT
200	0.9900D 00	0.1840D 05	0.9900D 00	0.9700D 00	0.9000D 01	0.0
	BO	BC	BHC	BHH	BL	WA
300	0.6000D-02	0.3000D-01	0.0	0.0	0.0	0.4800D 01
	DP/PHC	DP/PC	DP/PIT	DP/PD	DP/PHH	P10/PA
400	0.0	0.3000D-01	0.5000D-02	0.0	0.0	0.1040D 01
	P3/P2	ETA C	ETA T	T5	ETA PT	EHE
500	0.1500D 02	0.7700D 00	0.8450D 00	0.2960D 04	0.8880D 00	0.0
	NPT	N	(ETA-CP)I	(ETA-TP)I	(ETA-PTP)I	
600	0.2500D 05	0.5470D 05	0.0	0.0	0.0	

OUTPUT 30.038

TA	0.5187D 03	PA	0.1470D 02	N/RTH2	0.5470D 05	N/RTH5C	0.2329D 05
T2	0.5187D 03	P2	0.1470D 02	WRT/D2	0.4800D 01	WN/D605	0.2983D 03
T3	0.1270D 04	P3	0.2204D 03	NPT/T7C	0.1208D 05	DHT/T5C	0.3533D 02
T4	0.1270D 04	P4	0.2204D 03	WN/D607	0.5244D 03	DHT/N2	0.6513D-07
T5	0.2960D 04	P5	0.2138D 03	DHPT/T7	0.3689D 02	DH/N2PT	0.2530D-06
T6	0.2318D 04	P6	0.5755D 02	P3/P2	0.1500D 02	ETA C	0.7700D 00
T7	0.2287D 04	P7	0.5726D 02	P5/P6	0.3715D 01	ETA T	0.8450D 00
T8	0.1742D 04	P8	0.1528D 02	P7/P8	0.3747D 01	ETA PT	0.8880D 00
		P9	0.1528D 02	P10/PA	0.1040D 01	ETA N	0.9700D 00
T10	0.1742D 04	P10	0.1528D 02	DP/PHC	0.0	ETA COM	0.9900D 00
WA	0.4800D 01	P11	0.1527D 02	DP/PC	0.3000D-01		
W3	0.4627D 01	TAL	0.2219D 03	DP/PIT	0.5000D-02		
W5	0.4759D 01			DP/PD	0.0		
W7	0.4903D 01			DP/PHH	0.0		
W10	0.4903D 01			DP/PN	0.1050D-02		
WRT/P8	0.1339D 02	BO	0.6000D-02	EHE	0.0	F/A	0.2852D-01
FN	0.7266D 02	FG	0.7266D 02	AJ	0.6444D 02	WF	0.4750D 03
SHP	0.1056D 04	BSFC	0.4497D 00	ESHP	0.1085D 04	EBSFC	0.4377D 00
ETA-CP	0.8367D 00	ETA-TP	0.8242D 00	ETA-PTP	0.8712D 00		

DESIGN POINT CALCULATIONS-REGENERATED TURBOSHAFT ENGINE
SINGLE SPOOL,FREE TURBINE PROGRAM 30.038

DATE8-4-72 NAME L COX SQ68702

U.S. AMRDL ADV. TURBINE STUDY
FREE TURBINE TURBOSHAFT SLS 2A 170/2500

INPUT

	ALT	M	TA	PA	P2/P1	
100	0.0	0.0	0.5187D 03	0.1470D 02	0.1000D 01	
	ETA COMB	LHV	EM	ETA N	HPE	F/A CONT
200	0.9900D 00	0.1840D 05	0.9900D 00	0.9700D 00	0.9000D 01	0.0
	BO	BC	BHC	BHH	BL	WA
300	0.5000D-02	0.3000D-01	0.0	0.0	0.0	0.4800D 01
	DP/PHC	DP/PC	DP/PIT	DP/PD	DP/PHH	P10/PA
400	0.0	0.3500D-01	0.5000D-02	0.0	0.0	0.1040D 01
	P3/P2	ETA C	ETA T	T5	ETA PT	EHE
500	0.1200D 02	0.8040D 00	0.8400D 00	0.2960D 04	0.8880D 00	0.0
	NPT	N	(ETA-CP)I	(ETA-TP)I	(ETA-PTP)I	
600	0.2500D 05	0.5823D 05	0.0	0.0	0.0	

OUTPUT 30.038

TA	0.5187D 03	PA	0.1470D 02	N/RTH2	0.5823D 05	N/RTH5C	0.2481D 05
T2	0.5187D 03	P2	0.1470D 02	WRT/D2	0.4800D 01	WN/D605	0.4000D 03
T3	0.1162D 04	P3	0.1764D 03	NPT/T7C	0.1184D 05	DHT/T5C	0.3008D 02
T4	0.1162D 04	P4	0.1764D 03	WN/D607	0.5324D 03	DHT/N2	0.4889D-07
T5	0.2960D 04	P5	0.1702D 03	DHPT/T7	0.3669D 02	DH/N2PT	0.2615D-06
T6	0.2417D 04	P6	0.5684D 02	P3/P2	0.1200D 02	ETA C	0.8040D 00
T7	0.2380D 04	P7	0.5655D 02	P5/P6	0.2994D 01	ETA T	0.8400D 00
T8	0.1823D 04	P8	0.1528D 02	P7/P8	0.3700D 01	ETA PT	0.8880D 00
		P9	0.1528D 02	P10/PA	0.1040D 01	ETA N	0.9700D 00
T10	0.1823D 04	P10	0.1528D 02	DP/PHC	0.0	ETA COM	0.9900D 00
WA	0.4800D 01	P11	0.1527D 02	DP/PC	0.3500D-01		
W3	0.4632D 01	TAU	0.2297D 03	DP/PIT	0.5000D-02		
W5	0.4772D 01			DP/PD	0.0		
W7	0.4916D 01			DP/PHH	0.0		
W10	0.4916D 01			DP/PN	0.1050D-02		
WRT/P8	0.1373D 02	BO	0.5000D-02	EHE	0.0	F/A	0.3019D-01
FN	0.7451D 02	FG	0.7451D 02	AJ	0.6609D 02	WF	0.5034D 03
SHP	0.1093D 04	BSFC	0.4605D 00	ESHP	0.1123D 04	EBSFC	0.4483D 00
ETA-CP	0.8576D 00	ETA-TP	0.8225D 00	ETA-PTP	0.8715D 00		

DESIGN POINT CALCULATIONS-REGENERATED TURBOSHAFT ENGINE
SINGLE SPOOL,FREE TURBINE PROGRAM 30.038

DATE8-4-72 NAME L COX SQ68702

U.S. AMRDL ADV. TURBINE STUDY
FREE TURBINE TURBOSHAFT SLS 2A 200/2200

INPUT

	ALT	M	TA	PA	P2/P1	
100	0.0	0.0	0.5187D 03	0.1470D 02	0.1000D 01	
	ETA COMB	LHV	EM	ETA N	HPE	F/A CONT
200	0.9900D 00	0.1840D 05	0.9900D 00	0.9700D 00	0.9000D 01	0.0
	BO	BC	BHC	BHH	BL	WA
300	0.6000D-02	0.3000D-01	0.0	0.0	0.0	0.4800D 01
	DP/PHC	DP/PC	DP/PIT	DP/PD	DP/PHH	P10/PA
400	0.0	0.3000D-01	0.5000D-02	0.0	0.0	0.1040D 01
	P3/P2	ETA C	ETA T	T5	ETA PT	EHE
500	0.1550D 02	0.7890D 00	0.8450D 00	0.2660D 04	0.8880D 00	0.0
	NPT	N	(ETA-CP)I	(ETA-TP)I	(ETA-PTP)I	
600	0.2500D 05	0.6088D 05	0.0	0.0	0.0	

OUTPUT 30.038

TA	0.5187D 03	PA	0.1470D 02	N/RTH2	0.6088D 05	N/RTH5C	0.2730D 05
T2	0.5187D 03	P2	0.1470D 02	WRT/D2	0.4800D 01	WN/D605	0.3195D 03
T3	0.1265D 04	P3	0.2278D 03	NPT/T7C	0.1294D 05	DHT/T5C	0.3889D 02
T4	0.1265D 04	P4	0.2278D 03	WN/D607	0.5990D 03	DHT/N2	0.5220D-07
T5	0.2660D 04	P5	0.2210D 03	DHPT/T7	0.3325D 02	DH/N2PT	0.1984D-06
T6	0.2004D 04	P6	0.5012D 02	P3/P2	0.1550D 02	ETA C	0.7890D 00
T7	0.1982D 04	P7	0.4987D 02	P5/P6	0.4409D 01	ETA T	0.8450D 00
T8	0.1540D 04	P8	0.1528D 02	P7/P8	0.3263D 01	ETA PT	0.8880D 00
		P9	0.1528D 02	P10/PA	0.1040D 01	ETA N	0.9700D 00
T10	0.1540D 04	P10	0.1528D 02	DP/PHC	0.0	ETA COM	0.9900D 00
WA	0.4800D 01	P11	0.1527D 02	DP/PC	0.3000D-01		
W3	0.4627D 01	TAU	0.1741D 03	DP/PIT	0.5000D-02		
W5	0.4733D 01			DP/PD	0.0		
W7	0.4877D 01			DP/PHH	0.0		
W10	0.4877D 01			DP/PN	0.1050D-02		
WRT/P8	0.1252D 02	BO	0.6000D-02	EHE	0.0	F/A	0.2287D-01
FN	0.6795D 02	FG	0.6795D 02	AJ	0.6026D 02	WF	0.3809D 03
SHP	0.8286D 03	BSFC	0.4597D 00	ESHP	0.8558D 03	EBSFC	0.4451D 00
ETA-CP	0.8509D 00	ETA-TP	0.8205D 00	ETA-PTP	0.8725D 00		

APPENDIX B

COMPUTER OUTPUT FOR PRELIMINARY TURBINE DESIGN

The computer output for the preliminary (baseline) turbine design from Program 08.058 is included in this appendix.

```
IEF653I SUBSTITUTION JCL - SYSOUT=(P,,WHIT),DCB=(RECFM=F,LRECL=80,BLKSIZE=80)
XXFT03F001 DD SYSOUT=(&OUTPUT,,&FORM),                                  00000160
IEF653I SUBSTITUTION JCL - SYSOUT=(A,,1PRT),
XX              DCB=(RECFM=FA,LRECL=133,BLKSIZE=133)                    00000170
XXFT04F001  DD  DSN=&&FT04F001,UNIT=SPOOL,DISP=(OLD,DELETE,DELETE),     00000180
XX  DCB=(LRECL=80,RECFM=FB,BLKSIZE=800)                                 00000190
//
IEF236I ALLOC. FOR SEQ70268 EX
IEF237I 230   ALLOCATED TO STEPLIB
IEF237I 234   ALLOCATED TO FT01F001
IEF237I 233   ALLOCATED TO FT02F001
IEF237I 234   ALLOCATED TO FT03F001
IEF237I 233   ALLOCATED TO FT04F001
```

DATE 8-12-72 NAME HANS DUE SQ70268
ENGINE NO 14/1 180 BTU AMRDL
DESIGN NO 2400 DEG F
PART NO

INPUT DATA

SPEED - (RPM)	0.60000000D 05	WORK - BTU/LB.	0.18000000D 03
TEMPERATURE	0.28600000D 04	PRESSURE	0.18860000D 03
AIR COOLING	0.10000000D 01	INCIDENCE -1	0.0
INCIDENCE -5	0.0	A5/A9	0.70000000D 00
NOZZLE CLEARENCE	0.0	ROTOR CLEARENCE	0.11000000D-01
FUEL-AIR RATIO	0.28000000D-01	WEIGHT FLOW	0.48000000D 01
BETA -1	0.0	VELOCITY	-.35000000D 03
NOZZLE LOAD COEFF.	0.75000000D 00	ROTOR LOAD COEFF.	0.10000000D 01
CASCADE AXIAL WIDTH (NOZZ)	0.35000000D 00	CASCADE AXIAL WIDTH (ROT)	0.60000000D 00
THICK-CHORD RATIO (NOZZ)	0.18000000D 00	THICK-CHORD RATIO (ROT)	0.20000000D 00
TRAILING EDGE THICK. (NOZ)	0.30000000D-01	TRAILING EDGE THICK. (ROT)	0.30000000D-01
NO. OF NOZZLE BLADES	0.0	NO OF ROTOR BLADES	0.0
VX9/VCR9	0.50000000D 00	VX1/VCR1	0.15000000D 00
NOZZLE LOAD FACTOR RATIO	0.70000000D 00	ROTOR LOAD FACTOR RATIO	0.12000000D 01
PERCENT TIP SHROUD WIDTH	0.0	TAPER FACTOR	0.70000000D 00
WORK FACTOR	0.0	WORK FACTOR AT HUB	0.50000000D 01

OUTPUT DATA

CRIT VEL RAT 1 =0.14999633D 00	WHEEL SPEED =0.15212681D 04
MEAN RADIUS =0.29054079D 01	EFFICIENCY =0.80161688D 00
NOZ LOSS COEF =0.11993016D 01	ROT LOSS COEF =0.14148079D 01
OPT NO.BLADES N=0.18683637D 02	OPT NO.BLADES R=0.41050447D 02
REYNOLDS NO N =0.80339970D 06	REYNOLDS NO R =0.18830043D 06
STATION 4	
CRIT VEL RATIO =0.12011804D 01	CRIT VEL RAT A =0.46185534D 00
GAS ANGLE =0.67387198D 02	
STATION 5	
OUTER RADIUS =0.31445621D 01	INNER RADIUS =0.25662536D 01
GAS ANGLE =0.69636266D 02	CRIT VEL RATIO =0.11827583D 01
CRIT VEL RAT A =0.41157430D 00	CRIT VEL RAT T =0.11088390D 01
REL GAS ANGLE =0.48309504D 02	REL TOTAL PRESS=0.91456675D 02
REL VEL RATIO =0.66522885D 00	WHEEL SPEED RAT=0.64597124D 00
NOZ PROF LOSS 0=0.37652302D-01	NOZ PROF LOSS 5=0.37652302D-01
NOZ SEC LOSS =0.14118911D 00	NOZ SEC+CL LOSS=0.14118911D 00
NOZ T.E. LOSS =0.19137805D-01	NOZ TOTAL PRESS=0.16939785D 03
STATION 8	
REL VEL RATIO =0.10313406D 01	REL VEL RAT A =0.58479258D 00
REL GAS ANGLE =0.55457178D 02	
STATION 9	
OUTER RADIUS =0.32470568D 01	INNER RADIUS =0.25637589D 01
GAS ANGLE =-.18470949D 02	CRIT VEL RATIO =0.52688530D 00
CRIT VEL RAT A =0.49974248D 00	CRIT VEL RAT T =-.16692984D 00

```
REL GAS ANGLE  =0.60753628D 02      REL TOTAL TEMP =0.24925306D 04
REL VEL RATIO  =0.97476881D 00      WHEEL SPEED RAT=0.72555725D 00
REL TOTAL PRESS=0.76900466D 02      TOTAL PRESS    =0.50144799D 02
REL VEL RAT TAN=0.85051208D 00      LIMIT LOAD     =0.11178182D 01
TOTAL TEMP     =0.22635890D 04      HUB CENT STRESS=0.41112330D 05
ROT PROF LOSS 0=0.77240886D-01      ROT PROF LOSS 5=0.77240886D-01
ROT SEC LOSS   =0.27937136D 00      ROT SEC+CL LOSS=0.33029682D 00
ROT T.E. LOSS  =0.64450168D-01
```

FORCE CALCULATIONS

```
NOZ AXIAL FORCE=0.10546083D 04      ROT AXIAL FORCE=0.28503664D 03
NOZ TAN FORCE  =0.38958054D 03      ROTOR TAN FORCE=0.44179662D 03
```

HUB CALCULATIONS

	STATION 5	STATION 9
GAS ANGLE	0.71163338D 02	-.20732074D 02
CRIT VEL RATIO A	0.41297183D 00	0.49978502D 00
REL GAS ANGLE	0.56189676D 02	0.58927530D 02
REL.TOTAL.TEMPERATURE	0.24558362D 04	0.24578246D 04
REL.VELOCITY RATIO	0.79903472D 00	0.92923846D 00
CRIT VELOCITY RATIO (TAN)	0.12105562D 01	-.18917277D 00
WHEEL SPEED RATIO	0.59390685D 00	0.64023070D 00
TOTAL REL PRESSURE	0.87681905D 02	0.71439139D 02
STATIC PRESSURE	0.60145106D 02	0.42530561D 02
REL VELOCITY RATIO (TAN)		0.79590674D 00
CRIT VELOCITY RATIO	0.12790590D 01	0.53438882D 00
HUB REACTION		0.16383287D 00

TIP CALCULATIONS

	STATION 5	STATION 9
GAS ANGLE	0.68082338D 02	-.16639107D 02
CRIT VEL RATIO A	0.41298713D 00	0.49978544D 00
REL GAS ANGLE	0.38284212D 02	0.62503711D 02
REL.TOTAL.TEMPERATURE	0.25110108D 04	0.25314871D 04
REL.VELOCITY RATIO	0.56059010D 00	0.10235890D 01
CRIT VELOCITY RATIO (TAN)	0.10264226D 01	-.14936400D 00
WHEEL SPEED RATIO	0.70044987D 00	0.81086620D 00
TOTAL REL PRESSURE	0.95929987D 02	0.81123128D 02
STATIC PRESSURE	0.80036368D 02	0.42868587D 02
REL VELOCITY RATIO (TAN)		0.90796507D 00
CRIT VELOCITY RATIO	0.11063913D 01	0.52162735D 00

MECHANICAL DESIGN PARAMETERS

ROTOR ROOT AREA	0.83706053D-01	ROTOR TIP AREA	0.38160926D-01
TOTAL CENTRIFUGAL STRESS	0.35009990D 05	BLADE WEIGHT	0.10015318D-01
DISK WEIGHT	0.46900711D 01	ROOT ANGLE OF IMIN FROM ENGINE CENTERLINE	0.21330379D 02
ROTOR ROOT - IMAX	0.20142839D-02	ROTOR ROOT BENDING STRESS	0.16483756D 04
ROTOR ROOT - IMIN	0.37875187D-03		
ROTOR ROOT TOTAL STRESS	0.36658365D 05		
NOZZ HUB AXIAL WIDTH	0.88722365D 00	NOZZ TIP AXIAL WIDTH	0.83006264D 00
ROTOR HUB AXIAL WIDTH	0.61544118D 00	ROTOR TIP AXIAL WIDTH	0.58750598D 00
BLADE TEMP (TIP)	0.24791847D 04	BLADE TEMP (MEAN)	0.24397881D 04
BLADE TEMP (HUB)	0.24159579D 04	TAPER FACTOR	0.70129202D 00
(PHI-I/PHI-O)ROTOR	0.11929565D 01		

STEWARTS EFFICIENCY

```
TOTAL TO STATIC=0.75859142D 00      TOTAL TO TOTAL =0.84547810D 00

713C = NO LIFE,0.30458332D 03 DEGREES F COOLING REQUIRED FOR 100 HRS. LIFE
SM200= NO LIFE,0.24855477D 03 DEGREES F COOLING REQUIRED FOR 100 HRS. LIFE
```

INPUT - AIR COOLED SECTION

W NOZZLE COOLING-A	=0.0	W ROTOR COOLING-E	=0.13000000D-01
W NOZZLE COOLING-B	=0.40000000D-01	W ROTOR COOLING-F	=0.70000000D-02
W NOZZLE COOLING-C	=0.50000000D-02	W ROTOR COOLING-G	=0.0
W NOZZLE COOLING-D	=0.50000000D-02	W ROTOR COOLING-H	=0.30000000D-01
COOL AIR TEMP-C	=0.12060000D 04	COOL PRESS-B	=0.19550000D 03
DELTA BETA NOZZLE-5	=0.0	DELTA ALPHA ROTOR-9	=0.0

OUTPUT -

ROTOR MEAN COOLANT TEMP	=0.15686423D 04	HUB BLADE TEMP UNCOOLED	=0.22747595D 04
ROTOR TIP COOLANT TEMP	=0.16589435D 04	MEAN BLADE TEMP UNCOOLED	=0.23109081D 04
ROTOR INLET TOTAL TEMP	=0.27621671D 04	TIP BLADE TEMP UNCOOLED	=0.23455162D 04
ROTOR EXIT TOTAL TEMP	=0.21204392D 04	EFFICIENCY	=0.76488379D 00
ROTOR INLET TOTAL PRESS	=0.16299578D 03	EFFICIENCY LOSS	=0.36735082D-01
ROTOR EXIT TOTAL PRESS	=0.46889630D 02		

APPENDIX C

COMPUTER OUTPUT FOR FLOW PATH STREAMLINE ANALYSIS

The streamline analysis for selecting the ASATT, detail, design, turbine flow path was performed using computer Program 08.086. The computer output from those runs is included in this appendix.

MASS-AVERAGE TOTAL PRESSURE= 27158.4 MASS-AVERAGE TOTAL TEMPERATURE= 2860.00
CUMULATIVE TOTAL PRESSURE RATIO= 1.0000

STATOR INLET

LOCATION	RADIUS	MERIDIONAL VELOCITY	AXIAL VELOCITY	ABSOLUTE VELOCITY	VEL REL TO NEXT BLADE	VEL REL TO THIS BLADE	ABSOLUTE MACH NUMBER	MACH NO REL NEXT BLADE	MACH NO REL THIS BLADE	RAD OF CURVTRE	STRMLNE SLOPE ANGLE	AXIAL BLADE LOING	TANGEN BLADE LOING
1	0.2220	390.16	390.14	390.16	390.35	390.16	0.15505	0.15513	0.15505	********	0.0	0.1	0.0
2	0.2270	390.07	390.07	390.07	390.24	390.07	0.15502	0.15508	0.15502	-31.395	-0.1055	0.1	0.0
3	0.2319	389.77	389.77	389.77	389.90	389.77	0.15490	0.15495	0.15490	-10.242	-0.2651	0.1	0.0
4	0.2366	389.22	389.21	389.22	389.30	389.22	0.15468	0.15471	0.15468	-5.107	-0.4132	0.1	0.0
5	0.2413	388.36	388.35	388.33	388.40	388.38	0.15434	0.15436	0.15434	-3.068	-0.6057	0.1	0.0
6	0.2459	387.21	387.17	387.21	387.17	387.21	0.15387	0.15388	0.15387	-2.058	-0.8161	0.1	0.0
7	0.2504	385.68	385.61	385.68	385.60	385.68	0.15326	0.15323	0.15326	-1.488	-1.0354	0.0	0.0
8	0.2549	383.77	383.68	383.77	383.66	383.77	0.15250	0.15246	0.15250	-1.134	-1.2574	-0.0	0.0
9	0.2593	381.48	381.35	381.48	381.36	381.48	0.15159	0.15154	0.15159	-0.895	-1.4797	-0.2	0.0
10	0.2637	378.77	378.60	378.77	378.67	378.77	0.15051	0.15047	0.15051	-0.724	-1.7001	-0.4	0.0
11	0.2680	375.99	375.99	375.99	375.93	375.99	0.14940	0.14938	0.14940	-0.597	0.0	0.1	0.0

LOCATION	STAGN PRESSR	STAGN TEMPTRE	STATIC PRESSRE	STATIC TEMPTRE	STATIC DENSITY	DELTA P OVER Q	DE HALL NUMBER	LOSS COEFF	DIFFUS FACTOR	RELATIVE EXIT ANG	ABSOLUTE FLOW ANG	NEXT-INL-ANGLE ACTUAL
1	27158.40	2860.00	26740.23	2849.96	0.17573	-0.02083	1.01043	0.0	0.0	0.0	0.0	0.0
2	27158.40	2860.00	26740.47	2849.96	0.17573	-0.02033	1.01026	0.0	0.0	0.0	0.0	0.0
3	27158.40	2860.00	26741.13	2849.98	0.17573	-0.01914	1.00987	0.0	0.0	0.0	0.0	0.0
4	27158.40	2860.00	26742.27	2850.00	0.17574	-0.01683	1.00912	0.0	0.0	0.0	0.0	0.0
5	27158.40	2860.00	26744.05	2850.05	0.17574	-0.01314	1.00787	0.0	0.0	0.0	0.0	0.0
6	27158.40	2860.00	26746.95	2850.11	0.17576	-0.00706	1.00602	0.0	0.0	0.0	0.0	0.0
7	27158.40	2860.00	26749.73	2850.18	0.17577	-0.00073	1.00405	0.0	0.0	0.0	0.0	0.0
8	27158.40	2860.00	26753.78	2850.28	0.17579	0.00333	0.99589	0.0	0.0	0.0	0.0	0.0
9	27158.40	2860.00	26758.58	2850.40	0.17582	0.01947	0.99025	0.0	0.0	0.0	0.0	0.0
10	27158.40	2860.00	26764.20	2850.53	0.17585	0.03293	0.98344	0.0	0.0	0.0	0.0	0.0
11	27158.40	2860.00	26769.93	2850.67	0.17588	0.04674	0.97630	0.0	0.0	0.0	0.0	0.0

TOTAL AXIAL FORCE ON BLADES = 0.00 TOTAL TANGENTIAL FORCE ON BLADES = 0.0

STREAMLINE ANALYSIS RUN 1 CONSTANT MEAN LINE, CONSTANT ΔP/P, CONSTANT WORK

BEST AVAILABLE COPY

* * * STATION 8 * * *

MASS-AVERAGE TOTAL PRESSURE= 24459.7 MASS-AVERAGE TOTAL TEMPERATURE= 2960.00
CUMULATIVE TOTAL PRESSURE RATIO= 0.9006

ROTOR INLET

LOCATION	RADIUS	MERIDIONAL VELOCITY	AXIAL VELOCITY	ABSOLUTE VELOCITY	VEL REL TO NEXT BLADE	VEL REL TO THIS BLADE	ABSOLUTE MACH NUMBER	MACH NO REL NEXT BLADE	MACH NO REL THIS BLADE	RAD OF CURVTRE	STRMLNE SLOPE ANGLE	AXIAL BLADE LOING	TANGEN BLADE LOING
1	0.2220	993.96	993.96	3041.51	1782.65	3041.51	1.38010	0.79717	1.38010	-0.206	0.0	-0.4	-1.6
2	0.2268	985.42	985.26	2935.42	1707.04	2935.42	1.32818	0.76946	1.32818	-0.442	-1.0415	-1.5	-1.3
3	0.2313	979.96	979.95	2934.73	1638.65	2934.73	1.29977	0.72590	1.29977	-1.729	-0.2537	-1.0	-1.3
4	0.2357	977.87	977.86	2886.26	1575.79	2886.26	1.27296	0.69502	1.27296	1.530	0.3406	-1.1	-1.7
5	0.2399	976.23	976.13	2840.84	1518.10	2840.84	1.24816	0.66702	1.24816	0.616	0.8219	-1.4	-2.2
6	0.2439	979.01	978.79	2800.38	1466.67	2800.38	1.22631	0.64228	1.22631	0.412	1.2270	-2.1	-2.6
7	0.2473	979.44	979.27	2767.66	1423.13	2767.66	1.20880	0.62158	1.20880	0.320	1.5716	-2.6	-3.0
8	0.2513	980.39	980.37	2735.51	1382.10	2735.51	1.19174	0.60212	1.19174	0.267	1.8837	-3.2	-3.2
9	0.2551	984.48	983.81	2705.27	1345.13	2705.27	1.17581	0.58464	1.17581	0.231	2.1113	-3.7	-3.1
10	0.2586	990.20	989.39	2676.95	1312.32	2676.95	1.16099	0.56914	1.16099	0.205	2.3212	-4.1	-2.7
11	0.2620	997.54	996.60	2650.35	1283.37	2650.35	1.14717	0.55546	1.14717	0.184	2.4991	-4.7	-2.0

LOCATION	STAGN PRESSRE	STAGN TEMPTRE	STATIC PRESSRE	STATIC TEMPTRE	STATIC DENSITY	DELTA P UPON Q	DE HALL NUMBER	LOSS COEFF	DIFFUS FACTOR	RELATIVE EXIT ANG	ABSOLUTE FLOW ANG	NEXT-INL-ANGLE ACTUAL
1	24395.61	2860.00	8412.35	2227.35	0.07077	-0.00071	1.00037	0.0	-0.00026	70.9306	70.9306	56.119
2	24397.12	2860.00	8757.64	2281.79	0.07313	-0.00017	0.99995	0.0	0.00013	70.7346	70.7346	54.732
3	24401.16	2860.00	9143.19	2272.63	0.07538	0.00029	0.99952	0.0	0.00046	70.4006	70.4006	53.254
4	24410.34	2860.00	9481.87	2292.33	0.07753	0.00057	0.99939	0.0	0.00071	70.2015	70.2015	51.616
5	24423.00	2860.00	9805.42	2310.63	0.07951	0.00076	0.99926	0.0	0.00087	69.8651	69.8651	49.842
6	24440.18	2860.00	10096.63	2326.70	0.08132	0.00073	0.99929	0.0	0.00086	69.5466	69.5466	48.118
7	24462.18	2860.00	10340.91	2339.47	0.08282	0.00050	0.99946	0.0	0.00071	69.2870	69.2870	46.518
8	24488.96	2860.00	10592.02	2351.05	0.08431	0.00005	0.99978	0.0	0.00040	69.0024	69.0024	44.819
9	24520.74	2860.00	10814.75	2359.35	0.08574	-0.00060	1.00023	0.0	-0.00006	68.6777	68.6777	43.017
10	24557.55	2860.00	11038.47	2370.99	0.08710	-0.00144	1.00081	0.0	-0.00066	68.3118	68.3118	41.117
11	24598.92	2860.00	11247.20	2383.87	0.08840	-0.00246	1.00151	0.0	-0.00140	67.9142	67.9142	39.139

TOTAL AXIAL FORCE ON BLADES = -0.09 TOTAL TANGENTIAL FORCE ON BLADES = -0.09

BEST AVAILABLE COPY

* * * STATION 7 * * *

MASS-AVERAGE TOTAL PRESSURE= 24459.7 MASS-AVERAGE TOTAL TEMPERATURE= 2860.00
CUMULATIVE TOTAL PRESSURE RATIO= 0.9006

STATOR EXIT

LOCATION	RADIUS	MERIDNAL VELOCITY	AXIAL VELOCITY	ABSOLUTE VELOCITY	VEL REL TO NEXT BLADE	VEL REL TO THIS BLADE	ABSOLUTE MACH NUMBER	MACH NO REL NEXT BLADE	MACH NO REL THIS BLADE	RAD OF CURVTRE	STRMLNE SLOPE ANGLE	AXIAL BLADE LOING	TANGEN BLADE LOING
1	0.2221	989.96	989.96	3040.38	3040.34	3040.38	1.35939	1.35936	1.35939**********		0.0	-23744.5	8589.2
2	0.2263	984.77	984.77	2993.58	2993.69	2993.58	1.33820	1.33826	1.33820	17.467	-0.0417	-23715.1	8776.5
3	0.2314	982.19	982.19	2938.25	2938.37	2938.25	1.30983	1.30995	1.30983	5.830	-0.1081	-23679.6	8991.1
4	0.2357	981.76	981.75	2888.03	2888.30	2888.03	1.27767	1.27802	1.27737	3.008	-0.1527	-23650.1	9011.3
5	0.2391	982.68	982.65	2842.04	2843.23	2842.04	1.24924	1.24940	1.24924	1.674	-0.2042	-23613.5	9173.8
6	0.2439	982.90	982.89	2802.38	2802.63	2802.38	1.22733	1.22747	1.22733	1.304	-0.2698	-23443.4	9222.0
7	0.2477	981.65	981.63	2769.15	2769.39	2769.15	1.20955	1.20967	1.20955	0.980	-0.3551	-23430.0	9304.3
8	0.2515	980.51	980.47	2736.11	2736.30	2736.11	1.19201	1.19210	1.19201	0.776	-0.4658	-23360.5	9379.5
9	0.2551	980.01	979.96	2704.64	2704.73	2704.64	1.17543	1.17548	1.17543	0.630	-0.6068	-23318.9	9449.8
10	0.2586	982.70	982.61	2674.70	2674.74	2674.76	1.15982	1.15980	1.15982	0.539	-0.7809	-23289.0	9517.6
11	0.2620	985.77	985.62	2646.36	2646.15	2646.36	1.14507	1.14495	1.14507	0.464	-0.9892	-23144.1	9622.3

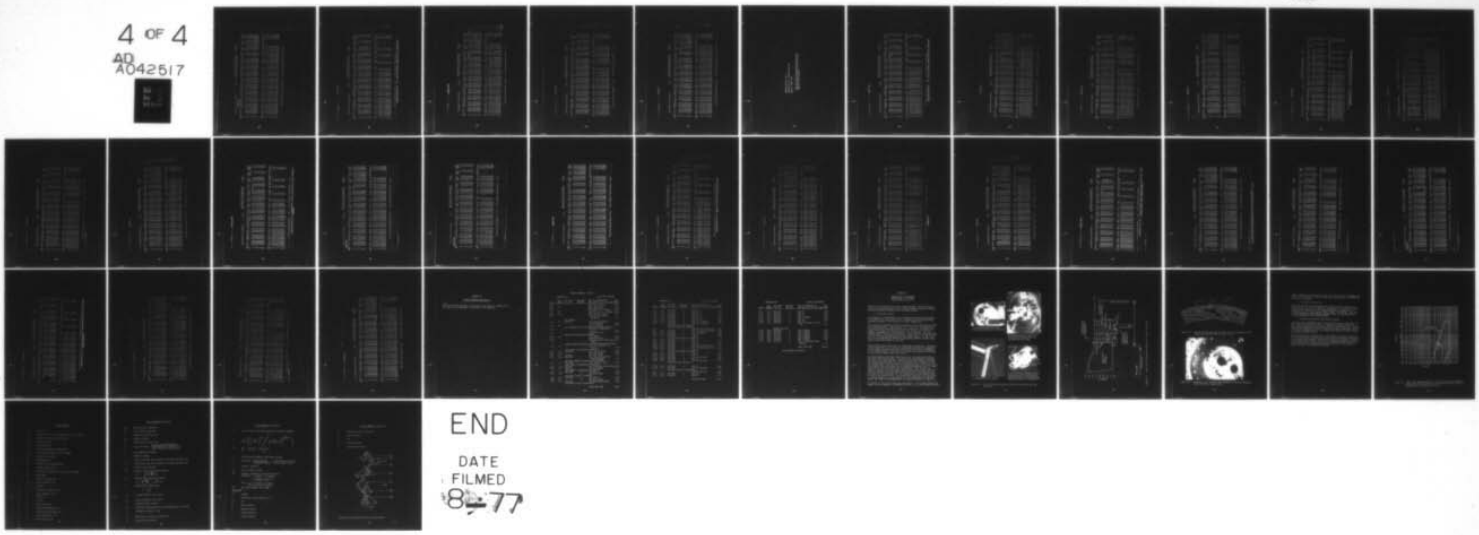
LOCA- TION	STAGN PRESSURE	STAGN TEMPTRE	STATIC PRESSURE	STATIC TEMPTRE	STATIC DENSITY	DELTA P UNCORD	DF FALL NUMBER	LOSS COEFF	DIFFUS FACTOR	RELATIVE EXIT ANG	ABSOLUTE FLOW ANG	NEXT-INL ACTUAL	-ANGLE
1	24495.61	2860.00	9423.71	2228.09	0.07092-43.79822		7.79260	6.60000-11.34126		71.0229	71.0229		71.026
2	24477.19	2860.00	8795.35	2291.46	0.07318-42.93003		7.65593	6.60000-11.11417		70.7460	70.7460		70.746
3	24451.65	2860.00	8132.29	2272.26	0.07539-42.17514		7.53219	6.60000-10.91378		70.4601	70.4601		70.459
4	24431.39	2860.00	7673.30	2281.99	0.07743-41.49143		7.41757	6.60000-10.72743		70.1320	70.1320		70.131
5	24415.23	2860.00	7241.36	2313.04	0.07942-40.90036		7.31998	6.60000-10.55596		69.7032	69.7032		69.702
6	24399.11	2860.00	10850.10	2326.12	0.08124-40.44803		7.23742	6.60000-10.42115		69.4728	69.4728		69.471
7	24382.13	2860.00	10333.92	2339.09	0.08276-40.16594		7.17996	6.60000-10.32420		69.2429	69.2429		69.242
8	24366.99	2860.00	10342.13	2351.81	0.08429-39.95971		7.12950	6.60000-10.23813		69.0063	69.0063		69.006
9	24352.74	2860.00	10322.95	2363.77	0.08577-39.84947		7.08693	6.60000-10.16851		68.7437	68.7437		68.747
10	24341.55	2860.00	11055.84	2374.98	0.08720-39.84133		7.06176	6.60000-10.11601		68.4518	68.4518		68.459
11	24328.42	2860.00	11279.69	2385.52	0.08857-39.86705		7.03835	6.60000-10.07034		68.1381	68.1381		68.150

TOTAL AXIAL FORCE ON BLADES =-1010.11 TOTAL TANGENTIAL FORCE ON BLADES = 393.79

BEST AVAILABLE COPY

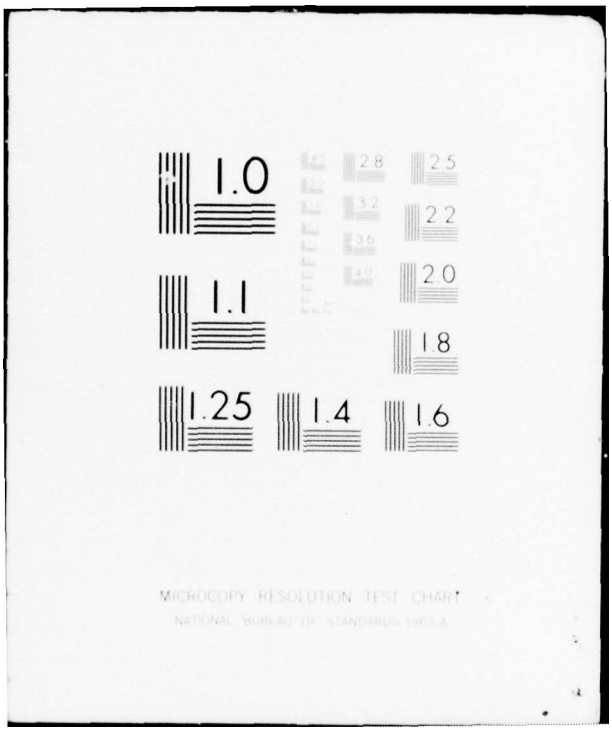
AD-A042 517 TELEDYNE CAE TOLEDO OHIO F/G 21/5
ADVANCED SMALL AXIAL TURBINE TECHNOLOGY.(U)
MAY 77 H F DUE, C ROGO, C L KOSIER DAAJ02-72-C-0117
UNCLASSIFIED TCAE-1508 USAAMRDL-TR-77-1 NL

4 OF 4
AD
A042517



END

DATE
FILMED
8-77


1.0
1.1
1.25
1.4
1.6
2.8
2.5
3.2
2.2
3.6
2.0
4.0
1.8
MICROCOPY RESOLUTION TEST CHART
NATIONAL BUREAU OF STANDARDS 1963-A

MASS-AVERAGE TOTAL PRESSURE= 7526.2 MASS-AVERAGE TOTAL TEMPERATURE= 2263.00
CUMULATIVE TOTAL PRESSURE RATIO= 0.2771

ROTOR EXIT

LOCATION	RADIUS	MERIDNAL VELOCITY	AXIAL VELOCITY	ABSOLUTE VELOCITY	VEL REL TO NEXT BLADE	VEL REL TO THIS BLADE	ABSOLUTE MACH NUMBER	MACH NO REL NEXT BLADE	MACH NO REL THIS BLADE	RAD OF CURVTRE	STRMLNE SLOPE ANGLE	AXIAL BLADE LOING	TANGEN BLADE LOING
1	0.2143	624.07	620.71	673.57	677.69	1727.46	0.30316	0.30276	0.77448	0.455	-5.9501	-3094.5	-5837.6
2	0.2232	779.66	779.49	829.74	827.59	1857.42	0.37156	0.37114	0.83253	0.481	-1.2224	-3644.7	-7312.7
3	0.2306	887.55	887.35	935.77	934.03	1957.62	0.42065	0.41984	0.87993	0.549	1.2269	-4139.9	-8100.4
4	0.2373	969.13	967.90	1017.49	1016.17	2043.14	0.45749	0.45736	0.92125	0.948	2.8906	-4630.7	-8737.5
5	0.2428	1033.14	1030.43	1082.37	1081.64	2117.10	0.48673	0.48837	0.95744	1.564	4.1511	-5110.2	-9257.3
6	0.2481	1084.23	1079.83	1139.74	1133.62	2179.05	0.51281	0.51274	0.98813	3.483	5.1823	-5561.5	-9690.3
7	0.2532	1125.97	1119.64	1173.79	1174.20	2227.46	0.53168	0.53185	1.01254	-166.914	6.0764	-5946.6-10051.4
8	0.2579	1160.95	1152.59	1207.98	1208.85	2272.81	0.54785	0.54824	1.03554	-4.021	6.8847	-6360.1-10377.7
9	0.2624	1190.41	1179.85	1236.99	1238.26	2314.51	0.56161	0.56219	1.05684	-2.204	7.6383	-6775.0-10678.4
10	0.2668	1214.95	1202.05	1261.35	1262.96	2352.91	0.57320	0.57394	1.07664	-1.582	8.3592	-7194.2-10957.4
11	0.2710	1235.62	1220.23	1282.04	1283.93	2388.68	0.58307	0.58395	1.09523	-1.255	9.0538	-7618.2-11211.6

LOCATION	STAGN PRESSRE	STAGN TEMPTRE	STATIC PRESSRE	STATIC TEMPTRE	STATIC DENSITY	DELTA P UPON Q	DE HALL NUMBER	LOSS COEFF	DIFFUS FACTOR	RELATIVE EXIT ANG	ABSOLUTE FLOW ANG	NEXT-INL-ANGLE ACTUAL
1	6844.01	2263.00	6450.13	2231.73	0.05411	-0.47971	0.99300	0.72000	0.00041	-60.9312	-23.2735	-23.279
2	7038.27	2263.00	6647.91	2231.13	0.05443	-0.61811	1.08851	0.72000	-0.15969	-60.1938	-20.0142	-20.107
3	7201.72	2263.00	6807.25	2230.24	0.05462	-0.75784	1.19486	0.72000	-0.30469	-63.0990	-13.4751	-13.550
4	7346.43	2263.00	6418.91	2142.27	0.05482	-0.90951	1.29713	0.72000	-0.44828	-61.7190	-17.7577	-17.829
5	7474.15	2263.00	6412.92	2152.87	0.05501	-1.06793	1.39514	0.72000	-0.58400	-60.8595	-17.3924	-17.456
6	7585.22	2263.00	6409.79	2175.02	0.05518	-1.22589	1.48619	0.72000	-0.71316	-60.2661	-17.0615	-17.123
7	7676.24	2263.00	6408.42	2158.64	0.05534	-1.37152	1.56553	0.72000	-0.82613	-59.7808	-16.4967	-16.559
8	7765.35	2263.00	6410.67	2163.03	0.05550	-1.52368	1.64454	0.72000	-0.94010	-59.4687	-16.1517	-16.211
9	7844.49	2263.00	6414.74	2150.16	0.05566	-1.67601	1.72027	0.72000	-1.05097	-59.2768	-15.9043	-15.972
10	7916.27	2263.00	6420.78	2154.00	0.05581	-1.82477	1.79187	0.72000	-1.15760	-59.1857	-15.7487	-15.816
11	7980.34	2263.00	6427.67	2150.41	0.05596	-1.96878	1.85931	0.72000	-1.25975	-59.1712	-15.6514	-15.726

TOTAL AXIAL FORCE ON BLADES = -254.00 TOTAL TANGENTIAL FORCE ON BLADES = -442.49

BEST AVAILABLE COPY

* * * STATION 6 * * * STATOR INLET

MASS-AVERAGE TOTAL PRESSURE= 27158.4 MASS-AVERAGE TOTAL TEMPERATURE= 2860.00
CUMULATIVE TOTAL PRESSURE RATIO= 1.0000

LOCATION	RADIUS	MERIDNAL VELOCITY	AXIAL VELOCITY	ABSOLUTE VELOCITY	VEL REL TO NEXT BLADE	VEL REL TO THIS BLADE	ABSOLUTE MACH NUMBER	MACH NO REL NEXT BLADE	MACH NO REL THIS BLADE	RAD OF CURVTRE	STRMLNE SLOPE ANGLE	AXIAL BLADE LOING	TANGEN BLADE LOING
1	0.2220	389.17	389.17	389.17	389.19	389.17	0.15465	0.15466	0.15465	*********	0.0	0.0	0.0
2	0.2270	389.20	389.20	389.20	389.22	389.20	0.15467	0.15467	0.15467	23.881	-0.0064	0.0	0.0
3	0.2318	389.19	389.19	389.19	389.20	389.19	0.15466	0.15467	0.15466	-203.083	-0.1148	0.0	0.0
4	0.2366	388.97	388.97	388.97	388.98	388.97	0.15458	0.15458	0.15458	-8.813	-0.2090	0.0	0.0
5	0.2413	388.42	388.41	388.42	388.42	388.42	0.15436	0.15436	0.15436	-3.724	-0.3110	0.0	0.0
6	0.2459	387.47	387.44	387.47	387.47	387.47	0.15398	0.15398	0.15398	-2.189	-0.7593	-0.0	0.0
7	0.2504	386.08	386.02	386.08	386.07	386.08	0.15342	0.15342	0.15342	-1.498	-1.0150	-0.1	0.0
8	0.2549	384.22	384.13	384.22	384.22	384.22	0.15268	0.15268	0.15268	-1.119	-1.2638	-0.2	0.0
9	0.2593	381.91	381.78	381.91	381.90	381.91	0.15176	0.15176	0.15176	-0.882	-1.4988	-0.3	0.0
10	0.2637	379.14	378.97	379.14	379.13	379.14	0.15066	0.15065	0.15066	-0.716	-1.7173	-0.5	0.0
11	0.2680	376.28	376.28	376.28	376.28	376.28	0.14952	0.14952	0.14952	-0.597	0.0	0.0	0.0

LOCATION	STAGN PRESSRE	STAGN TEMPTRE	STATIC PRESSRE	STATIC TEMPTRE	STATIC DENSITY	DELTA P UPON Q	DF HALL NUMBER	LOSS COEFF	DIFFUS FACTOR	RELATIVE EXIT ANG	ABSOLUTE FLOW ANG	NEXT-INL-ANGLE ACTUAL
1	27158.40	2860.00	26742.33	2850.00	0.17574	-0.01554	1.00760	0.0	0.0	0.0	0.0	0.0
2	27158.40	2860.00	26742.26	2850.00	0.17574	-0.01562	1.00794	0.0	0.0	0.0	0.0	0.0
3	27158.40	2860.00	26742.27	2850.00	0.17574	-0.01617	1.00806	0.0	0.0	0.0	0.0	0.0
4	27158.40	2860.00	26742.74	2850.01	0.17574	-0.01450	1.00778	0.0	0.0	0.0	0.0	0.0
5	27158.40	2860.00	26743.90	2850.04	0.17574	-0.01326	1.00670	0.0	0.0	0.0	0.0	0.0
6	27158.40	2860.00	26745.92	2850.09	0.17575	-0.00824	1.00465	0.0	0.0	0.0	0.0	0.0
7	27158.40	2860.00	26748.87	2850.16	0.17577	-0.00291	1.00147	0.0	0.0	0.0	0.0	0.0
8	27158.40	2860.00	26752.77	2850.26	0.17579	0.00577	0.99711	0.0	0.0	0.0	0.0	0.0
9	27158.40	2860.00	26757.60	2850.37	0.17581	0.01687	0.99149	0.0	0.0	0.0	0.0	0.0
10	27158.40	2860.00	26763.37	2850.51	0.17584	0.03049	0.98456	0.0	0.0	0.0	0.0	0.0
11	27158.40	2860.00	26769.27	2850.66	0.17587	0.04476	0.97724	0.0	0.0	0.0	0.0	0.0

TOTAL AXIAL FORCE ON BLADES = -0.00 TOTAL TANGENTIAL FORCE ON BLADES = 0.0

STREAMLINE ANALYSIS RUN 2 CML STATOR LOSS VARIABLE, CONSTANT ROTOR LOSS, CONSTANT WORK

BEST AVAILABLE COPY

* * * STATION 7 * * * **STATOR EXIT**

MASS-AVERAGE TOTAL PRESSURE= 24508.5 MASS-AVERAGE TOTAL TEMPERATURE= 2860.00
CUMULATIVE TOTAL PRESSURE RATIO= 0.9024

LOCA-TION	RADIUS	MERIDNAL VELOCITY	AXIAL VELOCITY	ABSOLUTE VELOCITY	VEL REL TO NEXT BLADE	VEL REL TO THIS BLADE	ABSOLUTE MACH NUMBER	MACH NO REL NEXT BLADE	MACH NO REL THIS BLADE	RAD OF CURVTRE	STRMLNE SLOPE ANGLE	AXIAL BLADE LOING	TANGEN BLADE LOING
1	0.2220	924.36	924.36	3021.36	3021.73	3021.36	1.44832	1.34853	1.34832*********		0.0	-24170.1	8157.0
2	0.2271	952.00	951.99	2973.23	2973.49	2973.23	1.32107	1.32121	1.32107	16.344	0.1931	-23913.7	8442.4
3	0.2317	974.33	974.31	2930.66	2930.78	2930.66	1.20727	1.29733	1.29727	4.121	0.3473	-23639.2	8759.6
4	0.2360	991.01	990.99	2888.93	2889.01	2888.99	1.27424	1.27425	1.27424	2.014	0.4944	-23453.8	9102.3
5	0.2401	1001.64	1001.60	2847.33	2847.29	2847.33	1.25148	1.25145	1.25146	1.261	0.6366	-23305.3	9257.8
6	0.2440	1004.49	1004.45	2810.30	2810.22	2810.30	1.23145	1.23140	1.23145	0.906	0.4961	-23227.6	9368.7
7	0.2477	999.72	999.71	2776.77	2776.71	2776.77	1.21347	1.21344	1.21347	0.747	0.2831	-23261.8	9430.7
8	0.2514	990.52	990.51	2741.46	2741.43	2741.46	1.19471	1.19469	1.19471	0.691	-0.1950	-23312.2	9446.6
9	0.2550	980.57	980.52	2706.49	2706.49	2706.49	1.17628	1.17628	1.17628	0.624	-0.5942	-23330.5	9468.3
10	0.2585	971.32	971.23	2672.36	2672.40	2672.36	1.15844	1.15846	1.15844	0.534	-0.7781	-23346.7	9445.5
11	0.2620	962.55	962.41	2638.95	2639.03	2638.95	1.14112	1.14116	1.14112	0.464	-0.9892	-23382.7	9472.3

LOCA-TION	STAGN PRESSRE	STAGN TEMPTRE	STATIC PRESSRE	STATIC TEMPTRE	STATIC DENSITY	DELTA P UPON Q	DE HALL NUMBER	LOSS COEFF	DIFFUS FACTOR	RELATIVE EXIT ANG	ABSOLUTE FLOW ANG	NEXT-INL-ANGLE ACTUAL
1	23746.13	2860.00	8334.23	2236.89	0.06975-44.24172		7.78370	8.20000-11.32631		72.1905	72.1905	72.171
2	24237.42	2860.00	8831.63	2257.29	0.07324-43.03869		7.63938	7.01839-11.10678		71.3310	71.3310	71.322
3	24458.54	2860.00	9205.62	2275.02	0.07575-42.14186		7.53912	6.43751-10.91394		70.5873	70.5873	70.586
4	24628.36	2860.00	9561.39	2292.00	0.07809-41.33413		7.42724	6.00440-10.73577		69.9441	69.9441	69.962
5	24804.22	2860.00	9882.42	2308.87	0.08014-40.67557		7.33048	5.93522-10.58623		69.4094	69.4094	69.416
6	24727.93	2860.00	10161.03	2323.57	0.08187-40.20681		7.25289	5.88750-10.43423		69.0033	69.0033	69.070
7	24704.02	2860.00	10391.24	2336.68	0.08325-39.94132		7.19227	5.99424-10.33422		68.7032	68.7032	68.809
8	24630.84	2860.00	10601.89	2350.30	0.08445-39.81535		7.13503	6.30523-10.24184		68.8245	68.8245	68.828
9	24523.19	2860.00	10820.54	2363.59	0.08571-39.76239		7.08664	6.57508-10.16390		68.7643	68.7243	68.765
10	24453.52	2860.00	11036.28	2376.38	0.08695-39.81150		7.04847	6.84741-10.10160		68.6935	68.6935	68.693
11	24355.67	2860.00	11233.84	2388.73	0.08805-39.92221		7.01320	7.20060-10.04408		68.6158	68.6158	68.614

TOTAL AXIAL FORCE ON BLADES =-1008.73 TOTAL TANGENTIAL FORCE ON BLADES = 394.18

BEST AVAILABLE COPY

• • STATION 3 • • • ROTOR INLET

MASS-AVERAGE TOTAL PRESSURE= 24508.5 MASS-AVERAGE TOTAL TEMPERATURE= 2860.00
CUMULATIVE TOTAL PRESSURE RATIO= 0.9024

A-N	RADIUS	MERIDNAL VELOCITY	AXIAL VELOCITY	ABSOLUTE VELOCITY	VEL REL TO NEXT BLADE	VEL REL TO THIS BLADE	ABSOLUTE MACH NUMBER	MACH NO REL NEXT BLADE	MACH NO REL THIS BLADE	RAD OF CURVTRE	STRMLNE SLOPE ANGLE	AXIAL BLADE LOING	TANGEN BLADE LOING
	0.2220	912.63	912.63	3017.62	1740.82	3017.62	1.34621	0.77663	1.34621	-0.206	0.0	-0.1	-0.5
	0.2271	935.15	935.08	2967.04	1674.04	2967.04	1.31761	0.74383	1.31761	-0.508	-0.6372	-1.3	-2.8
	0.2319	954.69	954.68	2922.62	1617.99	2922.62	1.29283	0.71573	1.29283	-1.056	0.2040	-1.1	-6.4
	0.2362	971.06	970.94	2879.95	1566.24	2879.95	1.26931	0.69087	1.26931	2.323	0.8723	-1.2	-9.5
	0.2403	984.29	983.99	2838.49	1515.69	2838.49	1.24670	0.66571	1.24670	0.833	1.4136	2.0	-11.2
	0.2443	997.54	997.32	2813.24	1481.99	2813.24	1.23305	0.64956	1.23305	0.921	1.3607	-61.2	22.0
	0.2483	1013.39	1012.70	2756.63	1429.09	2756.63	1.20383	0.62363	1.20333	0.376	2.1046	225.4	-101.1
	0.2515	1013.89	1013.21	2701.19	1371.17	2701.19	1.17351	0.59569	1.17351	0.281	2.0967	541.2	-222.0
	0.2550	994.84	994.15	2716.57	1358.66	2716.57	1.18159	0.59095	1.18159	0.230	2.1329	-63.9	22.0
	0.2595	978.21	977.41	2674.58	1305.64	2674.58	1.15961	0.56608	1.15961	0.203	2.3182	-3.7	-1.3
	0.2620	970.46	969.53	2641.70	1264.61	2641.70	1.14256	0.54695	1.14256	0.184	2.4991	-3.6	-0.6

A-N	STAGN PRESSRE	STAGN TEMPTRE	STATIC PRESSRE	STATIC TEMPTRE	STATIC DENSITY	DELTA P UPON Q	DE HALL NUMBER	LOSS COEFF	DIFFUS FACTOR	RELATIVE EXIT ANG	ABSOLUTE FLOW ANG	NEXT-INL ANGLE ACTUAL
	23746.18	2860.00	8257.59	2230.41	0.06990	0.00151	0.99876	0.0	0.00127	72.4015	72.4015	58.344
	24237.42	2860.00	8872.53	2259.31	0.07350	0.00265	0.99792	0.0	0.00227	71.6349	71.6349	56.837
	24455.54	2860.00	9260.07	2278.26	0.07568	0.00357	0.99726	0.0	0.00309	70.7896	70.7896	55.329
	24628.34	2860.00	9623.72	2295.63	0.07768	0.00413	0.99687	0.0	0.00364	70.3023	70.3023	51.768
	24693.22	2860.00	9845.30	2312.33	0.08052	0.00416	0.99699	0.0	0.00375	69.7213	69.7213	49.521
	24729.93	2860.00	10138.68	2322.34	0.08174	-0.00153	1.00105	0.0	-0.00229	69.2403	69.2403	47.710
	24704.02	2860.00	10520.85	2343.63	0.08405	0.00905	0.99347	0.0	0.01205	68.4660	68.4660	44.023
	24600.54	2860.00	10891.99	2365.53	0.08621	0.02070	0.98531	0.0	0.02653	67.9724	67.9724	42.365
	24523.19	2860.00	10746.49	2359.71	0.08527	-0.00540	1.00373	0.0	-0.00692	68.5363	68.5363	42.472
	24453.52	2860.00	11019.01	2375.49	0.08685	-0.00129	1.00083	0.0	-0.00076	68.5675	68.5675	41.523
	24356.67	2860.00	11212.75	2387.66	0.08793	-0.00161	1.00104	0.0	-0.00101	68.4707	68.4707	39.926

TOTAL AXIAL FORCE ON BLADES = 2.16 TOTAL TANGENTIAL FORCE ON BLADES = -1.13

BEST AVAILABLE COPY

* * * STATION 9 * * * ROTOR EXIT

MASS-AVERAGE TOTAL PRESSURE= 7558.8 MASS-AVERAGE TOTAL TEMPERATURE= 2263.00
CUMULATIVE TOTAL PRESSURE RATIO= 0.2783

LOCATION	RADIUS	MERIDNAL VELOCITY	AXIAL VELOCITY	ABSOLUTE VELOCITY	VEL REL TO NEXT BLADE	VEL REL TO THIS BLADE	ABSOLUTE MACH NUMBER	MACH NO REL NEXT BLADE	MACH NO REL THIS BLADE	RAD OF CURVTRE	STRMLNE SLOPE ANGLE	AXIAL BLADE LOING	TANGEN. BLADE LOING
1	0.2140	508.45	505.72	574.37	574.07	1690.84	0.25835	0.25599	0.75649	0.455	-5.9501	-2880.3	-4773.1
2	0.2240	776.06	776.06	826.45	826.23	1541.10	0.37047	0.37037	0.83404	0.423	-0.1401	-3632.5	-7297.6
3	0.2313	917.03	916.53	963.99	964.05	1975.90	0.43371	0.43374	0.88912	0.577	1.8360	-4179.6	-8262.9
4	0.2375	1008.28	1006.65	1055.11	1055.35	2065.47	0.47603	0.47614	0.93269	0.709	3.2559	-4707.0	-9994.7
5	0.2430	1070.32	1067.26	1118.53	1118.87	2136.68	0.50569	0.50585	0.96856	1.177	4.3333	-5190.0	-9544.3
6	0.2482	1113.40	1109.72	1158.16	1158.58	2193.32	0.52433	0.52453	0.99102	1.998	5.2939	-5601.8	-9957.2
7	0.2531	1143.81	1137.37	1198.21	1198.66	2258.07	0.54324	0.54346	1.02736	6.418	6.0336	-6340.5-10364.5	
8	0.2578	1164.18	1155.87	1229.30	1229.82	2326.51	0.55799	0.55823	1.06071	-4.865	6.8520	-6765.0-10630.2	
9	0.2623	1181.14	1170.77	1225.43	1225.92	2300.78	0.55615	0.55639	1.05014	-2.050	7.6000	-6522.3-10667.5	
10	0.2667	1196.95	1184.30	1243.84	1244.30	2342.74	0.56490	0.56512	1.07133	-1.511	8.3394	-7202.6-10900.6	
11	0.2710	1208.33	1193.29	1255.85	1256.27	2374.97	0.57062	0.57082	1.08798	-1.255	9.0538	-7495.1-10933.0	

LOCATION	STAGN PRESSRE	STAGN TEMPTRE	STATIC PRESSRE	STATIC TEMPTRE	STATIC DENSITY	DELTA P UPON Q	DE HALL NUMBER	LOSS COEFF	DIFFUS FACTOR	RELATIVE EXIT ANG	ABSOLUTE FLOW ANG	NEXT-INL-ANGLE ACTUAL
1	6740.51	2263.00	6457.84	2240.37	0.05399	-0.49703	0.97163	0.72000	-0.00297	-72.5036	-27.0460	-27.050
2	7058.27	2263.00	6457.41	2216.18	0.05458	-0.65701	1.11146	0.72000	-0.12676	-65.3601	-20.1120	-20.109
3	7262.66	2263.00	6432.24	2199.29	0.05478	-0.80429	1.22146	0.72000	-0.23590	-62.3651	-17.9791	-17.958
4	7435.23	2263.00	6426.33	2186.45	0.05505	-0.95046	1.31073	0.72000	-0.47288	-60.8242	-17.1914	-17.150
5	7565.32	2263.00	6419.75	2177.17	0.05523	-1.09602	1.41107	0.72000	-0.60325	-60.0452	-16.9301	-16.921
6	7647.07	2263.00	6411.32	2170.46	0.05532	-1.20231	1.47313	0.72000	-0.69204	-59.4490	-16.8458	-16.838
7	7747.36	2263.00	6413.66	2164.46	0.05550	-1.33679	1.57569	0.72000	-0.85365	-59.7117	-17.4283	-17.413
8	7825.67	2263.00	6412.91	2159.24	0.05563	-1.62660	1.69028	0.72000	-1.02777	-60.1566	-18.2630	-18.254
9	7820.49	2263.00	6416.80	2159.89	0.05565	-1.62152	1.69313	0.72000	-1.01471	-59.3382	-15.6383	-15.579
10	7890.89	2263.00	6434.91	2156.75	0.05589	-1.83835	1.77405	0.72000	-1.16061	-59.5460	-15.9436	-15.936
11	7928.64	2263.00	6439.45	2154.67	0.05598	-2.02623	1.87777	0.72000	-1.28413	-59.7354	-16.0019	-15.994

TOTAL AXIAL FORCE ON BLADES = -255.56 TOTAL TANGENTIAL FORCE ON BLADES = -443.34

BEST AVAILABLE COPY

STREAMLINE ANALYSIS RUN 3

CONSTANT MEAN LINE, STATOR AND ROTOR LOSS

VARIABLE, CONSTANT WORK

This run would not converge because of severe axial velocity gradients imposed by the radial losses and high work of the hub section.

* * * STATION 6 * * * STATOR INLET

MASS-AVERAGE TOTAL PRESSURE= 27158.4 MASS-AVERAGE TOTAL TEMPERATURE= 2860.00
CUMULATIVE TOTAL PRESSURE RATIO= 1.0000

LOCATION	RADIUS	MERIDNAL VELOCITY	AXIAL VELOCITY	ABSOLUTE VELOCITY	VEL REL TO NEXT BLADE	VEL REL TO THIS BLADE	ABSOLUTE MACH NUMBER	MACH NO REL NEXT BLADE	MACH NO REL THIS BLADE	RAD OF CURVTRE	STRMLNE SLOPE ANGLE	AXIAL BLADE LOADG	TANGEN BLADE LOADG
1	0.2220	390.58	390.58	390.58	390.74	390.58	0.15522	0.15528	0.15522*********		0.0	0.4	0.0
2	0.2270	390.46	390.46	390.46	390.59	390.46	0.15517	0.15522	0.15517	-27.869	-0.0534	0.4	0.0
3	0.2318	390.09	390.09	390.09	390.15	390.09	0.15502	0.15505	0.15502	-8.027	-0.1996	0.4	0.0
4	0.2366	389.43	389.42	389.43	389.41	389.43	0.15476	0.15475	0.15476	-3.963	-0.3842	0.4	0.0
5	0.2413	388.43	388.41	388.43	388.35	388.43	0.15436	0.15432	0.15436	-2.435	-0.6309	0.4	0.0
6	0.2459	387.11	387.07	387.11	386.98	387.11	0.15383	0.15378	0.15383	-1.691	-0.8864	0.4	0.0
7	0.2504	385.44	385.38	385.44	385.31	385.44	0.15317	0.15312	0.15317	-1.269	-1.0717	0.3	0.0
8	0.2549	383.46	383.36	383.46	383.35	383.46	0.15238	0.15234	0.15238	-1.005	-1.3018	0.2	0.0
9	0.2593	381.16	381.03	381.16	381.13	381.16	0.15146	0.15145	0.15146	-0.826	-1.5201	0.1	0.0
10	0.2637	378.57	378.39	378.57	378.65	378.57	0.15043	0.15046	0.15043	-0.696	-1.7256	-0.1	0.0
11	0.2680	375.94	375.94	375.94	376.13	375.94	0.14938	0.14946	0.14938	-0.597	0.0	0.5	0.0

LOCATION	STAGN PRESSRE	STAGN TEMPTRE	STATIC PRESSRE	STATIC TEMPTRE	STATIC DENSITY	DELTA P UPON Q	DF HALL NUMBER	LOSS COEFF	DIFFUS FACTOR	RELATIVE EXIT ANG	ABSOLUTE FLOW ANG	NEXT-INL-ANGLE ACTUAL
1	27158.40	2860.00	26739.59	2849.94	0.17572	-0.02367	1.01217	0.0	0.0	0.0	0.0	0.0
2	27158.40	2860.00	26739.83	2849.94	0.17572	-0.02313	1.01190	0.0	0.0	0.0	0.0	0.0
3	27158.40	2860.00	26740.62	2849.96	0.17573	-0.02138	1.01103	0.0	0.0	0.0	0.0	0.0
4	27158.40	2860.00	26742.04	2850.00	0.17573	-0.01816	1.00943	0.0	0.0	0.0	0.0	0.0
5	27158.40	2860.00	26744.15	2850.05	0.17574	-0.01337	1.00703	0.0	0.0	0.0	0.0	0.0
6	27158.40	2860.00	26746.96	2850.12	0.17576	-0.00689	1.00379	0.0	0.0	0.0	0.0	0.0
7	27158.40	2860.00	26750.46	2850.20	0.17578	0.00130	0.99967	0.0	0.0	0.0	0.0	0.0
8	27158.40	2860.00	26754.63	2850.30	0.17580	0.01115	0.99470	0.0	0.0	0.0	0.0	0.0
9	27158.40	2860.00	26759.43	2850.42	0.17582	0.02260	0.98890	0.0	0.0	0.0	0.0	0.0
10	27158.40	2860.00	26764.81	2850.55	0.17585	0.03559	0.98225	0.0	0.0	0.0	0.0	0.0
11	27158.40	2860.00	26770.23	2850.68	0.17588	0.04879	0.97548	0.0	0.0	0.0	0.0	0.0

TOTAL AXIAL FORCE ON BLADES = 0.01 TOTAL TANGENTIAL FORCE ON BLADES = 0.0

STREAMLINE ANALYSIS RUN 4 CML STATOR LOSS VARIABLE, CONSTANT ROTOR LOSS, VARIABLE WORK

BEST AVAILABLE COPY

STATOR EXIT

MASS-AVERAGE TOTAL PRESSURE= 24507.1 MASS-AVERAGE TOTAL TEMPERATURE= 2860.00
CUMULATIVE TOTAL PRESSURE RATIO= 0.9024

LOCATION	RADIUS	MERIDNAL VELOCITY	AXIAL VELOCITY	ABSOLUTE VELOCITY	VEL REL TO NEXT BLADE	VEL REL TO THIS BLADE	ABSOLUTE MACH NUMBER	MACH NO REL NEXT BLADE	MACH NO REL THIS BLADE	RAD OF CURVTR	STAGGR SLOPE ANGLE	AXIAL BLADE LOADG	TANGEN BLADE LOADG
1	0.2220	939.09	939.09	3026.79	3027.78	3026.79	1.35130	1.35180	1.35130	*********	0.0	-24176.5	8182.4
2	0.2270	958.93	958.93	2977.43	2979.67	2977.93	1.32861	1.32953	1.32861	15.305	-0.0145	-23870.7	8029.6
3	0.2316	975.24	975.24	2934.17	2936.25	2934.17	1.29912	1.30022	1.29912	4.366	-0.0370	-23537.6	7864.2
4	0.2359	987.91	987.91	2891.32	2893.46	2891.32	1.27543	1.27656	1.27543	2.217	-0.0150	-23471.2	7832.9
5	0.2400	996.64	996.64	2849.82	2851.86	2849.82	1.25274	1.25380	1.25274	1.401	-0.0226	-23333.5	7764.5
6	0.2439	999.66	999.66	2811.00	2812.55	2811.00	1.23174	1.23253	1.23174	1.012	-0.0027	-23239.6	7361.4
7	0.2477	996.13	996.12	2777.52	2778.86	2777.52	1.21379	1.21446	1.21379	0.813	-0.1472	-23267.5	7436.2
8	0.2514	988.29	988.25	2742.34	2743.47	2742.34	1.19609	1.19665	1.19609	0.709	-0.3473	-23325.3	7563.0
9	0.2550	979.80	979.71	2707.55	2708.48	2707.55	1.17676	1.17720	1.17676	0.620	-0.7674	-23322.4	7552.4
10	0.2585	972.02	971.91	2673.65	2674.36	2673.65	1.15904	1.15937	1.15904	0.531	-0.8645	-23338.1	7581.9
11	0.2620	964.68	964.54	2640.47	2640.95	2640.47	1.14184	1.14205	1.14184	0.464	-0.9992	-23376.3	7620.4

LOCATION	STAGN PRESSRE	STAGN TEMPTRE	STATIC PRESSRE	STATIC TEMPTRE	STATIC DENSITY	DELTA P UPON Q	DF HALL NUMBER	LOSS COEFF	DIFFUS FACTOR	RELATIVE EXIT ANG	ABSOLUTE EXIT ANG	NEXT-ITE-ANGLE ACTUAL
1	23719.05	2860.00	8295.53	2234.99	0.06945-44.00915		7.74947	8.20000-11.29704		71.9305	71.9305	71.930
2	24207.10	2860.00	8795.29	2255.71	0.07296-42.84245		7.63665	7.04156-11.08370		71.2207	71.2207	71.217
3	24434.09	2860.00	9178.69	2273.94	0.07563-42.00825		7.52171	6.51454-10.90077		70.5423	70.5423	70.534
4	24628.13	2860.00	9551.47	2291.50	0.07800-41.25042		7.42459	6.07367-10.73183		70.0257	70.0257	70.021
5	24805.89	2860.00	9871.93	2305.23	0.08003-40.70159		7.33869	5.68474-10.57954		69.5349	69.5349	69.535
6	24735.93	2860.00	10164.97	2323.63	0.08186-40.27502		7.26157	5.33763-10.45130		69.1733	69.1733	69.170
7	24717.67	2860.00	10398.07	2336.73	0.08327-40.05853		7.20601	5.98337-10.35826		68.9985	68.9985	68.991
8	24615.41	2860.00	10608.24	2350.29	0.08447-39.96233		7.15158	6.23744-10.26950		68.8820	68.8820	68.885
9	24535.82	2860.00	10824.75	2363.52	0.08571-39.91245		7.10343	6.57006-10.19109		68.7913	68.7913	68.803
10	24461.45	2860.00	11036.80	2376.22	0.08692-39.93375		7.06257	6.84449-10.12386		68.6885	68.6885	68.694
11	24358.77	2860.00	11230.01	2388.48	0.08799-40.00751		7.02371	7.20000-10.05962		68.5791	68.5791	68.570

TOTAL AXIAL FORCE ON BLADES =-1009.06 TOTAL TANGENTIAL FORCE ON BLADES = 394.27

* * * STATION 8 * * * ROTOR INLET

MASS-AVERAGE TOTAL PRESSURE= 24507.1 MASS-AVERAGE TOTAL TEMPERATURE= 2860.00
CUMULATIVE TOTAL PRESSURE RATIO= 0.9024

LOCATION	RADIUS	MERIDNAL VELOCITY	AXIAL VELOCITY	ABSOLUTE VELOCITY	VEL REL TO NEXT BLADE	VEL REL TO THIS BLADE	ABSOLUTE MACH NUMBER	MACH NO REL NEXT BLADE	MACH NO REL THIS BLADE	RAD OF CURVTRE	STRMLNE SLOPE ANGLE	AXIAL BLADE LOING	TANGEN BLADE LOING
1	0.2220	944.69	944.69	3029.11	1760.01	3029.11	1.35254	0.78590	1.35254	-0.206	0.0	1.3	1.7
2	0.2270	956.47	956.07	2977.75	1692.86	2977.75	1.32343	0.75246	1.32343	-0.279	-1.6936	-1.2	2.0
3	0.2316	965.95	965.81	2931.46	1632.45	2931.46	1.29754	0.72268	1.29754	-0.443	-0.3536	-0.6	1.2
4	0.2359	973.69	973.68	2886.47	1575.26	2886.47	1.27270	0.69467	1.27270	-0.995	-0.2346	-0.2	-0.2
5	0.2401	980.48	980.45	2843.74	1522.08	2843.74	1.24938	0.66882	1.24938	6.988	0.4413	0.4	-1.0
6	0.2440	988.00	987.84	2806.32	1475.35	2806.32	1.22916	0.64626	1.22916	0.932	1.0364	-1.6	-2.3
7	0.2473	998.59	998.26	2760.96	1427.86	2760.86	1.20492	0.62227	1.20402	0.440	1.4753	169.0	-75.4
8	0.2514	999.71	999.26	2697.03	1382.29	2697.03	1.17119	0.59156	1.17119	0.307	1.7184	564.8	-229.4
9	0.2553	983.98	983.42	2714.62	1353.14	2714.62	1.18042	0.58840	1.18042	0.241	1.9415	-59.4	24.0
10	0.2585	970.05	969.30	2673.46	1301.64	2673.46	1.15859	0.56424	1.15859	0.206	2.2468	-1.8	2.4
11	0.2620	954.98	954.06	2641.06	1261.83	2641.06	1.14210	0.54566	1.14210	0.184	2.4991	-2.5	2.2

LOCATION	STAGN PRESSRE	STAGN TEMPTRE	STATIC PRESSRE	STATIC TEMPTRE	STATIC DENSITY	DELTA P UPON Q	DF HALL NUMBER	LOSS COEFF	DIFFUS FACTOR	RELATIVE EXIT ANG	ABSOLUTE FLOW ANG	NEXT-IBL-ANGLE ACTUAL
1	23719.05	2860.00	8284.50	2234.27	0.06936	-0.00071	1.00077	0.0	-0.00089	71.8332	71.8332	57.476
2	24207.10	2860.00	8800.80	2256.05	0.07297	0.00036	0.99764	0.0	-0.00037	71.2766	71.2766	56.571
3	24434.09	2860.00	9201.70	2275.31	0.07565	0.00151	0.99608	0.0	0.00004	70.7686	70.7686	53.709
4	24613.13	2860.00	9589.89	2293.71	0.07821	0.00254	0.99532	0.0	0.00168	70.2910	70.2910	51.524
5	24696.89	2860.00	9919.43	2310.89	0.08030	0.00319	0.99787	0.0	0.00224	69.8370	69.8370	48.617
6	24729.93	2860.00	10202.77	2325.70	0.08207	0.00259	0.99834	0.0	0.00179	69.3847	69.3847	48.012
7	24717.67	2860.00	10521.70	2343.34	0.08400	0.00062	0.99904	0.0	0.01012	68.8079	68.8079	45.738
8	24615.41	2860.00	10940.24	2367.70	0.08645	-0.00367	0.99848	0.0	0.02049	68.2569	68.2569	42.660
9	24535.82	2860.00	10777.86	2351.07	0.08541	-0.00341	1.00251	0.0	-0.00397	68.7639	68.7639	43.396
10	24481.45	2860.00	11042.21	2376.50	0.08694	0.00040	0.99893	0.0	-0.00006	68.7456	68.7459	41.953
11	24358.77	2860.00	11229.76	2388.47	0.08797	-0.00002	1.00022	0.0	-0.00034	68.5923	68.5923	40.143

TOTAL AXIAL FORCE ON BLADES = 2.51 TOTAL TANGENTIAL FORCE ON BLADES = -0.99

* * * STATION 9 * * * ROTOR EXIT

MASS-AVERAGE TOTAL PRESSURE= 7562.9 MASS-AVERAGE TOTAL TEMPERATURE= 2265.08

CUMULATIVE TOTAL PRESSURE RATIO= 0.2785

LOCATION	RADIUS	MERIDNAL VELOCITY	AXIAL VELOCITY	ABSOLUTE VELOCITY	VEL REL TO NEXT BLADE	VEL REL TO THIS BLADE	ABSOLUTE MACH NUMBER	MACH NO REL NEXT BLADE	MACH NO REL THIS BLADE	RAD OF CURVTRE	STRMLNE SLOPE ANGLE	AXIAL BLADE LOING	TANGEN BLADE LOING
1	0.2140	924.20	919.23	924.62	927.37	1608.71	0.41102	0.41228	0.71760	0.455	-5.9501	-1582.2	-5[illegible]
2	0.2211	882.36	880.83	899.68	899.27	1796.09	0.40243	0.40222	0.80423	0.440	-3.3731	-3076.5	-7415.5
3	0.2280	875.70	875.60	913.57	911.68	1905.88	0.40895	0.40906	0.85510	0.466	-3.8599	-3402.6	-7850.4
4	0.2347	904.69	904.48	958.94	956.47	2007.49	0.43162	0.43045	0.90349	0.553	1.2104	-4647.3	-9417.4
5	0.2409	941.44	940.25	1005.59	1003.39	2090.45	0.45366	0.45241	0.94366	0.733	2.7013	-5200.9	-8816.4
6	0.2467	981.57	978.84	1048.90	1046.93	2155.72	0.47399	0.47306	0.97595	1.126	4.2727	-5843.3	-8355.9
7	0.2521	1023.41	1018.80	1092.71	1092.71	2223.39	0.49592	0.49444	1.00894	2.430	5.4435	-6518.6	-7832.2
8	0.2573	1065.14	1058.36	1147.09	1146.99	2303.04	0.51978	0.51872	1.04767	-26.015	6.4695	-6970.1-10217.8
9	0.2621	1110.84	1101.54	1161.93	1161.03	2276.82	0.52642	0.52599	1.03720	-2.544	7.4130	-6601.6-10394.9
10	0.2667	1170.15	1157.92	1216.32	1215.33	2323.55	0.55158	0.55110	1.06095	-1.542	8.2397	-7151.1-10714.5
11	0.2710	1240.89	1225.44	1274.93	1274.06	2349.49	0.57323	0.57279	1.07438	-1.255	8.9836	-7199.5-11115.0

LOCATION	STAGN PRESSRE	STAGN TEMPTRE	STATIC PRESSRE	STATIC TEMPTRE	STATIC DENSITY	DELTA P UPON Q	DE HALL NUMBER	LOSS COEFF	DIFFUS FACTOR	RELATIVE EXIT ANG	ABSOLUTE FLOW ANG	NEXT-BL-ANGLE ACTUAL
1	7236.05	2213.30	6579.99	2255.06	0.05464	-0.43815	0.91472	0.72000	0.12477	-55.0348	1.7205	2.024
2	7233.72	2281.54	6518.76	2226.10	0.05485	-0.61109	1.06232	0.72000	-0.10427	-60.6230	-11.2202	-10.054
3	7270.06	2268.50	6529.07	2211.33	0.05530	-0.75090	1.16927	0.72000	-0.26437	-62.6541	-16.5577	-14.232
4	7350.92	2260.37	6526.43	2197.44	0.05562	-0.90299	1.27539	0.72000	-0.42254	-63.2241	-19.3719	-18.149
5	7438.05	2256.05	6516.79	2186.92	0.05570	-1.05526	1.37544	0.72000	-0.56876	-63.2678	-20.4012	-23.[illegible]
6	7526.35	2254.39	6517.49	2179.28	0.05599	-1.19763	1.46255	0.72000	-0.69581	-63.9825	-20.6940	-20.[illegible]
7	7622.79	2254.73	6515.04	2172.86	0.05613	-1.36988	1.55057	0.72000	-0.83908	-62.7341	-20.9602	-21.[illegible]
8	7747.32	2256.82	6519.83	2166.93	0.05632	-1.62297	1.66040	0.72000	-1.03180	-62.6063	-21.9171	-22.[illegible]
9	7782.47	2259.95	6519.08	2167.64	0.05631	-1.68683	1.68305	0.72000	-1.08926	-61.8070	-17.1911	-17.542
10	7919.82	2264.66	6523.19	2163.45	0.05645	-1.82316	1.78566	0.72000	-1.15073	-60.0269	-15.9972	-16.280
11	8097.50	2274.20	6544.30	2162.87	0.05665	-1.99767	1.86241	0.72000	-1.25297	-58.4448	-13.4325	-13.658

TOTAL AXIAL FORCE ON BLADES = -266.05 TOTAL TANGENTIAL [illegible]

BEST AVAILABLE COPY

* * * STATION 6 * * * STATOR INLET

MASS-AVERAGE TOTAL PRESSURE= 27158.4 MASS-AVERAGE TOTAL TEMPERATURE= 2860.00
CUMULATIVE TOTAL PRESSURE RATIO= 1.0000

LOCATION	RADIUS	MERIDNAL VELOCITY	AXIAL VELOCITY	ABSOLUTE VELOCITY	VEL REL TO NEXT BLADE	VEL REL TO THIS BLADE	ABSOLUTE MACH NUMBER	MACH NO REL NEXT BLADE	MACH NO REL THIS BLADE	RAD OF CURVTRE	STRMLNE SLOPE ANGLE	AXIAL BLADE LOSS	TANGEN BLADE LOSS
1	0.2220	389.14	389.14	389.14	389.15	389.14	0.15464	0.15465	0.15464	*********	0.0	0.0	0.0
2	0.2273	389.18	389.18	389.13	389.19	389.18	0.15466	0.15466	0.15466	23.217	-0.0042	0.0	0.0
3	0.2318	389.18	389.13	389.13	389.18	389.18	0.15466	0.15466	0.15466	-258.583	-0.1109	0.0	0.0
4	0.2366	388.97	388.96	388.97	388.97	388.97	0.15458	0.15458	0.15458	-8.955	-0.2954	0.0	0.0
5	0.2413	388.43	388.41	388.43	388.43	388.43	0.15436	0.15436	0.15436	-3.722	-0.4991	0.0	0.0
6	0.2459	387.48	387.45	387.48	387.48	387.48	0.15398	0.15398	0.15398	-2.185	-0.7591	-0.0	0.0
7	0.2504	386.09	386.03	386.09	386.08	386.09	0.15343	0.15342	0.15343	-1.405	-1.0145	-0.1	0.0
8	0.2547	384.24	384.14	384.24	384.23	384.24	0.15269	0.15269	0.15269	-1.119	-1.2648	-0.2	0.0
9	0.2593	381.92	381.79	381.92	381.92	381.92	0.15177	0.15177	0.15177	-0.881	-1.4900	-0.3	0.0
10	0.2637	379.15	378.98	379.15	379.14	379.15	0.15066	0.15066	0.15066	-0.717	-1.7175	-0.5	0.0
11	0.2680	376.29	376.29	376.29	376.29	376.29	0.14952	0.14952	0.14952	-0.597	0.0	0.0	0.0

LOCATION	STAGN PRESSRE	STAGN TEMPTRE	STATIC PRESSRE	STATIC TEMPTRE	STATIC DENSITY	DELTA P UPON Q	DE HALL NUMBER	LOSS COEFF	DIFFUS FACTOR	RELATIVE EXIT ANG	ABSOLUTE FLOW ANG	NEXT-INL-ANGLE ACTUAL
1	27158.40	2860.00	26742.38	2850.01	0.17574	-0.01548	1.00776	0.0	0.0	0.0	0.0	0.0
2	27158.40	2860.00	26742.30	2850.00	0.17574	-0.01578	1.00791	0.0	0.0	0.0	0.0	0.0
3	27158.40	2860.00	26742.30	2850.00	0.17574	-0.01610	1.00807	0.0	0.0	0.0	0.0	0.0
4	27158.40	2860.00	26742.75	2850.01	0.17574	-0.01561	1.00778	0.0	0.0	0.0	0.0	0.0
5	27158.40	2860.00	26743.93	2850.04	0.17574	-0.01338	1.00671	0.0	0.0	0.0	0.0	0.0
6	27158.40	2860.00	26745.90	2850.09	0.17575	-0.00928	1.00466	0.0	0.0	0.0	0.0	0.0
7	27158.40	2860.00	26748.65	2850.16	0.17577	-0.00294	1.00148	0.0	0.0	0.0	0.0	0.0
8	27158.40	2860.00	26752.74	2850.26	0.17579	0.00574	0.99711	0.0	0.0	0.0	0.0	0.0
9	27158.40	2860.00	26757.58	2850.37	0.17581	0.01605	0.99149	0.0	0.0	0.0	0.0	0.0
10	27158.40	2860.00	26763.35	2850.51	0.17584	0.02848	0.98456	0.0	0.0	0.0	0.0	0.0
11	27158.40	2860.00	26769.25	2850.66	0.17587	0.04477	0.97724	0.0	0.0	0.0	0.0	0.0

TOTAL AXIAL FORCE ON BLADES = -0.00 TOTAL TANGENTIAL FORCE ON BLADES = 0.0

STREAMLINE ANALYSIS RUN 5 CML STATOR AND ROTOR LOSS VARIABLE, VARIABLE WORK

* * * STATION 7 * * * STATOR EXIT

MASS-AVERAGE TOTAL PRESSURE= 24509.7 MASS-AVERAGE TOTAL TEMPERATURE= 2460.00

CUMULATIVE TOTAL PRESSURE RATIO= 0.9329

LOCATION	RADIUS	MERIDNAL VELOCITY	AXIAL VELOCITY	ABSOLUTE VELOCITY	VEL REL TO NEXT BLADE	VEL REL TO THIS BLADE	ABSOLUTE MACH NUMBER	MACH NO REL NEXT BLADE	MACH NO REL THIS BLADE	RAD OF CURVTRE	STAGGER ANGLE	AXIAL BLADE LOING	TANGEN BLADE LOING
1	0.2220	922.51	922.51	3020.71	3021.05	3020.71	1.34796	1.34815	1.34766	**********	0.0	-24171.7	8148.2
2	0.2271	951.14	951.14	2972.81	2973.04	2972.81	1.32004	1.32047	1.32004	24.269	0.1[illegible]	-23813.7	[illegible]
3	0.2317	974.25	974.24	2930.47	2930.58	2930.47	1.29716	1.29727	1.29713	4.639	[illegible]	[illegible]	[illegible]
4	0.2360	991.42	991.40	2888.98	2889.00	2888.98	1.27425	1.27425	1.27425	3.178	0.4371	-23463.4	8133.7
5	0.2401	1002.27	1002.24	2847.43	2847.39	2847.43	1.25154	1.25152	1.25154	1.246	0.4666	-23339.0	8256.5
6	0.2440	1005.10	1005.06	2810.42	2810.36	2810.42	1.23152	1.23140	1.23152	0.917	0.4672	-23237.5	8330.6
7	0.2477	1000.18	1000.17	2776.86	2776.81	2776.86	1.21553	1.21550	1.21553	0.752	0.2651	-23261.6	8432.1
8	0.2514	990.77	990.76	2741.43	2741.45	2741.48	1.19473	1.19471	1.19473	0.803	-0.2362	-23317.1	8447.4
9	0.2550	980.62	980.57	2705.44	2706.44	2706.44	1.17626	1.17626	1.17626	0.624	-0.5[illegible]	-23330.3	8459.4
10	0.2585	971.17	971.03	2672.24	2672.27	2672.24	1.15839	1.15840	1.15839	0.534	-0.7[illegible]	-23346.6	8468.4
11	0.2620	962.21	962.07	2638.76	2638.83	2638.76	1.14103	1.14106	1.14103	0.464	-0.9[illegible]	-23362.3	8470.7

LOCATION	STAGN PRESSRE	STAGN TEMPTRE	STATIC PRESSRE	STATIC TEMPTRE	STATIC DENSITY	DELTA P UPON Q	DF HALL NUMBER	LOSS COEFF	DIFFUS FACTOR	RELATIVE EXIT ANG	ABSOLUTE FLOW ANG	NEXT-IN L-ANGLE ACTUAL
1	23746.77	2860.00	8338.10	2237.13	0.06577-44.23824		7.76254	8.20000	1.32532	72.2235	72.2235	72.206
2	24238.26	2860.00	8834.26	2267.43	0.07326-43.03736		7.63972	7.01743	1.13612	71.3456	71.3456	71.337
3	24459.21	2860.00	9206.57	2275.06	0.07576-42.14233		7.52790	6.48655	0.91260	70.5875	70.5875	70.594
4	24628.60	2860.00	9560.93	2292.06	0.07809-41.33627		7.42721	6.03615	0.73365	69.9352	69.9352	69.933
5	24693.24	2860.00	9842.32	2308.80	0.08013-40.67820		7.33069	5.93511	0.56622	69.3955	69.3955	69.394
6	24729.82	2860.00	10159.48	2323.48	0.08186-40.20908		7.25309	5.88750	0.43420	69.0509	69.0509	69.057
7	24703.84	2860.00	10389.94	2336.61	0.08325-39.94250		7.19252	5.93827	0.33404	68.8939	68.8939	68.899
8	24600.67	2860.00	10501.04	2350.26	0.08446-39.81530		7.13491	6.30518	0.24150	68.8190	68.8190	68.823
9	24523.32	2860.00	10820.19	2363.58	0.08571-39.76122		7.08835	6.57500	0.16341	68.7929	68.7929	68.7[illegible]
10	24453.38	2860.00	11036.48	2376.40	0.08695-39.80932		7.04302	6.84734	0.10116	68.8060	68.8060	68.806
11	24355.53	2860.00	11234.61	2388.77	0.08806-39.91901		7.01258	7.20000	0.04328	68.8222	68.8222	68.820

TOTAL AXIAL FORCE ON BLADES =-1006.73 TOTAL TANGENTIAL FORCE ON BLADES = 394.17

BEST AVAILABLE COPY

* * * STATION 8 * * * ROTOR INLET

MASS-AVERAGE TOTAL PRESSURE= 24508.7 MASS-AVERAGE TOTAL TEMPERATURE= 2860.00
CUMULATIVE TOTAL PRESSURE RATIO= 0.9224

LOCATION	RADIUS	MERIDNAL VELOCITY	AXIAL VELOCITY	ABSOLUTE VELOCITY	VEL REL TO NEXT BLADE	VEL REL TO THIS BLADE	ABSOLUTE MACH NUMBER	MACH NO REL NEXT BLADE	MACH NO REL THIS BLADE	RAD OF CURVTRE	STRMLNE SLOPE ANGLE	AXIAL BLADE LOING	TANGEN BLADE LOING
1	0.2220	914.28	914.23	3018.10	1741.62	3018.10	1.34649	0.77702	1.34649	-0.206	0.0	0.1	-0.3
2	0.2271	936.40	936.28	2967.47	1675.67	2967.47	1.31786	0.74419	1.31786	-0.425	-0.4997	-1.5	-2.2
3	0.2319	955.38	955.38	2922.92	1618.49	2922.92	1.29300	0.71507	1.29300	-1.104	-0.8732	-1.0	-4.6
4	0.2362	971.19	971.12	2880.09	1565.43	2880.09	1.26938	0.68906	1.26938	5.829	0.6995	-0.9	-7.7
5	0.2403	983.96	983.71	2838.46	1515.58	2838.46	1.24668	0.66556	1.24668	0.959	1.2180	2.1	-10.4
6	0.2443	997.24	996.75	2813.03	1481.67	2813.08	1.23296	0.64941	1.23296	0.557	1.7147	-90.9	22.6
7	0.2480	1012.68	1012.02	2758.48	1428.71	2758.48	1.20375	0.62346	1.20375	0.385	2.0624	224.4	-100.3
8	0.2515	1013.20	1012.53	2700.90	1370.68	2700.90	1.17337	0.59647	1.17337	0.282	2.0335	541.3	-221.0
9	0.2550	994.23	993.54	2716.34	1358.24	2716.34	1.18147	0.59076	1.18147	0.239	2.1368	-54.3	22.2
10	0.2585	977.74	976.94	2674.39	1305.32	2674.39	1.15952	0.56593	1.15952	0.203	2.3274	-3.6	-1.1
11	0.2620	970.16	969.24	2641.57	1264.42	2641.57	1.14249	0.54686	1.14249	0.184	2.4091	-3.5	-0.4

LOCATION	STAGN PRESSRE	STAGN TEMPTRE	STATIC PRESSRE	STATIC TEMPTRE	STATIC DENSITY	DELTA P UPON Q	DE HALL NUMBER	LOSS COEFF	DIFFUS FACTOR	RELATIVE EXIT ANG	ABSOLUTE FLOW ANG	NEXT-INL-ANGLE ACTUAL
1	23746.77	2860.00	8354.49	2238.20	0.06983	0.00106	0.99913	0.0	0.00089	72.3714	72.3714	58.299
2	24238.26	2860.00	8864.70	2259.52	0.07349	0.00230	0.99820	0.0	0.00194	71.6131	71.6131	55.006
3	24659.21	2860.00	9258.04	2278.12	0.07608	0.00337	0.99742	0.0	0.00287	70.9270	70.9270	53.012
4	24623.60	2860.00	9622.69	2295.61	0.07858	0.00410	0.99692	0.0	0.00354	70.2996	70.2996	51.697
5	24693.24	2860.00	9945.35	2312.33	0.08052	0.00425	0.99685	0.0	0.00375	69.7271	69.7271	49.532
6	24727.82	2860.00	10139.60	2322.39	0.08174	-0.00136	1.00094	0.0	-0.00222	69.2515	69.2515	47.720
7	24703.84	2860.00	10521.67	2343.68	0.08405	0.00919	0.99338	0.0	0.01209	68.4799	68.4799	44.905
8	24690.67	2860.00	10693.82	2355.43	0.08522	0.00980	0.99320	0.0	0.01263	67.9855	67.9855	42.383
9	24523.32	2860.00	10747.92	2359.77	0.08528	-0.00527	1.00365	0.0	-0.00486	68.5483	68.5483	42.606
10	24453.38	2860.00	11020.11	2375.55	0.08686	-0.00122	1.00080	0.0	-0.00074	68.5769	68.5769	41.536
11	24356.53	2860.00	11213.44	2387.70	0.08793	-0.00161	1.00107	0.0	-0.00104	68.4785	68.4785	39.933

TOTAL AXIAL FORCE ON BLADES = 2.17 TOTAL TANGENTIAL FORCE ON BLADES = -1.11

* * * STATION 7 * * *

• • • STATION 9 • • • ROTOR EXIT

MASS-AVERAGE TOTAL PRESSURE= 7564.5 MASS-AVERAGE TOTAL TEMPERATURE= 2264.05
CUMULATIVE TOTAL PRESSURE RATIO= 0.2785

LOCATION	RADIUS	MERIONAL VELOCITY	AXIAL VELOCITY	ABSOLUTE VELOCITY	VEL REL TO NEXT BLADE	VEL REL TO THIS BLADE	ABSOLUTE MACH NUMBER	MACH NO REL NEXT BLADE	MACH NO REL THIS BLADE	RAD OF CURVTRE	STRMLNE SLOPE ANGLE	AXIAL BLADE LOING	TANGEN BLADE LOING
1	0.2140	592.44	589.25	593.86	592.78	1431.64	0.26209	0.26161	0.62446	0.455	-5.0691	-2726.9	-4773.6
2	0.2234	799.42	799.40	824.78	824.54	1794.08	0.36859	0.36848	0.80158	0.766	-0.3348	-3504.5	-7176.4
3	0.2304	896.08	896.39	941.20	941.24	1952.45	0.42301	0.42303	0.87753	0.443	1.6851	-4193.0	-8892.9
4	0.2370	973.04	971.38	1029.43	1029.67	2068.02	0.46456	0.46467	0.92412	0.592	3.3463	-4743.2	-9852.6
5	0.2427	1035.27	1032.18	1097.84	1098.21	2155.10	0.49655	0.49702	0.97705	0.866	4.4297	-5265.6	-10405.5
6	0.2480	1084.67	1080.00	1144.04	1144.47	2206.79	0.51868	0.51889	1.00816	1.455	5.3214	-5626.1-11015.7	
7	0.2530	1118.41	1112.06	1186.89	1187.34	2279.87	0.53805	0.53806	1.03866	4.071	6.1072	-6437.8-11995.8	
8	0.2573	1143.55	1135.41	1219.47	1219.96	2341.12	0.55404	0.55428	1.06831	-5.223	6.8400	-6796.0-12645.1	
9	0.2623	1166.42	1156.25	1214.82	1215.29	2304.54	0.55146	0.55169	1.05205	-1.934	7.5735	-6516.8-12066.2	
10	0.2669	1193.66	1181.09	1238.05	1238.49	2332.88	0.56191	0.56212	1.06614	-1.431	8.3230	-7196.5-13242.1	
11	0.2710	1229.42	1214.11	1262.88	1263.29	2340.17	0.57253	0.57273	1.06972	-1.255	9.0932	-7394.7-13603.2	

LOCATION	STAGN PRESSRE	STAGN TEMPTRE	STATIC PRESSRE	STATIC TEMPTRE	STATIC DENSITY	DELTA P UPON Q	DE HALL NUMBER	LOSS COEFF	DIFFUS FACTOR	RELATIVE EXIT ANG	ABSOLUTE FLOW ANG	NEXT-INL-ANGLE ACTUAL
1	6803.65	2313.30	6506.69	2289.27	0.05323	-0.48302	0.82228	0.90000	0.22041	-55.6760	3.0948	4.013
2	7098.94	2276.91	6473.33	2230.34	0.05436	-0.65137	1.07095	0.78031	-0.12484	-63.6665	-14.2677	-14.251
3	7251.73	2264.88	6460.28	2204.17	0.05490	-0.79528	1.20697	0.73239	-0.31483	-62.5717	-17.4886	-17.662
4	7413.47	2258.14	6451.37	2185.46	0.05529	-0.94251	1.32119	0.69913	-0.48017	-61.9772	-19.3543	-19.070
5	7543.31	2255.22	6436.76	2172.50	0.05550	-1.09289	1.42200	0.67995	-0.62475	-61.3562	-19.4927	-19.486
6	7665.65	2254.30	6450.53	2164.45	0.05582	-1.19046	1.48430	0.65831	-0.72153	-60.6700	-18.3147	-18.607
7	7748.81	2255.31	6433.80	2158.28	0.05604	-1.39097	1.59558	0.65844	-0.88096	-60.7661	-19.8421	-19.051
8	7840.51	2257.20	6442.56	2155.06	0.05600	-1.61761	1.70768	0.66243	-1.04767	-60.9391	-20.4435	-20.488
9	7832.26	2260.21	6447.27	2158.37	0.05584	-1.61163	1.69845	0.68511	-1.02215	-55.8156	-16.3847	-16.755
10	7890.73	2264.88	6448.27	2159.62	0.05593	-1.83439	1.78698	0.73766	-1.15061	-59.4952	-15.5475	-15.542
11	7975.38	2274.20	6468.74	2164.71	0.05597	-2.01483	1.85060	0.80000	-1.23945	-58.6322	-13.3007	-13.376

TOTAL AXIAL FORCE ON BLADES = -255.70 TOTAL TANGENTIAL FORCE ON BLADES = -442.36

BEST AVAILABLE COPY

• • • STATION 6 • • • STATOR INLET

MASS-AVERAGE TOTAL PRESSURE= 27158.4 MASS-AVERAGE TOTAL TEMPERATURE= 2849.33
CUMULATIVE TOTAL PRESSURE RATIO= 1.0000

LOCA-TION	RADIUS	MERIDNAL VELOCITY	AXIAL VELOCITY	ABSOLUTE VELOCITY	VEL REL TO NEXT BLADE	VEL REL TO THIS BLADE	ABSOLUTE MACH NUMBER	MACH NO REL NEXT BLADE	MACH NO REL THIS BLADE	RAD OF CURVTRE	STRMLNE SLOPE ANGLE	AXIAL BLADE LDING	TANGEN BLADE LDING
1	0.2220	363.22	363.22	363.22	364.64	363.22	0.15308	0.15368	0.15308	*********	0.0	0.1	0.0
2	0.2268	373.65	373.62	373.65	374.92	373.65	0.15329	0.15381	0.15329	2.057	0.6376	0.0	0.0
3	0.2316	382.50	382.47	382.50	383.37	382.50	0.15349	0.15383	0.15349	1.842	0.6924	0.0	0.0
4	0.2363	388.74	388.72	388.74	389.16	388.74	0.15421	0.15437	0.15421	2.561	0.4650	0.1	0.0
5	0.2411	392.80	392.80	392.80	392.83	392.80	0.15421	0.15422	0.15421	7.524	0.1014	0.1	0.0
6	0.2457	394.64	394.63	394.64	394.34	394.64	0.15412	0.15400	0.15412	-5.551	-0.3234	0.2	0.0
7	0.2504	393.77	393.74	393.77	393.25	393.77	0.15358	0.15338	0.15358	-1.935	-0.7583	0.1	0.0
8	0.2549	390.28	390.20	390.28	389.62	390.28	0.15290	0.15264	0.15290	-1.171	-1.1661	-0.0	0.0
9	0.2594	384.43	384.30	384.43	383.72	384.43	0.15175	0.15147	0.15175	-0.851	-1.5166	-0.2	0.0
10	0.2638	375.68	375.50	375.68	374.99	375.68	0.15027	0.14999	0.15027	-0.686	-1.7801	-0.4	0.0
11	0.2680	364.35	364.35	364.35	363.69	364.35	0.14942	0.14915	0.14942	-0.597	0.0	0.2	0.0

LOCA-TION	STAGN PRESSRE	STAGN TEMPTRE	STATIC PRESSRE	STATIC TEMPTRE	STATIC DENSITY	DELTA P UPON Q	DE HALL NUMBER	LOSS COEFF	DIFFUS FACTOR	RELATIVE EXIT ANG	ABSOLUTE FLOW ANG	NEXT-INL-ANGLE ACTUAL
1	27158.40	2529.00	26748.76	2520.14	0.19878	0.00304	0.99857	0.0	0.0	0.0	0.0	0.0
2	27158.40	2675.36	26748.62	2666.06	0.18790	-0.00064	1.00042	0.0	0.0	0.0	0.0	0.0
3	27158.40	2802.20	26748.42	2792.52	0.1793	-0.00761	1.00392	0.0	0.0	0.0	0.0	0.0
4	27158.40	2870.69	26748.07	2860.73	0.1750	-0.01333	1.00678	0.0	0.0	0.0	0.0	0.0
5	27158.40	2933.98	26748.48	2923.85	0.17132	-0.01606	1.00815	0.0	0.0	0.0	0.0	0.0
6	27158.40	2966.39	26748.16	2956.13	0.16945	-0.01496	1.00760	0.0	0.0	0.0	0.0	0.0
7	27158.40	2974.36	26749.05	2964.19	0.16901	-0.00974	1.00499	0.0	0.0	0.0	0.0	0.0
8	27158.40	2946.41	26752.44	2936.41	0.17063	-0.00065	1.00043	0.0	0.0	0.0	0.0	0.0
9	27158.40	2900.25	26758.21	2890.53	0.17337	0.01177	0.99416	0.0	0.0	0.0	0.0	0.0
10	27158.40	2820.70	26765.41	2811.37	0.17830	0.02677	0.98654	0.0	0.0	0.0	0.0	0.0
11	27158.40	2677.00	26768.89	2668.16	0.18790	0.04135	0.97907	0.0	0.0	0.0	0.0	0.0

TOTAL AXIAL FORCE ON BLADES = 0.00 TOTAL TANGENTIAL FORCE ON BLADES = 0.0

STREAMLINE ANALYSIS RUN 6 CONSTANT MEANLINE, VARIABLE LOSSES AND WORK WITH INLET TEMPERATURE DISTORTION

MASS-AVERAGE TOTAL PRESSURE= 24540.7 MASS-AVERAGE TOTAL TEMPERATURE= 2849.33
CUMULATIVE TOTAL PRESSURE RATIO= 0.9036

STATOR EXIT

LOCATION	RADIUS	MERIDNAL VELOCITY	AXIAL VELOCITY	ABSOLUTE VELOCITY	VEL REL TO NEXT BLADE	VEL REL TO THIS BLADE	ABSOLUTE MACH NUMBER	MACH NO REL NEXT BLADE	MACH NO REL THIS BLADE	RAD OF CURVTRE	STRMLNE SLOPE ANGLE	AXIAL BLADE LOING	TANGEN BLADE LOING
1	0.2220	509.48	509.48	2920.50	2921.06	2920.50	1.39706	1.39732	1.39706*********	0.0	-26289.0		5791.5
2	0.2290	706.16	706.15	2884.13	2887.02	2884.13	1.32589	1.32743	1.32589	-1.186	-0.2517-24947.0		7689.6
3	0.2341	903.10	903.09	2883.21	2886.22	2883.21	1.28736	1.28892	1.28736	-1.066	-0.3132-23885.2		8711.5
4	0.2382	1060.72	1060.70	2891.51	2893.83	2891.51	1.27277	1.27394	1.27277	-1.435	-0.3578-23286.8		9345.6
5	0.2419	1164.63	1164.59	2891.71	2893.03	2891.71	1.25588	1.25650	1.25588	-3.332	-0.4228-22844.4		9717.7
6	0.2453	1214.67	1214.62	2882.63	2883.04	2882.63	1.24262	1.24278	1.24262	5.918	-0.5106-22671.6		9922.3
7	0.2486	1215.96	1215.89	2855.12	2855.09	2855.12	1.22607	1.22600	1.22607	1.516	-0.6107-22681.4		9992.8
8	0.2518	1175.87	1175.78	2810.49	2810.09	2810.49	1.20958	1.20933	1.20958	0.880	-0.7132-22839.9		9984.1
9	0.2551	1099.42	1099.31	2751.08	2750.43	2751.08	1.18983	1.18943	1.18983	0.637	-0.8126-23073.9		9878.0
10	0.2584	989.67	989.55	2679.52	2678.74	2679.52	1.17185	1.17138	1.17185	0.519	-0.9061-23636.1		9661.1
11	0.2620	862.21	862.08	2603.40	2602.65	2603.40	1.16768	1.16723	1.16768	0.464	-0.9892-24721.6		9163.5

LOCATION	STAGN PRESSRE	STAGN TEMPTRE	STATIC PRESSRE	STATIC TEMPTRE	STATIC DENSITY	DELTA P UPON Q	DE HALL NUMBER	LOSS COEFF	DIFFUS FACTOR	RELATIVE EXIT ANG	ABSOLUTE FLOW ANG	NEXT-INL-ANGLE ACTUAL
1	23770.40	2529.00	7769.11	1936.34	0.07514-46.29801		8.04060	8.20000-11.92703		79.9592	79.9592	79.964
2	24330.89	2675.36	8790.57	2102.90	0.07828-43.79194		7.71887	6.84796-11.33858		75.8331	75.8331	75.897
3	24597.62	2802.20	9374.16	2234.40	0.07857-42.34742		7.53782	6.21315-10.95665		71.7517	71.7517	71.851
4	24671.21	2870.69	9593.32	2301.81	0.07805-41.46597		7.43825	5.99976-10.70966		68.4845	68.4845	68.601
5	24718.37	2933.98	9835.24	2367.13	0.07781-40.92302		7.36177	5.90410-10.52122		66.2555	66.2555	66.373
6	24738.62	2966.39	10019.90	2404.28	0.07805-40.54515		7.30455	5.87452-10.39369		65.0842	65.0842	65.194
7	24673.09	2974.36	10213.60	2423.52	0.07892-40.36505		7.25070	6.08325-10.30025		64.7992	64.7992	64.904
8	24596.21	2946.41	10400.53	2412.32	0.08074-40.25082		7.20123	6.32845-10.23066		65.2737	65.2737	65.373
9	24534.76	2900.25	10638.56	2387.79	0.08344-40.25088		7.15621	6.57569-10.20554		66.4519	66.4519	66.547
10	24479.73	2820.70	10854.80	2333.05	0.08713-40.45661		7.13250	6.83633-10.22396		68.3322	68.3322	68.422
11	24362.08	2677.00	10848.31	2213.51	0.09178-40.84343		7.14536	7.20000-10.30716		70.6671	70.6671	70.749

TOTAL AXIAL FORCE ON BLADES =-1015.33 TOTAL TANGENTIAL FORCE ON BLADES = 392.97

* * * STATION 8 * * *

MASS-AVERAGE TOTAL PRESSURE= 24540.7 MASS-AVERAGE TOTAL TEMPERATURE= 2849.33
CUMULATIVE TOTAL PRESSURE RATIO= 0.9036

ROTOR INLET

LOCATION	RADIUS	MERIDIONAL VELOCITY	AXIAL VELOCITY	ABSOLUTE VELOCITY	VEL REL TO NEXT BLADE	VEL REL TO THIS BLADE	ABSOLUTE MACH NUMBER	MACH NO REL NEXT BLADE	MACH NO REL THIS BLADE	RAD OF CURVTRE	STRMLNE SLOPE ANGLE	AXIAL BLADE LDING	TANGEN BLADE LDING
1	0.2220	547.64	547.64	2927.29	1579.52	2927.29	1.40132	0.75614	1.40132	-0.206	0.0	8.4	-0.4
2	0.2287	732.56	731.63	2892.86	1548.38	2892.86	1.33100	0.71249	1.33100	-0.216	-2.8899	8.5	5.7
3	0.2333	912.66	911.58	2883.76	1567.54	2838.76	1.29048	0.70034	1.29048	-0.245	-2.7032	4.3	8.7
4	0.2379	1054.59	1053.74	2891.55	1556.69	2891.55	1.27280	0.70290	1.27280	-0.314	-2.3039	-3.7	9.4
5	0.2417	1147.51	1147.04	2886.57	1611.00	2886.57	1.25313	0.69941	1.25313	-0.495	-1.6322	0.9	7.9
6	0.2451	1191.63	1191.49	2874.13	1604.73	2874.13	1.23813	0.69129	1.23813	-1.495	-0.8550	2.6	5.5
7	0.2484	1191.23	1191.23	2845.47	1569.54	2845.47	1.22101	0.67349	1.22101	1.283	-0.0338	3.0	3.9
8	0.2517	1153.01	1152.91	2801.47	1506.69	2801.47	1.20487	0.64798	1.20487	0.453	0.7694	2.6	2.3
9	0.2550	1081.43	1081.06	2744.14	1418.24	2744.14	1.18621	0.61302	1.18621	0.284	1.4975	1.1	0.9
10	0.2584	978.71	978.05	2675.48	1305.54	2675.48	1.16973	0.57074	1.16973	0.216	2.0958	-1.7	-0.1
11	0.2620	858.75	857.93	2602.17	1179.23	2602.17	1.16703	0.52883	1.16703	0.184	2.4991	-2.8	-0.4

LOCATION	STAGN PRESSRE	STAGN TEMPTRE	STATIC PRESSRE	STATIC TEMPTRE	STATIC DENSITY	DELTA P UPON Q	DE HALL NUMBER	LOSS COEFF	DIFFUS FACTOR	RELATIVE EXIT ANG	ABSOLUTE FLOW ANG	NEXT-INL-ANGLE ACTUAL
1	23770.40	2529.00	7721.88	1933.44	0.07430	-0.00295	1.00233	0.0	-0.00230	79.2234	79.2234	69.705
2	24330.87	2675.36	8723.41	2099.27	0.07787	-0.00400	1.00303	0.0	-0.00350	75.3546	75.3546	61.877
3	24597.62	2802.20	9234.19	2232.09	0.07832	-0.00262	1.00192	0.0	-0.00250	71.6083	71.6083	54.569
4	24671.21	2870.69	9592.25	2301.74	0.07805	-0.00007	1.00001	0.0	-0.00054	68.6308	68.6308	48.861
5	24719.37	2933.98	9870.53	2369.16	0.07803	0.00237	0.99822	0.0	0.00138	66.5893	66.5893	44.775
6	24738.62	2966.39	10078.83	2407.65	0.07840	0.00400	0.99705	0.0	0.00268	65.5128	65.5128	42.236
7	24673.09	2974.36	10280.72	2427.31	0.07932	0.00464	0.99662	0.0	0.00320	65.2559	65.2559	40.809
8	24596.21	2946.41	10463.61	2415.80	0.08112	0.00444	0.99679	0.0	0.00310	65.7030	65.7030	40.259
9	24534.76	2900.25	10687.52	2390.41	0.08373	0.00352	0.99748	0.0	0.00248	66.8030	66.8030	40.517
10	24479.73	2820.70	10883.44	2334.51	0.08731	0.00210	0.99849	0.0	0.00151	68.5609	68.5609	41.654
11	24362.08	2677.00	10856.74	2213.92	0.09184	0.00062	0.99953	0.0	0.00050	70.7527	70.7527	43.473

TOTAL AXIAL FORCE ON BLADES = 0.11 TOTAL TANGENTIAL FORCE ON BLADES = 0.18

* * * STATION 9 * * *

* * * STATION 9 * * * **ROTOR EXIT**

MASS-AVERAGE TOTAL PRESSURE= 7325.0 MASS-AVERAGE TOTAL TEMPERATURE= 2243.22
CUMULATIVE TOTAL PRESSURE RATIO= 0.2697

LOCATION	RADIUS	MERIDNAL VELOCITY	AXIAL VELOCITY	ABSOLUTE VELOCITY	VEL REL TO NEXT BLADE	VEL REL TO THIS BLADE	ABSOLUTE MACH NUMBER	MACH NO REL NEXT BLADE	MACH NO REL THIS BLADE	RAD OF CURVTRE	STRMLNE SLOPE ANGLE	AXIAL BLADE LOING	TANGEN BLADE LOING
1	0.2140	898.42	893.58	1053.15	1058.62	1193.25	0.49945	0.50430	0.56367	0.455	-5.9501	-336.2	-4705.5
2	0.2202	1056.77	1052.26	1061.33	1065.91	1663.83	0.49230	0.49420	0.77362	0.340	-5.2950	-1867.5	-6999.9
3	0.2260	1090.42	1088.11	1110.47	1110.82	1950.72	0.50671	0.50670	0.89577	0.292	-3.7301	-3566.8	-8548.1
4	0.2317	1079.88	1079.24	1132.41	1133.68	2095.93	0.51151	0.51204	0.94691	0.290	-1.9658	-4699.4	-9344.2
5	0.2375	1059.66	1059.65	1160.90	1163.26	2233.36	0.51997	0.52105	1.00012	0.330	-0.2352	-5698.0	-9883.5
6	0.2434	1033.25	1032.95	1170.34	1173.81	2321.02	0.52218	0.52382	1.03554	0.442	1.3853	-6466.5	-10160.4
7	0.2493	1012.96	1011.67	1178.00	1181.87	2392.19	0.52596	0.52779	1.06857	0.779	2.8905	-7083.6	-10327.9
8	0.2551	1004.51	1001.62	1159.34	1162.51	2401.36	0.52020	0.52173	1.07901	3.233	4.3493	-7482.8	-10352.7
9	0.2607	1005.30	1000.09	1146.44	1148.88	2408.59	0.51908	0.52028	1.09364	-2.171	5.8363	-7832.6	-10329.7
10	0.2660	1017.24	1008.76	1122.07	1123.62	2373.81	0.51538	0.51618	1.09588	-1.153	7.4048	-7791.8	-10163.3
11	0.2710	1032.72	1019.86	1078.94	1079.82	2264.07	0.50852	0.50901	1.07637	-1.255	9.0538	-7183.7	-10008.9

LOCATION	STAGN PRESSRE	STAGN TEMPTRE	STATIC PRESSRE	STATIC TEMPTRE	STATIC DENSITY	DELTA P UPON Q	DE HALL NUMBER	LOSS COEFF	DIFFUS FACTOR	RELATIVE EXIT ANG	ABSOLUTE FLOW ANG	NEXT-INL-ANGLE ACTUAL
1	7325.00	2067.36	6251.77	1990.86	0.05872	-0.44016	0.75569	0.90000	0.42799	-41.3128	32.0337	32.847
2	7325.00	2141.60	6270.63	2064.15	0.05987	-0.74909	1.07506	0.82390	-0.05544	-50.6933	5.3374	6.734
3	7325.00	2220.77	6208.49	2135.76	0.05447	-0.52756	1.25226	0.75552	-0.34734	-56.2715	-10.9265	-10.023
4	7325.00	2269.33	6190.97	2181.22	0.05318	-0.97408	1.31344	0.72715	-0.46577	-59.0066	-17.5306	-17.274
5	7325.00	2312.06	6160.53	2219.91	0.05197	-1.04395	1.38638	0.69730	-0.60245	-61.6800	-24.1082	-24.237
6	7325.00	2330.97	6155.68	2237.74	0.05150	-1.10928	1.44580	0.67635	-0.70604	-63.5769	-28.0187	-28.380
7	7325.00	2328.82	6143.19	2234.60	0.05145	-1.21534	1.52317	0.64885	-0.82658	-64.9804	-30.7289	-31.162
8	7325.00	2303.03	6166.06	2211.66	0.05217	-1.35001	1.59238	0.66202	-0.92648	-65.3397	-30.0249	-30.425
9	7325.00	2260.17	6168.76	2170.51	0.05319	-1.56822	1.69635	0.67645	-1.06865	-65.4481	-28.8583	-29.175
10	7325.00	2193.11	6180.64	2106.77	0.05492	-1.86950	1.81582	0.72863	-1.22318	-64.8159	-25.1492	-25.357
11	7325.00	2077.33	6204.39	1996.86	0.05818	-2.17990	1.91735	0.80000	-1.34230	-63.1571	-17.0320	-17.129

TOTAL AXIAL FORCE ON BLADES = -261.63 TOTAL TANGENTIAL FORCE ON BLADES = -446.86

* * * STATION 6 * * * STATOR INLET

MASS-AVERAGE TOTAL PRESSURE= 27158.4 MASS-AVERAGE TOTAL TEMPERATURE= 2860.00
CUMULATIVE TOTAL PRESSURE RATIO= 1.0000

LOCATION	RADIUS	MERIDNAL VELOCITY	AXIAL VELOCITY	ABSOLUTE VELOCITY	VEL REL TO NEXT BLADE	VEL REL TO THIS BLADE	ABSOLUTE MACH NUMBER	MACH NO REL NEXT BLADE	MACH NO REL THIS BLADE	RAD OF CURVTRE	STREMLNE SLOPE ANGLE	AXIAL BLADE LOSS	TANGEN BLADE LOSS
1	0.2220	389.38	389.38	389.38	389.44	389.38	0.15474	0.15477	0.15474*********		0.0	0.0	0.0
2	0.2270	389.37	389.37	389.37	389.44	389.37	0.15474	0.15476	0.15474	48.991	-0.0348	0.0	0.0
3	0.2319	389.29	389.29	389.29	389.34	389.29	0.15471	0.15472	0.15471	-41.186	-0.1472	0.0	0.0
4	0.2366	389.00	388.99	389.00	389.02	389.00	0.15459	0.15460	0.15459	-7.372	-0.3195	0.0	0.0
5	0.2413	388.39	388.37	388.39	388.39	388.39	0.15434	0.15435	0.15434	-3.561	-0.5217	0.0	0.0
6	0.2459	387.40	387.37	387.40	387.39	387.40	0.15395	0.15395	0.15395	-2.202	-0.7603	0.0	0.0
7	0.2504	385.99	385.93	385.99	385.97	385.99	0.15339	0.15338	0.15339	-1.519	-1.0152	-0.1	0.0
8	0.2549	384.15	384.05	384.15	384.11	384.15	0.15265	0.15264	0.15265	-1.135	-1.2571	-0.1	0.0
9	0.2593	381.85	381.72	381.85	381.81	381.85	0.15174	0.15172	0.15174	-0.891	-1.4846	-0.2	0.0
10	0.2637	379.09	378.93	379.09	379.06	379.09	0.15064	0.15063	0.15064	-0.722	-1.7124	-0.2	0.0
11	0.2680	376.25	376.25	376.25	376.22	376.25	0.14951	0.14949	0.14951	-0.597	0.0	0.1	0.0

LOCATION	STAGN PRESSRE	STAGN TEMPTRE	STATIC PRESSRE	STATIC TEMPTRE	STATIC DENSITY	DELTA P UPON Q	DF HALL NUMBER	LOSS COEFF	DIFFUS FACTOR	RELATIVE EXIT ANG	ABSOLUTE FLOW ANG	NEXT-INL-ANGLE ACTUAL
1	27158.40	2860.00	26741.90	2849.99	0.17573	-0.01643	1.00325	0.0	0.0	0.0	0.0	0.0
2	27158.40	2860.00	26741.90	2849.99	0.17573	-0.01655	1.00331	0.0	0.0	0.0	0.0	0.0
3	27158.40	2860.00	26742.08	2850.00	0.17573	-0.01650	1.00329	0.0	0.0	0.0	0.0	0.0
4	27158.40	2860.00	26742.70	2850.01	0.17574	-0.01554	1.00781	0.0	0.0	0.0	0.0	0.0
5	27158.40	2860.00	26744.00	2850.05	0.17574	-0.01314	1.00661	0.0	0.0	0.0	0.0	0.0
6	27158.40	2860.00	26746.09	2850.10	0.17576	-0.00938	1.00468	0.0	0.0	0.0	0.0	0.0
7	27158.40	2860.00	26749.06	2850.17	0.17577	-0.00252	1.00129	0.0	0.0	0.0	0.0	0.0
8	27158.40	2860.00	26752.94	2850.26	0.17579	0.00611	0.99695	0.0	0.0	0.0	0.0	0.0
9	27158.40	2860.00	26757.75	2850.38	0.17581	0.01712	0.99137	0.0	0.0	0.0	0.0	0.0
10	27158.40	2860.00	26763.48	2850.52	0.17584	0.03067	0.98448	0.0	0.0	0.0	0.0	0.0
11	27158.40	2860.00	26769.35	2850.66	0.17587	0.04488	0.97720	0.0	0.0	0.0	0.0	0.0

TOTAL AXIAL FORCE ON BLADES = -0.00 TOTAL TANGENTIAL FORCE ON BLADES = 0.0

STREAMLINE ANALYSIS RUN 7 CONSTANT TIP RADIUS WITH VARIABLE LOSSES AND WORK

BEST AVAILABLE COPY

* * * STATION 7 * * * STATOR EXIT

MASS-AVERAGE TOTAL PRESSURE= 24507.9 MASS-AVERAGE TOTAL TEMPERATURE= 2860.00
CUMULATIVE TOTAL PRESSURE RATIO= 0.9024

LOCATION	RADIUS	MERIDNAL VELOCITY	AXIAL VELOCITY	ABSOLUTE VELOCITY	VEL REL TO NEXT BLADE	VEL REL TO THIS BLADE	ABSOLUTE MACH NUMBER	MACH NO REL NEXT BLADE	MACH NO REL THIS BLADE	RAD OF CURVTRE	STREAMLINE SLOPE ANGLE	AXIAL BLADE LOING	TANGEN BLADE LOING
1	0.2220	956.50	956.50	3031.09	3031.26	3031.09	1.35391	1.35400	1.35391	-0.221	0.0	-24139.3	9313.7
2	0.2270	970.46	963.05	2979.93	2979.87	2979.83	1.32402	1.32404	1.32402	-0.275	-7.0	-23856.1	9683.1
3	0.2316	981.07	976.15	2933.66	2933.59	2933.66	1.29897	1.29893	1.29897	-0.350	-5.7	-23554.6	9854.0
4	0.2359	988.97	986.05	2888.68	2888.75	2888.88	1.27421	1.27414	1.27421	-0.502	-4.4	-23401.7	9972.4
5	0.2400	994.07	992.66	2844.92	2844.92	2844.97	1.25022	1.25014	1.25022	-0.963	-3.0	-23314.6	9221.2
6	0.2440	994.72	994.29	2806.73	2806.65	2806.73	1.22955	1.22950	1.22955	-52.579	-1.6	-23242.4	9329.4
7	0.2477	990.87	990.86	2773.26	2773.26	2773.26	1.21163	1.21163	1.21163	0.375	-0.3	-23187.3	9394.3
8	0.2514	985.33	985.19	2739.09	2739.18	2739.09	1.19368	1.19352	1.19368	0.480	0.0	-23122.5	9421.9
9	0.2550	981.57	980.55	2706.32	2706.48	2706.32	1.17622	1.17629	1.17622	0.306	2.4	-23062.0	9453.3
10	0.2586	980.32	977.21	2675.40	2675.60	2675.40	1.16005	1.16015	1.16005	0.208	4.9	-23006.8	9481.6
11	0.2620	982.30	973.59	2646.00	2646.23	2646.00	1.14479	1.14491	1.14479	0.154	7.6	-22956.2	9507.9

LOCATION	STAGN PRESSRE	STAGN TEMPTRE	STATIC PRESSRE	STATIC TEMPTRE	STATIC DENSITY	DELTA P UPON Q	DE HALL NUMBER	LOSS COEFF	DIFFUS FACTOR	RELATIVE EXIT ANG	ABSOLUTE FLOW ANG	NEXT-TAL-ACTUAL
1	23741.65	2860.00	8266.86	2232.61	0.06932	-44.35474	7.78448	8.20000	-11.34419	71.6104	71.6104	71.603
2	24223.83	2860.00	8781.88	2254.40	0.07293	-43.11863	7.65226	7.03108	-11.11930	71.1336	71.1336	71.134
3	24451.93	2860.00	9120.43	2273.67	0.07560	-42.17934	7.53587	6.49893	-10.91981	70.5526	70.5526	70.555
4	24536.56	2860.00	9363.40	2292.32	0.07810	-41.32795	7.42649	6.09534	-10.73375	70.0403	70.0403	70.049
5	24603.09	2860.00	9558.48	2309.71	0.08024	-40.64730	7.32506	5.78541	-10.56169	69.5603	69.5603	69.563
6	24730.92	2860.00	10185.09	2324.86	0.08202	-40.16360	7.24504	5.58750	-10.42700	69.2562	69.2562	69.261
7	24704.58	2860.00	10415.02	2337.94	0.08341	-39.90101	7.18476	5.49407	-10.32704	69.0712	69.0712	69.071
8	24631.30	2860.00	10617.26	2351.10	0.08455	-39.79390	7.13033	6.30751	-10.23712	68.9243	68.9243	68.920
9	24523.35	2860.00	10819.96	2363.56	0.08571	-39.77691	7.08735	6.57771	-10.16435	68.7963	68.7963	68.791
10	24453.70	2860.00	11012.52	2375.15	0.08681	-39.88132	7.05732	6.84960	-10.11039	68.5705	68.5705	68.581
11	24357.49	2860.00	11181.39	2386.04	0.08774	-40.06397	7.03253	7.20000	-10.06338	68.3483	68.3483	68.378

TOTAL AXIAL FORCE ON BLADES =-1009.42 TOTAL TANGENTIAL FORCE ON BLADES = 394.05

BEST AVAILABLE COPY

• • • STATION 8 • • • ROTOR INLET

MASS-AVERAGE TOTAL PRESSURE= 24507.9 MASS-AVERAGE TOTAL TEMPERATURE= 2860.00
CUMULATIVE TOTAL PRESSURE RATIO= 0.9024

LOCATION	RADIUS	MERIDNAL VELOCITY	AXIAL VELOCITY	ABSOLUTE VELOCITY	VEL REL TO NEXT BLADE	VEL REL TO THIS BLADE	ABSOLUTE MACH NUMBER	MACH NO REL NEXT BLADE	MACH NO REL THIS BLADE	RAD OF CURVTRE	STRMLNE SLOPE ANGLE	AXIAL BLADE LOING	TANGEN BLADE LOING
1	0.2190	873.56	857.35	3007.36	1738.12	3007.36	1.34020	0.77460	1.34020	-1.074	-11.0572	383.3	3.4
2	0.2245	878.24	868.79	2954.49	1662.30	2954.49	1.31642	0.73717	1.31042	1.299	-8.4119	305.1	19.1
3	0.2296	879.11	873.55	2906.53	1592.65	2906.53	1.28377	0.70346	1.28377	0.760	-6.4596	235.1	17.4
4	0.2345	876.04	873.10	2859.11	1525.32	2859.11	1.25776	0.67101	1.25776	0.723	-4.6037	125.7	23.9
5	0.2391	869.70	868.49	2812.97	1460.32	2812.97	1.23277	0.63997	1.23277	0.844	-3.0240	37.5	32.7
6	0.2435	860.99	860.73	2769.54	1398.69	2769.54	1.20950	0.61062	1.20950	1.516	-1.4106	-5.3	27.6
7	0.2478	850.96	850.96	2724.80	1337.15	2724.80	1.18580	0.58100	1.18580	-61.321	0.1730	27.2	-7.0
8	0.2520	827.16	826.84	2638.84	1239.16	2638.84	1.14097	0.53573	1.14097	-1.431	1.5087	524.7	-154.0
9	0.2562	783.28	781.97	2650.58	1210.45	2650.58	1.14704	0.52382	1.14704	-0.567	3.3263	-174.8	37.7
10	0.2605	738.01	734.56	2601.24	1131.77	2601.24	1.12164	0.49802	1.12164	-0.248	5.5437	-219.5	15.4
11	0.2650	700.40	700.40	2556.01	1059.20	2556.01	1.09860	0.45927	1.09860	-0.176	0.0	-206.3	3.2

LOCATION	STAGN PRESSRE	STAGN TEMPTRE	STATIC PRESSRE	STATIC TEMPTRE	STATIC DENSITY	DELTA P UPON Q	DE HALL NUMBER	LOSS COEFF	DIFFUS FACTOR	RELATIVE EXIT ANG	ABSOLUTE FLOW ANG	NEXT-INL-ANGLE ACTUAL
1	23741.65	2860.00	8433.16	2243.40	0.07033	0.01074	0.98217	0.0	0.00753	73.4150	73.4150	60.256
2	24228.83	2860.00	8964.54	2265.64	0.07403	0.01132	0.98156	0.0	0.00776	72.8476	72.8476	58.361
3	24451.90	2860.00	9379.01	2285.43	0.07676	0.01299	0.96375	0.0	0.00806	72.3045	72.3045	56.424
4	24636.56	2860.00	9783.94	2304.64	0.07943	0.01462	0.98869	0.0	0.00875	72.2188	72.2188	55.054
5	24698.09	2860.00	10137.25	2322.98	0.08165	0.01612	0.98875	0.0	0.00919	72.0192	72.0192	53.817
6	24731.92	2860.00	10463.11	2339.93	0.08367	0.01610	0.98475	0.0	0.01155	71.8982	71.8982	52.053
7	24704.98	2860.00	10775.85	2357.02	0.08555	0.02523	0.98263	0.0	0.01785	71.8073	71.8073	50.815
8	24631.30	2860.00	11055.54	2373.17	0.08694	0.05276	0.98340	0.0	0.04784	71.7443	71.7443	48.167
9	24523.37	2860.00	11234.14	2384.86	0.08815	0.13020	0.97940	0.0	0.01928	72.8441	72.8441	46.732
10	24494.70	2860.00	11561.04	2402.66	0.09004	0.34076	0.97228	0.0	0.02651	73.5963	73.5963	48.332
11	24357.48	2860.00	11844.66	2419.01	0.09163	0.05031	0.96599	0.0	0.03372	74.1017	74.1017	48.521

TOTAL AXIAL FORCE ON BLADES = 4.37 TOTAL TANGENTIAL FORCE ON BLADES = -0.35

STATOR EXIT

* * * STATION 9 * * * ROTOR EXIT

MASS-AVERAGE TOTAL PRESSURE= 7690.7 MASS-AVERAGE TOTAL TEMPERATURE= 2263.75

CUMULATIVE TOTAL PRESSURE RATIO= 0.2632

LOCATION	RADIUS	MERIONAL VELOCITY	AXIAL VELOCITY	ABSOLUTE VELOCITY	VEL REL TO NEXT BLADE	VEL REL TO THIS BLADE	ABSOLUTE MACH NUMBER	MACH NO REL NEXT BLADE	MACH NO REL THIS BLADE	RAD OF CURVTRE	STRMLNE SLOPE ANGLE	AXIAL BLADE LOADG	TANGEN BLADE LOADG
1	0.2080	539.87	539.87	539.87	538.82	1413.31	0.23805	0.23759	0.62289	0.175	0.0	-2570.6	-4231.4
2	0.2191	778.72	778.29	817.88	818.03	1797.42	0.36557	0.36564	0.80354	0.264	-1.3947	-3306.8	-5647.2
3	0.2256	889.31	889.71	947.02	947.30	1955.66	0.42582	0.42595	0.87920	0.386	-0.8654	-3564.6	-7005.4
4	0.2321	980.71	980.69	1046.96	1047.32	2071.27	0.47282	0.47298	0.93522	0.592	-0.2757	-4415.9	-8662.9
5	0.2378	1055.55	1055.55	1124.27	1124.68	2156.87	0.50931	0.50950	0.97639	0.974	0.2433	-4975.4	-9175.0
6	0.2430	1114.79	1114.78	1182.63	1183.07	2221.47	0.53692	0.53713	1.00838	1.662	0.2834	-5294.0	-9647.0
7	0.2479	1158.83	1158.81	1225.06	1225.53	2272.35	0.55694	0.55716	1.03289	6.221	0.3693	-5707.3	-9934.5
8	0.2525	1193.78	1193.75	1274.71	1275.10	2357.73	0.58033	0.58051	1.07320	-6.584	0.4000	-6469.8	-10145.1
9	0.2569	1228.83	1228.80	1279.86	1280.28	2323.17	0.58250	0.58269	1.05717	-3.223	0.3056	-6166.2	-10014.4
10	0.2611	1274.88	1274.87	1318.71	1319.07	2352.52	0.60039	0.60055	1.07088	-4.104	0.2241	-6460.6	-9954.6
11	0.2650	1330.27	1330.27	1363.56	1363.83	2372.27	0.62074	0.62086	1.07977********		0.0	-8626.9	-10027.9

LOCATION	STAGN PRESSRE	STAGN TEMPTRE	STATIC PRESSRE	STATIC TEMPTRE	STATIC DENSITY	DELTA P UPON Q	DE HALL NUMBER	LOSS COEFF	DIFFUS FACTOR	RELATIVE EXIT ANG	ABSOLUTE FLOW ANG	NEXT-INL ANGLE ACTUAL
1	6796.38	2313.30	6550.36	2293.43	0.05348	-0.49118	0.81342	0.90000	0.23254	-67.5403	0.0351	-0.160
2	7087.96	2275.37	6893.15	2229.51	0.05461	-0.67751	1.03179	0.77245	-0.13434	-64.3446	-17.3125	-17.870
3	7267.08	2263.63	6981.22	2202.10	0.05513	-0.84593	1.22306	0.72717	-0.33630	-62.9429	-20.0212	-20.035
4	7478.26	2257.36	6975.39	2182.12	0.05559	-1.02885	1.35788	0.69461	-0.51512	-61.7444	-20.4969	-20.432
5	7632.18	2254.89	6960.90	2168.09	0.05582	-1.22531	1.47674	0.67395	-0.67869	-60.7039	-20.1379	-20.113
6	7790.53	2254.32	6976.27	2158.24	0.05621	-1.42518	1.58785	0.65866	-0.83170	-59.8837	-19.5302	-19.470
7	7873.73	2255.30	6960.19	2152.16	0.05623	-1.66617	1.69858	0.66001	-0.98631	-59.1431	-19.0217	-19.[illegible]
8	8025.25	2257.62	6971.53	2145.98	0.05650	-2.13947	1.90225	0.66498	-1.27543	-58.5155	-20.9278	-20.860
9	8030.22	2259.89	6964.86	2147.20	0.05641	-2.21710	1.91021	0.69519	-1.26019	-58.0707	-19.2203	-19.202
10	8149.82	2265.40	6974.46	2145.69	0.05654	-2.67401	2.07926	0.74149	-1.49154	-57.1897	-14.9141	-14.766
11	8296.74	2274.20	6989.64	2146.15	0.05666	-3.18589	2.24147	0.80000	-1.70239	-55.8959	-12.6875	-12.671

TOTAL AXIAL FORCE ON BLADES = -251.70 TOTAL TANGENTIAL FORCE ON BLADES = -447.45

BEST AVAILABLE COPY

* * STATION 6 * * * STATOR INLET

MASS-AVERAGE TOTAL PRESSURE= 27158.4 MASS-AVERAGE TOTAL TEMPERATURE= 2860.00
CUMULATIVE TOTAL PRESSURE RATIO= 1.0000

A-IN	RADIUS	MERIDNAL VELOCITY	AXIAL VELOCITY	ABSOLUTE VELOCITY	VEL REL TO NEXT BLADE	VEL REL TO THIS BLADE	ABSOLUTE MACH NUMBER	MACH NO REL NEXT BLADE	MACH NO REL THIS BLADE	RAD OF CURVTRE	STRMLNE SLOPE ANGLE	AXIAL BLADE LDING	TANGEN BLADE LDING
	0.2220	390.58	390.58	390.58	390.74	390.58	0.15517	0.15523	0.15517*********		0.0	0.4	0.0
	0.2270	390.46	390.46	390.46	390.59	390.46	0.15512	0.15517	0.15512	-23.144	-0.0745	0.4	0.0
	0.2318	390.08	390.08	390.08	390.15	390.08	0.15497	0.15500	0.15497	-7.649	-0.2089	0.4	0.0
	0.2366	389.41	389.40	389.41	389.40	389.41	0.15470	0.15470	0.15470	-3.918	-0.3885	0.4	0.0
	0.2413	388.42	388.39	388.42	388.34	388.42	0.15431	0.15428	0.15431	-2.443	-0.5989	0.4	0.0
	0.2459	387.09	387.05	387.09	386.97	387.09	0.15378	0.15373	0.15378	-1.705	-0.8268	0.4	0.0
	0.2504	385.44	385.37	385.44	385.30	385.44	0.15312	0.15307	0.15312	-1.282	-1.0597	0.3	0.0
	0.2549	383.46	383.37	383.46	383.35	383.46	0.15233	0.15229	0.15233'	-1.015	-1.2880	0.2	0.0
	0.2593	381.17	381.04	381.17	381.13	381.17	0.15142	0.15140	0.15142	-0.832	-1.5075	0.1	0.0
	0.2637	378.57	378.40	378.57	378.65	378.57	0.15038	0.15042	0.15038	-0.699	-1.7177	-0.1	0.0
	0.2680	375.94	375.94	375.94	376.13	375.94	0.14933	0.14941	0.14933	-0.597	0.0	0.5	0.0

A-IN	STAGN PRESSRE	STAGN TEMPTRE	STATIC PRESSRE	STATIC TEMPTRE	STATIC DENSITY	DELTA P UPON Q	DF HALL NUMBER	LOSS COEFF	DIFFUS FACTOR	RELATIVE EXIT ANG	ABSOLUTE FLOW ANG	NEXT-INL-ANGLE ACTUAL
	27158.40	2860.00	26739.56	2849.92	0.17572	-0.02373	1.01219	0.0	0.0	0.0	0.0	0.0
	27158.40	2860.00	26739.82	2849.92	0.17572	-0.02317	1.01190	0.0	0.0	0.0	0.0	0.0
	27158.40	2860.00	26740.63	2849.94	0.17573	-0.02137	1.01101	0.0	0.0	0.0	0.0	0.0
	27158.40	2860.00	26742.07	2849.98	0.17573	-0.01813	1.00940	0.0	0.0	0.0	0.0	0.0
	27158.40	2860.00	26744.18	2850.03	0.17575	-0.01332	1.00699	0.0	0.0	0.0	0.0	0.0
	27158.40	2860.00	26746.97	2850.10	0.17576	-0.00686	1.00376	0.0	0.0	0.0	0.0	0.0
	27158.40	2860.00	26750.46	2850.18	0.17578	0.00129	0.99967	0.0	0.0	0.0	0.0	0.0
	27158.40	2860.00	26754.61	2850.28	0.17580	0.01109	0.99472	0.0	0.0	0.0	0.0	0.0
	27158.40	2860.00	26759.40	2850.40	0.17582	0.02251	0.98893	0.0	0.0	0.0	0.0	0.0
	27158.40	2860.00	26764.79	2850.53	0.17585	0.03551	0.98229	0.0	0.0	0.0	0.0	0.0
	27158.40	2860.00	26770.21	2850.66	0.17588	0.04873	0.97550	0.0	0.0	0.0	0.0	0.0

TOTAL AXIAL FORCE ON BLADES = 0.01 TOTAL TANGENTIAL FORCE ON BLADES = 0.0

STREAMLINE ANALYSIS RUN 7A CONSTANT TIP RADIUS BLADE WITH VARIABLE LOSSES AND WORK AND CONSTANT EXIT TOTAL PRESSURE (DESIGN VELOCITY TRIANGLES)

* * * STATION 7 * * *

MASS-AVERAGE TOTAL PRESSURE= 24506.3 MASS-AVERAGE TOTAL TEMPERATURE= 2860.00
CUMULATIVE TOTAL PRESSURE RATIO= 0.9023

LOCATION	RADIUS	MERIDNAL VELOCITY	AXIAL VELOCITY	ABSOLUTE VELOCITY	VEL REL TO NEXT BLADE	VEL REL TO THIS BLADE	ABSOLUTE MACH NUMBER	MACH NO REL NEXT BLADE	MACH NO REL THIS BLADE	RAD OF CURVTRE	STRMLNE SLOPE ANGLE	AXIAL BLADE LOING	TANGEN BLADE LOING
1	0.2220	964.96	964.96	3034.48	3035.12	3034.48	1.35629	1.35660	1.35629	-0.221	0.0	-24101.8	8290.4
2	0.2269	975.23	967.53	2983.17	2984.55	2983.17	1.32736	1.32808	1.32736	-0.283	-7.2041	-23817.0	8620.6
3	0.2315	983.27	978.11	2936.75	2938.54	2936.75	1.30151	1.30246	1.30151	-0.378	-5.8733	-23641.6	8847.7
4	0.2359	989.91	986.83	2891.74	2893.71	2891.74	1.27674	1.27778	1.27674	-0.592	-4.5258	-23441.3	9050.7
5	0.2400	995.13	993.64	2848.83	2850.80	2848.83	1.25338	1.25441	1.25338	-1.482	-3.1394	-23301.3	9202.3
6	0.2439	997.24	996.80	2809.53	2811.10	2809.53	1.23221	1.23301	1.23221	2.535	-1.6886	-23207.1	9328.9
7	0.2477	995.31	995.31	2776.51	2777.94	2776.51	1.21456	1.21528	1.21456	0.660	-0.1393	-23227.9	9411.8
8	0.2514	991.44	991.07	2742.71	2743.96	2742.71	1.19664	1.19726	1.19664	0.371	1.5531	-23282.7	9452.1
9	0.2550	988.99	987.23	2710.17	2711.18	2710.17	1.17953	1.18002	1.17953	0.255	3.4160	-23312.9	9493.8
10	0.2585	989.04	984.56	2679.29	2680.01	2679.29	1.16340	1.16374	1.16340	0.192	5.4592	-23350.7	9532.9
11	0.2620	990.83	982.04	2649.77	2650.15	2649.77	1.14808	1.14824	1.14808	0.154	7.6388	-23415.3	9572.5

LOCATION	STAGN PRESSRE	STAGN TEMPTRE	STATIC PRESSRE	STATIC TEMPTRE	STATIC DENSITY	DELTA P UPON Q	DE HALL NUMBER	LOSS COEFF	DIFFUS FACTOR	RELATIVE EXIT ANG	ABSOLUTE FLOW ANG	NEXT-INL-ANGLE ACTUAL
1	23718.99	2860.00	8279.44	2251.60	0.06892	-44.04629	7.76907	8.20000	-11.31585	71.4633	71.4633	71.451
2	24204.80	2860.00	8791.10	2272.00	0.07242	-42.85242	7.64007	7.04707	-11.09704	71.0637	71.0637	71.071
3	24432.65	2860.00	9190.21	2290.16	0.07510	-41.98276	7.52851	6.51816	-10.90752	70.5387	70.5387	70.559
4	24627.95	2860.00	9576.17	2307.49	0.07767	-41.20457	7.42598	6.07440	-10.73297	70.0441	70.0441	70.072
5	24697.08	2860.00	9904.73	2323.76	0.07978	-40.62662	7.33448	5.94059	-10.57674	69.5880	69.5880	69.617
6	24736.09	2860.00	10199.31	2338.45	0.08163	-40.19427	7.25803	5.88760	-10.44657	69.2231	69.2231	69.246
7	24716.68	2860.00	10427.13	2350.64	0.0830	-39.90823	7.20349	5.90589	-10.35456	68.9986	68.9986	69.016
8	24614.03	2860.00	10625.59	2362.97	0.084	-39.91836	7.15249	6.30067	-10.26905	68.8210	68.8210	68.832
9	24534.59	2860.00	10824.45	2374.69	0.085	-39.91091	7.11013	6.57301	-10.19643	68.6371	68.6371	68.643
10	24460.55	2860.00	11013.43	2385.69	0.08641	-39.99132	7.07735	6.84673	-10.13753	68.4315	68.4315	68.434
11	24358.80	2860.00	11179.47	2396.08	0.08733	-40.13664	7.04837	7.20000	-10.08360	68.2233	68.2233	68.223

TOTAL AXIAL FORCE ON BLADES =-1008.11 TOTAL TANGENTIAL FORCE ON BLADES = 394.08

* * * STATION 8 * * *

THE STAGE EFFICIENCY PRINTED BELOW REFERS TO THE TWO PRECEDING BLADE ROWS
THE RELATIVE VELOCITIES AND MACHNUMBERS REFER TO THE BLADE-ROW FOLLOWING THIS STATION

MASS-AVERAGE TOTAL PRESSURE= 24506.3 MASS-AVERAGE TOTAL TEMPERATURE= 2860.00
CUMULATIVE TOTAL PRESSURE RATIO= 0.9023

LOCATION	RADIUS	MERIONAL VELOCITY	AXIAL VELOCITY	ABSOLUTE VELOCITY	VEL REL TO NEXT BLADE	VEL REL TO THIS BLADE	ABSOLUTE MACH NUMBER	MACH NO REL NEXT BLADE	MACH NO REL THIS BLADE	RAD OF CURVTRE	STRMLNE SLOPE ANGLE	AXIAL BLADE LDING	TANGEN BLADE LDING
1	0.2190	901.44	884.72	3016.50	1751.92	3016.50	1.34590	0.78166	1.34590	-1.074	-11.0572	384.2	4.2
2	0.2244	899.70	887.52	2963.14	1675.27	2963.14	1.31597	0.74402	1.31597	-0.789	-9.4419	304.8	11.5
3	0.2295	894.64	886.27	2914.00	1604.02	2914.00	1.28877	0.70942	1.28877	-0.641	-7.8473	208.5	18.7
4	0.2343	886.36	881.19	2865.11	1534.22	2865.11	1.26205	0.67581	1.26205	-0.543	-6.1911	135.0	24.8
5	0.2389	874.64	871.99	2817.12	1468.96	2817.12	1.23611	0.64325	1.23611	-0.469	-4.4629	56.2	29.3
6	0.2434	857.89	856.97	2770.52	1408.72	2770.52	1.21122	0.61149	1.21122	-0.408	-2.6542	-1.9	27.4
7	0.2477	835.47	835.40	2730.44	1335.98	2730.44	1.19003	0.58227	1.19003	-0.352	-0.7522	-60.7	26.9
8	0.2521	809.68	809.48	2688.94	1271.44	2688.94	1.16828	0.55241	1.16828	-0.300	1.2649	-111.3	24.8
9	0.2564	783.80	782.41	2647.64	1207.53	2647.64	1.14685	0.52305	1.14685	-0.253	3.4135	-159.9	20.4
10	0.2607	758.98	755.22	2606.83	1144.92	2606.83	1.12585	0.49449	1.12585	-0.213	5.7004	-194.4	13.4
11	0.2650	734.88	734.88	2566.46	1083.58	2566.46	1.10526	0.46667	1.10526	-0.176	0.0	-195.9	4.3

LOCATION	STAGN PRESSRE	STAGN TEMPTRE	STATIC PRESSRE	STATIC TEMPTRE	STATIC DENSITY	DELTA P UPON Q	DE HALL NUMBER	LOSS COEFF	DIFFUS FACTOR	RELATIVE EXIT ANG	ABSOLUTE FLOW ANG	NEXT-INL-ANGLE ACTUAL
1	23718.99	2860.00	8407.97	2259.49	0.06958	0.00831	0.99408	0.0	0.00558	72.9213	72.9213	59.530
2	24204.80	2860.00	8937.67	2280.55	0.07329	0.00950	0.99329	0.0	0.00589	72.5543	72.5543	57.918
3	24432.55	2860.00	9359.39	2299.61	0.07611	0.01102	0.99225	0.0	0.00648	72.2827	72.2827	56.413
4	24627.95	2860.00	9774.39	2318.26	0.07885	0.01315	0.99079	0.0	0.00760	72.0827	72.0827	54.938
5	24697.08	2860.00	10141.16	2335.26	0.08119	0.01596	0.98887	0.0	0.00928	71.9687	71.9687	53.522
6	24736.09	2860.00	10490.01	2353.44	0.08337	0.01997	0.98611	0.0	0.01218	71.9853	71.9853	52.251
7	24716.68	2860.00	10769.96	2367.99	0.08507	0.02396	0.98341	0.0	0.01493	72.1893	72.1893	51.319
8	24614.03	2860.00	11024.28	2382.83	0.08654	0.02846	0.98039	0.0	0.01806	72.4848	72.4848	50.439
9	24534.59	2860.00	11286.89	2397.37	0.08807	0.03368	0.97693	0.0	0.02178	72.8143	72.8143	49.517
10	24460.55	2860.00	11548.08	2411.53	0.08958	0.03971	0.97296	0.0	0.02616	73.1576	73.1576	48.504
11	24358.80	2860.00	11792.08	2425.31	0.09096	0.04642	0.96856	0.0	0.03110	73.3664	73.3664	47.119

TOTAL AXIAL FORCE ON BLADES = 1.82 TOTAL TANGENTIAL FORCE ON BLADES = 0.86

* * * STATION 9 * * *

* * * TION 9 * * *

MASS-AVERAGE TOTAL PRESSURE= 7325.0 MASS-AVERAGE TOTAL TEMPERATURE= 2262.15
CUMULATIVE TOTAL PRESSURE RATIO= 0.2697

ROTOR EXIT

LOCATION	RADIUS	MERIONAL VELOCITY	AXIAL VELOCITY	ABSOLUTE VELOCITY	VEL REL TO NEXT BLADE	VEL REL TO THIS BLADE	ABSOLUTE MACH NUMBER	MACH NO REL NEXT BLADE	MACH NO REL THIS BLADE	RAD OF CURVTRE	STRMLNE SLOPE ANGLE	AXIAL BLADE LOING	TANGEN BLADE LOING
1	0.2083	1033.14	1033.14	1043.98	1038.17	1550.83	0.46235	0.46017	0.68675	0.175	0.0	-1735.7	-6512.0
2	0.2145	1066.70	1064.10	1069.21	1073.61	1776.75	0.47338	0.48057	0.79607	0.197	-3.9998	-2628.0	-7479.7
3	0.2207	1071.24	1069.26	1093.51	1100.83	1930.71	0.49297	0.49638	0.87130	0.223	-3.4925	-3434.6	-8106.4
4	0.2268	1068.27	1066.83	1111.18	1117.93	2033.53	0.50341	0.50701	0.92170	0.258	-2.9725	-4223.3	-8510.2
5	0.2326	1063.48	1062.50	1125.44	1131.46	2116.24	0.51186	0.51512	0.96286	0.309	-2.4659	-4971.4	-8810.5
6	0.2383	1058.14	1057.50	1135.76	1141.53	2183.50	0.51815	0.52084	0.99632	0.387	-1.9882	-5695.8	-9018.4
7	0.2439	1056.09	1055.70	1142.68	1146.96	2234.18	0.52257	0.52458	1.02174	0.513	-1.5448	-6293.2	-9160.3
8	0.2494	1058.23	1058.02	1142.68	1145.45	2260.84	0.52296	0.52427	1.03461	0.733	-1.1290	-6788.5	-9192.5
9	0.2547	1061.55	1061.47	1144.86	1146.27	2289.89	0.52445	0.52510	1.04879	1.185	-0.7353	-7304.0	-9211.7
10	0.2599	1065.72	1065.69	1143.12	1143.61	2307.24	0.52368	0.52389	1.05676	2.560	-0.3620	-7810.1	-9185.6
11	0.2650	1070.56	1070.56	1140.09	1139.93	2318.72	0.52209	0.52197	1.06159	********	0.0	-8306.2	-9167.1

LOCATION	STAGN PRESSRE	STAGN TEMPTRE	STATIC PRESSRE	STATIC TEMPTRE	STATIC DENSITY	DELTA P UPON Q	DE HALL NUMBER	LOSS COEFF	DIFFUS FACTOR	RELATIVE EXIT ANG	ABSOLUTE FLOW ANG	NEXT-INL-ANGLE ACTUAL
1	7325.00	2365.79	6388.20	2293.35	0.05220	-0.52157	0.88452	0.90000	0.19742	-48.2304	8.2650	4.375
2	7325.00	2322.41	6334.59	2246.99	0.05278	-0.70024	1.06038	0.82016	-0.06222	-53.1748	-3.9361	-6.645
3	7325.00	2292.05	6280.31	2213.29	0.05312	-0.89075	1.20343	0.74953	-0.27473	-56.3532	-11.6031	-13.499
4	7325.00	2272.87	6240.28	2191.58	0.05330	-1.09129	1.32506	0.72136	-0.45471	-58.3484	-15.9966	-17.460
5	7325.00	2257.98	6206.90	2174.57	0.05343	-1.30595	1.44299	0.69257	-0.62834	-59.8596	-19.1184	-20.227
6	7325.00	2246.18	6181.10	2161.16	0.05354	-1.54500	1.56030	0.67140	-0.79979	-61.0325	-21.3192	-22.136
7	7325.00	2236.95	6161.99	2150.76	0.05364	-1.79058	1.67158	0.64681	-0.96011	-61.8038	-22.4580	-23.033
8	7325.00	2233.86	6158.17	2147.49	0.05371	-2.07064	1.77776	0.66264	-1.11103	-62.1002	-22.1712	-22.545
9	7325.00	2230.46	6149.65	2143.54	0.05375	-2.40225	1.89659	0.67674	-1.27986	-62.3680	-21.9960	-22.172
10	7325.00	2230.11	6150.18	2143.26	0.05378	-2.78362	2.01653	0.72734	-1.44995	-62.4952	-21.2082	-21.241
11	7325.00	2231.53	6154.30	2144.94	0.05379	-3.22300	2.14282	0.80000	-1.62896	-62.5077	-20.1154	-20.032

TOTAL AXIAL FORCE ON BLADES = -272.08 TOTAL TANGENTIAL FORCE ON BLADES = -443.57

* * * STATION10 * * *

* * * STATION 6 * * * STATOR INLET

MASS-AVERAGE TOTAL PRESSURE= 27158.4 MASS-AVERAGE TOTAL TEMPERATURE= 2860.00
CUMULATIVE TOTAL PRESSURE RATIO= 1.0000

LOCATION	RADIUS	MERIDIONAL VELOCITY	AXIAL VELOCITY	ABSOLUTE VELOCITY	VEL REL TO NEXT BLADE	VEL REL TO THIS BLADE	ABSOLUTE MACH NUMBER	MACH NO REL NEXT BLADE	MACH NO REL THIS BLADE	RAD OF CURVTRE	STREAM SLOPE ANGLE	AXIAL BLADE LOAD	TANGEN BLADE LOAD
1	0.2220	402.93	402.93	402.93	402.55	402.93	0.16014	0.15999	0.16014	*********	0.0	0.1	0.0
2	0.2263	402.01	401.97	402.01	401.65	402.01	0.15978	0.15963	0.15978	-1.998	-3.2267	0.1	0.0
3	0.2316	399.49	399.34	399.49	399.18	399.49	0.15877	0.15865	0.15877	-1.043	-1.6083	0.0	0.0
4	0.2363	396.81	396.52	396.81	396.57	396.81	0.15730	0.15721	0.15730	-0.734	-2.2234	-0.1	0.0
5	0.2407	391.40	390.96	391.40	391.26	391.40	0.15524	0.15519	0.15524	-0.587	-2.6054	-0.4	0.0
6	0.2455	386.65	386.12	386.65	386.63	386.65	0.15365	0.15364	0.15365	-0.512	-3.0165	-0.6	0.0
7	0.2501	381.94	381.37	381.94	382.03	381.94	0.15177	0.15181	0.15177	-0.482	-3.1264	-0.8	0.0
8	0.2546	377.51	376.98	377.51	377.69	377.51	0.15001	0.15009	0.15001	-0.483	-3.0165	-0.9	0.0
9	0.2591	373.50	373.03	373.50	373.76	373.50	0.14841	0.14851	0.14841	-0.513	-3.7134	-1.0	0.0
10	0.2636	369.93	369.62	369.93	370.23	369.93	0.14699	0.14711	0.14699	-0.558	-2.3155	-0.6	0.0
11	0.2680	366.90	366.90	366.90	367.22	366.90	0.14578	0.14591	0.14578	-0.597	0.0	0.2	0.0

LOCATION	STAGN PRESSRE	STAGN TEMPTRE	STATIC PRESSRE	STATIC TEMPTRE	STATIC DENSITY	DELTA P UPON Q	DF HALL NUMBER	LOSS COEFF	DIFFUS FACTOR	RELATIVE EXIT ANG	ABSOLUTE FLOW ANG	NEXT-TAL-ANGLE ACTUAL
1	27158.40	2860.00	26713.62	2849.29	0.17558	-0.08322	1.04111	0.0	0.0	0.0	0.0	0.0
2	27158.40	2860.00	26714.64	2849.33	0.17560	-0.07873	1.03994	0.0	0.0	0.0	0.0	0.0
3	27158.40	2860.00	26720.14	2849.47	0.17562	-0.06651	1.03300	0.0	0.0	0.0	0.0	0.0
4	27158.40	2860.00	26725.13	2849.66	0.17566	-0.04877	1.02432	0.0	0.0	0.0	0.0	0.0
5	27158.40	2860.00	26737.62	2849.89	0.17571	-0.02766	1.01389	0.0	0.0	0.0	0.0	0.0
6	27158.40	2860.00	26747.69	2850.13	0.17576	-0.00518	1.00268	0.0	0.0	0.0	0.0	0.0
7	27158.40	2860.00	26757.59	2850.37	0.17581	0.01702	0.99148	0.0	0.0	0.0	0.0	0.0
8	27158.40	2860.00	26766.79	2850.60	0.17586	0.03780	0.98089	0.0	0.0	0.0	0.0	0.0
9	27158.40	2860.00	26775.01	2850.79	0.17590	0.05662	0.97119	0.0	0.0	0.0	0.0	0.0
10	27158.40	2860.00	26782.27	2850.97	0.17594	0.07361	0.96236	0.0	0.0	0.0	0.0	0.0
11	27158.40	2860.00	26788.37	2851.12	0.17597	0.08833	0.95464	0.0	0.0	0.0	0.0	0.0

TOTAL AXIAL FORCE ON BLADES = -0.02 TOTAL TANGENTIAL FORCE ON BLADES = 0.0

STREAMLINE ANALYSIS RUN 8 CONSTANT TIP RADIUS WITH VARIABLE LOSSES AND WORK AND NON-FREE VORTEX WHIRL AT STATOR EXIT

BEST AVAILABLE COPY

BEST AVAILABLE COPY

* * * S ..ION 7 * * * STATOR EXIT

MASS-AVERAGE TOTAL PRESSURE= 24451.8 MASS-AVERAGE TOTAL TEMPERATURE= 2360.00
CUMULATIVE TOTAL PRESSURE RATIO= 0.9003

LOCATION	RADIUS	MERIDNAL VELOCITY	AXIAL VELOCITY	ABSOLUTE VELOCITY	VEL REL TO NEXT BLADE	VEL REL TO THIS BLADE	ABSOLUTE MACH NUMBER	MACH NO REL NEXT BLADE	MACH NO REL THIS BLADE	RAD OF CURVTRE	STRMLNE SLOPE ANGLE	AXIAL BLADE LOING	TANGEN. BLADE LOING
1	0.2223	1957.81	1957.81	3115.50	3116.12	3115.50	1.40236	1.40273	1.40236	-0.221	0.0	-20357.8	9613.3
2	0.2247	1820.03	1900.01	3079.17	3079.14	3079.17	1.38120	1.38117	1.38120	-0.242	-8.9367	-20922.3	9809.7
3	0.2275	1566.14	1647.93	3047.71	3047.14	3047.71	1.36305	1.36272	1.36305	-0.304	-8.4766	-21502.9	10020.3
4	0.2306	1491.94	1475.61	3020.89	3019.89	3020.89	1.34772	1.34714	1.34772	-0.532	-8.6681	-22266.6	10270.2
5	0.2339	1303.54	1289.11	2991.91	2990.82	2991.91	1.32564	1.32502	1.32564	-0.760	-8.5360	-22979.0	10503.6
6	0.2375	1112.54	1100.13	2965.09	2964.25	2965.09	1.31618	1.31571	1.31618	-1.102	-8.8089	-24054.9	9874.2
7	0.2417	940.55	930.67	2936.99	2936.37	2936.99	1.30049	1.30014	1.30049	-1.771	-8.3132	-24824.8	9214.5
8	0.2463	806.36	799.96	2909.29	2909.07	2909.29	1.28514	1.28501	1.28514	-40.367	-7.2206	-25557.6	8736.0
9	0.2515	720.99	718.31	2883.40	2882.98	2883.40	1.27060	1.27066	1.27060	0.859	-4.4616	-25972.9	8566.4
10	0.2568	684.69	684.65	2803.98	2804.01	2803.98	1.22780	1.22781	1.22780	0.292	-0.6136	-25563.2	8280.6
11	0.2620	676.57	670.57	2728.47	2729.06	2728.47	1.18762	1.18793	1.18762	0.154	7.6308	-25377.7	8280.1

LOCATION	STAGN PRESSRE	STAGN TEMPTRE	STATIC PRESSRE	STATIC TEMPTRE	STATIC DENSITY	DELTA P UPON Q	DF HALL NUMBER	LOSS COEFF	DIFFUS FACTOR	RELATIVE EXIT ANG	ABSOLUTE FLOW ANG	NEXT-INL-ANGLE ACTUAL
1	23509.35	2360.00	7653.61	2197.15	0.06520-42.72609		7.73214	8.20000-10.44401		51.0708	51.0708	51.058
2	23053.12	2360.00	8013.65	2213.11	0.06767-42.14299		7.65345	7.46072-10.47318		54.0720	54.0720	54.076
3	24121.05	2360.00	8509.41	2229.75	0.06976-43.00357		7.62496	6.96050-10.57218		57.1516	57.1516	57.132
4	24312.30	2360.00	8554.23	2233.27	0.07143-42.23295		7.62215	6.62183-10.72870		60.6793	60.6793	60.732
5	24547.44	2360.00	8603.33	2236.73	0.07303-42.37335		7.61667	6.20211-10.84838		64.3325	64.3325	64.403
6	24687.16	2360.00	9070.33	2261.82	0.07498-43.03574		7.66358	6.01706-11.05641		68.1902	68.1902	68.253
7	24790.66	2360.00	9304.54	2273.49	0.07652-43.53395		7.68869	5.90392-11.19642		71.5104	71.5104	71.566
8	24839.06	2360.00	9517.74	2284.87	0.07789-44.04036		7.70558	5.91587-11.27735		74.0354	74.0354	74.064
9	24733.90	2360.00	9660.02	2295.40	0.07869-44.63558		7.71095	6.31419-11.33296		75.5672	75.5672	75.593
10	24633.35	2360.00	10184.30	2327.03	0.08184-44.12303		7.57988	6.70134-11.11713		75.8729	75.8729	75.844
11	24439.15	2360.00	10654.55	2356.18	0.08465-43.56901		7.43658	7.20000-10.88370		75.7705	75.7705	75.726

TOTAL AXIAL FORCE ON BLADES =-1025.04 TOTAL TANGENTIAL FORCE ON BLADES = 397.86

MASS-AVERAGE TOTAL PRESSURE= 24451.8 MASS-AVERAGE TOTAL TEMPERATURE= 2860.00
CUMULATIVE TOTAL PRESSURE RATIO= 2.9003

LOCATION	RADIUS	MERIONAL VELOCITY	AXIAL VELOCITY	ABSOLUTE VELOCITY	VEL REL TO NEXT BLADE	VEL REL TO THIS BLADE	ABSOLUTE MACH NUMBER	MACH NO REL NEXT BLADE	MACH NO REL THIS BLADE	RAD OF CURVTRE	STREAMLIN SLOPE ANGLE	AXIAL BLADE LOADG	TANGEN BLADE LOADG
1	0.2190	1762.32	1730.10	2995.76	2053.46	2995.76	1.33357	0.91427	1.33357	-1.074	-11.0572	244.2	-7.4
2	0.2219	1663.03	1642.20	2934.11	1987.90	2934.11	1.32700	0.88416	1.32700	0.436	-9.6831	392.7	-31.4
3	0.2249	1552.61	1540.13	2874.02	1920.34	2876.02	1.32244	0.85342	1.32244	0.108	-7.2804	332.3	-65.7
4	0.2280	1421.13	1413.75	2813.45	1849.80	2870.45	1.31931	0.81983	1.31931	0.130	-5.0418	477.5	-84.1
5	0.2313	1264.84	1260.23	2845.69	1767.74	2845.69	1.30533	0.77450	1.20533	0.108	-4.8865	465.5	-93.5
6	0.2350	1082.19	1079.17	2824.01	1644.32	2824.01	1.29339	0.72720	1.29339	0.098	-4.2739	511.0	-123.2
7	0.2393	868.30	866.32	2808.64	1545.38	2808.64	1.28489	0.68251	1.28489	0.093	-3.8203	498.3	-42.0
8	0.2443	710.05	709.08	2874.63	1438.86	2876.43	1.28729	0.63384	1.28729	0.110	-2.9341	105.6	-23.9
9	0.2504	570.55	570.46	2862.53	1357.29	2862.53	1.28559	0.59721	1.28559	0.163	-1.0213	-102.6	31.4
10	0.2574	479.02	478.48	2776.50	1215.95	2776.50	1.21318	0.53128	1.21318	0.947	2.7369	-284.8	24.7
11	0.2653	419.18	419.18	2675.44	1084.79	2675.44	1.15992	0.46164	1.15992	-0.176	0.0	-321.6	-4.9

LOCATION	STAGN PRESSRE	STAGN TEMPTRE	STATIC PRESSRE	STATIC TEMPTRE	STATIC DENSITY	DELTA P UPON Q	DE HALL NUMBER	LOSS COEFF	DIFFUS FACTOR	RELATIVE EXIT ANG	ABSOLUTE FLOW ANG	NEXT-INL ANGLE ACTUAL
1	22595.35	2860.00	8429.43	2263.51	0.07012	0.04616	0.96157	0.0	0.03869	54.4569	54.4569	31.125
2	23453.12	2860.00	8830.22	2293.62	0.07164	0.03897	0.96913	0.0	0.03227	56.4686	56.4686	33.290
3	24121.05	2860.00	8781.32	2256.73	0.07279	0.02983	0.97548	0.0	0.02717	58.7729	58.7729	35.187
4	24312.30	2860.00	9009.35	2334.17	0.07380	0.02119	0.98430	0.0	0.02044	61.9673	61.9673	38.747
5	24547.66	2860.00	9147.32	2268.58	0.07500	0.01557	0.98778	0.0	0.01673	64.6543	64.6543	42.115
6	24687.16	2860.00	9349.72	2279.45	0.07626	0.01783	0.98615	0.0	0.02053	68.3379	68.3379	46.057
7	24790.66	2860.00	9497.12	2294.76	0.07776	0.01229	0.99035	0.0	0.01231	72.2601	72.2601	50.145
8	24839.06	2860.00	9742.51	2297.76	0.07932	0.01462	0.98877	0.0	0.01286	75.7340	75.7340	60.529
9	24733.90	2860.00	9801.26	2303.43	0.07960	0.00834	0.99276	0.0	0.00439	78.5106	78.5106	65.234
10	24633.35	2860.00	10374.68	2337.39	0.08304	0.01313	0.99020	0.0	0.00633	80.0922	80.0922	66.034
11	24489.15	2860.00	11040.95	2375.80	0.08695	0.02714	0.98056	0.0	0.01963	80.9919	80.9919	66.741

TOTAL AXIAL FORCE ON BLADES = 6.79 TOTAL TANGENTIAL FORCE ON BLADES = -1.23

* * * STATION 8 * * *

BEST AVAILABLE COPY

BEST AVAILABLE COPY

* * * STATION 9 * * * ROTOR EXIT

MASS-AVERAGE TOTAL PRESSURE= 7288.1 MASS-AVERAGE TOTAL TEMPERATURE= 2264.30

CUMULATIVE TOTAL PRESSURE RATIO= 0.2684

LOCATION	RADIUS	MERIDNAL VELOCITY	AXIAL VELOCITY	ABSOLUTE VELOCITY	VEL REL TO NEXT BLADE	VEL REL TO THIS BLADE	ABSOLUTE MACH NUMBER	MACH NO REL NEXT BLADE	MACH NO REL THIS BLADE	RAD OF CURVTRE	STRMLNE SLOPE ANGLE	AXIAL BLADE LOADG	TANGEN BLADE LOADG
1	0.2060	618.99	618.98	1039.17	1086.56	2050.71	0.47972	0.47600	0.91605	0.175	0.0	-597.6	-[illegible]
2	0.2156	634.17	634.17	1048.21	1090.38	2062.75	0.47421	0.47673	0.92225	0.300	-1.3774	-[illegible]	-[illegible]
3	0.2253	854.67	854.66	1062.45	1097.92	2104.64	0.47004	0.47956	0.93479	-3.467	0.1412	-[illegible]	-[illegible]
4	0.2325	959.00	959.52	1089.76	1091.06	2198.32	0.49693	0.49350	0.99443	-0.393	1.3229	-[illegible]	-9106.5
5	0.2389	1082.02	1080.52	1170.26	1170.19	2226.73	0.53109	0.53112	1.01119	-0.262	3.0038	-5300.5	-9500.7
6	0.2443	1191.45	1188.04	1243.93	1244.10	2235.96	0.56606	0.56621	1.01867	-0.210	3.7182	-5165.6	-10134.7
7	0.2491	1280.63	1277.57	1300.27	1308.08	2227.40	0.59570	0.59662	1.01715	-0.201	3.9036	-4991.5	-9772.5
8	0.2535	1345.70	1342.88	1353.17	1360.71	2228.38	0.62036	0.62162	1.01901	-0.217	3.7114	-4134.1	-8071.9
9	0.2576	1389.80	1387.98	1405.10	1405.83	2213.34	0.64179	0.64314	1.01305	-0.278	2.9228	-3994.4	-8105.6
10	0.2614	1468.57	1467.98	1471.58	1473.97	2274.12	0.67435	0.67555	1.04224	-0.501	1.6337	-4651.7	-7656.8
11	0.2650	1549.12	1549.12	1552.65	1554.39	2351.63	0.71295	0.71384	1.07971	********	0.0	-5135.6	-7483.1

LOCATION	STAGN PRESSRE	STAGN TEMPTRE	STATIC PRESSRE	STATIC TEMPTRE	STATIC DENSITY	DELTA P UPON Q	DE HALL NUMBER	LOSS COEFF	DIFFUS FACTOR	RELATIVE EXIT ANG	ABSOLUTE FLOW ANG	NEXT-INL-ANGLE ACTUAL
1	6704.58	2313.30	5805.11	2236.40	0.06863	-0.46566	1.00324	0.72000	-0.16026	-63.3910	-20.8167	-30.632
2	6580.61	2278.35	5687.80	2208.13	0.06836	-0.46230	1.00854	0.72000	-0.20009	-67.3300	-37.0379	-35.330
3	6521.44	2264.19	5742.25	2189.30	0.06915	-0.40923	1.13856	0.72000	-0.32105	-66.3745	-36.5816	-35.325
4	6754.21	2357.01	5773.86	2174.93	0.06975	-0.67738	1.14166	0.72000	-0.37278	-64.1517	-23.3700	-25.197
5	6696.92	2254.63	5834.63	2160.12	0.06963	-0.79607	1.27369	0.72000	-0.44938	-60.9851	-22.4227	-21.[illegible]
6	7237.69	2254.44	5804.68	2147.89	0.06942	-0.93614	1.35956	0.72000	-0.52363	-57.5599	-15.7371	-16.225
7	7459.13	2255.78	5565.35	2136.35	0.06917	-1.08699	1.43975	0.72000	-0.59945	-54.9727	-11.3374	-11.[illegible]
8	7707.71	2253.25	6032.69	2131.30	0.06903	-1.31131	1.54735	0.72000	-0.69875	-52.9126	-7.7067	-7.[illegible]
9	7841.95	2260.56	6035.09	2125.03	0.06921	-1.50037	1.62966	0.72000	-0.77780	-50.8100	-3.9342	-3.[illegible]
10	8123.52	2256.09	6089.53	2116.90	0.06939	-2.00983	1.86973	0.72000	-1.08156	-49.7912	-3.6636	-3.501
11	8425.74	2274.20	6112.08	2107.98	0.06933	-3.05402	2.21072	0.72000	-1.52080	-48.7995	-3.8619	-3.710

TOTAL AXIAL FORCE ON BLADES = -267.80 TOTAL TANGENTIAL FORCE ON BLADES = -449.15

APPENDIX D

TESTING SEQUENCE FOR PHASE II

The actual testing sequence of all tests run in Phase II, together with the test time for each test, is included in this appendix.

TESTING SEQUENCE - PHASE II

CONDENSED LOG				ASATT TEST PROGRAM	
DATE	RUN NUMBER	DACS TAPE I.D. NO.	MTS EQUATION NO.	TEST NO./DESCRIPTION (See Table II for Test Disc)	TEST TIME
4/20				Null Sta. 9 Probe	1.33
4-27	0.1			Eqpt. Check Run	1.83
4-30				Null Check of Sta. 9	0.75
5-2	0.2			Run Check, Sta. 9 Survey	6.40
5-4	0.3			Null Sta. 9, Sta. 9 Survey	4.03
5-10	0.4			Leak and Eqpt. Check	1.92
5-11				Load Cell Cal. While Pressurize	1.97
		Test Number 1			
5-14	0.5	A4473134		Full Survey with MTS System Removed	5.90
5-15	0.6			Hot Film Survey	1.85
		Ball Bearings and Silicon Rubber Diaphragm Installed			
5-18				Null Sta. 9; Calibrate Force	0.95
5-21				Calibrated Force	1.25
		Replaced Failed Rubber Diaphragm			
5-22	1.0			Test Number 1	4.38
5-23				Calibrated Force	0.92
5-24				Calibrate Force & Rig Press. Press.	2.42
		Replaced Rubber Diaphragm and Added Diaphragm Restraint			
5-25	1.2			Test 1 with Recal. of Force	2.00
		Test Number 2 Configuration Installed			
5-29	2.0	A4473149		Full Sta. 8 Survey	5.88
6-6	2.1			Hot Film Survey	0.62
6-8	2.2	A4473159		Hot Film Survey	2.27
6-12	3.0	A4473163		Full Sta. 8 Survey MTS System Removed	7.97
		MTS Vane Assembly Re-operated per X604054-1			
6-13	3.1	A4473164		Full Survey of Sta. 8	3.00
		Test Number 3 Configuration Installed			
6-21	4.0	A4473172		Sta. 8 and Hot Film Surveys	6.07
6-25	4.1	A4473176		Hot Film Survey	1.77
		Test Number 4 Configuration Installed			
6-29	5.0	A4473180	5	Test No. 4	4.42
7-2	5.1		5	Hot Film Survey	2.58
		Turbulence Screen 2 Installed			
7-12	6.0	A4473193	5	Test No. 6	5.63
7-13	6.1		5	Hot Film Survey	3.75
7-14	6.2	A4473195	5	Hot Film Survey Repeat	2.50
		Turbulence Screen 1 Reinstalled			
				TOTAL TEST TIME	84.36

CONDENSED LOG — ASATT TEST PROGRAM

DATE	RUN NUMBER	DACS TAPE L.D. NO.	MTS EQUATION NO.	TEST NO./DESCRIPTION (see Table II for Test Disc)	TEST TIME
7-14	7.0	A4473195	5	Test No. 7	1.50
7-14	8.0	A4473195	5	Test No. 8	1.33
7-16	9.0	A4473197	5	Test No. 9	2.17
7-17	10.0	A4473198	5	Test No. 10	2.42
7-17	11.0	A4473198	5	Test No. 11	1.75
7-18	12.0	A4473199	5	Test No. 12	3.00
7-18	10.1	A4473199	5	Test No. 10 Repeat	1.50
7-19	11.1	A4473200	5	Test No. 11 Repeat	1.50
		Labyrinth Seal Was Installed			
		Actuator Nozzle Was Installed			
9-7				Leak and Inst. Check Run	0.83
9-8	13.0	A4473251	4	Test 13; A Leak was Noted	3.08
9-17	13.1	A4473260	3	Test 13 Repeat	2.92
9-17	14.0	A4473260	3	Test 14	0.50
9-21	15.0	A4473264	3	Test 15	2.83
		Rotor Configuration Was Installed			
10-8	16.0	A4473281	2	Test 16	5.33
10-9	17.0	A4473282	2	Test 17	1.67
10-10	18.0	A4473283	2	Test 18	2.17
10-11	18.1	A4473284	2	Test 18 with Bypass Flow	2.17
10-15	18.2	A4473288	2	Test 18 with Bypass Flow	1.33
10-16	19.0	A4473288	2	Test 19	3.00
		Cooling Flow Manifold Installed			
10-23	26.0	A4473296	2	Test 26	2.53
10-24	27.0	A4473297	2	Test 27	2.92
10-25	27.1	A4473298	2	Test 27 Continued	2.42
10-25	28.0	A4473298	2	Test 28	1.83
10-26	28.1	A4473299	2	Test 28 Continued	1.33
		Slave Rotor Was Installed			
10-29	25.0	A4473302	1	Test 25	3.00
10-30	25.0	A4473303	1	Test 25 Continued	3.50
		Installed Shroud Configuration 4			
11-2				System Check Run	0.92
11-5	20.0	A4473309	1	Test 20	7.57
11-6	22.0	A4473310	1	Test 22	1.52
				TOTAL TEST TIME	152.95

CONDENSED LOG — ASATT TEST PROGRAM

DATE	RUN NUMBER	DACS TAPE I.D. NO.	MTS EQUATION NO.	TEST NO./DESCRIPTION (See Table II for Test Disc)	TEST TIME
11-6	21.0	A4473310	1	Test 21	1.28
11-9	23.0	A4473313	1	Test 23	1.28
11-9	24.0	A4473313	1	Test 24	1.28
11-9	22.1	A4473313	1	Test 22 Repeat	2.75
11-13	24.1	A4473317	1	Test 24a	1.58
11-16	24.2	A4473320	1	Test 24b	4.33
11-19	24.3	A4473323	1	Test 24b Similar to Test 24a	1.92
		Repeat Test Runs			
11-25	3R.0	A4473329	1	Test 2 Repeat	3.29
11-26	5R.0	A4473330	1	Test 4 Repeat	4.50
11-27	6R.0	A4473331	1	Test 6 Repeat	2.45
11-27	8R.0	A4473331	1	Test 8 Repeat	3.28
11-29	9R.0	A4473333	1	Test 9 Repeat	2.83
11-30	7R.0	A4473334	1	Test 7 Repeat	4.92
12-3	BL.0	A4473337	1	Test 2 with Inlet Rakes Removed	2.34
				TOTAL TEST TIME	188.42

END OF PHASE II TESTING

APPENDIX E

PROBLEM AREAS ENCOUNTERED DURING PHASE III TESTING

Several of the problems encountered during the Phase III testing effort are briefly described below to assist future similar programs in applying testing techniques developed during the ASATT Program.

1. Nozzle Exit Survey

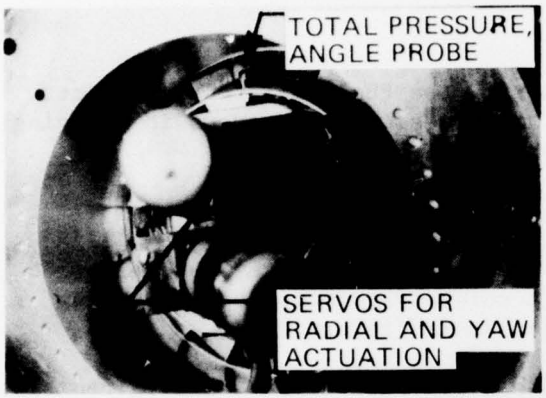
The radial and circumferential total pressure/angle survey was performed on the ASATT full round nozzle using a uniquely constructed traversing mechanism fastened to the turbine rotor shaft (Figure E-1).

The probe was constructed such that the survey could be regulated radially and circumferentially. The probe was free to pivot in two dimensions to a nulled position determined by side taps on the probe. Because of the length of the probe from the pivot point, the sensing end's position changed considerably as it was rotated to a null position. The probe projections tend to focus toward mid-channel. Figure E-2 illustrates the axial shift of the probe sensing end as the null angle changes. At 10%, this axial shift indicates flow affecting the nulling could be from 5% to 10% height projections instead of just 10%.

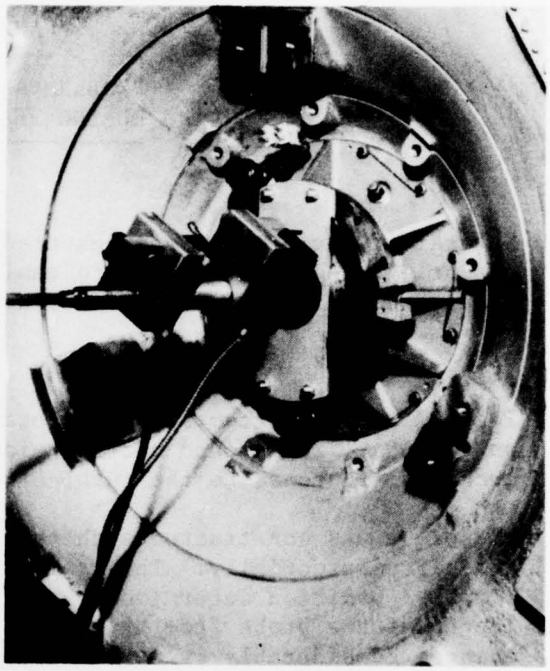
Regions where survey data exist are illustrated in Figure E-3. The projections incorporated in this pictoral representation ignored the change of percent height associated with the axial-radial shift of the sensing end in the flaring annulus. The regions of missing data present an indeterminant problem in constructing loss contours.

The total pressure probe was redesigned to move the probe head closer to the nozzle vane trailing edge. The design was accomplished by extending the probe in an axial direction toward the nozzle approximately 1¼ inches and curving the probe head into the flow direction for a distance of 3/8 inch (Figure E-4). With the traverse mechanism mounted on the turbine rotor shaft (Figure E-1(a)) the probe tip was spaced approximately 0.25 in. (measured axially) from the nozzle vane trailing edge. That location was chosen to simulate the rotor leading edge axial location so that the loss profiles measured would approximate the loss profiles entering the rotor. The probe tip was fabricated with the same geometry as the original probe to achieve the same recovery. The surveys were conducted at a fixed angle (a nulling system was not incorporated on the redesigned probe) and the vacant data areas are discussed above and shown pictorially in Figure E-3.

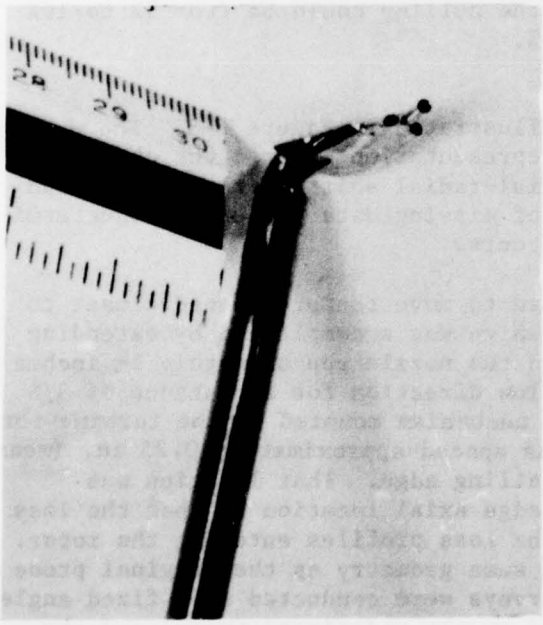
The results of the surveys were very satisfactory. Even though measured air angles were not obtained, the improved accuracy of the total pressure measure-



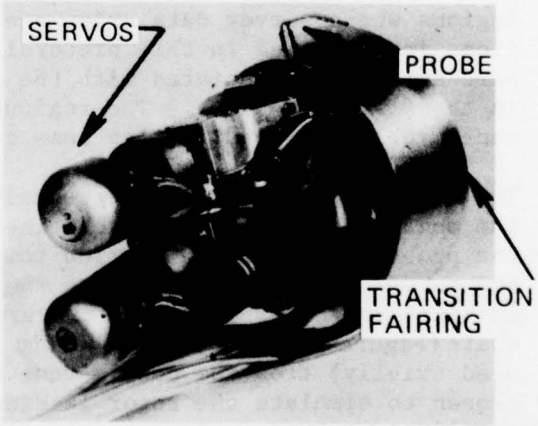
(a) VIEW INTO NOZZLE EXIT WITH TRAVERSING MECHANISM INSTALLED



(b) CIRCUMFERENTIAL ACTUATOR INSTALLED ON ROTOR SHAFT AT OPPOSITE SIDE OF PLENUM



(d) SUPERSONIC PITOT, ANGLE



(c) TRAVERSE MECHANISM PROVIDES UNIQUE SOLUTION TO RADIAL AND CIRCUMFERENTIAL TOTAL PRESSURE AND ANGLE SURVEY AT NOZZLE EXIT

Figure E-1. Test 1 (Nozzle Performance) Facility Installation and Test Equipment.

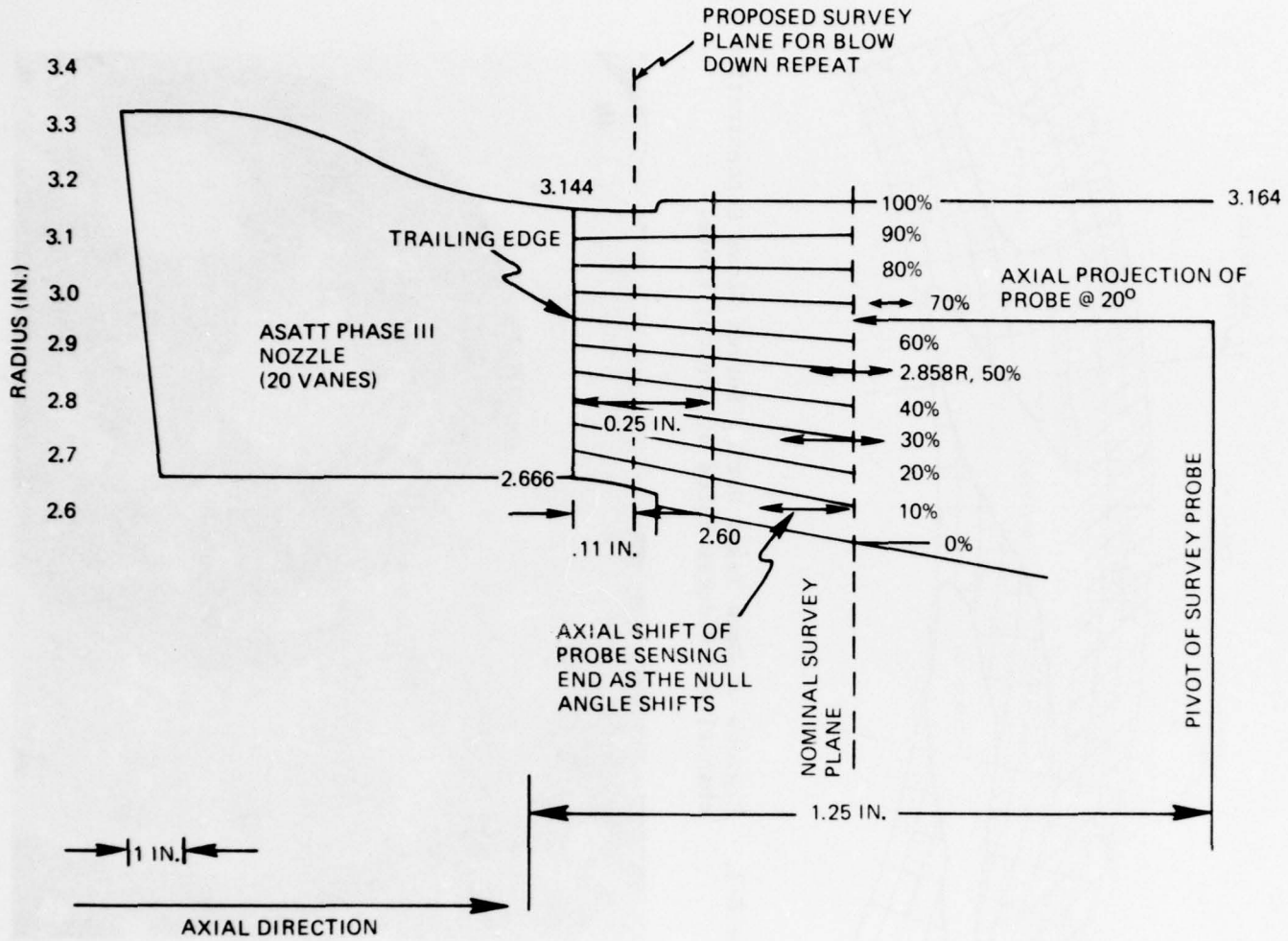


Figure E-2. Axial shift in Measurement Plane as a Result of Nulling.

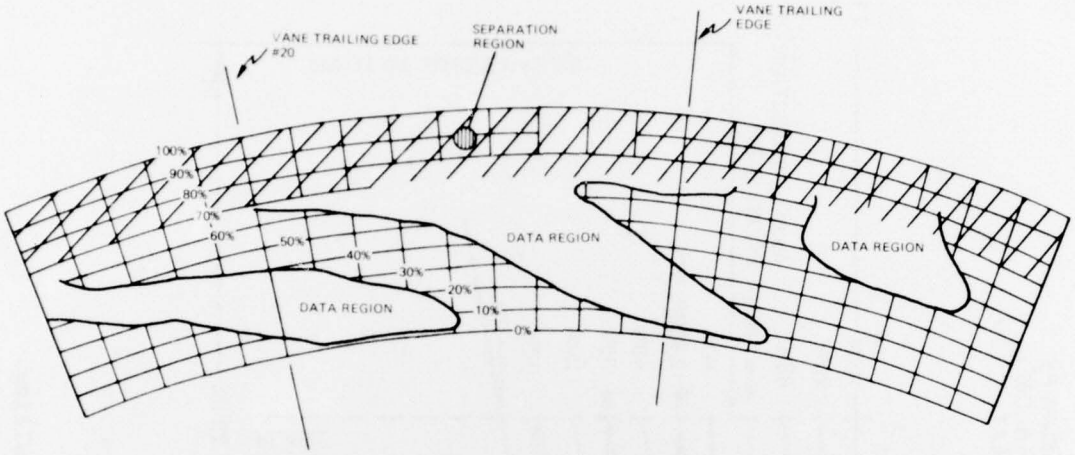


Figure E-3. Regions of Data Taken During Survey Shows Concentration in Mid-channel and Reduces Value of Contour Plots.

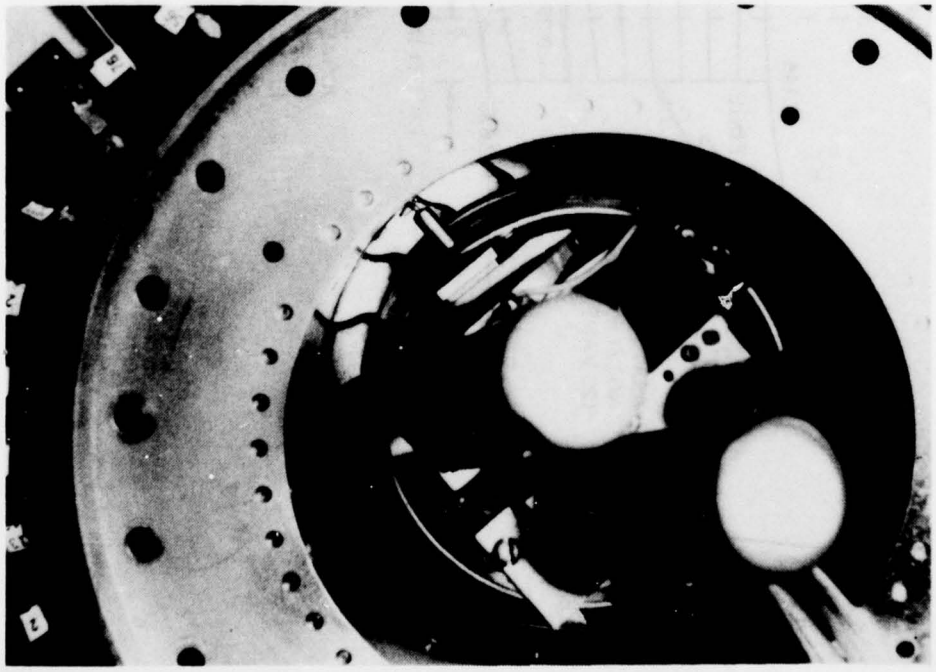


Figure E-4. Redesigned Total Pressure Probe Installed in Traverse Mechanism (shown in Phase V installation).

ments, together with the measured inner and outer wall static pressure, permitted a good estimate of the air angle distribution using a continuing of mass flow calculation.

2. Torque-meter Vibrations

During the initial rotating turbine stage tests vibratory problems were experienced at the in-line Himmelstein torquemeter. An extensive investigative effort revealed that the cantilever-mounted torquemeter had a resonance near the turbine design speed (26,000 - 28,000 RPM). The problem was resolved by constructing a bracket fixing the cantilevered end of the torquemeter to the plenum housing.

3. Water Brake Vibrations and Bearing Failures

The water brake dynamometer used to load the turbine was a Kahn Model 401-015. This unit was selected since it adequately covered the power and speed range determined for the ASATT turbine testing (Figure E-5). Several problems were experienced during testing which caused considerable delays in the test schedule; however, the problems were resolved and the program was completed satisfactorily.

The two most critical problems were: high vibrations caused by unbalance of the rotating disk, and bearing failures caused by inadequate lubrication of the water brake bearings. The balance problem was resolved by rebalancing the smooth disk to within 0.001 oz-in. The bearing lubrication problem was solved at the Kahn Company by modifying the oil mist supply to permit lubricant flow through the bearing.

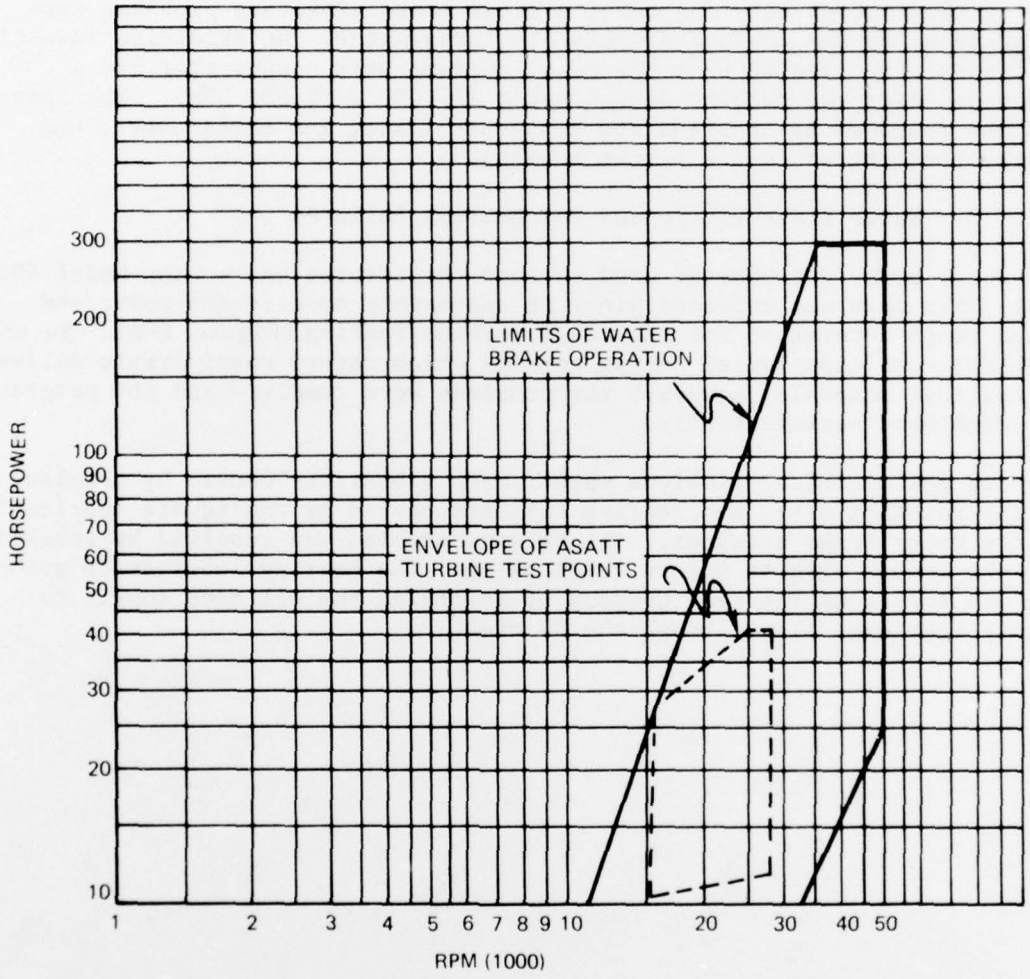


Figure E-5. Water Brake Operating Envelope - The Power Absorption Requirements of the ASATT Turbine Fall Within the Water Brake Operating Envelope for all Planned Test Points.

LIST OF SYMBOLS

A	area, $in.^2$
C_o	isentropic velocity corresponding to total head, fps.
c_p	specific heat at constant pressure
c,b	actual chord, in.
C_x	axial chord, in.
D	diffusion parameter, dimensionless
g	gravitational constant, 32.17 ft/sec^2
ΔH	turbine work, Btu/lb
h,	blade height, in.
K_B	blockage factor dimensionless
i	incidence angle, deg.
J	mechanical equivalent of heat, 778.2 ft-lb/Btu
M	Mach number
N	rotational speed, rpm
σ, d_o	throat dimension, in.
σ	solidity
P	stagnation pressure, psia
ρ	static pressure, psia
R	radius, in.
S	entropy
s	pitch spacing, in.
T	stagnation temperature, °R
t	trailing edge thickness, in.
t	static temperature, °R
U	blade velocity, fps

LIST OF SYMBOLS (continued)

ϕ_n	nozzle Zweifel coefficient
ϕ_r	rotor Zweifel coefficient
V	absolute gas velocity, fps
W_a	airflow, lbs/sec.
W	relative gas velocity, fps
Y_T	Loss coefficient, $\frac{\text{Loss of total head pressure}}{\text{Total pressure at blade outlet} - \text{Static pressure at blade outlet}}$
w	gas weight flow, lbs/sec.
z	number of blades
α	relative gas flow angle measured from axial direction, deg.
β	absolute gas glow angle measured from axial direction, deg.
δ	boundary layer thickness
δ^*	boundary layer displacement thickness $\delta^* = \int_o^\delta (1+\frac{\rho_X W_X}{\rho W})\, dy$
θ	boundary layer momentum thickness $\theta = \int_o^\delta \frac{\rho_X W_X}{\rho W} \quad (1 - \frac{W_X}{W})\, dy$
H	boundary layer shape factor $H = \frac{\delta^*}{\theta}$
H_i	incompressible form factor
W_X	velocity parallel to the wall
W	theoretical wall velocity
X,Y	coordinate system parallel to and perpendicular to the wall
T	turbulence intensity $T = \frac{u'}{U}$
u'	RMS velocity in thru flow direction
U	Mean thru flow velocity

LIST OF SYMBOLS (continued)

δ ratio of inlet stagnation pressure to sea level standard

ϵ $$\frac{\gamma_{s1}}{\gamma}\left[\left(\frac{\gamma+1}{2}\right)^{\frac{\gamma}{\gamma-1}} \Big/ \left(\frac{\gamma_{s1}+1}{2}\right)^{\frac{\gamma_{s1}}{\gamma_{s1}-1}}\right]$$

θ_{cr} $$\frac{T}{T_{s1}}\quad\frac{(\ \gamma\ )}{(\gamma+1)}\quad\frac{(\ \gamma_{s1}+1\ )}{(\ \gamma_{s1}\ )}$$

η total-to-total adiabatic efficiency, percent

ψ efficiency, $\frac{\text{Actual velocity}}{\text{Isentropic velocity}}$, corresponding to-total-to static pressure ratio

ρ density, slugs/ft^3

γ,k ratio of specific heats

TDF Combustor temperature distribution factor, defined as: $\dfrac{T_5 \text{ maximum} - T_5 \text{ average}}{T_5 \text{ average} - T_{CDT}}$

Where, 5 is at turbine rotor inlet
CDT is compressor discharge

Ω_H Hub stage loading = $2gJ\ H/U^2h$

Subscripts:

av average

cr conditions at Mach number of 1.0

h,H hub

m mean condition

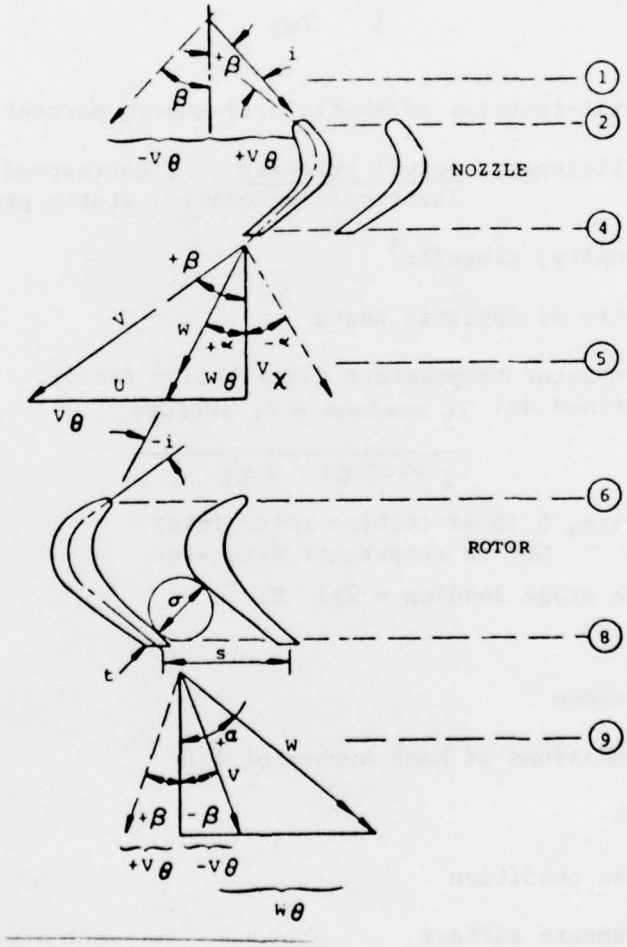
p pressure surface

r radial direction

s suction surface

LIST OF SYMBOLS (continued)

sl	standard sea level conditions
T	total condition
t	tip
x	axial direction
θ	tangential direction



Turbine Velocity Diagram Station and Sign Notation

5828-77